

AN ASSESSMENT OF INDOOR GEOLOCATION SYSTEMS

by

Illir Fiqiri Progri

A Dissertation

Submitted to the Faculty

of the

WORCESTER POLYTECHNIC INSTITUTE

in partial fulfillment of the requirements for the

Degree of Doctor of Philosophy

in

Electrical Engineering

by

May 2003

APPROVED:

Prof. William R. Michalson, Advisor

Prof. John A. Orr, Head of Department

Prof. Kaveh Pahlavan, Dissert. Committee

Prof. Reinhold Ludwig, Dissert. Committee

Dr. Pratap N. Misra, Dissert. Committee

Abstract

CURRENTLY there is a need to design, develop, and deploy autonomous and portable indoor geolocation systems to fulfil the needs of military, civilian, governmental and commercial customers where GPS and GLONASS signals are not available due to the limitations of both GPS and GLONASS signal structure designs.

The goal of this dissertation is (1) to introduce geolocation systems; (2) to classify the state of the art geolocation systems; (3) to identify the issues with the state of the art indoor geolocation systems; and (4) to propose and assess four WPI indoor geolocation systems. It is assessed that the current GPS and GLONASS signal structures are inadequate to overcome two main design concerns; namely, (1) the *near-far* effect and (2) the *multipath* effect. We propose four WPI indoor geolocation systems as an alternative solution to *near-far* and *multipath* effects. The WPI indoor geolocation systems are (1) a DSSS/CDMA indoor geolocation system, (2) a DSSS/CDMA/FDMA indoor geolocation system, (3) a DSSS/OFDM/CDMA/FDMA indoor geolocation system, and (4) an OFDM/FDMA indoor geolocation system. Each system is researched, discussed, and analyzed based on its principle of operation, its transmitter, the indoor channel, and its receiver design and issues associated with obtaining an observable to achieve indoor navigation. Our assessment of these systems concludes the following.

First, a DSSS/CDMA indoor geolocation system is inadequate to neither overcome the *near-far* effect nor mitigate cross-channel interference due to the *multipath*. Second, a DSSS/CDMA/FDMA indoor geolocation system is a potential candidate for indoor positioning, with data rate up to 3.2 KBPS, pseudorange error, less than 2 m and phase error less than 5 mm. Third, a DSSS/OFDM/CDMA/FDMA indoor geolocation system is a potential candidate to achieve similar or better navigation accuracy than a DSSS/CDMA indoor geolocation system and data rate up to 5 MBPS. Fourth, an OFDM/FDMA indoor geolocation system is another potential candidate with a totally different signal structure than the previous three WPI indoor geolocation systems, but with similar pseudorange error performance.

Acknowledgments

“Jesus saith unto him, I am the way, the truth, and the life: no man cometh unto the Father, but by me.”—John 14:6

I WOULD like to express my sincere gratitude and thanks to several people for assisting, guiding, directing, and inspiring me towards my completion of the degree of the Doctor of Philosophy.

My deepest gratitude and thanks goes to my good friend and advisor, Professor Bill Michalson who is a unique example of a down to earth person with great sense of humor, solid worker, great motivator, and honest advisor despite our differences in beliefs and in cultural and technical backgrounds. Thank you Bill, for frequently revising my drafts, clarifying my thoughts, improving my technical writing skills, and orienting me over baffling phenomena encountered in this tremendous project. Thank you Bill, for supporting me in so many technical conferences and sharing part of your personal life with me.

On a more personal note, I am very grateful of Professor John A. Orr as a great example of an honest and just person, who lives in the “Fear of God,” and who treats colleges equally and fairly. I would like to thank you, John, for your wisdom and courage, for believing in me and for being my academic advisor for the early part of my Ph.D. program.

I am very grateful to Professor Fred J. Looft who is a good and a solid administrator with good heart and willing to do good to young teaching assistants and help them gain their confidence in their teaching experience.

On a more personal note, I would like to thank the dissertation committee members, Professor Reinhold Ludwig, Professor Kaveh Pahlavan, and Dr. Pratap Misra.

I would also like to thank my past advisors Professor Alex E. Emanuel and Professor Kevin Clements who have continued to support and encourage me. My sincere thanks goes to Professor David Cygancki, Professor Rich Brown, and Dr. Matthew Bromberg, for assisting in my area research committee examination. I would like to thank Professor

Hossein Hakim, Professor Peder Pedersen, Professor Dennis Nicoletti, Professor Bob Labonté, Professor Jonathan Hill, Professor Jim Duckworth, Dr. Rulph Chassaing, Dr. Duncan Cox, Jr., Gene Bogdanov, Vikram Rammanna, Dr. Bob Swarz, Dr. Richard Stanley, Cathy Emmerton, Brenda McDonald, and Patricia LeBreton.

I would also like to thank my friend David Anderson who was my roommate for the first three years of my Ph.D. program and inspired me during this time and is a great friend.

I would like to thank the Institute of Navigation and the IEEE Communication Society. These institutions have been my inspiration in my carrier goals as a scholar and researcher.

My sincere thanks goes also to my mother, Lumturi, to my father, Fiqiri, to my sister Adriana, my brother-in-law, Anesti, and my two beautiful nieces, Rafailia and Aleksia. I would like to thank my dear relatives, Dr. Peter Demir, his wife, Elizabeth Demir, and my cousins, Kristen and Alex. I am also very thankful to my brethren and sisters of my local assembly (Walnut Street Gospel Hall) in Saugus, MA. I am also very thankful to my brethren and sisters to other local assemblies such as Midland Park, NJ; Worcester, MA; Watertown, MA; Methuen, MA, and Cambridge, MA.

I would also like to thank my karate master, Dr. Johnson Chung, Dr. Reinhard Bartelmann, and Marion M Taylor and my karate friends at MIT, Worcester, and Amherst Dojos.

Last but not least, thanks be unto God for his unspeakable gift, the Lord Jesus Christ. Thank you Lord for your faithfulness, for your provision and for your precious word "HOLY BIBLE:" Its doctrines are holy, its precepts are binding, its histories are true, and its decisions are immutable. Read it to be wise, believe it to be safe, practice it to be holy. It contains light to direct you, food to support you, and comfort to cheer you.

Finally, I have reserved a few words to share with every WPI community member. This has been a very friendly and nice community; it has offered me unlimited opportunities, true friendship, and inspiring and consistent leadership.

Table of Content

CHAPTER 1. INTRODUCTION.....	1
1.0 GEOLOCATION SYSTEM.....	1
1.1 HISTORY AND BACKGROUND.....	2
1.2 GEOLOCATION SYSTEM CONCEPT.....	3
1.3 TECHNICAL DEFINITION AND CLASSIFICATION OF RADIO GEOLOCATION SYSTEMS	6
1.3.1 OUTDOOR GEOLOCATION SYSTEMS.....	7
1.3.2 INDOOR GEOLOCATION SYSTEMS.....	9
1.3.3 UNDERWATER GEOLOCATION SYSTEMS	10
1.4 A GENERIC RADIO GEOLOCATION SYSTEM.....	11
1.4.1 TRANSMITTER.....	12
1.4.2 CHANNEL	14
1.4.3 RECEIVER	15
1.5 OUTDOOR GEOLOCATION SYSTEMS	16
1.5.1 THE GLOBAL POSITIONING SYSTEM	17
1.5.1.1 GPS Description.....	17
1.5.2 THE GLOBAL NAVIGATION SATELLITE SYSTEM	19
1.5.2.1 GLONASS Description	20
1.5.3 GALILEO: THE EUROPEAN SATELLITE RADIO NAVIGATION SYSTEM	21
1.5.3.1 Galileo Description	22
1.5.4 MTSAT OR MSAS	24
1.5.5 SATELLITE/PSEUDOLITE OUTDOOR GEOLOCATION SYSTEM.....	24
1.5.5.1 GPS Satellite/Pseudolite Outdoor Geolocation System.....	24
1.5.5.2 GLONASS Satellite/Pseudolite Outdoor Geolocation System.....	26
1.6 INDOOR GEOLOCATION SYSTEMS	26
1.6.1 INDOOR SATELLITE/PSEUDOLITE GEOLOCATION SYSTEM.....	27
1.6.1.1 SnapTrack™ Indoor Geolocation System.....	28
1.6.1.2 US Coast Guard Indoor Geolocation System.....	29
1.6.2 WIRELESS INDOOR GEOLOCATION SYSTEMS.....	30
1.6.2.1 Wireless Networks (IEEE 802.11).....	31
1.6.2.2 Mobile Phone Positioning for 3G Systems	33
1.6.2.3 Cell-ID Positioning Method	35
1.6.2.4 TDOA Positioning Method	35
1.6.2.5 Aided GPS Positioning Methods.....	37
1.6.3 OTHER INDOOR GEOLOCATION SYSTEMS.....	38
1.6.3.1 MIT Relay Indoor Geolocation System.....	38
1.6.3.2 Precise RF Positioning System.....	39
1.6.3.3 UWB Indoor Geolocation System.....	40
1.7 INDOOR GEOLOCATION SYSTEM SPECIFICATIONS	41

1.7.1	REQUIREMENTS.....	41
1.7.1.1	Accuracy.....	42
1.7.1.2	Integrity.....	43
1.7.1.3	Availability.....	43
1.7.1.4	Compatibility.....	43
1.7.1.5	Interoperability.....	43
1.7.1.6	Continuity.....	44
1.7.1.7	Communication.....	44
1.7.2	APPLICATIONS.....	44
1.7.2.1	Indoor, Indoors/Outdoors, and Outdoors/Indoors.....	44
1.7.2.2	Interference.....	45
1.7.2.3	Jamming/Spoofing.....	45
1.7.3	NOVELTY.....	45
1.7.3.1	Signal Structure.....	45
1.7.3.2	Code Selection.....	46
1.7.3.3	Frequency Selection.....	46
1.7.3.4	Equalization.....	46
1.7.3.5	Anti-jamming/Anti-spoofing.....	46
1.8	WPI INDOOR GEOLOCATION SYSTEM.....	46
	CHAPTER 2. RADIO GEOLOCATION SYSTEMS.....	60
2.0	INTRODUCTION.....	60
2.1	SELECTION OF EXAMPLES OF OUTDOOR GEOLOCATION SYSTEMS.....	60
2.2	GPS.....	61
2.2.1	PRINCIPLE OF OPERATION OF GPS.....	61
2.2.2	GPS TRANSMITTER (SATELLITE).....	64
2.2.2.1	Signal Structure and Design.....	64
2.2.2.2	Message Format, Content, and GPS Time.....	66
2.2.2.2.1	Satellite Ephemerides.....	70
2.2.2.2.2	Satellite Almanacs.....	71
2.2.2.2.3	GPS UTC Parameters.....	71
2.2.2.3	GPS Satellite Onboard Clocks.....	72
2.2.3	GPS RECEIVER.....	73
2.2.4	EXTRACTION OF OBSERVABLE(S).....	75
2.2.4.1	GPS Receiver Signal Acquisition.....	77
2.2.4.1.1	The Acquisition Search Space.....	77
2.2.4.1.2	The Detection Criterion.....	79
2.2.4.1.3	DFT (FFT) Search Method.....	86
2.2.4.2	Code and Carrier Tracking Loops.....	86
2.2.4.2.1	I/Q Demodulation.....	86
2.2.4.2.2	Generic Tracking Loop.....	90
2.2.4.2.3	GPS Receiver Code Tracking Loop.....	94
2.2.4.2.4	GPS Receiver Frequency Lock Loop.....	97
2.2.4.2.5	GPS Receiver Carrier Tracking Loop.....	102
2.2.4.3	GPS Receiver Bit Synchronization.....	103
2.2.4.4	GPS Receiver Subframe Alignment.....	105
2.2.5	ISSUES.....	106
2.3	GLONASS.....	106
2.3.1	PRINCIPLE OF OPERATION OF GLONASS.....	106
2.3.2	GLONASS TRANSMITTER (SATELLITES).....	107
2.3.2.1	Signal Structure Design.....	107
2.3.2.2	Message Format, Content, and GLONASS Time.....	110

2.3.2.3	<i>Satellite Ephemerides</i>	111
2.3.2.4	<i>Satellite Almanac</i>	112
2.3.2.5	<i>Onboard Clocks</i>	113
2.3.3	GLONASS RECEIVER.....	113
2.3.4	EXTRACTION OF OBSERVABLE(S)	114
2.3.5	ISSUES.....	114
2.4	EXAMPLES FOR (INDOOR) GEOLOCATION SYSTEMS.....	114
2.5	A PSEUDOLITE GEO LOCATION SYSTEM.....	114
2.5.1	PRINCIPLES OF OPERATION OF A PSEUDOLITE GEOLOCATION SYSTEM	115
2.5.2	TRANSMITTER (PSEUDOLITE).....	118
2.5.2.1	<i>Conventional Pseudolite Signal Design</i>	119
2.5.2.2	<i>Pseudolite Time Synchronization</i>	120
2.5.2.3	<i>Message Format, Type, and Content</i>	121
2.5.3	RECEIVER	123
2.5.4	EXTRACTION OF OBSERVABLE(S)	123
2.5.5	ISSUES.....	124
2.5.5.1	<i>Interference Caused by Crosscorrelation Between C/A Codes</i>	124
2.5.5.2	<i>Interference Caused by Pseudolite Signal Level</i>	128
2.6	MIT INDOOR GEOLOCATION SYSTEM.....	130
2.6.1	PRINCIPLE OF OPERATION	131
2.6.1.1	<i>The Forward Problem</i>	131
2.6.1.2	<i>The Inverse Problem</i>	132
2.6.2	TRANSMITTER.....	134
2.6.2.1	<i>Signal Structure</i>	134
2.6.2.2	<i>Generation of Stable Signals</i>	135
2.6.2.3	<i>Distribution of Stable Signals</i>	136
2.6.3	RECEIVER	136
2.6.4	EXTRACTION OF OBSERVABLE(S)	137
2.6.4.1	<i>Logarithmic Detection and RSSI A/D Conversion</i>	137
2.6.4.2	<i>Frame Alignment</i>	138
2.6.4.3	<i>Framing Error Conditions</i>	138
2.6.4.4	<i>Frame Data Interval</i>	138
2.6.4.5	<i>Signal Processing</i>	139
2.6.5	ISSUES.....	139
CHAPTER 3. CHANNEL MODELS.....		143
3.0	INTRODUCTION.....	143
3.1	WIRELESS COMMUNICATION CHANNEL MODELS	143
3.1.1	THE PHYSICS OF PROPAGATION FOR MACROCELLULAR GEOLOCATION SYSTEMS	144
3.1.1.1	<i>Path Loss</i>	145
3.1.1.2	<i>Multipath Distribution of a Macrocellular Geolocation System</i>	152
3.1.2	THE PHYSICS OF PROPAGATION FOR MICROCELLULAR GEOLOCATION SYSTEMS.....	157
3.1.2.1	<i>Path Loss</i>	158
3.1.2.2	<i>Multipath Distribution for Microcellular Geolocation Systems</i>	165
3.1.3	THE PHYSICS OF PROPAGATION FOR INDOOR GEOLOCATION SYSTEMS.....	167
3.1.3.1	<i>Path Loss Model for Indoor Geolocation Systems</i>	167
3.1.3.2	<i>Multipath Distribution for Indoor Geolocation Systems</i>	171
3.2	UNIFIED CHANNEL MODEL.....	174
3.2.1	UNIFIED PATH LOSS MODEL	174
3.2.2	UNIFIED MULTIPATH DISTRIBUTION MODEL	179

CHAPTER 4. WPI INDOOR GEOLOCATION SYSTEMS	188
4.0 INTRODUCTION.....	188
4.1 A DSSS/CDMA/FDMA INDOOR GEOLOCATION SYSTEM.....	191
4.1.1 PRINCIPLE OF OPERATION OF A DSSS/CDMA/FDMA INDOOR GEOLOCATION SYSTEM.....	192
4.1.2 TRANSMITTER.....	192
4.1.3 RECEIVER	199
4.2 A DSSS/OFDM/CDMA/FDMA INDOOR GEOLOCATION SYSTEM.....	202
4.2.1 PRINCIPLE OF OPERATION	202
4.2.2 TRANSMITTER.....	202
4.2.3 RECEIVER	206
4.3 AN OFDM/FDMA INDOOR GEOLOCATION SYSTEM.....	208
4.3.1 PRINCIPLE OF OPERATION	209
4.3.2 TRANSMITTER.....	211
4.3.3 RECEIVER	215
CHAPTER 5. A DSSS/CDMA/FDMA INDOOR GEOLOCATION SYSTEM.....	219
5.0 INTRODUCTION.....	219
5.1 COMMUNICATION PERFORMANCE ANALYSES (C CODE)	220
5.1.1 RECEIVER'S FRONT END AND BASEBAND SAMPLING.....	221
5.1.2 DOPPLER REMOVAL AND PHASE ROTATION.....	223
5.1.3 CORRELATION WITH THE LOCALLY GENERATED C CODE	224
5.1.4 (FIRST) INTEGRATION AFTER THE CORRELATION WITH THE LOCALLY GENERATED C CODE...	225
5.1.5 CORRELATION WITH THE LOCALLY GENERATED P CODE	228
5.1.6 (SECOND) INTEGRATION AFTER THE P CODE CORRELATION.....	229
5.1.7 SIGNAL TO INTERFERENCE PLUS NOISE RATIO	231
5.1.8 BIT ERROR PROBABILITY	234
5.2 COMMUNICATION PERFORMANCE ANALYSES (C AND B CODES).....	235
5.2.1 CORRELATION WITH THE LOCALLY GENERATED B CODE	236
5.2.2 (THIRD) INTEGRATION AFTER THE CORRELATION WITH THE LOCALLY GENERATED B CODE..	236
5.2.3 SIGNAL TO INTERFERENCE PLUS NOISE RATIO	238
5.2.4 BIT ERROR PROBABILITY	241
5.3 NAVIGATION PERFORMANCE ANALYSES	241
5.3.1 RECEIVER'S CODE ERROR.....	241
5.3.2 RECEIVER'S PHASE ERROR	242
5.4 QUANTITATIVE ASSESSMENT.....	242
5.4.1 SELECTION OF PARAMETERS.....	243
5.4.2 QUANTITATIVE REQUIREMENTS ON THEORETICAL PERFORMANCE	244
5.4.2.1 <i>Quantitative Requirements on Communication Performance</i>	245
5.4.2.2 <i>Navigation Performance</i>	250
5.5 SUMMARY AND CONCLUSIONS	261
CHAPTER 6. A DSSS/OFDM/CDMA/FDMA INDOOR GEOLOCATION SYSTEM.....	264
6.0 INTRODUCTION.....	264

6.1	COMMUNICATION PERFORMANCE ANALYSES	264
6.1.1	RECEIVER'S FRONT END AND BASEBAND SAMPLING.....	266
6.1.2	DOPPLER REMOVAL AND PHASE ROTATION.....	267
6.1.3	CORRELATION WITH THE LOCALLY GENERATED C CODE	268
6.1.4	INTEGRATION AFTER THE CORRELATION WITH THE LOCALLY GENERATED C CODE	269
6.1.5	TIME OF ARRIVAL ESTIMATION.....	272
6.1.6	SIGNAL TO INTERFERENCE PLUS NOISE RATIO	272
6.1.7	BIT ERROR PROBABILITY	276
6.2	NAVIGATION PERFORMANCE ANALYSES	277
6.2.1	RECEIVER'S CODE ERROR.....	278
6.2.2	RECEIVER'S PHASE ERROR	278
6.3	QUANTITATIVE ASSESSMENT.....	279
6.3.1	SELECTION OF PARAMETERS.....	279
6.3.2	QUANTITATIVE REQUIREMENTS ON THEORETICAL PERFORMANCE	281
6.3.2.1	<i>Quantitative Requirements on Communication Performance</i>	<i>281</i>
6.3.2.2	<i>Quantitative Requirements on Navigation Performance.....</i>	<i>287</i>
6.4	SUMMARY AND CONCLUSIONS	297
CHAPTER 7. AN OFDM/FDMA INDOOR GEOLOCATION SYSTEM.....		299
7.0	INTRODUCTION.....	299
7.1	COMMUNICATION PERFORMANCE ANALYSES	300
7.1.1	RECEIVER'S FRONT END AND INTERMEDIATE FREQUENCY SAMPLING.....	300
7.1.2	DIGITAL SIGNAL PROCESSING.....	303
7.1.3	QUANTITATIVE ASSESSMENT	304
7.2	NAVIGATION PERFORMANCE ANALYSES	311
7.2.1	A QUANTITATIVE APPROACH FOR TIME DELAY ESTIMATION	312
7.2.2	PSEUDORANGE ESTIMATION AND PSEUDORANGE ERROR	314
7.3	SUMMARY AND CONCLUSIONS	316
CHAPTER 8. CONCLUSIONS AND FUTURE WORK.....		318
8.0	INTRODUCTION.....	318
8.1	A DSSS/CDMA/FDMA INDOOR GEOLOCATION SYSTEM.....	319
8.2	A DSSS/OFDM/CDMA/FDMA INDOOR GEOLOCATION SYSTEM.....	320
8.3	AN OFDM/FDMA INDOOR GEOLOCATION SYSTEM.....	320
8.4	ASSESSMENT OF ALL WPI INDOOR GEOLOCATION SYSTEMS	321
8.5	FUTURE WORK.....	323
APPENDIX A. HISTORY AND BACKGROUND		325
A.0	INTRODUCTION.....	325
A.1	HISTORY AND BACKGROUND.....	325

A.1.1	ANCIENT ERA.....	325
A.1.2	MEDIEVAL ERA.....	326
A.1.3	SCIENTIFIC REVOLUTION.....	327
A.1.4	DYNAMO.....	329
A.1.5	GREATEST SCIENTIFIC DISCOVERIES BETWEEN 1800–1951.....	330
A.1.6	GREATEST TECHNOLOGICAL INVENTIONS BETWEEN 1800–1951.....	330
A.1.7	MODERN LOCALIZATION IDEA.....	331
APPENDIX B. TRANSMITTER DESIGN CONSIDERATIONS		333
B.0	INTRODUCTION.....	333
B.1	CODE DIVERSITY.....	334
B.2	FREQUENCY DIVERSITY.....	335
B.3	TIME DIVERSITY.....	336
B.4	PHASE DIVERSITY.....	337
B.5	AMPLITUDE DIVERSITY.....	337
B.6	PULSE DIVERSITY.....	337
B.7	ENCODING DIVERSITY.....	338
B.8	ANTENNA DIVERSITY.....	338
B.9	POLARIZATION DIVERSITY.....	338
APPENDIX C. FORWARD ERROR CORRECTION (FEC).....		341
C.0	FORWARD ERROR CORRECTION.....	341
APPENDIX D. SPREADING CODES		350
D.0	SPREADING CODES.....	350
APPENDIX E. CHANNEL CONSIDERATIONS		364
E.0	INTRODUCTION.....	364
E.1	PATH LOSS.....	365
E.2	MULTIPATH.....	368
E.3	AUTO-REGRESSIVE.....	369
E.4	INTERFERENCE.....	370
APPENDIX F. RECEIVER DESIGN CONSIDERATIONS		375
F.0	INTRODUCTION.....	375
F.1	EQUALIZATION.....	375

F.2 FREQUENCY DIVERSITY.....378

F.3 CODE DIVERSITY.....379

F.4 ANTENNA DIVERSITY.....382

F.5 PHASE DIVERSITY.....383

F.6 TIME DIVERSITY.....384

F.7 BLIND384

F.8 OTHER385

REFERENCES.....390

A.....390

B.....391

C.....392

D.....393

E.....394

F.....394

G.....395

H.....396

I.....397

J.....397

K.....397

L.....398

M.....399

N.....400

O.....401

P.....401

Q.....403

R.....403

S.....404

T.....405

U	406
V	406
W	407
X	408
Y	408
Z	408

Table of Figures

FIGURE 1.1 AN OVERVIEW OF A GEOLOCATION SYSTEM.	1
FIGURE 1.2 GEOLOCATION SYSTEM MAIN COMPONENTS: DOMAIN, ENVIRONMENT, AND METHODOLOGY.	3
FIGURE 1.3 A GENERIC INDOOR GEOLOCATION SYSTEM DIAGRAM.	5
FIGURE 1.4 TECHNICAL CLASSIFICATION OF GEOLOCATION SYSTEMS.	7
FIGURE 1.5 A CLASSIFICATION OF THE MOST IMPORTANT OUTDOOR GEOLOCATION SYSTEMS.	8
FIGURE 1.6 A CLASSIFICATION OF INDOOR GEOLOCATION SYSTEMS.	10
FIGURE 1.7 COMPONENTS OF A GENERIC RADIO GEOLOCATION SYSTEM.	11
FIGURE 1.8 COMPONENTS OF A GENERIC INDOOR GEOLOCATION SYSTEM.	12
FIGURE 1.9 A BLOCK DIAGRAM OF A GENERIC TRANSMITTER.	13
FIGURE 1.10 A BLOCK DIAGRAM OF A GENERIC CHANNEL.	14
FIGURE 1.11 A BLOCK DIAGRAM OF A GENERIC RECEIVER.	16
FIGURE 1.12 A DESCRIPTION AND DEFINITION OF GPS.	18
FIGURE 1.13 THE GPS OPERATIONAL SEGMENTS- - USING ELEMENTS FROM [10].	19
FIGURE 1.14 A DESCRIPTION AND DEFINITION OF GLONASS.	21
FIGURE 1.15 A DESCRIPTION AND DEFINITION OF GALILEO- - USING INFORMATION FROM [18] AND [19].	23
FIGURE 1.16 A GPS/GLONASS SATELLITE/PSEUDOLITE OUTDOOR GEOLOCATION SYSTEM.	25
FIGURE 1.17 A SNAP TRACK INDOOR GEOLOCATION SYSTEM- - TAKEN FROM [52].	28
FIGURE 1.18 US COAST GUARD INDOOR GEOLOCATION SYSTEM- - TAKEN AND MODIFIED FROM [55].	30
FIGURE 1.19 AN IEEE 802.11 WIRELESS SYSTEM- - TAKEN AND MODIFIED FROM [58].	32
FIGURE 1.20 A MOBILE PHONE GEOLOCATION SYSTEM.	34

FIGURE 1.21 THE ARCHITECTURE OF A MOBILE PHONE GEOLOCATION SYSTEM- - TAKEN FROM [47].	34
FIGURE 1.22 CLASSIFICATION OF MOBILE PHONE POSITIONING METHODS.	35
FIGURE 1.23 A DESCRIPTION OF CELL-ID MOBILE PHONE GEOLOCATION SYSTEM SYSTEMS.	36
FIGURE 1.24 A TDOA MOBILE PHONE GEOLOCATION SYSTEM.	36
FIGURE 1.25 AN AIDED GPS MOBILE PHONE GEOLOCATION SYSTEM- - MODIFIED FROM [71].	37
FIGURE 1.26 A CLASSIFICATION OF OTHER INDOOR GEOLOCATION SYSTEMS.	38
FIGURE 1.27 MIT RELAY INDOOR GEOLOCATION SYSTEM.	39
FIGURE 1.28 A PRECISE RF POSITIONING SYSTEM- - TAKEN AND MODIFIED FROM [59]. ...	40
FIGURE 1.29 AN UWB INDOOR GEOLOCATION SYSTEM.	41
FIGURE 1.30 INDOOR GEOLOCATION SYSTEM SPECIFICATIONS.	42
FIGURE 1.31 THE RATIONAL FOR WPI INDOOR GEOLOCATION SYSTEM.	47
FIGURE 2.1 THE PRINCIPLE OF OPERATION OF GPS.	62
FIGURE 2.2 GPS SATELLITE DESIGN.	65
FIGURE 2.3 GPS SIGNAL STRUCTURE AND FREQUENCY ALLOCATION- - TAKEN AND MODIFIED FROM [8].	66
FIGURE 2.4 GPS MESSAGE FORMAT, CONTENT AND TIMING- - TAKEN AND MODIFIED FROM [9].	67
FIGURE 2.5 GPS NAVIGATION MESSAGE DATA-FRAME STRUCTURE- - TAKEN AND MODIFIED FROM [11].	69
FIGURE 2.6 GPS TLM AND HOW MESSAGE DATA-FRAME STRUCTURE- - TAKEN AND MODIFIED FROM [11].	69
FIGURE 2.7 GPS SATELLITE ONBOARD CLOCK CORRECTION MODEL.	72
FIGURE 2.8 A BLOCK DIAGRAM OF A GENERIC GPS/GLONASS RECEIVER- - TAKEN AND MODIFIED FROM [5].	73
FIGURE 2.9 GPS RECEIVER SIGNAL PROCESSING MODEL.	76
FIGURE 2.10 GPS RECEIVER ACQUISITION PROCESS- - TAKEN AND MODIFIED FROM [9] AND [11].	78
FIGURE 2.11 GPS RECEIVER ACQUISITION SEARCH SPACE- - TAKEN AND MODIFIED FROM [11].	78

FIGURE 2.12 PROBABILITY DENSITY FUNCTION FOR SNR = - {30, 20, 10} DB, $P_{FA} = - 0.01$, AND $N_S = 1023$.....	85
FIGURE 2.13 STANDARD I/Q DEMODULATION- - TAKEN AND MODIFIED FROM [11]......	87
FIGURE 2.14 STANDARD TRACKING LOOP- - TAKEN AND MODIFIED FROM [11].	90
FIGURE 2.15 PLL IN LAPLACE DOMAIN- - TAKEN AND MODIFIED FROM [11]......	92
FIGURE 2.16 GPS CODE TRACKING LOOP- - TAKEN AND MODIFIED FROM [11].	95
FIGURE 2.17 GPS CARRIER TRACKING LOOP- - TAKEN AND MODIFIED FROM [11].	98
FIGURE 2.18 COSTAS PHASE LOCK LOOP- - TAKEN AND MODIFIED FROM [11]......	103
FIGURE 2.19 ILLUSTRATION OF BIT CELL STATISTICS - WITH NOISE- - TAKEN AND MODIFIED FROM [11]......	104
FIGURE 2.20 THE PRINCIPLE OF OPERATION OF GLONASS.....	108
FIGURE 2.21 THE GLONASS SIGNAL STRUCTURE AND FREQUENCY ALLOCATION.	108
FIGURE 2.22 GLONASS MESSAGE CONTENT AND FORMAT- - TAKEN AND MODIFIED FROM [10].	111
FIGURE 2.23 THE PRINCIPLE OF OPERATION OF A PSEUDOLITE INDOOR GEOLOCATION SYSTEM.	116
FIGURE 2.24 THE NEAR-FAR EFFECT- - TAKEN AND MODIFIED FROM [23]......	118
FIGURE 2.25 MASTER/SLAVE PSEUDOLITE CONFIGURATION- - TAKEN AND MODIFIED FROM [30].	122
FIGURE 2.26 PSEUDOLITE MESSAGE STRUCTURE- - TAKEN AND MODIFIED FROM [30].	122
FIGURE 2.27 THE BLOCK DIAGRAM OF THE SIGNAL-PROCESSING MODEL OF A PSEUDOLITE RECEIVER- - TAKEN AND MODIFIED FROM [30].	124
FIGURE 2.28 THE CROSSCORRELATION POWER RATIO, DP_{IJ} (DB), VS. INPUT POWER RATIO, P_{IJ} (DB).	128
FIGURE 2.29 INTERFERENCE CAUSED BY THE PSEUDOLITE SIGNAL LEVEL.....	130
FIGURE 2.30 THE PRINCIPLE OF OPERATION OF THE MIT INDOOR GEOLOCATION SYSTEM.	132
FIGURE 2.31 MIT SIGNAL STRUCTURE- - TAKEN AND MODIFIED FROM [33]......	135
FIGURE 2.32 MIT TRANSMITTER BLOCK DIAGRAM- - TAKEN AND MODIFIED FROM [33].	135
FIGURE 2.33 MIT RECEIVER BLOCK DIAGRAM- - TAKEN AND MODIFIED FROM [33]. ...	137

FIGURE 3.1 THE (A) TOP (OR HORIZONTAL) AND (B) VIEW VERTICAL VIEW OF THE PROPAGATION PATH BETWEEN THE TRANSMITTER AND THE RECEIVER—TAKEN AND MODIFIED FROM [18].	144
FIGURE 3.2 FREE SPACE PATH LOSS MODEL (A) VS. R AND (B) VS. F FOR A MACROCELLULAR GEOLOCATION SYSTEM.	146
FIGURE 3.3 FACTOR Q_2 VS. (A) BUILDING HEIGHT AND (B) F FOR A MACROCELLULAR GEOLOCATION SYSTEM.	148
FIGURE 3.4 NORMALIZED Q_2 VS. (A) ANTENNA HEIGHT AND (B) F FOR A MACROCELLULAR GEOLOCATION SYSTEM.	148
FIGURE 3.5 FACTOR Q_1 VS. (A) BUILDING HEIGHT AND (B) F FOR A MACROCELLULAR GEOLOCATION SYSTEM.	150
FIGURE 3.6 TOTAL PATH LOSS Q (DB) VS. (A) R (KM) AND (B) F (GHZ) FOR A MACROCELLULAR GEOLOCATION SYSTEM.	150
FIGURE 3.7 TOTAL PATH LOSS Q (DB) VS. (A) BUILDING HEIGHT (M) AND (B) F (GHZ) FOR A MACROCELLULAR GEOLOCATION SYSTEM.	151
FIGURE 3.8 TOTAL PATH LOSS Q (DB) VS. (A) ANTENNA HEIGHT (M) AND (B) F (GHZ) FOR A MACROCELLULAR GEOLOCATION SYSTEM.	151
FIGURE 3.9 THE LOGNORMAL PDF AND CDF OF THE PATH GAIN, A_K, FOR $m = \{0.3, 0.6\}$ AND $s = \{1.57, 6.26\} * 1E-2$.	155
FIGURE 3.10 THE EXPONENTIAL PDF AND CDF OF INTERARRIVAL TIMES, X_K, FOR $l = \{0.5, 1\}$.	157
FIGURE 3.11 THE UNIFORM PDF AND CDF OF PATH PHASES, q_K.	157
FIGURE 3.12 TWO RAY MODEL SHOWING THE FRESNEL ELLIPSE ABOUT THE DIRECT RAY—TAKEN AND MODIFIED FROM [18].	158
FIGURE 3.13 THE LOS PATH LOSS, Q_{Los}, VS. THE DISTANCE BETWEEN TX AND RX, R...	160
FIGURE 3.14 THE LOS PATH LOSS, Q_{Los}, VS. THE FREQUENCY, F (GHZ).....	160
FIGURE 3.15 FOOTPRINTS OF FOUR RECTANGULAR MULTIPLE STORY BUILDINGS—MODIFIED FROM [18].	163
FIGURE 3.16 TWO TURN ROUTES FROM THE TRANSMITTER TO THE RECEIVER—MODIFIED FROM [18].	163
FIGURE 3.17 THE RICIAN PDF AND CDF OF PATH GAIN, A_K, FOR $V = \{0.3, 0.6\}$ AND $a = \{0.0521, 0.1041\}$.	166
FIGURE 3.18 THE FRESNEL ZONE FOR PROPAGATION BETWEEN THE TX AND RX IN CLEAR SPACE BETWEEN BUILDING FURNISHINGS AND CEILING FIXTURES—TAKEN AND MODIFIED FROM [18].	168
FIGURE 3.19 THE TWO DIMENSIONAL RAY-TRACING ACCOUNTING FOR SPECULAR REFLECTION AND TRANSMISSION AT WALLS—TAKEN AND MODIFIED FROM [18].	169

FIGURE 3.20 THE CDF AND PDF OF A RAYLEIGH FADING CHANNEL.....	172
FIGURE 3.21 THE CDF AND PDF OF A LOGNORMAL, RICIEN, AND RAYLEIGH FADING CHANNEL FOR $m_A = 0.6$ AND $s_A = 0.0626$.....	172
FIGURE 3.22 THE NUMBER OF RESOLVABLE PATHS AS A FUNCTION OF THE CHIPPING RATE, R_C, AND RMS DELAY SPREAD, s.....	173
FIGURE 3.23 UNIFIED PATH LOSS MODEL FOR A MACROCELLULAR GEOLOCATION SYSTEM, $s = 0.5$.....	175
FIGURE 3.24 UNIFIED PATH LOSS MODEL FOR A MICROCELLULAR GEOLOCATION SYSTEM, $s = 2$.....	176
FIGURE 3.25 UNIFIED PATH LOSS MODEL FOR AN INDOOR GEOLOCATION SYSTEM, $s = 1$.....	176
FIGURE 3.26 UNIFIED PATH LOSS MODEL FOR A MACROCELLULAR GEOLOCATION SYSTEM, $s = 0.5$.....	178
FIGURE 3.27 UNIFIED PATH LOSS MODEL FOR A MICROCELLULAR GEOLOCATION SYSTEM, $s = 2$.....	178
FIGURE 3.28 UNIFIED PATH LOSS MODEL FOR AN INDOOR GEOLOCATION SYSTEM, $s = 1$.....	178
FIGURE 3.29 THE COMPOSITE CDF AND PDF WHICH CONTAINS A LOGNORMAL, RICIEN, AND RAYLEIGH FADING CHANNEL FOR $m_A = 0.6$ AND $s_A = 0.0626$ AND $N = \{0.25, 0.35, 0.4\}$.....	183
FIGURE 3.30 THE UNIFORM CDF AND PDF WHICH IS NOT A SUPERPOSITION OF A LOGNORMAL, RICIEN, AND RAYLEIGH FADING CHANNEL FOR $m_A = 0.6$ AND $s_A = 0.0626$.....	183
FIGURE 4.1 FIREFIGHTER IN RESCUE MISSION WORKING IN THE SAME FLOOR (LEFT) AND AT DIFFERENT FLOORS (RIGHT)^{3/4}TAKEN FROM [1].....	188
FIGURE 4.2 THE WPI PSEUDOLITE INDOOR GEOLOCATION SYSTEM WITHOUT THE CONTROL SEGMENT.....	189
FIGURE 4.3 THE SIGNAL STRUCTURE OF A DSSS/CDMA/FDMA INDOOR GEOLOCATION SYSTEM.....	193
FIGURE 4.4 A BLOCK DIAGRAM OF A DSSS/CDMA/FDMA TRANSMITTER—TAKEN FROM [12].....	194
FIGURE 4.5 A BLOCK DIAGRAM OF A QPSK MODULATOR.....	195
FIGURE 4.6 THE TIMING DIAGRAM OF P, C, B, AND DATA SYMBOL-- TAKEN FROM [13].....	197
FIGURE 4.7 THE SMALLEST ORDER OF GENERATING POLYNOMIAL, M_{C0}, VS. THE NUMBER OF TRANSMITTERS, I.....	198

FIGURE 4.8	A BLOCK DIAGRAM OF A CHANNEL OF A C AND P CODE RECEIVER.....	199
FIGURE 4.9	THE SIGNAL STRUCTURE OF A DSSS/OFDM/CDMA/FDMA INDOOR GEOLOCATION SYSTEM.	203
FIGURE 4.10	THE SMALLEST ORDER OF GENERATING POLYNOMIAL, M_{C0}, VS. (A) THE NUMBER OF TRANSMITTERS, I, (B) THE NUMBER OF OFDM FREQUENCIES, N.....	204
FIGURE 4.11	A BLOCK DIAGRAM OF A DSSS/OFDM/CDMA/FDMA TRANSMITTER.....	205
FIGURE 4.12	A BLOCK DIAGRAM OF A CHANNEL A DSSS/OFDM/CDMA/FDMA RECEIVER.	206
FIGURE 4.13	GPS AND UWB FREQUENCY ALLOCATION- - TAKEN FROM [23].	209
FIGURE 4.14	GPS AND UWB FREQUENCY ALLOCATION- - TAKEN FROM [23].	210
FIGURE 4.15	A BLOCK DIAGRAM OF AN OFDM/FDMA INDOOR GEOLOCATION SYSTEM... ..	211
FIGURE 4.16	A BLOCK DIAGRAM OF AN OFDM/FDMA TRANSMITTER- - TAKEN FROM [23].	212
FIGURE 4.17	CROSSCORRELATION FUNCTION g FOR $t = \{-204.8$ (DASH ^), 0 (SOLID +), 204.8 (DASH O)} NSEC.....	214
FIGURE 4.18	A BLOCK DIAGRAM OF AN OFDM/FDMA RECEIVER.....	216
FIGURE 5.1	BLOCK DIA GRAM OF THE FIRST CHANNEL OF A DSSS/CDMA/FDMA RECEIVER.	221
FIGURE 5.2	BLOCK DIAGRAM OF THE RECEIVER'S FRONT END AND BASE BAND SAMPLING.	222
FIGURE 5.3	DOPPLER REMOVAL AND PHASE ROTATION BLOCK DIAGRAM.....	223
FIGURE 5.4	BLOCK DIAGRAM OF THE CORRELATION WITH THE LOCALLY GENERATED C CODE.	224
FIGURE 5.5	BLOCK DIAGRAM OF THE INTEGRATION AFTER THE CORRELATION WITH THE C CODE.	225
FIGURE 5.6	BLOCK DIAGRAM OF THE CORRELATION WITH THE LOCALLY GENERATED P CODE.....	228
FIGURE 5.7	INTEGRATION WITH THE P CODE BLOCK DIAGRAM.....	229
FIGURE 5.8	TRANSMITTER RECEIVER GEOMETRY OF BOTH A CDMA AND A CDMA/FDMA INDOOR GEOLOCATION SYSTEMS.....	243
FIGURE 5.9	THE SYNCHRONIZATION COEFFICIENT VS. SYNCHRONIZATION PARAMETER, dt (NSEC).....	245
FIGURE 5.10	BEP VS. IDEAL SNR, E_B/N_0 (DB), FOR (A) GOLD AND (B) KASAMI SEQUENCES	245

FIGURE 5.11 BEP VS. RELATIVE ADJACENT DISTANCE, R_I (M), FOR (A) GOLD AND (B) KASAMI SEQUENCES.	246
FIGURE 5.12 BEP VS. NUMBER OF TRANSMITTERS, I, FOR (A) GOLD AND (B) KASAMI SEQUENCES.	247
FIGURE 5.13 BEP VS. NUMBER PATHS, K, FOR (A) GOLD AND (B) KASAMI SEQUENCES.	248
FIGURE 5.14 BEP VS. SYNCHRONIZATION PARAMETER, dt, FOR (A) GOLD AND (B) KASAMI SEQUENCES.	249
FIGURE 5.15 BEP VS. FREQUENCY ERROR, F_E, (HZ) FOR (A) GOLD AND (B) KASAMI SEQUENCES.	250
FIGURE 5.16 PSEUDORANGE ERROR VS. IDEAL SNR, E_B/N_0 (DB), FOR (A) GOLD AND (B) KASAMI SEQUENCES.	251
FIGURE 5.17 PSEUDORANGE ERROR VS. ADJACENT DISTANCE (M) FOR (A) GOLD AND (B) KASAMI SEQUENCES.	252
FIGURE 5.18 PSEUDORANGE ERROR VS. NUMBER OF TRANSMITTERS, I, FOR (A) GOLD AND (B) KASAMI SEQUENCES.	252
FIGURE 5.19 PSEUDORANGE ERROR VS. NUMBER OF PATHS, K, FOR (A) GOLD AND (B) KASAMI SEQUENCES.	254
FIGURE 5.20 PSEUDORANGE ERROR VS. dt FOR (A) GOLD AND (B) KASAMI SEQUENCES...	254
FIGURE 5.21 PSEUDORANGE ERROR VS. THE FREQUENCY ERROR (HZ) FOR (A) GOLD AND (B) KASAMI SEQUENCES.	255
FIGURE 5.22 PHASE ERROR VS. THE IDEAL SNR (DB) FOR (A) GOLD AND (B) KASAMI SEQUENCES.	256
FIGURE 5.23 PHASE ERROR VS. THE ADJACENT DISTANCE, R_I, (M) FOR (A) GOLD AND (B) KASAMI SEQUENCES.	257
FIGURE 5.24 PHASE ERROR VS. NUMBER OF TRANSMITTERS, I, FOR (A) GOLD AND (B) KASAMI SEQUENCES.	258
FIGURE 5.25 PHASE ERROR VS. NUMBER PATHS, K, FOR (A) GOLD AND (B) KASAMI SEQUENCES.	258
FIGURE 5.26 PHASE ERROR VS. SYNCHRONIZATION PARAMETER, dt, FOR (A) GOLD AND (B) KASAMI SEQUENCES.	259
FIGURE 5.27 PHASE ERROR VS. FREQUENCY ERROR (HZ) FOR (A) GOLD AND (B) KASAMI SEQUENCES.	260
FIGURE 6.1 A DSSS/OFDM/CDMA/FDMA RECEIVER DESIGN.	265
FIGURE 6.2 BLOCK DIAGRAM OF THE RECEIVER'S FRONT END AND BASE BAND SAMPLING.	266

FIGURE 6.3 DOPPLER REMOVAL AND PHASE ROTATION BLOCK DIAGRAM.....	267
FIGURE 6.4 CORRELATION WITH THE C CODE BLOCK DIAGRAM.....	268
FIGURE 6.5 INTEGRATION OF THE C CODE BLOCK DIAGRAM.....	269
FIGURE 6.6 TRANSMITTER RECEIVER GEOMETRY OF AN OFDM/CDMA/FDMA INDOOR GEOLOCATION SYSTEM.	280
FIGURE 6.7 THE SYNCHRONIZATION COEFFICIENT VS. SYNCHRONIZATION PARAMETER, dt (NSEC).....	282
FIGURE 6.8 BEP VS. IDEAL SNR, E_B/N_0 (DB), FOR (A) GOLD AND (B) KASAMI SEQUENCES.	282
FIGURE 6.9 BEP VS. RELATIVE ADJACENT DISTANCE, R_I (M), FOR (A) GOLD AND (B) KASAMI SEQUENCES.....	283
FIGURE 6.10 BEP VS. NUMBER OF TRANSMITTERS, I, FOR (A) GOLD AND (B) KASAMI SEQUENCES.....	284
FIGURE 6.11 BEP VS. NUMBER PATHS, K, FOR (A) GOLD AND (B) KASAMI SEQUENCES.....	285
FIGURE 6.12 BEP VS. SYNCHRONIZATION PARAMETER, dt, FOR (A) GOLD AND (B) KASAMI SEQUENCES.....	286
FIGURE 6.13 BEP VS. FREQUENCY ERROR (HZ) FOR (A) GOLD AND (B) KASAMI SEQUENCES.....	286
FIGURE 6.14 PSEUDORANGE ERROR VS. IDEAL SNR, E_B/N_0 (DB), FOR (A) GOLD AND (B) KASAMI SEQUENCES.....	288
FIGURE 6.15 PSEUDORANGE ERROR VS. ADJACENT DISTANCE (M) FOR (A) GOLD AND (B) KASAMI SEQUENCES.....	288
FIGURE 6.16 PSEUDORANGE ERROR VS. NUMBER OF TRANSMITTERS, I, FOR (A) GOLD AND (B) KASAMI SEQUENCES.....	289
FIGURE 6.17 PSEUDORANGE ERROR VS. NUMBER OF PATHS, K, FOR (A) GOLD AND (B) KASAMI SEQUENCES.....	290
FIGURE 6.18 PSEUDORANGE ERROR VS. dt FOR (A) GOLD AND (B) KASAMI SEQUENCES...	291
FIGURE 6.19 PSEUDORANGE ERROR VS. THE FREQUENCY ERROR (HZ) FOR (A) GOLD AND (B) KASAMI SEQUENCES.....	292
FIGURE 6.20 PHASE ERROR VS. THE IDEAL SNR (DB) FOR (A) GOLD AND (B) KASAMI SEQUENCES.....	293
FIGURE 6.21 PHASE ERROR VS. THE ADJACENT DISTANCE (M) FOR (A) GOLD AND (B) KASAMI SEQUENCES.....	293
FIGURE 6.22 PHASE ERROR VS. NUMBER OF TRANSMITTERS, I, FOR (A) GOLD AND (B) KASAMI SEQUENCES.....	294

FIGURE 6.23 PHASE ERROR VS. NUMBER PATHS, K, FOR (A) GOLD AND (B) KASAMI SEQUENCES.....	295
FIGURE 6.24 PHASE ERROR VS. SYNCHRONIZATION PARAMETER, dt, FOR (A) GOLD AND (B) KASAMI SEQUENCES.....	296
FIGURE 6.25 PHASE ERROR VS. FREQUENCY ERROR (HZ) FOR (A) GOLD AND (B) KASAMI SEQUENCES.....	297
FIGURE 7.1 THE BLOCK DIAGRAM OF AN OFDM/FDMA RECEIVER.....	301
FIGURE 7.2 THE BLOCK DIAGRAM OF THE RECEIVER'S FRONT END AND INTERMEDIATE FREQUENCY SAMPLING.	302
FIGURE 7.3 AN EXAMPLE OF AN OFDM/FDMA INDOOR GEOLOCATION SYSTEM- - MODIFIED FROM [6].	305
FIGURE 7.4 THE IF SIGNAL FROM THE 1ST TRANSMITTER IN THE TIME AND FREQUENCY DOMAIN.	305
FIGURE 7.5 THE IF SIGNAL FROM THE 2ND TRANSMITTER IN THE TIME AND FREQUENCY DOMAIN.	306
FIGURE 7.6 THE IF SIGNAL FROM THE 3RD TRANSMITTER IN THE TIME AND FREQUENCY DOMAIN.	307
FIGURE 7.7 THE CROSSCORRELATION FUNCTION g FOR $t = \{-435.2$ (BLUE O), 0 (RED +), 435.2 (GREEN ^)} NSEC.	307
FIGURE 7.8 THE TOTAL NOISELESS RF SIGNAL IN THE TIME AND FREQUENCY DOMAIN.	308
FIGURE 7.9 THE TOTAL NOISY RF SIGNAL IN THE TIME AND FREQUENCY DOMAIN.....	309
FIGURE 7.10 THE RECEIVED NOISY IF SIGNAL OF THE 1ST CHANNEL IN THE TIME AND FREQUENCY DOMAIN.	309
FIGURE 7.11 THE RECEIVED NOISY IF SIGNAL OF THE 2ND CHANNEL IN THE TIME AND FREQUENCY DOMAIN.	310
FIGURE 7.12 THE RECEIVED NOISY IF SIGNAL OF THE 3RD CHANNEL IN THE TIME AND FREQUENCY DOMAIN.	310
FIGURE 7.13 THE CROSSCORRELATION FUNCTION g FOR $t = \{-435.2$ (BLUE O), 0 (RED +), 435.2 (GREEN ^)} NSEC.	311
FIGURE 7.14 A SNAPSHOT OF THE CROSSCORRELATION FUNCTION g FOR $t = \{-434$ (BLUE O), -2 (RED +), 436 (GREEN ^)} NSEC AFTER THE ALGORITHM AS CONVERGED.....	313
FIGURE 7.15 THE CUMULATIVE DISTRIBUTION FUNCTION CORRESPONDING TO THE THREE SCENARIOS FOR 1000 RUNS.....	314
FIGURE 7.16 THE CUMULATIVE DISTRIBUTION FUNCTION CORRESPONDING TO THE THREE SCENARIOS FOR 1000 RUNS.....	315

FIGURE 8.1 DATA RATE, R_D, VS. THE ORDER OF THE GENERATING POLYNOMIAL, M.	321
FIGURE B.1 AN OVERVIEW OF TRANSMITTER MODULATION TECHNIQUES	333
FIGURE C.1 A $R=0.5$, CONVOLUTIONAL CODE WITH CONSTRAIN LENGTH OF L_S	343
FIGURE C.2 STATE DIAGRAM FOR AN $R = 1/2$, $N = 4$, CONVOLUTIONAL CODE	344
FIGURE C.3 SIGNAL FLOW GRAPH FOR AN $R = 1/2$, $N = 4$, CONVOLUTIONAL CODE	345
FIGURE C.4 AN ILLUSTRATION IN MATLAB FOR COMPUTING THE TRANSFER FUNCTION $T(L,W,O)$	347
FIGURE C.5 THE BER_{WCC} VS. BER_{NCC} FOR A 0.5 RATE CONVOLUTIONAL CODE WITH $N = \{3, 5, \dots, 9\}$.	348
FIGURE D.1 AN M-STAGE SHIFT REGISTER WITH LINEAR FEEDBACK—TAKEN FROM [1].	350
FIGURE D.2 GENERATION OF A GOLD SEQUENCE AS DEPICTED IN THEOREM 3	358
FIGURE D.3 GENERATION OF A SMALL SET KASAMI SEQUENCE AS DEPICTED IN THEOREM 4	361
FIGURE E.1 AN OVERVIEW OF THE INDOOR COMMUNICATION CHANNEL	365
FIGURE F.1 AN OVERVIEW OF INDOOR COMMUNICATION AND LOCALIZATION RECEIVER DESIGNS	375

Table of Tables

TABLE 2.1	GPS SATELLITE EPHEMERIDES - - TAKEN AND MODIFIED FROM [6].....	70
TABLE 2.2	GPS SATELLITE ALMANAC MESSAGE- - TAKEN FROM [6] AND [10]......	71
TABLE 2.3	GLONASS SATELLITE ALMANAC MESSAGE- - TAKEN AND MODIFIED FROM [10].	113
TABLE 2.4	PSEUDOLITE MESSAGE TYPES - - TAKEN AND MODIFIED FROM [30].	123
TABLE 4.1	TRUTH TABLE FOR THE XOR WITH THREE INPUTS AND THE XOR WITH TWO INPUTS.....	195
TABLE 8.1	QUANTITATIVE RESULTS FOR THE PSEUDORANGE ERROR PERFORMANCE.....	322
TABLE 8.2	QUANTITATIVE RESULTS FOR THE PHASE ERROR PERFORMANCE.....	322
TABLE C.1	GENERATORS (IN OCTAL) AND WEIGHT STRUCTURE OF AN $R = 0.5$ CONVOLUTIONAL CODE—TAKEN AND MODIFIED FROM [1]......	343
TABLE D.1	SHIFT REGISTER CONNECTIONS FOR GENERATING M-SEQUENCES—TAKEN FROM [1].....	351
TABLE D.2	M-SEQUENCES AND MAXIMAL CONNECTED SET FOR $M = \{3,4,\dots,16\}$ - TAKEN FROM [1].....	357
TABLE D.3	THE PRIMITIVE POLYNOMIALS (OCTAL) FOR GENERATING GOLD SEQUENCES.....	359
TABLE D.4	THE PRIMITIVE POLYNOMIALS (OCTAL) FOR GENERATING KASAMI SEQUENCES.....	361

Chapter 1. Introduction

“Perseverance (Patience) must finish its work so that you might be mature and complete not lacking anything.”—James 1:4 (NIV)

1.0 Geolocation System

A GEOLOCATION System just like any other system requires a proper technical definition, is needed for its usage, has a progression in the present time, has a historical background and moment of conception in the past, and has a certain field of applicability and vision towards the future (see Figure 1.1).

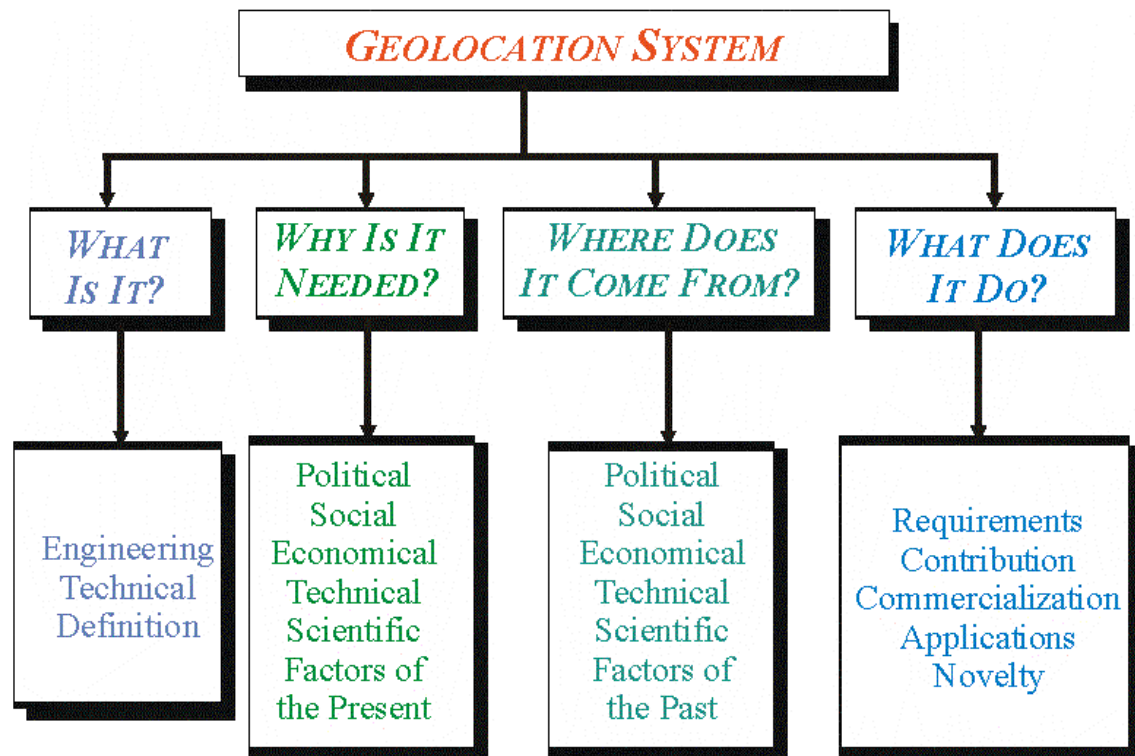


Figure 1.1 An overview of a geolocation system.

The purpose of this study is to investigate the navigation and communication properties of several candidate radio frequency (RF) signals in open indoor environments. This research can be later extended for closed indoor environments. To do this efficiently it is necessary (1) to introduce the state of the art geolocation systems in Chapter 1; (2) to address the limitations of the some of the state of the art geolocation systems for indoor applications in Chapter 2; (3) to introduce channel models with emphasis on indoor applications in Chapter 3; and propose and assess three candidates radio frequency signals in Chapters 4 through 7.

Chapter 1 is organized as follows. We briefly provide a history and background of geolocation systems in §1.1. We discuss the geolocation system concept, which includes the domain environment and the methodology and we illustrate under ideal conditions the generic principle of operation of an indoor geolocation system in §1.2. We provide a proper technical definition and classification of geolocation systems into outdoor, indoor, and underwater geolocation system in §1.3. We consider the components of a generic geolocation system, which are transmitter, channel, and receiver, and we assess the prior art issues associated with every component in §1.4. We introduce and describe the existing outdoor geolocation systems in §1.5. We introduce and describe existing indoor geolocation systems in §1.6. We summarize the specifications of geolocation systems in §1.7. We introduce WPI indoor geolocation systems in §1.8.

1.1 History and Background

People have always had an interest in localizing themselves, objects, plants, animals, cities, planets, stars, etc. The level of science and technology determined the practicality, the understanding, the capability, and other issues related to a means or systems of the time to achieve localization and exchange information from one point to another. We take a long walk to uncover the individuals, the scientific wisdom, and some of the political, philosophical and religious implications from the ancient times until the modern era (see Appendix A). Even though humans have been developing these ingenious ways of navigating to remote locations for the past six thousand years, in the context of geolocation systems that we are so much familiar with, these ways of navigating remained out of reach for the public and a privilege to only a few individuals. This is

extremely important as although we live in a technologically, economically driven society we have a great difficulty relating our modern technology and ideas or assertions that were made perhaps some hundred or thousand years ago (see Appendix A) [1]-[5].

1.2 Geolocation System Concept

There are three main components that constitute any geolocation system: (1) the *domain*, (2) the *environment*, and (3) the *methodology* as shown in Figure 1.2.

The *domain* of any geolocation system is the fabric of space and time, which means that any geolocation system exists and operates in a well defined space and time coordinate system. Such a space-time coordinate system is defined as the reference system. For example, the World Geodetic System 1984 (or WGS'84) is an Earth-Centered-Earth-Fixed (ECEF) coordinate system [4]-[7]. The WGS'84 system is fixed with respect to the Earth but it is moving with respect to the Sun. Another well-known reference system is an Earth-Centered-Inertial (ECI) and in general the Earth is not fixed with respect to this system [4]-[7]. A space-time reference system can also be a local system such as a North East Down (NED) frame, which is widely used for local positioning and navigation.

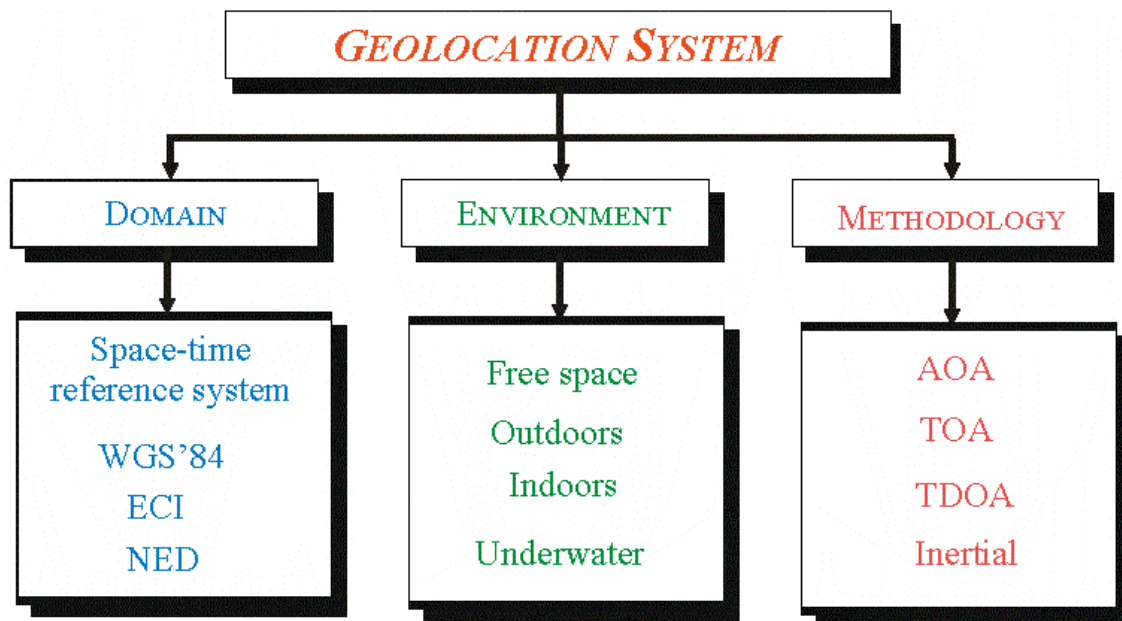


Figure 1.2 Geolocation system main components: domain, environment, and methodology.

The *environment* is the set of local or global physical properties of the medium of operation of any geolocation system. For example, the free-space physical properties of the medium are different from those in the air, from those on the surface of the Earth, from those inside buildings, and from those underwater and so forth.

The *methodology* for achieving geolocation is the technology that maps the appropriate theoretical approach (or the idea or concept) to the appropriate application. For example, commonly studied radio techniques for geolocation are the *angle of arrival* (AOA) positioning, the *time of arrival* (TOA) positioning, and the *time difference of arrival* (TDOA) positioning. The TOA and TDOA techniques become applicable methodologies only after the invention of the radio in the beginning of the 20th century. For example satellite based geolocation systems use TOA for localization and Loran C and mobile phone positioning systems employ TDOA for doing the same thing.

Now that we know which are the main components of a geolocation system we shall illustrate its concept. For that we have assumed that the domain is a hypothetical NED frame, the environment is indoors, and the methodology is a TOA positioning. In this case we have obtained an indoor geolocation system, which is shown in Figure 1.3.

There are four transmitters, one receiver and four channels shown in Figure 1.3. All transmitters are positioned in fixed locations, (X_i, Y_i, Z_i) , $i = \{1, 2, 3, 4\}$. The direct path between the transmitter and receiver is called the line-of-sight (LOS) path. The signal transmitted from the transmitter and received from the receiver forms an observable (or measurement), ρ_i , which can result from observing the signal strength, TOA, code, phase, or Doppler. The environment between the transmitter and receiver is called *channel*. For example, walls, floors, and roof, or open air can be viewed as individual indoor channels. The receiver collects all measurements and solves for the receiver location (x_r, y_r, z_r) and local time, τ_r .

Let R_i denote the geometric distance between the i th transmitter and the receiver. From Euclidean geometry R_i can be written as

$$(1.1.1) \quad R_i = \sqrt{(X_i - x_r)^2 + (Y_i - y_r)^2 + (Z_i - z_r)^2}, \quad i = \{1, 2, 3, 4\}.$$

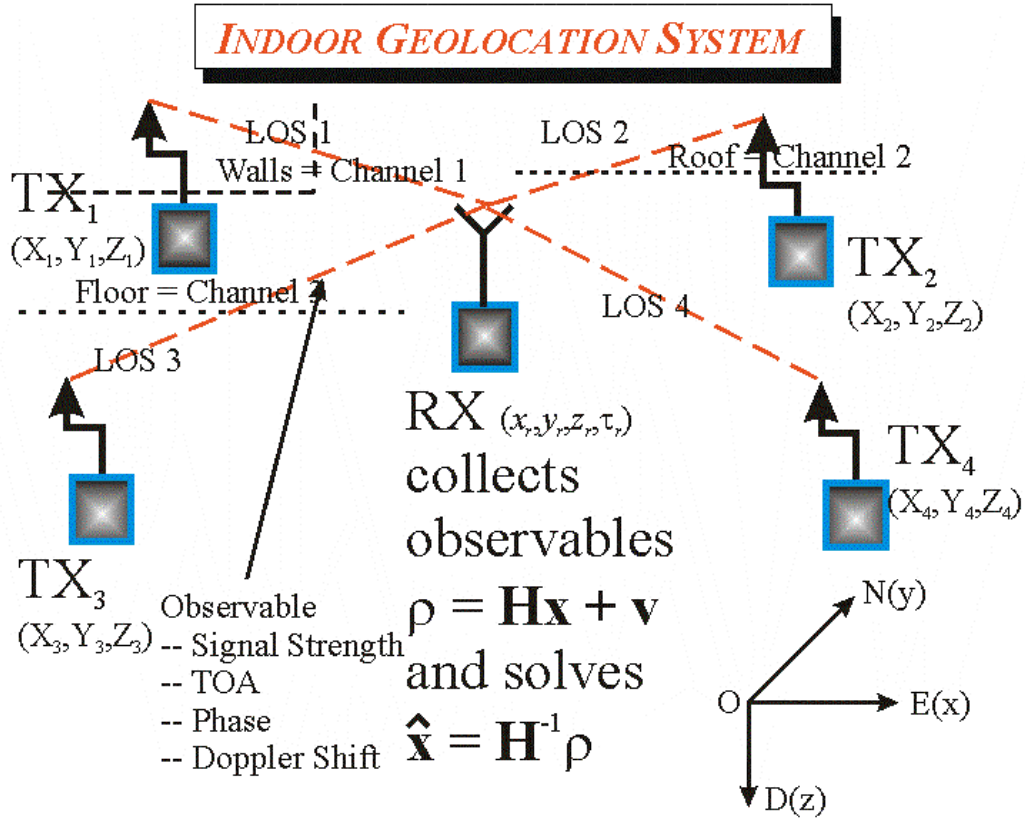


Figure 1.3 A generic indoor geolocation system diagram.

If the TOA positioning is used then the quantity observed by the receiver is, in its simplest form, given by

$$(1.1.2) \quad \rho_i = R_i + c\tau_r + v_i, \quad i = \{1, 2, 3, 4\}$$

where c is the speed of light (see Appendix A), τ_r is the receiver's clock offset from the reference time, v_i is the receiver noise (which is assumed to be white Gaussian). The above equation is a non-linear equation with respect to (x_r, y_r, z_r) . Linearizing with respect to some initial location (x_{r0}, y_{r0}, z_{r0}) yields

$$(1.1.3) \quad \rho_i \approx \left. \frac{\partial R_i}{\partial x_r} \right|_{x_r=x_{r0}} x_r + \left. \frac{\partial R_i}{\partial y_r} \right|_{y_r=y_{r0}} y_r + \left. \frac{\partial R_i}{\partial z_r} \right|_{z_r=z_{r0}} z_r + c\tau_r + v_i, \quad i = \{1, 2, 3, 4\}.$$

Define the following:

$$(1.1.4) \quad \mathbf{x} = [x_r \ y_r \ z_r \ \tau_r]^t$$

$$(1.1.5) \quad \mathbf{r} = [\rho_1 \ \rho_2 \ \rho_3 \ \rho_4]^t$$

$$(1.1.6) \quad \mathbf{v} = [v_1 \ v_2 \ v_3 \ v_4]^t$$

$$(1.1.7) \quad \mathbf{H} = \begin{bmatrix} \frac{\partial R_1}{\partial x_r} & \frac{\partial R_1}{\partial y_r} & \frac{\partial R_1}{\partial z_r} & c \\ \frac{\partial R_2}{\partial x_r} & \frac{\partial R_2}{\partial y_r} & \frac{\partial R_2}{\partial z_r} & c \\ \frac{\partial R_3}{\partial x_r} & \frac{\partial R_3}{\partial y_r} & \frac{\partial R_3}{\partial z_r} & c \\ \frac{\partial R_4}{\partial x_r} & \frac{\partial R_4}{\partial y_r} & \frac{\partial R_4}{\partial z_r} & c \end{bmatrix}_{\{x_r=x_{r0}, y_r=y_{r0}, z_r=z_{r0}\}}$$

Then equation (1.1.3) can be written in vector form as

$$(1.1.8) \quad \mathbf{?} = \mathbf{H}\mathbf{x} + \mathbf{v}.$$

If the noise autocovariance matrix, $\mathbf{R} = E\{\mathbf{v}^t\mathbf{v}\}$, is known then an approximated solution for (x_r, y_r, z_r, τ_r) is derived from the well known least squares algorithm [12]

$$(1.1.9) \quad \hat{\mathbf{x}} = (\mathbf{H}^t\mathbf{R}^{-1}\mathbf{H})^{-1}\mathbf{H}^t\mathbf{R}^{-1}\mathbf{?}.$$

Since \mathbf{H} and \mathbf{R} are both 4×4 matrices and if the inverse of \mathbf{H} exists then

$$(1.1.10) \quad \hat{\mathbf{x}} = \mathbf{H}^{-1}\mathbf{?}.$$

From equations (1.1.9) and (1.1.10) we conclude that at least four independent measurements are required to solve for receiver location (x_r, y_r, z_r) and local time (or clock offset, τ_r), if TOA positioning is applied. If more than four measurements are employed then equation (1.1.9) should be used instead of equation (1.1.10). For fewer than four measurements equation (1.1.9) is underdetermined. In that case we can only solve for fewer than four unknowns. For example if the number of measurements is only two then we can solve for only one of six combinations $\{(x_r, y_r), (x_r, z_r), (y_r, z_r), (x_r, \tau_r), (y_r, \tau_r), (z_r, \tau_r)\}$.

1.3 Technical Definition and Classification of Radio Geolocation Systems

Radio is the practice or science of communicating over a distance by converting localization information into electromagnetic waves and transmitting these directly through space, without connecting wires, to a receiving set, which changes these into signals appropriate for performing localization—taken and modified from [13]. A *radio*

geolocation system is a navigation system which employs either *radio* transmitters to broadcast ranging signal(s) continuously and utilizes a *radio* receiver to resolve at a minimum for its 3-D position and its own local time (see Figure 1.3). Since we are interested in radio geolocation systems the coin term *radio* is understood to mean a *radio system*, a *radio transmitter*, a *radio receiver*, or a *radio channel*; and therefore, it is dropped and it is no longer used later on. Based on the application *environment*, a geolocation system can be classified into three main categories: *outdoor*, *indoor*, or *underwater geolocation system* (see Figure 1.4).

Although in some geolocation systems it is also possible to use the same channel both for navigation and communication applications, the focus of this work is to discuss the channel mainly for navigation applications. Each geolocation system is discussed in order below starting with outdoor geolocation systems (see §1.3.1), indoor geolocation systems (see §1.3.2), and underwater geolocation systems (see §1.3.3).

1.3.1 Outdoor Geolocation Systems

An outdoor geolocation system is a geolocation system that operates outdoors such as open air and anywhere on the surface of the Earth except indoors. As such outdoor geolocation systems can have either global or local coverage.

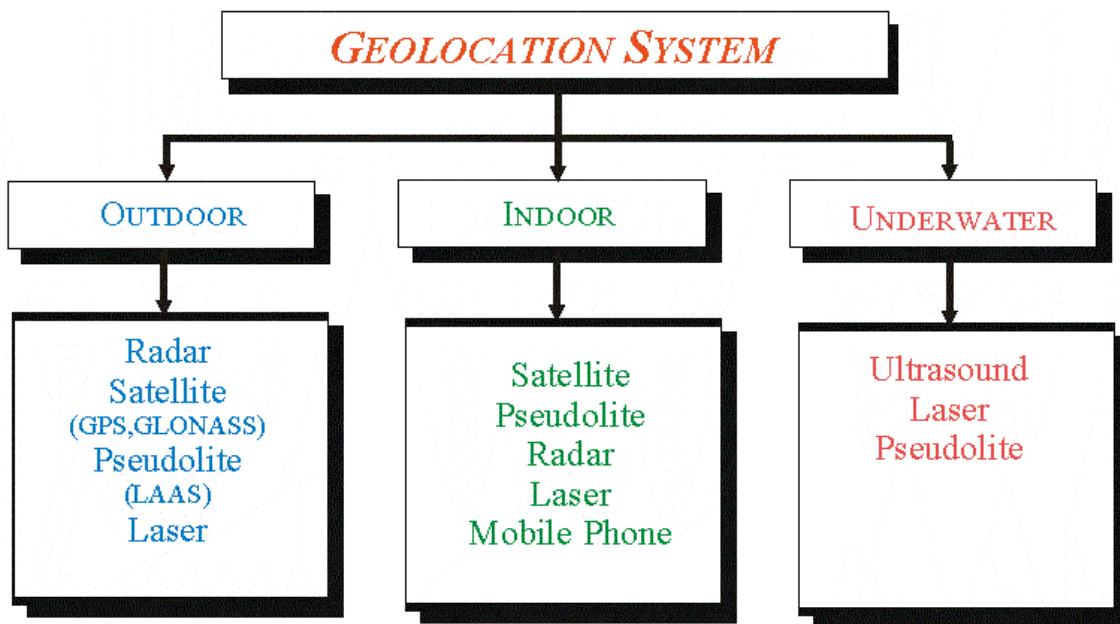


Figure 1.4 Technical classification of geolocation systems.

There are a variety of outdoor geolocation systems, which are grouped into five categories: *satellite*, *pseudolite*, *wireless*, *laser*, and *radar*. However, we are most interested in the first three categories depicted in Figure 1.5.

The most recognized *satellite* outdoor geolocation systems are the Global Positioning System (GPS) fielded by the United States of America, the Russian Global Navigation Satellite System (GLONASS), the European Galileo, and the Japanese Multifunctional Transport Satellite (MTSAT).

The first three outdoor geolocation systems provide global coverage and the last outdoor geolocation system provides regional coverage [4]-[8],[14]-[20]. Today, only GPS is fully operational, containing over 24 active satellites. This system provides a very respectable accuracy of 30 m 95% of the time using the C/A code with selective availability turned off under any weather and view conditions [5]. The Russian GLONASS [16] has lost almost half of its satellites as a result of the difficult economics in Russia as reported by the Ministry of Defense of the Russian Federation Coordination Scientific Information Center. The European Galileo system is currently in the development and validation phase (phase II) [17]. The Japanese MTSAT is a dual aeronautical and meteorological system with only two satellites [20].

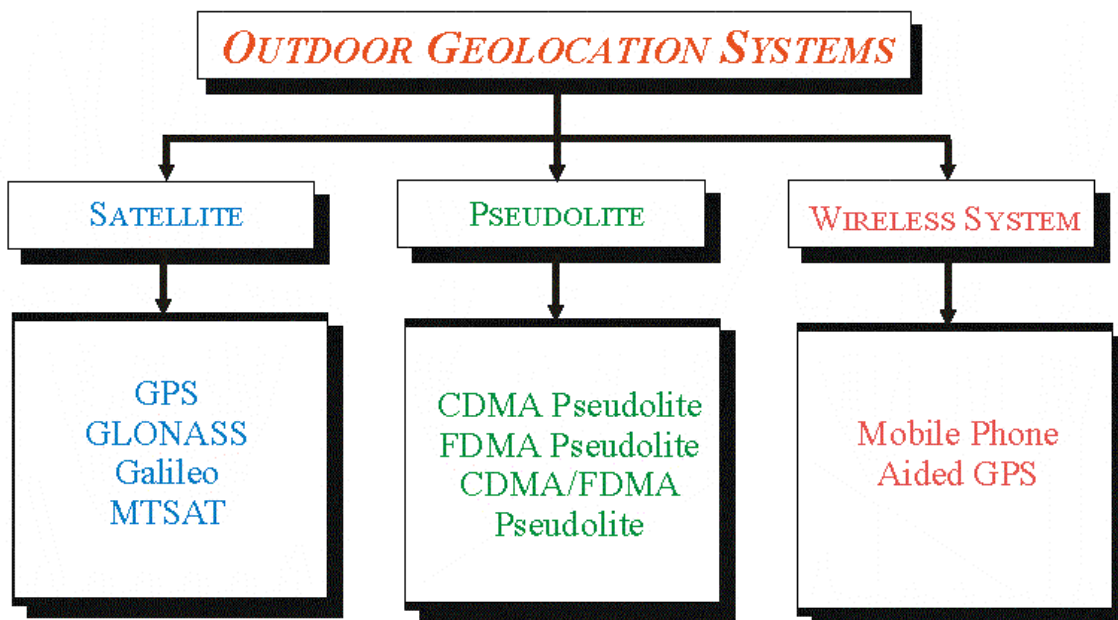


Figure 1.5 A classification of the most important outdoor geolocation systems.

Outdoor *pseudolite* geolocation systems are: (1) the Local Area Augmentation System (LAAS) based on pseudolites developed by Stanford University, (2) the LAAS based on pseudolites developed by Ohio University, (3) the pseudolite system for Category III Precision Landing (CAT III) proposed by WPI [21], [22]; and (4) others developed by public or private companies [23]-[21]. The Stanford University and Ohio University systems are GPS-like pseudolite systems as they utilize pseudolites which transmit a signal that is identical to the signal transmitted by the GPS satellites. In contrast, the WPI outdoor (later indoor see §1.8) pseudolite geolocation system uses pseudolites that transmit a signal that is specially engineered to avoid problems associated with the GPS signal structure. As such the WPI pseudolite outdoor geolocation system is treated extensively in Chapters 4 through 8.

Mobile phone positioning for 3G systems and aided GPS systems, which fulfil the requirements of the Enhanced (or emergency) 911/112 as mandated by the Federal Communication Commission (FCC), are generally considered as outdoor wireless geolocation systems [46]-[50].

Other local outdoor geolocation systems are OMEGA, Loran C, and other classical radio navigation aids. The outdoor laser geolocation systems are very expensive and are used by NASA for very precise navigation and landing of space shuttles and personnel. The outdoor radar geolocation systems are also very expensive and are currently used by the US, Canadian, or European military forces.

1.3.2 Indoor Geolocation Systems

An indoor geolocation system is a geolocation system that operates indoors. Indoor geolocation systems have emerged as a means to render localization and navigation inside buildings to people and personnel due to limited capabilities of outdoor systems in such environments. These systems may contain fixed transmitters, wireless networks, or mobile units, in cases such as *ad hoc networks* as depicted in Figure 1.6. Such systems can be classified as *satellite/pseudolite*, *wireless* and *other* indoor geolocation systems.

Satellite/pseudolite indoor geolocation systems include GPS/GLONASS/Galileo, SnapTrack™, and US Coast Guard indoor geolocation systems [52]-[58].

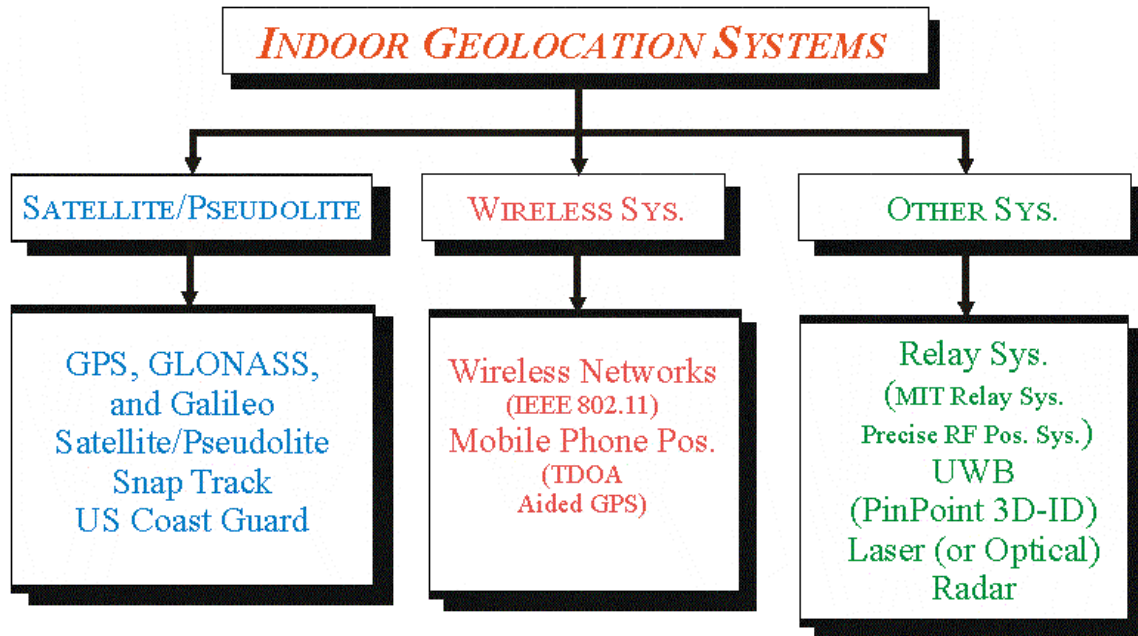


Figure 1.6 A classification of indoor geolocation systems.

Wireless indoor geolocation systems, include IEEE 802.11 such as IEEE 802.11 (a), (b), (c), etc. and the mobile phone positioning system and aided GPS, which fulfil the E911/E112 requirements [46]-[50]. We discuss these systems in section §1.6 in great detail.

Other indoor geolocation systems include relay indoor geolocation systems such as the MIT relay system and the precise Radio Frequency (RF) positioning system [59]-[61]; Ultra Wide Band (UWB) systems with PinPoint 3D-ID system as an example [62]-[70]; radar and laser indoor geolocation systems (very specialized and expensive systems and as such they fall outside the scope of this work).

Conceptually, an *indoor pseudolite geolocation system* is similar to its outdoor counterpart. We would desire to design a seamless technology which would yield an indoor to outdoor or outdoor to indoor pseudolite geolocation system.

1.3.3 Underwater Geolocation Systems

An *underwater geolocation system* is a geolocation system that operates underwater. Underwater geolocation systems are less familiar to us because they are currently used for ships, submarines and other uncommon applications [71]-[94]. They can be grouped

into three main categories: *ultrasound*, *pseudolite*, and *laser*. *Underwater ultrasound geolocation systems* are perhaps the most common examples and are currently used by the Navy and the US Coast Guard for national security purposes. An *underwater pseudolite geolocation system* will probably emerge as the technology of the future to partially or fully replace underwater ultrasonic geolocation systems due to advantages such as signal robustness and encryption; important features for avoiding detection by enemy ships or submarines. Similarly, *underwater laser geolocation systems* are used for very specialized and restricted manned operations.

1.4 A Generic Radio Geolocation System

Regardless of the specific details of an outdoor, an indoor or an underwater geolocation system, each one of these systems contains three main components, as shown in Figure 1.7 and Figure 1.8. These components are *transmitter(s)*, *channel*, and *receiver(s)*.

A *transmitter* is a device (or apparatus), which generates electromagnetic waves, based on a signal that is encoded in a manner that improves its ability to render localization, and sends them through space by means of an antenna. Important characteristics of a transmitter include modulation type, power level, and data rate.

A *receiver* is a device (or apparatus) that captures electromagnetic waves by means of an antenna and converts them into electric signals for extracting localization information. Electromagnetic waves are received by means of an antenna and they are converted into electric signals, which are demodulated and utilized for tracking the code and the phase of the transmitted signal.

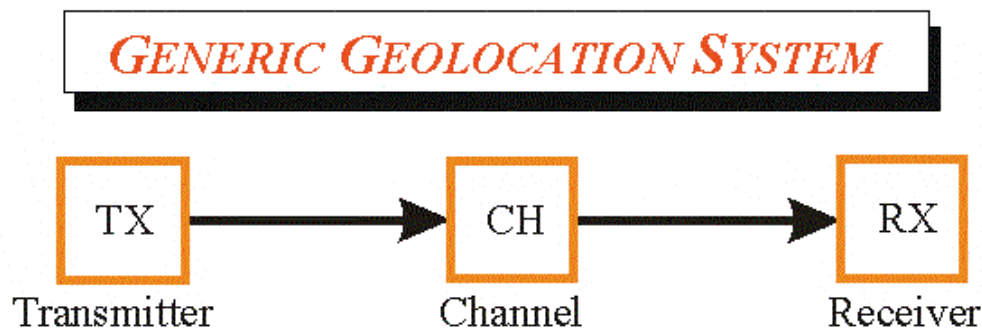


Figure 1.7 Components of a generic radio geolocation system.

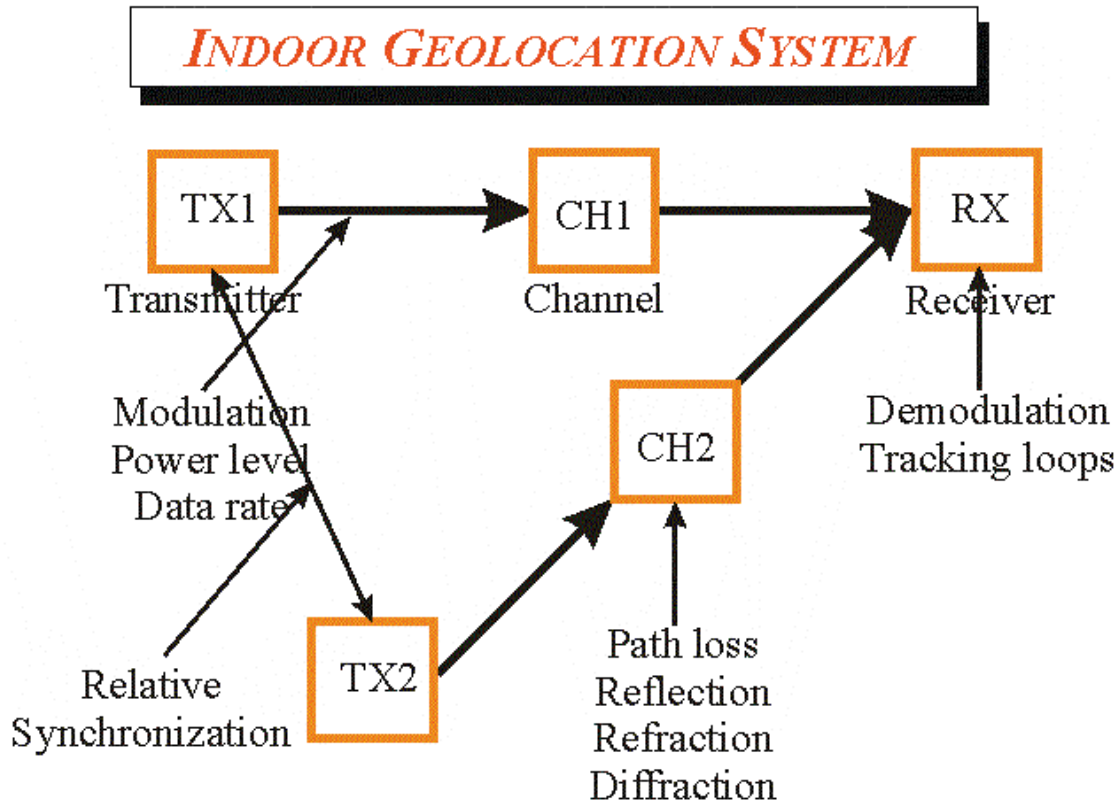


Figure 1.8 Components of a generic indoor geolocation system.

A *channel* is the medium that enables the electromagnetic waves to propagate from the transmitting antenna to the receiving antenna. The transmitted electromagnetic waves, passing through a channel, are subject to various channel impairments such as (1) path loss, (2) reflection, (3) refraction, and (4) scattering.

1.4.1 Transmitter

A geolocation system, which uses a TOA positioning methodology (see §1.2), must contain at least four transmitters to solve for the receiver's 3D position and local time. A block diagram of a generic transmitter is shown in Figure 1.9. The reader may refer to Appendix B for further detail on transmitter design considerations.

Regardless of the application, a geolocation transmitter contains seven critical components: (1) reference oscillator (REF OSC), (2) a frequency synthesizer (FREQ. SYN.) (or a multiplier), (3) code generator(s) (CODER), (4) modulator(s) (MOD), (5) RF combiner (RF COMB.), (6) power amplifier (POWER AMP), and (7) antenna(e).

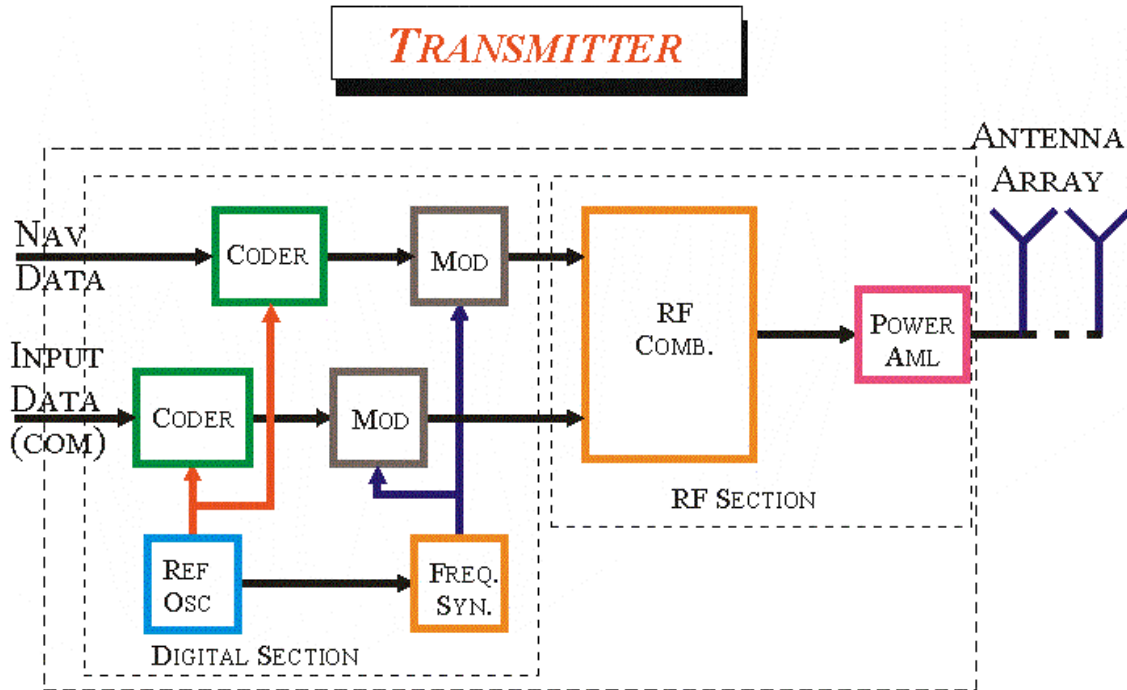


Figure 1.9 A block diagram of a generic transmitter.

Typically, a reference oscillator is a crystal oscillator for driving the transmitter local clock, which is used to synchronize all processes that take place for generating a transmitted signal. A transmitter has a frequency synthesizer for increasing the frequency of the reference oscillator to the desired carrier frequency.

The transmitted data (or information) is either in the form of communication or navigation messages. The rate of the communication data messages is usually different from the rate of the navigation data messages. A transmitter contains two code generators for coding the input data messages. The input communication data is often encoded using forward error correction (FEC) encoding to improve the quality of the data on the receiving side (see Appendix C). Typically the navigation data messages are spread either in time or in frequency employing spreading codes (see Appendix D) to ensure data robustness. The transmitter has two modulators one for changing the amplitude, phase, or frequency of the signal of the output of the communication CODER and the other for the navigation CODER. The process of combining information with the radio frequency carrier of the transmitter is called modulation, which takes place in the modulator. Four well-known modulation schemes, the *code division multiple access*

(CDMA), the *frequency division multiple access* (FDMA), the *orthogonal frequency division multiplexing* (OFDM), and the *time division multiple access* (TDMA) [95]-[124], are the most-applied and appropriate modulation schemes for geolocation applications [4]-[69].

The output signal coming from the first modulator and the output signal coming from the second modulator are combined in the RF combiner. A power amplifier is utilized to raise the power of the output signal from the RF combiner. The output of the power amplifier goes to either the transmitter antenna or antenna array. The underlying term that identifies the process that takes place in the transmitter is called *signal structure*. For a complete classification of transmitter designs the reader may refer to Appendix B. Chapters 2 and 4 discuss several transmitters in great detail, which are either implemented or are currently being designed.

1.4.2 Channel

The channel is the medium (or the environment) between the transmitting antenna and the receiving antenna. An electromagnetic wave propagating through a channel undergoes *loss* in power and *dispersion* in direction (see Figure 1.10) [125]-[172].

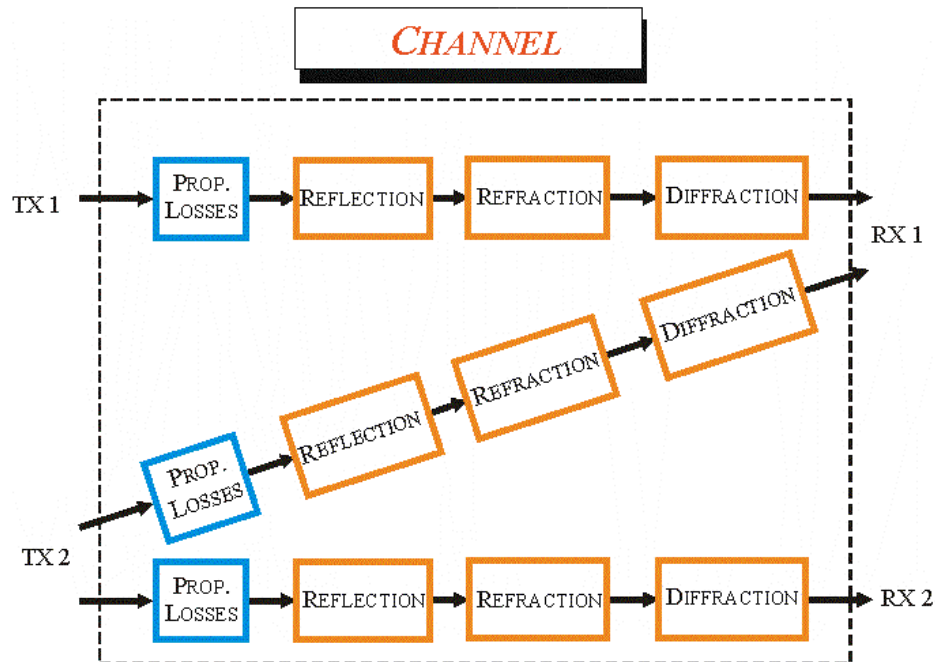


Figure 1.10 A block diagram of a generic channel.

The ability of the medium to absorb an electromagnetic wave depends on its physical properties, which is known as propagation power loss. The power loss (in dB) can be inversely proportional with the twice, three times, 4 times, or n times the distance or with m times the signal frequency where n and m are real; therefore, the power loss can be of a quadratic, cubic, biquadratic, or n^{th} order law of the inverse distance [125]-[158].

The *dispersion* of an electromagnetic wave results from non-uniformity of the geometry and physical properties of the environment. The three most common phenomena that perturb an electromagnetic wave are *reflection*, *refraction*, and *scattering* (or *diffraction*). When there is a direct path between the transmitter and the receiver, the signal is received through the LOS path. A signal that is received through the LOS path loses power as a result of the lack of conductivity of the medium and through refraction which occurs as a result of the existence of physical layers with different refractive coefficients. Part of the LOS signal may also be reflected and scattered. When a signal is received through paths different from the LOS path it is said that the signal is received through *non line-of-sight* (NLOS) paths. Like the LOS path, these paths also undergo reflection, refraction, and diffraction. Generically, the outcome of the signal dispersion is called *multipath* [159]-[172]. For more details on the classification of channel models the reader may refer to Appendix E and Chapter 3.

1.4.3 Receiver

Just like a transmitter, a receiver is a physical device, which is characterized by its *sensitivity*, *noise factor* and *signal structure*. The signal structure of a receiver is selected to be compatible with the signal structure of the designated transmitter. The signal structure of a receiver can also be classified into many categories, such as CDMA, FDMA, OFDM, TDMA, and Blind, which are the five main categories relevant to this work [173]-[186]. The reader may refer to Appendix F for more details on the classification of receiver designs.

A block diagram of a generic receiver is shown in Figure 1.11. A receiver contains six main components (or units): (1) antenna (or antenna array, ANTENNA(E)); (2) front end (FE); (3) mixer (MIXER); (4) local oscillator (LO); (5) code/carrier tracking loops (CCTL); and (6) demodulator (DMOD).

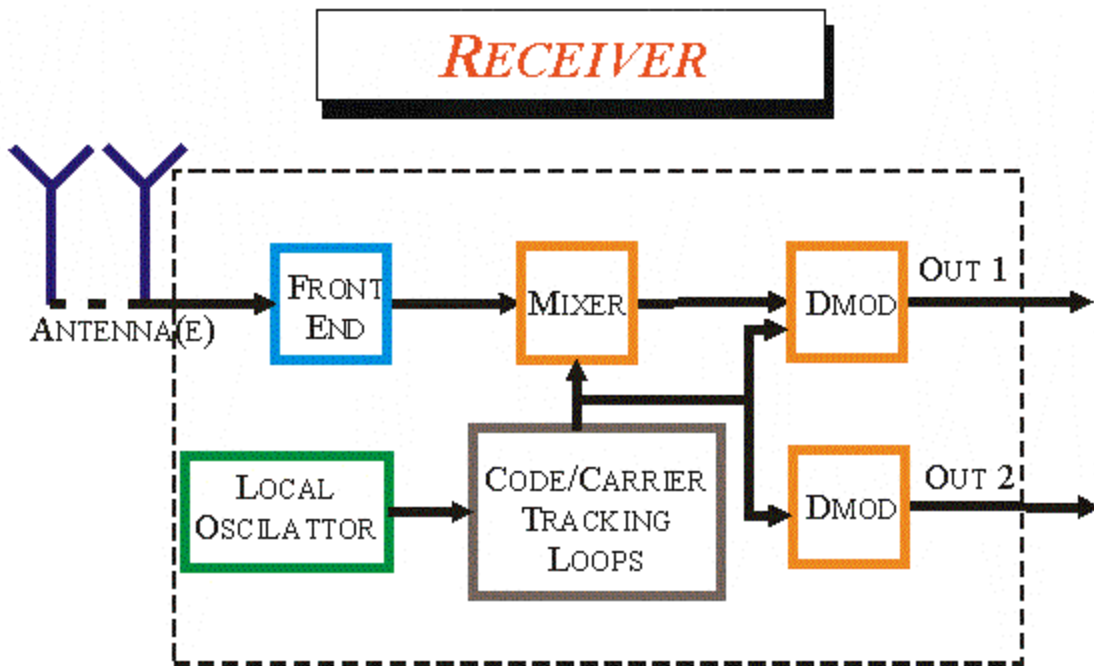


Figure 1.11 A block diagram of a generic receiver.

A localization signal received at the antenna port is amplified in the front end section of the receiver. Then, the output signal of the front end is down-converted and filtered in the mixer using a reference signal coming from code carrier tracking loops. A local oscillator drives the code and carrier tracking loops. Each demodulator demodulates the mixer output signal based on the code carrier and tracking loops output signal. The output signal of each demodulator is the desired signal, which contains localization information.

Chapters 2 and 4 discuss several receiver designs and illustrate the process of obtaining an observable in great detail.

1.5 Outdoor Geolocation Systems

Only the invention and development of radios forged the era of *precise line-of-sight* radio based navigation technology in the 20th century. Among many technologies of the time, the US Navy's Navigation Satellite System, called *Transit*, realized this promise in the 1960's [4], [5] when the John Hopkins Applied Physics Laboratory (APL) developed the first operational, innovative navigation satellite system. The second system, called

Cicada, was developed by the USSR, as part of the cold war response and was very similar to the Transit concept [4], [5].

A few years later, *TIMATION* by the Naval Research Laboratory and program *621B* by the Air Force Space and Missile Organization (SAMSO) were the next two satellite navigation concepts and together with *Transit* became the prototypes for the development and success of *NAVSTAR* (currently known as the Global Positioning System (GPS)) [4], [5].

1.5.1 The Global Positioning System

Almost exactly 30 years ago, during the 1973 Labor Day weekend, a group of ten or so individuals put the final touches on a plan that would revolutionize the art and science of navigation [6]. These individuals were members of a newly formed JPO created to develop the NAVSTAR GPS, having, as a first priority to meet all the US Department of Defense (DoD) needs [6]. Although the GPS concept was based partially on the predecessor navigation systems, the new added feature – *radio ranging* – would revolutionize radio based navigation technology. Radio ranging measurements were anticipated to render greater accuracy than angular measurements to natural stars [4], [5].

1.5.1.1 GPS Description

GPS consists of three main segments (divisions or sections) (see Figure 1.12): the *space* segment (see Figure 1.13), the *control* segment (see Figure 1.13), and the *user* segment (see Figure 1.13) [5].

The *space* segment, which is what most people think of GPS, is the system of 24 GPS satellites. A GPS satellite is a man made object put into orbit around the earth which continuously transmits a spread spectrum signal on two carrier frequencies, $L_1 = 1575.42$ MHz and $L_2 = 1227.6$ MHz (see Figure 1.13) [5]-[10]. At times, the number of satellites can be different from 24. Several satellites are designated as active and a few of them as active spares. The L_1 carrier is modulated by two pseudorandom sequences, the C/A (or coarse acquisition) code and the P (or precise) code. The L_2 carrier is modulated only with the P code. The C/A codes are selected from a family of Gold codes with length equal to 1023 and each one of which repeats once every millisecond. The P code is a

much longer code resulting in a code that has a repeat period of several weeks. The information contained in one week of the P code period is assigned to one satellite; the following week of the P code is assigned to another satellite and so forth. The chipping rate for modulating the C/A code is 1.023 MHz and the chipping rate for the P code is 10.23 MHz. The power associated with the C/A code is 15 dB higher than the power associated with the P code. In Chapter 2 we provide a detailed description of the GPS operation and the C/A code signal specifications.

The *control* segment (see Figure 1.13); i.e., the system of ground-based antennae and monitoring stations is designed to accomplish the following tasks [5]:

- Maintain each satellite in its proper orbit through infrequent small command maneuvers.
- Make corrections and adjustments to the satellite clocks and payload as needed.
- Track all GPS satellites and generate and upload the navigation data to each of the GPS satellites.
- Command major satellite relocations in the event of satellite failure to minimize its impact in the GPS system. (This is the reason why spare satellites are required.)

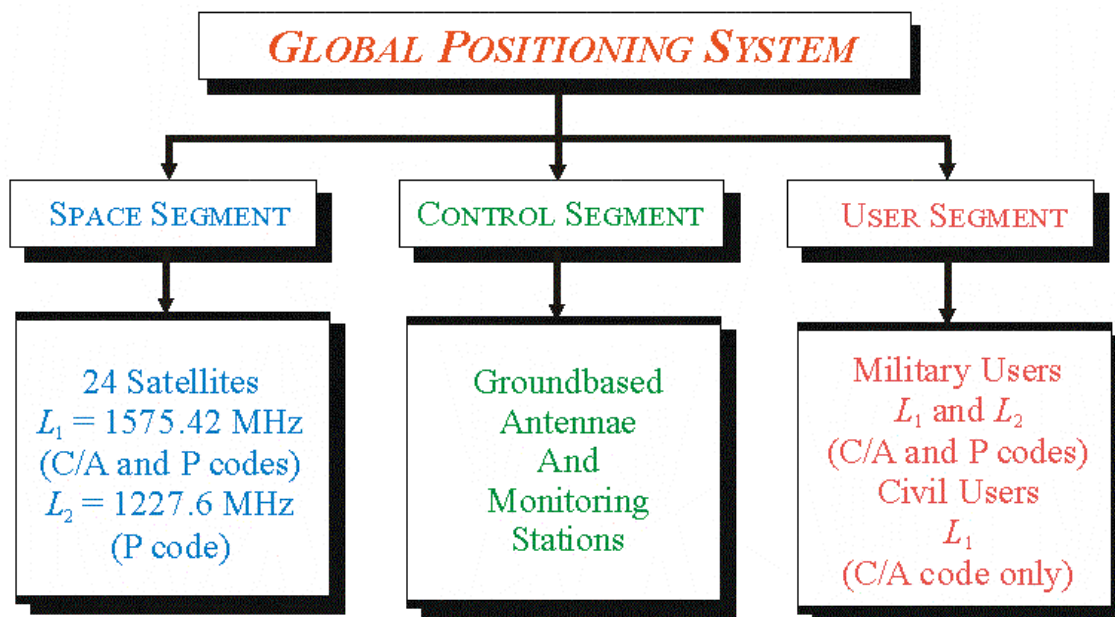


Figure 1.12 A description and definition of GPS.

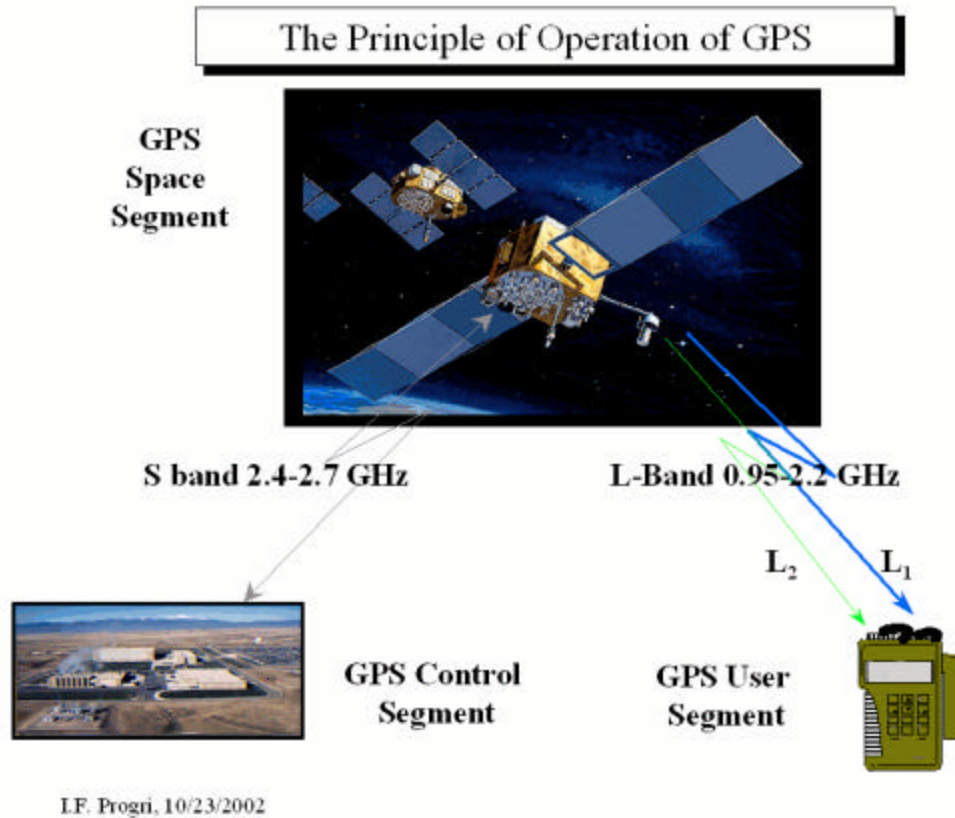


Figure 1.13 The GPS operational segments - - using elements from [10].

The *user* segment consists of all GPS receivers every one of which tracks ranging GPS signals and computes its 2-D or 3-D position and its local clock correction (or local time, see Figure 1.13) with respect to the GPS time. The user segment consists of military receivers and civilian receivers. The military receivers have access to both C/A and P(Y) codes as opposed to the civilian receivers which have access only to the C/A code; therefore, the civilian receivers are prone to larger position errors than the military receivers are.

1.5.2 The Global Navigation Satellite System

Close in concept, but quite different in signal structure and satellite frequency selection, is, the Russian equivalent to GPS, GLONASS. GLONASS can achieve similar or better accuracy for users on the surface of the earth, in the air or in space. Both GPS and GLONASS are part of the Global Satellite Navigation Systems (GNSS); nevertheless, GLONASS is primarily designed to provide a navigation role for maritime

and aviation interests and as such has many features in common with GPS. The orbital plan allows for 24 satellites with 8 satellites in each of three orbital planes separated by 120° with spacing of 45° within the plane. Clearly the orbital planning enables users' access to at least four satellites anywhere, which is the minimum for navigation purposes. If combined together both GPS and GLONASS would offer about 8 satellites in view for the greater part of the day, which offers a greater level of independence, redundancy, and cross-checking that enhances certain global applications of GNSS such as civil aviation [16].

GLONASS had the potential to be a great competitor of GPS. However, GLONASS has been plagued with several outages, which have reduced the number of available satellites in the space segment to approximately half of what is needed. This situation has been exacerbated by the state of the Russian economy since 1990. Currently GLONASS has only 7 operating satellites, which is insufficient for GLONASS receivers to reliably extract simultaneous positioning and timing information.

1.5.2.1 GLONASS Description

Like GPS, GLONASS also consists of three main segments: the *space segment*, the *control segment*, and the *user segment* as shown in Figure 1.14.

The *space segment* contains 24 satellites each one of which transmits two spread-spectrum ranging signals one at $L_1 = 1600$ MHz and the other at $L_2 = 1250$ MHz at around the same power levels as the GPS signals. Radio frequency channels, rather than spread-spectrum codes, distinguish satellites; i.e., GLONASS uses FDMA rather than CDMA. A single narrowband code of length 511 repeats every 1 ms, which is the same as the repetition period of the GPS C/A code. Information is differentially encoded in a return-to-zero (RZ) format with a final data rate of 50 baud. A separate broadband code is used to transmit differentially encoded data at 50 baud. A narrowband code is found only at the L_1 -band as opposed to the broadband code, which is found at both L -bands; hence, it enables correcting for ionospheric delay in a manner analogous to that used by GPS. The GLONASS C/A-code (coarse/acquisition) spectrum covering 1 MHz bandwidth is superimposed on the P-code (precise) signal transmitted in phase quadrature and covering 10 times the C/A-code bandwidth.

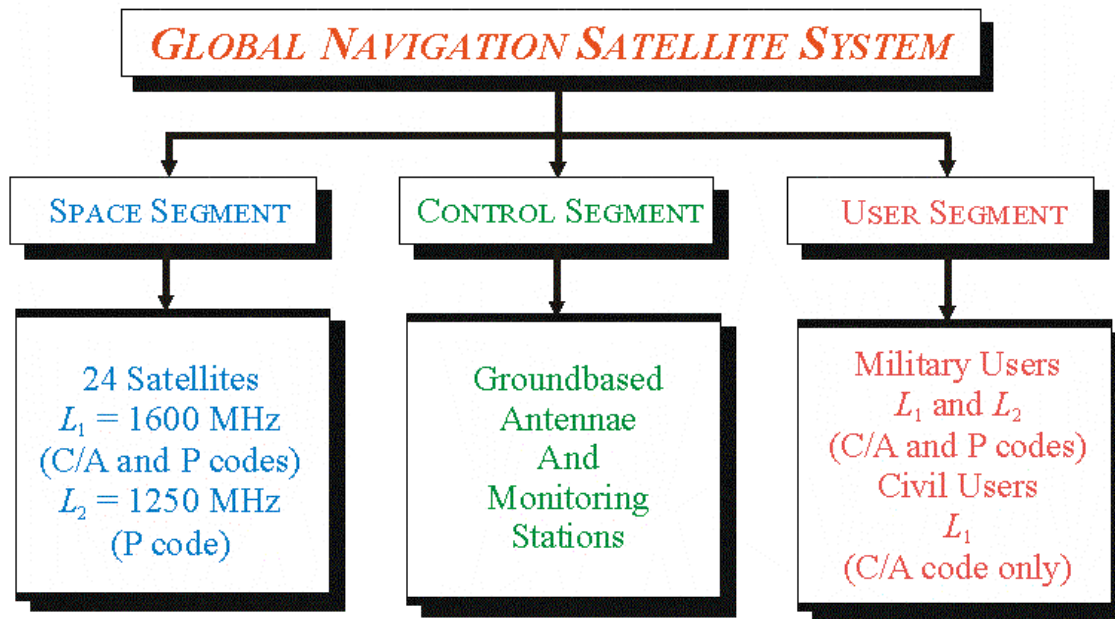


Figure 1.14 A description and definition of GLONASS.

The *control segment* consists of ground antennae and monitoring stations. The GLONASS control segment is designated to accomplish tasks similar to the GPS control segment.

The *user segment* consists of all the GLONASS users; i.e., all users who own a GLONASS receiver.

1.5.3 Galileo: The European Satellite Radio Navigation System

In February 1999 the European Commission presented an autonomous program on satellite radio navigation—Galileo. On July 19, 1999 the European Council passed a resolution to call the Commission to develop a civilian system for global use managed by civil authorities and offering both compatibility and significantly added value in relation to existing systems, such as GPS and GLONASS [17]. On November 2000, the Commission reaffirmed the importance of this technology on the future economy and security of the European Union. The European Union approved Galileo on March 23rd,

2002, once it was demonstrated that Galileo would be profitable by generate €¹ 10,000 million annually [17].

Galileo is planned to become operational after the completion of four phases. The 1st Phase (the system definition) is already completed (1998–2002). The 2nd Phase (the development and validation) includes the launch of the first experimental satellite in 2004 (2002–2005). The 3rd Phase (the deployment) starts in 2006 and ends 2007 with construction and launch of satellites and installation of the complete ground segment. The 4th Phase (the commercialization) starts in 2008 and onward [17].

1.5.3.1 Galileo Description

Galileo also consists of three segments, (1) the *space segment*, (2) the *ground* (or control) *segment*, and (3) the *user segment* as depicted in Figure 1.15.

The Galileo *space segment* consists of 30 satellites (27 operational and 3 spare) positioned in three circular medium Earth orbit planes at an altitude of 23,616 km and at an inclination of 56° with reference to the equatorial plane [17]. Each satellite contains a navigation payload and a search and rescue transponder. It also contains two onboard atomic clocks that calculate time within a few hundred microseconds per day; one based on Rubidium atomic frequency standard (6 GHz) and the other using hydrogen maser (1.4 GHz). These clocks were chosen because they present very good stability to within a day or so. These clocks are regularly synchronized to a network of even more stable ground-based reference clocks, based on a Cesium frequency standard [17].

Galileo provides five navigation signals. Each signal contains one or two ranging codes and one additional information message, which may be *navigation*, *commercial* or *search and rescue* data. Galileo provides four categories of services: *open*, *safety*, *commercial* and *public regulated service*. The *open* service is free of charge and gives users their exact location on the planet to within 5-m accuracy. The *safety* service includes the search and rescue services. In this case the open signals could be encrypted to provide integrity information. The *commercial* service sends encrypted data over the open signals and provides access to a third navigation signal to enable users to apply the

¹ The symbol for European Current Unit (ECU) is €

three carrier phase ambiguity resolution technique which results in nearly instantaneous ambiguity resolution. As such, the commercial service is not free, but offers quality of service (QoS) features, which are neither offered by GPS nor GLONASS. The last two navigation signals provide the *public regulated service* that offers position and timing to specific users requiring high continuity of service [17].

Galileo is also equipped with data encryption, systems of keys managed by the European governments, spectral separation between two different navigation signals, and service denial capacity to meet European and global security concerns. These concerns are defined as (1) security of infrastructure; (2) security of signals against jamming and spoofing and management of the potential keys used to access the service; (3) security to guaranty a high level of continuity; and (4) global security [17].

The Galileo *ground (or control) segment* consists of: (1) two control centers to be implemented on European soil to provide satellite control and navigation mission management; (2) 20 sensor stations and 15 uplink stations installed around the world for data exchange [17].

The Galileo *user segment* consists of all of the civil or military Galileo users, who will poses a Galileo receiver.

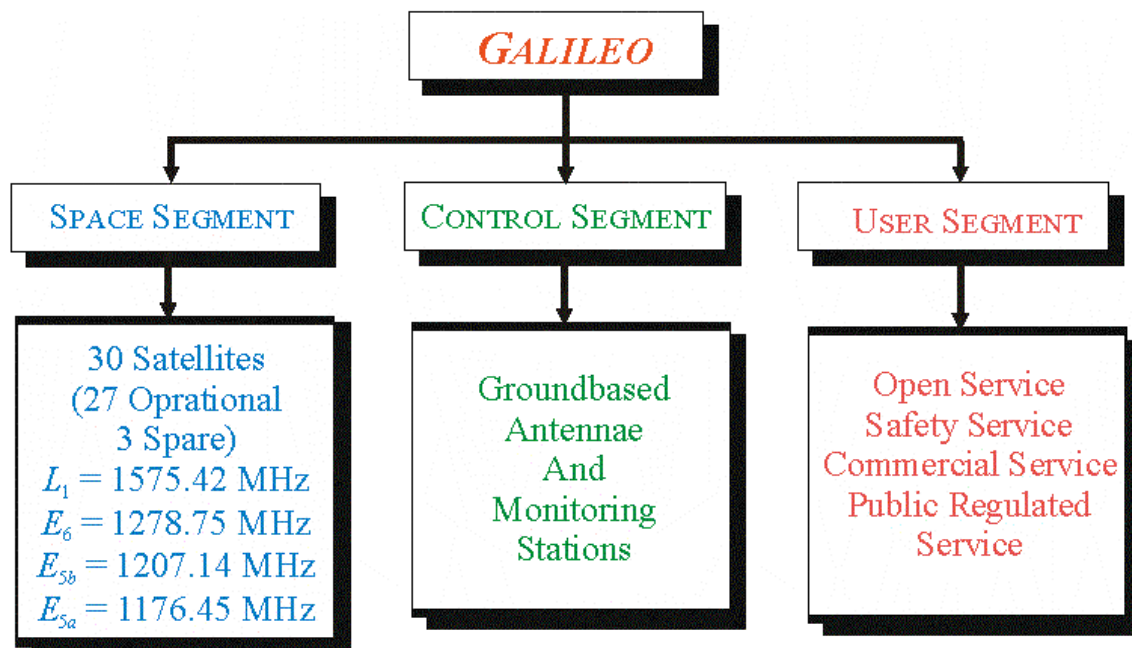


Figure 1.15 A description and definition of Galileo- - using information from [18] and [19].

1.5.4 MTSAT or MSAS

MTSAT has a two-fold mission: aeronautical and meteorological [20]. These two payloads work on board independently. The owner and operator of the MTSAT are the Japanese Civil Aviation Bureau (JCAB) and the Japanese Meteorological Bureau (both belonging to Japanese Ministry of Land, Infrastructure, and Transport (MLIT)) [20]. The MSAT aeronautical program objective is to provide safe and efficient aircraft operation in rapid growing areas of the Asia/Pacific airspace [20].

1.5.5 Satellite/Pseudolite Outdoor Geolocation System

The pseudolite idea is just as old as the GPS idea itself. A pseudolite is a GPS-like signal transmitter that can be placed on the ground, on the top of buildings, indoors, underground, or underwater. Initially, a pseudolite is seen as a means for increasing navigation accuracy in the vicinity of airports by using pseudolites to form a Local Area Augmentation System (LAAS) [24]. Pseudolites greatly improve the geometry especially the vertical component, and thus enable the aircraft to perform precision approach and landing [24]-[26].

1.5.5.1 GPS Satellite/Pseudolite Outdoor Geolocation System

There are several authors who have proposed GPS satellite/pseudolite systems. Stain and Tsang propose a GPS aided with pseudolites and demonstrate the capability of using Commercial Off-the-Shelf (COTS) GPS receivers with pseudolites [28]-[29]. Van Dierendonck envisions a role for pseudolites in differential GPS [30]. Brown and Van Diggelen [32] and Cohen et al. [33] propose a similar integrated system of GPS satellites/pseudolites for category II and III precision approach and landing employing a differential carrier ranging technique. McGraw has analyzed the pseudolite code interference effects for aircraft precision approaches [34]. Bartone and Van Graas have proposed ranging airport pseudolite for local area augmentation [36]. Bartone and Kiran have discussed the flight test results of an integrated wideband airport pseudolite for LAAS [37].

A GPS satellite/pseudolite outdoor geolocation system for Category II and III precision landing is illustrated in Figure 1.16. As shown in the figure, we note system components: GPS satellites, GPS airport pseudolites, airport runway, and the airplane.

Typically, an airplane has a dual GPS satellite/pseudolite receiver with two antennae, one mounted on the top of the airplane to track GPS satellites and the other mounted on the bottom of the airplane to track GPS pseudolites. Pseudolites offer potentially several improvements and benefits to the airplane approach, which are mentioned in order.

The geometry of such a system is greatly improved because to a large extent we have control over the pseudolite placement. This enhances the vertical accuracy and the receiver clock correction to GPS time by almost an order of magnitude. The system integrity, continuity, and availability are enhanced because pseudolites provide additional ranging sources, thus offering more redundancy. For definitions of accuracy, integrity, continuity, and availability, the reader may refer to §1.7.

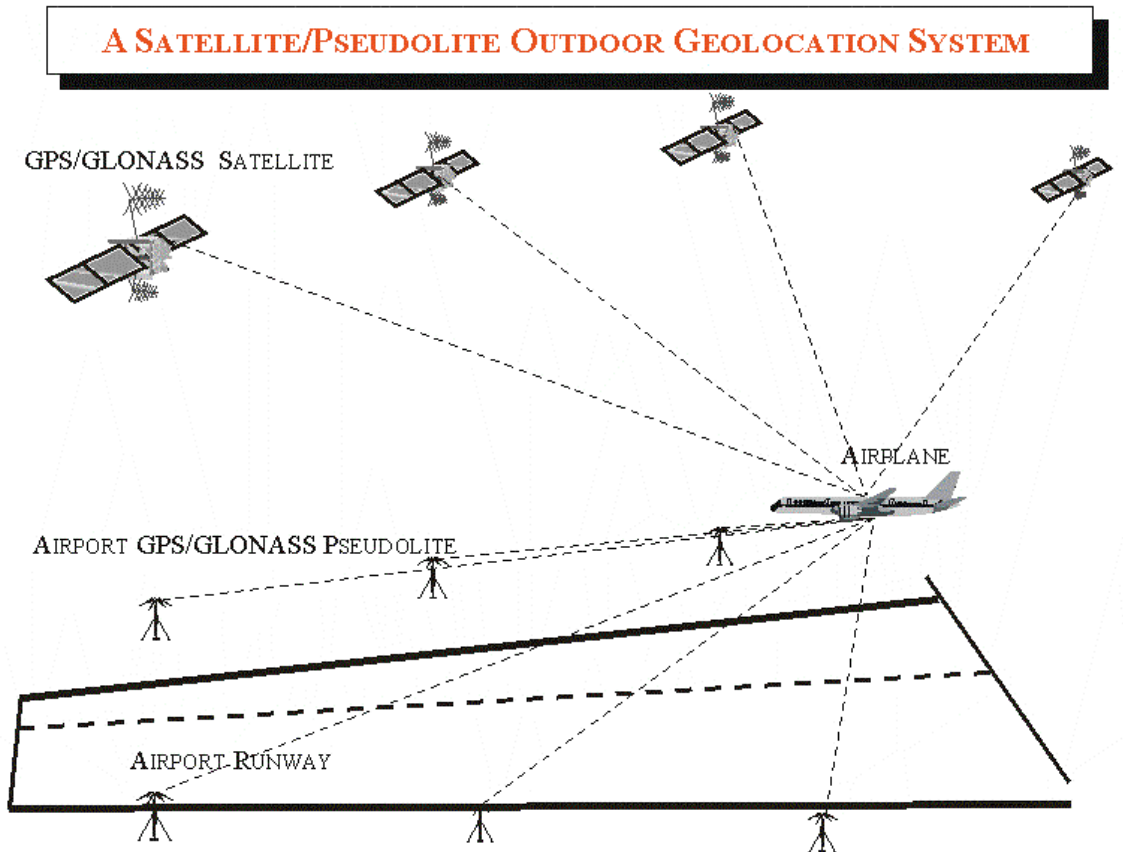


Figure 1.16 A GPS/GLONASS satellite/pseudolite outdoor geolocation system.

Nevertheless, there are several technical issues that pseudolites impose. Pseudolites may or may not be synchronized to the GPS time. Past experience has demonstrated that all pseudolites must be synchronized to allow a normal operation of the system [23]-[37]. Any pseudolite system requires additional infrastructure and real estate. The infrastructure includes the pseudolite cost, the synchronization cost and the maintenance cost. The real estate includes the land cost and availability. Other technical issues of this technology are addressed in Chapter 2.

1.5.5.2 GLONASS Satellite/Pseudolite Outdoor Geolocation System

Galijan and Lucha, suggest an approach for augmenting GNSS category III approaches and landings based on a GPS/GLONASS and a GLONASS pseudolite system [31].

A GLONASS satellite/pseudolite outdoor geolocation system for category III approach and landing is depicted in Figure 1.16. The operation of this system and the issues associated with this system are very similar to the GPS satellite/pseudolite outdoor geolocation system.

1.6 Indoor Geolocation Systems

Despite superior advantages for outdoor applications, current satellite-based systems **cannot** provide accurate indoor geolocation simply because they were not designed to operate indoors. In principle, there are at least three solutions to this problem. One would be to redesign the satellite-based systems to provide accurate indoor geolocation (GPS modernization, GPS III, and Galileo programs). The second approach would be to invent new indoor geolocation systems based on technologies such as relay, UWB, mobile phone, IEEE 802.11, etc. The third approach would be to integrate current indoor geolocation systems with current satellite systems (for example Aided GPS mobile phone positioning). The answer to the first approach is that GPS modernization, GPS III, or Galileo will presumably provide an indoor geolocation capability; however, this is not expected to be available until at least the year 2010 or onwards. The answer to the third approach is based on the answer to the first approach anyway. Therefore, the

investigation of indoor technologies that utilize ground-based transmitters is critical for the needs of indoor positioning of the current decade [46]-[69].

A technology that provides accurate indoor geolocation is particularly needed for military, public safety, commercial, and scientific applications. In public safety applications, indoor geolocation systems may be used to track people afflicted with diseases such as Alzheimer's, to monitor inmates in prison and provide useful information to policemen, firemen and emergency personnel. Moreover, emergency workers performing rescue missions or soldiers on the battlefield may depend on such systems to accomplish their civilian duties or military objectives. In residential and commercial applications, such systems can be utilized to locate personal, portable equipment, to navigate under emergency conditions, and pinpoint specific items inside buildings. In other commercial applications indoor geolocation systems can render accurate localization of equipment and items and can be utilized by security personnel to monitor guests or personnel with restricted privileges. Nursing homes and hospitals can benefit from this technology and use it to track people with special needs, children who are away from visual supervision, the elderly, the blind, or to better assist people in case of emergency etc. Scientists, such as geologists, or cave explorers, can employ indoor geolocation system for their scientific missions to locate themselves or equipment inside caves or in underground environments.

A classification of indoor geolocation systems based on the signal structure is depicted in Figure 1.6. As shown in Figure 1.6 these systems can be classified into three main groups: (1) Satellite/Pseudolite indoor geolocation systems (see §1.5.5); (2) wireless indoor geolocation systems (see §1.6.2); (3) Relay indoor geolocation systems (see §1.6.1.2); and (4) UWB indoor geolocation systems (see §1.6.1.2).

1.6.1 Indoor Satellite/Pseudolite Geolocation System

Although outdoor satellite/pseudolite geolocation systems were not designed to operate indoors, in principle they can be utilized to operate indoors with limited accuracy and benefits to indoor users. Until outdoor geolocation systems will become fully operational indoors, indoor users have three options: (1) extend the capabilities of outdoor geolocation systems, (2) rely on the state of the art indoor positioning

technologies, or (3) invent new technologies, which are investigated in this work in Chapters 4 through 8. The following system, called SnapTrack™, is presented as an alternative to indoor positioning using GPS and a non-conventional GPS receiver design.

1.6.1.1 SnapTrack™ Indoor Geolocation System

The SnapTrack™ system is a GPS based indoor geolocation system, which uses a SnapTrack™ receiver as illustrated in Figure 1.17 [52]–[54]. As shown in the figure, the SnapTrack™ system uses a reference receiver to obtain GPS navigation data and differential corrections. These data feed a Terrain Database and Location Server that provides aided data to a handset device. The handset produces pseudorange measurements and feeds them back to the terrain database and location server. Finally, the location server produces the handset navigation solution, which is passed in the external application [52].

It is claimed that the SnapTrack™ system can acquire and provide position fixes in environments with up to 25-dB attenuation [52]. In a worst case scenario, a SnapTrack™ system can provide the first fix in a few seconds [52]. Also a SnapTrack™ system performs localization on demand; thus, minimizing the power consumption.

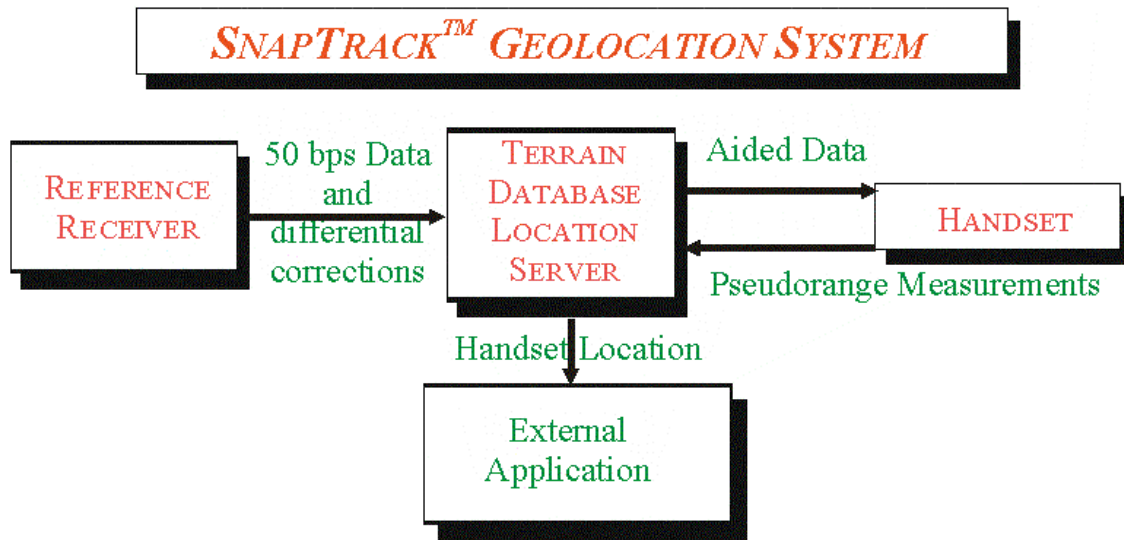


Figure 1.17 A snap track indoor geolocation system-- taken from [52].

1.6.1.2 US Coast Guard Indoor Geolocation System

In the late 1990s the United States Coast Guard Academy developed an indoor, spread spectrum geolocation system to track personnel inside buildings under a project funded by the Defense Advanced Research Projects Agency (DARPA) Small Unit Operations Geolocation program. This system is illustrated in Figure 1.18 [55].

The system evolved from a single time difference (TD) engineering testbed to a fully functional, six-receiver indoor geolocation system [55]. The system consists of one reference transmitter, one handheld transmitter and six wideband receivers. The reference transmitter is placed outside of the area of interest and supplies sampling time synchronization to all receivers. This is explained later in this section. The soldier, who is depicted in the figure inside the building, carries a hand-held transmitter, which is placed inside a backpack along with a long-life battery. Six wideband receiver antennae are placed outside the area of interest in surveyed positions, which are selected to provide adequate three-dimensional geometry. Six receivers are grouped into three groups of two and each group is equipped with a GPS receiver. The GPS receiver provides a one-pulse-per-second (1 PPS) signal to trigger the start of the data acquisition. Even though the stability of the 1 PPS signal may vary among receivers by as much as ± 50 ns, the coarse triggering of 1 PPS ensures that all receivers start data acquisition within the same pseudorandom (PRN) sequence from the transmitter, whose duration is 80 μ s. To further synchronize the receiver clocks a reference transmitter is placed in a known location. A clear view to each receiver is desired to minimize the effects of multipath for the reference transmitter. The reference transmitter also housed a GPS receiver supplying 1 PPS to reset the start of its PRN transmission. Using the known locations of the reference transmitter and the receiver antennae, a theoretical TOA was calculated for each receiver. This theoretical TOA was compared with the measured TOA to determine the clock errors of each receiver with respect to the reference transmitter's clock. This error was then applied to each receiver clock to synchronize it to the reference transmitter's clock.

The first major drawback of this approach is its reliance on GPS for synchronization. The second major drawback is its complexity (six receivers and at least two transmitters).

US COAST GUARD INDOOR GEOLOCATION SYSTEM

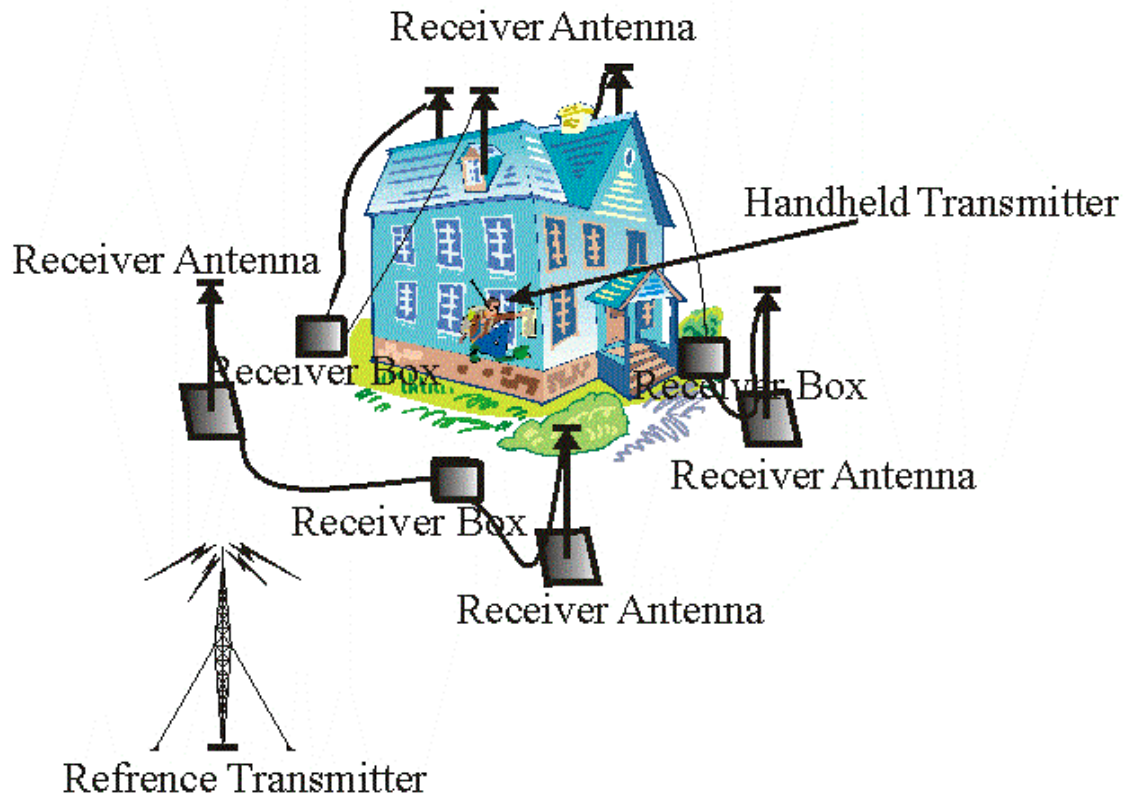


Figure 1.18 US Coast Guard indoor geolocation system- - taken and modified from [55].

Nevertheless, utilizing over 3,000 samples taken at 28 different points throughout the test area a solution converges within 1 second and 90 % of the fixes fell within a 2.86-m (1 sigma) error [55].

1.6.2 Wireless Indoor Geolocation Systems

Wireless indoor geolocation systems contain the IEEE 802.11 wireless networks, which are generally **not** considered as indoor geolocation systems, in contrast to the mobile phone geolocation systems, which are typically considered as dual outdoor-indoor communications and geolocation systems. Nevertheless, IEEE 802.11 wireless networks can be utilized as indoor geolocation systems.

1.6.2.1 Wireless Networks (IEEE 802.11)

IEEE Standard 802.11 was initially conceived to operate at 1 and 2 MBPS in the license-exempt 2.4-GHz industrial, scientific, and medical (ISM) band and also in the infrared in 1997 as an extension technology for conventional wired local area networks (LANs). In its early days IEEE 802.11 was envisioned as a few PCs with wireless capabilities connected to an Ethernet LAN through a single network access point. Today, it has grown into something much more capable, complex, and confusing [56]. Something more capable because IEEE 802.11 operates in both 2.4 and 5-GHz bands [56]. Something more complex and confusing because service companies are stringing these networks together to create what soon will be the world's largest wireless data network [56],[57].

In 1990, the IEEE 802.11 standards committee was established to set up task groups to design specifications for systems operating in the 2.4-GHz and 5-GHz bands, systems currently known as (a) and (b).

IEEE 802.11a was finalized in 1997 and was devised in parallel with the (b) variant, partly because (b) shares spectrum with applications such as cordless phones, microwave ovens, and Bluetooth [56]. IEEE 802.11a, the fastest flavor of the standard, operates at data rates ranging from 6 MBPS to 54 MBPS and in the 5-GHz band (known in US as the Unlicensed National Information Infrastructure (UNII) band) [56]. The physical layer uses OFDM modulation and is similar to that for HiperLAN II, the wireless standard of the European Telecommunications Standards Institute in France [56].

IEEE 802.11b was finalized in 1997 and was trademarked commercially by the Wireless Ethernet Compatibility Alliance (WECA) as Wi-Fi. This variant operates in the ISM band at 5.5 MBPS and 11 MBPS. The physical layer combines Complementary Code Keying (CCK) and Packet Binary Convolution Coding (PBCC) [56].

A draft of IEEE 802.11g proposes an improvement of the data rate of IEEE 802.11a to Wi-Fi (54 MBPS) in the 2.4-GHz ISM band. IEEE 802.11g adopts OFDM from the (a) variant and two modulation schemes: PBCC and CCK-OFDM from the (b) one [56].

IEEE 802.11c, d, and h working groups address regulatory and networking issues. IEEE 802.11e working group addresses time-sensitive applications such as voice and

video, IEEE 802.11f with communications among access points to support roaming, and IEEE 802.11i with advanced encryption standards to support stronger privacy [56].

IEEE 802.11 Wireless Networks can be augmented (or modified) to offer position accuracy from 100 m to 50 m in most cases. It is important to emphasize that this technology must be enhanced or integrated with other technologies or have a close interface with a user to refine its position [58].

Typically, most IEEE 802.11 Wireless Networks contain several base stations deployed around the city (see Figure 1.19). Each base station consists of a server equipped with two network interfaces: one network interface provides wireless access to the client, and the other to connect to a fixed network [58]. Each cell server also periodically broadcasts a beacon—a simple datagram that encapsulates a location identifier—to inform the end-user system of his or her cell location. In the worst case scenario this system provides an accuracy of approximately 350 meters, which reflects the transmission range of the WaveLAN network cards. In general 802.11 Wireless Networks provide a much better accuracy.

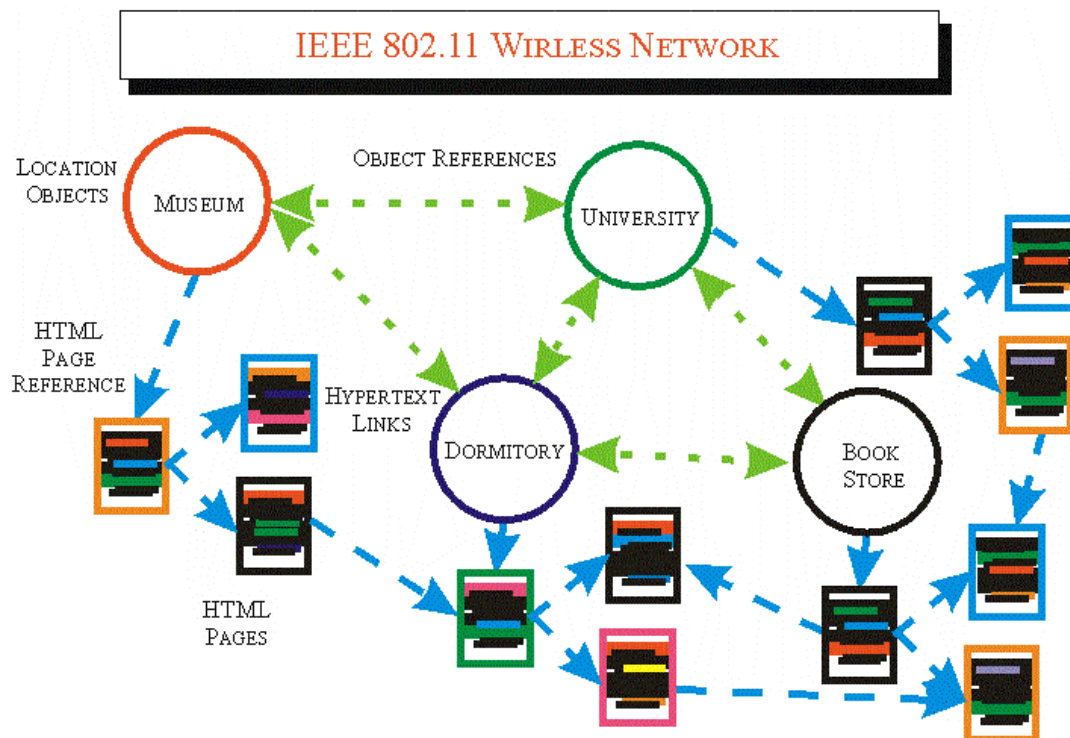


Figure 1.19 An IEEE 802.11 wireless system - - taken and modified from [58].

If an end user can receive beacon signal from multiple sources then a smoothing function could be used to avoid this issue. Such smoothing function dictates that an end-user must see at least N consecutive beacons from a new cell server before reporting the cell as its new location.

1.6.2.2 Mobile Phone Positioning for 3G Systems

Finding the location of mobile phones is one of the important features of the 3G mobile communication system (see Figure 1.20). This new feature can enable many valuable location-based services.

The architecture of such a system is illustrated in Figure 1.21. The acronyms applied to Figure 1.21 are explained in order. UTRAN stands for Universal Terrestrial Radio Access Network. UE depicts the user equipment, which is handheld apparatus or handset. Node B is the term for base station. LMU stands for location measurement unit. LMU type A is a standalone LMU as opposed to LMU type B, which is an integrated LMU with a base station. SAS stands for standalone serving mobile location center (SMLC). RNC depicts radio network controller; thus, SRNC stands for standalone RNC. CN stands for core network [47]. The deployment of all units is mandatory with exception of the SAS, whose deployment is optional. If SAS is not included in the system, then the SMLC is integrated in either RNC or SRNC.

There are five types of interfaces that enable communications among all units in UTRAN: (1) Uu, (2) Iub, (3) Iur, (4) Iupc, and (5) Iu. Uu enables the communications between the user equipment and the base station (or Node B). Also, LMU type A communicates through Uu with the Node B (or LMU type B). Iub enables the communications between Node B and either RNC or SRNC. Iur ensures the communications between RNC and SRNC. Iupc (optional) enables the communications between SRNC and (optional) SAS. Iu ensures the communications between SRNC and CN [47].

Mobile phone positioning methods for 3G systems include cell-ID-based, assisted GPS, and TDOA-based methods (such as OTDOA, E-OTD, and A-FLT) as illustrated in Figure 1.22 [46]-[51].

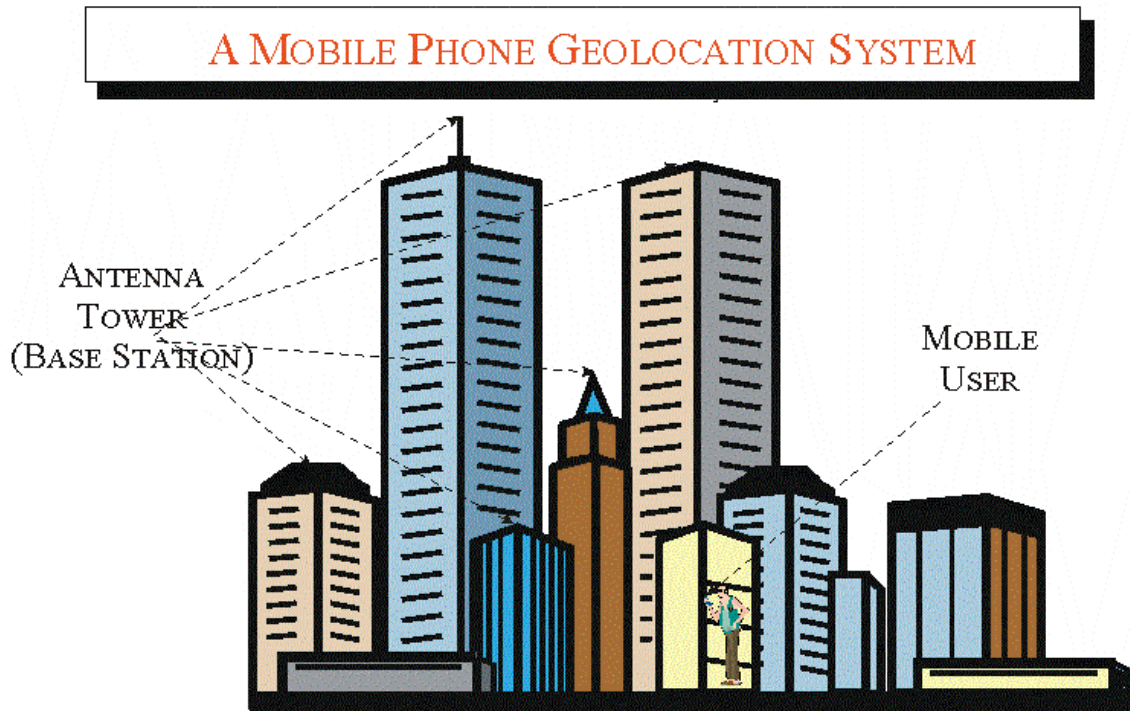


Figure 1.20 A mobile phone geolocation system.

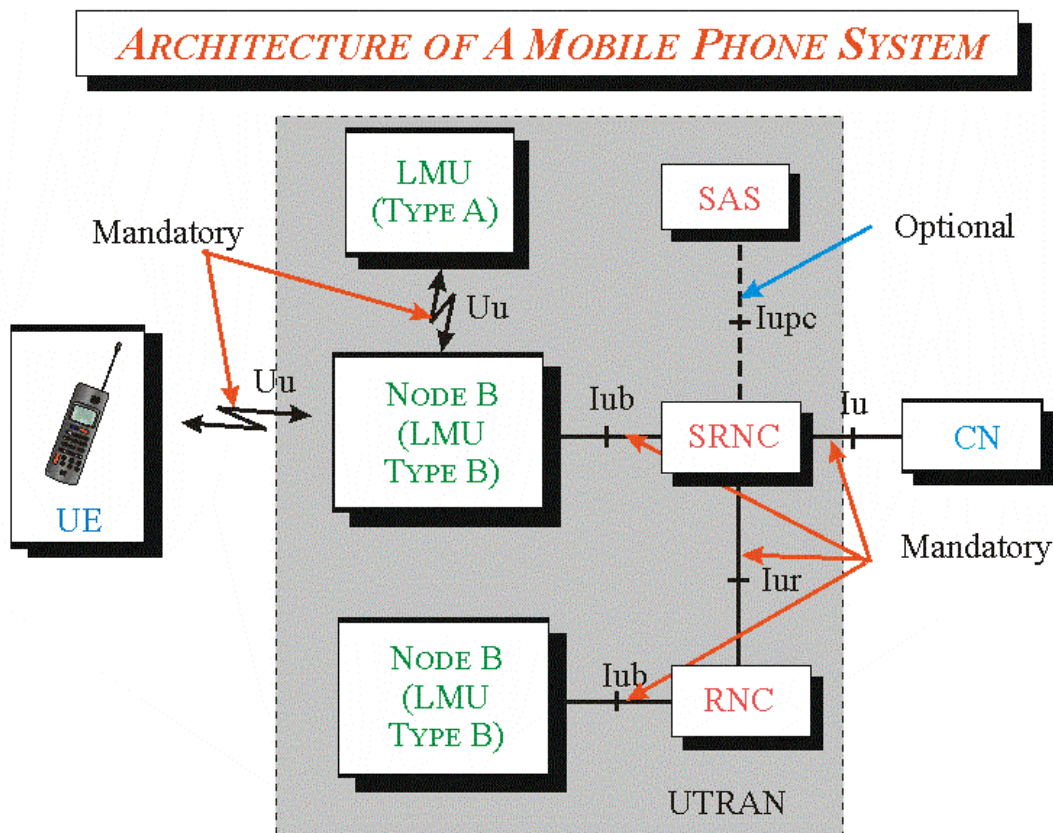


Figure 1.21 The architecture of a mobile phone geolocation system-- taken from [47].

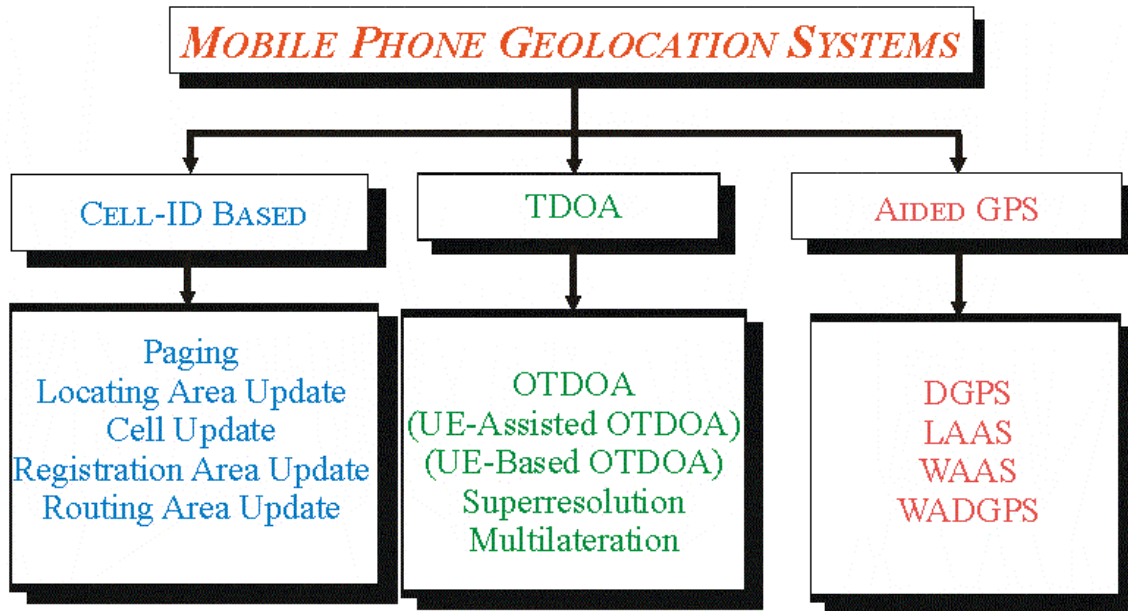


Figure 1.22 Classification of mobile phone positioning methods.

We discuss the mobile positioning based on cell-ID in §1.6.2.3. We investigate the mobile positioning based on TDOA scheme in §1.6.2.3. We discuss the GPS aided (or assisted) mobile positioning in §1.6.2.5.

1.6.2.3 Cell-ID Positioning Method

Mobile phone systems are classified into 3 categories based on the cell size: (1) macrocell systems; (2) microcell systems; and (3) picocell systems as shown in Figure 1.23 [51]. This classification is exploited in Chapter 3 to model the channel impairments as a function of the cell radius. It is conceivable that the smaller the cell radius the better the accuracy; i.e., the smaller the position error.

1.6.2.4 TDOA Positioning Method

The FCC has issued an order requiring wireless providers to locate wireless 911 callers to within 100 m (67 % of the time) by October 2001 [48]. One alternative of mobile phone positioning is proposed by Klukas *et al.* [49]-[50], which underlines the efforts of the Cell-Loc Inc., and the Department of Geomatics Engineering at the University of Calgary. The system that Klukas *et al.* proposes consists of a telephone positioning using superresolution to estimate time of arrival and hyperbolic multilateration [49].

CELL-ID MOBILE PHONE GEOLOCATION SYSTEM

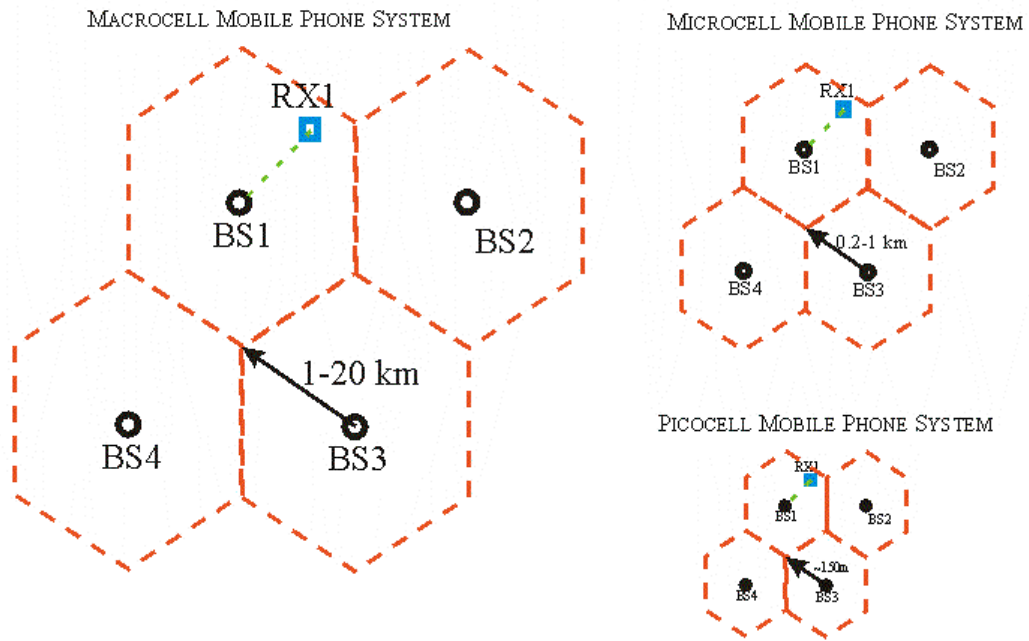


Figure 1.23 A description of cell-ID mobile phone geolocation system systems.

TDOA MOBILE PHONE GEOLOCATION SYSTEM

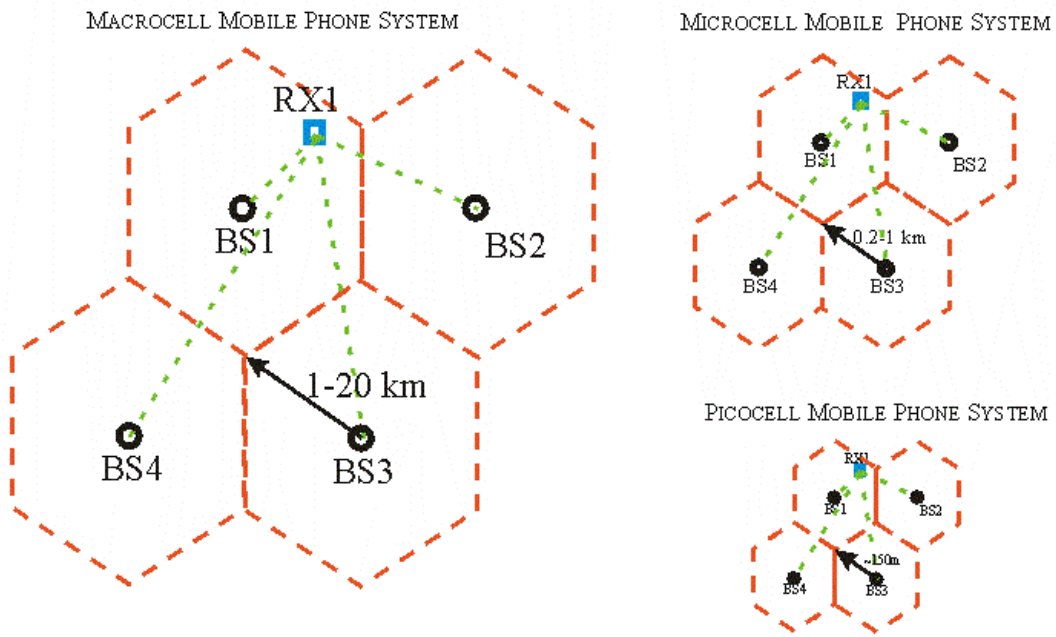


Figure 1.24 A TDOA mobile phone geolocation system.

1.6.2.5 Aided GPS Positioning Methods

The aided (or assisted) GPS positioning methods include Differential GPS (DGPS), Wide Area Differential GPS (WADDGPS), the Wide Area Augmentation System (WAAS) and the Local Area Augmentation System (LAAS). An illustration of an assisted GPS mobile indoor geolocation system is shown in Figure 1.25. This system attempts to establish a GPS reference network (or a wide-area DGPS network) whose receivers have clear views of the sky and operate continuously. This reference network is connected with the mobile phone infrastructure, monitors the constellation status in real-time, and provides data such as handset position (or base station location), ephemeris and clock correction, satellite visibility, Doppler, and even the pseudorandom noise for each visible satellite at a particular epoch [71]. A mobile phone or a specific location based application can request the GPS reference network to transmit assist data back to the mobile phone to aid fast start up and increase sensor sensitivity [71]. Since the reference network and reference receiver predicts the Doppler vs. code phase acquisition time the acquisition time is reduced to yield a rapid search speed and a much narrower signal search bandwidth [71]. Ultimately, the received signal sensitivity is enhanced and the receiver power consumption is reduced [71].

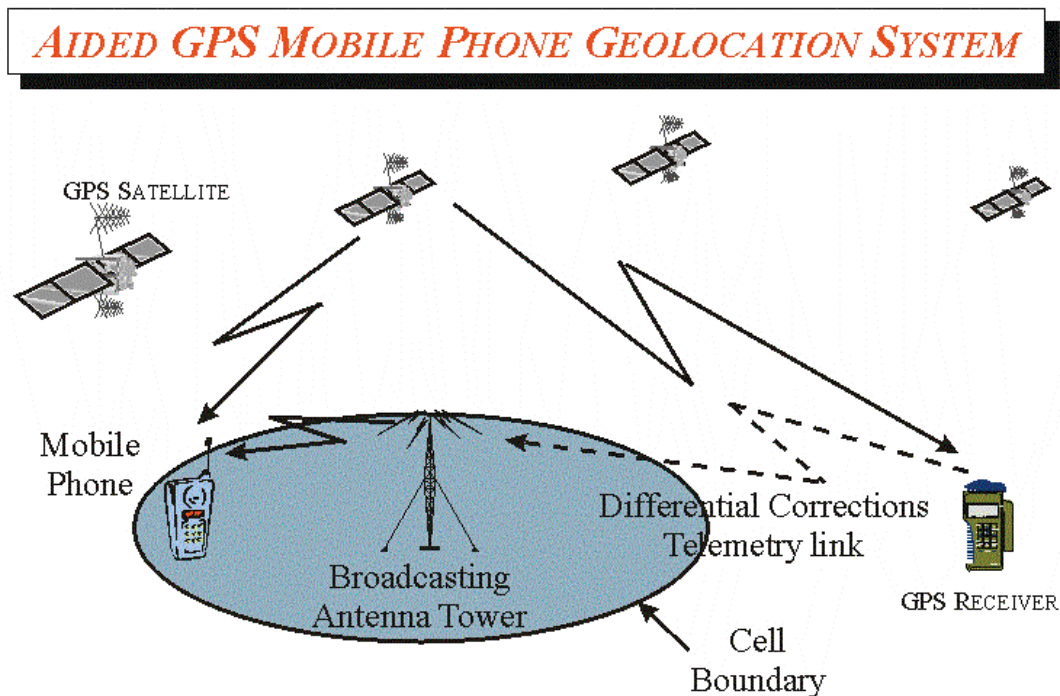


Figure 1.25 An aided GPS mobile phone geolocation system - modified from [71].

1.6.3 Other Indoor Geolocation Systems

Other indoor geolocation systems that we discuss are relay indoor geolocation system and UWB indoor geolocation systems as depicted in Figure 1.26.

A relay is a device or apparatus by means of which a change of current or a variation in conditions of an electric circuit causes a change in conditions of another circuit or operates another or other devices in the same or another circuit [13].

Based on this definition, we highlight two relay systems: namely, (1) the MIT relay system (see §1.6.3.1) and (2) the precise RF positioning system (see §1.6.3.2).

UWB systems are discussed in §1.6.3.3.

1.6.3.1 MIT Relay Indoor Geolocation System

Reynolds (MIT) proposes a low frequency radio navigation system based on phase measurements called a building positioning system [61]. This system provides good accuracy 5 cm for a 50-m radius area and it is intended for asset tracking, security and human computer interface, robot navigation, and management of services as diverse as medical care. A conceptual description of the MIT indoor geolocation system is illustrated in Figure 1.27. The system contains at least 4 low frequency relay transmitters and more that one low frequency receiver.

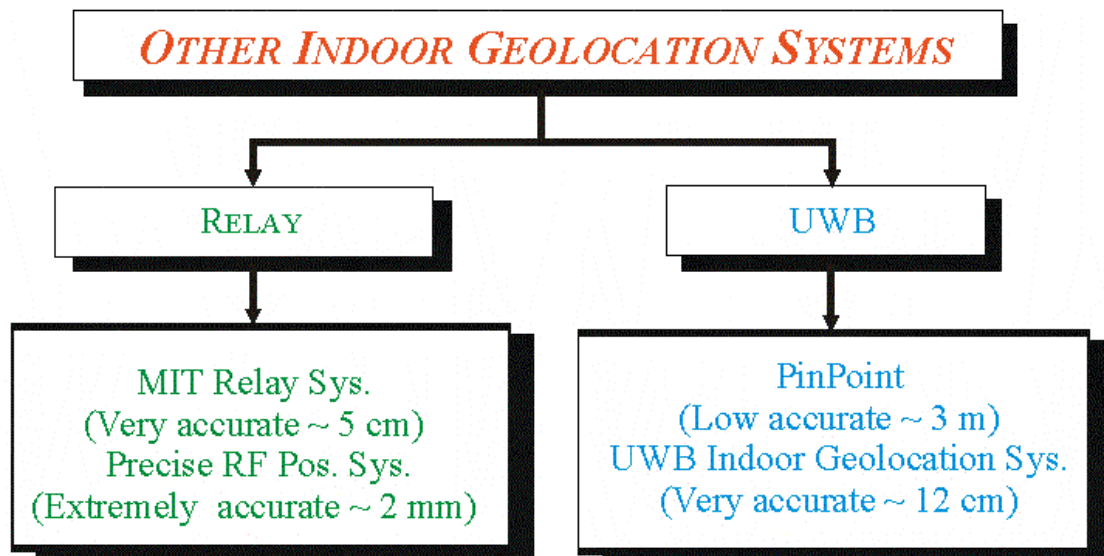


Figure 1.26 A classification of other indoor geolocation systems.

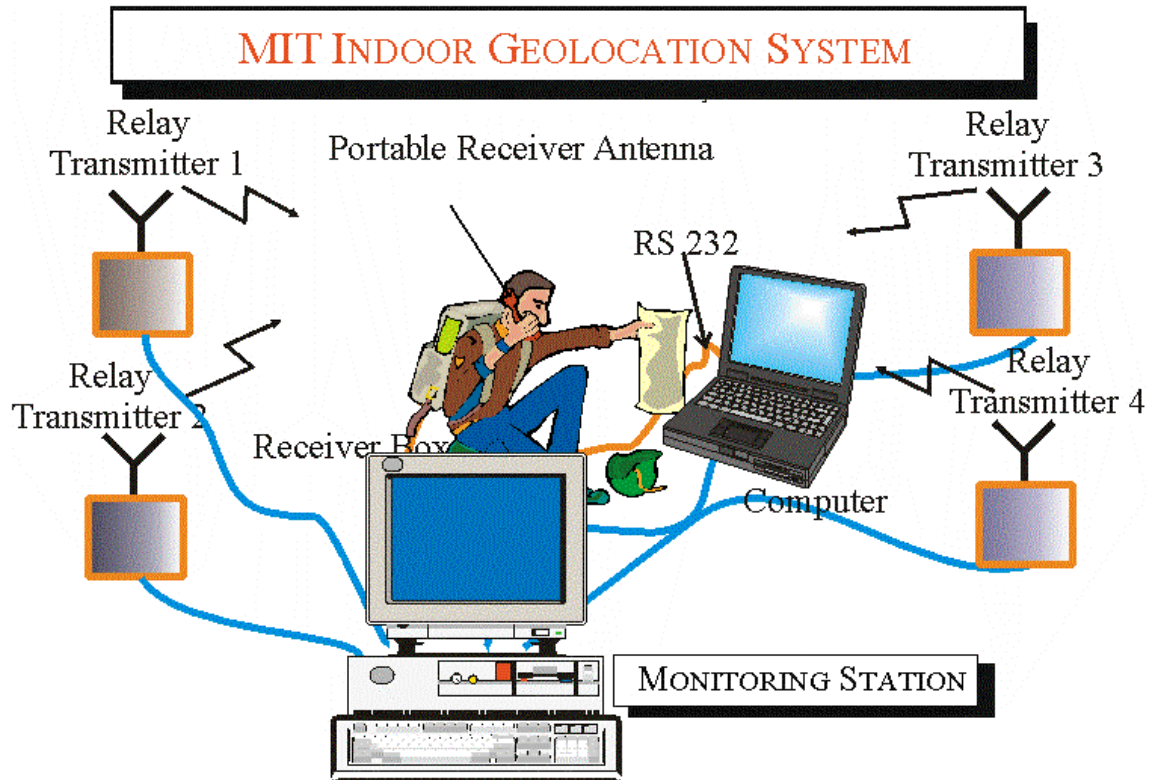


Figure 1.27 MIT relay indoor geolocation system.

It is believed that the monitoring station monitors all transmitters. The portable low frequency receiver computes the navigation solution and passes that solution to a computer (or laptop) for other applications. The system operational frequency is either 1.9 MHz or 13.56 MHz [61].

1.6.3.2 Precise RF Positioning System

Advanced Position Systems, Inc. has patented an idea which is called “A precise RF positioning system,” [59]-[60]. This system employs a wireless link and it operates at ranges greater than 5 m with resolution of 1 mm. The reported accuracy is 2-mm rms. The latency is less than 1 ms and the update rate is greater than 500 Hz. This system can accommodate more than 10 users simultaneously [59] as presented in Figure 1.28.

As shown in the figure there are four relays used for receiving the signal coming from the user (who poses the transmitter device). All relays pass the received signal to the central station, which contains the data processing unit and the computer (or the operator).

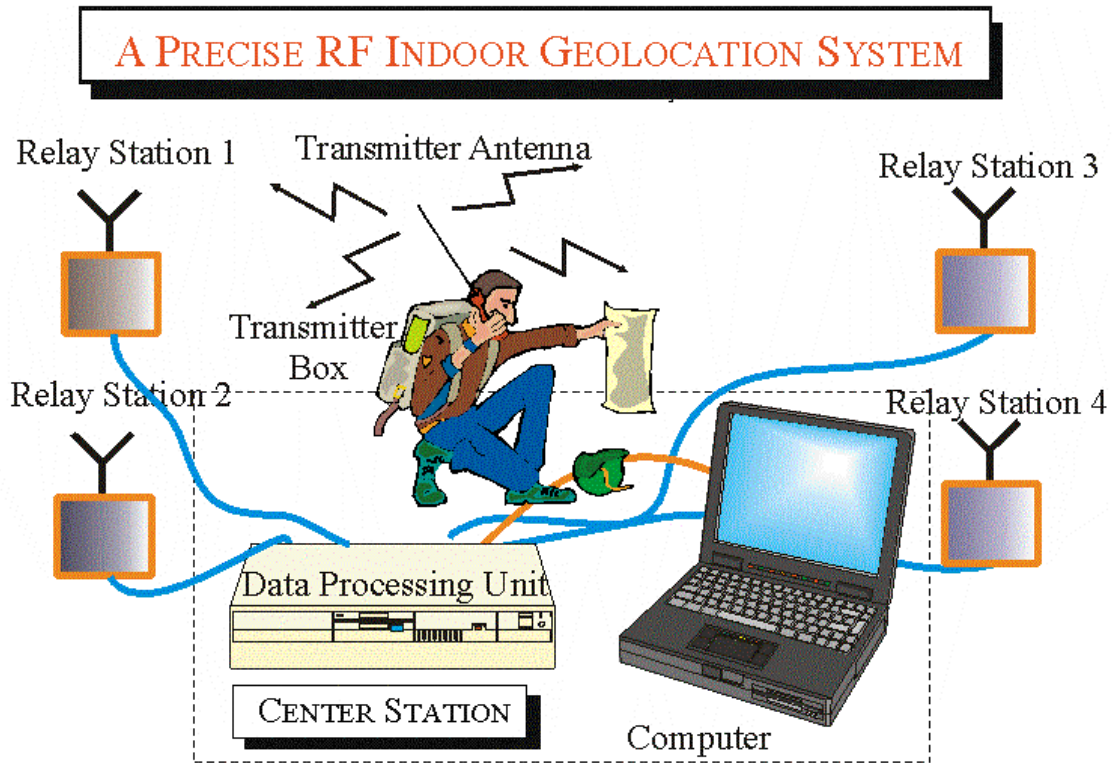


Figure 1.28 A precise RF positioning system- - taken and modified from [59].

Potential applications to this system would be (1) 3D games and entertainment, (2) military/professional training, (3) video recording prototype for airplane, houses, and tourism [59].

1.6.3.3 UWB Indoor Geolocation System

An UWB indoor geolocation system is very distinct from the previous geolocation systems from the frequency allocation and the modulation scheme [62]-[64]. An UWB system is depicted in Figure 1.29. An UWB indoor geolocation system employs at least 4 UWB transmitters. Each transmitter broadcasts a 1–2 ns pulse, which results in a signal bandwidth of several GHz; i.e., at least 1000 times the C/A code signal bandwidth. An UWB indoor geolocation system uses a central transmitter, which employs time division multiple access to control the transmission of every pulse from each transmitter. The receiver receives the pulse from each transmitter and determines the range between each transmitter and itself to an accuracy of ± 6 cm.

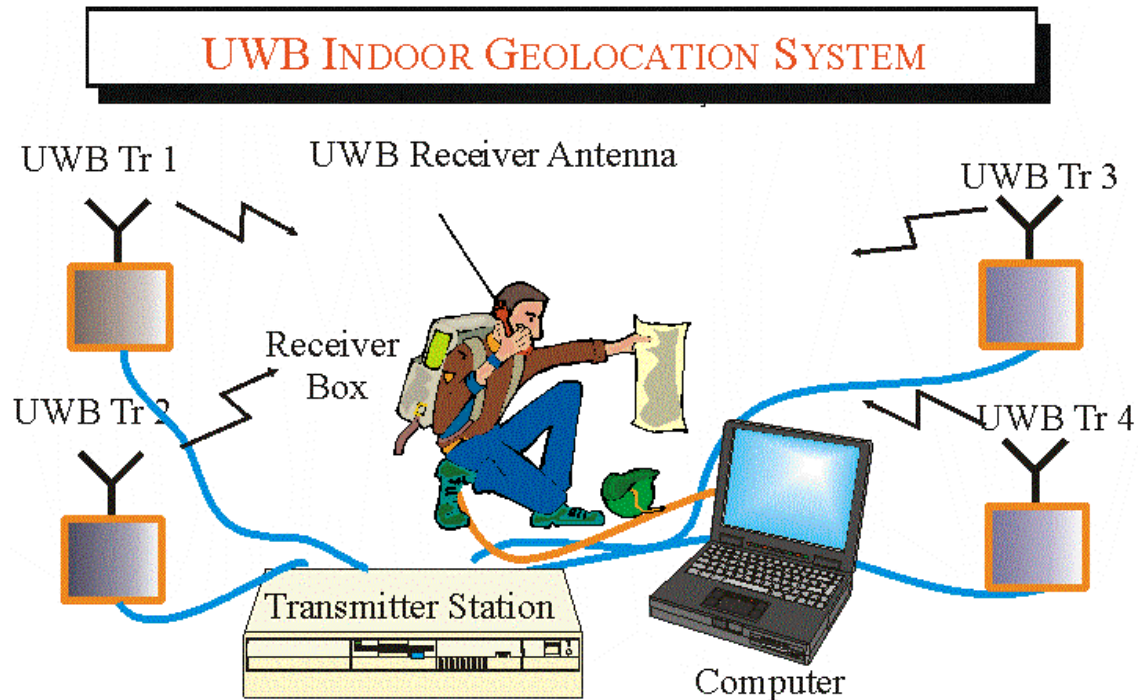


Figure 1.29 An UWB indoor geolocation system.

1.7 Indoor Geolocation System Specifications

So far we have discussed some of the most important ideas and inventions, which led to the idea of an indoor geolocation system, we have commented on the need for such technology in today's markets, and we have provided the technical definition of an indoor geolocation system. Finally, we shall discuss the indoor geolocation system specifications (see Figure 1.30) which include system *requirements*, *applications*, and *novelty*.

1.7.1 Requirements

Requirements consist of the set of technical merits that an indoor geolocation system should achieve to satisfy commercial, governmental, and private customers. Because an indoor geolocation system may be a dual communication and navigation system, we have specified navigation requirements as well as communication requirements. The most accepted technical navigation requirements of a geolocation system are *accuracy*, *integrity*, *availability*, and *continuity*.

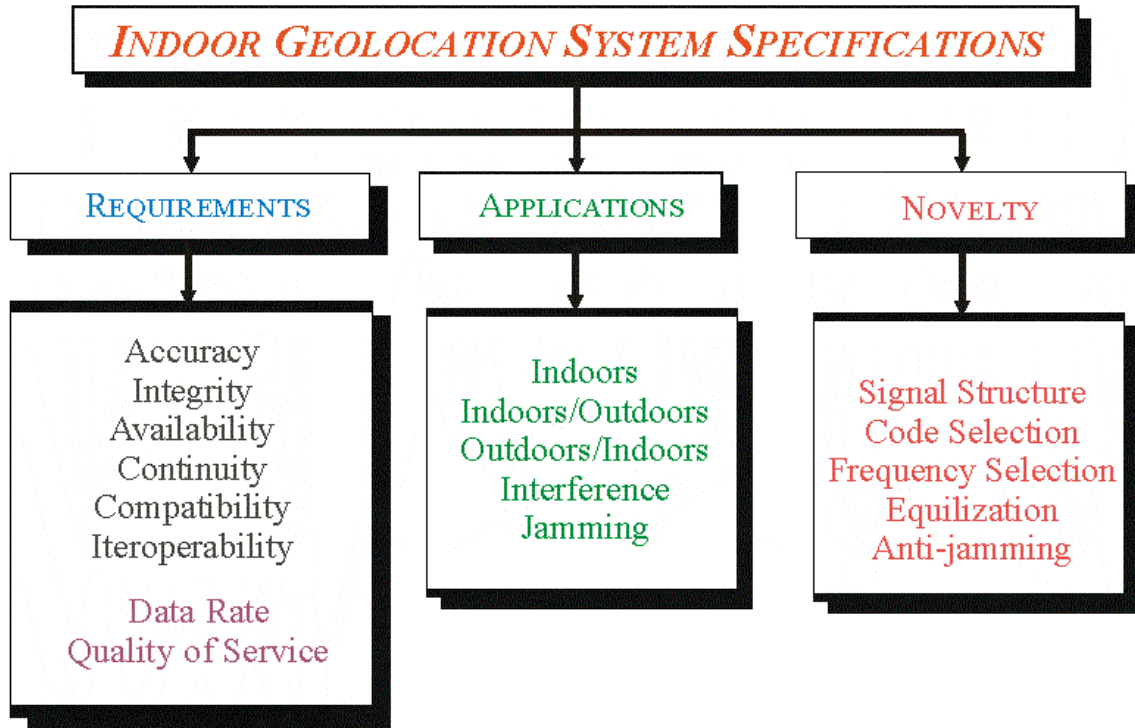


Figure 1.30 Indoor geolocation system specifications.

Other secondary technical requirements are *compatibility* and *interoperability* of indoor geolocation systems among themselves. The communication requirements are given in terms of *data rate* and QoS. These requirements are based on our preliminary investigations [38]-[21].

1.7.1.1 Accuracy

Accuracy is a measure of correctness placed on an estimated navigation solution, which quantifies how close the estimated navigation solution is to the true navigation solution. If no other errors are present in the system then accuracy should be equal to *navigation system error* (NSE).

Accuracy consists of the horizontal and vertical accuracy and local time. For indoor geolocation systems under investigation, distances are in the order of from a few meters to a few tens or hundreds of meters. The navigation accuracy depends upon the application. Based upon our investigation we believe that a system horizontal and vertical accuracy of 10 cm 95% of the time and the local time accuracy less than 10 ns 95% of the time would be adequate for most indoor applications.

1.7.1.2 Integrity

Integrity is a measure of trust that can be placed on the correctness of the signals coming from the transmitters. The receiver should be equipped with an integrity flag to indicate whether the signal is the correct signal or not. *Integrity* can be further enhanced utilizing encryption and scrambling of the signal to protect the signal from spoofing although we do not discuss this issue in detail in this treatment. The basic approach for achieving *integrity* is the proper utilization of the signal structure, frequency and code selection, and proper transmitter and receiver design [38]-[21].

1.7.1.3 Availability

Availability is the fraction of time that the system will be operational during the time of the mission [38]-[21].

1.7.1.4 Compatibility

Compatibility is measure of the system interference on other systems and vice versa. If the system is 100 % compatible it means that it is not influenced by the presence of signals from other existing systems and it does not influence others also. Hence, compatibility is bi-directional: (1) it assesses how our system affects other systems and (2) it assesses how other systems affect ours.

The International Telecommunication Union (ITU) provides the allowed interference levels.

1.7.1.5 Interoperability

Interoperability is a measure of the receiver operating more than one system. For example, if a GPS/GLONASS receiver is said to be GPS and GLONASS interoperable because it can operate as a GPS receiver and as a GLONASS receiver. This requirement may impose design complexity on the receiver. Initially we will require that the device be non-operable with other systems and later require that the device be operable at least with GPS (or other systems).

1.7.1.6 Continuity

Continuity is a measure of interruptions that is places in the system once a mission is being initiated. A measure of continuity is the *outage probability*.

1.7.1.7 Communication

Communication is a measure of information transmission between a transmitter and a receiver and information exchange between a transceiver and a base station (or a central processing computer). This quantity is known as the *data rate*. The quality is known as the QoS.

We are dealing here with two kinds of data rate: *geolocation data rate* and *communication data rate*. *Geolocation data rate* is the amount of information that a transmitter (pseudolite) broadcasts during a second to the receiving part of the transceiver. *Communication data rate* is the amount of information that the transmitter part of a transceiver passes to the base station or the base station passes to the receiving part of a transceiver.

The QoS is given in terms of Bit Error Rate (BER) for the geolocation data information and Frame Error Rate (FER) for the communication information. The emphasis in this work is given only to geolocation information and thus QoS is measured only using BER.

1.7.2 Applications

Applications will include the set of all mission/approaches/etc. and the conditions in which these missions/approaches are carried. Besides applications under normal conditions, we require that an indoor geolocation system should operate indoors, indoors/outdoors, outdoors/indoors, interference and jamming conditions.

1.7.2.1 Indoor, Indoors/Outdoors, and Outdoors/Indoors

Indoor here refers to all the interior space of residential, commercial, and governmental owned buildings. For example, a typical indoor residence would be the area inside a typical home or apartment. For example a typical indoor commercial would be the area inside a university, institution, factory, bank, hospital, nursing home, etc. For

example, a typical governmental owned building would be city hall, all federal buildings, The White House, etc.

Indoors/Outdoors refers to ability of the system to operate when transmitters are placed indoors and the receiver is outdoors.

Outdoor/Indoors refers to ability of the system to operate when transmitters are placed outdoors and the receiver is indoors.

1.7.2.2 Interference

To some extent interference is treated as part of the compatibility of the system with other existing FCC or ITU approved systems which are operational. *Interference* here is seen as multiple access interference effects caused by channel distortion or impairments. The system should be designed to overcome the widely known channel distortion or impairments. Chapter 3 is dedicated for treating such effects and Chapter 4 through 7 discusses the extent to which such effects can be overcome.

1.7.2.3 Jamming/Spoofing

Jamming is a real concern for any geolocation system. It is the intentional/hostile action of deliberately degrading the signal using an external device called jammer. Spoofing on the other hand is also a deliberate action of transmitting the same signal with bogus information. To a large extent an adaptive array can mitigate jamming effects. Scrambling and encryption can overcome spoofing. As part of system integrity these conditions will be considered at a later development stage of the system but not initially.

1.7.3 Novelty

Novelty is the characteristic of the technology that will enable the system to meet its requirements in the field of application. As such we should seek novelty in *signal structure, code selection, frequency selection, equalization, and anti-jamming capability*.

1.7.3.1 Signal Structure

The novelty of *signal structure* and system concept should enable the system to meet its accuracy, integrity, availability, and continuity, requirements and for all applications

(but jamming and spoofing) discussed earlier. A novel signal should lead to a novel *transmitter* or *receiver* design. *Signal structure* is discussed extensively in Chapter 4 and its applications in Chapters 5 through 7.

1.7.3.2 Code Selection

Code selection should enable the system to be compatible with other geolocation systems such as GPS, GLONASS, etc. *Code selection* should also enable the system to meet its accuracy requirements. *Code selection* is discussed extensively in Chapter 4 and its applications in Chapters 5 through 7.

1.7.3.3 Frequency Selection

Frequency selection should enable the system to be compatible with other geolocation systems such as GPS, GLONASS, etc. *Frequency selection* should also enable the system to meet its accuracy requirements. *Frequency selection* is discussed extensively in Chapter 4 and its applications in Chapters 5 through 7.

1.7.3.4 Equalization

Equalization should enable the receiver to achieve its accuracy and QoS requirements. As such *equalization* should have a priority on the receiver design. Chapters 4 through 7 discuss in great detail ways of designing low quality receiver equalizers and assess the system performance for each one of them.

1.7.3.5 Anti-jamming/Anti-spoofing

Anti-jamming/anti-spoofing should enable the system to operate under jamming and spoofing conditions. This aspect of the system novelty is left for future work.

1.8 WPI Indoor Geolocation System

So far, we have elaborated why non-of these indoor geolocation systems are the solution to indoor positioning. Therefore, we propose the WPI indoor geolocation system as a solution to indoor positioning and this is going to be the focus of this work in Chapters 4 through 7.

The WPI indoor geolocation system utilizes four or more ground-based pseudolites (or transmitters) and one or more receivers as shown in Figure 1.3. Pseudolites can be placed either indoors or outdoors and the receiver can operate either indoors or outdoors. There are several issues that are pertinent to this system, which are addressed in the indoor geolocation system specifications. The detailed treatment of all issues related to an indoor geolocation system goes far beyond the scope of this work. This work is going to focus on the following important issues:

1. Chapter 2, Transmitter/Receiver signal structure and design for state of the art systems relevant to WPI indoor geolocation system. The extraction of observable quantities is discussed and illustrated for these systems.
2. Chapter 3: Indoor/outdoor channel model.
3. Chapter 4: Extraction of observable quantities for three WPI indoor geolocation systems (i) DSSS/CDMA/FDMA, (ii) DSSS/CDMA/OFDM/FDMA, and (iii) OFDM/FDMA.

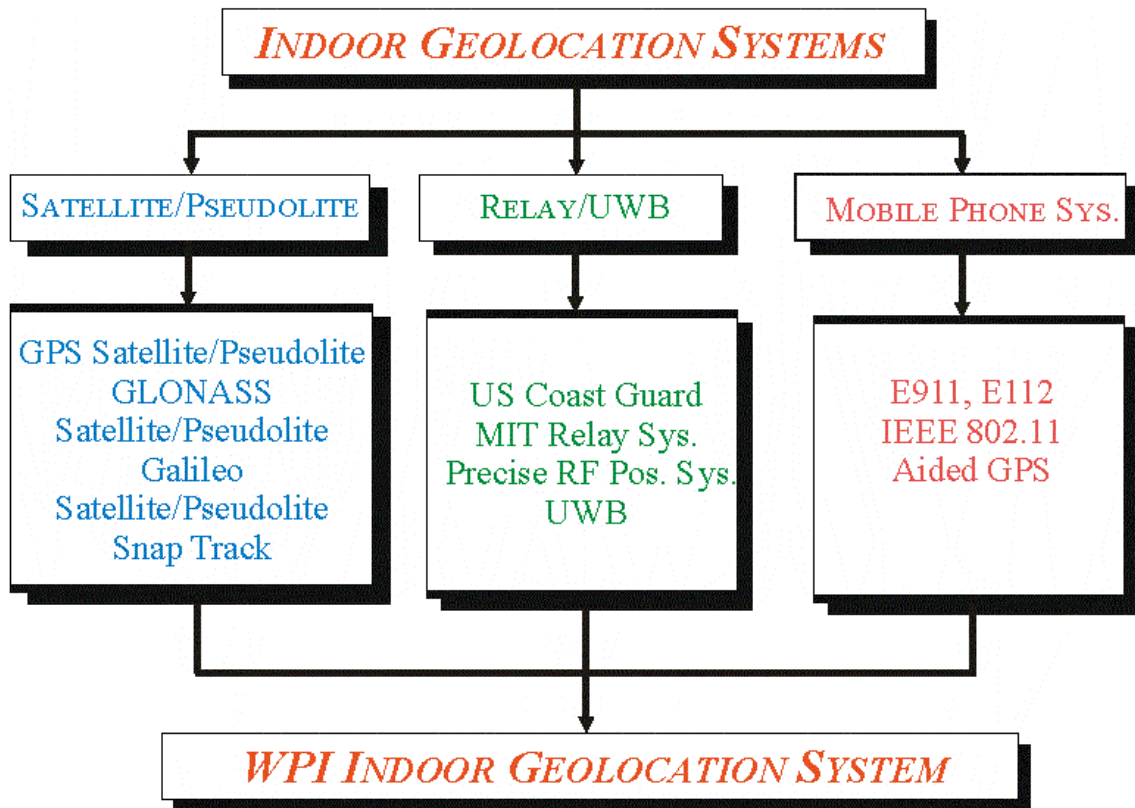


Figure 1.31 The rationale for WPI indoor geolocation system.

4. Chapter 5: Qualitative and quantitative objectives on the performance requirements of a DSSS/CDMA/FDMA indoor geolocation system.
5. Chapter 6: Qualitative and quantitative objectives on the performance requirements of a DSSS/CDMA/OFDM/FDMA indoor geolocation system.
6. Chapter 7: Qualitative and quantitative objectives on the performance requirements of an OFDM/FDMA indoor geolocation system.
7. Chapter 8: Conclusions and future work.

Other issues such as relative synchronization and implementation are not discussed in this work.

CITED REFERENCES AND FURTHER READING:

- [1] N. Davies, *Europe a History*, New York, NY: Oxford University Press, 1996.
- [2] H. Butterfield, *The Origins of Modern Science, 1300-1800*, London, 1947.
- [3] F. Nebeker, "September and October in EE history," *IEEE The Institute*, vol. 25, pp. 9, Oct. 2001.
- [4] B. Parkinson, K. Gromov, T. Stansell, and R. Beard, "A history of satellite navigation," in *Proc. ION-AM*, pp. 17-65, Colorado Springs, Co, June 1995.
- [5] B.W. Parkinson, J.J. Spilker, P. Axelrad, and P. Enge, *Global Positioning System: Theory and Applications*, vol. 1 and 2, Washington, DC: AIAA, 1996.
- [6] B. Parkinson and S.W. Gilbert, "NAVSTAR: Global Positioning System—ten years later," in *IEEE*, vol. 71, pp. 1177-1186, Oct. 1983.
- [7] B.W. Parkinson, J.J. Spilker, Jr, et al., *The Global Positioning System-Theory and Applications*, Washington, DC: American Institute of Aeronautics and Astronautics, (vol. 1, chap. 2, "Overview of GPS operation and design") 1996.
- [8] P. Misra and P. Enge, *Global Positioning System-Signals Measurements and Performance*, Lincoln, MA: Ganga-Jamuna Press, 2001.
- [9] Anon., Department of Defense, *Global Positioning System (GPS) Standard Positioning Service (SPS)*, Signal Specification, Dec. 8, 1993.
- [10] R.M. Lollock, "Global Positioning System (GPS) Modernization," civil GPS service interface committee, Washington, DC, 27-29 Mar. 2001. (unclassified presentation)

- [11] J.M. Hill, "Development of an experimental Global Positioning System (GPS) receiver platform for navigation algorithm evaluation," Ph.D. Dissertation, Worcester Polytechnic Institute, Aug. 2001.
- [12] R.C. Brown and P.Y.C. Hwang, *Introduction to Random Signals and Applied Kalman Filtering*, 3rd ed., New York: John Wiley & Sons, 1981.
- [13] *Webster's New World Dictionary of the American Language*. College Edition, Cleveland, OH: World Publishing Co., 1957.
- [14] J.J. Spilker, *Digital Communications by Satellite*. Englewood Cliffs, NJ: Prentice-Hall, 1977.
- [15] V.K. Bhargava, D. Hancoun, R. Matyas, and P.P. Nuspl, *Digital Communications by Satellite*. New York, NY: John Wiley & Sons, 1981.
- [16] B.W. Parkinson, J.J. Spilker, Jr, et al., *The Global Positioning System-Theory and Applications*, Washington, DC: American Institute of Aeronautics and Astronautics, (vol. 2, chap. 9, "GPS and Global Navigation Satellite System (GLONASS)") 1996.
- [17] C. Lopez-Bravo and M.-D. Cano, "Galileo: The European satellite radio navigation system," *Global Comm. News.*, vol. 40, no. 7, pp. 2-4, Jul. 2002.
- [18] K. Kovac, "GNSS signal compatibility and interoperability: GPS person's view," *ION-GPS 2002* (panel presentation), Portland, OR, Sep. 24, 2002.
- [19] C. Hegarty, "GPS-Galileo signal compatibility," *ION-GPS 2002* (panel presentation), Portland, OR, Sep. 24, 2002.
- [20] Anon, "JCAB MTSAT functions and current status," the 4th meeting of the allpigr advisory Y group, Montreal, 6 - 8 February 2001.
- [21] I.F. Proгри and W.R. Michalson, "Performance evaluation of category III precision landing using airport pseudolites," in *Proc. IEEE PLANS*, San Diego, CA, pp. 262-269, Mar. 2000.
- [22] I.F. Proгри and W.R. Michalson, "A combined GPS satellite/pseudolite system for category III precision landing," in *Proc. IEEE PLANS*, pp. 212-218, April 15-17, 2002.
- [23] B.W. Parkinson and K.T. Fitzgibbon, "Optimal locations of pseudolites for differential GPS," *J. Inst. Nav.*, vol. 33, no. 4, pp. 259-283, winter 1986-87.
- [24] D. Klein and B.W. Parkinson, "The use of pseudo-satellites for improving GPS performance," in *Global Positioning System*, vol. II., pp. 135-146, Silver Spring, MD: Institute of Navigation, 1986.
- [25] T. Stansell, Jr., "RTCM SC-104 recommended pseudolite signal specification," in *Global Positioning System*, vol. III. Silver Spring, MD: Institute of Navigation, 1986.

- [26] L. Schuchman, B.D. Elrod, and A.J. Van Dierendonck, "Applicability of an augmented GPS for navigation in the national airspace system," in *Proc. IEEE*, vol. 77, pp. 1709-1727, Nov, 1989.
- [27] A.J. Van Dierendonck, B.D. Elrod, and W.C. Melton, "Improving the integrity, availability and accuracy of GPS using pseudolites," in *Proc. NAV*, Royal Institute of Navigation, London, UK, Oct. 1989.
- [28] B.A. Stain and W.L. Tsang, "Pseudolite-aided GPS: a comparison," in *Proc. IEEE PLANS*, pp. 329-333, 1988.
- [29] B.A. Stain and W.L. Tsang, "COTS GPS C/A-code receivers with pseudolites for range PSL applications," in *Proc. IEEE PLANS*, pp. 101-107, 1990.
- [30] A.J. Van Dierendonck, "The role of pseudolites in the implementation of differential GPS," in *Proc. IEEE PLANS*, pp. 370-377, 1990.
- [31] R.C. Galijan and G.V. Lucha, "A suggested approach for augmenting GNSS category III approaches and landings: the GPS/GLONASS and GLONASS pseudolite system," in *Proc. ION-GPS*, pp. 157-853, 1993.
- [32] A. Brown, F. Van Diggelen, and C. LaBerge, "Test results of a GPS/pseudolite precision approach and landing system," in *Proc. ION-GPS*, pp. 157-853, 1993.
- [33] C.A. Cohen et al., "Real-time cycle ambiguity resolution using a pseudolite for precision landing of aircraft using GPS," in *Proc. DSNS*, Amsterdam, The Netherlands, Mar.-Apr. 1993.
- [34] G.A. McGraw, "Analysis of pseudolite code interference effects for aircraft precision approaches," in *Proc. ION AM*, Colorado Springs, CO, June 1994.
- [35] B.W. Parkinson, J.J. Spilker, Jr, et al., *The Global Positioning System-Theory and Applications*, Washington, DC: American Institute of Aeronautics and Astronautics, (vol. 2, chap. 2, "Pseudolites") 1996.
- [36] C. Bartone and F., Van Graas, "Ranging airport pseudolite for local area augmentation," *IEEE Trans. Aer. Elect. Sys.*, vol. 36, pp. 278 -286, Jan. 2000.
- [37] C.G. Bartone and S. Kiran, "Flight test results of an integrated wideband airport pseudolite for the local area augmentation system," *J. Inst. Nav.*, vol. 48, no. 1, pp. 35-48, Spring 2001.
- [38] I.F. Proгри, W.R. Michalson, and M.C. Bromberg, "A DSSS/CDMA/FDMA indoor geolocation system," in *Proc. ION-GPS*, Portland, OR, Sep. 2002.

- [39] I.F. Progri and W.R. Michalson, "An alternative approach to multipath and near-far problem for indoor geolocation systems" in *Proc. ION-GPS*, Salt Lake City, UT, pp. 1434-1443, Sep. 2001.
- [40] I.F. Progri and W.R. Michalson, "The impact of proposed pseudolite's signal structure on the receiver's phase and code error," in *Proc. ION-AM*, Albuquerque, NM, pp. 414-422, June 2001.
- [41] I.F. Progri, J.M. Hill, and W.R. Michalson, "An investigation of the pseudolite's signal structure for indoor applications," in *Proc. ION-AM*, Albuquerque, NM, pp. 453-462, June 2001.
- [42] I.F. Progri, W.R. Michalson, and J. Hill, "Assessing the accuracy of navigation algorithms using a combined system of GPS satellites and pseudolites," in *Proc. ION-NTM*, Long Beach, CA, pp. 473-481, Jan. 2001.
- [43] I.F. Progri, J. Hill, and W.R. Michalson, "A Doppler based navigation algorithm," in *Proc. ION-NTM*, Long Beach, CA, pp. 482-490, Jan. 2001.
- [44] I.F. Progri and W.R. Michalson, "An innovative navigation algorithm using a system of fixed pseudolites," in *Proc. ION-NTM*, Long Beach, CA, pp. 619-627, Jan. 2001.
- [45] I.F. Progri, W.R. Michalson et al, "A system for tracking and locating emergency personnel inside buildings," in *Proc. ION-GPS*, Salt Lake City, UT, pp. 560-568, Sep. 2000.
- [46] C.-S. Li, "Emerging pervasive technologies for e-commerce," in *Proc. IEEE ISCAS*, pp. 7.3.1-7.3.14, 2001.
- [47] Y. Zhao, "Standardization of mobile phone positioning for 3G systems," *IEEE Comm. Mag.*, vol. 40, no. 7, pp. 108-116, Jul. 2002.
- [48] Federal Communications Commission, Memorandum Opinion and Order FCC 97-402, Revision of the Commission's Rules To Ensure Compatibility with Enhanced 911 Emergency Calling Systems, Washington, DC, adopted December 1, 1997, revised Sep. 1999.
- [49] R. Klukas, G. Lachapelle, and M. Fattouche, "Estimation noise of a cellular telephone positioning system," *J. Inst. Nav.*, vol. 47, no. 3, pp. 167-174, fall 2000.
- [50] R. Klukas, "Cellular telephone positioning using GPS time synchronization," in *Proc. ION-GPS*, Kansas City, MO, pp. 1405-1414, Sep. 1997.
- [51] H.L. Bertoni, W. Honcharenko, L.R. Macel, and H.H. Xia, "UHF propagation prediction for wireless personal communications," in *Proc. IEEE*, vol. 82, no. 9, pp. 1333-1359, Sep. 1994.

- [52] M. Moeglein and N. Krasner, "An introduction to SnapTrack™ server-aided GPS technology," in *Proc. ION-GPS*, pp. 333-342, Sep. 1998.
- [53] L. Shaynblat and N. Krasner, "Description of a wireless integrated SmartServer™/client system architecture," in *Proc. ION-AM*, pp. 667-675, Cambridge, MA, June 1999.
- [54] Anon., "Location technologies for GSM, GPRS, and WCDMA networks," SnapTrack™ a QUALCOM company, white paper.
- [55] B.B. Peterson, C.G. Kmiecik, H. Nguyen, and B. Kaspar, "Indoor geolocation system operational test results," *J. Inst. Nav.*, vol. 47, no. 3, pp. 157-166, Fall 2000.
- [56] M.J. Riezenman, "The ABCs of the IEEE 802.11," *IEEE Spectrum Mag.*, p. 20, Sep. 2002.
- [57] J. Blau, "Wi-Fi hotspot networks sprout like mushrooms," *IEEE Spectrum Mag.*, pp18–20, Sep. 2002.
- [58] N. Davies, K. Cheverst, K. Mitchell, and A. Efrat, "Using and determining location in a context-sensitive tour guide," *Comp.*, vol. 34, pp 35-41, Aug. 2001.
- [59] J. Fen, "A precise RF positioning system," *Pres. at ION-NES*, Jan. 17, 2001.
- [60] J. Fen, "Security system," *United States Patent*, no. 5,374,936, Dec. 20, 1994.
- [61] M.S. Reynolds, "A phase measurement radio positioning system for indoor use," MS Thesis, Dep. Elec. and Comput. Eng., MIT, Cambridge, MA, Feb. 1999.
- [62] G.R. Opshaug and P. Enge, "GPS and UWB for indoor navigation," in *Proc. ION-GPS*, Salt Lake City, UT, pp. 1427–1433, Sep. 11-14, 2001.
- [63] P. Enge, "A global challenge—Protect GNSS noise floor a.k.a. spectrum stewardship," ION-GPS 2002 (panel presentation), Portland, OR, Sep. 24, 2002.
- [64] Anon. "UWB threatens from the sideline," *ION-GPS 2002*, Show Daily, p. 2, Wed., Sep. 25, 2002.
- [65] R. Fontana, "Advances in ultra wideband indoor geolocation systems," *3rd IEEE Wksp. WLAN*, Boston, MA, Sept. 2001.
- [66] M. Win and R. Scholtz, "On the performance of ultra-wide bandwidth signals in dense multipath environment," *IEEE Commun. Letters*, vol. 2, no. 2, Feb. 1998, pp. 51–53.
- [67] I. Koffman and V. Roman, "Broadband wireless access solutions based on OFDM access in IEEE 802.16," *IEEE Comm. Mag.*, vol. 40, no. 4, pp. 96-103, Apr. 2002.
- [68] K. Pahlavan, X. Li, J.-P. Makela, "Indoor geolocation science and technology," *IEEE Comm. Mag.*, vol. 40, no. 2, pp. 112-118, Feb. 2002.

- [69] P. Bahl and V. Padmanabhan, "RADAR: an in-building RF-based user location and tracking system," *IEEE INFOCOM*, Israel, Mar. 2000.
- [70] C. Matchumoto, "PinPoint debuts local positioning system," *EE Times*, Sept. 14, 1998.
- [71] G. Rand, "Sonar and the fourth dimension," *J. Inst. Nav.*, vol. 6, no. 4, pp. 203-216, spring 1959.
- [72] E. Durbin, "Current development in the Loran C system," *J. Inst. Nav.*, vol. 9, no. 2, pp. 138-150, summer 1962.
- [73] R.J. Alexander, "Navigation requirements for oceanography," *J. Inst. Nav.*, vol. 10, no. 2, pp. 161-166, summer 1963.
- [74] D.M. Holmes, "Surface controlled-deep ocean navigation techniques for precise bottom site determination and relocation," *J. Inst. Nav.*, vol. 12, no. 4, pp. 287-298, winter 1965-66.
- [75] S. Wisotsky AND J.A. Dolan, "Subloran-a sonic underwater long range aid to navigation employing cross-correlation of FM-CW signals," *J. Inst. Nav.*, vol. 13, no. 2, pp. 148-153, Summer 1966.
- [76] E.E. Turner, B.J. Thompson, and O.H. Jackson, "The Raytheon acoustic Doppler navigator," *J. Inst. Nav.*, vol. 13, no. 3, pp. 210-221, autumn 1966.
- [77] A.G. Mourad and N.A. Frazier, "Improving navigational systems through establishment of a marine geodetic range," *J. Inst. Nav.*, vol. 14, no. 2, pp. 187-194, summer 1967.
- [78] M.J. Tonkel, "Navigation in ocean surveys," *J. Inst. Nav.*, vol. 14, no. 4, pp. 368-375, winter 1967-68.
- [79] J.A. Cestone, "Deep submergence navigation," *J. Inst. Nav.*, vol. 15, no. 1, pp. 3-15, spring 1968.
- [80] L.W. Griswold, "Underwater logs," *J. Inst. Nav.*, vol. 15, no. 2, pp. 127-135, summer 1968.
- [81] K.V. Mackenzie, "Early history of deep submergence navigation a board Trieste," *J. Inst. Nav.*, vol. 17, no. 2, pp. 3-12, spring 1970.
- [82] D.E. Boegeman, "The offset method of sonar ranging," *J. Inst. Nav.*, vol. 17, no. 1, pp. 47-51, spring 1970.
- [83] B. Saltzer, "A deep submergence divers' navigation system," *J. Inst. Nav.*, vol. 17, no. 1, pp. 76-82, spring 1970.
- [84] D.E. Campbell, "Precise acoustic navigation and position keeping," *J. Inst. Nav.*, vol. 17, no. 2, pp. 124-135, summer 1970.

- [85] T.A. Goulet, "The use of pulsed Doppler sonar for navigation of manned deep submergence vehicles," *J. Inst. Nav.*, vol. 17, no. 2, pp. 136-141, summer 1970.
- [86] G.D. Dunlap, "Major developments in marine navigation during the last 25 years," *J. Inst. Nav.*, vol. 18, no. 1, pp. 63-76, spring 1971.
- [87] M.H. Damon, "SANS, ships acoustic navigation system," *J. Inst. Nav.*, vol. 19, no. 1, pp. 11-18, spring 1972.
- [88] J.A. Cestone and E.st. George, jr., "Hydrospheric navigation," *J. Inst. Nav.*, vol. 19, no. 3, pp. 199-208, fall 1972.
- [89] D.L. Mckeown, "Survey techniques for acoustic positioning arrays," *J. Inst. Nav.*, vol. 22, no. 1, pp. 59-67, spring 1975.
- [90] H.E. Lee, "Application of optimal estimation techniques to acoustic transponder navigation systems," *J. Inst. Nav.*, vol. 22, no. 3, pp. 201-207, fall 1975.
- [91] J.A. Cestone, R.J. Cyr, G. Roesler, and E.st. George, jr., "Latest highlights in acoustic underwater navigation," *J. Inst. Nav.*, vol. 24, no. 1, pp. 7-39, spring 1977.
- [92] M. Higgins and D.M. Harrell, "Integrated navigation for deep ocean positioning," *J. Inst. Nav.*, vol. 35, no. 1, pp. 1-13, spring 1988.
- [93] J.W. Youngberg, "A novel method for extending GPS to underwater applications," *J. Inst. Nav.*, vol. 38, no. 3, pp. 263-271, fall 1991.
- [94] J.S. Stambaugh and R.B. Thibault, "Navigation requirements for autonomous underwater vehicles," *J. Inst. Nav.*, vol. 39, no. 1, pp. 79-92, spring 1992.
- [95] D.I. Kim, "On the performance of common spreading code CDMA packet radio systems with multiple capture capability," Ph.D. dissertation, Dept. Elect. Eng., Univ. Southern California, Los Angeles, CA, 1990.
- [96] D.C. Lee, "Power-efficient coded modulation for wireless infrared communication," Ph.D. Dissertation, Univ. California, Berkeley, 1998.
- [97] M. Schwartz, W.R. Bennet, and S. Stein, *Communication Systems and Techniques*. New York: McGraw-Hill, 1966.
- [98] R.W. Lucky, J. Salz, and E.J. Weldon, Jr., *Principles of Data Communication*. New York: McGraw Hill, 1968.
- [99] R.G. Gallager, *Information Theory and Reliable Communications*, New York: Wiley, 1968.
- [100] K.W. Cattermole, *Principles of Pulse Code Modulation*, London: Illife Books, 1969.

- [101] W.C. Lindsey and M.K. Simon, *Telecommunication Systems Engineering*. Englewood Cliffs, NJ: Prentice-Hall, 1973.
- [102] W. Jakes, Jr., *Microwave Mobile Communications*. New York: Wiley-Interscience, 1974.
- [103] R. Gagliardi, *Introduction to Communication Engineering*. New York: Wiley, 1978.
- [104] M.B. Pursley, "Spread spectrum multiple access communications," in *Multi-User Communications*, G. Longo, Ed. Vienna and New York: Springer-Verlag, 1981.
- [105] F.G. Stremler, *Introduction to Communication Systems*. Reading, MA: Addison-Wesley, 1982.
- [106] J.G. Proakis, *Digital Communications*. 1st, 2nd, and 3rd, ed., New York: McGraw-Hill, 1983, 1989, and 1995.
- [107] W.C.Y. Lee, *Mobile Communications Design Fundamentals*. New York: Howard W. Sams, 1986.
- [108] G.R. Cooper and C.D. McGillem, *Modern Communications and Spread Spectrum*. New York: McGraw-Hill, 1986.
- [109] S. Benedetto, E. Biglieri, and V. Castellani, *Digital Transmission Theory*. Englewood Cliffs, NJ: Prentice-Hall, 1987.
- [110] S. Haykin, *An Introduction to Analog and Digital Communications*. New York: Wiley, 1989.
- [111] G.E. Keiser, *Local Area Networks*. New York: McGraw-Hill, 1989.
- [112] W.C.Y. Lee, *Mobile Cellular Telecommunications Systems*. New York: McGraw-Hill, 1989.
- [113] R.D. Gitlin, J.F. Hayes, and S.B. Weinstein, *Data Communications Principles*. New York: Plenum, 1992.
- [114] R. Steele, *Mobile Radio Communications*. London, U.K.: Pentech Press, 1992.
- [115] J.-P. Linnartz, *Narrowband Land-Mobile Radio Networks*. Boston, MA: Artech House, 1993.
- [116] E.A. Lee and D.G. Messerschmitt, *Digital Communications*, Second Edition, Boston: Kluwer Academic Publishers, 1994.
- [117] J.R. Barry, *Wireless Infrared Communications*, Boston: Kluwer Academic Publishers, 1994.
- [118] M.K. Simon, J.K. Omura, R.A. Scholtz, and B.K. Levitt, *Spread Spectrum Communications*, vol. 3. Rockville, MD: Comput. Sci., 1984 and 1994.
- [119] K. Pahlavan and A. H. Levesque, *Wireless Information Networks*. New York: Wiley, 1995.

- [120] P.T. Davis and C.R. McGuffin, *Wireless Local Area Networks: Technology, Issues, and Strategies*. New York: McGraw-Hill, 1995.
- [121] A.J. Viterbi, *CDMA, Principles of Spread Spectrum Communication*. Reading, MA: Addison Wesley, 1995.
- [122] G. L. Stüber, *Principles of Mobile Communication*. Dordrecht, NL: Kluwer Academic, 1996.
- [123] T.S. Rappaport, *Wireless Communications: Principles and Practice*. NJ: Prentice-Hall, 1996.
- [124] W.H. W. Tuttlebee, Ed., *Cordless Telecommunications Worldwide*. New York: Springer-Verlag, 1997.
- [125] M.D. Kotzin, "Short-range communications using diffusely scattered infrared radiation," Ph.D. dissertation, Northwestern Univ., June 1981.
- [126] T.S. Rappaport, "Characterization the UHF factory multipath channels," Ph.D. dissertation, School of Elec. Eng., Purdue Univ., West Lafayette, IN, Dec. 1987.
- [127] R.J. Davies, "In-building UHF propagation studies," M.Sc. thesis, Univ. Calgary, 1989, unpublished.
- [128] P.A. Sharples, "The modeling of terrain diffraction phenomena at microwave frequencies," Ph.D. dissertation, Univ. Birmingham, Birmingham, U.K., 1989.
- [129] P. Boisvert, "The ambient electromagnetic environment in metropolitan hospitals," MS thesis, Dept. Elect. Eng., McGill Univ., Montreal, Canada, 1991.
- [130] P. Vlach, "Measurement, prediction, and analysis of the radio frequency electromagnetic environment outside and inside hospitals," Master's thesis, Dept. Elect. Eng., McGill Univ., Montreal, Canada, 1994.
- [131] T. Miller, "Radio frequency interference suppression for foliage penetration radar imaging," MS thesis, Ohio State University, Columbus, OH, Dec. 1994.
- [132] C.A. Zelle, "Radiowave propagation over irregular terrain using the parabolic equation method," Ph.D. dissertation, Univ. Birmingham, Birmingham, U.K., 1996.
- [133] D.E. Kerr, Ed., *Propagation of Short Radio Waves*. New York: McGraw-Hill, vol. 13, 1951 (Radiation Lab. Series).
- [134] R.E. Collin, *Field Theory of Guided Waves*. New York: McGraw-Hill, 1960.
- [135] *Antenna Engineering Handbook*, H. Jasik, Ed., MacGraw-Hill, New York, 1961.
- [136] C.E. Cook, *Radar Signals: An Introduction to Theory and Application*. New York: Academic Press, 1967.

- [137] L.B. Felsen and N. Marcuvitz, *Radiation and Scattering of Waves*. Englewood Cliffs, NJ: Prentice-Hall, 1973.
- [138] E.N. Skomal, *Man-Made Radio Noise*. New York: Van Nostrand Reinhold, 1978.
- [139] M.J. Wenninger, *Spherical Models*. New York: Cambridge Univ. Press, 1979.
- [140] J. Bahl and P. Bhartia, *Microstrip Antennas*. Norwood, MA: Artech House, 1980
- [141] W.L. Stutzman and G.A. Thiele, *Antenna Theory and Design*. New York: Wiley, 1981.
- [142] R.E. Collin, *Antennas and Radiowave Propagation* New York: McGraw-Hill, 1985.
- [143] E.N. Skomal and A.A. Smith, *Measuring the Radio Frequency Environment*. New York: Van Nostrand Reinhold, 1985.
- [144] J.A. Kong, *Electromagnetic Waves Theory*. New York: Wiley, 1986.
- [145] D.R. Wehner, *High Resolution Radar*. Norwood, MA: Artech House, Inc, 1987.
- [146] J.D. Kraus, *Antennas*, 1st ed. New York: McGraw-Hill, 1950, 2nd ed., 1988.
- [147] Y.T. Lo and S.W. Lee Ed., *Antenna Handbook*. New York: Van-Nostrand Reinhold, 1988.
- [148] J.P. Fitch, *Synthetic Aperture Radar*. New York: Springer-Verlag, 1988.
- [149] W. Goj, *Synthetic Aperture Radar and Electronic Warfare*. Dedham, MA: Artech House, 1989.
- [150] C.A. Balanis, *Advanced Engineering Electromagnetics*. New York: Wiley, 1989.
- [151] J. Curlander and R. McDonough, *Synthetic Aperture Radar*. New York: Wiley, 1991.
- [152] N.C. Currie, R.D. Hayes, and R.N. Trebits, *Millimeter-Wave Radar Clutter*. Boston, MA: Artech House, 1992.
- [153] T.S.M. Maclean and Z. Wu, *Radiowave Propagation over Ground*. London, U.K.: Chapman Hall, 1993.
- [154] R.J. Mailloux, *Phased Array Antenna Handbook*. Boston: Artech House, 1994.
- [155] W. Carrara, R. Goodman, and R. Majewski, *Spotlight Synthetic Aperture Radar*. Boston, MA: Artech House, 1995.
- [156] K. Siwiak, *Radio Wave Propagation and Antennas for Personal Communications*. New York: Artech House, 1995.
- [157] J.D. Taylor, *Introduction to Ultrawide-Band (UWB) Radar Systems*. Boca Raton, FL: CRC Press, 1995.

- [158] M. Soumekh, *Synthetic Aperture Radar Signal Processing with MATLAB Algorithms*. New York: Wiley, 1999.
- [159] J.A. Roberts, "Packet Radio Performance over Fading Channels," Ph.D. dissertation, Dep. Elec. Eng. Comput. Sci., Santa Carla Univ., Santa Carla, CA, May 1979.
- [160] T.A. Sexton and K. Pahlavan, "Channel modeling and adaptive equalization of indoor radio channels," *IEEE J. Select. Areas Commun.*, vol. SAC-5, pp. 128-137, Feb. 1987.
- [161] T.A. Sexton, "Channel modeling and high speed data transmission performance for indoor radio channel," Ph.D. dissertation, Worcester Polytech. Inst., Aug. 1989.
- [162] S.Y. Seidel, "UHF indoor radio channel models for manufacturing environments," Master thesis in Elec. Eng., Virginia Polytech. Inst. State Univ., Blacksburg, VA, Aug. 1989.
- [163] S.J. Howard, "Frequency domain characteristics and autoregressive modeling of the indoor radio channel," Ph.D. dissertation, Worcester Polytech. Inst., 1991.
- [164] S.J. Howard and K. Pahlavan, "Autoregressive modeling of wide-band indoor radio propagation," *IEEE Trans. Comm.*, vol. 40, no. 9, pp. 1540-1552, Sep. 1992.
- [165] M.S. Braach, "On the characterization of multipath error in satellite-based precision approach and landing systems," Ph.D. dissertation, Ohio University, Athens, OH, June 1992.
- [166] R. Van Nee, "Multipath and multi-transmitter interference in spread-spectrum communication and navigation systems," Ph.D. dissertation, Delft University of Technology, Delft, The Netherlands, 1995.
- [167] J. Sun, "Analyses of digital transmissions over wireless fading channels," Ph.D. dissertation, Commun. Sci. Inst., Univ. Southern California, Feb. 1996.
- [168] R.S. Kennedy, *Fading Dispersive Communication Channel*. New York: Wiley-Interscience, 1969.
- [169] W. Elenbass, *Fluorescent Lamps*. London: Macmillan, 2nd ed., 1971.
- [170] K. Brayer, Ed., *Data Communications via Fading Channels*. New York: IEEE Press, 1975.
- [171] J.B. Murdoch, *Illumination Engineering*, New York: Macmillan, 1985.
- [172] J.D. Parson, *The Mobile Radio Propagation Channel*, New York: Halsted Press, 1992.
- [173] B.G. Agee, "The property-restoral approach to blind adaptive signal extraction," Ph.D. dissertation, University of California, Davis, 1989.

- [174] N.W.K. Lo, "Adaptive Equalization for a Multipath Fading Channel in the Presence of Interference," Ph.D. dissertation, Dept. of Systems and Computer Eng., Carleton University, May 1994.
- [175] G.W. Marsh, "High-speed wireless infrared communication links," Ph.D. dissertation, Univ. California, Berkeley, Dec. 1995.
- [176] H. Park, "Coded modulation and equalization for wireless infrared communications," Ph.D. dissertation, Georgia Inst. Technol., 1997.
- [177] R. Rau, "Postprocessing tools for ultra-wideband SAR images," Ph.D. dissertation, Georgia Inst. Tech., Atlanta, 1998.
- [178] F.M. Gardner, *Phaselock Techniques*. New York: John Wiley, 1979.
- [179] R.E. Best, *Phase-Locked Loops*. New York: McGraw-Hill, 1984.
- [180] S.U.H. Qureshi, "Adaptive equalization," Ch. 12 of *Advanced Digital Communications* by K. Feher, Englewood Cliffs, NJ: Prentice-Hall, 1987.
- [181] S.S. Haykin, *Adaptive Filter Theory*. Englewood Cliffs, NJ: Prentice-Hall, 1987.
- [182] S. Verdú, "Recent progress in multiuser detection," in *Advances in Communication and Signal Processing*. New York: Springer-Verlag, 1989.
- [183] A.V. Oppenheim and R.W. Schaffer, *Discrete-Time Signal Processing*. Englewood Cliffs, NJ: Prentice-Hall, 1989.
- [184] J.G. Proakis and D.G. Manolakis, *Digital Signal Processing: Principles, Algorithms and Applications*, 2nd ed. New York: Macmillan, 1992.
- [185] H.V. Poor, *An Introduction to Signal Detection and Estimation*. 2nd ed., New York: Dowden & Culver, 1994.
- [186] C.W. Helstrom, *Elements of Signal Detection and Estimation*. Englewood Cliffs, NJ: Prentice-Hall, 1995.

Chapter 2. Radio Geolocation Systems

“Be ye transformed by the renewing of your mind.”^{3/4}Romans 12-2

2.0 Introduction

THE ability to measure line-of-sight range using radios forged a new successful era for navigation technology in the 20th century. The most successful among all geolocation systems built are GPS (see §2.2) and GLONASS (see §2.3), which stand unique both in historical significance and in operation. These two systems motivated other outdoor geolocation systems and techniques such as pseudolites, LAAS, WAAS, DGPS, etc. In this chapter we discuss the principle of operation, the transmitter design, receiver design, the method used for extracting the observable and issues related with the prior art of all geolocation systems that are relevant to the WPI indoor geolocation system.

The discussion starts with the selection of examples of outdoor geolocation systems (see §2.1). The discussion continues with GPS (see §2.2) and then GLONASS (see §2.3). Next, we investigate two indoor geolocation systems (see §2.4), which include a pseudolite indoor geolocation system (see §2.5) and the MIT indoor geolocation system (see §2.6).

2.1 Selection of Examples of Outdoor Geolocation Systems

Although there are several outdoor geolocation systems that were designed and deployed in the 20th century, we have selected only two systems to investigate in this chapter: GPS and GLONASS. As we already know from chapter 1 both GPS and GLONASS are part of GNSS. Both GPS and GLONASS are designed to provide accurate positioning and timing information to users anywhere on the surface of the earth, in the air, and in space using very distinct signal structure design and frequency allocation. Nevertheless, both GPS and GLONASS are very similar as far as their principle of operation is concerned; therefore, we will explain the GPS operation in

greater detail and emphasize the GLOANSS differences in the GLONASS section. The discussion presented here is based to some extent on [1]-[22] with enhancement and detailed treatment for the average reader.

2.2 GPS

In chapter 1 we have described the GPS as a system with three main segments: the space segment, the control segment, and the user segment. Here we discuss the GPS principle of operation (see §2.2.1), the GPS satellite (see §2.2.2), the GPS receiver (see §2.2.3), the method for extracting the observable(s) (see §2.2.4), and issues related to using GPS for indoor positioning (see §2.2.5).

2.2.1 Principle of Operation of GPS

The principle of operation of GPS is illustrated in Figure 2.1. In this figure the true and measured time of arrival are shown. The *true time of arrival* between the i th GPS satellite and the GPS receiver, t_{OAi} , is defined as difference between the GPS time, $T_{GPS}(TX)$, when signal transmission occurs at the transmitter with the GPS time, $T_{GPS}(RX)$, when signal reception occurs at the receiver. Note that in this definition, for ease of understanding, we do not include both general and special relativistic effects with the exception of one principle. The speed of light is constant despite the motion of the reference system or despite the relative motion between the i th GPS satellite and a GPS receiver. Analytically, the true time of arrival can be written as

$$(2.1.1) \quad t_{OAi} = T_{GPS}(TX) - T_{GPS}(RX).$$

The actual satellite time, T_i , when signal transmission occurs, is determined from

$$(2.1.2) \quad T_i = T_{GPS}(TX) - \Delta T_i$$

where ΔT_i is offset of the clock of the i th GPS satellite from the GPS time, $T_{GPS}(TX)$. The actual receiver time, t_r , when signal reception occurs, is given by

$$(2.1.3) \quad t_r = T_{GPS}(RX) - \Delta t_r$$

where Δt_r is the receiver clock offset from the GPS time, $T_{GPS}(RX)$, when signal reception occurs at the receiver. Therefore, the measured (or actual) time of arrival, t_{OAi} , between the i th GPS satellite and a GPS receiver is

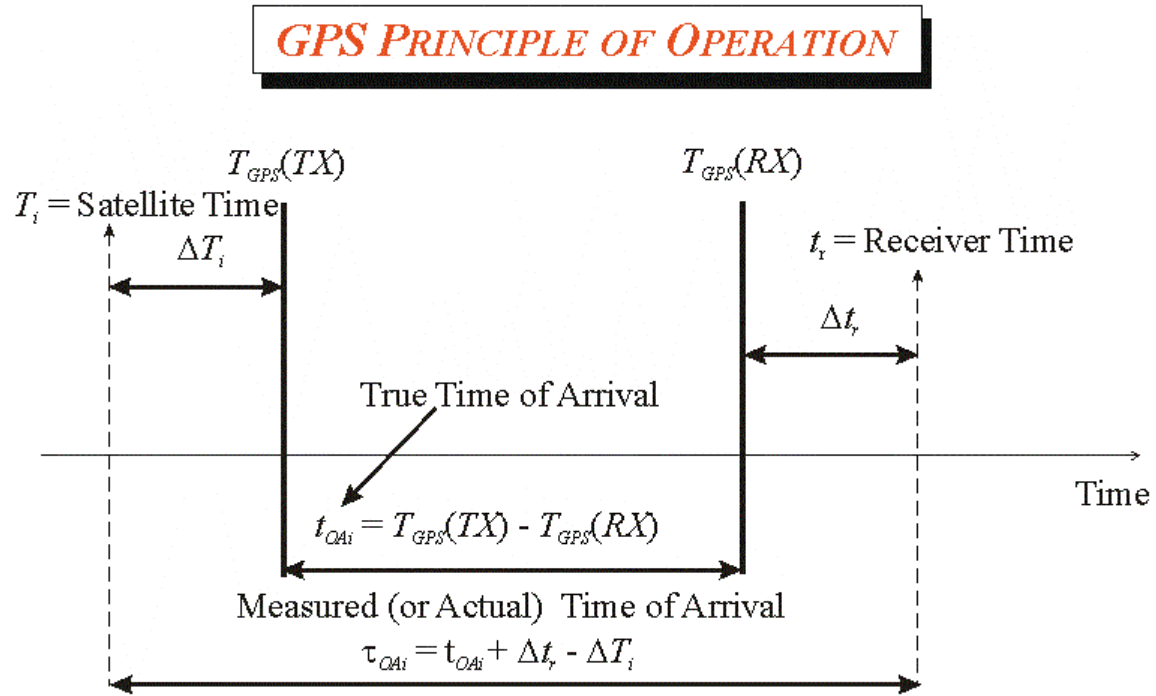


Figure 2.1 The principle of operation of GPS.

$$(2.1.4) \quad \tau_{OAi} = t_r - t_i = t_{OAi} + \Delta t_r - \Delta T_i.$$

The true time of the arrival when multiplied with the speed of light, c , produces the true range, R_i , between the i th GPS satellite and the GPS receiver as

$$(2.1.5) \quad R_i = c t_{OAi} = c [T_{GPS}(TX) - T_{GPS}(RX)].$$

The measured time of the arrival when multiplied with the speed of light, c , produces the measured range (or pseudorange), ρ_i , between the i th GPS satellite and the GPS receiver as

$$(2.1.6) \quad \rho_i = c \tau_{OAi} = c(t_r - t_i) = c(t_{OAi} + \Delta t_r - \Delta T_i) = R_i + c(\Delta t_r - \Delta T_i).$$

The above quantity is the first crude measurement that any GPS receiver must initially produce in order to provide a navigation solution.

The process for producing this measurement is explained in the remainder of this section. This process is overwhelming and the full details of it may easily span the pages of many textbooks. However, its main steps are addressed below:

1. How does a GPS receiver know what the GPS time is?
2. How does a GPS receiver know what the satellite clock offset from the GPS time is?

3. How does a GPS receiver account for the satellite motion and achieve synchronization between the satellite clock and its own internal clock?
4. How does a GPS receiver know what the satellite location and motion parameters are?

Here we briefly outline the general idea behind these questions and leaving the details to be answered in the remainder of the section.

First, any GPS receiver does not know that the GPS time is unless this information is contained in the transmitted signal. Also, any GPS satellite does not know what the GPS time is unless this information is provided from the control segment (see chapter 1). That is why we investigate the GPS satellite signal design and signal format in §2.2.2.

However, it is not enough that the GPS time is contained in the transmitted signal. Any GPS receiver must perform a well-defined procedure to extract this information. This is why we discuss the GPS receiver design and operation in §2.2.3.

Second, the receiver would similarly know what the satellite clock offset is if this information is contained in the transmitted signal and if the receiver has a well-defined procedure for extracting this information. This is why we discuss the GPS satellite onboard clocks as part of the GPS satellite in §2.2.2 and the GPS receiver design and operation in §2.2.3.

Third, although the GPS time and the satellite clock offset are included in the transmitted signal and although any GPS receiver may have in place a well-defined procedure for extracting this information, a GPS receiver must account for the relative motion between the GPS satellite and the receiver because the transmitted signal at the receiver is corrupted by this information. At the very least, the Doppler phenomenon occurs as a consequence of the relative motion between the transmitter and the receiver. This component will shift the spectrum of the transmitted signal at the receiver by the amount of Doppler. Thus, we will see that a GPS receiver performs an acquisition process to recursively determine this Doppler component and achieve synchronization between the transmitter clock (contained in the transmitted signal) and receiver clock (see §2.2.3).

Fourth, the information about the satellite position and motion parameters must be contained in the transmitted signal and the receiver must have a well-defined procedure

for extracting this information. This information is contained in the satellite ephemeris and almanac message and the procedure for extracting this information is explained in the GPS message format and content (see §2.2.2) and GPS receiver design (see §2.2.3).

Fifth, we discuss the how the actual measurement is obtained and how this process is put together to produce the actual measurement (see §2.2.4).

And last, we discuss some of the issues associated with the accuracy of this measurement for indoor positioning (see §2.2.5).

2.2.2 GPS Transmitter (Satellite)

For reasons explained earlier, the discussion on the GPS satellite design includes the GPS satellite signal structure and design (see §2.2.2.1), message format and content (see §2.2.2.2), and the GPS satellite onboard clocks (see §2.2.2.3) as shown in Figure 2.2.

2.2.2.1 Signal Structure and Design

The purpose of the GPS signal structure and design is to ensure propagation of the GPS signal from the Satellite to everywhere on the surface of the Earth, to guarantee reception of the signal from commercially built receivers (i.e., synchronization), and to ensure signal robustness against cross-channel interference and to some extent to external interference and jamming.

Each GPS satellite continuously transmits two signals, one at the $L_1 = 1575.42$ MHz frequency and the other at the $L_2 = 1227.6$ MHz frequency as depicted in Figure 2.3. These frequencies are selected because they ensure signal propagation through ionosphere and troposphere. The “critical” frequency of the ionosphere is around 30 MHz and any signal whose frequency is greater than 30 MHz can propagate through ionosphere. Also frequencies smaller than 10 GHz can propagate through troposphere or through clouds, rain, snow, etc. Both GPS L frequencies can easily satisfy these two requirements.

Spreading codes or pseudorandom sequences ensures signal robustness against cross-channel interference and multipath. For this reason, the signal at L_1 contains two pseudorandom sequences: C/A (in phase) and P codes (in quadrature), which are also used for synchronization purposes explained later in the receiver design. The C/A and P codes are unique for every satellite. The signal at L_2 contains only the P code. Because

both codes carry roughly the same power however they differ by a factor of 10 in bandwidth, the C/A code is roughly 10–15 times stronger than the P code (see Figure 2.3).

Every signal also contains a navigation message. Dual frequency navigation transmissions at L_1 and L_2 enables the GPS receiver to correct for the propagation effects caused by the ionosphere. GPS uses a CDMA modulation scheme to achieve multiaccess capability; i.e., every C/A or P code is unique for every satellite. The signal generated from every satellite is spread on a known pseudorandom sequence (Gold code) of a length of 1,023 for the C/A code and 6,187,104,000 for the P code. A C/A code sequence lasts only 1 ms so that the C/A code (chipping) rate is 1023 KBPS (or 1.023 MBPS) and the P code chipping rate 10.23 MBPS. The power spectrum of the C/A code and P code approximate the sinc_2 function with the first nulls occur at \pm the chipping rate; therefore, the bandwidth for the C/A code or the P code is 2 MHz or 20 MHz respectively. The data is commonly sent at a 50-baud rate. A binary phase shift keying (BPSK) technique is employed to transmit encoded data.

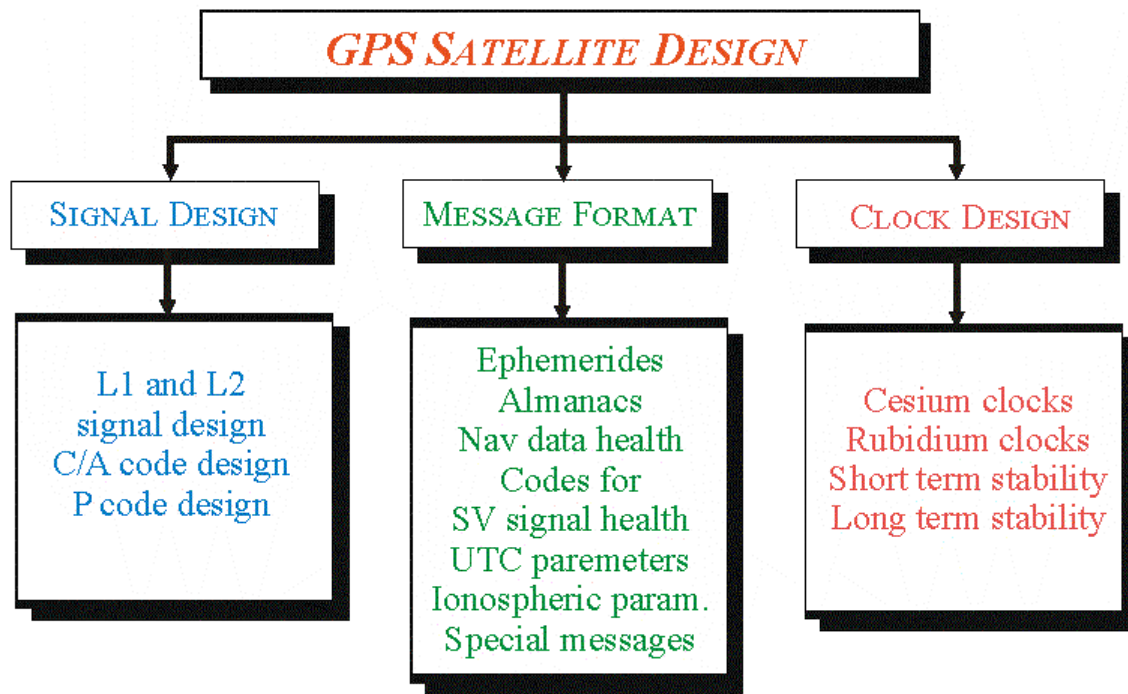


Figure 2.2 GPS satellite design.

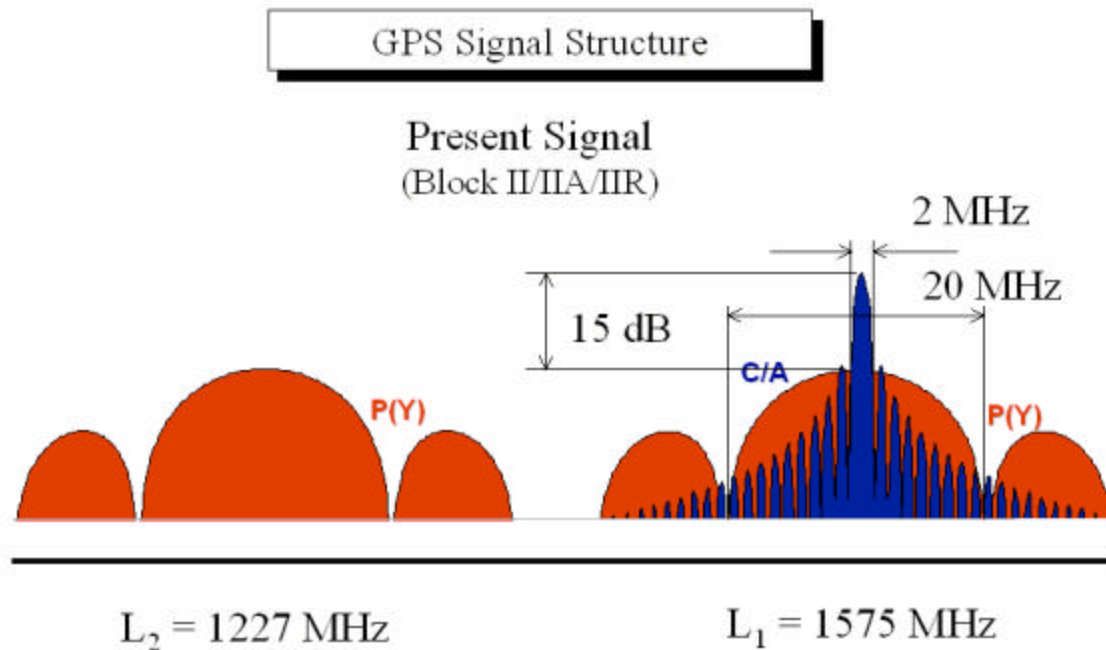


Figure 2.3 GPS signal structure and frequency allocation- - taken and modified from [8].

2.2.2.2 Message Format, Content, and GPS Time

GPS navigation messages ensure transmission of the necessary satellite orbital, clock, and health parameters, of the GPS time, and the ionospheric propagation parameters. The satellite orbital and clock parameters are contained in the ephemerides and almanacs. The GPS time is contained in the UTC message. The navigation health message contains health information. The ionospheric message contains ionospheric parameters. According to the GPS ICD 200 there are other special messages, which are not discussed here [6].

The GPS navigation message format, content, and timing are illustrated in Figure 2.4 [4]. The GPS navigation message contains 5 subframes, which require 30 seconds for transmission (or reception). One subframe contains ten (10) GPS words, which requires 6 seconds for transmission. A GPS word contains thirty (30) bits, which requires 600 milliseconds for transmission. One (1) GPS data bit period contains twenty (20) C/A code periods, which requires 20 milliseconds for transmission. A C/A code period consists of 1023 chips (or transitions) and it requires 1 millisecond for transmission.

The first and the second words in a subframe are the telemetry word (TLM) and the hand-over word (HOW), respectively (see Figure 2.5). Each subframe conveys the time of week (TOW) for the beginning of the next subframe, but since a subframe is sent in exactly six seconds, the two least significant bits of the TOW will be zero at the start of each subframe. Only the upper 17 bits of the TOW are contained in the actual navigation message.

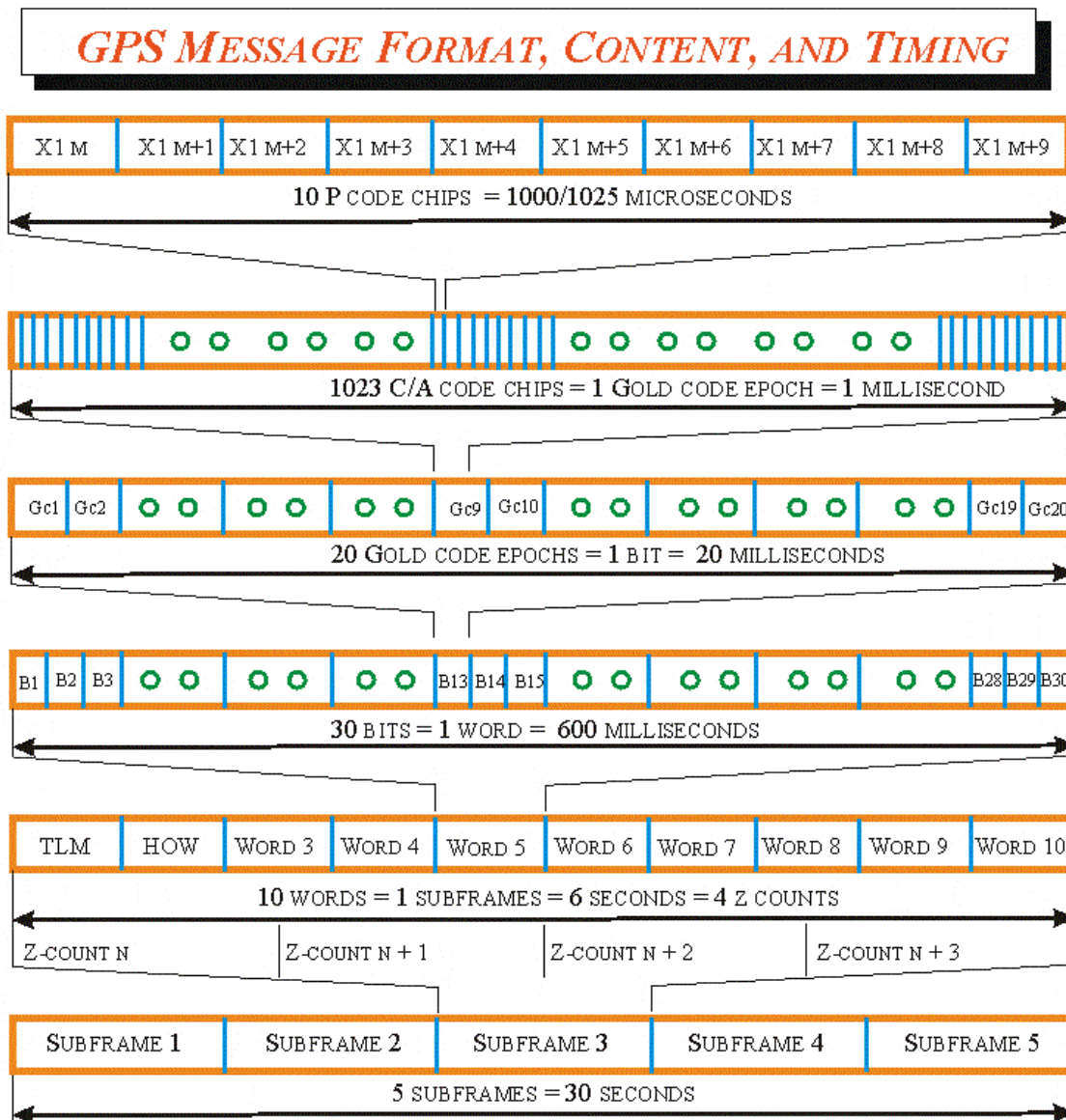


Figure 2.4 GPS message format, content and timing - - taken and modified from [9].

Subframes are contained into five types that are sent in order; such a grouping of five subframes is referred to as a *minor frame* (see Figure 2.5). Subframe types 1, 2, and 3 convey precision clock parameters and ephemeris data. Note that each satellite transmits its own clock and precision ephemeris data. Each type 1 subframe contains the week number. Subframe 4 and 5 convey all the almanac data for all participating satellites. A pairing of a type 4 and 5 subframe is known as a *page*. Type 4 and type 5 subframes are sub-communicated with 25 such pairings; therefore, there are 25 pages that convey the entire almanac, which requires 12.5 minutes.

Figure 2.6 illustrates the structure for the TLM and HOW words. The TLM word is the first word in each subframe, occurs every six seconds in the data frame and is 30 bits long. Each TLM word begins with a preamble followed by the TLM message, two reserved bits and six parity bits. Apparently in [20] the reserved bits are set to '1'. The HOW word is the second word in the subframe, immediately preceded by the TLM word, occurs every six seconds in the data frame and is 30 bits long. The most significant bits (MSB) are transmitted first and the least significant bits are transmitted next. The HOW word begins with the seventeen MSBs of the TOW count. Bit 18 is the momentum flag (for SV configuration 000) or "alert" flag (for SV configuration 001) and bit 19 is the synchronization flag (for SV configuration 000) or anti-spoof flag for (SV configuration 001) [5].

GPS time is referenced to the UTC zero time-point defined as midnight on the night of January 5, 1980. The largest unit used in stating GPS time is one week defined as 604,800 seconds. The Z-count is convenient for precisely counting and communicating GPS time (see Figure 2.4). The Z-count is given as a 29-bit binary number consisting of two parts: the 19 least significant bits and 10 most significant bits.

The 19 least significant bits (LSB) of the 29-bit Z-count form the GPS time of week. The time of week count range is from 0 to 403,199 X1 epochs (equaling one week) and is reset to zero at the end of each week. To aid rapid ground lock-on to the P-code signal, a truncated version of the TOW-count, consisting of the 17 most significant bits, is contained in the HOW word. The symbol '*' is used to identify the last 2 bits of the previous word of the subframe; D25, D26,..., D30 are the computed parity bits; D1,

D2,..., D29, D30 are the bits transmitted by the SV; G is the modulo-2 or exclusive-or (XOR) operation.

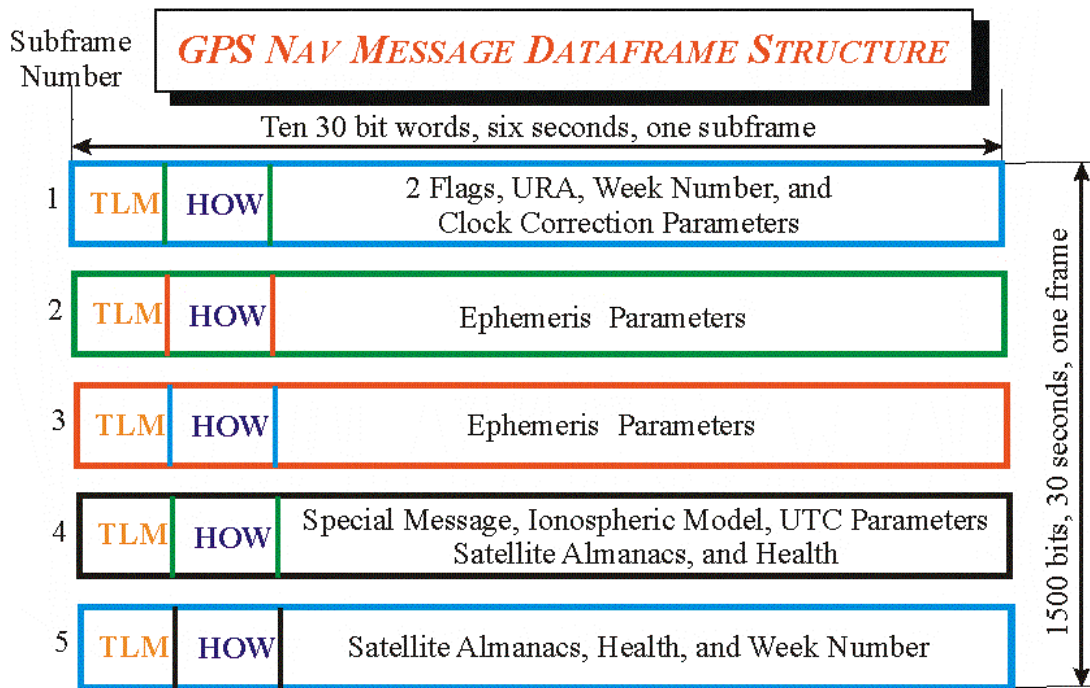


Figure 2.5 GPS navigation message data-frame structure- - taken and modified from [11].

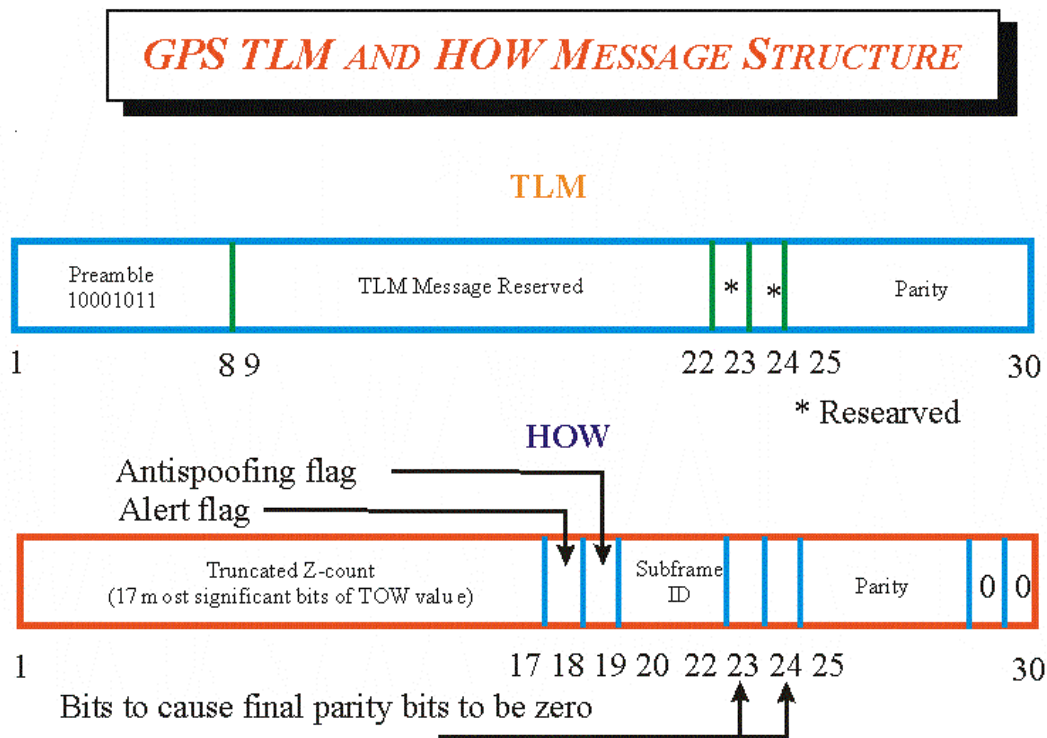


Figure 2.6 GPS TLM and HOW message data-frame structure- - taken and modified from [11].

The 10 most significant binary bits of the Z-count are assigned to a sequential number representing the present GPS week (modulo 1024). The range is from 0 to 1023 with its zero state defined as the week, which began with the X1 epoch occurring at approximately midnight on the night of January 5, 1980.

2.2.2.2.1 Satellite Ephemerides

The GPS ephemeris data describe a Kepler ellipse with additional corrections that allow the satellite's position to be calculated in an ECEF frame at any time during the period of validity of the data. This message is updated frequently most often on hour boundaries, following an upload from the control segment; however, an update may occur at any time [6]. According to Hill [9], updates (or cutovers) of the ephemerides have been observed to occur after periods of approximately one to two hours, but in one case a cutover was observed to occur after eleven minutes. This may presume that there is a suitable overlap between precision ephemeris data sets.

The GPS ephemeris message is illustrated in Table 2.1.

Table 2.1 GPS satellite ephemerides - - taken and modified from [6].

<i>GPS SATELLITE EPHEMERIS</i>	
M_0	Mean anomaly at reference time
Δn	Mean motion difference from computed value
E	Eccentricity
$(A)^{1/2}$	Square root of the semi-major axis
Ω_0	Longitude of ascending node of orbit plane at weekly epoch
i_0	Inclination angle at reference time
ω	Argument of perigee
$\dot{\Omega}$	Rate of right ascension
\dot{i}	Rate of inclination angle
C_{uc}	Amplitude of the cosine harmonic correction term to the argument of latitude
C_{us}	Amplitude of the sine harmonic correction term to the argument of latitude
C_{rc}	Amplitude of the cosine harmonic correction term to the orbit radius
C_{rs}	Amplitude of the sine harmonic correction term to the orbit radius
C_{ic}	Amplitude of the cosine harmonic correction term to the angle of inclination
C_{is}	Amplitude of the sine harmonic correction term to the angle of inclination
t_{oe}	Reference time ephemeris
IDOE	Issue of data (ephemeris)

2.2.2.2.2 Satellite Almanacs

GPS provides a second message, namely the satellite almanac message, for computing a less accurate satellite position and velocity for three reasons. It contains fewer orbital parameters than the precision ephemeris message does. It is updated less frequently than the ephemerides message is because the GPS satellite almanacs are valid for several days. Old almanac data is still useful for calculating initial satellite visibility. It requires only one subframe to be transmitted unlike precision ephemeris, which requires three subframes.

The almanac message (see Table 2.2) contains: (1) week of validity; (2) identifier; (3) eccentricity; (4) inclination; (5) time of almanac; (6) health; (7) right ascension (RA); (8) rate of change of RA (RRA); (9) root of semi-major axis; (10) argument of perigee; (11) mean anomaly; (12) time offset; and (13) frequency offset.

2.2.2.2.3 GPS UTC Parameters

As far as timing is concerned the GPS satellites transmit satellite clock corrections to a GPS time and corrections from GPS time to a national time reference. GPS represents the satellite clock behavior in terms of a clock-offset (a_0), frequency-offset (a_1), and rate of change of frequency (a_2). The difference of the GPS system time from the Universal Time Coordinated at the U.S. Naval Observatory, UTC (USNO), is given as A_0 , and its first derivative as A_1 . Updates of the UTC parameters are performed as necessary.

Table 2.2 GPS satellite almanac message-- taken from [6] and [10].

GPS SATELLITE ALMANAC

WEEK	WEEK OF VALIDITY
IDEN	IDENTIFIER
e	ECCENTRICITY
i_o	INCLINATION
t_o	TIME OF ALMANAC
H	HEALTH
Ω_o	RIGHT ASCENSION
$\dot{\Omega}$	RATE OF CHANGE OF RIGHT ASCENSION
$(A)^{1/2}$	ROOT OF SEMI-MAJOR AXIS
ω	ARGUMENT OF PERIGEE
M_o	MEAN ANOMALY
a_{f0}	TIME OFFSET
a_{f1}	FREQUENCY OFFSET

2.2.2.3 GPS Satellite Onboard Clocks

GPS offers precise location and time transfer continuously anywhere on the surface of the earth and in space. The time transfer from GPS is achieved in a straightforward manner. Each satellite transmits signals referenced to its own onboard clock. The GPS control segment monitors the satellite clocks and determines their offsets from the common GPS time. The GPS clock correction model is illustrated in Figure 2.7.

GPS satellites carry two cesium and two rubidium atomic clocks as frequency/time standards. The i th satellite clock correction, ΔT_i , from the GPS time, T_{GPS} , at the time of signal transmission is computed from any GPS receiver based on the equation

$$(2.1.7) \quad \Delta T_i = a_{f0} + a_{f1}(T_{GPS} - t_{OC}) + a_{f2}(T_{GPS} - t_{OC})^2 + \Delta t_r$$

where a_{f0} , a_{f1} , and a_{f2} are the coefficients from the navigation message; t_{OC} is the reference time for the current parameter set; and Δt_r is the relativistic correction parameter (sheet 73 of [6]).

The control segment uploads the a_{f0} , a_{f1} , and a_{f2} clock parameters to every satellite as part of the satellite transmitted data message. When a GPS receiver receives signals from a satellite, it decodes the datastream modulated onto the transmission and it obtains the position of the satellite, as well as the satellite's clock correction from the GPS system time. The signal propagation can be calculated at an instant. The data message contains the time of signal transmission. By combining this time with the propagation time and correcting first for atmospheric effects, other delays, and for the satellite's own clock offset, the user can effectively transfer the GPS time of transmission to the GPS time of reception.

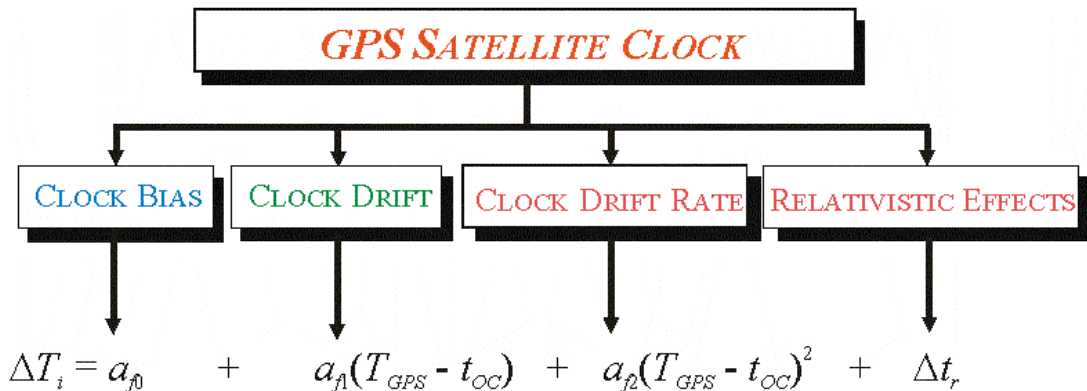


Figure 2.7 GPS satellite onboard clock correction model.

Correction to an external time scale [such as UTC (USNO) or UTC (SU)] is possible because the relevant offset is one of the transmitted data parameters. Any other user who has the same visible satellite is also able to transfer to the same GPS time scale. Clearly if two users access the same satellite simultaneously (common-view reception), the difference between the two users' measurements eliminates the systematic errors common to both, such as satellite ephemeris error or dither clock errors. In this way, time transfer between users in common view offers increased accuracy.

2.2.3 GPS Receiver

Every GPS receiver is designed to track either the C/A code only or both the C/A and P codes for a limited number of satellites. The number of available channels of the receiver may limit the maximum number of visible satellites that a GPS receiver can track. Typically, the number of visible satellites is smaller than 10 most of the time. Every channel performs the same process simultaneously; therefore, the receiver clock correction is common to all channels and when more than four simultaneous measurements are available the receiver starts the computation of the navigation solution.

In §2.2.1 we address the main issues associated with the design of a GPS receiver. A generic design of a GPS receiver is depicted in Figure 2.8.

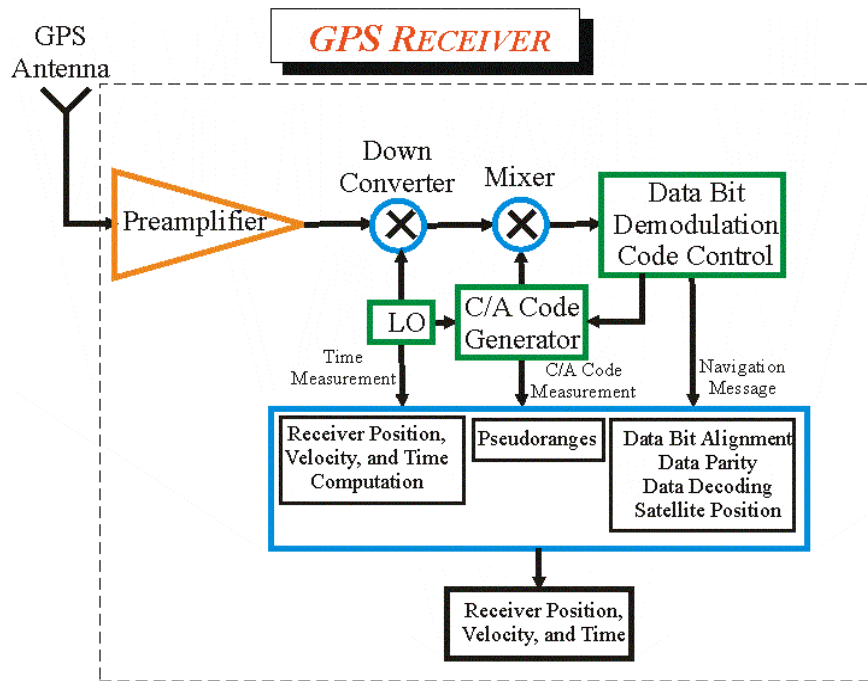


Figure 2.8 A block diagram of a generic GPS/GLONASS receiver-- taken and modified from [5].

Because the GPS signal may come from positive elevation directions then the antenna of a GPS receiver must have positive gain (in dB) for positive elevation angles. The GPS signal is already very weak when it reaches at the entrance of a GPS antenna and the antenna gain is not sufficient to bring the GPS signal to a level appropriate for analog and digital processing. A preamplifier amplifies both the signal and thermal noise (introduced from the electronics of the radio frequency (RF) section). The signal at this point is ready for analog processing. The down-conversion stage brings the RF signal into the intermediate-frequency (IF) band, since, we know that the signal center frequency is either L_1 or L_2 .

However, the IF signal will still contain a Doppler component due to relative motion of the satellite with respect to the GPS receiver. Moreover, the signal also contains the unwanted receiver clock errors (bias, first and higher order derivatives). Every GPS receiver must be able to accurately replicate the C/A code or P code (limited only to military users) contained in the transmitted signal in order to acquire and track that particular signal. The locally generated C/A code in the C/A code generator multiplies the IF signal based on a Doppler estimation from the data bit demodulation and code control. During this iterative process which ends when the GPS receiver is able to align its own generated code with the satellite generated code to within half of a C/A code chipping period (or roughly 500 ns equal to 150 m) then a good estimation of the Doppler frequency is obtained. Next comes the bit alignment process when the detection of the navigation message is achieved. The details of this process are explained in the following section. Next the receiver performs subframe alignment. During this process the start and the end of a subframe is determined. The knowledge of the GPS navigation message makes the decoding of the navigation message possible. The navigation message contains information on the GPS time, satellite position and velocity, satellite clock errors, ionospheric, and tropospheric corrections. The satellite position and velocity information can be extracted from decoding and processing two messages: satellite ephemerides or satellite almanac messages. The computed satellite position and velocity from the satellite ephemerides message is more accurate than the computed satellite position and velocity from the almanac message.

Thus far we have discussed the GPS operation, the satellite signal design, and the receiver design, which provide all the background information to link them into the most important section that of the extraction of the observable(s) or see how a measurement is obtained.

2.2.4 Extraction of Observable(s)

In determining the accuracy with which the time of arrival (or its equivalent, pseudorange) can be measured, it is important to remember that two basic quantities are available: (1) *code phase* and (2) *carrier phase* [10]. We can use a GPS receiver to measure *code phase*, meaning the time interval between local and transmitted epochs, to an accuracy limited by the code frequency, the SNR, and the bandwidth of the measurement. We can use a GPS receiver to measure *carrier phase* meaning a fraction of a wavelength at the carrier frequency.

If all satellite onboard frequency clocks are locked to the same frequency standard, the stability of that standard limits the available accuracy [10]. In the *carrier phase* approach where onboard standards are synchronized atomic clocks, range, and hence, position can be established to a fraction of a wavelength at the carrier frequency. At the L_1 frequency of 1.57542 GHz, the free-space wavelength is around 19 cm [10]. Because carrier-phase measurements are fractional, range to a satellite can only be found by inclusion of the integer number of carrier wavelengths between the satellite and receiver. In practice, these integers may only be resolved if two or more receivers are operating simultaneously (differential operation) on the same satellite [5],[10]. The remainder of this section is dedicated on the detailed discussion of how a code phase measurement or a carrier phase measurement, namely an observable, is obtained.

There are several steps that a GPS receiver performs to produce an observable as shown in Figure 2.9. After the down-conversion process the noisy signal is digitized, which is represented by the signal and noise model. A received GPS signal at the output of the IF stage, $x(t)$, is a combination of carrier, C/A code, P(Y) code, navigation data, and noise. A typical, L_1 signal looks like [11]

$$(2.1.8) \quad x(t) = A \sin(\mathbf{w}_r t + \mathbf{q}_r) D(t) C(t) + \frac{A}{\sqrt{2}} [\cos(\mathbf{w}_r t + \mathbf{q}_r) D(t) P(t)] + \mathbf{u}(t)$$

where A is the signal amplitude; w_i is the IF carrier frequency adjusted for Doppler; q_i is the phase offset for the carrier at time $t = 0$; $D(t)$ is the navigation data; $C(t)$ is the C/A code; $P(t)$ is the P(Y) code; and $u(t)$ represents the noise term.

The $1/\sqrt{2}$ in front of the cosine term represents the -3dB attenuation applied by the GPS transmitter to the P(Y)-code signal. The reader is also reminded that we are dealing with an IF GPS signal rather than the actual GPS signal at the RF (L_1) frequency.

Suppose that this signal are sampled at a rate [5]

$$(2.1.9) \quad R = \frac{4f_i}{N}$$

where N is an odd number. Now we can easily determine the times in which the samples are taken as

$$(2.1.10) \quad t_k = \frac{kN}{4f_i} \text{ sec}; k = \{0, 1, \dots\}.$$

Hence, the discrete-time signal x_k (ignoring the P(Y) code) is obtained from [5]:

$$(2.1.11) \quad x_k = x(t_k) = AC(t_k)D(t_k)\cos\left[2p(f_i + \Delta f)\frac{kN}{4f_i} + q_i\right] + u_k$$

$$= AC_k D_k \cos\left[\frac{kpN}{2} + q_k\right] + u_k$$

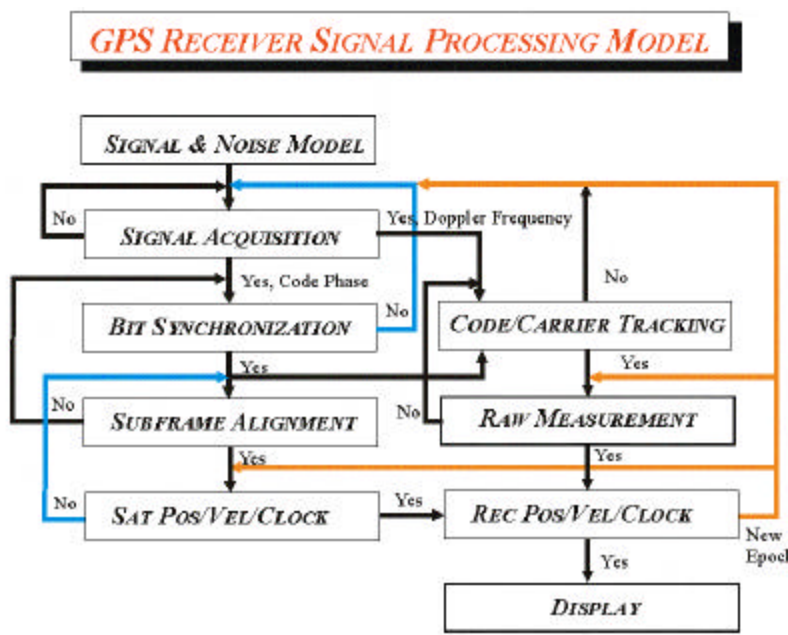


Figure 2.9 GPS receiver signal processing model.

where Δf is an intentional frequency offset (included Doppler), C_k and D_k are the code and data at time t_k , and

$$(2.1.12) \quad \mathbf{q}_k = \mathbf{q}_i + \frac{\mathbf{p}kN\Delta f}{2f_i} = \mathbf{q}_i + \Delta \mathbf{w}t_k = \mathbf{q}_i + \Delta \mathbf{q}_k$$

where $\Delta \mathbf{w} = 2\mathbf{p}\Delta f$ is called a residual frequency offset. If we ignore the Δf from the above equation then we observe that the IF signal is sampled at exactly 90° phases depending only on the values of N . The Δf results in a phase rotation $\Delta \mathbf{q}_k$ of the samples that is removed after the sampling process.

2.2.4.1 GPS Receiver Signal Acquisition

The *signal acquisition*, during which coarse estimates of the locally generated code offset, t_i , and the carrier Doppler frequency, f_i , are obtained, is depicted in Figure 2.10. This information is exploited to initialize the carrier tracking process. The signal acquisition is a two dimensional search process, in which the signal code replica and carrier are coarsely aligned with the received signal [11].

The heart of the acquisition process is the synchronization control scheme (see Figure 2.10) three important elements of which are (1) the acquisition search space, (2) the detection criterion, and (3) the Discrete Fourier Transform (DFT) or Fast Fourier Transform (FFT) search algorithm [11].

2.2.4.1.1 The Acquisition Search Space

The acquisition search space is illustrated in Figure 2.11. Since the C/A code is fairly short, 1023 chips; hence, the acquisition search space includes all C/A code chips. Moreover, the resolution of the code search is typically 1/2-chip increments; however, the sampling frequency determines the resolution of the code search. In theory the Doppler corresponding to the i th satellite, is given by, [14]

$$(2.1.13) \quad f_i = -\frac{(\mathbf{v}_i - \mathbf{v}_u) \cdot \mathbf{1}_i}{c} L_k, \text{ for } k = \{1,2\}$$

where \mathbf{v}_i and \mathbf{v}_u are the Satellite velocity and user vector respectively, $\mathbf{1}_i$ is the line of sight unit vector and L_k is the GPS operation frequency either L_1 or L_2 . The ratio, L_k/c is 5.255 for the L_1 and 4.0948 for the L_2 or in a more compact form

$$(2.1.14) \quad \alpha_k = \frac{L_k}{c} = \begin{cases} 5.255 \text{ m}^{-1}, & k = 1, \\ 4.0948 \text{ m}^{-1}, & k = 2. \end{cases}$$

Therefore, the Doppler is largely determined from the inner product $(\mathbf{v}_i - \mathbf{v}_u) \cdot \mathbf{1}_i$, i.e.;

$$(2.1.15) \quad (\mathbf{v}_i - \mathbf{v}_u) \cdot \mathbf{1}_i = |\mathbf{v}_i - \mathbf{v}_u| \cos \theta_i$$

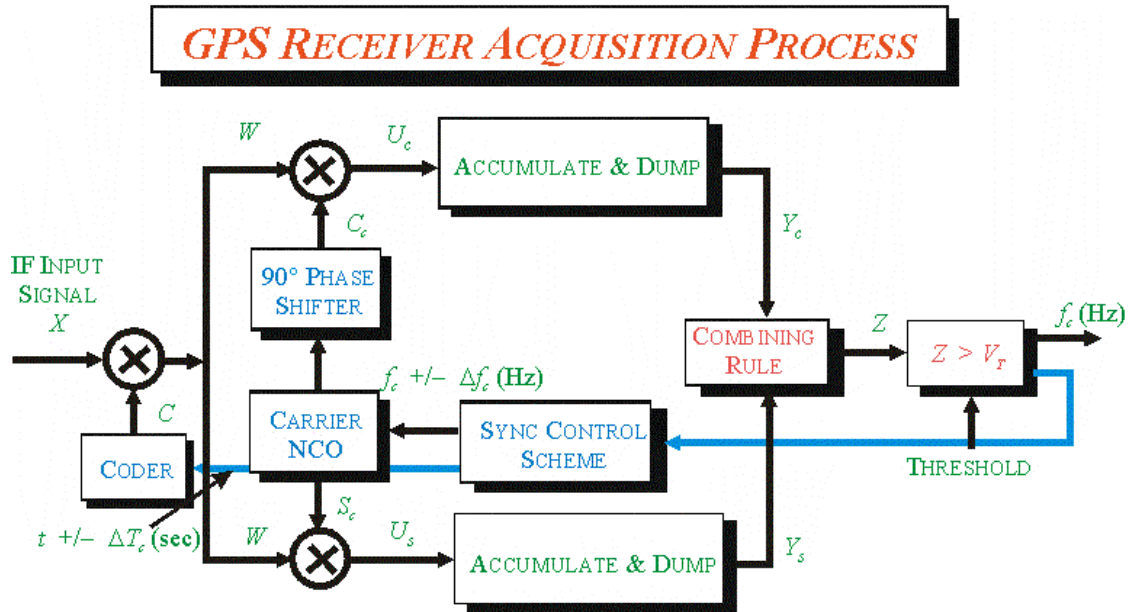


Figure 2.10 GPS receiver acquisition process-- taken and modified from [9] and [11].

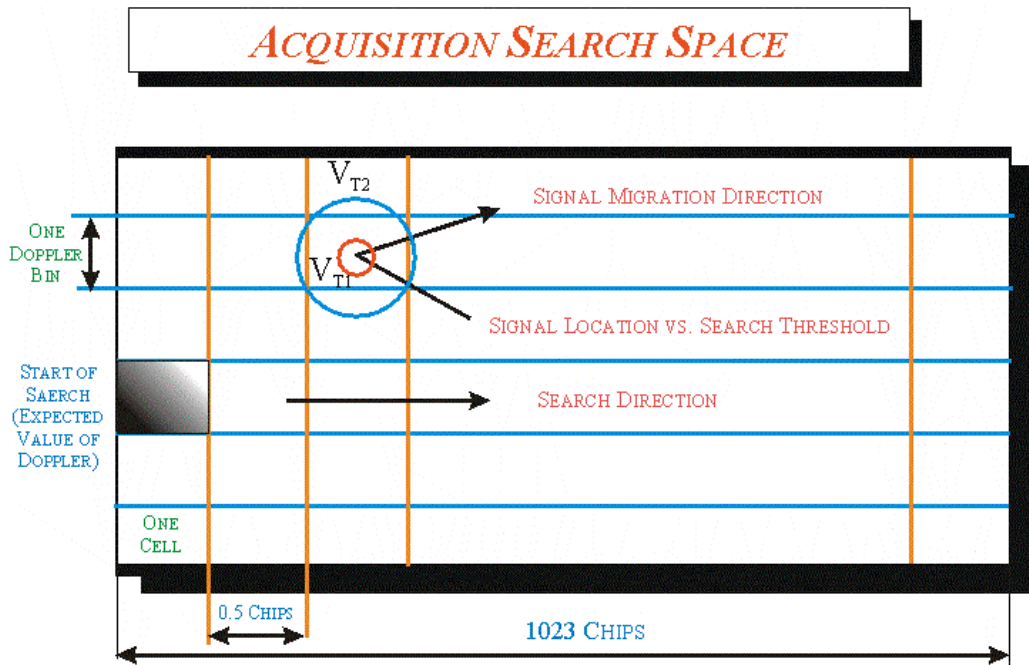


Figure 2.11 GPS receiver acquisition search space-- taken and modified from [11].

where θ_i is the angle between the vector $\mathbf{v}_i - \mathbf{v}_u$ and the vector, $\mathbf{1}_i$. Substituting equation (2.1.14) and equation (2.1.15) into equation (2.1.13) and knowing that $-1 \leq \cos \theta_i \leq 1$ we conclude that the Doppler satisfies the following inequality

$$(2.1.16) \quad -\alpha_k |\mathbf{v}_i - \mathbf{v}_u| \leq f_i \leq \alpha_k |\mathbf{v}_i - \mathbf{v}_u|, \text{ or } |f_i| \leq \alpha_k |\mathbf{v}_i - \mathbf{v}_u|, \text{ for } k = \{1,2\}.$$

Based on equation (2.1.16) we conclude that Doppler is largely dependent on the magnitude of the vector $\mathbf{v}_i - \mathbf{v}_u$, which means that the Doppler resolution, in theory, is largely dependent by the user and GPS satellite dynamics [11]. In practice, however, the Doppler resolution is also dependent by the stability of the receiver oscillator [11].

To get a better understanding of the Doppler value we find another upper bound for the absolute value of the vector, $\mathbf{v}_i - \mathbf{v}_u$, as

$$(2.1.17) \quad |\mathbf{v}_i - \mathbf{v}_u| \leq |\mathbf{v}_i| + |\mathbf{v}_u|$$

so then the final upper bound for the Doppler is given by

$$(2.1.18) \quad |f_i| \leq \alpha_k (|\mathbf{v}_i| + |\mathbf{v}_u|), \text{ for } k = \{1,2\}.$$

Typically, a GPS satellite velocity is approximately 3870.4 m/sec [3] and a terrestrial, civilian GPS user moves no faster than 360 m/sec (which is the speed of sound in the air). Therefore, the Doppler value would be

$$(2.1.19) \quad |f_i| < \begin{cases} 22 \text{ kHz,} & \text{for } L_1, \\ 17 \text{ kHz,} & \text{for } L_2. \end{cases}$$

The above Doppler values are comparable with the 5-10 kHz Doppler values for terrestrial users reported in [11]. The coherent integration time (or the dwell time in seconds), T , determines the frequency resolution (or the bin size), Δf_i , as [11]

$$(2.1.20) \quad \Delta f_i = \frac{2}{3T}.$$

The C/N0 of the transmitters to be acquired determines the dwell time, T .

2.2.4.1.2 The Detection Criterion

First, the IF input signal, x_k , multiplies the reference code replica, $C_{kr,j}$, to yield a signal, w_k , that contains only Doppler information if both the code replica and the code contained in the received signal are aligned. The analytical expression of w_k is given by [5]

$$(2.1.21) \quad w_k = \frac{A}{\sqrt{2}} C_k C_{kr,j} D_k \cos \theta_k + C_{kr,j} v_k.$$

The signal, w_k , contains both the actual Doppler frequency, f_i , and the code phase offset, t_i . The signal, w_k , is simultaneously multiplied by an in-phase signal and a quadrature signal coming from the carrier numerically controlled oscillator (NCO), which contains the estimate of the Doppler frequency to produce the u_{ck} signal and u_{sk} signal. The analytical expressions of these signals are given by [5]

$$(2.1.22) \quad u_{ck} = w_k \cos \theta_{kr}$$

$$(2.1.23) \quad u_{sk} = w_k \sin \theta_{kr}.$$

These signals are lowpass filtered and whose analytical expressions become [5]

$$(2.1.24) \quad u_{ck} = \frac{A}{\sqrt{2}} C_k C_{kr,j} D_k \cos(\theta_k - \theta_{kr}) + C_{kr,j} v_k \cos \theta_{kr}$$

$$(2.1.25) \quad u_{sk} = \frac{A}{\sqrt{2}} C_k C_{kr,j} D_k \sin(\theta_k - \theta_{kr}) + C_{kr,j} v_k \sin \theta_{kr}.$$

Let $\mathbf{j}(\mathbf{t}_{kj})$ denote the crosscorrelation function between C_k and $C_{kr,j}$ [5]

$$(2.1.26) \quad \varphi(\tau_{kj}) = E\{C_k C_{kr,j}\} \approx \begin{cases} 1 - |\tau_{kj}|, & |\tau_{kj}| \leq 1 \\ 0, & |\tau_{kj}| > 1 \end{cases}$$

where \mathbf{t}_{kj} is the time offset at time t_k .

Unless full correlation is achieved, the correlated signal components are still pseudorandom. Therefore, this accumulation process serves as a time average of the components in equations (2.1.24) and (2.1.25). Henceforth, we can only evaluate the result as an expected value given by [5]

$$(2.1.27) \quad y_{ci} = E\left\{\sum_{k=1}^M u_{ck}\right\} = y_{cDi} + y_{cNi}$$

$$(2.1.28) \quad y_{si} = E\left\{\sum_{k=1}^M u_{sk}\right\} = y_{sDi} + y_{sNi}$$

where

$$(2.1.29) \quad y_{cDi} = E\left\{\sum_{k=1}^M \frac{A}{\sqrt{2}} C_k C_{kr,j} D_k \cos(\theta_k - \theta_{kr})\right\} = \frac{A}{\sqrt{2}} \varphi(\tau_i) D_i \sum_{k=1}^M \cos(\theta_k - \theta_{kr})$$

$$(2.1.30) \quad y_{sDi} = E \left\{ \sum_{k=1}^M \frac{A}{\sqrt{2}} C_k C_{kr,j} D_k \sin(\theta_k - \theta_{kr}) \right\} = \frac{A}{\sqrt{2}} \varphi(\tau_i) D_i \sum_{k=1}^M \sin(\theta_k - \theta_{kr})$$

$$(2.1.31) \quad y_{cNi} = E \left\{ \sum_{k=1}^M \frac{A}{\sqrt{2}} C_{kr,j} \nu_k \cos \theta_{kr} \right\}$$

$$(2.1.32) \quad y_{sNi} = E \left\{ \sum_{k=1}^M \frac{A}{\sqrt{2}} C_{kr,j} \nu_k \sin \theta_{kr} \right\}.$$

Assumed a constant frequency and phase error Δf_i and $\Delta \theta_i$ respectively. Then the change in the difference between the signal phase, θ_i , and the reference phase, θ_r , over the interval, T , is given by

$$(2.1.33) \quad (\theta_i - \theta_{ri}) - (\theta_{i-1} - \theta_{r,i-1}) = 2\pi\Delta f_i T + \Delta \theta_i.$$

Now we can approximate the sums of the sine and cosine samples as finite integrals [5]

$$(2.1.34) \quad \frac{1}{T} \sum_{k=1}^M [\cos(\theta_k - \theta_{kr})] T \approx \frac{1}{T} \int_0^T \cos(2\pi\Delta f_i t + \Delta \theta_i) dt$$

$$(2.1.35) \quad \frac{1}{T} \sum_{k=1}^M [\sin(\theta_k - \theta_{kr})] T \approx \frac{1}{T} \int_0^T \sin(2\pi\Delta f_i t + \Delta \theta_i) dt.$$

Integration of equations (2.1.29) and (2.1.30) produces [5]

$$(2.1.36) \quad y_{cDi} = \frac{A}{\sqrt{2}} M \frac{\sin(\pi\Delta f_i T)}{\pi\Delta f_i} \varphi(\tau_i) D_i \cos(\Delta \theta_i)$$

$$(2.1.37) \quad y_{sDi} = \frac{A}{\sqrt{2}} M \frac{\sin(\pi\Delta f_i T)}{\pi\Delta f_i} \varphi(\tau_i) D_i \sin(\Delta \theta_i).$$

And the noise samples have the following variances

$$(2.1.38) \quad E\{y_{cNi}^2\} = E\{y_{sNi}^2\} = \frac{N_0}{2T} M.$$

To aid our performance analysis we define a new set of I and Q samples which normalizes the noise power as

$$(2.1.39) \quad E\{\mathbf{h}_{ci}^2\} = E\{\mathbf{h}_{si}^2\} = 1$$

and produces for the early-minus-late samples [5]

$$(2.1.40) \quad E\{\mathbf{h}_{ci,e-l}^2\} = E\{\mathbf{h}_{si,e-l}^2\} = 2(1 - \mathbf{r}_{n,e-l}).$$

Define the signal power, S , by $S = P_s = A^2/2$. Multiply the samples by a factor of $\sqrt{2T/MN_0}$, then we have [5]

$$(2.1.41) \quad y_{ci} = \sqrt{\frac{2T}{MN_0}}(y_{cDi} + y_{cNi}) = \sqrt{\frac{2ST}{N_0}} \frac{\sin(\pi\Delta f_i T)}{\pi\Delta f_i T} \varphi(\tau_i) D_i \cos(\Delta\theta_i) + \eta_{ci}$$

$$(2.1.42) \quad y_{si} = \sqrt{\frac{2T}{MN_0}}(y_{sDi} + y_{sNi}) = \sqrt{\frac{2ST}{N_0}} \frac{\sin(\pi\Delta f_i T)}{\pi\Delta f_i T} \varphi(\tau_i) D_i \sin(\Delta\theta_i) + \eta_{si}.$$

For convenience, S/N_0 = signal-to-noise density is given in ratio-Hz; $C/N_0 = 10\log_{10}S/N_0$ = carrier-to-noise density is given in dB-Hz; and, $(S/N_0)T$ = signal-to-noise ratio is given in a $1/T$ Hz two-sided noise bandwidth [5].

The final results (the y_{ci} signal and y_{si} signal) are combined to yield the signal, z , whose amplitude is compared with the threshold V_t .

$$(2.1.43) \quad z = \sqrt{y_{ci}^2 + y_{si}^2}.$$

The output of the detection criterion unit is an estimate of the Doppler frequency, f_i , and code phase offset, τ_i . This Doppler frequency is used to feed the synchronization control scheme, which controls both the coder process and the carrier NCO.

Typically the Doppler is set to its expected value and the code is searched over all possible delays. If the detection criterion fails, then the search is continued in the next bin higher from the starting point. If this also fails then the search is continued in the next bin lower from the starting point. And so forth the search continues on higher and lower Doppler bins until success is achieved. The following section explains the detection criterion for determining a success or failure during the Doppler search procedure.

The detection criterion consists of a measurement from the correlator outputs. The correlators provide a measure of the total Y_c and Y_s signal amplitude voltages over the coherent integration time, T , (equations (2.1.27) and (2.1.28)). The envelope of $Z = \sqrt{Y_c^2 + Y_s^2}$ renders the total amplitude for determining the presence or absence of the C/A code signal. When the replica and the reference signals are aligned, the amplitude of the aligned signal, Z , is close to its maximum. During the dwell time in each cell, stripping off the reference code and the carrier from the received signal respectively forms

the in-phase and quadrature components. The envelope signal, Z , which is a measure of the incoming signal amplitude, is computed and compared with a threshold, V_T . Care must be shown to set the threshold of the signal based on an acceptable probability that the noisy measurement does not contain a signal, which matches the replica. Let P_{fa} denote the probability of the false alarm of a single trial when no signal is present and \mathbf{s}_Y depict the noise amplitude of the y_{cN} and y_{sN} signal voltages. It is a well known result that if no signal is present, and assuming that y_{cN} and y_{sN} are normally distributed, then $f_z(z)$ is Rayleigh distributed [9],[11]-[13]

$$(2.1.44) \quad f_z(z) = \frac{z}{\sigma_Y^2} e^{-\frac{z^2}{2\sigma_Y^2}} U(z)$$

where $U(z)$ is unit step function. The mean of this distribution is given by [13]

$$(2.1.45) \quad \mu_z = \int_0^{\infty} z f_z(z) dz = \frac{1}{\sigma_Y^2} \int_0^{\infty} z^2 e^{-\frac{z^2}{2\sigma_Y^2}} dz = \sqrt{\frac{\pi}{2}} \sigma_Y$$

and variance is given by [13]

$$(2.1.46) \quad \sigma_z^2 = \int_0^{\infty} z^2 f_z(z) dz - \mu_z^2 = \frac{1}{\sigma_Y^2} \int_0^{\infty} z^3 e^{-\frac{z^2}{2\sigma_Y^2}} dz - \mu_z^2 = \left(2 - \frac{\pi}{2}\right) \sigma_Y^2.$$

In particular, the higher order moments of z are [13]

$$(2.1.47) \quad E\{z^n\} = \begin{cases} 1 \cdot 3 \cdots n \sigma_Y^n \sqrt{\frac{\pi}{2}}, & n = 2k + 1 \\ 2^k k! \sigma_Y^{2k}, & n = 2k \end{cases}$$

Hill [9] proposes that the probability of false alarm (or false detection) P_{fa} be given by

$$(2.1.48) \quad P_{fa} = \int_{V_T}^{\infty} f_z(z) dz = \int_{V_T}^{\infty} \frac{z}{\sigma_Y^2} e^{-\frac{z^2}{2\sigma_Y^2}} dz = e^{-\frac{V_T^2}{2\sigma_Y^2}}.$$

Hence, an amplitude threshold for acquisition is computed from [11]

$$(2.1.49) \quad V_t = \sigma_Y \sqrt{-2 \ln P_{fa}}.$$

For the chosen threshold, V_t , any cell envelope that is at or above the threshold is detected as the presence of the signal. Any cell envelope that is below the threshold is detected as noise. The detection of the signal is a statistical process because each cell

either contains noise with signal present or noise with the signal absent. Hence, in the absence of the desired signal the envelope has a Rayleigh distribution.

If the noise is Gaussian y_c and y_s signals are normally distributed [9], [11]. Therefore, let the joint distribution of $f(y_c, y_s)$ is given by [13]

$$(2.1.50) \quad f(y_c, y_s) = \frac{1}{2\pi\sigma_y^2} e^{-\frac{[(y_c - \mu_c)^2 + (y_s - \mu_s)^2]}{2\sigma_y^2}}.$$

Since in the region DD_z is such that $z < \sqrt{y_c^2 + y_s^2} < z + dz$; hence, it can be seen as a circular ring with radius z and thickness dz . If we select

$$(2.1.51) \quad y_c = z \cos \phi, \quad y_s = z \sin \phi, \quad dy_c dy_s = z dz d\phi$$

the following is obtained

$$(2.1.52) \quad f_z(z) dz = \iint_{\Delta D_z} f(y_c, y_s) dy_c dy_s = \frac{z dz}{2\pi\sigma_y^2} \int_0^{2\pi} e^{-\frac{[(z \cos \phi - \mu_c)^2 + (z \sin \phi - \mu_s)^2]}{2\sigma_y^2}} d\phi.$$

Therefore, the pfd function is given by

$$(2.1.53) \quad f_z(z) = \frac{ze^{-\frac{z^2 + \mu_c^2 + \mu_s^2}{2\sigma_y^2}}}{2\pi\sigma_y^2} \int_0^{2\pi} e^{\frac{z\mu_c \cos \phi + z\mu_s \sin \phi}{\sigma_y^2}} d\phi.$$

If we define

$$(2.1.54) \quad x = \frac{z\mu_c}{\sigma_y^2} \quad \text{and} \quad y = \frac{z\mu_s}{\sigma_y^2}$$

then we can write

$$(2.1.55) \quad x \cos \phi + y \sin \phi = x \left(\cos \phi + \frac{y}{x} \sin \phi \right) = x (\cos \phi + \tan \gamma \sin \phi) = \frac{x}{\cos \gamma} \cos(\phi - \gamma)$$

where

$$(2.1.56) \quad \tan \mathbf{g} = \frac{y}{x} \Rightarrow \gamma = \tan^{-1} \left(\frac{y}{x} \right) \Rightarrow \cos \gamma = \cos \left[\tan^{-1} \left(\frac{y}{x} \right) \right] = \cos \left[\tan^{-1} \left(\frac{\mu_s}{\mu_c} \right) \right].$$

Let w be defined as

$$(2.1.57) \quad w = \frac{x}{\cos \mathbf{g}}$$

and let, $I(w)$ denote a function defined as

$$(2.1.58) \quad I(w) = \int_0^{2\pi} e^{w \cos(\phi - \gamma)} d\phi = \int_0^{2\pi} e^{w \cos(\phi)} d\phi = I_0(w)$$

which is the modified Bessel function and the distribution of the envelope, z , is the well known Rician distribution [9],[11]-[13]

$$(2.1.59) \quad f_z(z) = \frac{z e^{-\frac{z^2 + \mu_c^2 + \mu_s^2}{2\sigma_Y^2}}}{2\pi\sigma_Y^2} I_0 \left(\frac{z\mu_c}{\sigma_Y^2 \cos \left[\tan^{-1} \left(\frac{\mu_s}{\mu_c} \right) \right]} \right) U(z).$$

The distributions of the envelope z for the cases $\mathbf{m}_s = 0$ (Rician distribution) and $\{\mathbf{m}_s = 0, \mathbf{m}_c = 0\}$ (Rayleigh) have been developed previously [9],[11]-[13]. Another case we are also interested in is when both $\{\mathbf{m}_s \neq 0, \mathbf{m}_c \neq 0\}$, which again produces a Rician distribution given by equation (2.1.59), which is different from the previous case only when $\mathbf{m}_c = 0$.

Figure 2.12 illustrates three probability density functions of the envelope signal z given by equation (2.1.59). We have assumed that we have 1023 samples for performing the integration. The input SNR is given by SNR $\{-30, -20, -10\}$ dB and the $P_{fa} = 0.01$;

If the SNR is high, it is easy to set a threshold, which results in a low probability of false alarm and also a low probability of a missed detection. As the SNR is reduced, this is no longer possible due to the significant overlap of the signal distributions. If the threshold is set very high to avoid false detection, then there is a high probability that weak signals will not be detected.

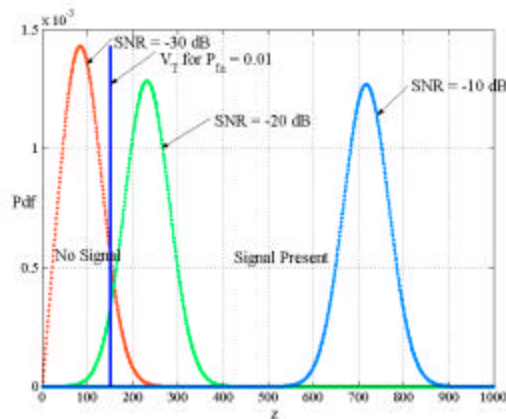


Figure 2.12 Probability density function for SNR = $\{-30, -20, -10\}$ dB, $P_{fa} = 0.01$, and $N_s = 1023$.

2.2.4.1.3 DFT (FFT) Search Method

The DFT (FFT) search method has the advantage of calculating the correlation for an entire range dimension in a single step in contrast to other methods which require more than one step. When Doppler is non-zero this approach has a disadvantage, because the reference signal when convolved produces some error. In this technique a DFT is applied to the incoming GPS signal and multiplied by the conjugate DFT of the reference signal. Taking the inverse DFT of the product gives the correlation result of the product [11].

2.2.4.2 Code and Carrier Tracking Loops

The acquisition process gives a coarse estimate of the carrier Doppler and PRN code offset of the incoming signal. Control is then handed over to the tracking loops, the function of which are to track the variations in the carrier Doppler and code offset due to line of sight dynamics between the satellite and the receiver. The unknown parameters of interest in the incoming GPS signal are the carrier Doppler, carrier phase, the PRN code Doppler, and PRN code phase. These parameters are functions of time because of the relative motion between the satellite and the user receiver. Hence it is important to track these parameters and get a very good estimate of the same. Another important function of the tracking loops is to demodulate the Navigation data from the incoming GPS signal. The PRN code phase can be used to determine the pseudorange whereas the carrier phase is used to accurately determine the small changes in the pseudorange.

2.2.4.2.1 I/Q Demodulation

We use I/Q demodulation in all of the standard GPS tracking loops. This simple process has two functions:

- Demodulates the navigation data from the carrier;
- Provides an indicator of the frequency and phase errors between the reference and input signals.

This section discusses I/Q demodulation outside the scope of GPS to simplify the later tracking loop sections. Figure 2.13 shows a typical time-domain I/Q demodulation circuit. Our discussion in this section uses the continuous time domain, but it applies equally well to digital processing.

Let us assume a noiseless input signal $x(t)$ given by

$$(2.1.60) \quad x(t) = D(t) \cdot \sin(\omega_c t)$$

where t is the time, $D(t)$ is the modulated data signal, ω is the radian frequency and the subscripts c , r , and e refer to the carrier, reference, and error respectively.

Assume that $\omega_e = \omega_r - \omega_c$ is fairly small. The signal $x(t)$ is split into the in-phase channel (I) and quadrature (Q) channel. The I signal, multiplied by the reference signal, $\sin(\omega_r t + \theta)$, and then lowpass filtered, produces

$$(2.1.61) \quad I(t) = \frac{1}{2} \cos(\omega_e t + \theta) \cdot D(t)$$

where θ is the phase between the carrier signal and the reference signal. The Q channel when multiplied by the reference signal plus a 90° phase offset, $\cos(\omega_r t + \theta)$, and then lowpass filtered, yields

$$(2.1.62) \quad Q(t) = -\frac{1}{2} \sin(\omega_e t + \theta) \cdot D(t).$$

These two output values are combined to form the complex number

$$(2.1.63) \quad \tilde{x}(t) = I(t) + jQ(t).$$

The phase of the signal $\tilde{x}(t)$ is an indicator the phase between the input and the reference carriers. Hence, we can use the $\tilde{x}(t)$ in the phase detector portion of the tracking loop to provide the phase error

$$(2.1.64) \quad \theta_e(t) = k_p \text{atan2}(Q(t), I(t))$$

where k_p is the discriminator gain and $\text{atan2}(y,x)$ is defined in [15]. (This is explored further in the tracking loop sections below)

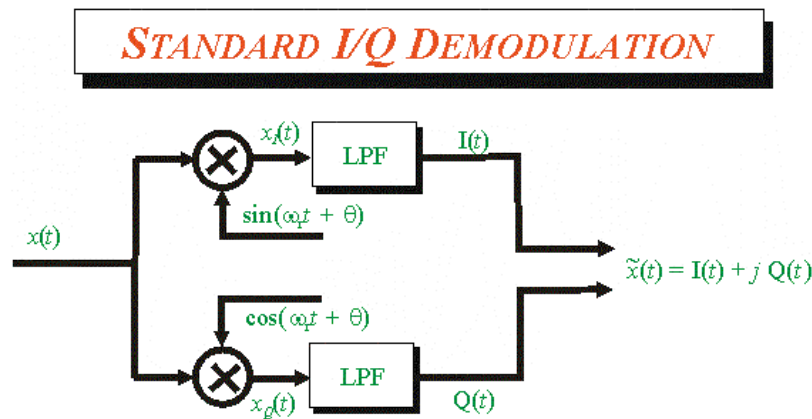


Figure 2.13 Standard I/Q demodulation- - taken and modified from [11].

Once, the lock is achieved; i.e., ω_e and θ have been minimized, the I-channel contains the navigation data at half amplitude and the Q-channel contains only noise. Hence,

$$(2.1.65) \quad I(t) \cong \frac{1}{2} D(t) + \text{noise}$$

and

$$(2.1.66) \quad Q(t) \cong \text{noise} .$$

The above results assume a continuous time domain with $\tilde{x}(t)$ updating instantly in response to changes in the reference signal or input signal. The digital GPS receiver, however, integrates the input data over a time interval and then dumps the single, $\tilde{x}(t)$, value—which changes the characteristics of the signal, $\tilde{x}(t)$. Here, we examine the effect of the integration and dump on the phase angle of $\tilde{x}(t)$. For ease of understanding we assume that there is no noise in the data and that the navigation data equals 1 for the duration of the integration.

Let us assume an initial phase offset q and a constant frequency error w_e . The signal, $\tilde{x}_{ni}(t)$, without the integration and dump is defined as

$$(2.1.67) \quad \tilde{x}_{ni}(t) = \frac{1}{2} e^{-j(\omega_e t + \theta)}$$

with the phase angle

$$(2.1.68) \quad \theta_{\tilde{x}_{ni}} = -(\omega_e t + \theta).$$

Given an integration interval, $T > 0$, a start time, t_1 , a stop time, $t_2 = t_1 + T$, and a scale factor, $\frac{1}{T}$, the integration is

$$(2.1.69) \quad \tilde{x}(t) = \frac{1}{T} \int_{t_1}^{t_2} \tilde{x}_{ni}(t) dt = \frac{1}{T} \int_{t_1}^{t_2} \left[\frac{1}{2} e^{-j(\omega_e t + \theta)} \right] dt .$$

The solution to the above integral is simply

$$(2.1.70) \quad \tilde{x}(t) = \frac{1}{2T\omega_e} \left[e^{j\left(\frac{p}{2} - w_e t_2 - q\right)} - e^{j\left(\frac{p}{2} - w_e t_1 - q\right)} \right] .$$

This expression can be written as

$$(2.1.71) \quad \tilde{x}(t) = \frac{e^{j\left(\frac{p-q}{2}\right)}}{2T\omega_e} \left[e^{-j\omega_e t_2} - e^{-j\omega_e t_1} \right].$$

Now the expression in the brackets can be written as

$$(2.1.72) \quad e^{-j\omega_e t_2} - e^{-j\omega_e t_1} = (\cos \omega_e t_2 - \cos \omega_e t_1) + j(\sin \omega_e t_1 - \sin \omega_e t_2).$$

Now using the trigonometric identities we find

$$(2.1.73) \quad \cos \omega_e t_2 - \cos \omega_e t_1 = 2 \sin \left(\omega_e \frac{t_1 - t_2}{2} \right) \sin \left(\omega_e \frac{t_1 + t_2}{2} \right)$$

$$(2.1.74) \quad \sin \omega_e t_1 - \sin \omega_e t_2 = 2 \sin \left(\omega_e \frac{t_1 - t_2}{2} \right) \cos \left(\omega_e \frac{t_1 + t_2}{2} \right).$$

Therefore, combining the above two equations together produces

$$(2.1.75) \quad e^{-j\omega_e t_2} - e^{-j\omega_e t_1} = 2 \sin \left(\omega_e \frac{t_1 - t_2}{2} \right) e^{j\left(\frac{p-q}{2} - \omega_e \frac{t_1 + t_2}{2}\right)}.$$

Substituting equation (2.1.75) into equation (2.1.71) yields

$$(2.1.76) \quad \tilde{x}(t) = \frac{1}{T\omega_e} \sin \left(\omega_e \frac{t_1 - t_2}{2} \right) e^{j\left(\pi - \omega_e \frac{t_1 + t_2}{2} - \theta\right)} = \frac{1}{T\omega_e} \sin \left(\omega_e \frac{t_2 - t_1}{2} \right) e^{j\left(\omega_e \frac{t_1 + t_2}{2} + \theta\right)}.$$

Since, $t_2 = t_1 + T$, then we have

$$(2.1.77) \quad \tilde{x}(t) = \frac{1}{T\omega_e} \sin \left(\omega_e \frac{T}{2} \right) e^{j\left(\omega_e \frac{2t_1 + T}{2} + \theta\right)}.$$

Hence, the phase of the signal $\tilde{x}(t)$ is given by

$$(2.1.78) \quad \theta_{\tilde{x}(t)} = \begin{cases} \omega_e \frac{2t_1 + T}{2} + \theta, & 2n\pi \leq \omega_e \frac{T}{2} \leq 2n\pi + \pi, \\ \pi + \omega_e \frac{2t_1 + T}{2} + \theta, & 2n\pi - \pi < \omega_e \frac{T}{2} < 2n\pi, \end{cases} \text{ for } n = \{0, \pm 1, \pm 2, \dots\}.$$

A simple example will show the significance of this difference. For example, if $\theta = 0$ and $t_1 = 0$, but $\omega_e \neq 0$. After a period of time, we perform integration and dump and we get the following

$$(2.1.79) \quad |\theta_{\tilde{x}_{int}(t)}| = |\omega_e T + \theta|$$

$$(2.1.80) \quad |\theta_{\tilde{x}}| = \left| \frac{\omega_e T}{2} + \theta \right|.$$

As we can see the phase angles are quite different; we should keep that in mind when analyzing the tracking loops.

2.2.4.2.2 Generic Tracking Loop

The goal of the tracking loop is to produce a replica (reference) signal that matches some input θ . Figure 2.14 shows the block diagram for a generic-tracking loop. The digital signal, θ , is run through a discriminator (shown as a dotted box) to produce the error value $\delta\theta_{i+1}$. The discriminator is represented as a single subtraction with an associated gain of k_p but actual GPS discriminators are more complex. The output is lowpass filtered to reduce noise. The NCO, with a gain of k_v utilizes the resulting value to produce a new replica of the signal for the next loop iteration. We want the loop output, $\Delta\hat{\theta}_i$, to be as close to zero as possible—at which point the replica signal will equal the input carrier.

Note that the following discussion is applicable to PLL tracking loops and to other loops as well such as GLONASS receiver's [16].

The performance analysis is quite complex, especially during the pull-in process or in the presence of noise; therefore, simplified analysis is considered here. Because the signs of the received databits are unknown a typical discriminator is given by [5]

$$(2.1.81) \quad \delta\theta_i = y_{ci}y_{si}.$$

The product eliminates dependence on the signs of the databits, because they effect I and Q alike, until their noise components dominate their signal components. This leads to a loss-of-lock.

The expected value of equation (2.1.81) in terms of equations (2.1.41) and (2.1.42) yields [5]

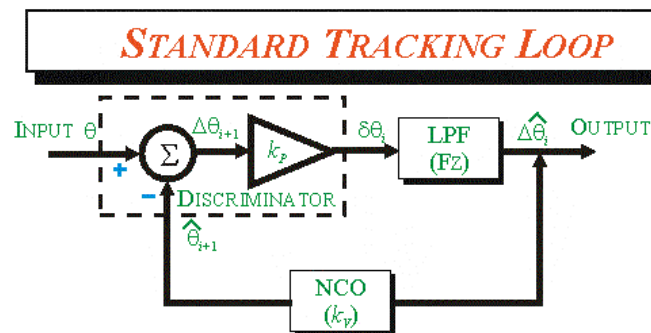


Figure 2.14 Standard tracking loop - taken and modified from [11].

$$\begin{aligned}
(2.1.82) \quad E\{\delta\theta_i\} &= \frac{2T}{MN_0} [E\{y_{cDi}\}E\{y_{sDi}\} + E\{y_{cDi}\}E\{y_{sNi}\} + E\{y_{sDi}\}E\{y_{cNi}\} + E\{y_{cNi}y_{sNi}\}] \\
&= \frac{2T}{MN_0} [E\{y_{cDi}\}E\{y_{sDi}\}] = \frac{S}{N_0} T\phi(\tau_i) \frac{\sin^2(\pi\Delta f_i T)}{(\pi\Delta f_i T)^2} \sin(2\Delta\theta_i) \\
&\approx 2\frac{S}{N_0} T\Delta\theta_i
\end{aligned}$$

in linearized form for small frequency errors and small code- and phase-tracking errors. If the PLL is truly tracking, the frequency errors have to be small. If the code tracking errors are not small, the amplitude of the above discriminator is simply reduced; hence, we see the importance of simultaneous code and carrier tracking.

The variance of that discriminator is as follows [5]

$$\begin{aligned}
(2.1.83) \quad V\{\delta\theta_i\} &= E\{y_{ci}^2 y_{si}^2\} - E^2\{y_{ci} y_{si}\} \\
&= \left(\frac{2T}{MN_0}\right)^2 [E\{y_{cDi}^2\}E\{y_{sDi}^2\} + E\{y_{cDi}^2\}E\{y_{sNi}^2\} \\
&\quad + E\{y_{sDi}^2\}E\{y_{cNi}^2\} + E\{y_{cNi}^2 y_{sNi}^2\} - E^2\{y_{cDi} y_{sDi}\}] \\
&= \left(\frac{2T}{MN_0}\right)^2 [E\{y_{cDi}^2\}E\{y_{sNi}^2\} + E\{y_{sDi}^2\}E\{y_{cNi}^2\} + E\{y_{cNi}^2 y_{sNi}^2\}] \\
&= 2\frac{S}{N_0} T \frac{\sin^2(\pi\Delta f_i T)}{(\pi\Delta f_i T)^2} + 1 \\
&\approx 2\frac{S}{N_0} T + 1 = 2\frac{S}{N_0} T \left(1 + \frac{1}{2TS/N_0}\right).
\end{aligned}$$

The second term in the parenthesis of the variance equation is attributable to squaring loss, which is proportional to the predetection bandwidth $1/T$.

For ease of implementation, based on the results of equations (2.1.82) and (2.1.83) a linear model of the feedback-tracking loop, illustrated in Figure 2.15, is often used [17]. For this linear model the discriminator gain, k_p , would be

$$(2.1.84) \quad k_p = 2\frac{S}{N_0} T.$$

If the NCO gain is k_v and the filter transfer function is $F(s)$ then the loop transfer function is given by

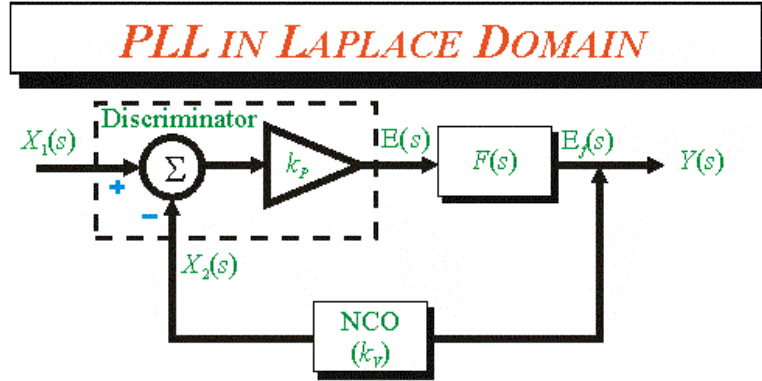


Figure 2.15 PLL in Laplace domain- - taken and modified from [11].

$$(2.1.85) \quad H(s) = \frac{k_v k_p F(s)}{1 + k_v k_p F(s)}.$$

Because of the ease of implementation and because of the presence of an integrator in its transfer function the active proportional-integrator filter is employed as a loop filter.

Akos [16] provides the following derivations for the filter transfer function:

$$(2.1.86) \quad F(s) = \frac{sT_2 + 1}{sT_1}$$

therefore the loop transfer function is given by

$$(2.1.87) \quad H(s) = \frac{2\zeta\omega_n s + \omega_n^2}{s^2 + 2\zeta\omega_n s + \omega_n^2}$$

where the loop natural frequency, ω_n , is determined from

$$(2.1.88) \quad \omega_n = \sqrt{\frac{k_p k_v}{T_1}}$$

and the damping ratio, z , is given by

$$(2.1.89) \quad z = \frac{\omega_n T_2}{2} = \sqrt{\frac{k_p k_v}{T_1}} \frac{T_2}{2}.$$

From this the filter parameters, T_1 and T_2 , can be picked to taking into account the gain, $k_p k_v$, to achieve the desired response. These parameters define a number of key properties associated with the tracking loop such as: lock-in time, pull-in range, and pull-out range from which the performance of the implementation can be accurately predicted. The steady-state error of this loop to a step change in phase or frequency (i.e., the first or second order derivative of the phase angle) is zero [18].

It is a second order-tracking loop since the denominator of the tracking loop, $H(s)$, is a second order of s . A first order loop is not used for tracking GPS signals since the PLL steady state error due to a frequency step or ramp (second or higher order derivatives of the phase angle) does not go to zero due to the presence of only one integrator.

In order to implement this loop in software, the continuous system must be changed into a discrete system. To transfer from the 's' domain into discrete domain 'z' we use the bilinear transformation, $s = \frac{2(1-z^{-1})}{t_s(1+z^{-1})}$, where t_s is the sampling interval (i.e., the coherent integration time, T). The loop filter transfer function in the z domain is

$$(2.1.90) \quad F(z) = \frac{C_1 + C_2 - C_1 z^{-1}}{1 - z^{-1}}$$

where

$$(2.1.91) \quad C_1 = \frac{8\zeta\omega_n t_s}{K[4 + 4\zeta\omega_n t_s + (\omega_n t_s)^2]}$$

and

$$(2.1.92) \quad C_2 = \frac{4(\omega_n t_s)^2}{K[4 + 4\zeta\omega_n t_s + (\omega_n t_s)^2]}$$

and $K = k_v k_p$ [16].

This provides the most accurate discrete implementation of the linear phase lock loop model, which is implemented in the software receiver of *Data Fusion Co.* [11].

The damping ratio plays an important role in the dynamics performance of the tracking loop. When working with an underdamped system ($0 < \zeta < 1$) the step response is rapid and will overshoot the desired state, oscillating before settling down to the desired state. If the system is overdamped ($\zeta > 1$), the step response will be slow to achieve the desired state, but will do so without any oscillation. The optimally flat response is achieved using $\zeta > 0.707$, which corresponds to a second order Butterworth lowpass filter.

The selection of the natural frequency of the loop filter is a compromise. A relatively small natural frequency will provide excellent noise performance but will be unable to track dynamics induced on the signal. A relatively large natural frequency will be able to track signal dynamics but will have poor noise performance. These conclusions are

based strongly on the noise bandwidth, B_l , approximation for the tracking loop given by [11]

$$(2.1.93) \quad B_l = 0.5\omega_n(\zeta + 1/4\zeta).$$

Based on expected dynamics, typical noise bandwidths for the code and carrier loops are 1 Hz and 25 Hz respectively. For a damping ratio of 0.707 this corresponds to a natural frequency of 2 Hz and 50 Hz for the code and carrier tracking loops [11].

2.2.4.2.3 GPS Receiver Code Tracking Loop

Figure 2.16 illustrates a typical GPS code early/late delay lock loop (DLL) [11]. It is a combination of the I/Q demodulation shown in Figure 2.13 and a tracking loop with 2-error terms (early and late). This implementation of the DLL is very similar to the generic feedback structure shown in Figure 2.14. The majority of components in the block diagram represent the phase detector (shaded area of Figure 2.16). The linear PLL model has been shown to be a good approximation of the early/late non-coherent delay lock loop [16].

The code-tracking loop plays a dual purpose in the software receiver: (1) to despread the incoming signal and (2) to render time of arrival measurements, which are directly linked with range measurements and navigation solution.

The code-tracking loop is thus the popular non-coherent early-late gate delay lock loop. The input to the loop is the composite signal consisting of the carrier modulated with the navigation data and the pseudorandom sequence. The input signal is split into two paths and is correlated with two versions (one early and one late) of the locally generated pseudorandom sequence. The two versions are equally spaced, typically ± 0.5 of the chipping period of the *prompt* pseudorandom related sequence (C/A code).

Each of these two paths is mixed to baseband, generating in-phase and quadrature components. The energy of the early and late paths is differenced and the result is filtered and input to NCO, which adjusts the rate of the pseudorandom code generator. In this case, the NCO bias indicates which path, early or late, contains more energy and thus whether the NCO needs to speed up or slow down the locally generated pseudorandom sequence. Ideally, when these two paths are balanced, the resulting difference is zero.

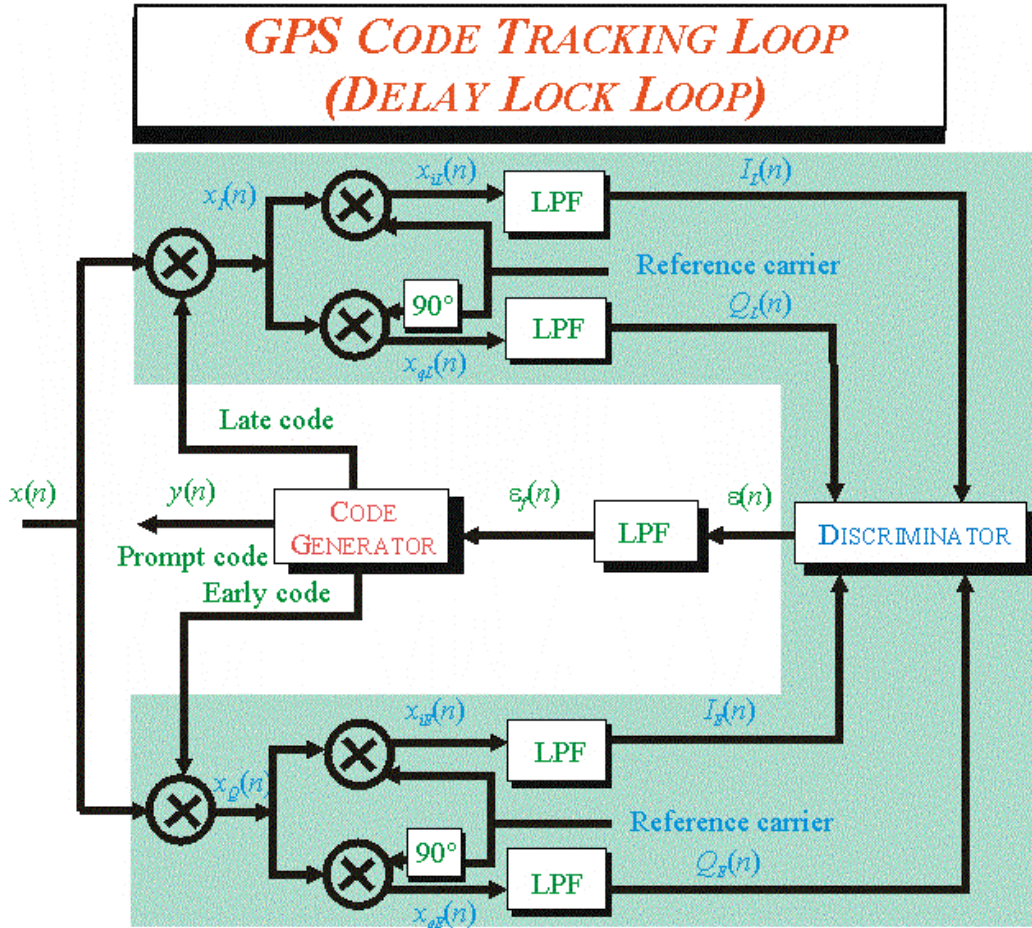


Figure 2.16 GPS code tracking loop - taken and modified from [11].

Three of the most popular code-tracking discriminators are the non-coherent discriminators (early-minus-late power) [5]

$$(2.1.94) \quad \delta\tau_i = I_{E,i}^2 + Q_{E,i}^2 - I_{L,i}^2 - Q_{L,i}^2$$

the dot product

$$(2.1.95) \quad \delta\tau_i = I_{E-L,i} I_{P,i} + Q_{E-L,i} Q_{P,i}$$

and the coherent DLL

$$(2.1.96) \quad \delta\tau_i = I_{E-L,i} \text{sign}(I_{P,i})$$

where E , L , $E-L$, and P indicate early, late, early-minus-late, and punctual phases of the reference code used in the cross correlation (see Figure 2.16) and $\text{sign}(I_{P,i})$ is the sign of the GPS navigation message databit demodulation in the PLL or FLL. The coherent DLL requires parallel carrier-phase tracking (and thus the coherent qualifier). However, the noncoherent discriminators require no carrier tracking as long as the frequency offset is

small with respect to the predetection bandwidth. This is an important feature in the presence of jamming using an external aiding source.

The advantages and disadvantages of each of these three discriminators are discussed in order. First, the noncoherent early-minus-late discriminator is the most robust discriminator because it has the largest linear range of the three. Its expected value is equal to [5]

$$(2.1.97) \quad \begin{aligned} E\{\mathbf{d}t_i\} &= E\{I_{E,i}^2\} + E\{Q_{E,i}^2\} - E\{I_{L,i}^2\} - E\{Q_{L,i}^2\} \\ &= 2S/N_0 T_i [R^2(\tau_i - d/2) - R^2(\tau_i + d/2)] \\ &\approx 4S/N_0 T_i (2 - d)\tau_i \end{aligned}$$

in the range of $|\tau_i| \leq d/2$, where $d < 2$ is the spacing between the late and early correlators (in units of PN chips), and where

$$(2.1.98) \quad T_i = MT$$

is the predetection integration interval after summing M I and Q samples in software, providing a predetection bandwidth of $1/T_i$. The closed loop-noise variance of a DLL using the early-minus-late power discriminator is given by [5]

$$(2.1.99) \quad V\{\delta\tau_i\} = \frac{B_L d}{2S/N_0} \left(1 + \frac{2}{(2-d)S/N_0 T_i} \right)$$

for simultaneously measured early and late samples and a precorrelation bandwidth that is wide relative to the chipping rate of the code. The squaring loss term in the brackets is the largest of the three discriminators. Two correlators are required to measure early and late power simultaneously. In order to track the carrier at the correlation peak a third correlator would be required. However, the performance is best when d is small, in which case either the early or late correlator is near the correlation peak.

The noncoherent dot-product DLL discriminator has an expected value of [5]

$$(2.1.100) \quad \begin{aligned} E\{\delta\tau_i\} &= E\{I_{E-L,i} I_{P,i}\} + E\{Q_{E-L,i} Q_{P,i}\} \\ &= 2S/N_0 T_i [R(\tau_i - d/2) - R(\tau_i + d/2)]R(\tau_i) \\ &\approx 4S/N_0 T_i \tau_i (1 - |\tau_i|) \end{aligned}$$

in the range of $|\tau_i| \leq d/2$. The closed-loop noise variance of the dot-product DLL is given by [5]

$$(2.1.101) \quad V\{\delta\tau_i\} = \frac{B_i d}{2S/N_0} \left(1 + \frac{1}{S/N_0 T_i} \right)$$

for simultaneous measured early-minus-late and punctual samples.

The coherent DLL discriminator has an expected value of [5]

$$(2.1.102) \quad E\{\delta\tau_i\} \approx E\{I_{E-L,i}\} = \sqrt{2S/N_0 T_i} [R(\tau_i - d/2) - R(\tau_i + d/2)] \approx 2\sqrt{2S/N_0 T_i} \tau_i$$

in the range of $|\tau_i| \leq d/2$ for low bit error rates as long as phase lock is maintained and a closed-loop noise variance of [5]

$$(2.1.103) \quad V\{\delta\tau_i\} \approx \frac{B_i d}{2S/N_0}$$

for simultaneous measured early-minus-late and punctual samples under the same conditions.

The three implementations of the DLL presented here have the same noise performance at higher signal-to-noise conditions at times when squaring loss is minimal in the noncoherent designs. Of course, when the squaring loss in a coherent DLL would be significant, the performance of the coherent DLL would also be marginal and equation (2.1.103) would not apply.

2.2.4.2.4 GPS Receiver Frequency Lock Loop

A Frequency Lock Loop (FLL) employs frequency error to track the input carrier, unlike a PLL which utilizes the phase error. In Figure 2.17, the discriminator output $\varepsilon(n)$ is the frequency error $\delta\omega_i$, which is then filtered and provided as an input to the NCO. In general, a Costas PLL tracks more tightly, but the FLL can track a larger noise bandwidth and is more robust in the presence of dynamic stress [9], [19].

Much of the available GPS literature suggests that under normal conditions a PLL may be sufficient to track the carrier [5], [9], [11], [19]. However, in situations where noise is an issue or where a large noise bandwidth is required, the receiver may not be able to track without an FLL [5], [9], [11], [19]. The GPS literature recommends using a PLL/FLL combination that closes the bandwidth with an FLL and then switches to the PLL [19].

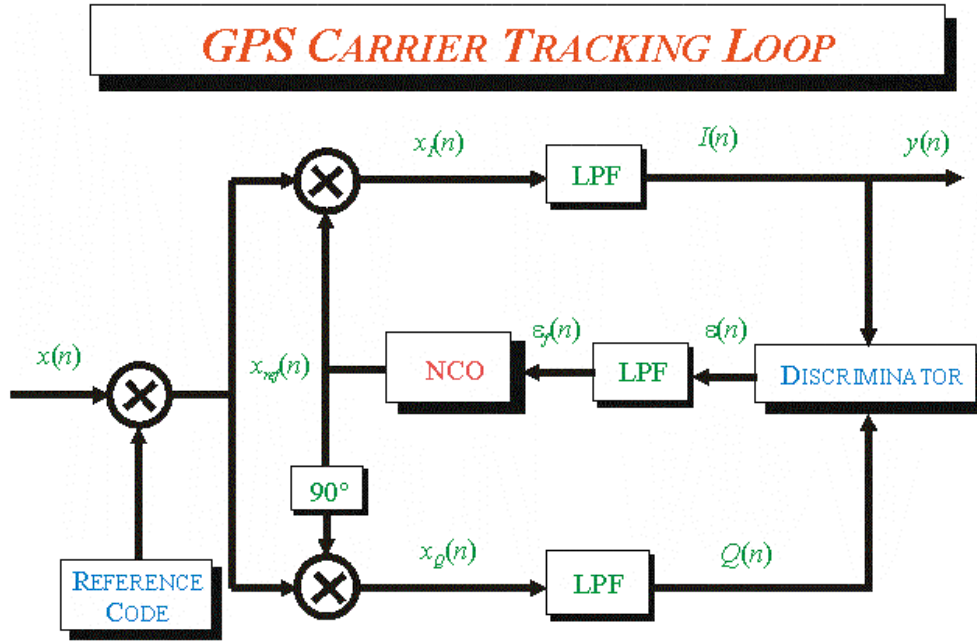


Figure 2.17 GPS carrier tracking loop - taken and modified from [11].

In continuous-time systems, a frequency $\omega(t)$ is defined as the change in phase angle over time

$$(2.1.104) \quad \omega(t) = \frac{d\theta}{dt}.$$

In digital systems, we approximate the derivative by using the change in phase angle over two consecutive inputs

$$(2.1.105) \quad \omega_i = \frac{\Delta\theta_i}{\Delta t_i} = \frac{\theta_i - \theta_{i-1}}{t_i - t_{i-1}}.$$

The phase angles are available via the atan2() function, and for GPS the denominator in equation (2.1.105) is the coherent integration time T . Thus, the FLL discriminator will collect and demodulate (see 2.2.4.2.1.) two consecutive input values, then compute the frequency error

$$(2.1.106) \quad \delta f_i = \frac{\Delta\theta_i}{2\pi T} = \frac{\text{atan2}(Q_i, I_i) - \text{atan2}(Q_{i-1}, I_{i-1})}{2\pi T}.$$

We switched from frequency $[w]$ to error frequency $[w_i]$ because the complex phase angles of the \tilde{x} terms (see equation (2.1.63)) correspond to the phase error $d\mathbf{q}_i$.

The general discriminator (a.k.a. differential arctangent discriminator), given by equation (2.1.106), is computationally inefficient. Kaplan [19] provides a list of

discriminators requiring fewer calculations. Here we address two of those discriminators, one of which is equivalent to equation (2.1.106)

$$(2.1.107) \quad \delta f_i = \frac{\text{atan2}(I_{i-1}I_i + Q_{i-1}Q_i, I_{i-1}Q_i - Q_{i-1}I_i)}{2\pi T}$$

and the other of which is known as the cross-product discriminator given by

$$(2.1.108) \quad \delta f_i = \frac{I_{i-1}Q_i - Q_{i-1}I_i}{2\pi T}.$$

First, it is not obvious how equation (2.1.106) and equation (2.1.107) are similar, so some additional explanation is required.

In order for equation (2.1.107) to equal the frequency error $\Delta \mathbf{w}_i$, the following must be true

$$(2.1.109) \quad \text{atan2}(y, x) = \theta_i - \theta_{i-1}.$$

It can be easily seen that $\text{atan2}(y, x)$ is equal to the phase angle of the complex number $x + jy$, which, in fact, is

$$(2.1.110) \quad x + jy = \tilde{x}_i \cdot \tilde{x}_{i-1}^* = e^{j\theta_i} e^{-j\theta_{i-1}} = e^{j[\theta_i - \theta_{i-1}]}$$

We assume that a databit interval is T_b , and its relationship to the predetection interval T is given by

$$(2.1.111) \quad T_b = KT.$$

The expected value of the cross-product discriminator summed over a databit period, in terms of equations [5]

$$(2.1.112) \quad E\{\mathbf{df}'_k\} = E\left\{\sum_{i=1}^{K-1} \mathbf{df}_i\right\}$$

$$= 2 \frac{S}{N_0} TD_k \frac{\sin^2(\pi \Delta f_k T)}{(\pi \Delta f_k T)^2} \sum_{i=1}^{K-1} [\cos(\Delta \theta_{i-1}) \sin(\Delta \theta_i) - \cos(\Delta \theta_{i-1}) \sin(\Delta \theta_i)]$$

$$= 2 \frac{S}{N_0} TD_k \frac{\sin^2(\pi \Delta f_k T)}{(\pi \Delta f_k T)^2} \sum_{i=1}^{K-1} \sin(\Delta \theta_i - \Delta \theta_{i-1})$$

$$\approx 2 \frac{S}{N_0} TD_k \frac{\sin^2(\pi \Delta f_k T)}{(\pi \Delta f_k T)^2} (K-1) \sin(2\pi \Delta f_k T)$$

$$\approx 4\pi \frac{S}{N_0} T^2 D_k (K-1) \Delta f_k$$

for small Δf_i and assuming that [5]

$$(2.1.113) \quad \Delta \mathbf{q}_i - \Delta \mathbf{q}_{i-1} = 2\mathbf{p}\Delta f_i T = 2\mathbf{p}\Delta f_k T$$

over $K-1$ samples, with the first sample of the bit period being discarded. Also note that the discriminator is proportional to $\sin(2\pi\Delta f_k T)$ attenuated by the sinc^2 function and has more than one zero point as a function of Δf_k , some with some positive slope and some with some negative slope. Care must be taken when initializing the tracking loop with a large initial frequency because in order to avoid large phase errors T should be as small as possible and gradually increased to a minimum value of 10 ms for the cross-product discriminators.

Tracking error variance for the cross-product discriminator, in Hz, is [5]

$$(2.1.114) \quad V\{\delta f_k'\} = \frac{1}{2\pi^2} \frac{K}{K-1} \frac{B_l B^2}{S/N_0} \left(\frac{1}{K-1} + \frac{B}{2S/N_0} \right)$$

where $B = 1/T$ is the predetection noise bandwidth with a minimum of 100 Hz if $K = 2$. Prior to bit synchronization, when the times of bit edges are unknown, a predetection bandwidth of 1 KHz is used. In this case the first sample per bit would be discarded, and the variance becomes [5]

$$(2.1.115) \quad V\{\delta f_k'\} = \frac{1}{2\pi^2} \frac{B_l B^2}{S/N_0} \left(\frac{1}{20} + \frac{B}{2S/N_0} \right).$$

As discussed in [19] the FLL ignores navigation data, *provided that the input samples do not straddle a bit flip*. When this occurs, the $\Delta \mathbf{q}$ value is offset by n which (for $T = 1$ msec) is an unfiltered frequency error of 500 Hz – a significant amount.

Using a standard coherent integration time of $T = 1$ msec, we have at most 1 bit flip per 20 inputs, meaning 1 out of every 10 outputs may be in incorrect. The loop filter helps alleviate this. If we modify the FLL to provide an output for every input (see previous section), then it becomes 1 in 20. Also, once we get past initial tracking and complete the bit synchronization process, we know when the bit flips will occur and can adjust for them.

The situation becomes exacerbated, however, when we utilize a larger coherent integration time. For $T = 3$ msec, there is the possibility of a bit flip every 6.7 input samples, meaning every 3rd or 4th output may be invalid.

As the coherent integration time increases, FLL tracking performance is degraded. The effects of the navigation bits become more significant, and we may lose lock and/or tracking.

Depending upon the quality of lock, the Data Fusion Company's software receiver switches between FLLs and PLLs with varying bandwidth [11]. When these transitions occur the tracking loop is reset and restarted with new parameters. Similarly to the switch from acquisition to tracking, the loops are especially vulnerable for a short period immediately after restarting. If a loop fails due to an ill-timed navigation bit flip, tracking is lost and the receiver returns to the lengthy acquisition process. This algorithm provides an alternative fallback position by continuing to run the previous tracking loop in parallel.

A close look at equation (2.1.106) brings up another interesting point about FLL tracking loop - it does not provide any phase information. Thus, although the NCO-generated reference signal may be the correct frequency, it will most likely have some phase offset from the input carrier.

As mentioned previously, the $\text{atan2}()$ function returns a value between $\pm\pi$. Equation (2.1.107), therefore, limits the maximum frequency error to $500 \text{ Hz}/n$ (where ' n ' is the number of msec of coherent integration). Thus, $T = 1$ msec is 500 Hz, 3 msec is 167 Hz, and 10 msec is 50 Hz. This value is the maximum error the discriminator can handle before it starts to return invalid results. (Note the difference between this and the Costas PLL which tracks very well when it is exactly 180° out of phase due to its use of the $\text{atan}()$ function instead of $\text{atan2}()$.)

As long as the frequency error is within this boundary, the loop will function nicely. If we exceed the maximum error, however, $\text{atan2}()$ returns the wrong value. For example, if $\Delta\theta$ is 1.2π , the $\text{atan2}()$ function returns -0.8π and the reference frequency is adjusted in the wrong direction.

Once again we see that FLLs and coherent integration don't mix well. For $T = 3$ msec, our maximum error is 167 Hz – a reasonable value in the early stages of tracking.

2.2.4.2.5 GPS Receiver Carrier Tracking Loop

So far we have seen the GPS receiver code tracking (DLL) and frequency tracking (AFC) loops. A DLL is a code-tracking loop whose discriminator measures code phase time delay. An AFC is a FLL whose discriminator measures frequency (essentially the Doppler) of the carrier. In order to track the carrier phase, a PLL should use phase tracking discriminators that measure carrier phase. Three carrier tracking discriminators are provided below [5]

$$(2.1.116) \quad \delta\theta_i = Q_i I_i \text{ (Generic Costas discriminator)}$$

which is presented earlier (see 2.2.4.2.2) [5]

$$(2.1.117) \quad \delta\theta_i = Q_i \text{sign}(I_i) \text{ (Decision-directed Costas discriminator)}$$

where $\text{sign}(I_i)$ is also the sign of the databit D_i with an ambiguity of 180°

$$(2.1.118) \quad \delta\theta_i = \text{atan2}(Q_i, I_i) = \text{atan}(Q_i, I_i) \text{ (arctangent discriminator)}.$$

The computation of all of the above discriminators must be performed within a databit period. Except for the possible operation prior to achieving bit synchronization, they are usually computed over the entire bit period [5].

Figure 2.17 depicts a standard GPS carrier-tracking loop, which is a combination of a generic tracking loop shown in Figure 2.14 and of I/O demodulation shown in Figure 2.13. From the input signal $x(n)$ we strip the code and the carrier leaving the navigation data as the output signal, $y(n)$. The complex signal $I(n) + jQ(n)$ is passed through a discriminator and filtered to determine the carrier tracking error, $\varepsilon_f(n)$, which is then used by the NCO to generate a new GPS reference signal.

A block diagram of the Costas loop implementation is given in Figure 2.18 [18]. It is very similar to the structure shown in Figure 2.17. The main difference is in the main phase detection function, which is an arctangent discriminator function. This is the optimal (maximum likelihood estimator) phase detector, but also the most computationally expensive [19]. Assuming that the loop operates in the lock mode, the modulated data bits are present on the in-phase arm of the Costas loop directly after the low pass filter.

The advantage of a Costas PLL over a regular PLL is the usage of the two quadrant discriminator, $\text{atan}()$, over the fourth quadrant discriminator, $\text{atan2}()$, which enables the former to easily handle 180° phase shifts [9].

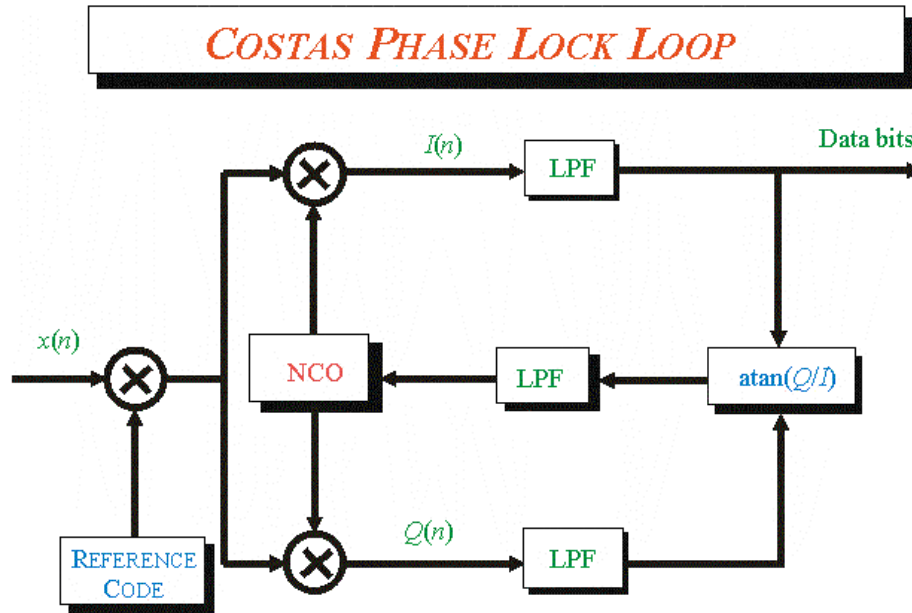


Figure 2.18 Costas phase lock loop - taken and modified from [11].

2.2.4.3 GPS Receiver Bit Synchronization

If the acquisition process succeeds then the next step is data bit alignment or synchronization. Since twenty C/A code periods are contained in one data bit transition then a special mechanism is in place to determine the data bit transition. This process continues until a successful data bit alignment is achieved. If this process fails then the signal acquisition should restart.

At this point the start of each C/A code period is known; however, the start of the navigation data bit is unknown, which contains several navigation C/A code periods. There are several techniques used to perform bit synchronization search; i.e., determining the data bit timing and eliminate the navigation bit offset ambiguity.

The algorithm senses sign changes between successive code periods and records these sign changes by incrementing the count in the bin corresponding to that particular code period. The code offset can be determined from a peak in the histogram that exceeds a pre-specified upper threshold. In the absence of noise, a peak will occur only at the true offset value. Due to random, noise-related perturbations to the signal, it is possible that peaks may appear at bins other than the true code offset. In the presence of noise, two possibilities exist: either the noise is weak enough that the noise-influenced bins appear as background noise about the dominant peak or it is strong enough such to result in more

than one dominant peak, with each of these peaks exceeding a pre-specified lower threshold.

The procedure for histogram implementation in the Data Fusion Company receiver is as follows: [5].

1. A cell counter is arbitrary set to run from 0 to 19.
2. Each sensed sign cell is recorded by adding 1 to the histogram cell corresponding to K_{cell} .
3. The procedure continues until one of the following occurs
 - (a) Two cell counts exceed the threshold NSB_2 .
 - (b) Loss of lock
 - (c) One cell count exceeds the threshold NSB_1 .
4. If (a) occurs then bit synchronization fails because of low C/N_0 or lack of bit sign transition, and bit synchronization is reinitialized. If (b) occurs then lock is reestablished. If (c) occurs then bit synchronization is successful, and C/A code period count is set to the correct offset.

Figure 2.19 illustrates a successful GPS receiver bit synchronization histogram. The code navigation ambiguity is resolved and the NAV bit offset is set to 8. The NAV bit offset is defined as the number of C/A code periods preceding the first code period of a complete bit.

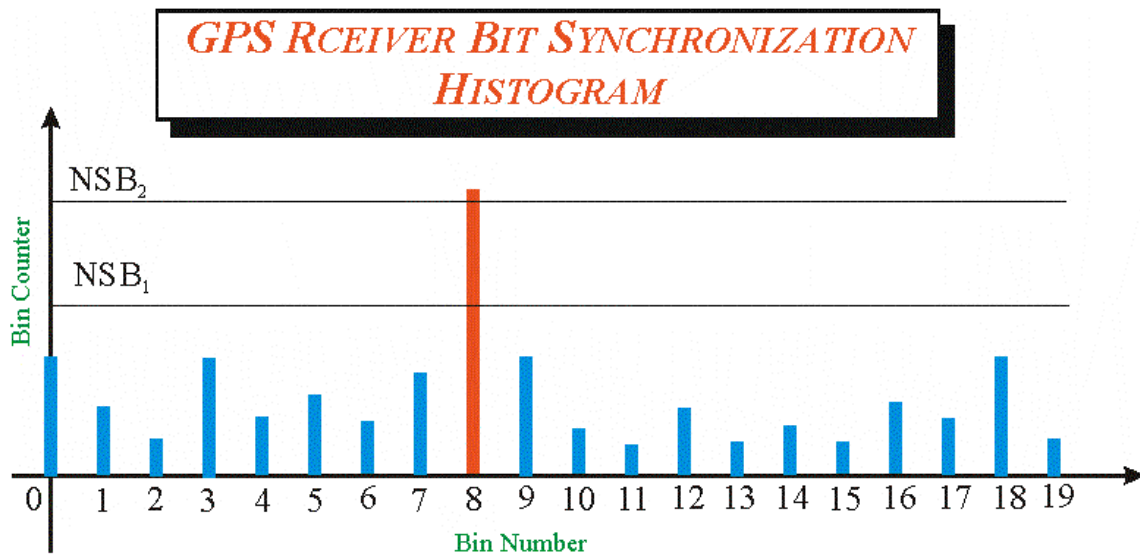


Figure 2.19 Illustration of bit cell statistics - with noise- - taken and modified from [11].

For example, a C/A code sequence with an offset of 0 would begin with the first code period of a complete bit. An offset of 5 would have five preceding code periods of the previous bit and then begin with the 6th period of the current bit.

Analysis for deriving the upper and lower histogram thresholds is provided in [11].

Subframe synchronization begins once data bit synchronization is established.

2.2.4.4 GPS Receiver Subframe Alignment

Frame synchronization is required in order to process the GPS data. When timing uncertainties are large, parity decoding is not possible since the boundaries of the words are unknown. The following section details the procedure necessary to synchronize frames.

The algorithm for positively finding the correct preamble and performing frame synchronization is as follows [5],[11]:

1. Search for either an upright or inverted preamble.
2. When one is found, which could be a legitimate pattern somewhere else in the data stream, a check is required to see if it is the beginning of a 30-bit word. This is accomplished by collecting the following 22 bits and checking parity. If parity does not pass, the candidate preamble is discarded.
3. If parity passes, it verifies that the preamble existed at the beginning of a word. The parity algorithm will also resolve the sign ambiguity. However, there are also legitimate such patterns at beginning of other words, so additional checks are required. If it is the correct TLM word, the following word must be a HOW word that contains a truncated Z-count. The first eight bits of this truncated Z-count can also resemble a preamble. (The reader is reminded that the structure for the TLM and HOW words is given in Figure 2.6)
4. Parity should pass on the HOW word. If not, the frame synchronization procedure should be restarted. Two checks can be made to verify a legitimate HOW word. First, the Z-count must be reasonable and second, it must agree with the sub-frame count. Of course, there is a small probability that these conditions could also occur elsewhere in the message. Thus, further checking is required.
5. If the HOW seems legitimate, provisional demodulation of the other words can commence, and they can be stored in memory. A final check on the next preamble

and next Z-count solidifies the frame synchronization. That is, the preamble is where it is supposed to be, and the Z-count increments by one.

2.2.5 Issues

Despite its success as a world navigation and positioning system, the GPS system was not intended to operate in areas of obstructed signal visibility, indoors, underground, or underwater. In these environments the GPS signal quality is deteriorated due to additional channel errors unaccounted for in the GPS design and signal specifications; hence, the reported GPS accuracy for such environments is questionable. Several alternatives can be pursued to overcome this disability of GPS. (1) The GPS modernization and GPS III is going to enhance the GPS signal structure and to some extent provide far better capabilities than what currently is offered by GPS. (2) A pseudolite geolocation system can be exploited to navigate and localize users indoors or underground. Wireless networks can be employed to provide localization indoors and outdoors.

2.3 GLONASS

In chapter 1 we have described the GLONASS as a system with three main segments: the space segment, the control segment, and the user segment. Here we discuss the principle of operation (see §2.3.1), the GLONASS satellite (see §2.3.2), the GLONASS receiver (see §2.3.3), the method for extracting the observable (see §2.3.4), and issues related to GLONASS for indoor positioning (see §2.3.5).

2.3.1 Principle of Operation of GLONASS

GLONASS seeks to provide high-precision position-fixing and time-reference capability on a worldwide and continuous basis to users on the Earth's surface, on land and at sea, in the air, and in space itself. Under the control of highly stable, onboard frequency references (clocks), timing signals (epochs) and data are transmitted simultaneously from all satellites. The data received from a particular satellite includes precise ephemerides for that satellite, which can result in precise position and velocity determination at a given time. In addition, each satellite provides information on the behavior of its own onboard clock. The receiver simultaneously performs time of arrival

(TOA) measurements from three satellites and employs the received data to compute the position of the satellites. Given a synchronized ground time reference, the observer can then, in principle, solve three range equations for three unknown position coordinates. In practice the user will not have a synchronized time reference; hence, the user will use the pseudorange measurements from four satellites to resolve its 3D position and local time [3].

The GLONASS principle of operation is illustrated in Figure 2.20. As depicted in Figure 2.20 the GLONASS principles of operation are almost identical to the GPS principles of operation. If the reader can substitute $T_{GLONASS}(TX)$ for $T_{GPS}(TX)$, $T_{GLONASS}(RX)$ for $T_{GPS}(RX)$, and GLONASS for GPS the rest of the GPS principles of operation in §2.2.1 would be in fact a discussion on the GLONASS principles of operation.

2.3.2 GLONASS Transmitter (Satellites)

The discussion on the GLONASS satellite includes a discussion on the signal structure and design (see §2.3.2.1), message format and content (see §2.3.2.2), satellite ephemeris (see §2.3.2.3), satellite almanac (see §2.3.2.4), and onboard clocks (see §2.3.2.5).

2.3.2.1 Signal Structure Design

Every GLONASS satellite transmits information continuously in form of messages on its position and GLONASS reference time. For military purposes such as hiding the user position from the adversary, first the GLONASS user just like the GPS user is expected to play a passive role. Second, the navigation message is protected to some extent from any deliberate interference or jamming by employing spreading codes, which increase the bandwidth occupied by the signal and that of a potential jammer. From the civilian point of view, spreading serves two purposes: it minimizes interference to others and it provides sufficient bandwidth for the definition of the epoch timing edge [10].

The two transmission carrier frequencies, chosen for the GLONASS satellite, lie in the L-band, around 1250 MHz (L_2) and 1607 MHz (L_1) as depicted in Figure 2.21. Dual-frequency navigation transmissions at L_1 and L_2 allow the user to correct for ionospheric propagation effects. A high-precision code is modulated into both carriers: whereas, the lower-precision civil code only appears at L_1 . Russian publications refer to the services

provided by low “C/A” and high “P” precision codes as the GLONASS Standard Positioning Service (SPS) and as the GLONASS PPS respectively. Spread-spectrum techniques are primarily intended to reduce the jamming and interference effects on these signals [10].

GLONASS employs FDMA as the modulation scheme as opposed to GPS, which relies on the CDMA modulation scheme to achieve multiple access capability. The radio frequencies used by GLONASS are channelized within the bands 1240–1260 MHz and 1597–1617. The channel spacing, Δf_i , is given by [10]

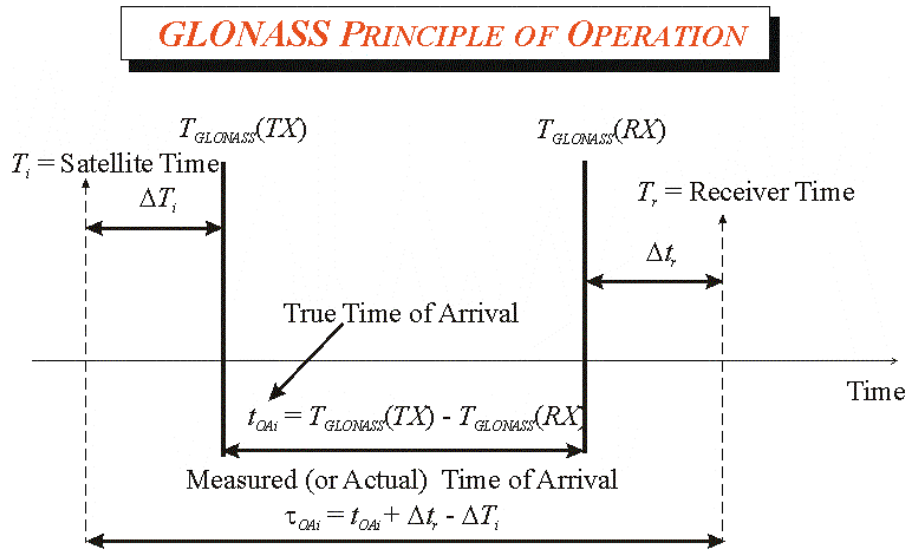


Figure 2.20 The principle of operation of GLONASS.

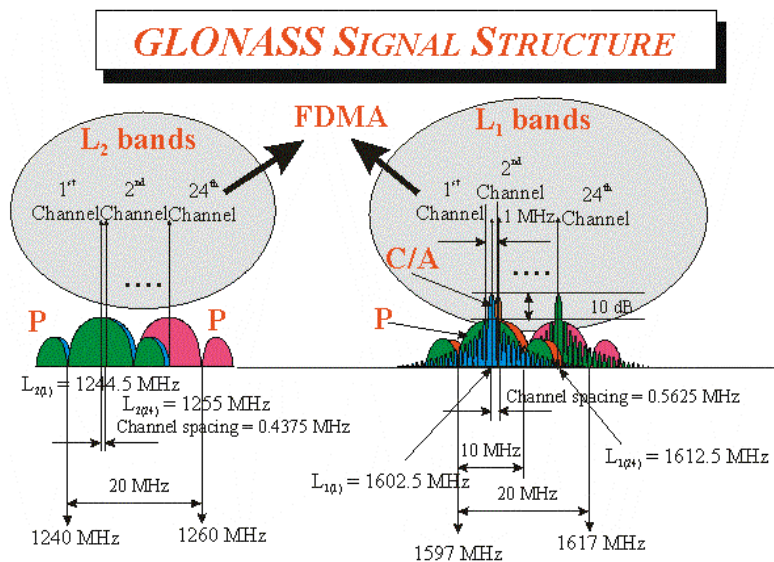


Figure 2.21 The GLONASS signal structure and frequency allocation.

$$(2.2.1) \quad \Delta f_i = \begin{cases} 7/16 \text{ MHz}, & L_2(i=2), \\ 9/16 \text{ MHz}, & L_1(i=1), \end{cases} = \begin{cases} 0.4375 \text{ MHz}, & L_2(i=2), \\ 0.5625 \text{ MHz}, & L_1(i=1). \end{cases}$$

The carrier frequencies themselves are also multiples of channel spacing, Δf_i , and the channel number, k , for $k = \{1, \dots, 24\}$. The relationship between channel number, k , and the L_i transmit frequencies, $L_{i(k)}$, is given by [10]

$$(2.2.2) \quad L_{i(k)} = f_i + k \times \Delta f_i, \text{ for } k = \{1, \dots, 24\}$$

where

$$(2.2.3) \quad f_i = \begin{cases} 1244 \text{ MHz}, & i = 2, \\ 1602 \text{ MHz}, & i = 1. \end{cases}$$

At the L_2 frequency, only the P code is carried, but at L_1 both codes are transmitted on the same carrier, one in phase and the other in quadrature. This results in a signal spectrum that superimposes the two individual spectra whose bandwidths differ by a factor of 10. Because both transmissions carry roughly the same power, a spectrum analyzer will display the narrow band-code at 10 times the strength of the wide-band code (see Figure 2.21) [10].

Each satellite sends data at 50-baud rate, superimposed on a pseudorandom related sequence, to enable the receiver to compute its own position at any reference time. The GLONASS low precision (C/A) code is 511 bits long. This code sequence lasts only 1 ms; therefore, the C/A code rate is 511 KBPS. The P code rate is 10 times the C/A code rate or 5.11 MBPS [10].

Both GLONASS codes are generated as maximum length sequences. For a complete discussion of the maximum length sequences the reader should refer to Appendix D “Spreading Codes.” The generating polynomials for both codes are [10]:

$$(2.2.4) \quad \text{C/A-code generator } g(x) = 1 + x^5 + x^9$$

$$(2.2.5) \quad \text{P-code generator } g(x) = 1 + x^3 + x^{25}$$

the latter being truncated every 1 second.

The first nulls in the transmitted spectrum occur at \pm the bit rate. Hence, bandwidths for GLONASS transmission can be taken at 1 MHz and 10 MHz for the C/A code and P codes, respectively (see Figure 2.21) [10].

Moreover, each data bit occupies 20 entire code sequences; i.e., when the data bit is a '0' 20 periods of the C/A code itself are sent and when the databit is a '1' 20 periods of the C/A code inverse are sent. In this manner the information spectrum is spread across a wide bandwidth. Due to the corruption of the signal with Gaussian noise whose power level is proportional to the bandwidth and other errors the signal will become immersed in the noise at the receiver's end and recoverable by reversing the coding operation applied at the transmitter. This implies that the receiver has knowledge of the pseudorandom codes [10]. To transmit the encoded data, a binary phase-shift keying (BPSK) modulation technique is employed. There is no need in GLONASS for HOW as with GPS to allow acquisition of the P-code [10].

2.3.2.2 Message Format, Content, and GLONASS Time

The 50-Hz data essentially provides information on accurate positions and the onboard frequency standard for the transmitting satellite. Data in form of low-precision almanacs of all satellites assists the GLONASS receiver to obtain signal acquisition. Data are sent in lines, subframes, and frames with preambles and parity checks at the end of each line. Essentially, each subframe divides into a 5-line set of ephemeris data (including clock correction) and a 10-line set of almanac data. In this way, the subframe accommodates the almanacs of five satellites; the full constellation of 24 satellites occupies five complete subframes, the last of the 25 almanacs always being set to zero (spare). The subframe format is shown in Figure 2.22.

The start of each line marks the beginning of a 2-second subframe synchronized to GLONASS system time. The leading bit is always '0' and followed by a line number, various databits, parity bits, and a preamble. Some information bits are flags (for example, words P1-P5) not used by the receiver. The flag H on line 2 is most important, referring to the "health" of the space vehicle ('1' means unhealthy).

The symbol TA gives the time of transmission in hours, minutes, and half-minutes Moscow Standard Time [MST (GMT + 3 h)]. The symbol TE gives the time of validity of the ephemeris in hours and quarter-hours (MST). Usually the ephemeris is valid at odd quarter-hours, but occasionally (when a satellite is temporarily unhealthy) the ephemeris will be valid only on the half-hour. The remaining databits are described in [10] and [21].

GLONASS C/A-CODE DATA MESSAGE											
1	0 1	Line 4	P4 2	P1 2	TA 12		\dot{X} 24	\dot{Y} 5	X 27	Parity 8	Post- amble 0.3s
2			H 1	P2 2	P1 1	TE 7	\dot{Y} 24	\dot{Y} 5	Y 27		
3			P3 1	a1 11			\dot{Z} 24	Z 5	Z 27		
4			a0 22			P5 5	A.ode 5				
5			Day No. 11		A0 28						
6			V 1	Alm 5	a0 10	East Long 21	Inclination 18	Eccentricity 15			
7			Perigee 16		Equator Time 21	P 22	\dot{P} 7	Chn 5	0 1		

Figure 2.22 GLONASS message content and format - taken and modified from [10].

2.3.2.3 Satellite Ephemerides

In GLONASS, the satellite's instantaneous position and velocity are computed in an ECEF frame and are updated at fixed intervals of time (usually one half-hour). Satellite positions and velocities at intermediate times are calculated using interpolation procedures and acceleration terms, if the latter are provided. The resolution in satellite position and velocity are 0.5 m and 1 mm/s respectively [10].

GLONASS only transmits, in the ephemeris, two parameters relating to the satellite clocks, a_0 and a_1 . The first time offset (with resolution 1 ns) refers to the instantaneous time difference between space vehicle time and GLONASS system time. The second parameter (with resolution 1 in 10^{-12}) gives the rate of change of space vehicle time offset. Use of both parameters allows the user to establish individual space vehicle time offsets at any required instant of observation. Reference to GLONASS system time to Universal Coordinate Time/Soviet Union, UTC (SU) is by a single time offset parameter, A_0 (with a resolution of 7 ns) [10].

An additional parameter called age-of-data of ephemeris (ADOE) gives the integer number of days starting at the previous local midnight since the ephemeris data was

updated. On a particular day, the parameter will normally be '0', increasing by '1' each successive midnight unless, in the interim, the ephemeris data are based on a current (same day) set of measurements. When the GLONASS operates normally, this parameter is always either '0' or '1'. On occasion it has been observed to grow as large as 25 [10].

2.3.2.4 Satellite Almanac

Each GLONASS satellite transmits the same basic elements of an osculating (reduced) Kepler ellipse, which can be used to compute the satellite position.

The almanac data consists of a validity flag (V), an almanac number, a reduced-precision satellite clock phase offset, a set of orbital elements, and a satellite channel number. The set of orbital elements is presented as follows (all angular quantities are in semicircles and times are in seconds): (1) equator-crossing longitude; (2) inclination (offset 0.35); (3) eccentricity; (4) argument of perigee; (5) equator-crossing time; (6) period P (offset from 12 h); and (7) rate of change of period. The equator-crossing time of the reference orbit is always the first of the day. The reference number occurs at the start of the line 5. Day 1 corresponds to the first day of the year at the start of the 4-year leap cycle (currently 1 January 1992). The reference day number does not necessarily change each day—a set of almanacs is often allowed to remain unchanged for 2 days. The almanac number just referred to ranges from 1–25, each number in sequence (except the last) referring to a satellite location within one of the three reference planes. The first 8 almanac numbers (1–8) refer to location within the orbital arc in plane *one* starting with phase “0” and working around clockwise in steps of 45°. The second set of almanac numbers (9–16) refers to satellites in plane *two*. And the third set of 8 almanac numbers (17–24) refer to satellites in plane *three* [10].

The reader is reminded that the primary goal of almanac data is to allow the user to predict in fairly crude terms which satellites are above his local horizon at a given time and whether their geometry is favorable for navigation as is the case of GPS almanacs. However, the inclusion of a luni-solar correction term in GLONASS almanac message implies a position error perhaps an order of magnitude better than GPS almanac [10]. Almanacs are usually changed once a day at local midnight.

Table 2.3 GLONASS Satellite almanac message-- taken and modified from [10].

GLONASS SATELLITE ALMANAC

Day of validity
 Channel number
 Eccentricity
 Inclination
 Equator time
 Validity of almanac
 Equator longitude
 Orbital period
 Argument of perigee
 Luni-solar term
 Time offset

2.3.2.5 Onboard Clocks

GLONASS satellites carry three cesium standards. For a performance comparisons of the GLONASS and GPS clocks [22]. Over the years 1986-1989, a steady improvement in performance has been demonstrated with clocks on board spacecraft launched during 1989 showing the qualities of high-quality cesium standards of roughly the same level of performance as the GPS block I cesium's. Since 1989, the level of performance of onboard clocks has been consistently high. It is planned to use improved cesium clocks on future GLONASS satellites. These new clocks "Malachite" atomic standards will offer long-term stability five times better than the ones are currently in operation.

2.3.3 GLONASS Receiver

Every GLONASS satellite, just like a GPS satellite, transmits a timing epoch every millisecond. This would imply that raw pseudorange measurements could be produced to a rate up to 1000 times a second. In most applications, such a high rate of raw measurements is either not necessary or very expensive to achieve.

The block diagram of a GLONASS receiver is very similar to the block diagram of a GPS receiver (see Figure 2.8). Therefore, for discussion on the GLONASS receiver the reader may refer to §2.2.3.

2.3.4 Extraction of Observable(s)

The process for extracting an observable for GLONASS receivers is very similar with the process for extracting an observable for GPS receivers; henceforth, the reader may refer to §2.2.4.

2.3.5 Issues

For indoor positioning, in principle, GLONASS and GPS have similar disadvantages. Nevertheless, the GLONASS signal structure (FDMA modulation scheme) provides larger signal dynamic range than the GPS signal structure does. Henceforth, it is to a large extent preferred than the GPS signal structure is.

Because multipath and interference are the main sources of impairments; hence, the GLONASS signal is just as susceptible as the GPS signal is for indoor applications. These issues become more apparent when we discuss the GPS/GLONASS Pseudolite signal structure for indoor applications.

2.4 Examples for (Indoor) Geolocation Systems

In chapter 1 we introduced several indoor geolocation systems, such as GPS or GLONASS, Pseudolite based systems, the system developed by the US Coast Guard, the MIT indoor geolocation system, Mobile Phone Positioning, IEEE 802.11, and UWB based systems. In this section we discuss the two systems which are the most relevant to understanding the proposed WPI indoor geolocation systems discussed in detail in chapters 4 through 7. First, systems based on GPS or GLONASS pseudolites are commonly used in both indoor and aviation applications (see §2.5). These systems use an approach that is related to the CDMA/FDMA and OFDM/CDMA/FDMA indoor geolocation systems discussed in chapters 4 through 6. Second, the MIT indoor geolocation system (see §2.6) is related to our OFDM/FDMA indoor geolocation system, which is discussed in chapters 4 and 7.

2.5 A Pseudolite Geolocation System

The classical embodiment of a pseudolite-based geolocation system is to create a GPS-like system in which all pseudolites broadcast on the same carrier frequency. In this case, the signal separation (or multiaccess capability) is achieved by creating a spread

spectrum system in which each transmitter modulates its carrier using a pseudorandom noise code selected from a set of near orthogonal codes such as Gold or Kasami sequences. Such a system creates independent channels between the transmitter and receiver using a technique commonly known as Code Division Multiple Access (CDMA). For a small number of pseudolites it is relatively easy to find pseudorandom sequences which have good autocorrelation and crosscorrelation properties. For large numbers of pseudolites finding acceptable codes may be much more difficult.

Another embodiment of the pseudolite system would involve channelizing the frequency spectrum as is done in the GLONASS system. In this case each pseudolite transmits its signal on a separate frequency and signal separation is achieved through the signal frequency separation between individual pseudolites. This technique is commonly known as Frequency Division Multiple Access (FDMA). In this case synchronization between the pseudolite and the receiver (i.e., signal acquisition) is achieved by means of a maximum length sequence.

Since the characteristics of the receiver, and the issues that must be resolved, are very similar for GPS and GLONASS pseudolite systems, the remainder of this chapter will assume the use of a GPS-based pseudolite system.

2.5.1 Principles of Operation of a Pseudolite Geolocation System

The principles of operation for a pseudolite geolocation system are similar to the principles of operation for the GPS system. Figure 2.23 depicts the main principle of operation of the pseudolite system. The reference time at the transmitter (pseudolite) or receiver ($T_{REF}(TX)$ or $T_{REF}(RX)$) can either be a local reference time or the GPS time if it is known. The receiver measures the TOA between the pseudolite and the receiver and then the receiver derives several measurements based on this initial observable. These measurements are the pseudorange, Doppler, and accumulated carrier phase.

There are several advantages to using a pseudolite system. In many applications, the location of the pseudolites can be known either with extremely good accuracy (millimeter-level) or with good accuracy (centimeter to meter-level). Moreover, the motion of the pseudolites may also be well known since the pseudolites are often in fixed locations with earth so any measured Doppler will be due to user motion. As a result, if

the user is initially static then the acquisition process for a pseudolite receiver is much faster than the one for a normal GPS receiver. Further, the designer has much better control of the position of the pseudolites and therefore can adjust the system geometry to optimize system accuracy. Because there is no need for ephemerides, the pseudolite signal design and message format can be simpler than either the GPS or GLONASS signal design and message format.

Despite the great benefits and advantages that a pseudolite system offers, there are a number of technical difficulties associated with pseudolite systems.

First, when a pseudolite is in close proximity to a receiver, that pseudolite can potentially jam the signal coming from a far away pseudolite. This phenomenon is known as the *near-far* effect and is introduced here to give the reader an understanding of the problem. A formal investigation of the near-far effect is presented in §2.5.5.

Suppose that the transmitted power is P_t (dB) above the noise floor, which is assumed to be at 0 dB (see Figure 2.24) and that the propagation losses from the 1st transmitter are p_1 . The signal coming from the 1st pseudolite will be received at a power level given by [23]:

$$(2.3.1) \quad P_{r1} = P_t - p_1.$$

Similarly, the signal coming from the 2nd pseudolite will be received at a power level given by

PRINCIPLE OF OPERATION OF A PSEUDOLITE INDOOR GEOLOCATION SYSTEM

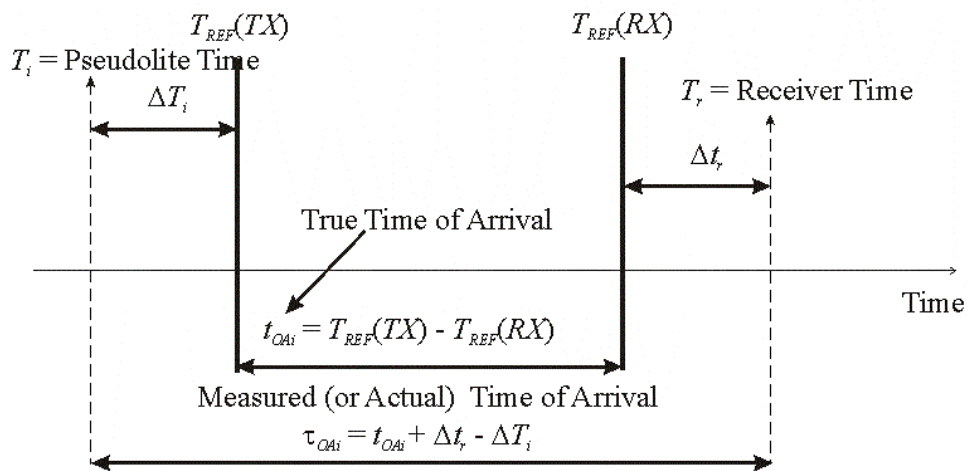


Figure 2.23 The principle of operation of a pseudolite indoor geolocation system.

$$(2.3.2) \quad P_{r_2} = P_t - p_2.$$

If we assume that a family of Gold code sequences of period 1023 is used, then the autocorrelation peak is approximately 30 dB and the maximum crosscorrelation is approximately 15 dB. The necessary conditions for acquisition of signals coming from the 1st and 2nd transmitters is [23]

$$(2.3.3) \quad P_{r_i} \geq -30 \text{ dB, for } i = \{1,2\}.$$

The sufficient condition for the near-far effect to occur is given by [23]

$$(2.3.4) \quad |P_{r_1} - P_{r_2}| > 15 \text{ dB.}$$

Assuming that the power P_{r_1} is constant, then variability of P_{r_2} can cause the near-far effect. Therefore, the necessary and sufficient condition for acquisition of both signals (accounting for the near-far effect) is given by [23]

$$(2.3.5) \quad P_{r_i} \geq -30 \text{ dB, for } i = \{1,2\}, \text{ and } |P_{r_1} - P_{r_2}| \leq 15 \text{ dB.}$$

It is important to mention that systems [24]-[28] assume that the pseudolites use a conventional GPS signal structure, which is basically a CDMA scheme based on a 1023-Gold code family running at a chipping rate of $R_c = 1.023 \text{ MHz}$ [2]. The signal separation achieved employing this Gold code family of period 1023 is approximately 15 dB. Moreover, it is well known that the Gold code set with a period of 1023 (which contains 1025 Gold sequences [29]) is sub-optimal with respect to the Sidelnikov and Welch lower bound formula by a factor of $\sqrt{2}$ because the order of the generating primitive polynomial is 10 (even) [29]. The near-far effect has always been an issue for conventional pseudolite systems because such systems have preserved the properties of a conventional GPS system. This is not a problem for the GPS satellites since the extreme separation between the satellites and the receiver means that the received signal strengths will be similar for each satellite. This is clearly not the situation in an indoor geolocation system [23].

Second, the pseudolite signal power level is stronger than the satellite signal power level on the ground. Hence, if the pseudolite signal occupies the same frequency bandwidth as the GPS or GLONASS do, then it can potentially jam either one of these signals. This is known as a *compatibility issue* of the pseudolite signal design (see §2.5.5.2 for further details).

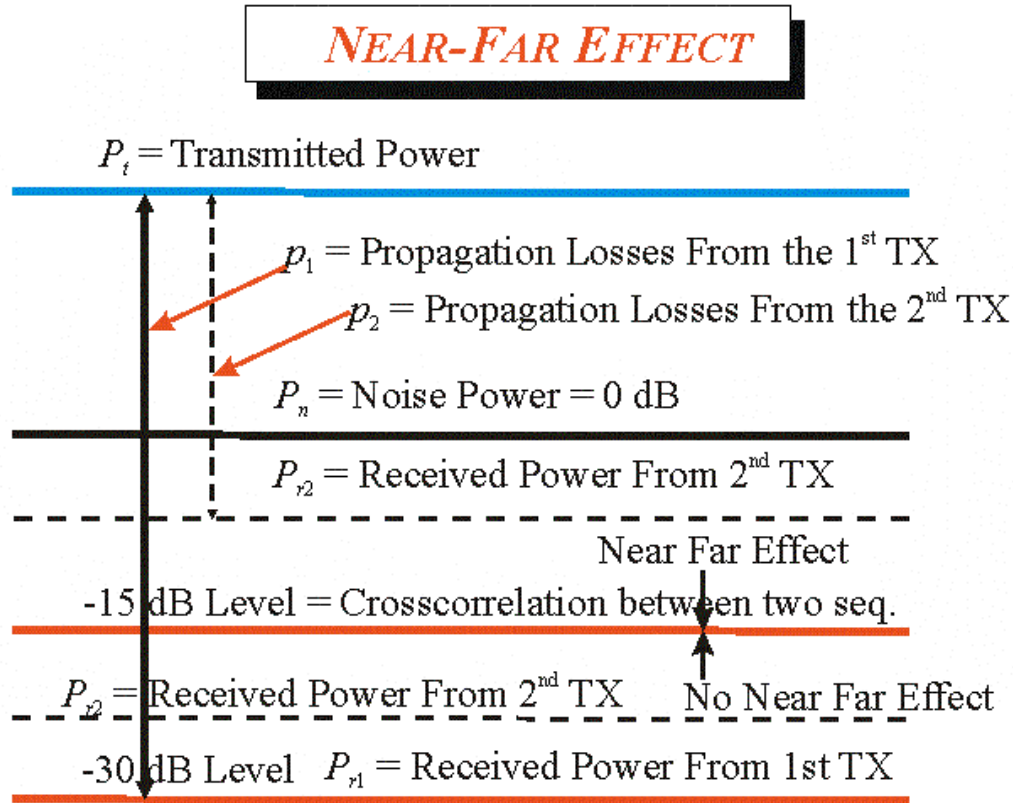


Figure 2.24 The near-far effect- - taken and modified from [23].

Other issues relevant to this system include the deployment requirements, relative synchronization between pseudolites, signal data rate, signal integrity monitoring, user antenna location and sensitivity, and system cost. We remind our readers that the focus of this research is on the signal structure, the steps that lead to obtaining the observable, and issues associated with this process.

2.5.2 Transmitter (Pseudolite)

Two approaches can be followed to design a pseudolite. A pseudolite can be designed to operate within or outside the GPS frequency bands (L_1 : 1565–1585 MHz or L_2 : 1217–1237 MHz). The main concern for designing a pseudolite to operate within the GPS frequency bands is the compatibility with the GPS system; i.e., pseudolites become potential interference sources to the GPS signal. The main concern for designing a pseudolite to operate outside the GPS frequency bands is the interoperability of pseudolite receivers with GPS receivers. In both cases the near-far problem remains an issue.

Some have favored the first approach because to them the interoperability issue was the most important and they have proposed a solution to the compatibility issue. Using the first approach pseudolites can be configured to cover a limited area with a power level low enough to preclude appreciable interference to standard GPS signals [30]. Moreover, a pulsing scheme with fixed or random duty cycle rates is utilized to make the impact of the pseudolite signal on the reception of GPS signals as transparent as possible.

Others have favored the second approach because to them the compatibility issue is more important than the interoperability issue. WPI indoor geolocation systems discussed in chapters 4 through 7 fall into the second approach.

We refer to the first approach as the conventional pseudolite signal design and the second approach as the novel pseudolite signal design.

2.5.2.1 Conventional Pseudolite Signal Design

There are five concerns which must be resolved for a conventional pseudolite signal design: C/A codes, frequency offset, pulsing scheme, pseudolite carrier tracking, and pseudolite transmit power [30].

First, a study referenced in [30] identifies 19 C/A codes with best crosscorrelation properties and 712 balanced codes with properties almost as good as the 19 best C/A codes.

Second, the pseudolite carrier frequency is proposed to have an offset of 1.023 MHz on either side of the L_1 , because the first null of the GPS spectrum occurs at the frequency $L_1 \pm 1.023$ MHz [30].

Third, the pulsing scheme is derived based on the pseudolite message bit rate of 50 N BPS (where $N = 1, 2, 4, 5, 10, \text{ or } 20$). Each pseudolite code cycle (1 ms) is divided into 11 slots, each with a width of $1/11,000$ s ($90.909090 \mu\text{s}$) and these pulses are never synchronous with a GPS bit pattern [30]. However, only one of the slots contain the pulse, so the duty cycle is $1/11$. Hence, there are $20/N$ pulses per bit, but only one is required because the receiver integrates the energy over the entire bit period. The C/A code is now received once every 11 ms. The clocking rate for the slots is $1/93$ of the C/A-code chipping rate of 1.023 MHz, or 11 kHz [30].

Fourth, there is a misconception that pulsing would prevent the tracking of the pseudolite signal carrier phase. This is not true if the pulses occur at a high enough rate, because one or more pulses will always be integrated along with noise over bit. This phenomenon is transparent to the tracking loop, because the phase change due to Doppler uncertainty over a bit is negligible. Hence, the pulsing signal looks continuous to the tracking loops [30].

Fifth, given an average power P_r through a receiving antenna (with gain G_a) at a distance d from a pseudolite, the average transmitted power, P_t , at the $L_1 \pm \Delta f$ is given by [30]:

$$(2.3.6) \quad P_t \approx P_r + 20 \log_{10} \left(\frac{4\pi d}{\lambda_1} \right) - G_a = P_r + 20 \log_{10} d + 101.75 - G_a$$

where $\lambda_1 = 19$ cm. For example, if we consider an average received power of -130 dBm at 37 km through an antenna gain of -10 dB, the average transmitted power is 7.77 dBm or about 6 mW. The peak power for a duty cycle of 1/11 is then 18.18 dBm, or about 66 mW. If we assume that a receiver receives two simultaneous signals from two pseudolites which transmit at the same signal level we have

$$(2.3.7) \quad P_{r1} \approx P_t - 20 \log_{10} d_1 - 101.75 + G_a \text{ and } P_{r2} \approx P_t - 20 \log_{10} d_2 - 101.75 + G_a$$

or

$$(2.3.8) \quad P_{r1} - P_{r2} = 20 \log_{10} \frac{d_2}{d_1}.$$

For example, if d_2/d_1 is taken from $\{0.01, 0.1, 1, 10, 100\}$ then the difference in power $P_{r1} - P_{r2}$ is given by $\{-40, -20, 0, 20, 40\}$ dBm. The difference in received power of the order of 20 dBm or higher can potentially lead to the near-far effect. The analysis of the near-far effect is more complicated than what is shown here and in §2.5.1. For a complete discussion of the near-far effect the reader should refer to §2.5.5.

2.5.2.2 Pseudolite Time Synchronization

Synchronizing a pseudolite clock to GPS time can be achieved in two ways: by collocating each pseudolite with a GPS reference receiver or by having a remote reference receiver that tracks the signals transmitted by each pseudolite [30]. In the latter case, the reference receiver sends corrections to the remote “slave” pseudolite to correct

itself and also sends message data (e.g., code- and/or carrier-based GPS corrections) to be transmitted. These two different pseudolite configurations are illustrated in Figure 2.25. In the collocated configuration, the reference receiver shares the transmit/receive antenna with the pseudolite, which also allows for self-calibration. Details of the master and slave pseudolite configuration are discussed in [30].

2.5.2.3 Message Format, Type, and Content

A pseudolite offers the possibility for an order of magnitude increase in the data rate (up to 1000 BPS vs. 50 BPS for the GPS) that can be supported via a GPS-compatible signal with essentially a firmware change in the user receiver [30].

The general format (see Figure 2.26) is patterned after the WAAS format with three differences—it may or may not include forward error correction (the addition of a 7 bit word see Appendix C) and the data rate can be higher than 250 BPS [30]. When the FEC is not included the data rate is up to 1 KBPS [30]; hence, an order of magnitude increase in the data rate. The time word is added as a convenience to the user receiver, because pseudolite time is not the same as GPS time. This is because the code-chipping rate is offset in frequency by approximately ± 664 chips per second, the feature that eliminates cross-correlation with the GPS signals. The actual pseudolite frequency can be chosen (at an offset from the spectral null of 710.4166667 Hz) so that the pseudolite week is exactly 393 s shorter than the GPS week. In fact, pseudolite time is, at any GPS time, given by [30]

$$(2.4.1) \quad t_{PL} = \left(1 \pm \frac{393}{604,800} \right) t_{GPS}$$

depending upon which null is selected. The pseudolite time is distributed over three 250-bit subframes making up a 21-bit word. The 21-bit time word represents the pseudolite time of week at the start of the currently transmitted 24-bit preamble with 0 at the beginning of the week. This pseudolite time word also serves as the reference time for the data in the messages. The data field consists of 205 information-bearing bits. The 24-bit parity is the same as the cyclic redundancy check (CRC) parity specified for the WAAS [30].

To avoid confusing the message types with those of the WAAS, the message type numbers starts at 40 [30] (see Table 2.4). Every message type would include a certain number GPS/ pseudolite signal integrity flags to provide a short time to alarm capability.

Every message broadcast contains integrity flags for several PRN numbers, with a minimum of 11, including the transmitting pseudolite. This allows for a positive integrity indication at least once per 0.5 s. Each can accommodate four satellites and/or pseudolites. Therefore, both pseudorange and carrier phase can be broadcast [30].

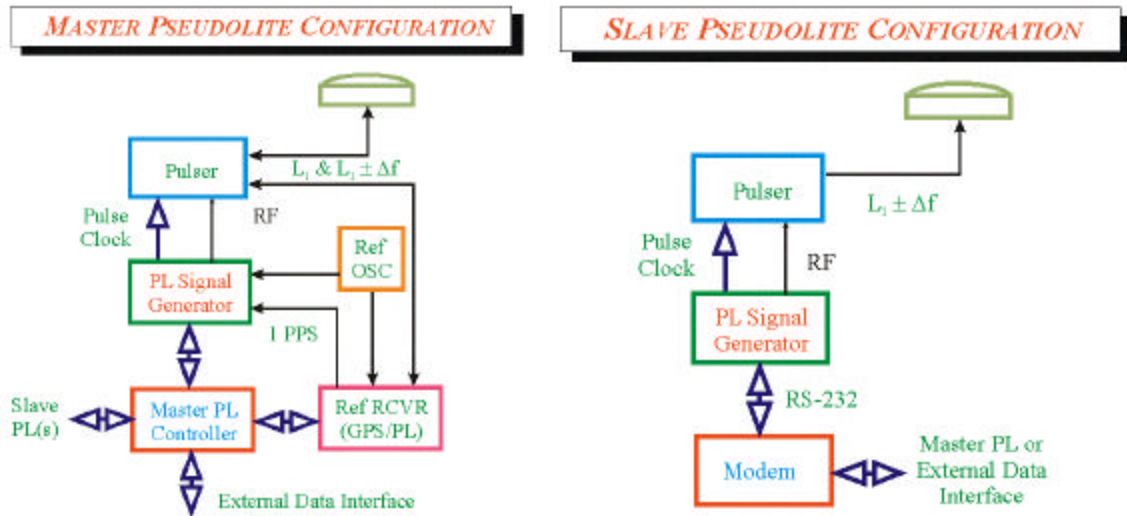


Figure 2.25 Master/Slave Pseudolite configuration-- taken and modified from [30].

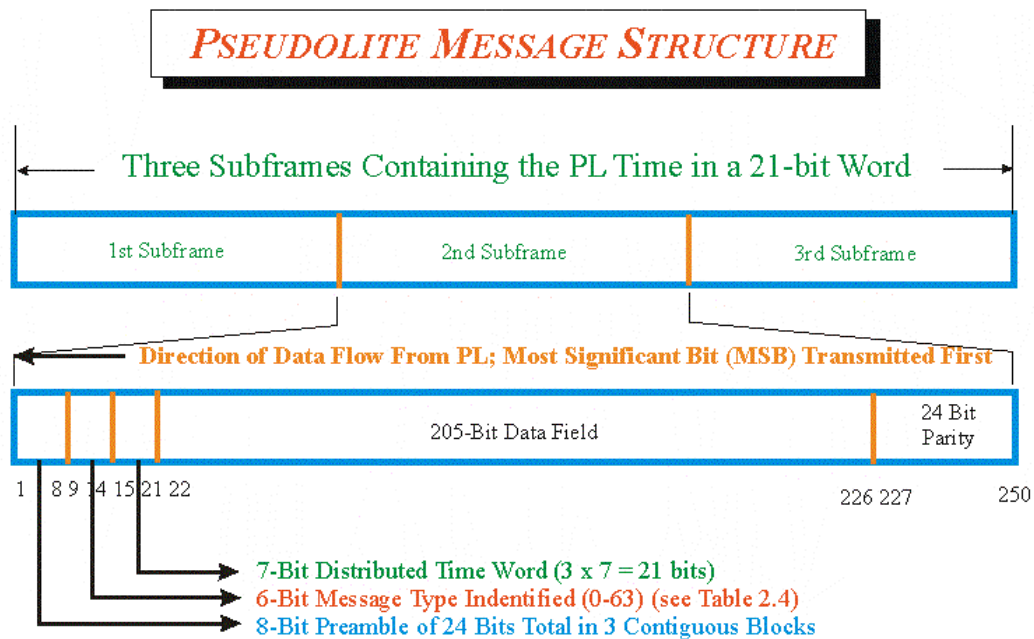


Figure 2.26 Pseudolite message structure-- taken and modified from [30].

Table 2.4 Pseudolite message types - - taken and modified from [30].

<i>PSEUDOLITE MESSAGE TYPES</i>	
TYPE	CONTENTS
40	Do not use this PL for anything (PL testing)
41	Integrity flags/Pseudorange corrections
42	Integrity flags/Carrier-phase corrections (if required)
43	Integrity flags/PL location and PRN assignment
44	Integrity flags/PL almanacs
45	Integrity flags/Precision approach path definition
46	Integrity flags/Special messages
63	Null message--Alternating '1' and '0'

2.5.3 Receiver

The design of a pseudolite receiver is similar to the design of a GPS receiver, which is extensively discussed in §2.2.3 and §2.2.4. However, for the purposes of discussing the interference between two pseudolite signals, and the impact of the pseudolite signal interference on the GPS signal, we use the simplified model of a pseudolite receiver shown in Figure 2.27.

There are five modules in the simplified receiver model: a Doppler removal and phase rotation module, a NCO, a correlator, a code generator, and an integrate and dump module. The input signal consists of a desired signal $s_i(t)$ and an undesired signal, $s_j(t)$. The reference phase consists of signal, $2\pi\Delta f_i t + \phi_i$, and the reference code consists of the signal, $C_i(t)$. The following section discusses these signals and modules in great detail.

2.5.4 Extraction of Observable(s)

The steps for obtaining an observable using a pseudolite receiver are exactly the same as the steps described in the GPS section for the extraction of observable(s) §2.2.4. Assuming that the receiver has reached a steady state condition (see Figure 2.27), the focus of this section is to present an analytical model necessary to address two main concerns of the pseudolite signal structure; namely, the near-far effect and the interference between the pseudolite and the GPS signals (see §2.5.5).

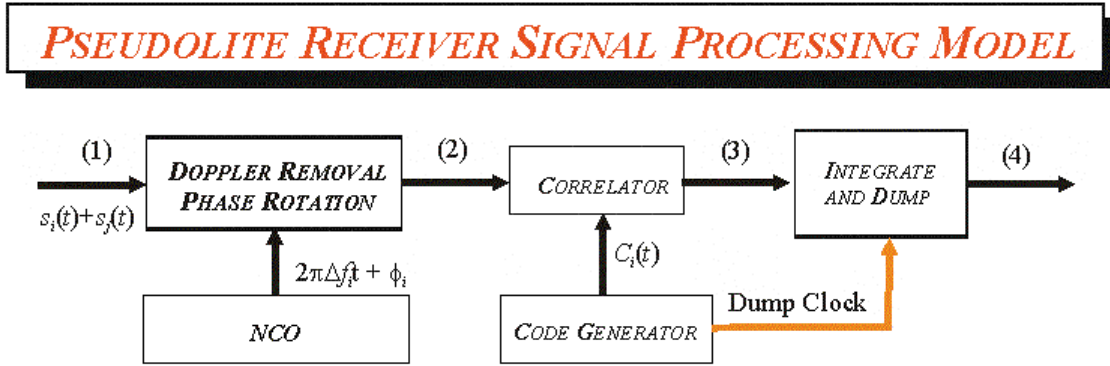


Figure 2.27 The block diagram of the signal-processing model of a pseudolite receiver-- taken and modified from [30].

Based on equation (2.1.8), ignoring the noise term, the P code, and the databit component, the desired in-phase and quadrature components of the input signals at (1), are given by [30]:

$$(2.4.2) \quad I_{i1}(t) = A_i C_i(t) \cos(2p\Delta f_i + \mathbf{f}_i) \quad \text{and} \quad Q_{i1}(t) = A_i C_i(t) \sin(2p\Delta f_i + \mathbf{f}_i)$$

and the undesired signal components are

$$(2.4.3) \quad I_{j1}(t) = A_j C_j(t + \mathbf{t}_j(t)) \cos[2p(\mathbf{d}f_j + \Delta f_j) + \mathbf{f}_j] \quad \text{and} \\ Q_{j1}(t) = A_j C_j(t + \mathbf{t}_j(t)) \sin[2p(\mathbf{d}f_j + \Delta f_j) + \mathbf{f}_j]$$

where the unknowns are: A_i , A_j are the signal amplitudes; $C_i(t)$, $C_j(t)$ are the signal C/A codes; Δf_i , Δf_j are the signal Doppler shifts; $\Delta \mathbf{f}_i$, $\Delta \mathbf{f}_j$ are the signal phases; δf_j frequency offset of undesired signal; and $\delta \mathbf{t}_j(t)$ time offset between signals.

2.5.5 Issues

By now the reader is very familiar as with the two main concerns of the pseudolite signal structure: the interference caused by cross correlation between C/A codes and the interference between a pseudolite signal and other to the GPS or pseudolite signals (near-far effect).

2.5.5.1 Interference Caused by Crosscorrelation Between C/A Codes

The reader is reminded that the pseudolite frequency of operation is within the GPS signal frequency and the spreading codes are selected from the C/A code family. The similarity of pseudolite and satellite signal structure is the cause of the interference between C/A codes. In essence there are two kinds of interference between C/A codes.

One is the interference of one or more C/A pseudolite code(s) on another C/A pseudolite code and the other is the interference of one or more C/A pseudolite code(s) on a GPS C/A code.

We recognize that interference caused by crosscorrelation between C/A codes is directly linked with the signal structure properties and the Doppler deference, which is going to become more apparent in the reminder of this section. The signal model illustrated in Figure 2.27 is employed to analyze the interference effect.

The Doppler removal and phase rotation process eliminates the desired signal's Doppler and phase shift so that the signal components at (2) in Figure 2.27 are given by [30]:

$$(2.4.4) \quad I_{i2}(t) = A_i C_i(t) \text{ and } Q_{i2}(t) = 0,$$

and the undesired signal components [30]

$$(2.4.5) \quad I_{j2}(t) = A_j C_j(t + \tau_j(t)) \cos[2\pi\Delta f_{ij} + \phi_j - \phi_i] \text{ and}$$

$$(2.4.6) \quad Q_{j2}(t) = A_j C_j(t + \tau_j(t)) \sin[2\pi\Delta f_{ij} + \phi_j - \phi_i].$$

where the Doppler difference is determined from [30]:

$$(2.4.7) \quad \Delta f_{ij} = \delta f_j + \Delta f_j - \Delta f_i.$$

For simplicity we assume that the code chips line up; i.e., the time offset between the i th and the j th signal is an integer number of chipping periods or [30]

$$(2.4.8) \quad \tau_j(t) = nT_c$$

where n is an integer, and T_c is a chip width (1/1,023,000 s). Also, assume full correlation for signal i . Then, at (3) we have the following [30]:

$$(2.4.9) \quad I_{i3}(t) = A_i \text{ and } Q_{i3}(t) = 0,$$

and the undesired signal [30]

$$(2.4.10) \quad I_{j3}(t) = A_j C_j(t + nT_c) C_i(t) \cos[2\pi\Delta f_{ij} + \phi_j - \phi_i] \text{ and}$$

$$Q_{j3}(t) = A_j C_j(t + nT_c) C_i(t) \sin[2\pi\Delta f_{ij} + \phi_j - \phi_i].$$

The signal components at (4) are then determined from [30]:

$$(2.4.11) \quad I_{i4}(t) = A_i T \text{ and } Q_{i4}(t) = 0,$$

$$(2.4.12) \quad I_{j4}(t) = A_j \int_0^T C_j(t+nT)C_i(t) \cos[2\pi\Delta f_{ij} + \phi_j - \phi_i] dt \text{ and}$$

$$Q_{j4}(t) = A_j \int_0^T C_j(t+nT)C_i(t) \sin[2\pi\Delta f_{ij} + \phi_j - \phi_i] dt ,$$

where T is a multiple M of 1 ms C/A-code repetition periods.

The power in the two correlated signals is given by [30]:

$$(2.4.13) \quad 2P_{i4} = I_{i4}^2 + Q_{i4}^2 = A_i^2 T^2$$

$$(2.4.14) \quad 2P_j(\Delta f_{ij}) = A_j^2 \left\{ \left[\int_0^T C_j(t+nT_c)C_i(t) \cos(2\pi\Delta f_{ij}t) dt \right]^2 \right. \\ \left. + \left[\int_0^T C_j(t+nT_c)C_i(t) \sin(2\pi\Delta f_{ij}t) dt \right]^2 \right\} .$$

Note that, through expansion using trigonometric identities, the dependence upon the phase difference has been removed in equation (2.4.14), which resembles the expression for a Fourier power spectrum component at the Doppler difference. For indoor applications, the pseudolites are stationary and the user motion can be characterized with small Doppler values; hence, assuming that:

$$(2.4.15) \quad \Delta f_{ij} \ll \frac{1}{T} \implies \Delta f_{ij} \ll 1 \text{ kHz}$$

we can make the following approximations

$$(2.4.16) \quad \cos(2\pi\Delta f_{ij}t) \approx 1 \text{ and } \sin(2\pi\Delta f_{ij}t) \approx 2\pi\Delta f_{ij}t .$$

Substituting equation (2.4.16) into equation (2.4.14) yields

$$(2.4.17) \quad 2P_j(\Delta f_{ij}) \approx A_j^2 \left\{ \left[\int_0^T C_j(t+nT_c)C_i(t) dt \right]^2 + \left[2\pi\Delta f_{ij} \int_0^T C_j(t+nT_c)C_i(t) t dt \right]^2 \right\} .$$

Next, we make the following approximations [29]:

$$(2.4.18) \quad \int_0^T C_j(t+nT_c)C_i(t) dt \cong M \sum_{k=1}^N C_{j+n} C_i T_c \leq M T_c [1 + \sqrt{2(N+1)}]$$

$$(2.4.19) \quad \int_0^T C_j(t+nT_c)C_i(t) t dt \cong M \sum_{k=1}^{M_E} C_{j+n} C_i \frac{T_c^2}{2} \leq M \frac{T_c^2}{2} [1 + \sqrt{2(N+1)}]$$

where N is the length of the C/A code (1023 chips), M is the number of C/A code periods within a bittransition (20 chips per bit), and T_c is the chipping period frequency (equal to $1/1.023 \mu\text{s}$).

Substituting the results of equations (2.4.18) and (2.4.19) into equation (2.4.17) yields

$$(2.4.20) \quad 2P_j(\Delta f_{ij}) \leq A_j^2 \left[1 + \sqrt{2(N+1)}\right]^2 \left[M^2 T_c^2 + M^2 \pi^2 (\Delta f_{ij})^2 T_c^4\right].$$

Thus the ratio of equation (2.4.20) to equation (2.4.13) (i.e., the crosscorrelation power ratio, ΔP_{ij}) is given by

$$(2.4.21) \quad \Delta P_{ij}(\Delta f_{ij}) \leq \frac{A_j^2 \left[1 + \sqrt{2(N+1)}\right]^2}{A_i^2 T^2} \left[M^2 T_c^2 + M^2 \pi^2 (\Delta f_{ij})^2 T_c^4\right]$$

$$= \frac{P_{ij} \left[1 + \sqrt{2(N+1)}\right]^2}{N^2} \left[1 + \pi^2 (\Delta f_{ij})^2 T_c^2\right]$$

where T is the integration period equal to MNT_c and P_{ij} is the input power ratio equal to A_j^2/A_i^2 . Assume that $\Delta f_{ij} = 50$ Hz we present the crosscorrelation power ratio, ΔP_{ij} (dB), versus the input power ratio, P_{ij} (dB), in Figure 2.28. The crosscorrelation power ratio, ΔP_{ij} (dB), increases proportionally with the input power ratio, P_{ij} (dB). For this particular example equation (2.4.21) is simply written as

$$(2.4.22) \quad \Delta P_{ij} = P_{ij} - 27 \text{ (dB)}.$$

As shown in Figure 2.28, the upper-bound crosscorrelation power ratio is about -27 dB for 0 dB input power ratio.

Assuming 0 dB input power ratio and based on experimental computations, Elrod and Van Dierendonck proposes that the average crosscorrelation power ratio vary as [30]

$$(2.4.23) \quad \langle \Delta P_{ij}(\Delta f) \rangle = \frac{1}{N} \text{sinc}^2 \left(\frac{\Delta f}{N} \right) \text{ or } \langle \Delta P_{ij}(\Delta f) \rangle_{dB} = -10 \log_{10} N + 20 \log_{10} \text{sinc} \left(\frac{\Delta f}{N} \right)$$

and Δf is given in kHz. The above closed form expression can be easily modified to include the input power ratio, P_{ij} (dB), hence we have

$$(2.4.24) \quad \langle \Delta P_{ij}(\Delta f) \rangle = \frac{P_{ij}}{N} \text{sinc}^2 \left(\frac{\Delta f}{N} \right) \text{ or } \langle \Delta P_{ij}(\Delta f) \rangle_{dB} = 10 \log_{10} \frac{P_{ij}}{N} + 20 \log_{10} \text{sinc} \left(\frac{\Delta f}{N} \right).$$

The above closed form expression is employed to produce the dashed line in Figure 2.28. As shown in the figure there is a very good agreement between the upper bound and the modified result from Elrod and Van Dierendonck [30].

Equation (2.4.24) suggests that the first null occurs at $f = 1.023$ MHz [30]. Based on this discussion, without changing the receiver structure, the pseudolite transmission frequency is selected at $L_1 \pm 1.023$ MHz. Although this solves the problem of crosscorrelation interference between a pseudolite signal and satellite signal, there is still a crosscorrelation problem between pairs of pseudolite signals.

Although a pseudolite can transmit at this frequency, there is potentially another problem, which is addressed next.

2.5.5.2 Interference Caused by Pseudolite Signal Level

So far we have treated the problem of interference based only on the code properties of the pseudolite signal. However, if a pseudolite signal is strong enough it can also interfere with the satellite signal simply because both signals carrier frequencies are almost the same. The simple mechanism to explain this problem is illustrated below.

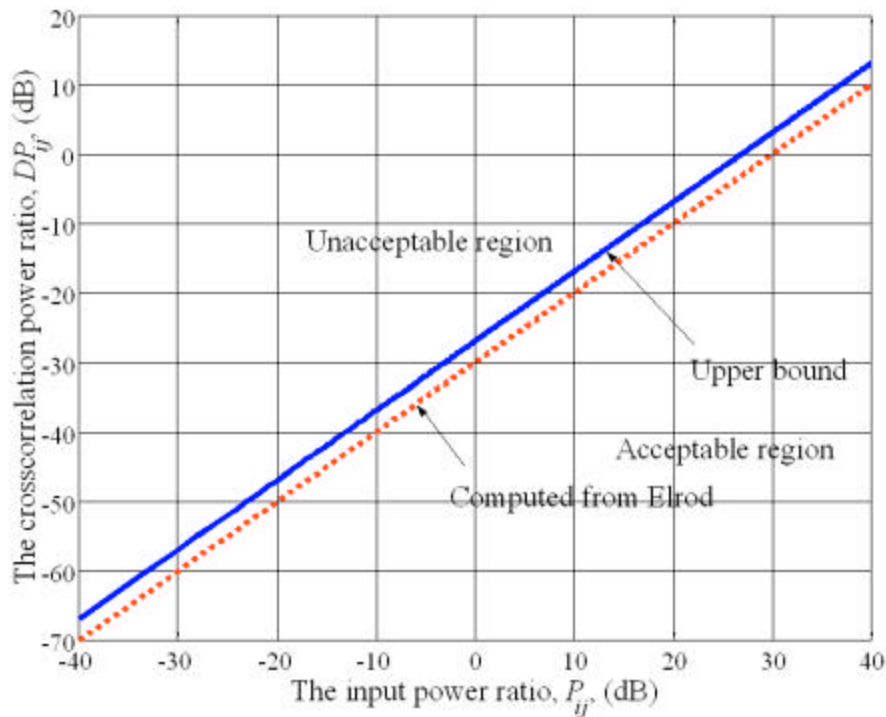


Figure 2.28 The crosscorrelation power ratio, DP_{ij} (dB), vs. input power ratio, P_{ij} (dB).

Let P_s/P_r denote the satellite/pseudolite signal power at the port of the receiver's antenna. Let N_0 denote the noise power spectrum density caused by the receiver electronics and channel impairments. In the absence of a pseudolite signal the signal to noise ratio is given by

$$(2.4.25) \quad SNR_0 = \frac{P_s}{N_0}.$$

When a pseudolite signal is present then the signal to noise ratio is given by

$$(2.4.26) \quad SNR_1 = \frac{P_s}{N_0 + P_r}.$$

If a duty cycle ι is applied to the pseudolite signal, as usually suggested by [30], then the signal to noise ratio becomes

$$(2.4.27) \quad SNR_2 = \frac{P_s}{N_0 + \iota P_r}.$$

Rewriting the above equation in dB we obtain

$$(2.4.28) \quad SNR_{2dB} = 10\log_{10} P_s - 10\log_{10}(N_0 + \iota P_r).$$

If we assume that the noise power is -170 dBm, the satellite signal power is -185 dBW, and the duty cycle is $1/11$ then equation (2.4.28) is given by

$$(2.4.29) \quad SNR_{2dB} = -10\log_{10}(1e^{-17} + 1/11 P_r) - 185$$

Varying the received pseudolite power we produce the graph shown in Figure 2.29. For pseudolite signal power smaller than -153 dBm the satellite signal can be detected and for pseudolite signal power greater than -153 dBm the satellite signal cannot be detected.

If we want to compute the pseudolite transmitted power in light of equation (2.3.6) we have

$$(2.4.30) \quad P_t \approx -153 + 20\log_{10} d + 111.75 = 20\log_{10} d - 41.25 \text{ (dBm)}.$$

For indoor applications the smallest reference distance between the transmitter and the receiver is $d = 1$ m. Hence, we find the requirement on the pseudolite transmitted power equal to $P_t = -41.25$ dBm or 75 nW.

As indicated by our simplified analysis, pulsing of the pseudolite signal is one way to reduce the interference caused by the pseudolite. Although this is a preferred technique for LAAS and WAAS applications would not be the desired method at all for indoor

geolocation applications for multiple reasons. First, if any duty cycle imposes restrictions on the number of pseudolites. For example the 1/11 duty cycle quite often applied will not allow more than 11 pseudolites to operate in the same proximity. Second, if we were to reduce the duty cycle then the dwell time becomes so small risking loss of signal detection during the acquisition and tracking process. Third, any duty cycle would impose tough restrictions of the pseudolite signal level. Therefore, for these reasons we propose a novel pseudolite signal structure and design when we discuss the WPI indoor geolocation system in chapters 4 through 7.

2.6 MIT Indoor Geolocation System

Here we discuss the principles of operation of the MIT indoor geolocation system (see §2.6.1), the transmitter (see §2.6.2), the receiver (see §2.6.3), the method for extracting the observable(s) (see §2.6.4), and issues related to the MIT indoor geolocation system (see §2.6.5).

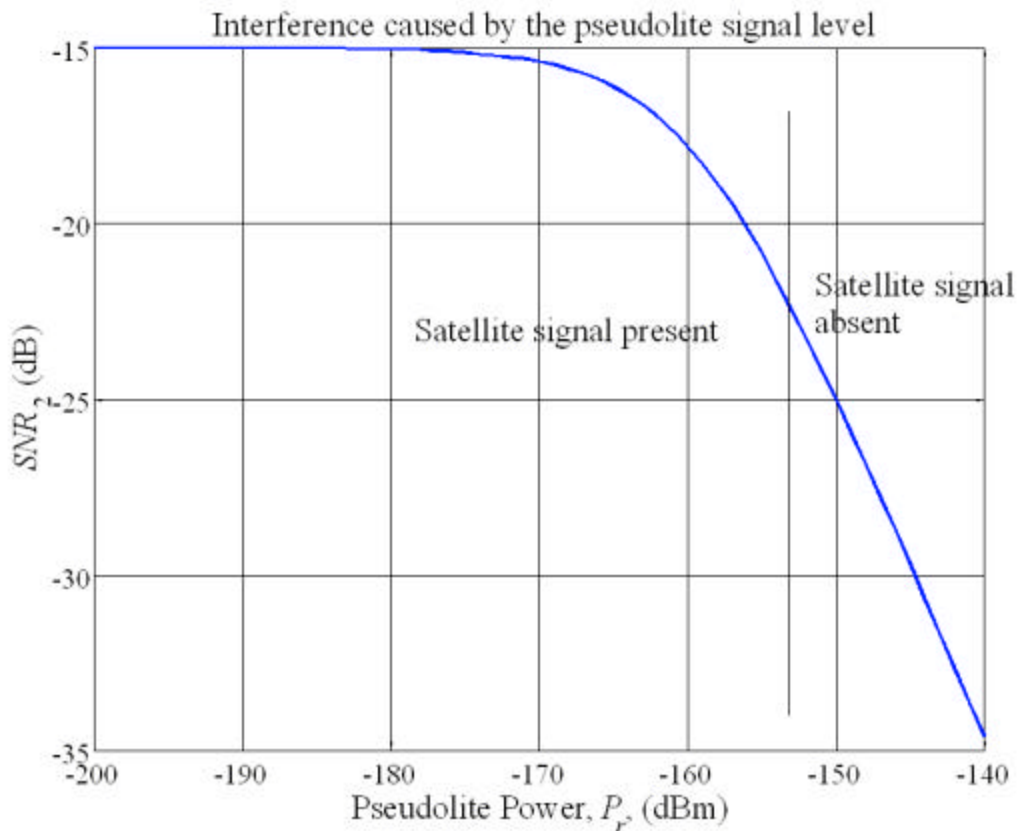


Figure 2.29 Interference caused by the pseudolite signal level.

2.6.1 Principle of Operation

The MIT positioning system employs phase information to determine the receiver position from a set of fixed transmitters. In order to understand how this system works, we consider both the forward and the inverse positioning problem. First, we consider the forward problem; given the transmitter and receiver geometry what are the relative phases of signals from the transmitters as seen by the receiver. Second, we consider the inverse problem; given the relative phases of the signals seen by the receiver, and the location of the transmitters, how do we determine the location of the receiver.

Consider the MIT indoor geolocation system as illustrated in Figure 2.30. We assume that each transmitted signal is a spherical electromagnetic wave with a wavelength smaller than the maximum distance between the transmitter and the receiver. For signals whose frequency is smaller than 1.9 MHz the corresponding wavelength is larger than 157 m.

2.6.1.1 The Forward Problem

Assume that each transmitter emits a pure sinusoidal signal with the same frequency, f , and the same initial phase offset, ϕ_0 . Assume that the relative distance between the i th transmitter and the receiver is d_i . We express this delay as the fraction of the signal's wavelength and denote it with the symbol ϕ_i given by [33]

$$(2.5.1) \quad \phi_i = \frac{2\pi f d_i}{c} = k d_i .$$

where k is defined as [33]

$$(2.5.2) \quad k = \frac{2\pi f}{c} .$$

Hence, the expression for the transmitted signal $s_i(t)$ from the i th transmitter is given by [33]

$$(2.5.3) \quad s_i(t) = \sin(2\pi f t + \phi_i + \phi_0), \quad \forall i \in \{1, 2, 3, 4\} .$$

Let $\phi_i(t)$ denote the total phase of the received signal coming from the i th transmitter [33]

$$(2.5.4) \quad \phi_i(t) = 2\pi f t + \phi_i + \phi_0, \quad \forall i \in \{1, 2, 3, 4\} .$$

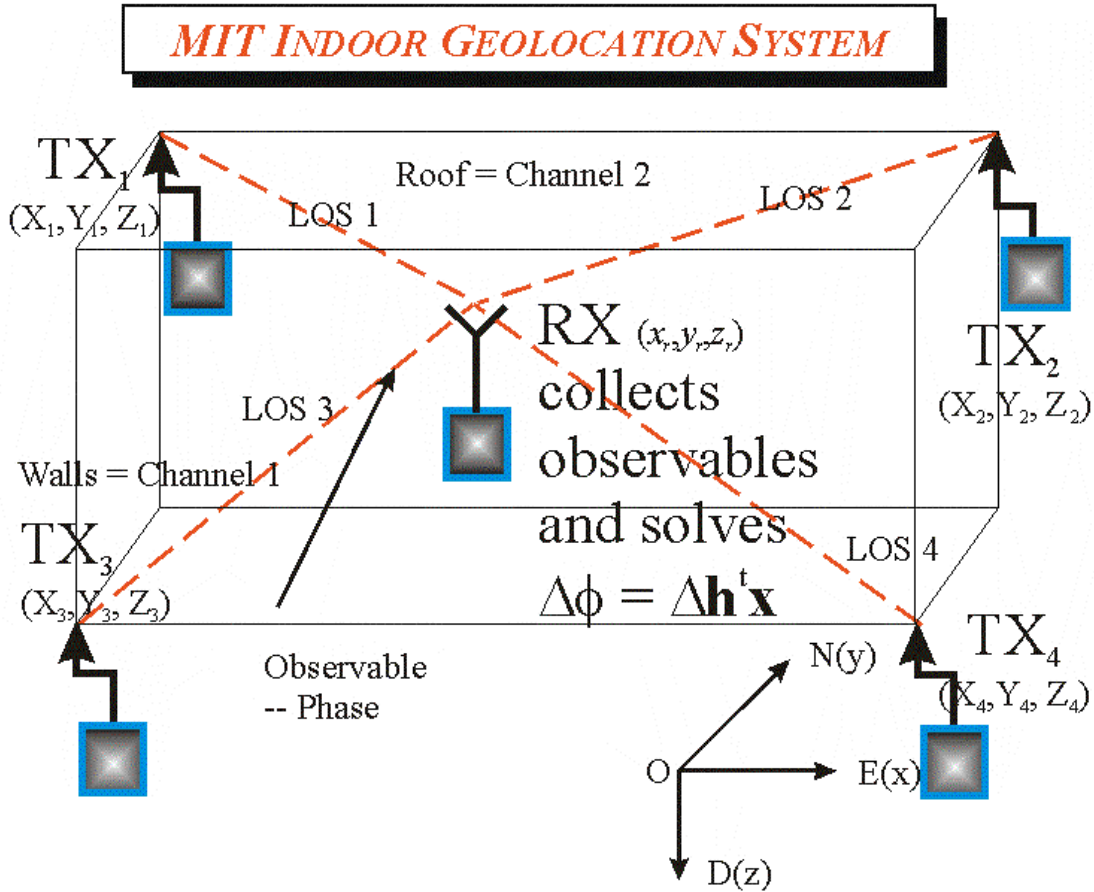


Figure 2.30 The principle of operation of the MIT indoor geolocation system.

Assume that the signal from the 1st transmitter is the reference signal; hence, the phase from the 1st transmitter is the reference phase. Let $\Delta\phi_{i-1}(t)$ denote the difference of the phase of the signal from the i th transmitter with the phase of the signal from the 1st transmitter. The expression for $\Delta\phi_{i-1}(t)$ is given by [33]

$$(2.5.5) \quad \Delta\phi_{i-1}(t) = \phi_i - \phi_1 = k(d_i - d_1), \quad \forall i \in \{2, 3, 4\}.$$

As long as $d_i \neq d_1, \forall i \in \{2, 3, 4\}$, we have independent measurements for the phase difference $\Delta\phi_{i-1}(t)$, which is in fact the observable.

Next, we discuss the inverse problem; i.e., given the transmitter locations and the independent measurements $\Delta\phi_{i-1}(t)$ we compute the receiver location.

2.6.1.2 The Inverse Problem

As long as the transmitted signal wavelength is longer than the diagonal of the cubic building (see Figure 2.30), we notice that the transmit time of the signals from each

transmitter to the receiver adds a nonzero phase offset, ϕ_i , given by equation (2.5.1) to the measured signal [33]. The reader is reminded here that we can only measure phase with respect to a reference signal; hence, between two pairs. In fact, the receiver measures phase differences between two pairs of stations.

Let $\Delta\phi_{i-j}$ be the phase difference between the station i and the station j . Based on equation (2.5.1) this phase difference can be written as [33]

$$(2.5.6) \quad \Delta\phi_{i-j} = \phi_i - \phi_j = k(d_i - d_j) + \Delta v_{i-j}, \quad \forall i \neq j \cap \forall i, j \in \{1, 2, 3, 4\}$$

where Δv_{i-j} is the difference on the phase measurement noise v_i and v_j . Assuming that the first station is selected as the reference station, we can measure up to three independent phase differences. Using the first two terms of the Taylor series expansion, the distance difference, $d_i - d_1$, can be written as

$$(2.5.7) \quad d_i - d_1 \approx \left[\frac{\partial d_i}{\partial x_r} - \frac{\partial d_1}{\partial x_r} \quad \frac{\partial d_i}{\partial y_r} - \frac{\partial d_1}{\partial y_r} \quad \frac{\partial d_i}{\partial z_r} - \frac{\partial d_1}{\partial z_r} \right]_{(x_{r0}, y_{r0}, z_{r0})} \begin{bmatrix} x_r \\ y_r \\ z_r \end{bmatrix}$$

or in vector form

$$(2.5.8) \quad d_i - d_1 \approx \mathbf{h}_i^t \mathbf{x}$$

where

$$(2.5.9) \quad \mathbf{h}_i^t = \left[\frac{\partial d_i}{\partial x_r} - \frac{\partial d_1}{\partial x_r} \quad \frac{\partial d_i}{\partial y_r} - \frac{\partial d_1}{\partial y_r} \quad \frac{\partial d_i}{\partial z_r} - \frac{\partial d_1}{\partial z_r} \right]_{(x_{r0}, y_{r0}, z_{r0})}, \quad \mathbf{x} = \begin{bmatrix} x_r \\ y_r \\ z_r \end{bmatrix}.$$

In vector form equation (2.5.6) can be written as

$$(2.5.10) \quad \begin{bmatrix} \Delta\phi_1 \\ \Delta\phi_2 \\ \Delta\phi_3 \end{bmatrix} \approx \begin{bmatrix} \mathbf{h}_1^t \\ \mathbf{h}_2^t \\ \mathbf{h}_3^t \end{bmatrix} \mathbf{x} + \begin{bmatrix} \Delta v_1 \\ \Delta v_2 \\ \Delta v_3 \end{bmatrix} \text{ or } \mathbf{f} \approx \mathbf{H}\mathbf{x} + \mathbf{v}.$$

Referring to the solution in Chapter 1 we have the following: If the noise autocovariance matrix, $\mathbf{R} = E\{\mathbf{v}^t \mathbf{v}\}$, is known then an approximated solution for (x_r, y_r, z_r) is derived from the well known least squares algorithm [34]

$$(2.5.11) \quad \hat{\mathbf{x}} = (\mathbf{H}^t \mathbf{R}^{-1} \mathbf{H})^{-1} \mathbf{H}^t \mathbf{R}^{-1} \mathbf{f}.$$

Since \mathbf{H} and \mathbf{R} are both 3×3 matrices and if the inverse of \mathbf{H} exists then

$$(2.5.12) \quad \hat{\mathbf{x}} = \mathbf{H}^{-1} \mathbf{f} .$$

From equations (2.5.11) and (2.5.12) we conclude that at least three independent measurements are required to solve for the receiver location. If more than three measurements are employed, then equation (2.5.11) should be used instead of equation (2.5.12). For fewer than three measurements equation (2.5.11) is underdetermined. In that case we can only solve for fewer than three unknowns. For example if the number of measurements is only two then we can solve for only one of three combinations $\{(x_r, y_r), (x_r, z_r), (y_r, z_r)\}$.

2.6.2 Transmitter

The transmitter is responsible for generating a stable carrier signal, maintaining synchronization, and transferring data packets to the receiver. It is suggested that the power levels generated by the transmitter must be as high as +43 dBm [33]. The bandwidth of the signal is less than 14 kHz; hence, it is comparable with the signal of Amateur Radio stations [33].

2.6.2.1 Signal Structure

The signal structure of the MIT indoor geolocation system consists of a set of 10 ms frames, each of which is formed from four signal periods and one data period (see Figure 2.31). Hence, the modulation scheme is Time Division Multiple Access (TDMA). Each signal period is 1.5 ms long and consists of a pure sinusoidal signal [33]. The remaining 4 ms of each frame consists of 3.9 ms of data period, followed by 100 μ s of silence. The 3.9 ms data period consists of digital data transmitted by primary location service station 1, using an FSK modulation at 10.25 KBPS [33]. The silent period enables the receiver to recognize the end of the frame and to process the received data corresponding to each frame's data period. Also, based on equation (2.5.4) the initial phases on all transmitted signals must be equal; hence, all transmitted signals must be synchronized.

The block diagram of the MIT transmitter is depicted in Figure 2.32. As depicted in the figure, the transmitter contains two main sections: signal generation section and the signal distribution section.

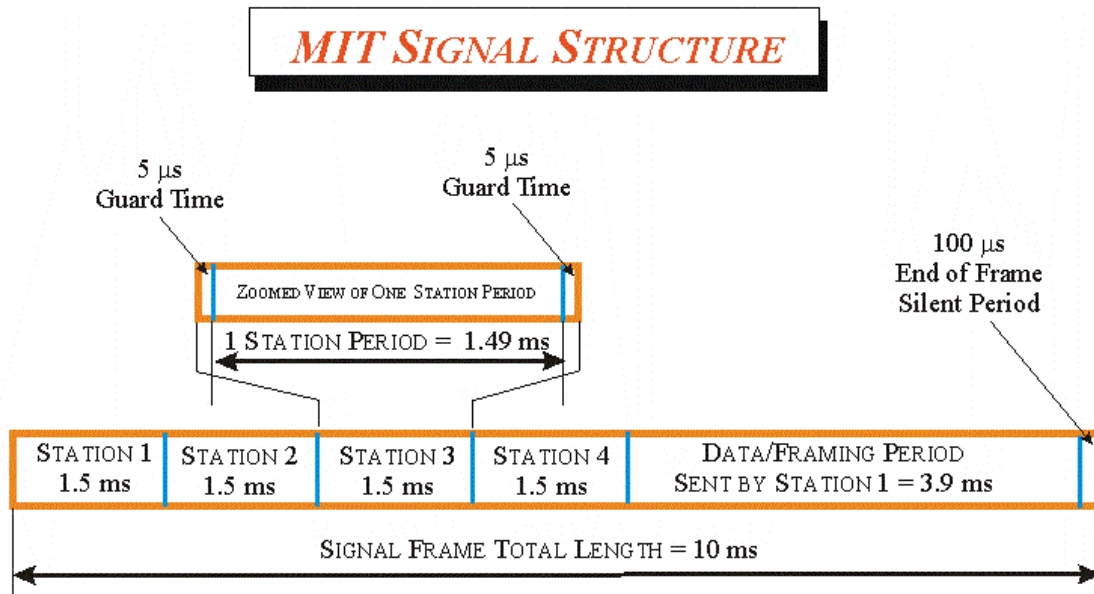


Figure 2.31 MIT Signal Structure-- taken and modified from [33].

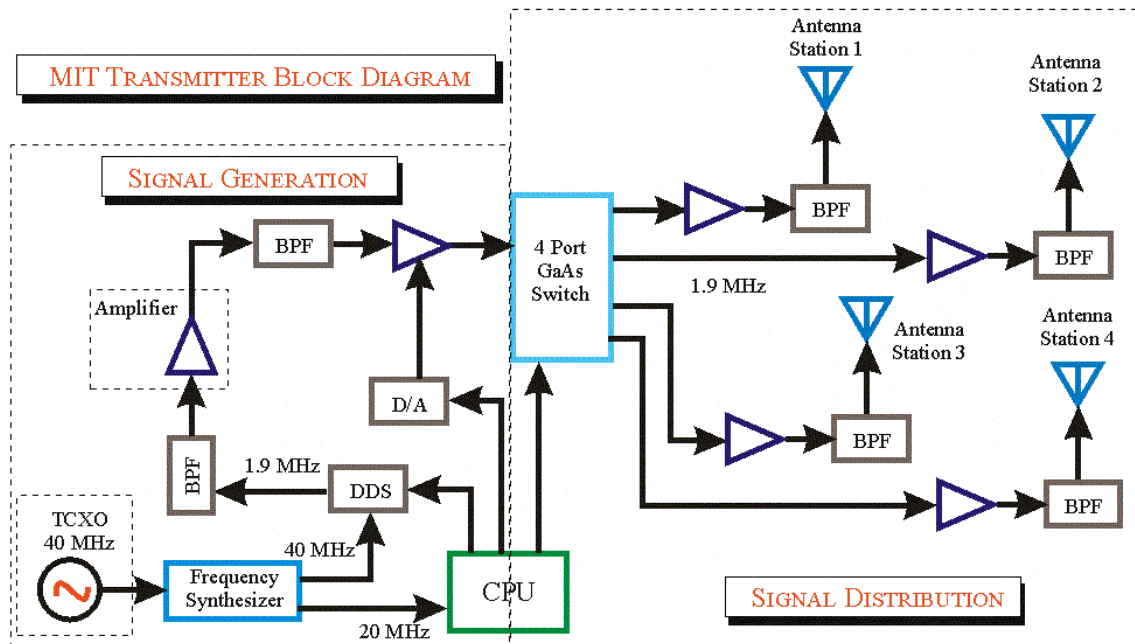


Figure 2.32 MIT transmitter block diagram-- taken and modified from [33].

2.6.2.2 Generation of Stable Signals

The Master Clock unit consists of a four-output source of timing signals whose frequency and power output are under microprocessor control. The unit's master oscillator is a quartz crystal based 40 MHz TCXO with a stated short-term stability

limited by the oscillator's phase noise. A typical phase noise of -140 dBc at 10 kHz offset is quite sufficient for our application; this corresponds to a short-term phase variation that is negligible compared to propagation distortion phase. The unit's long term frequency stability is less than 10 ppm per day at room temperature range. This, coupled with the Direct Digital Synthesizer (DDS) is used to synthesize the carrier frequency, which ensures the long-term stability of the system. It is possible to update calibration values for the TCXO calibration input based on an external GPS reference signal at 10 MHz, as the system includes a 10-MHz phase-synchronous output that is ordinarily used as the A/D converter clock in the receiver. The system operator has access to this calibration output and can easily compare it to a high-accuracy external standard. Alternatively, if a source of extremely stable 40 MHz TTL level clock signals is available, it is very easy to inject this external reference and dispense with the onboard TCXO altogether [33].

2.6.2.3 Distribution of Stable Signals

With the help of a 4-port GaAs switch signals are distributed into four stations, each one of which serves as a transmitter. These signals are amplified, bandpass filtered, and broadcast by means of an antenna.

2.6.3 Receiver

The BPS Receiver Unit is based on a digitized IF software radio architecture. As shown in Figure 2.33, the received signal from an antenna is filtered, pre-amplified, mixed to a 455 kHz IF, and is then amplified by a limiting amplifier. This signal is then passed to a high speed ADC that feeds the CPU's Direct Memory Access (DMA) unit with a high speed streaming digitization of the incoming signal. The CPU acquires these signals in real time but processes them at leisure one signal frame at a time. This arrangement allows the use of a standard Hitachi SH-1 microcontroller instead of a dedicated DSP unit. Of course, this results in considerable cost and complexity savings. Another feature of this receiver is its direct digital synthesis (DDS) local oscillator unit, based on an Analog Devices DDS IC. This IC greatly simplifies the task of generating a clean local oscillator signal for the down-conversion [33].

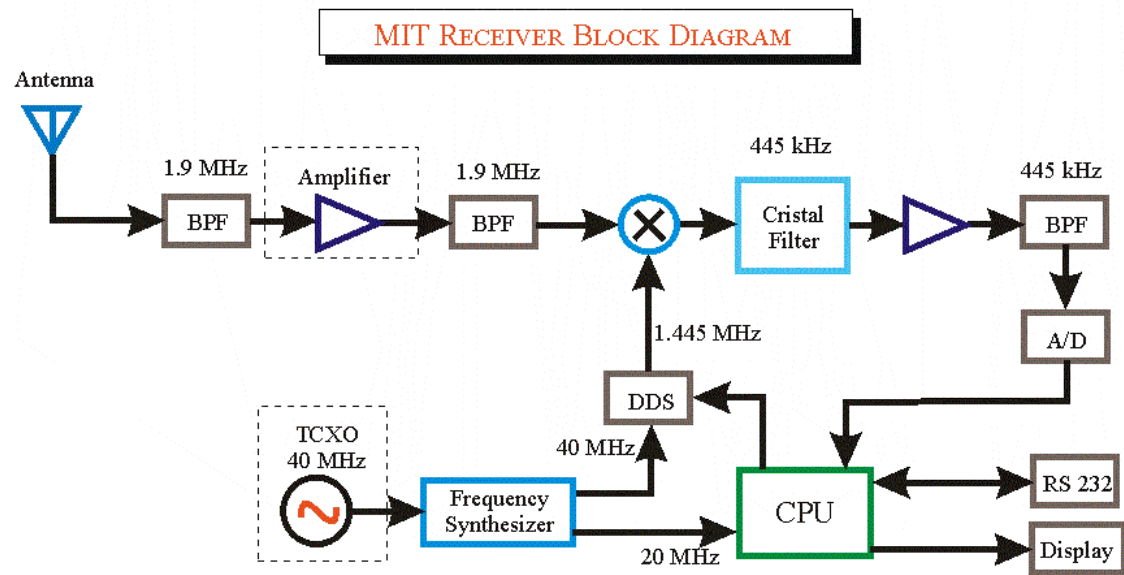


Figure 2.33 MIT receiver block diagram- - taken and modified from [33].

2.6.4 Extraction of Observable(s)

2.6.4.1 Logarithmic Detection and RSSI A/D Conversion

In order to detect the gaps in the transmitted signal which indicate the start and end of each transmitted frame, the CPU's internal 12-bit ADC is used to capture the received signal strength indicator (RSSI) voltage from the AD608 IF device. The RSSI output is logarithmic with respect with to the incoming signal over a range of 60 dB and is low pass filtered with a one-pole RC lowpass filter which has a cutoff frequency of 10 kHz. A filter removes frequency components 455 kHz and higher from the IF signal. This signal is then buffered by a high-speed operational amplifier, which is connected to the CPU's internal 12-bit low speed A/D converter for the digital measurement of RSSI. An appropriate compensation function is used to report actual RSSI in dBm units for test purposes. As the RSSI is used as a source of framing information the high cutoff frequency is important to allow the signal acquisition to occur within the 100 μ s inter-frame interval [33].

2.6.4.2 Frame Alignment

The RSSI looks for a 100- μ s period of silence from the receiver IF module signifying the imminent beginning of a signal frame. When a silent period of 100 μ s is detected, the high-speed acquisition system begins to acquire the signal on each of the four transmitter phase intervals. The receiver's DMA is capable of capturing 6.5 ms (65536 samples at 10 Msamples/sec) in a single shot measurement, but we capture only the first 6.0 ms of the signal frame with the fast ADC. This results in a buffer of 60 K 12-bit words, or 90 Kbytes of raw data. These DMA periods include 5.0 μ s dead times at the beginning and end of each subframe period, yielding a total of 10.0 μ s to allow for the transmitter switching and power control systems to settle [33].

2.6.4.3 Framing Error Conditions

If two entire frame periods (20 ms) pass with no silence interval, the receiver assumes that it is encountering a "Jam" condition; therefore, the receiver reports the last valid position, and raises the "Jam" indicator on the operator display [33]. It also reports an error code in its serial output stream. This could be the result of interference from environmental sources, including the close proximity of two or more MIT indoor geolocation systems [33]. If no frames are received at all, or if the RSSI shows too weak an incoming signal, a "No signal" is indicated to the user [33]. The same indication is also presented if, for some reason, the processor records an unexpected drop in signal levels during the processing of the acquired signal frame [33].

2.6.4.4 Frame Data Interval

The 3.9-ms data subframes, each containing data sent at 10.25 KBPS, transfer 40 bits of information to the receiver per frame. This occurs at a rate of 100 frames per second to form a 4.0 KBPS data downlink channel, which is used to communicate the system ID and operating health of the four primary channels. It is sent in a narrow-shift FSK data format in which a logic '1' is represented by shifting the carrier frequency of transmitter 1 down by 10.0 kHz. The transmitter unit performs this modulation by loading the transmitter's direct digital synthesizer with the appropriate new frequency value. This signal is demodulated by the simple expedient of digitizing the receiver's RSSI signal exactly as is done to locate the end-of-frame gaps and looking for the small deviations in

RSSI that occur as the received carrier shifts in and out of the 6.0 kHz passband of the IF filter. This is a digital version of slope-detected FM and is a crude but effective way to send small amounts of data to the receiver without requiring additional hardware [33].

An essential component of the downlink signal is the surveyed location of the transmitter group's origin point if the computations are required in global frame. The 1st transmitter as part of the data period sends this information as a string. Moreover, the position of each transmitter is computed with respect to the group origin point [33].

2.6.4.5 Signal Processing

The correlation engine is the processor's main task. It consists of a set of sliding multiply-accumulate operations that seek to achieve maximal correlation among the four transmit periods, and records the offset in samples between each pair of transmit periods. The subsample interpolation used to meet the target position resolution goals is based on a simple sine-fitting algorithm that tries to fit a maximal-amplitude sine wave to the given point set. For our four transmit periods we can derive six pairs of phase offsets, which are then used by the position solution task to calculate a position estimate. This process is limited by the bus fetch speed to retrieve the appropriate samples from the main memory [33].

2.6.5 Issues

There are several advantages and disadvantages of this system. The main advantage is its simplicity—the signal structure is very simple and both the transmitter and receiver designs are very simple also.

The main disadvantage of this system is the synchronization between all transmitters and interference between two identical indoor geolocation systems due to the restriction on same frequency operation. Another main disadvantage of this system is its vulnerability against any external intentional jamming sources.

CITED REFERENCES AND FURTHER READING:

- [1] B.W. Parkinson, J.J. Spilker, Jr, et al., *The Global Positioning System-Theory and Applications*, Washington, DC: American Institute of Aeronautics and Astronautics, (vol. 1, chap. 1, "Introduction and heritage of NAVSTAR, the Global Positioning System") 1996.

- [2] B.W. Parkinson, J.J. Spilker, Jr, et al., *The Global Positioning System-Theory and Applications*, Washington, DC: American Institute of Aeronautics and Astronautics, (vol. 1, chap. 2, "Overview of GPS operation and design") 1996.
- [3] B.W. Parkinson, J.J. Spilker, Jr, et al., *The Global Positioning System-Theory and Applications*, Washington, DC: American Institute of Aeronautics and Astronautics, (vol. 1, chap. 3, "GPS signal structure and theoretical performance") 1996.
- [4] B.W. Parkinson, J.J. Spilker, Jr, et al., *The Global Positioning System-Theory and Applications*, Washington, DC: American Institute of Aeronautics and Astronautics, (vol. 1, chap. 4, "GPS navigation data") 1996.
- [5] B.W. Parkinson, J.J. Spilker, Jr, et al., *The Global Positioning System-Theory and Applications*, Washington, DC: American Institute of Aeronautics and Astronautics, (vol. 1, chap. 8, "GPS receivers") 1996.
- [6] Anon., Department of Defense, *Global Positioning System (GPS) Standard Positioning Service (SPS)*, Signal Specification, Dec. 8, 1993.
- [7] B.W. Parkinson, J.J. Spilker, Jr, et al., *The Global Positioning System-Theory and Applications*, Washington, DC: American Institute of Aeronautics and Astronautics, (vol. 1, chap. 15, "Foliage attenuation for land mobile users") 1996.
- [8] R.M. Lollock, "Global Positioning System (GPS) Modernization," civil GPS service interface committee, Washington, DC, 27-29 Mar. 2001. (unclassified presentation)
- [9] J.M. Hill, "Development of an experimental Global Positioning System (GPS) receiver platform for navigation algorithm evaluation," Ph.D. Dissertation, Worcester Polytechnic Institute, Aug. 2001.
- [10] B.W. Parkinson, J.J. Spilker, Jr, et al., *The Global Positioning System-Theory and Applications*, Washington, DC: American Institute of Aeronautics and Astronautics, (vol. 2, chap. 9, "GPS and Global Navigation Satellite System (GLONASS)") 1996.
- [11] K. Kurmiveda et al., "A complete IF software GPS receiver," in *Proc. ION-GPS*, Salt Lake City, UT, pp. 789-829, Sep. 2001.
- [12] J.G. Proakis, *Digital Communications*. 1st, 2nd, and 3rd, ed., New York: McGraw-Hill, 1983, 1989, and 1995.
- [13] A. Papoulis, *Probability, Random Variables, and Stochastic Processes*. New York: McGraw-Hill, 1984.
- [14] B.W. Parkinson, J.J. Spilker, Jr, et al., *The Global Positioning System-Theory and Applications*, Washington, DC: American Institute of Aeronautics and Astronautics, (vol. 1, chap. 9, "GPS Navigation Algorithms ") 1996.
- [15] I.F. Proгри, "Special report: magnitude and phase relationship," EE2311, WPI, Nov. 25, 2002.

- [16] D. Akos, "A software radio approach to Global Navigation Satellite System receiver design," Ph.D. dissertation, Ohio University, August 1997.
- [17] J. Bao-Yen Tsui, *Fundamentals of Global Positioning Systems Receivers, A Software Approach*. New York, NY: Wiley Inter-Science, May 2000.
- [18] R.E. Best, *Phase Locked Loops: Design, Simulations, and Applications*. 4th Ed. Mc-Graw Hill, Jun. 1999.
- [19] E.D. Kaplan, *Understanding GPS: Principles and Applications*. Boston, MA: Artech House, 1996.
- [20] IRN-200C-001, ICD-GPS-200C, 13 Oct 1995.
- [21] A.S. Dale, P. Daly, and I.D. Kitching, "Understanding signals from GLONASS satellites," *Inter. J. of Sat. Comm.*, vol. 7, no. 1, pp. 11-22, 1989.
- [22] P. Daly, I.D. Kitching, D. Allan, and T. Pepler, "Frequency and time stability of GPS and GLONASS clocks," *Inter. J. of Sat. Comm.*, vol. 9, no. 1, pp. 11-22, 1991.
- [23] I.F. Proгри, W.R. Michalson, and M.C. Bromberg, "A DSSS/CDMA/FDMA indoor geolocation system," in *Proc. ION-GPS*, Portland, OR, Sep. 2002.
- [24] I.F. Proгри, W.R. Michalson et al, "A system for tracking and locating emergency personnel inside buildings," in *Proc. ION-GPS*, Salt Lake City, UT, pp. 560-568, Sep. 2000.
- [25] W.R. Michalson and I.F. Proгри, "Assessing the accuracy of underground positioning using pseudolites," in *Proc. ION-GPS*, Salt Lake City, UT, pp. 1007-1015, Sep. 2000.
- [26] I.F. Proгри and W.R. Michalson, "An innovative navigation algorithm using a system of fixed pseudolites," in *Proc. ION-NTM*, Long Beach, CA, pp. 619-627, Jan. 2001.
- [27] I.F. Proгри, J. Hill, and W.R. Michalson, "A Doppler based navigation algorithm," in *Proc. ION-NTM*, Long Beach, CA, pp. 482-490, Jan. 2001.
- [28] I.F. Proгри, W.R. Michalson, and J. Hill, "Assessing the accuracy of navigation algorithms using a combined system of GPS satellites and pseudolites," in *Proc. ION-NTM*, Long Beach, CA, pp. 473-481, Jan. 2001.
- [29] D.V. Sarwate and M.B. Pursley, "Crosscorrelation properties of pseudorandom and related sequences," in *Proc. of IEEE*, vol. 68, pp. 593-619, May 1980.
- [30] B.W. Parkinson, J.J. Spilker, Jr, et al., *The Global Positioning System-Theory and Applications*, Washington, DC: American Institute of Aeronautics and Astronautics, (vol. 2, chap. 2, "Pseudolites") 1996.
- [31] Anon., "Minimum aviation system performance standards—DGNS instrument approach system: special category I (SCAT-I)," RTCA/DO-217, RTCA, Inc., Washington, DC, Aug. 27, 1993.
- [32] Federal Communications Commission, *News*, "New public safety applications and broadband internet access among uses envisioned by FCC authorization of ultra-wideband technology," Washington, DC, Feb. 14, 2002.

- [33] M.S. Reynolds, "A phase measurement radio positioning system for indoor use," MS Thesis, Dep. Elec. and Comput. Eng., MIT, Cambridge, MA, Feb. 1999.
- [34] R.C. Brown and P.Y.C. Hwang, *Introduction to Random Signals and Applied Kalman Filtering*. 3rd ed., New York: John Wiley & Sons, 1981.

Chapter 3. Channel Models

“Wherefore let them that suffer according to the will of God commit the keeping of their souls to him in well doing, as unto a faithful Creator.”³⁴¹ Peter 4:19

3.0 Introduction

IN Chapter 2 we have discussed four geolocation systems, we have explained the process for obtaining an observable in detail, and we have addressed issues associated with each one of these technologies. However, in Chapter 2, we have assumed an impairment-free indoor environment. The purpose of this Chapter is twofold: to classify all channel models and to propose a unified channel model.

3.1 Wireless Communication Channel Models

The properties of wireless communication channels have been the focus of research performed by many communication and fields engineers for many years [1]-[43]. This has led to combined efforts from scientists and engineers to come up with channel models that are easy to model, allow for accurate predictions, and are computationally efficient. It is important to emphasize here that although there is yet to be found a unique and complete channel model, there are several models that offer good to very accurate prediction of channel behavior under certain conditions. Many channel models have been validated through experimental measurements. Nevertheless, there is a need to conduct more measurements and it is desirable to refine current analytical models in a way that leads to a unified channel model. Although we would like to address to some extent an approach that might lead to a unified wireless communication model, this is neither the objective of this book nor the objective of this Chapter (see §3.2).

Based on the current conventions in the wireless community (see Appendix E), channel models are classified into three categories: (1) macrocellular geolocation systems (see §3.1.1), (2) microcellular geolocation systems (see §3.1.2), and (3) indoor geolocation systems (see §3.1.3).

Although in Chapter 1 we have classified the geolocation systems as outdoor, indoor, and underwater geolocation systems, we keep the definition of macrocellular, microcellular, and indoors because this is the definition used in the communication community. Nevertheless, to establish the link between this Chapter and Chapter 1 we treat macrocellular and microcellular and outdoor geolocation systems and picocellular as indoor geolocation systems. Moreover, we assume that there is a direct LOS path between the transmitter and the receiver. The case when the LOS path is not observed is not treated here and will be treated in the future.

3.1.1 The Physics of Propagation for Macrocellular Geolocation Systems

A macrocellular geolocation system consists of a network of macrocells [16], [18]. The transmitting antenna in a macrocell has a coverage radius going from approximately 1 km to 20 km. As we have discussed in the first chapter, there are two primary channel effects: path loss (see §3.1.1.1) and multipath distribution (see §3.1.1.2).

The propagation path between a transmitter (TX) and a receiver (RX) is illustrated in Figure 3.1 (a) horizontal view (or looking from the top) and (b) vertical view (or looking from forward). There are four buildings, one transmitter, and one receiver as illustrated in Figure 3.1. As shown in Figure 3.1 (b) the distance between two consecutive buildings is d and the height of each building is z_b . The transmitter's height is z_t and the receiver's height is z_r . The ray coming from the transmitter is refracted from the rooftop of the third building; therefore, the receiver receives one refracted path whose length is r_1 and one reflected path whose length is r_2 as shown in Figure 3.1 (b).

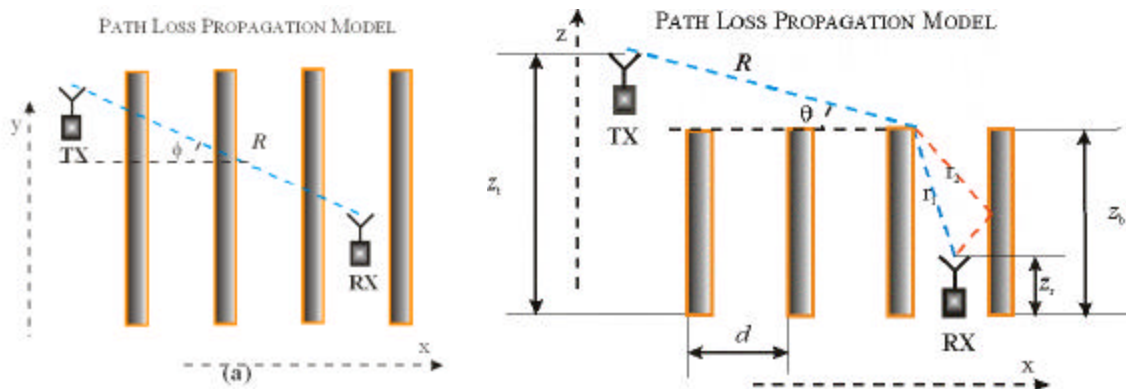


Figure 3.1 The (a) top (or horizontal) and (b) view vertical view of the propagation path between the transmitter and the receiver—taken and modified from [18].

The length of the direct path from the transmitter to the rooftop of the third building is R . The incident angle of the direct ray with the horizontal plane is ϕ Figure 3.1 (a) and the vertical phase is θ Figure 3.1 (b). Next, we shall see how to assess the path loss based on the model shown in Figure 3.1 (a) and (b).

3.1.1.1 Path Loss

The free-space path loss, Q_0 , is the ratio of received power, P_r , to radiated power, P_t , for isotropic antennae in free-space. Assume that the receiving antenna with gain, G_r , is located at a distance, R , from the transmitting antenna with gain, G_t . The sector average power, P_r , from the receiving antenna is, according to [1], equal to

$$(3.1.1) \quad P_r = \frac{G_t G_r P_t}{(4\pi)^2} \left(\frac{\lambda}{R} \right)^2 = G_t G_r P_t \left(\frac{c}{4\pi f R} \right)^2 = Q_0 G_t G_r P_t$$

where the free-space path loss, Q_0 , is determined from

$$(3.1.2) \quad Q_0 = \left(\frac{\lambda}{4\pi R} \right)^2 = \left(\frac{c}{4\pi R f} \right)^2.$$

Similarly, the average *path loss*, Q , is defined as the ratio of the sector average received power, P_r , to the radiated (or transmitted) power, P_t , times the factor $G_t G_r$. [18]. Employing Bertoni's definition [18], the path loss can be written as a product of three components: (1) free-space path loss, Q_0 ; (2) reduction factor due to previous rows propagation, Q_1^2 ; and (3) reduction due to diffraction, Q_2

$$(3.1.3) \quad Q = \frac{P_r}{G_t G_r P_t} = Q_0 Q_1^2 Q_2.$$

The free-space path loss, Q_0 , corresponds to the path loss from the transmitter to the rooftop of the third building as shown in Figure 3.1 (a) and (b). To give an intuitive explanation of the free space path loss we have considered the following example. Suppose that operating carrier frequency of the TX–RX is taken from the set $f = \{0.9, 1.17642, 1.2276, 1.57542, 20\}$ GHz. Suppose that the relative distance between the TX–RX is taken from the set $R = \{1, 2, \dots, 20\}$ km. Based on these assumptions we have computed the free space path loss Q_0 (dB) (see eq. (3.1.2)) versus $R = \{1, 2, \dots, 20\}$ km and the result is plotted in Figure 3.2 (a). As shown from Figure 3.2 (a) free space path losses can be as high as -91 dB ($R = 1$ km and $f = 900$ MHz) and as low as -145 dB ($R =$

20 km and $f = 20$ GHz). Suppose that the distance from the transmitter to the receiver is taken from the set $R = \{1, 5, 10, 15, 20\}$ km and that the operation frequency changes from $f = \{1, 2, \dots, 20\}$ GHz. Based on these assumptions we have computed the free space path loss Q_0 (dB) (see eq. (3.1.2)) versus $f = \{1, 2, \dots, 20\}$ GHz and the result is plotted in Figure 3.2 (b). Similar to Figure 3.2 (a) Q_0 (dB) can be as high as -92 dB and as low as -145 dB.

The field propagating through the rooftop of a building is approximated as a plane wave propagating parallel to the ground with an azimuth angle, $90^\circ - \phi$, where ϕ is the angle between the plane propagation vector and the horizontal direction x (see Figure 3.1 (a) and (b)). The receiver receives two paths of the same original plane wave: one diffracted path and the other reflected path, which are function of the elevation angle \mathbf{q} . The signal received at the receiver is reduced by the factor, Q_2 , given by [18]

$$(3.1.4) \quad Q_2 = \frac{1}{2\pi k \cos \phi} \left[\frac{1}{r_1} D^2(\theta_1) + \frac{1}{r_2} \Gamma^2 D^2(\theta_2) \right]$$

where Γ is the reflection coefficient at the building face. The wavelength λ is defined as the distance for which $k\lambda = 2\pi$, that yields the known expression for the wavenumber, k , equal to $k = 2\pi/\lambda$. The wavenumber k is interpreted as the number of wavelengths in a distance of 2π and its units are m^{-1} . The diffraction coefficient $D(\theta_i)$, $i = \{1, 2\}$ is determined from [18]

$$(3.1.5) \quad D(\theta_i) = \frac{1}{\theta_i} - \frac{1}{\theta_i + 2\pi}, \quad \forall i \in \{1, 2\}.$$

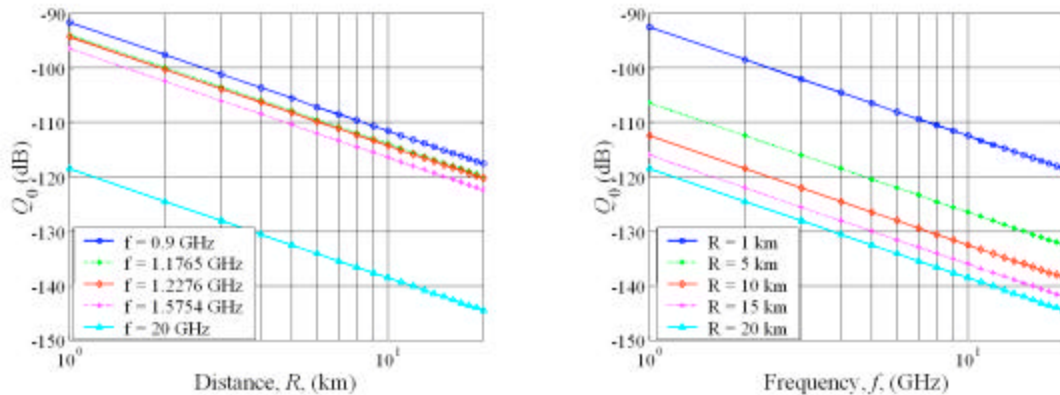


Figure 3.2 Free space path loss model (a) vs. R and (b) vs. f for a macrocellular geolocation system.

The expressions for the elevation angle θ_i and distance r_i are simply

$$(3.1.6) \quad \theta_i = \tan^{-1}\left(\frac{\Delta z_i}{\Delta x_i}\right) \text{ and } r_i = \sqrt{(\Delta x_i)^2 + (\Delta z_i)^2}, \quad \forall i \in \{1,2\}.$$

Signals reflected from next row of buildings have amplitude nearly equal to the diffracted path; therefore, the factor, Q_2 , is simply [18]

$$(3.1.7) \quad Q_2 = \frac{1}{\pi k \cos \phi} \frac{1}{r_1} D^2(\theta_1).$$

Further this relation is observed as deep fast fading and Q_2 given by (3.1.7) is twice the first term of Q_2 given by (3.1.4).

Suppose that the frequency changes from $f = \{0.9, 1.17642, 1.2276, 1.57542, 20\}$ GHz and that the building height changes from $z_b = \{10, 11, \dots, 100\}$ m. It is assumed that the building separation is approximately $d = 40$ m and that the building thickness is $w = 20$ m. Exploiting equations (3.1.4) through (3.1.6) yields the values of Q_2 shown in Figure 3.3 (a). Next, we change the building height from $z_b = \{10, 25, 50, 75, 100\}$ m and the frequency range from $f = \{1, 2, \dots, 20\}$ GHz and then compute the values of Q_2 shown in Figure 3.3 (b). The largest value of Q_2 is about -22.9 dB and the smallest value is about -53.6 dB.

Quite often we are interested in normalized values of Q_2 because a normalized value eliminates the dependence on a number of parameters and at the same time preserves the dependence of the parameter of interest such as building height and the frequency of operation. In addition to the parameters of the previous setup it is assumed that the average building height is $z_b = 12.5$ m. Therefore, utilizing the parameters of the previous setup we have normalized the values of Q_2 with respect to the antenna height of 3 m (see Figure 3.4 (a)) and also with respect to the 900 MHz operating frequency (see Figure 3.4 (b)). In general we observe that the losses Q_2 decrease with the increase of the antenna height or with decrease of the operating frequency.

Bertoni's simple diffraction model is validated with experimental results [18], which asserts that the diffraction model is the mechanism for explaining the signal reception at the street level coming from rooftop waves.

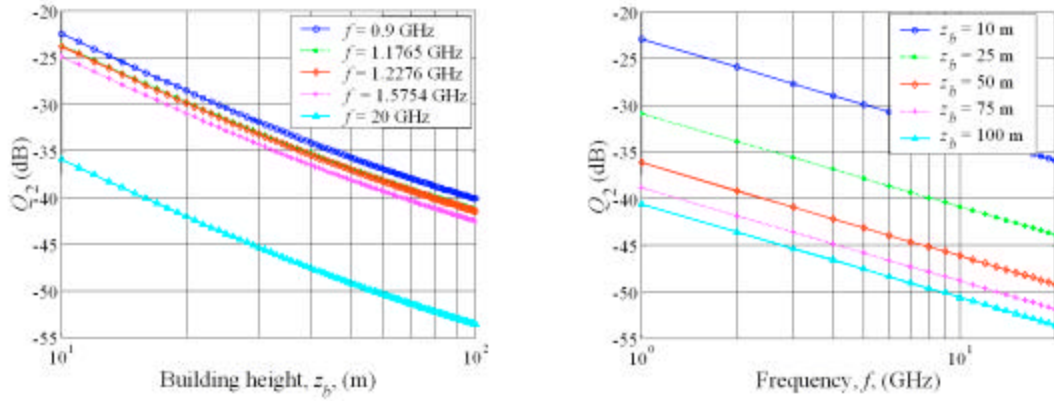


Figure 3.3 Factor Q_2 vs. (a) building height and (b) f for a macrocellular geolocation system.

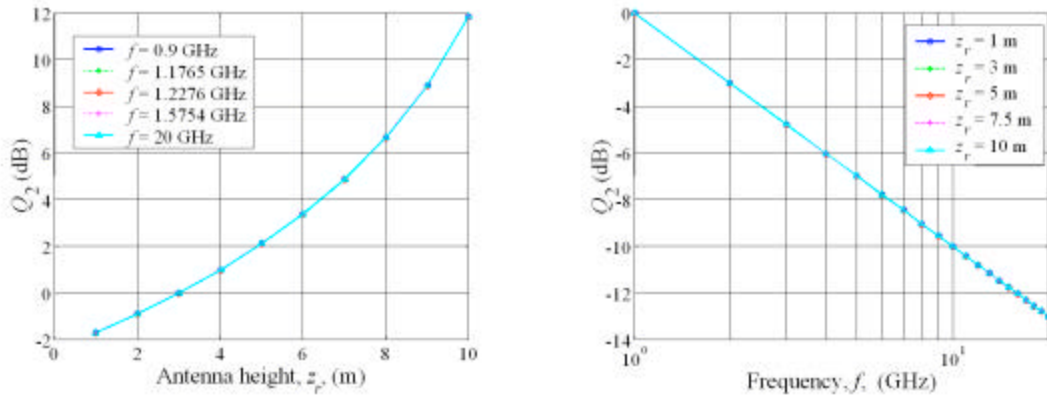


Figure 3.4 Normalized Q_2 vs. (a) antenna height and (b) f for a macrocellular geolocation system.

The field reaching the rooftop before the receiver is reduced by the factor, Q_1 . This factor depends on the row spacing, frequency, and path geometry given by the dimensionless parameter, g_p , which is determined from [18]

$$(3.1.8) \quad g_p = \mathbf{a} \sqrt{\frac{d}{l}} \cos \mathbf{f}$$

where \mathbf{a} is in radians and for flat terrain and building height, z_b , and \mathbf{a} is computed from

$$(3.1.9) \quad \alpha = \tan^{-1} \left(\frac{z_r - z_b}{R} \right) \cong \frac{z_r - z_b}{R}.$$

For $0.01 < g_p < 1.0$ a polynomial fit can be used to approximate the factor, Q_1 , as [18], [19]

$$(3.1.10) \quad Q_1(g_p) = 3.502g_p - 3.327g_p^2 + 0.962g_p^3.$$

Another useful expression for the factor, Q_1 , is obtained for $d = 50$ m, $z_t - z_b = 12$ m, and $1 < R < 10$ km

$$(3.1.11) \quad Q_1(g_p) \approx 2.35(g_p)^{0.9} = 2.35 \left(\alpha \sqrt{\frac{d}{\lambda}} \cos \phi \right)^{0.9} \approx 2.35 \left(\frac{z_t - z_b}{R} \sqrt{\frac{d}{\lambda}} \cos \phi \right)^{0.9}.$$

In order to get an intuitive understanding of the parameter, Q_1 , we consider the following example. Suppose that $R = 10$ km, $f = 60^\circ$, $d = 40$ m, $z_t = 120$ m, $z_b = \{10, 11, \dots, 100\}$, and $f = \{0.9, 1.17642, 1.2276, 1.57542, 20\}$ GHz. Based on these parameters and eq. (3.1.11) we have plotted the values of Q_1 (dB) versus z_b (m) Figure 3.5 in (a). We note that Q_1 decreases about 4 dB per meter of building height. In Figure 3.5 (b) we have considered $z_b = \{10, 25, 50, 75, 100\}$ m and have computed the values of Q_1 (dB) versus f (GHz). We note that Q_1 increases about 0.2 dB per GHz of operating frequency.

Combining the three factors together, eqs. (3.1.2), (3.1.4) or (3.1.7), (3.1.11), into eq. (3.1.3), yields, Q , given by

$$(3.1.12) \quad Q = \frac{P_r}{G_t G_r P_t} = Q_0 Q_1^2 Q_2 \\ = \frac{2.35^{1.8}}{8} \frac{\lambda^{2.1}}{(2\pi)^3} \frac{(z_t - z_b)^{1.8}}{R^{3.8}} \frac{d^{0.9}}{(\cos \phi)^{0.1}} \left[\frac{1}{r_1} D^2(\theta_1) + \frac{\Gamma^2}{r_2} D^2(\theta_1) \right]$$

or

$$(3.1.13) \quad Q = \frac{2.35^{1.8}}{4} \frac{\lambda^{2.1}}{(2\pi)^3} \frac{(z_t - z_b)^{1.8}}{R^{3.8}} \frac{d^{0.9}}{(\cos \phi)^{0.1}} \frac{1}{r_1} D^2(\theta_1).$$

Based on eq. (3.1.12), a range index 3.8 is close to what is reported in North American cities [18], [8]. The path loss, Q , varies proportionally to the wave length power of 2.1; thus, inverse proportionally to the frequency power of 2.1.

Finally, in order to illustrate the total path loss, Q , we have considered the following setup. Suppose that (azimuth angle) $\phi = 60^\circ$, (consecutive building distance) $d = 40$ m, (transmitter height) $z_t = 20$ m, (building height) $z_b = 12.5$ m, (antenna heights) $z_a = 1$ m and $f = \{0.9, 1.17642, 1.2276, 1.57542, 20\}$ GHz. Assuming that $R = \{1, 2, \dots, 20\}$ km we compute the path loss values Q for every frequency f as indicated in Figure 3.6 (a). Next,

assuming that frequency changes from $f = \{1, 2, \dots, 20\}$ GHz we compute the values of Q for every $R = \{1, 5, 10, 15, 20\}$ km as shown in Figure 3.6 (b).

According to the data shown in Figure 3.6 (a) path loss Q drops with a rate of 3 dB/km. According to the data shown in Figure 3.6 (b) path loss Q drops with a rate of approximately 1.25 dB/GHz.

Next suppose that $R = 10$ km, $z_b = \{10, 11, \dots, 100\}$ m, and using the parameters of the previous setup we compute the path loss, Q (dB), versus building height (m) for every $f = \{0.9, 1.17642, 1.2276, 1.57542, 20\}$ GHz as indicated in Figure 3.7 (a). Note a 2-dB/m drop of path loss Q . Next, assuming that the frequency changes from $f = \{1, 2, \dots, 20\}$ GHz we compute the path loss Q (dB) versus f (GHz) for $z_b = \{10, 25, 50, 75, 100\}$ m as shown in Figure 3.7 (b). Not surprisingly we note that on average there is approximately 1.5 dB/GHz drop in path loss Q .

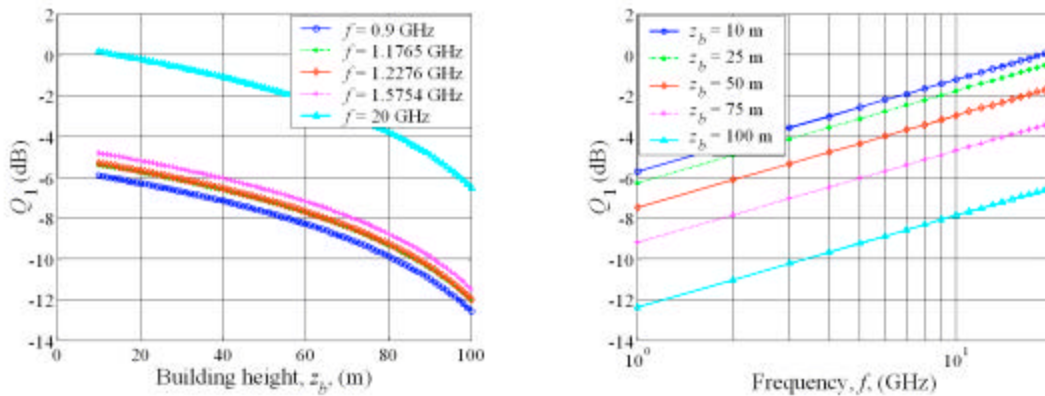


Figure 3.5 Factor Q_1 vs. (a) building height and (b) f for a macrocellular geolocation system.

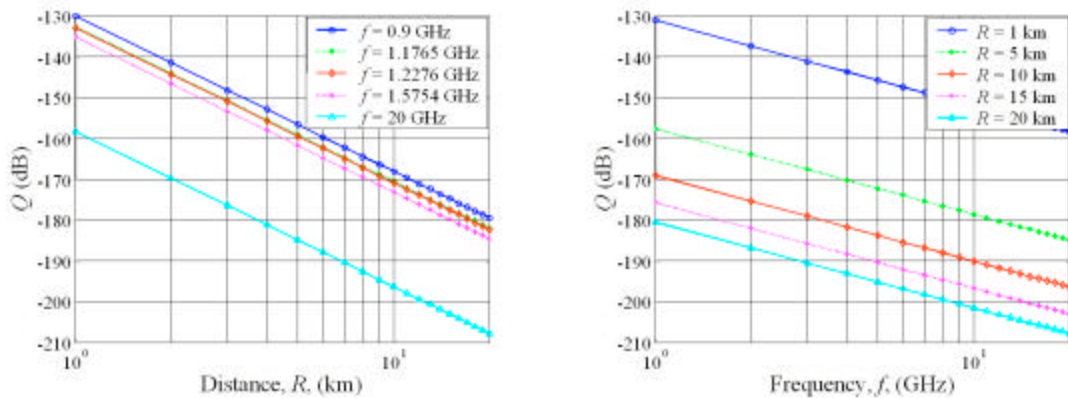


Figure 3.6 Total path loss Q (dB) vs. (a) R (km) and (b) f (GHz) for a macrocellular geolocation system.

Next suppose that $R = 10$ km, $z_b = 12.5$ m, and using the parameters of the previous example we compute the path loss, Q (dB), versus antenna height (m) for every $f = \{0.9, 1.17642, 1.2276, 1.57542, 20\}$ GHz as indicated in Figure 3.8 (a). Note a 1.5-dB/m increase of path loss Q . Next, assuming that the frequency changes from $f = \{1, 2, \dots, 20\}$ GHz we compute the path loss Q (dB) versus f (GHz) for $z_b = \{10, 25, 50, 75, 100\}$ m as shown in Figure 3.8 (b). Not surprisingly we note a 1.5-dB/GHz drop in path loss Q .

So far we have discussed the path loss model for the macrocellular geolocation system based on the ray-tracing model or on the field propagation and to some extent the geometry of buildings. Next, we discuss the multipath distribution model, which considers the statistical properties of the propagation such as path time of arrival distribution, phase of distribution, path gain, and number of paths.

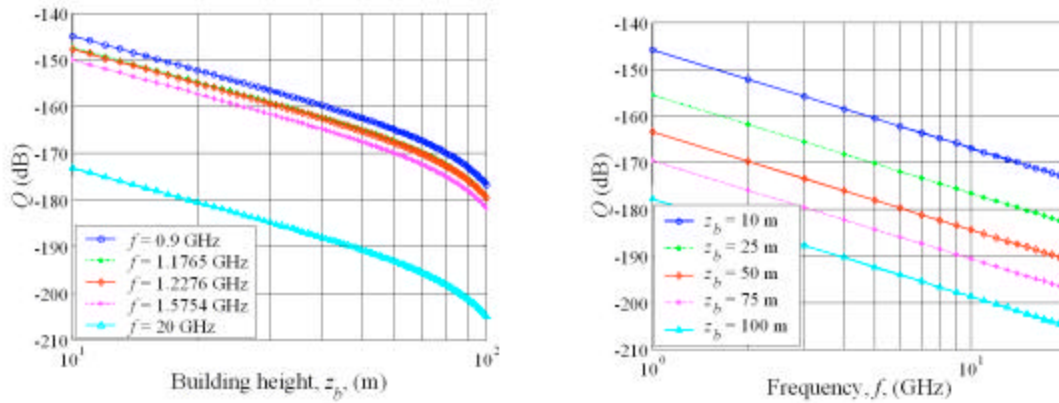


Figure 3.7 Total path loss Q (dB) vs. (a) building height (m) and (b) f (GHz) for a macrocellular geolocation system.

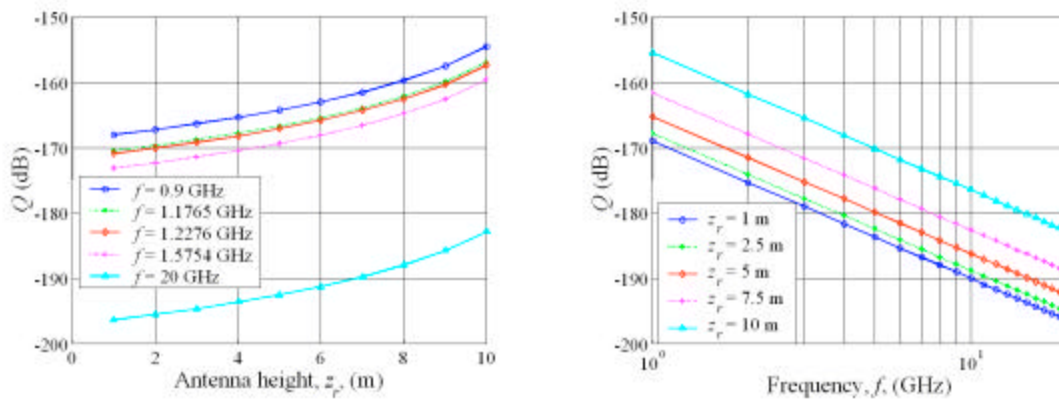


Figure 3.8 Total path loss Q (dB) vs. (a) antenna height (m) and (b) f (GHz) for a macrocellular geolocation system.

Let R_0 denote the known reference distance which is in the far field of the transmitting antenna (for example 1 km for the macrocellular systems) then the total path loss factor, Q , can be written as

$$(3.1.14) \quad Q(R_0) = \alpha_1(f) \beta_1(R_0) \frac{1}{R_0^{3.8}}$$

where α_1 is a coefficient that depends only on the operating frequency and β_1 is a coefficient that indirectly depends on the distance R_0 .

Suppose that for some distance $R > R_0$ the total path loss factor, Q , is given by

$$(3.1.15) \quad Q(R) = \alpha_1(f) \beta_1(R) \frac{1}{R^{3.8}} = Q(R_0) \left(\frac{R_0}{R} \right)^{3.8} \frac{\beta_1(R)}{\beta_1(R_0)}.$$

The above equation is written in dB as follows

$$(3.1.16) \quad Q(R)_{dB} = Q(R_0)_{dB} + 10 \times 3.8 \times \log_{10} \left(\frac{R_0}{R} \right) + 10 \log_{10} \frac{\beta_1(R)}{\beta_1(R_0)}.$$

Let f_0 denote the reference operation frequency of system. The total power loss factor, Q , (see (3.1.12)) can be expressed as

$$(3.1.17) \quad Q(f_0) = \delta_1(R) \epsilon_1(f_0) \frac{1}{f_0^{2.1}}.$$

Suppose that for some other frequency, $f > f_0$, the total path loss factor, Q , is given by

$$(3.1.18) \quad Q(f) = \delta_1(R) \epsilon_1(f) \frac{1}{f^{2.1}} = Q(f_0) \left(\frac{f_0}{f} \right)^{2.1} \frac{\epsilon_1(f)}{\epsilon_1(f_0)}.$$

Thus, the total power loss factor in dB is given by

$$(3.1.19) \quad Q(f)_{dB} = Q(f_0)_{dB} + 10 \times 2.1 \times \log_{10} \left(\frac{f_0}{f} \right) + 10 \log_{10} \frac{\epsilon_1(f)}{\epsilon_1(f_0)}.$$

3.1.1.2 Multipath Distribution of a Macrocellular Geolocation System

If $x(t)$ represents the transmitted waveform and $y(t)$ the received waveform then a multipath channel may be characterized as by its impulse response, $C(t, \tau)$. The received signal, $y(t)$, is an attenuated, time-delayed version of the transmitted signal, $x(t)$. For a discrete channel model this implies [14]

$$(3.1.20) \quad y(t) = \sum_{k=1}^{K(\tau)} a_k(t) x[t - \tau_k(t)].$$

where t and τ are the observation time and the application time of the impulse respectively, $K(\tau)$, is the number of multipath components, $\{a_k(t)\}, \{\tau_k(t)\}$ are the random time-varying amplitude (or gain) and arrival time of the k th path respectively.

Any indoor/outdoor channel is generally modeled as a time varying stochastic process described by the channel impulse response function [20],[21]

$$(3.1.21) \quad C(t, \tau) = \sum_{k=1}^{K(\tau)} a_k(t) \delta[t - \tau_k(t)] e^{j\theta_k(t)}$$

where $\{\theta_k(t)\}$ is the random phase of arrival of the k th path and δ is the Kronecker delta function. Although these parameters completely characterize any channel, the model given by equation (3.1.21) is very complicated due to the presence of four stochastic processes $K(\tau)$, $\{a_k(t)\}, \{\tau_k(t)\}$, and $\{\theta_k(t)\}$. Therefore, we must seek an approach to simplify it. If we assume that during the bit duration time the number of paths $K(\tau)$ and the path parameters $\{a_k(t)\}, \{\tau_k(t)\}$, and $\{\theta_k(t)\}$, fulfill the following

$$(3.1.22) \quad K \equiv E\{K(\tau)\}, a_k \equiv E\{a_k(t)\}, \tau_k \equiv E\{\tau_k(t)\}, \text{ and } \theta_k \equiv E\{\theta_k(t)\}$$

then the stochastic impulse response (3.1.21) is transformed into a time-invariant impulse response given by [3], [5]-[24]

$$(3.1.23) \quad C(t) \doteq \sum_{k=1}^K a_k \delta(t - \tau_k) e^{j\theta_k} .$$

The time-invariant impulse response model is more advantages than the time-varying one due to its simplicity. Now we can talk about the distribution of random path parameters a_k , τ_k , and θ_k , as opposed to stochastic processes $\{a_k(t)\}, \{\tau_k(t)\}$, and $\{\theta_k(t)\}$.

The total multipath power gain is given by [10], [22], [33]

$$(3.1.24) \quad G = \sum_{k=1}^K a_k^2 .$$

The power-weighted average multipath delay, τ , for sampled impulse response estimates is given by [10], [22], [33]

$$(3.1.25) \quad \tau = \frac{1}{G} \sum_{k=1}^K \tau_k a_k^2 .$$

The power-weighted second central moment (variance), σ^2 , of multipath component delays is given by [10], [22], [33]

$$(3.1.26) \quad \sigma^2 = \frac{1}{G} \sum_{k=1}^K \tau_k^2 a_k^2 - \tau^2.$$

The quantity, σ^2 , is also referred to as the static rms delay spread for the channel.

The above parameters can be estimated directly from the power profile $|h(t)|^2$ of the channel impulse response [11]. Defining the power profile moments [22]

$$(3.1.27) \quad M_n = \int_{-\infty}^{\infty} t^n |h(t)|^2 dt$$

we can obtain the power-weighted average multipath delay as [22]

$$(3.1.28) \quad \tau = \frac{M_1}{M_0}$$

and the power-weighted second central moment (variance) as [22]

$$(3.1.29) \quad \sigma^2 = \frac{M_2}{M_0} - \tau^2.$$

Some researchers utilize these parameters to evaluate the propagation characteristics of a given channel especially of indoor channels. Therefore we discuss them more extensively in §3.1.3.2.

Next we discuss the distribution of the path parameters, a_k , τ_k , and θ_k . We start first with the distribution of the path amplitude (or gain), a_k , for macrocellular geolocation systems. The average path loss is what remains after averaging the path loss over the fast fading due to multipath [16]. The macrocells were the basis for the first generation mobile systems with transmitters generally at high points like broadcasting systems with an area of coverage of several kilometers [16]. The key problem is to understand of the seemingly noise-like path loss existing over a variety of terrains such as land cover, mixed land and sea, and sea [16]. It is observed that the slow shadowing fading is remarkably close to a lognormal distribution, which implies that the average path loss in dB has a normal distribution [16]. Due to multipath reflections in a macrocell multipath environment, the fading phenomenon can be characterized as a multiplicative process, which renders the empirical explanation for the occurrence of this distribution. Moreover, multiplication of signal amplitudes give rise to a lognormal distribution, in the same manner that an additive process results in a normal distribution (central limit theorem) [16], [21].

It is widely accepted that for a macrocellular geolocation system the path amplitude, a_k , is log-normally distributed with the probability density function (pdf) given by [16], [21]

$$(3.1.30) \quad f(a_k) = \frac{1}{\sqrt{2\pi\alpha}a_k} \exp\left\{-\frac{(\log a_k - \eta)^2}{2\alpha^2}\right\}, \quad a_k \geq 0$$

where η is the mean and α is the standard deviation of $\log a_k$ not of a_k . The mean and variance of a_k are given by [25], [43]

$$(3.1.31) \quad \mu = \exp(\eta + \alpha^2/2) \text{ and } \sigma^2 = \exp(2\eta + \alpha^2)(\exp \alpha^2 - 1).$$

Given μ and σ^2 one can compute the parameters η and α^2 in the manner shown below

$$(3.1.32) \quad \alpha^2 = \log\left(\frac{\sigma^2}{\mu^2} + 1\right) \text{ and } \eta = \log \mu - \frac{\alpha^2}{2}.$$

The lognormal pdf and lognormal cumulative distribution function (cdf) for $\mu = \{0.3, 0.6\}$ and $\sigma = \{0.0157, 0.0626\}$ are illustrated in Figure 3.9. Hence, with a probability of 68 %, 95 % and 99 % the path gain values are centered around $(\mu - \sigma, \mu + \sigma)$, $(\mu - 2\sigma, \mu + 2\sigma)$, and $(\mu - 3\sigma, \mu + 3\sigma)$ respectively [25].

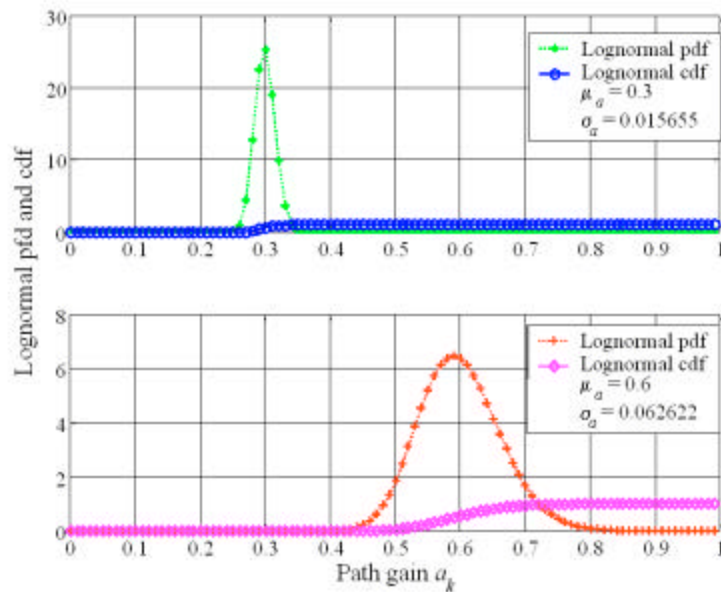


Figure 3.9 The lognormal pdf and cdf of the path gain, a_k , for $m = \{0.3, 0.6\}$ and $s = \{1.57, 6.26\}$ * $1e-2$.

Before we look at the interarrival time, τ_k , we should note that only the NLOS paths are randomly distributed as opposed to the LOS path, which is a deterministic function. Therefore, it makes sense to look at the $\{\tau_k - \tau_1\}$ for $k = \{2, \dots, \infty\}$. Typically, the distribution of the sequence $\{\tau_k - \tau_1\}$ for $k = \{2, \dots, \infty\}$ follows a Poisson model with pdf given by [16], [25], [43]

$$(3.1.33) \quad f(k) = \Pr(K = k) = \frac{\mu^k e^{-\mu}}{k!}$$

where $\mu \triangleq \int_T \lambda(t) dt$ is the Poisson parameter ($\lambda(t)$ is the mean arrival rate at time t). If, on the other hand, the process is stationary (for $\lambda(t) = \text{constant}$) then $E\{K\} = V\{K\} = \lambda$ [21]-[25], [43].

Let $x_k = \tau_k - \tau_{k-1}$ denote the interarrival time. For a standard, stationary Poisson process the interarrival times are independent, identically distributed with an exponential distribution given by

$$(3.1.34) \quad f_x(x_k) = \lambda e^{-\lambda x_k}, \quad x_k > 0.$$

Figure 3.10 illustrates the exponential pdf and cdf of the interarrival times for $\lambda = \{0.5, 1\}$. As we know that parameter λ determines the mean and the variance for this type of distribution.

There are no empirical data to date that provide an understanding of the distribution of the path phases, θ_k , due to difficulties associated with measuring the phase of individual multipath components [21]. Since the phase of every multipath component changes by 2π every time the path length changes by a wavelength (19 cm for the $L_1 = 1575.42$ MHz GPS frequency) it is reasonable to assume that the individual path phases, θ_k , are uniformly distributed over $[0, 2\pi)$. Figure 3.11 illustrates the uniform pdf and cdf of the path phases. The mean of the path phases is equal to π and the variance is equal to $\pi^2/3$.

Here we conclude the discussion on the macrocellular channel model and start the discussion on the microcellular channel model.

3.1.2 The Physics of Propagation for Microcellular Geolocation Systems

A microcellular geolocation system consists of a network of microcells. The transmitter antenna in a microcell has a coverage radius going from 100 m up to 1 km [15]-[18]. Similar to the macrocellular geolocation systems, physics of propagation for microcellular geolocation systems can be classified into two groups: (1) path loss (see §3.1.2.1) and (2) multipath distribution (see §3.1.2.2).

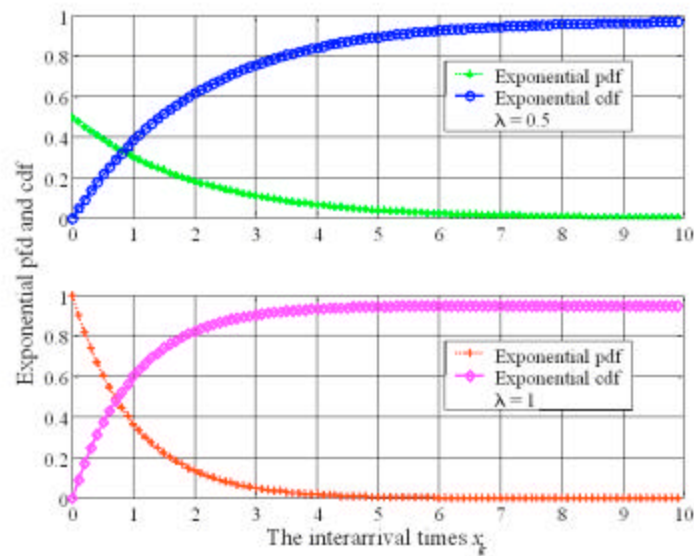


Figure 3.10 The exponential pdf and cdf of interarrival times, x_k , for $\lambda = \{0.5, 1\}$.

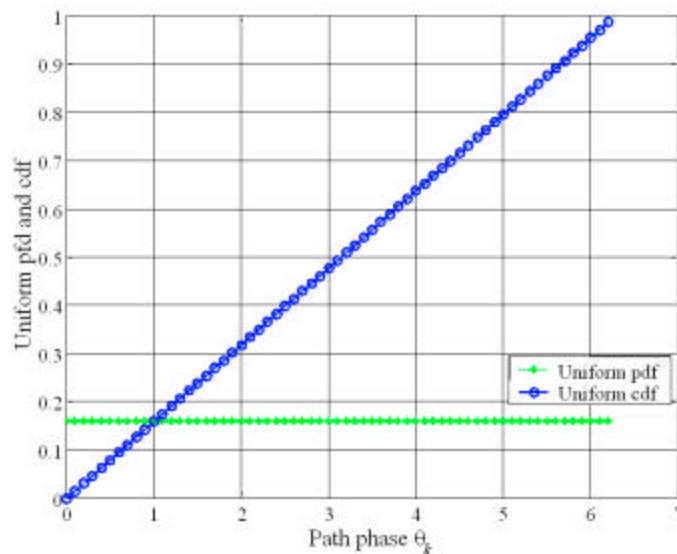


Figure 3.11 The uniform pdf and cdf of path phases, q_k .

3.1.2.1 Path Loss

The path loss model for the microcell geolocation systems is different from the path loss model of the macrocell geolocation systems. The discussion presented here is verified with experimental results, which confirms the accuracy of the prediction models.

Consider a simple two-ray model as illustrated in Figure 3.12. The receiver receives two rays: the line-of-sight (LOS) component and the non-line-of-sight component (NLOS). For isotropic antennae the line of sight path loss factor is given by [18]

$$(3.1.35) \quad Q_{LOS} = \left(\frac{\lambda}{4\pi} \right)^2 \left| \frac{1}{r_1} \exp(-jkr_1) + \Gamma \frac{1}{r_2} \exp(-jkr_2) \right|^2$$

where r_1 and r_2 are the direct and ground reflected ray paths and Γ is the ground reflection coefficient defined as [18]

$$(3.1.36) \quad \Gamma = \frac{\cos \theta - a\sqrt{\epsilon - \sin^2 \theta}}{\cos \theta + a\sqrt{\epsilon - \sin^2 \theta}}$$

where $a = 1$ for horizontal polarization and $a = 1/\epsilon$ for vertical polarization. For typical ground surfaces ϵ is equal to $\epsilon = 15 - j90/f$, where f is the frequency of operation in MHz [18].

In order to assess the line of sight path loss, Q_{LOS} (dB), as a function of the frequency and distance between the transmitting antenna and receiving antenna, R , we consider two examples. For these examples, the height of the transmitting/receiving antenna is 20/1.5 m.

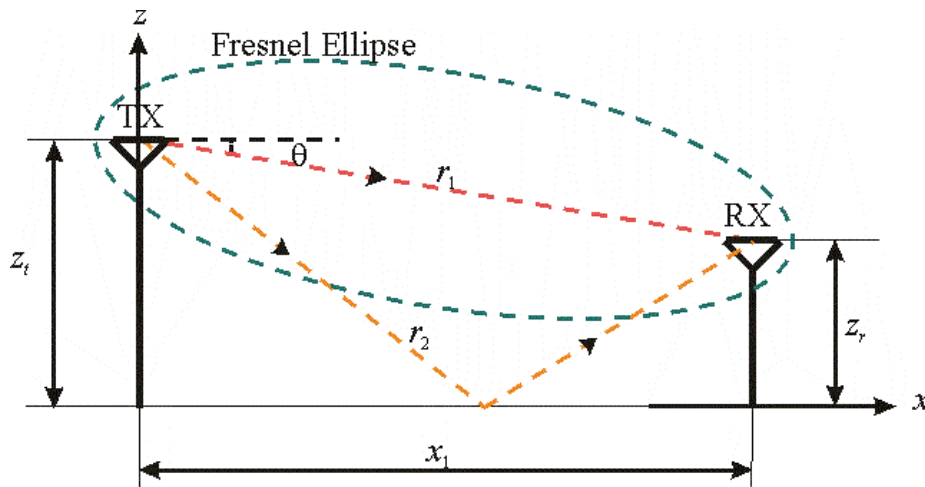


Figure 3.12 Two ray model showing the Fresnel ellipse about the direct ray—taken and modified from [18].

Figure 3.13 (a) and (b) illustrate the line of sight path loss, Q_{LOS} (dB), versus the distance between the transmitter and the receiver, R , for every $f = \{0.9, 1.17642, 1.2276, 1.57542, 10\}$ GHz, for horizontal polarization (a) and vertical polarization (b). The distance R changes from 10 m to 1000 m. The line of sight path loss at 900 MHz for $R = 10$ m is about $-47/-51$ dB and for $R = 1000$ m is about $-92/-89$ dB for horizontal/vertical polarization. The path loss corresponding to L_5 is almost the same as the path loss corresponding to L_2 and somewhat different from the one corresponding to the L_1 frequency. The LOS path loss at 10 GHz for $R = 10$ m is about $-80/-69$ dB and for $R = 1000$ m is about $-120/-108$ dB for horizontal/vertical polarization. The line of sight path loss numbers for R between 10 and 100 m are comparable with the numbers provided in Fig. 20 of [18]. The line of sight path loss at 900 MHz is about 20/15 dB higher than the path loss at 10 GHz for horizontal/vertical polarization. The line of sight path loss drops somewhat faster for horizontal polarization than for vertical polarization. Henceforth, vertical polarization would be a better choice than horizontal polarization.

Figure 3.14 (a) and (b) illustrate the line of sight path loss, Q_{LOS} (dB), versus the frequency, f , for every $R = \{10, 250, 500, 750, 1000\}$ m, for horizontal polarization (a) and vertical polarization (b). The frequency f changes from 1 to 10 GHz. The line of sight path loss for $R = 10$ m and $f = 1$ GHz is about -55 dB and for $f = 10$ GHz is about -75 dB for either horizontal or vertical polarization. The line of sight path loss for $R = 250$ m and $f = 1$ GHz is about $-80/-78$ dB and for $f = 10$ GHz is about $-108/-96$ dB for horizontal/vertical polarization. The line of sight path loss for $R = 500$ m and $f = 1$ GHz is about $-83/-90$ dB and for $f = 10$ GHz is about $-113/-102$ dB for horizontal/vertical polarization. The line of sight path loss for $R = 750$ m and $f = 1$ GHz is about $-88/90$ dB and for $f = 10$ GHz is about $-107/-111$ dB for horizontal/vertical polarization. The line of sight path loss for $R = 1000$ m and $f = 1$ GHz is about $-92/-90$ dB and for $f = 10$ GHz is about $-120/-108$ dB for horizontal/vertical polarization. The line of sight path loss at 10 m is about 40 dB higher than the path loss at 1000 m for either horizontal or vertical polarization. The minimums and maximums of the line of sight path loss depend on the distance as well as the frequency. The line of sight path loss drops somewhat faster for

horizontal polarization than for vertical polarization. Henceforth, vertical polarization would be a better choice than horizontal polarization.

Based on the data that is shown in Figure 3.13, we find the logarithmic power slope of the Q_{LOS}

$$(3.1.37) \quad Q_{LOS(R=10)} = Q_{R_0} + 10n = -50 \text{ dB and } Q_{LOS(R=100)} = Q_{R_0} + 20n = -70 \text{ dB}$$

Solving the above system produces, $Q_{R_0} = -30 \text{ dB}$ and $n = -2$; hence, the logarithmic power slope for the Q_{LOS} curves shown in Figure 3.13 is -2 . Similarly, we can find that the logarithmic power slope for the curves shown in Figure 3.14 is $m = -2$.

It is suggested that the Fresnel radius, R_b , is an important parameter that determines the degree of the logarithmic power slope defined as [18], [26]

$$(3.1.38) \quad R_b = \frac{4z_r z_r}{\lambda}.$$

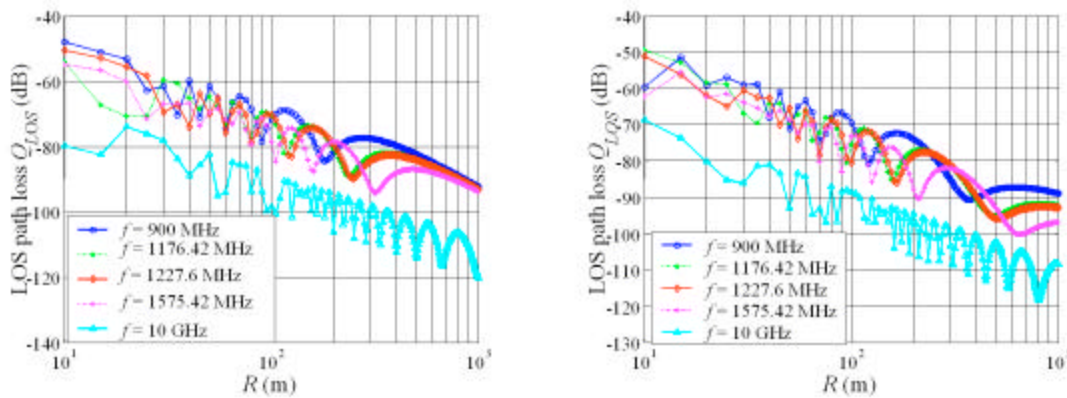


Figure 3.13 The LOS path loss, Q_{LOS} , vs. the distance between TX and RX, R .

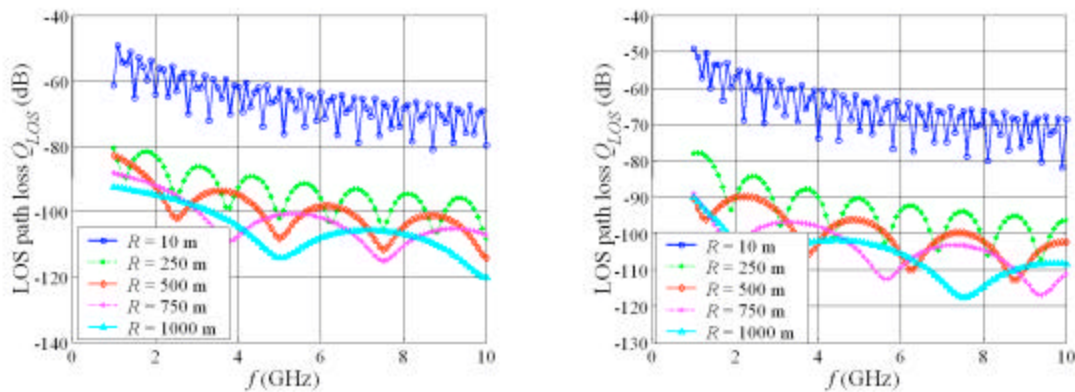


Figure 3.14 The LOS path loss, Q_{LOS} , vs. the frequency, f (GHz).

The Fresnel distances for the first experiment are $R_b = \{360, 470, 491, 630, 4000\}$ m which correspond to the frequencies $f = \{0.9, 1.17642, 1.2276, 1.57542, 10\}$ GHz. As shown in Figure 3.13 (a) and (b) the logarithmic power slope is near 2 for $x_r < R_b$ or equal to $x_r > R_b$.

For a given transmitting/receiving antenna height of 13.4/1.6 m, measuring the normalized signal strength (dB) at 800-MHz frequency for a transmitter receiver distance varying from 1 to 1000 m on a logarithmic scale produces a regression line slope less than 2 for $x_r < R_b$ and near 4 for $x_r > R_b$ [18], [27]. Nevertheless, the effect of traffic on all the ground-reflected rays is not fully understood. Measurements made in Manhattan and two experiments shown in Figure 3.13 and Figure 3.14 show a logarithmic power slope is near 2 at distances beyond, R_b [28]. Therefore this is currently a controversial issues to be resolved in the future.

The propagation over buildings for low antennae is treated next. The reduction Q_M in the rooftop field at the M^{th} row past the base station due to propagation past the previous rows depends on the signal frequency and path geometry. The last two parameters conspire the dimensionless parameter, g_c , given by [18], [29]

$$(3.1.39) \quad g_c = (z_t - z_b) \sqrt{\frac{\cos \phi}{\lambda d}}.$$

The reduction Q_M [19], [29] can be computed from the Boersma functions $I_{n,q}$ [30] given by

$$(3.1.40) \quad Q_M = \sqrt{M} \left| \sum_{q=0}^{\infty} \frac{1}{q!} (2g_c \sqrt{j\mathbf{p}})^q I_{M-1,q} \right|$$

where the recursion relation for the Boersma function is [19], [29], and [30]

$$(3.1.41) \quad I_{M-1,q} = \frac{(M-1)(q-1)}{2M} I_{M-1,q-2} + \frac{1}{2\sqrt{\mathbf{p}}M} \sum_{n=1}^{M-2} \frac{I_{M-1,q-1}}{\sqrt{M-1-n}}$$

with initial terms

$$(3.1.42) \quad I_{M-1,0} = M^{-3/2}$$

and

$$(3.1.43) \quad I_{M-1,1} = \frac{1}{4\sqrt{\mathbf{p}}} \sum_{n=0}^{M-1} \frac{1}{(nM - n^2)^{3/2}}.$$

If $g_c = 0$ then $Q_M(g_c = 0) = 1/M$, which is equivalent to $\log[Q_M(g_c = 0)] = -\log M$; the log of Q_M decreases linearly with the log of M . If $z_{TX} < z_B$ then the $\log Q_M$ (i.e., the slope of the curve of $\log Q_M$) decreases initially more rapidly than $\log M$ but it quickly approaches the $\log M$ variation. Conversely, if $z_{TX} > z_B$ then the $\log Q_M$ decreases initially less than $\log M$ but it quickly approaches the $\log M$ variation [18], [19]. Quantitatively, the slope of the curves is given by

$$(3.1.44) \quad s = -\frac{\log(Q_{M+1}/Q_M)}{\log[(M+1)/M]} = \frac{\log Q_M - \log Q_{M+1}}{\log(M+1) - \log M}.$$

The range index, n , is computed in terms of the slope, s , as follows:

$$(3.1.45) \quad n = 2(1 + s).$$

For low antennae the index, n , is greater than 4 and for high antennae the index, n , is close to 3.8 as predicted [18].

The approach presented here has a limitation because it does not account for crossing streets, which can form a significant fraction of all paths over a small area (see Figure 3.15). Also, the present approach does not account for high (or very tall) buildings (see Figure 3.16). For very tall buildings, the propagation is not carried out over the buildings but through the streets and around the corners [18].

Figure 3.15 depicts the approximate footprints of the houses in a typical downtown district and the propagation paths from a mid-block base station to several nearby subscriber locations. Paths 1–7 involve diffraction past rows of buildings parallel to the street on which the base station is located, and 1, 3, 4, 5, and 7 also involve diffraction at rows on perpendicular streets. Finally, line of sight propagation occurs on path 8, which is evaluated using the two-ray model for vertical polarization [18].

Replacing the buildings by absorbing screens located at the center of the building and oriented perpendicular to the propagation path is employed to evaluate the diffraction at the rooftops. Assuming a building height of 8 m, the -110 dB path loss contours are plotted in [18] for three base station heights 4, 8, and 14 m. It is observed that antenna height strongly affects the coverage area. Similar calculations for a base station located in a backyard rather than a street show that elimination of LOS path results in a more elliptical coverage area [18], [31], and [32].

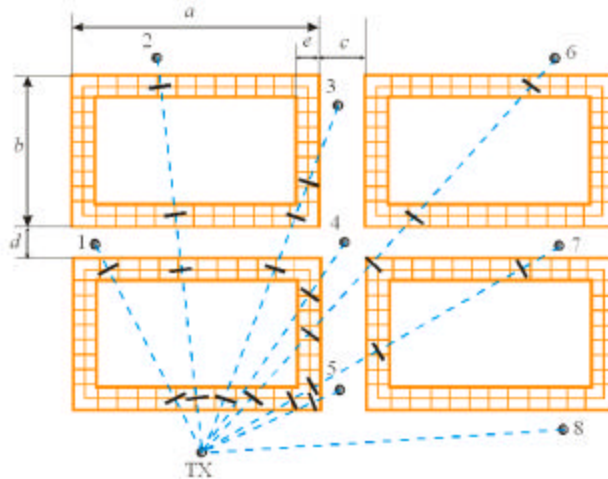


Figure 3.15 Footprints of four rectangular multiple story buildings—modified from [18].

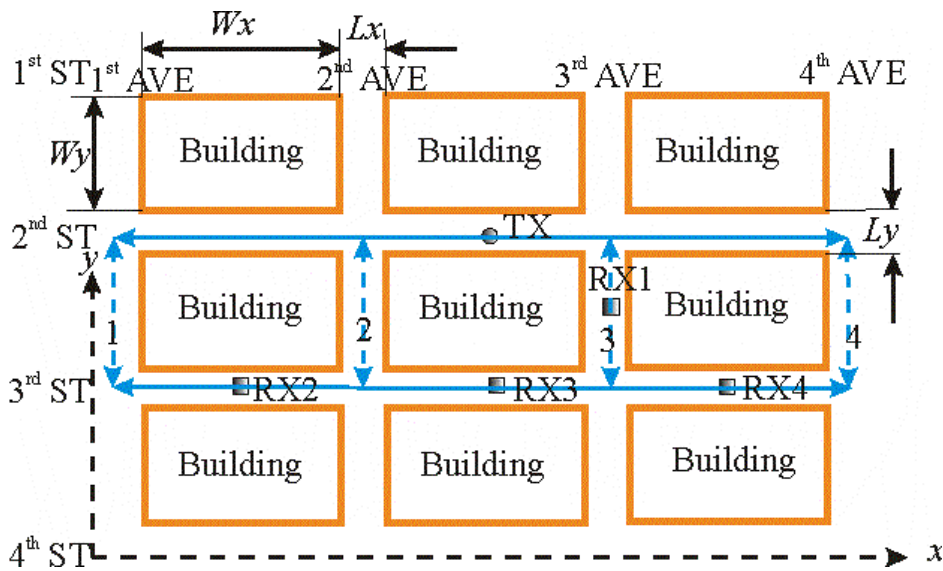


Figure 3.16 Two turn routes from the transmitter to the receiver—modified from [18].

It is found that the signal power level decreases by about 20 dB when the signal propagation path turns a corner. Thus the signal received by receivers on streets that cross the 2nd street on which the transmitter is located, such as RX1 is essentially due to signals that make a single turn off the 2nd street, as indicated by route 1. More turns are required to reach locations on streets parallel to the 2nd street, such as RX2, RX3, and RX4 which are all located in 3rd street [18].

Each one turn route is composed of an infinite number of two-dimensional (2D) ray paths that make m reflections at the buildings on the 2nd street followed by n reflections at the buildings on the 3rd avenue (RmDRn rays). Rays that are multiply diffracted at the

corners of one intersection are ignored since they are significantly weaker. Note that each 2D ray is composed of two rays, one of which is reflected from the ground and appears to come from the image of the transmitter in the ground plane [18].

On one hand, the path loss associated with a RmRn ray for vertically polarized antennae is given by [18]

$$(3.1.46) \quad Q_{mn} = |\Gamma(\phi_1)|^{2m} |\Gamma(\phi_2)|^{2n} Q_{LOS}$$

where $\Gamma(\phi_i)$, $\forall i \in \{1,2\}$, are the reflection coefficient at the building faces from the 2nd street and 3rd avenue. The factor Q_{LOS} is computed from eq. (3.1.35) and r_1 and r_2 are the total unfolded path lengths of the two three-dimensional (3D) rays. On the other hand, the path loss associated with a RmDRn ray is computed from [18]

$$(3.1.47) \quad Q_{mDn} = |\Gamma(\phi_1)|^{2m} |\Gamma(\phi_2)|^{2n} Q_{LOS} D^2(\psi) \frac{\rho_1 + \rho_2}{2\pi k \rho_1 \rho_2} = Q_{mn} D^2(\psi) \frac{\rho_1 + \rho_2}{2\pi k \rho_1 \rho_2}$$

where ρ_1 and ρ_2 are the unfolded 2D ray lengths between the diffracting edge and the transmitter or receiver respectively. For an absorbing boundary condition, the diffraction coefficient, $D(\psi)$, is given by (3.1.5). Also, the diffraction angel ψ is negative in the illuminated region and positive in the shadow region.

This model given by equations (3.1.46) and (3.1.47) can be transformed in the form of

$$(3.1.48) \quad Q_{mDn}(R) = \alpha_2(f) \beta_2(R) \frac{1}{R^n}$$

where $\alpha_2(f)$ and $\beta_2(R)$ are different from $\alpha_1(f)$ and $\beta_1(R)$ corresponding to the macrocellular systems. This is going to yield the following

$$(3.1.49) \quad Q_{mDn}(R)_{dB} = Q_{mDn}(R_0)_{dB} + 10n \log_{10} \frac{R_0}{R} + 10 \log_{10} \frac{\beta_2(R)}{\beta_2(R_0)}$$

where R_0 is the reference distance equal to 1 km.

Similarly, this model given by equations (3.1.46) and (3.1.47) can be transformed in the form of

$$(3.1.50) \quad Q_{mDn}(R) = \delta_2(R) \varepsilon_2(f) \frac{1}{f^m}$$

where $\delta_2(R)$ and $\varepsilon_2(f)$ are different from $\delta_1(R)$ and $\varepsilon_1(f)$ corresponding to the macrocellular systems. This is going to yield the following

$$(3.1.51) \quad Q_{mDn}(f)_{dB} = Q_{mDn}(f_0)_{dB} + 10m \log_{10} \frac{f_0}{f} + 10 \log_{10} \frac{\epsilon_2(f)}{\epsilon_2(f_0)}.$$

Note the n and m for microcellular geolocation systems can be different from n and m corresponding to macrocellular geolocation systems. For example, based on the measurements performed in five German cities [16] the slope n varies from -2 to -5 .

3.1.2.2 Multipath Distribution for Microcellular Geolocation Systems

The channel model for microcellular geolocation systems is essentially the same as the channel model for macrocellular geolocation systems given by equation (3.1.23). The difference here is the multipath distribution of the path gain, a_k , of the path interarrival time, τ_k , of the path phases, θ_k , and of the number of paths, K .

For most microcellular geolocation systems the distribution of the path gain, a_k , is Rician due to the presence of a strong LOS component or a path that goes through much less attenuation compare to other arriving paths [21]. In this case the received signal vector is modeled as the sum of two vectors: a deterministic vector in amplitude and phase and a scattered Rayleigh vector with random amplitude and phase. If the fixed component is denoted by $ve^{j\phi}$ (v and ϕ are not random) and the random component is denoted by $ue^{j\varphi}$ (u and φ are random) then the received signal vector $ae^{j\theta}$ is the phasor sum of the above two signals. The joint pdf of a (or a_k) and θ (or θ_k) is given by [2], [21]

$$(3.1.52) \quad f(a_k, \theta_k) = \frac{a_k}{2\pi\alpha^2} \exp\left[-\frac{a_k^2 + v^2 - 2a_kv \cos(\theta_k - \phi)}{2\alpha^2}\right], \quad a_k \geq 0, \quad -\pi \leq \theta - \phi \leq \pi.$$

Furthermore, since the length and the phase of the fixed path usually changes, ϕ , itself is a random variable uniformly distributed in the semi-interval $[0, 2\pi)$. Randomizing ϕ causes a_k and θ_k to become independent with θ_k having a uniform distribution and a_k have the Rician distribution given by [21]

$$(3.1.53) \quad f(a_k) = \frac{a_k}{\alpha^2} \exp\left[-\frac{a_k^2 + v^2}{2\alpha^2}\right] I_0\left(\frac{a_kv}{\alpha^2}\right), \quad a_k \geq 0$$

where I_0 is the zeroth-order of the modified Bessel function of the first kind, v is the magnitude (envelope) of the strong component and α^2 is proportional to the power of the scattered Rayleigh component [21].

When ν goes to zero (or if $\nu^2 \ll a_k^2$), the strong path is eliminated and the amplitude becomes Rayleigh as expected, which explains why the Rician distribution contains Rayleigh distribution as a special case. If, on the other hand, $\nu^2 \gg a_k^2$, power in the direct path is considerably higher than the combined random paths; hence, a_k and θ_k are both approximately Gaussian, r having a mean equal to ν_k and θ_k having a mean equal to zero [21].

Several measurements conducted in the factory environments have indicated that Rician distribution is a good fit for signal amplitudes of microcellular systems [13], [16], [20]. The rms delay spread is between 10 – 100 ns.

The Rician pdf and cdf for $\nu = \{0.6, 0.6\}$ and $\alpha = \{0.0521, 0.1041\}$ are pictured in Figure 3.17.

The mean and the variance of the Rician distribution are computed numerically and for our example the values are $\mu = \{0.3, 0.6\}$ and $\sigma = \{1.57, 6.26\} * 1e-2$. The Rician distribution is compared and contrasted to the lognormal and Rayleigh distribution in §3.1.3.2. Here we conclude our discussion on microcell propagation and distribution models and start our discussion on picocell propagation and distribution models.

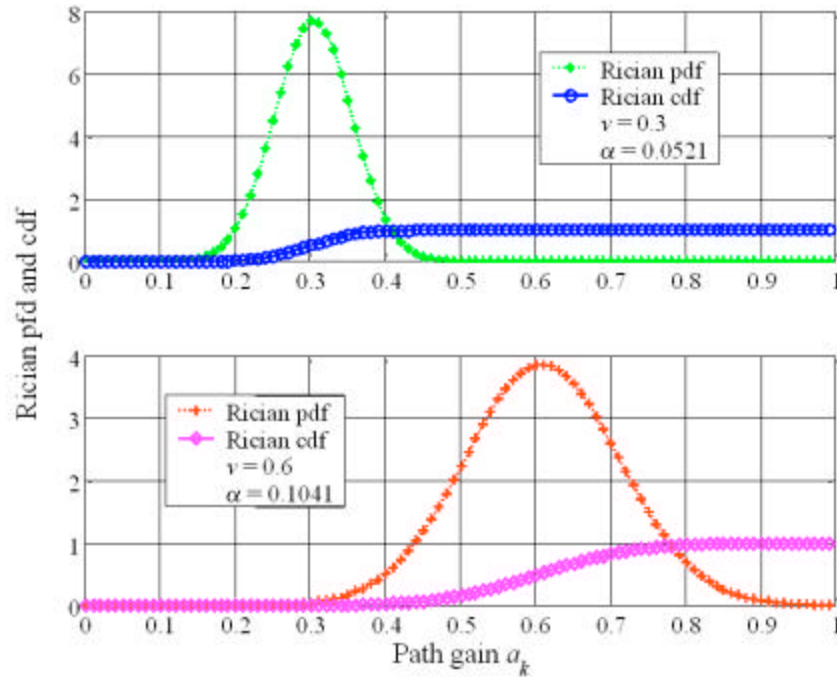


Figure 3.17 The Rician pdf and cdf of path gain, a_k , for $\nu = \{0.3, 0.6\}$ and $\alpha = \{0.0521, 0.1041\}$.

3.1.3 The Physics of Propagation for Indoor Geolocation Systems

An indoor geolocation system may be pictured as having one or several picocells. The transmitter antenna in a picocell has a coverage radius from 1 m up to 150 m [15]-[18]. As we are now already familiar with, the physics of propagation for indoor geolocation systems can be classified into two groups: (1) path loss model (see §3.1.3.1) and (2) multipath distribution model (see §3.1.3.2).

3.1.3.1 Path Loss Model for Indoor Geolocation Systems

The indoor propagation includes scattering inside rooms, refraction between rooms, penetration between floors, refraction from inside to outside, and refraction from outside to inside. It is suggested that either 2-D or 3-D ray tracing models can be applied to yield accurate indoor propagation predictions [18]. Due to the complexity associated with the analysis for the indoor channel model, we consider only the indoor propagation model due to scattering inside rooms and the most important one. Refraction between rooms, penetration between floors, refraction from inside to outside and from outside to inside have to some extent a similar behavior. Depending on the wall or floor material, thickness, and surface, a propagation loss of 10–15 dB is reported for these types of indoor propagation. The alternative to ray-tracing models is to create a model based on indoor experiments [17], [34], and [38] or on statistical models, which is discussed in §3.1.3.2.

The propagation inside rooms includes the influence of room furniture and ceiling fixtures. Due to the typical construction of modern buildings, the ray incident on the ceiling and on the floor will be scattered rather than reflected inside rooms [18], which is illustrated in Figure 3.18. As indicated in Figure 3.18, when the transmitter and receiver are placed in clear space it is suggested that the propagation can be explained through Fresnel ellipse mechanism [18]. For small distances between the transmitter and receiver the ellipse lies entirely within the clear space, and the presence of scattering will not affect the fields associated with the direct ray; therefore, the path loss will have the $1/R^2$ free-space dependence [18]. As we increase the separation between transmitter and receiver the ellipse becomes larger, and the scattering is contained within the ellipse (see Figure 3.18), which produces a path loss greater than that of the free-space [18].

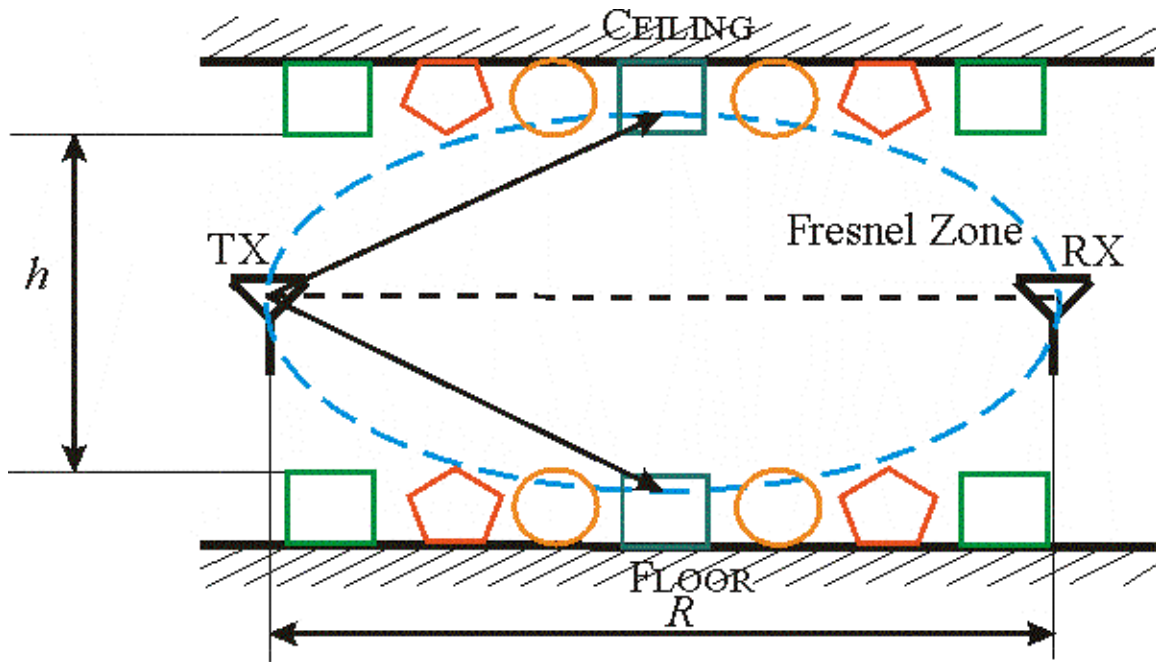


Figure 3.18 The Fresnel zone for propagation between the TX and RX in clear space between building furnishings and ceiling fixtures—taken and modified from [18].

The ellipse first encounters the scattering at a distance h^2/l . The path loss in excess to the free space is computed at 900 and 1800 MHz for $h = 1.5$ m and is plotted in Fig. 36 of [18] as a function of the transmitter receiver separation R . The path loss is small for small distances up to 40 m and then increases dramatically. The theoretical approach finds good agreement with the measurements made in an office building having very large open areas furnished with 1.57-m high cubicles but with no floor to ceiling walls [18].

Ray procedures have been used to account for reflection and transmission at interior and exterior walls, treating the interaction as a specular process. Use of the specular approach involves two approximations, the first being that the linear extent of the wall is large enough to act as a planar reflector, and that it is electrically smooth so that the scattering does not dominate. For ray paths whose unfolded length is up to 100 m, the maximum width of the Fresnel ellipse in the horizontal plane is less than 4.1 m at 900 MHz and 2.9 m at 1.8 GHz. Since the length of walls is commonly 4 m or more, they span most of the Fresnel zone, or several zones, so that they can reasonably be considered large [18].

Figure 3.19 shows the ray model dealing with wall reflections [18]. Five rays emanated from the transmitter reach the receiver after the transmission through and reflection from the walls. The total path length L is the sum of the path length of specular components. For example, the path loss of the signal associated with the r_1 and r_2 specular components, whose path length equal to $(r_1 + r_2)$, is proportional with the factor $1/(r_1 + r_2)^2$ is addition to the excess path loss of Fig. 36 of [18]. Nevertheless, scattering, associated with segments s_1 and s_2 , exhibits a multiplicative factor of $1/(s_1 s_2)^2$ [18]. Scattering influences the signal in the vicinity of the walls and its amplitude decreases more rapidly with distance than the amplitude of the reflected rays; therefore, it is neglected [18].

Ray shooting approach or *image theory* are usually suggested to determinate all possible 2D ray paths. In the first approach rays start off from the transmitter at one degree angular interval. Each ray is traced through its interaction with the first wall, where it generates a transmitted and reflected ray [18]. Both rays are then traced to the next interaction, and so on, building a binary tree of rays, which continues through some present number of interactions [18].

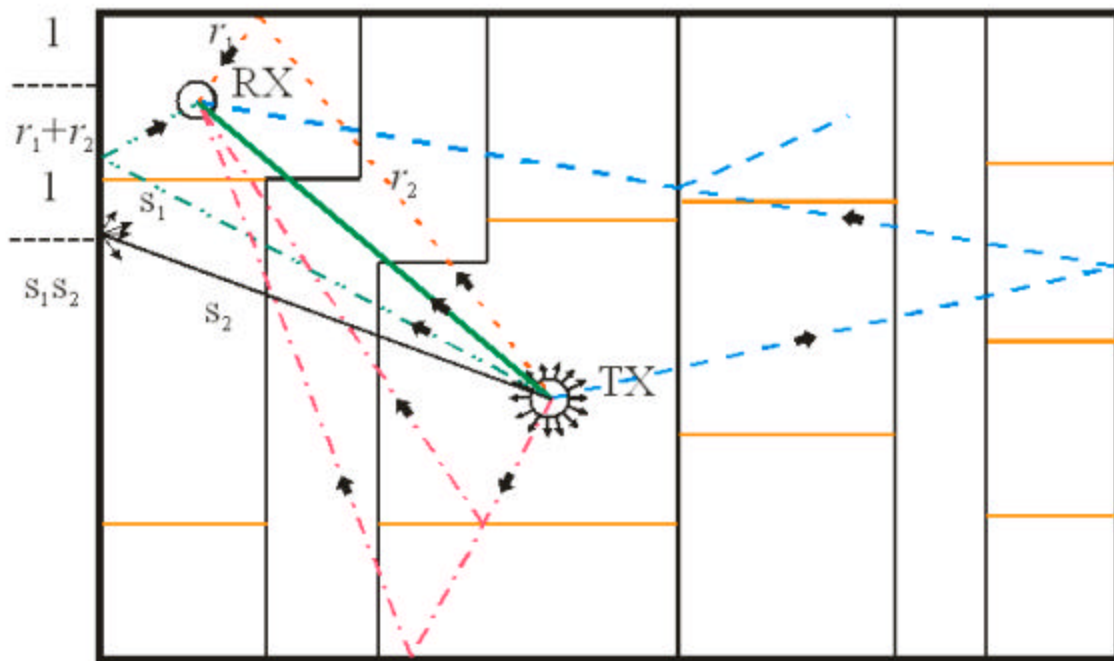


Figure 3.19 The two dimensional ray-tracing accounting for specular reflection and transmission at walls—taken and modified from [18].

It is known that discrete rays have zero probability of intercepting a given point; thus, a circle of finite radius proportional to the ray length is used to represent the receiver [18]. In the second approach the exact ray path between points is determined by imaging the source in the plane of each wall, one at a time, and checking that the plane between the image and the receiver intersects the wall in the physically existing segments. The same process is repeated for double/triple imaging of all combinations of the two/three walls etc [18]. It is reported that triple imaging is adequate for most cases [18].

Assuming isotropic antennae and having found the contributing rays, the path loss associated with the i th ray is computed from

$$(3.1.54) \quad Q_i = Q_0 E(L_i) \prod_n |G_n(\mathbf{f}_{ni})|^2 \prod_m |G_m(\mathbf{f}_{mi})|^2$$

where L_i is the total unfolded path length of the ray and Q_0 is the free-space factor given by (3.1.2). The coefficient $E(L_i)$ includes the excess path loss and the coefficients $G_n(\mathbf{f}_{ni})$ and $G_m(\mathbf{f}_{mi})$ are the reflection and refraction coefficients at the walls that the ray encounters [18].

The path loss associated with segments, L_0, L_1, \dots, L_M separated by diffraction at edges through angles, $\mathbf{b}_0, \mathbf{b}_1, \dots, \mathbf{b}_M$ provided that each edge lies outside the shadow boundary of the previous edge is determined from

$$(3.1.55) \quad Q = Q_0 \frac{L}{L_0} \prod_j \frac{1}{2\pi k L_j} D^2(\beta_j) = Q_0 \frac{L}{(2\pi k)^M L_0} \prod_j \frac{1}{L_j} D^2(\beta_j)$$

where L is the total path length; i.e., $L = \sum_j L_j$, Q_0 is the free-space factor given by

(3.1.2) for a distance L , and $D(\beta_j)$ is the diffraction coefficient given by (3.1.5).

This model given by equation (3.1.55) can be transformed in the form of

$$(3.1.56) \quad Q(R) = \alpha_3(f) \beta_3(R) \frac{1}{R^n}$$

where $\alpha_3(f)$ and $\beta_3(R)$ are different from $\alpha_1(f)$ and $\beta_1(R)$ corresponding to the macrocellular systems. This is going to yield the following

$$(3.1.57) \quad Q(R)_{dB} = Q(R_0)_{dB} + 10n \log_{10} \frac{R_0}{R} + 10 \log_{10} \frac{\beta_3(R)}{\beta_3(R_0)}$$

where R_0 is the reference distance equal to 1 m.

Similarly, the indoor propagation model given by equation (3.1.55) can be transformed in the form of

$$(3.1.58) \quad Q(R) = \delta_3(R) \epsilon_3(f) \frac{1}{f^m}$$

where $\delta_3(R)$ and $\epsilon_3(f)$ are different from $\delta_1(R)$ and $\epsilon_1(f)$ corresponding to the macrocellular systems. This is going to yield the following

$$(3.1.59) \quad Q(f)_{dB} = Q(f_0)_{dB} + 10m \log_{10} \frac{f_0}{f} + 10 \log_{10} \frac{\epsilon_3(f)}{\epsilon_3(f_0)}.$$

Note the n and m for microcellular geolocation systems can be different from n and m corresponding to macrocellular geolocation systems. For example based on the measurements summarized in [16] the slope n varies from -2 to -4 .

3.1.3.2 Multipath Distribution for Indoor Geolocation Systems

The indoor channel is perhaps very intriguing because multipath is ubiquitous due to high signal scattering, reflection, and refraction. We have summarized here the most widely used and accepted indoor channel models: Raleigh and Rician [33]-[42] and out of them we shall pick the most severe one, which is the Raleigh model.

We assume that every channel has fixed number of paths (also referred to as the number of resolvable paths), K , and that the properties of every channel are stationary over the longest symbol period. The channel bandwidth is assumed larger than the signal bandwidth prior to spreading.

The pdf of a Rayleigh distributed path gain, a_k , is given by [21], [43]

$$(3.1.60) \quad f(a_k) = \frac{a_k}{\alpha^2} \exp\left[-\frac{a_k^2 + v^2}{2\alpha^2}\right] U(a_k), \quad a_k \geq 0$$

where α is a positive parameter. As we shall see the parameter, α , plays an important role in computing the higher moments of \mathbf{a}_k which are [43]

$$(3.1.61) \quad E\{\mathbf{a}_k^n\} = \begin{cases} 1 \cdot 3 \cdots n \alpha^n, & n = 2m + 1, \\ 2^m m! \alpha^{2m}, & n = 2m. \end{cases}$$

In particular, the mean, μ , and the variance, σ^2 , are given by [43]

$$(3.1.62) \quad \mu = \alpha \sqrt{\pi/2}, \quad \sigma^2 = (2 - \pi/2) \alpha^2.$$

There is a close relation between the mean, μ , and the variance, σ^2 , for Rayleigh distributed random variables

$$(3.1.63) \quad \mu^2 = \frac{\sigma^2}{\left(\frac{4}{\pi} - 1\right)} = \alpha^2 \frac{\pi}{2}.$$

Figure 3.20 depicts the Rayleigh pdf and cdf for $\mu = \{0.3, 0.6\}$ and $\sigma = \{0.015, 0.063\}$. Figure 3.21 illustrates the pdf and cdf of the lognormal, Rician, and Rayleigh for $\mu = 0.6$ and $\sigma = 0.063$. As indicated in the figure the Rayleigh distribution is wider than Rician and Rician is wider than lognormal. This implies that the Rayleigh fading channel is the most severe and Rician fading is more severe than lognormal and lognormal is the least severe channel.

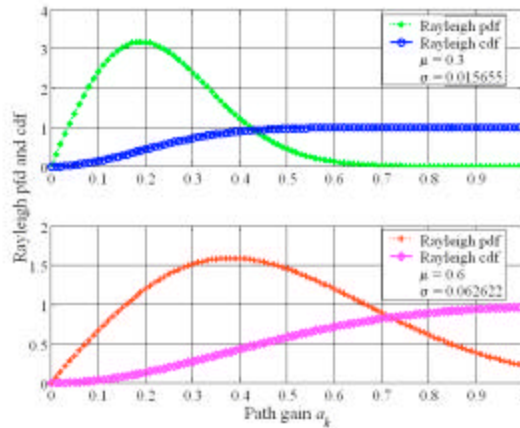


Figure 3.20 The cdf and pdf of a Rayleigh fading channel.

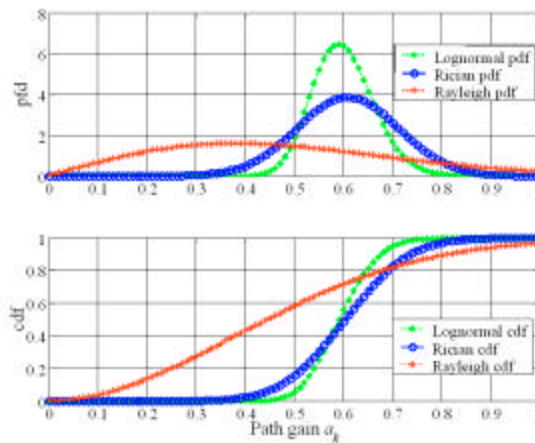


Figure 3.21 The cdf and pdf of a Lognormal, Rician, and Rayleigh fading channel for $m_a = 0.6$ and $S_a = 0.0626$.

The distribution of the path interarrival time is exponential (see Figure 3.10) and the path phases are uniform in $[0, 2\pi)$ (see Figure 3.11) as indicated in §3.1.1.2.

We recall that two other important parameters of the indoor channel are the mean excess delay spread, $\bar{\tau}$, (see equation (3.1.25)) and rms delay spread, $\bar{\sigma}$ (see equation (3.1.26)). The rms delay spread, $\bar{\sigma}$, is a very important parameter because it determines the number of resolvable paths, K , based on the findings of Kavehrad et al. [37] and upon the confirmation of Prasad et al. [33]

$$(3.1.64) \quad K = \left\lceil \frac{\bar{\sigma}}{T_c} \right\rceil + 1 = \lceil \bar{\sigma} R_c \rceil + 1$$

where T_c is the chipping period and R_c is the chipping rate.

To illustrate the impact of the chipping rate and rms delay spread we consider the following example. Suppose that the chipping rate is 1.023 MBPS and we vary the rms delay spread from 0.1 to 10 μs and note that K changes from 1 to 11. This is presented on the top of Figure 3.22. If we keep the rms delay spread equal to 50 ns and vary the chipping rate from 1 to 100 MBPS then the number of resolvable paths changes from 1 to 6. This indicates that for most indoor geolocation applications the number of paths will not exceed 10.

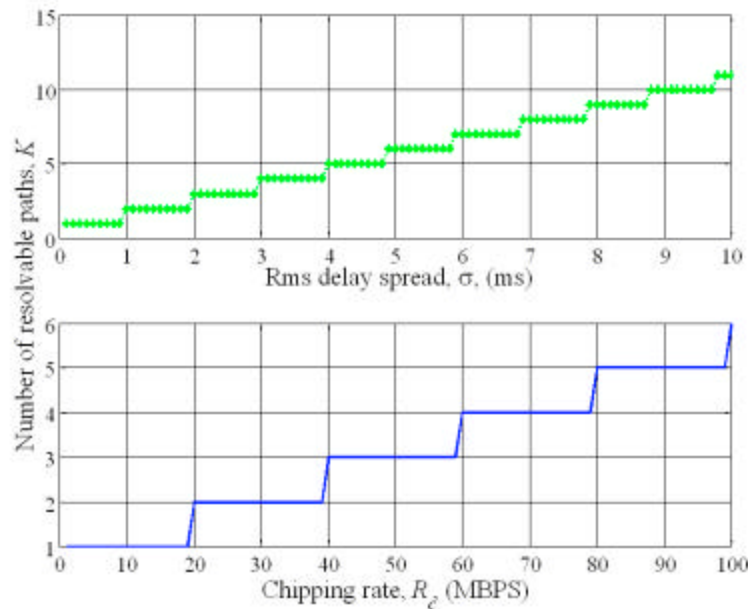


Figure 3.22 The number of resolvable paths as a function of the chipping rate, R_c , and rms delay spread, s .

3.2 Unified Channel Model

Although a unified channel model has not yet been found, in this section we make a first attempt to present a unified channel model which consists of a unified path loss model (see §3.2.1) and a unified multipath distribution model (see §3.2.2).

3.2.1 Unified Path Loss Model

The unified path loss model consists of an approach for linking together the path loss models of the three geolocation systems (macrocellular, microcellular, and indoor) with the distance between the transmitter and receiver, R , and the frequency of operation, f . Although there are several parameters that affect the power loss factor, we consider R and f as the most important parameters for two reasons. Most of the geolocation systems presented in chapter 1 and 2 are based on a direct measure of the time of travel; i.e., distance between the transmitter and receiver. The frequency of these systems varies; hence, the path loss factor varies as well.

Equations (3.1.16), (3.1.49), and (3.1.57) can be generalized as

$$(3.2.1) \quad Q(R)_{dB} = Q(R_0)_{dB} + 10n \log_{10} \frac{R_0}{R} + 10 \log_{10} \frac{\beta_i(R)}{\beta_i(R_0)}$$

where R_0 is the reference distance equal to 10 km (for macrocellular systems), 1 km (for microcellular systems), and 1 m (for indoor systems). Also, β_i is equal to β_1 (for macrocellular systems), β_2 (for microcellular systems), and β_3 (for indoor geolocation systems).

The term $10 \log_{10} [\beta_i(R)/\beta_i(R_0)]$ is very complicated and not very easy to be assessed. Nevertheless, it is proposed that a zero mean Gaussian noise fit reasonably well [16]

$$(3.2.2) \quad 10 \log_{10} \frac{\beta_i(R)}{\beta_i(R_0)} \cong \chi_\sigma$$

where χ_σ denotes a zero mean Gaussian random variable that reflects the variations in average received power that naturally occurs as well as indirect dependence of the distance. The standard deviation σ plays an important role on the accuracy of the propagation loss model [16].

The equation (3.2.1) is generalized as [16]

$$(3.2.3) \quad Q(R)_{dB} = Q(R_0)_{dB} + 10n \log_{10} \left(\frac{R_0}{R} \right) + \chi_\sigma$$

where n denotes the power law relationship between distance and received power.

In order to illustrate the unified path loss model given by equation (3.2.3) we consider three examples.

In the first example we consider a macrocellular geolocation system with the following parameters $Q(R_0)_{dB} = -140$ dB, $R_0 = 1$ km, and $\sigma = 0.5$. Figure 3.23 depicts the unified path loss, Q , versus the relative distance between the transmitter and the receiver, R , going from 1 km to 20 km and for $n = \{2, 3, \dots, 6\}$.

In the second example we consider a microcellular geolocation system with the following parameters $Q(R_0)_{dB} = -70$ dB, $R_0 = 100$ m, and $\sigma = 2.5$. Figure 3.24 depicts the unified path loss, Q , versus relative the distance between the transmitter and the receiver, R , going from 100 m to 1 km and for $n = \{2, 3, \dots, 6\}$.

In the third example we consider an indoor geolocation system with the following parameters $Q(R_0)_{dB} = 0$ dB, $R_0 = 1$ m, and $\sigma = 1$. Figure 3.25 depicts the unified path loss, Q , versus relative the distance between the transmitter and the receiver, R , going from 1 m to 100 m and for $n = \{2, 3, \dots, 6\}$.

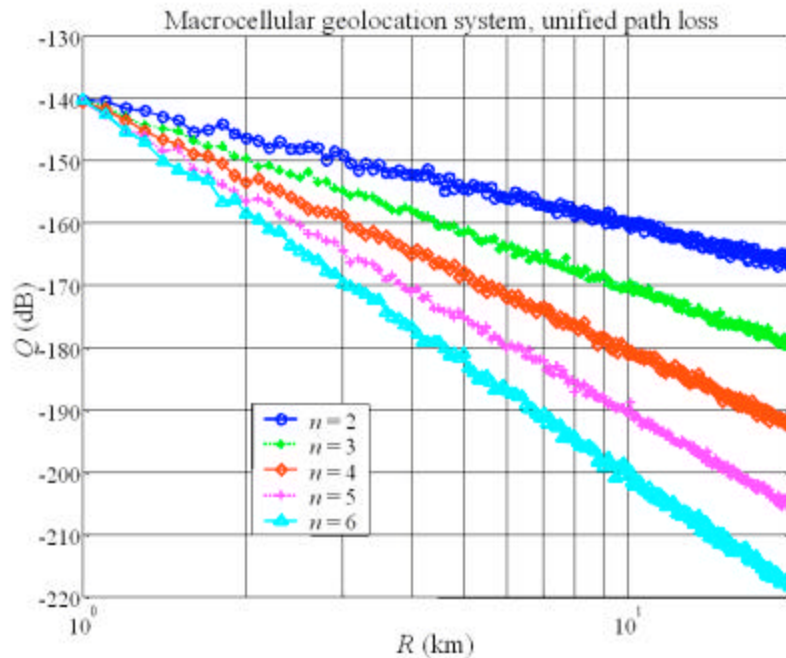


Figure 3.23 Unified path loss model for a macrocellular geolocation system, $s = 0.5$.

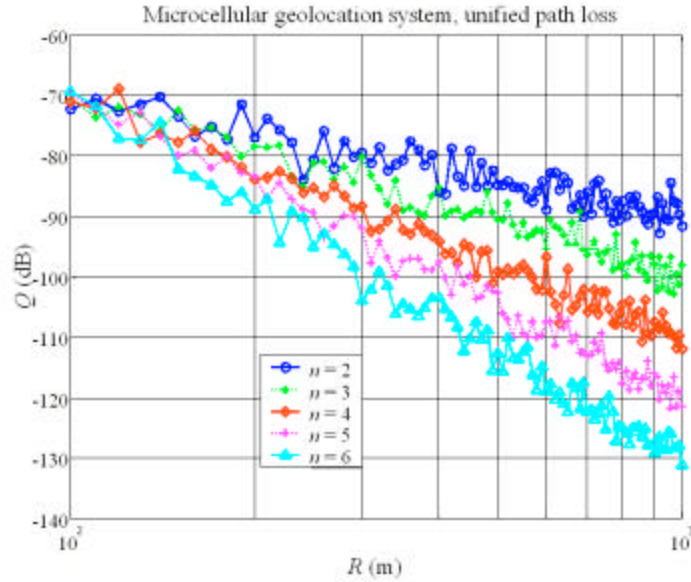


Figure 3.24 Unified path loss model for a microcellular geolocation system, $s = 2$.

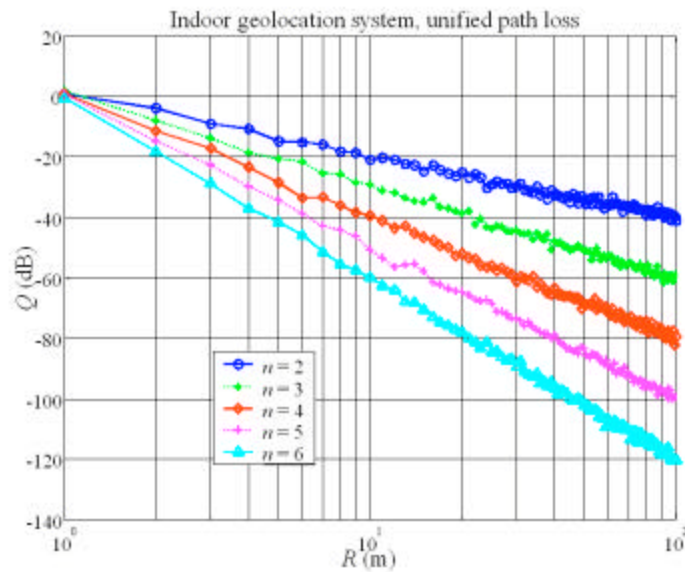


Figure 3.25 Unified path loss model for an indoor geolocation system, $s = 1$.

The reader is reminded that equation (3.2.3) shows the dependency between the power loss factor (in dB) and the distance between the transmitting antenna and the receiving antenna. Another important parameter that affects the power loss factor is the frequency of operation. Unfortunately, the dependency of the power loss factor on the frequency of operation is overlooked in the literature.

Equations (3.1.19), (3.1.51), and (3.1.59) can be generalized as

$$(3.2.4) \quad Q(f)_{dB} = Q(f_0)_{dB} + 10m \log_{10} \frac{f_0}{f} + 10 \log_{10} \frac{\epsilon_i(f)}{\epsilon_i(f_0)}$$

where f_0 is the reference frequency, ϵ_i is equal to ϵ_1 (for macrocellular systems), ϵ_2 (for microcellular systems), and ϵ_3 (for indoor geolocation systems).

The term $10 \log_{10} [\epsilon_i(f)/\epsilon_i(f_0)]$ is very complicated and not very easy to be assessed. Nevertheless, we model this term as a zero mean Gaussian process; hence, we have

$$(3.2.5) \quad 10 \log_{10} \frac{\epsilon_i(f)}{\epsilon_i(f_0)} \cong \gamma_\sigma$$

where γ_σ denotes a zero mean Gaussian random variable that reflects the variations in average received power that naturally occur and indirect dependence of the frequency. Similarly, we anticipate that the standard deviation σ will greatly influence the accuracy of the prediction of the path loss propagation model.

We can generalize equation (3.2.4) as follows

$$(3.2.6) \quad Q(f)_{dB} = Q(f_0)_{dB} + 10m \log_{10} \left(\frac{f_0}{f} \right) + \gamma_\sigma$$

where m denotes the power law relationship between the frequency and the power loss factor.

In order to illustrate the unified path loss model given by equation (3.2.6) we consider three examples.

In the first example we consider a macrocellular geolocation system with the following parameters $Q(f_0)_{dB} = -140$ dB, $f_0 = 1$ GHz, and $\sigma = 0.5$. Figure 3.26 depicts the unified path loss, Q , versus the frequency, f , going from 1 GHz to 10 GHz and for $m = \{2, 2.1, \dots, 2.4\}$.

In the second example we consider a microcellular geolocation system with the following parameters $Q(f_0)_{dB} = -70$ dB, $f_0 = 1$ GHz, and $\sigma = 2.5$. Figure 3.27 depicts the unified path loss, Q , versus the frequency, f , going from 1 GHz to 10 GHz and for $m = \{2, 2.1, \dots, 2.4\}$.

In the third example we consider an indoor geolocation system with the following parameters $Q(f_0)_{dB} = 0$ dB, $f_0 = 1$ GHz, and $\sigma = 1$. Figure 3.28 depicts the unified path loss, Q , versus the frequency, f , going from 1 GHz to 10 GHz and for $m = \{2, 2.1, \dots, 2.4\}$.

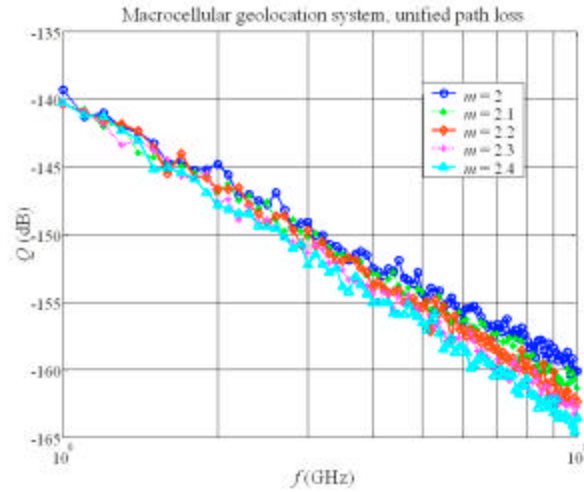


Figure 3.26 Unified path loss model for a macrocellular geolocation system, $s = 0.5$.

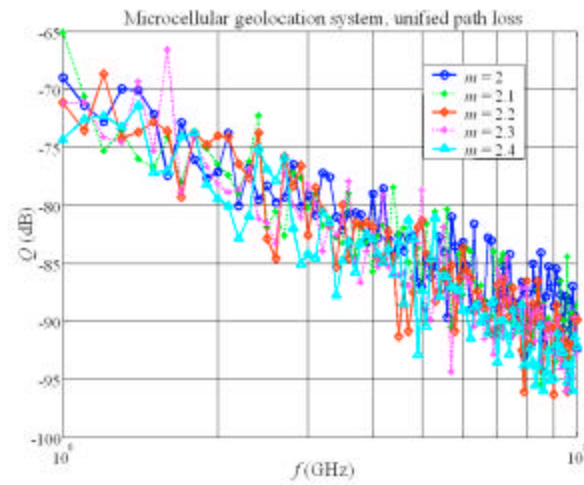


Figure 3.27 Unified path loss model for a microcellular geolocation system, $s = 2$.

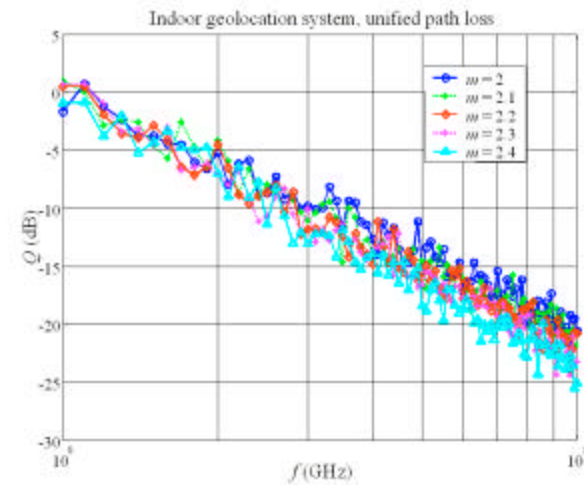


Figure 3.28 Unified path loss model for an indoor geolocation system, $s = 1$.

Sometimes we desire to have the path loss model be a function of both f and R . In this case, equations (3.2.3) and (3.2.6) are combined in one equation given by

$$(3.2.7) \quad Q(R(t), f)_{dB} = Q(R_0, f_0)_{dB} + 10n \log_{10} \frac{R_0}{R(t)} + 10m \log_{10} \frac{f_0}{f} + N(0, \sigma)$$

where $Q(R_0, f_0)_{dB}$ is the path loss corresponding to the frequency f_0 and distance R_0 and $N(0, \sigma)$ is a normal random variable. Clearly, if $R = R_0$ then equation (3.2.7) is the same as equation (3.2.3) as long as $N(0, \sigma)$ is the same as χ_σ . On the other hand if $f = f_0$ then equation (3.2.7) is the same as equation (3.2.6) as long as $N(0, \sigma)$ is the same as γ_σ . So then in general $N(0, \sigma)$ can be model as a sum of χ_σ and γ_σ . And since χ_σ and γ_σ are zero mean random variables then $N(0, \sigma)$ is also zero mean and with variance the sum of the variance of χ_σ and γ_σ .

Let $p(t)$ be defined as the ratio of the received power over the transmitted power as

$$(3.2.8) \quad p(t) = \frac{P_r(t)}{P_t(t)} = G_t G_r Q(t)$$

and in dB the above equation can be written as

$$(3.2.9) \quad p(t)_{dB} = G_{t,dB} + G_{r,dB} + Q(t)_{dB}$$

where $Q(t)_{dB}$ is given by equation (3.2.7). The parameter $p(t)$ is different from the total path loss factor only by the transmitting and receiving antenna gain. The benefit of using $p(t)$ is seen in Chapters 5 through 7.

3.2.2 Unified Multipath Distribution Model

While unifying the path loss model was to some extent initiated in the literature, unifying the multipath distribution model is currently a silent quest in the literature. It appears that the tendency is to come up with newer and more sophisticated models that would explain the characteristics of the old models. The approach that we present here to unify the multipath distribution models is rather simple.

Let $f_i(a_k)$ denote the multipath distribution model, which for the macrocellular systems ($i = 1$) is given by equations (3.1.30), for the microcellular systems ($i = 2$) is given by (3.1.52), and for the indoor geolocation systems ($i = 3$) is given by (3.1.60). Let $f(a_k)$

denote the unified multipath distribution model. If m_1 and m_2 are two real numbers between $[0,1]$ then

$$(3.2.10) \quad f(a_k) = (1 - m_2)[(1 - m_1)f_1(a_k) + m_1f_2(a_k)] + m_2f_3(a_k).$$

Clearly, $f(a_k)$, is a valid pdf function because it is greater than zero and because

$$(3.2.11) \quad \int_{-\infty}^{\infty} f(x)dx = (1 - m_2) \left[(1 - m_1) \int_{-\infty}^{\infty} f_1(x)dx + m_1 \int_{-\infty}^{\infty} f_2(x)dx \right] + m_2 \int_{-\infty}^{\infty} f_3(x)dx \\ = (1 - m_2)[(1 - m_1) + m_1] + m_2 = 1.$$

By selecting numbers m_1 and m_2 we can fit a wide number of distribution functions which come close to lognormal, Rician, and Rayleigh.

To aid our analysis we make the following definitions. Let r and n_i be defined as follows

$$(3.2.12) \quad r \equiv a_k, \quad n_1 = (1 - m_2)(1 - m_1), \quad n_2 = (1 - m_2)m_1, \quad \text{and} \quad n_3 = m_2$$

subject to the conditions

$$(3.2.13) \quad \sum_{i=1}^3 n_i = 1$$

$$(3.2.14) \quad 0 \leq n_i \leq 1.$$

Now equation (3.2.10) can be written as

$$(3.2.15) \quad f(r) = \sum_{i=1}^3 n_i f_i(r), \quad -\infty < r < \infty.$$

We will also assume that individual distribution functions are linearly independent; i.e., for any coefficients $\{a_1, a_2, a_3\}$ and for $-\infty < r < \infty$ the following holds

$$(3.2.16) \quad f_1(r) \neq a_2 f_2(r) + a_3 f_3(r), \quad f_2(r) \neq a_1 f_1(r) + a_3 f_3(r), \quad f_3(r) \neq a_1 f_1(r) + a_2 f_2(r).$$

It is interesting to note that the following theorems provides the relation between the mean and variance of \mathbf{r} based on the composite distribution, $f(r)$, and the mean and the variance of \mathbf{r} based on the individual distributions, $f_i(r)$, $\forall i \in \{1,2,3\}$, and condition for finding the solutions for the parameters n_i .

Before introducing our theorems let provide some useful definitions. Let μ and μ_i depict the following

$$(3.2.17) \quad \mu = \int_{-\infty}^{\infty} xf(x)dx, \quad \mu_i = \int_{-\infty}^{\infty} xf_i(x)dx, \quad \forall i \in \{1,2,3\}$$

and let υ and υ_i denote

$$(3.2.18) \quad \upsilon = \int_{-\infty}^{\infty} x^2 f(x) dx - \mu^2, \quad \upsilon_i = \int_{-\infty}^{\infty} x^2 f_i(x) dx - \mu_i^2, \quad \forall i \in \{1, 2, 3\}$$

Theorem 1: The mean of \mathbf{r} based on the composite distribution, $f(r)$, is the superposition of the mean \mathbf{r} based on the individual distribution functions, $f_i(r)$, $\forall i \in \{1, 2, 3\}$; i.e.,

$$(3.2.19) \quad \mu = \sum_{i=1}^3 n_i \mu_i.$$

Proof. Equation (3.2.19) is proved based on equations (3.2.17) and (3.2.15)

$$(3.2.20) \quad \mu = \int_{-\infty}^{\infty} x f(x) dx = \int_{-\infty}^{\infty} x \sum_{i=1}^3 n_i f_i(x) dx = \sum_{i=1}^3 n_i \int_{-\infty}^{\infty} x f_i(x) dx = \sum_{i=1}^3 n_i \mu_i.$$

Theorem 2: If the mean of \mathbf{r} based on the composite distribution, $f(r)$, is the same as the mean of \mathbf{r} based on the individual distribution functions, $f_i(r)$, $\forall i \in \{1, 2, 3\}$; i.e.,

$$(3.2.21) \quad \mu \equiv \mu_i \quad \forall i \in \{1, 2, 3\}$$

then variance of \mathbf{r} based on the composite distribution, $f(r)$, is the superposition of the variance of \mathbf{r} based on the individual distribution functions, $f_i(r)$, $\forall i \in \{1, 2, 3\}$; i.e.,

$$(3.2.22) \quad \upsilon = \sum_{i=1}^3 n_i \upsilon_i.$$

Proof. Similarly, based on equations (3.2.18), (3.2.15), and (3.2.22) we obtain

$$(3.2.23) \quad \begin{aligned} \upsilon &= \int_{-\infty}^{\infty} x^2 f(x) dx - \mu^2 = \int_{-\infty}^{\infty} x^2 \sum_{i=1}^3 n_i f_i(x) dx - \sum_{i=1}^3 n_i \mu^2 \\ &= \sum_{i=1}^3 n_i \left[\int_{-\infty}^{\infty} x^2 f_i(x) dx - \mu^2 \right] = \sum_{i=1}^3 n_i \left[\int_{-\infty}^{\infty} x^2 f_i(x) dx - \mu_i^2 \right] \\ &= \sum_{i=1}^3 n_i \upsilon_i. \end{aligned}$$

Theorem 3: If the mean and variance of \mathbf{r} based on the composite distribution, $f(r)$, is the same as the mean and variance of \mathbf{r} based on the individual distribution functions, $f_i(r)$, $\forall i \in \{1, 2, 3\}$, then it is possible to obtain a solution $\mathbf{n} = [n_1, n_2, n_3]^t$

$$(3.2.24) \quad \begin{bmatrix} n_1 \\ n_2 \\ n_3 \end{bmatrix} = \begin{bmatrix} f_1(r_1) & f_2(r_1) & f_3(r_1) \\ f_1(r_2) & f_2(r_2) & f_3(r_2) \\ f_1(r_3) & f_2(r_3) & f_3(r_3) \end{bmatrix}^{-1} \begin{bmatrix} f(r_1) \\ f(r_2) \\ f(r_3) \end{bmatrix}, \quad -\infty < r_1 < r_2 < r_3 < \infty \quad \text{and} \\ f_i(r_j) > 0, \forall i, j \in \{1,2,3\}.$$

Proof. Given the composite distribution, $f(r)$, and the mean and variance of \mathbf{r} based on $f(r)$, given also that $\mu \equiv \mu_i$, $v \equiv v_i$, and knowing each individual distributions $f_i(r)$, $\forall i \in \{1,2,3\}$, for $-\infty < r_1 < r_2 < r_3 < \infty$ we can obtain

$$(3.2.25) \quad \begin{bmatrix} f(r_1) \\ f(r_2) \\ f(r_3) \end{bmatrix} = \begin{bmatrix} f_1(r_1) & f_2(r_1) & f_3(r_1) \\ f_1(r_2) & f_2(r_2) & f_3(r_2) \\ f_1(r_3) & f_2(r_3) & f_3(r_3) \end{bmatrix} \begin{bmatrix} n_1 \\ n_2 \\ n_3 \end{bmatrix}, \quad -\infty < r_1 < r_2 < r_3 < \infty.$$

Since $f_i(r_j) > 0, \forall i, j \in \{1,2,3\}$ and since each individual distribution is linearly independent of the other two individual distributions then

$$(3.2.26) \quad \begin{vmatrix} f_1(r_1) & f_2(r_1) & f_3(r_1) \\ f_1(r_2) & f_2(r_2) & f_3(r_2) \\ f_1(r_3) & f_2(r_3) & f_3(r_3) \end{vmatrix} \neq 0$$

where equation (3.2.24) results.

Although the above theorem is very important it does not guarantee that we will always succeed in finding the desired solution. To accomplish this goal we have provided the following, important corollaries.

Corollary 1: If the solution \mathbf{n} is subject to the conditions of equations (3.2.13) and (3.2.14) then we have found the desired solution because the solution is **unique**; i.e., the solution \mathbf{n} falls within the desired subspace. In the case we **can** obtain the composite pdf as the superposition of the three-desired pdf functions.

Corollary 2: If the solution \mathbf{n} is **not** subject to the conditions of equations (3.2.13) and (3.2.14) then that is **not** the desired solution; i.e., the composite pdf **cannot** be obtained as the superposition of the three-desired pdf functions. In this case we could increase our subspace of the desired pdf functions to include more than three functions.

Let us illustrate the result of our analysis with an example. Consider the example presented in Figure 3.21. Using the parameters of Figure 3.21 and the vector $\mathbf{n} = \{0.25, 0.35, 0.4\}$ we form the composite pfd which is shown in Figure 3.29 the curve with a

triangular marker. Using the values of the composite pdf function and the values of the individual pdf functions we obtained the values of the vector $\mathbf{n} = \{0.25, 0.35, 0.4\}$. So for this case Theorem 3 and Corollary 1 are satisfied.

An example that satisfies both Theorem 3 and Corollary 2 is given next (see Figure 3.30). For this example we consider a uniform function with mean and variance equal to 0.6 and 0.0039 respectively. The values for $\mathbf{n} = \{0.4137, 0.5023, 4.3884\}$ or $\{-0.2136, 1.7936, -0.0015\}$.

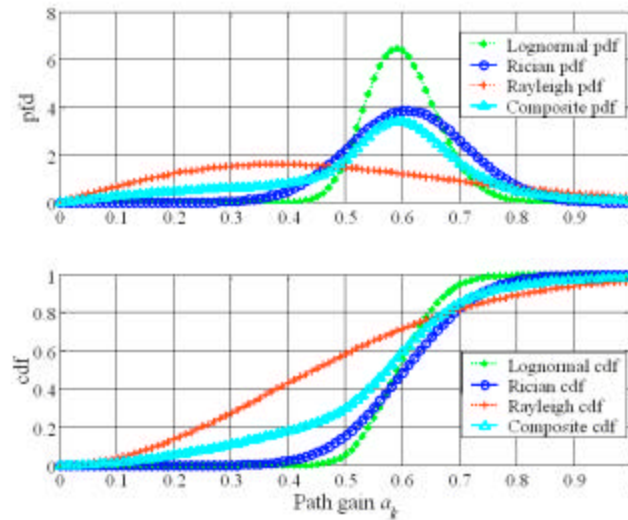


Figure 3.29 The composite cdf and pdf which contains a Lognormal, Rician, and Rayleigh fading channel for $m_a = 0.6$ and $s_a = 0.0626$ and $\mathbf{n} = \{0.25, 0.35, 0.4\}$.

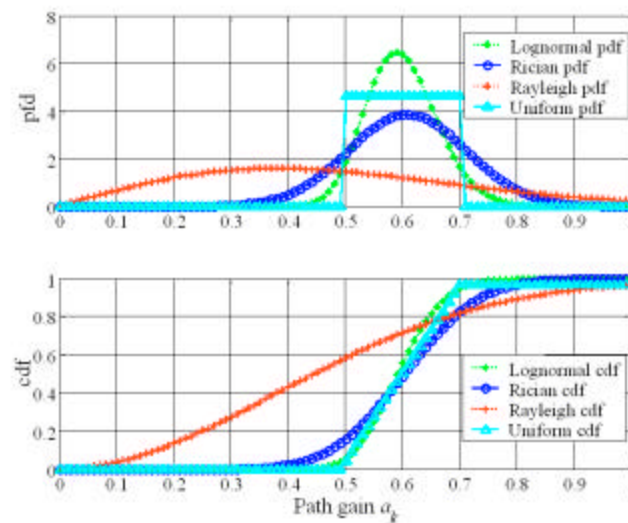


Figure 3.30 The uniform cdf and pdf which is not a superposition of a Lognormal, Rician, and Rayleigh fading channel for $m_a = 0.6$ and $s_a = 0.0626$.

Since the theorem 3 is the existence theorem because corollary 1 gave the desired solution and corollary 2 the undesired solution then we provide the following theorem which lays out the conditions for the unique solution of \mathbf{n} .

Theorem 4: Given the conditions of the theorem 3 then for a set of numbers $-\infty < r_1 < r_2 < r_3 < \infty$ there exists a vector $\mathbf{n} = [n_1, n_2, n_3]^t$ such that equation (3.2.24) is satisfied. Also for a different set of numbers $-\infty < r'_1 < r'_2 < r'_3 < \infty$ such that $f(r'_1) \neq f(r_1)$ or $f(r'_2) \neq f(r_2)$ or $f(r'_3) \neq f(r_3)$ there exists another vector $\mathbf{n}' = [n'_1, n'_2, n'_3]^t$ such that equation (3.2.24) is satisfied. The solution is unique if and only if $\mathbf{n} \equiv \mathbf{n}'$. Moreover the unique solution satisfies corollary 1 of theorem 3; i.e., equations (3.2.13) and (3.2.14).

Proof. In order to prove theorem 4 we have to prove both the necessary and the sufficient conditions. The proof the necessary condition is rather simple. We know that equation (3.2.15) is valid $-\infty < r < \infty$. Suppose that we can find $-\infty < r_1 \neq r_2 \neq r_3 < \infty$ such that $\mathbf{n} = [n_1, n_2, n_3]^t$ is a solution for (3.2.15). Suppose on the other hand we can find $-\infty < r'_1 \neq r'_2 \neq r'_3 < \infty$ such that $\mathbf{n}' = [n'_1, n'_2, n'_3]^t$ is another solution of (3.2.15). Since the solution of equation (3.2.15) is valid $-\infty < r < \infty$ then $\mathbf{n} \equiv \mathbf{n}'$. The proof of the sufficient condition is rather difficult therefore we have not provided here.

As a summary, we have provided a rather simple way to augment the set of the probability distribution functions based on the Lognormal, Rician, and Rayleigh distribution functions and we have derived the mathematical tools when such augmentation is valid. This is a way to attack the quest for a unified statistical channel model, which remains to be validated with real measurement data.

CITED REFERENCES AND FURTHER READING:

- [1] D.E. Kerr, *Propagation of Short Radio Waves*, 1st ed. New York, NY: McGraw-Hill, 1951.
- [2] S.O. Rice, "Mathematical analysis of random noise," *Bell. Sys. Tech. J.*, vol. 23, pp. 282-332, 1944 and pp. 46-156, 1954.
- [3] G.L. Turin, "Communication through noisy, random multipath varying channels," in *1956 IRE Convention Record*, part 4, pp. 154-166.
- [4] J.B. Keller, "Geometrical theory of diffraction," *J. Opt. Soc. Amer.*, vol. 52, pp. 116-131, 1962.

- [5] G.L. Turin, *et al.* "A statistical model of urban multipath propagation," *IEEE Trans. Veh. Technol.*, vol. VT-21, pp. 1-9, Feb. 1972.
- [6] L.B. Felsen and N. Markuvitz, *Radiation and Scattering of Waves*. Englewood Cliffs, NJ: Prentice Hall, pp. 652-665, 1973.
- [7] H. Suzuki, "A statistical model for urban radio propagation," *IEEE Trans. Commun.*, vol. COMM-25, pp. 673-685, July 1977.
- [8] G.D. Ott and A. Plitkins, "Urban path-loss characteristics at 820 MHz," *IEEE Trans. Veh. Technol.*, vol. VT-27, pp. 189-197, 1978.
- [9] H. Hashemi, "Simulation of the urban radio propagation channel," *IEEE Trans. Veh. Technol.*, vol. VT-28, pp. 213-224, Aug. 1979.
- [10] J.G. Proakis, *Digital Communications*. New York: McGraw-Hill, 1983.
- [11] A.A.M. Saleh and R.A. Valenzuela, "A statistical model for indoor multipath propagation," *IEEE J. Select. Areas Commun.*, vol. SAC-5, pp. 128-137, Feb. 1987.
- [12] T.S. Rappaport, "Indoor radio communications for factories of the future," *IEEE Comm. Mag.*, vol. 27, no. 2, pp. 15-24, May 1989.
- [13] P. Yegani and C.D. McGillem, "A statistical model for line-of-sight (LOS) factory radio channels," in *Proc. Vehicular Techn. Conf. VTC'89*, pp. 496-503, San Francisco, May 1989.
- [14] T.S. Rappaport, "Characterization of UHF multipath radio channels in factory buildings," *IEEE Trans. Ant. Prop.*, vol. 37, no. 8, pp. 1058-1069, Aug. 1989.
- [15] L.J. Greenstein *et al.*, "Microcells in personal communications systems," *IEEE Comm. Mag.*, vol. 30, no. 12, pp. 76-88, Dec. 1992.
- [16] J.B. Andersen, T.S. Rappaport, and S. Yoshida, "Propagation measurements and models for wireless communications channels," *IEEE Comm. Mag.*, vol. 33, no. 1, pp. 42-49, Jan. 1995.
- [17] K. Pahlavan, P. Krishnamurthy, and A. Beneat, "Wideband radio propagation modeling for indoor geolocation applications," *IEEE Comm. Mag.*, vol. 36, no. 4, pp. 60-65, Apr. 1998.
- [18] H.L. Bertoni, W. Honcharenko, L.R. Macel, and H.H. Xia, "UHF propagation prediction for wireless personal communications," in *Proc. IEEE*, vol. 82, no. 9, pp. 1333-1359, Sep. 1994.
- [19] L.R. Macel, H.L. Bertoni, and H.H. Xia, "Unified approach to prediction of propagation over building of all ranges of base station antenna height," *IEEE Trans. Veh. Technol.*, vol. 42, pp. 41-45, Feb. 1993.
- [20] P. Yegani and C.D. McGillem, "A statistical model for the factory radio channel," *IEEE Trans. Comm.*, vol. 39, no. 10, pp. 1445-1454, Oct. 1991.
- [21] H. Hashemi, "The indoor radio propagation channel," in *Proc. IEEE*, vol. 81, no. 7, pp. 943-968, July 1993.

- [22] T. Lo, J. Litva, and H. Leung, "A new approach for estimating indoor radio propagation characteristics," *IEEE Trans. Ant. Prop.*, vol. 42, no. 10, pp. 1369-1376, Oct. 1994.
- [23] F. Babich and G. Lombardi, "Statistical analysis and characterization of the indoor propagation channel," *IEEE Trans. Comm.*, vol. 48, no. 3, pp. 455-464, Mar. 2000.
- [24] T.S. Rappaport, S.Y. Seidel, and K. Takamizawa, "Statistical channel impulse response models for factory and open plan building radio communicate system design," *IEEE Trans. Comm.*, vol. 39, no. 5, pp. 794-807, May. 1991.
- [25] R. Jain, *The Art of Computer Systems Performance Analysis (Techniques for Experimentation Design, Measurements, Simulation, and Modeling)*. New York, NY: John Wiley & Sons, 1991 ("Chap. 29, Commonly Used Distributions").
- [26] T. Iwama *et al.*, "Investigation of propagation characteristics above 1 GHz for microcell land mobile radio," in *Proc. IEEE Veh. Technol. Conf.*, pp. 396-400, 1990.
- [27] D.M.J. Devasirvatham, C. Banerjee, R.R. Murray, and D.A. Rappaport, "Two frequency radio-wave propagation measurements in Brooklyn," in *Proc. IEEE Int. Conf. on Universal Personal Commun.*, pp. 23-27, Dallas, TX, 1992.
- [28] A.J. Rustako, Jr., N. Amitay, G.J. Owens, and R.S. Roman, "Radio propagation at microwave frequencies for line-of-sight microcellular mobile and personal communications," *IEEE Trans. Veh. Technol.*, vol. 40, pp. 203-210, 1991.
- [29] H.H. Xia and H.L. Bertoni, "Diffraction of cylindrical and plane waves by an array of absorbing half screens," *IEEE Trans. Ant. Prop.*, vol. 40, pp. 170-177, Feb, 1992.
- [30] J. Boersma, "On certain multiple integrals occurring in wave-guide scattering problem," *SIAM J. Math. Anal.*, vol. 9, no. 2, pp. 377-393, 1978.
- [31] L.R. Macel and H.L. Bertoni, "Cell shape for microcellular systems in residential and commercial environments," in *IEEE Conf. on Universal Personal Communications*, pp. 723-727, Ottawa, Ont., Canada, 1993.
- [32] L.R. Macel and H.L. Bertoni, "Cell shape for microcellular systems in residential and commercial environments," *IEEE Trans. Veh. Technol.*, vol. 43, no. 2, pp. 270-278, 1994.
- [33] R. Prasad, H.S. Misser, and A. Kegel, "Performance evaluation of direct-sequence spread spectrum multiple-access for indoor wireless communication in a Rician fading channel," *IEEE Trans. Comm.*, vol. 43, no. 2, pp. 581-592, Feb-Apr. 1995.
- [34] T.S. Rappaport and D.A. Hawbaker, "Wide-band microwave propagation parameters using circular and linear polarized antennas for indoor wireless channels," *IEEE Trans. Comm.*, vol. 40, no. 2, pp. 240-245, Feb. 1992.
- [35] G.J.M. Janssen, P.A. Stigter, and R. Prasad, "Wideband indoor channel measurements and BER analysis of frequency selective multipath channels at 2.4, 4.75, and 11.5 GHz," *IEEE Trans. Comm.*, vol. 44, no. 10, pp. 1272-1288, Oct. 1996.

- [36] J.G. Durgin, T.S. Rappaport, and H. Xu, "Measurements and models for radio path loss and penetration loss in and around homes and trees at 5.85 GHz," *IEEE Trans. Comm.*, vol. 46, no. 11, pp. 1484-1496, Nov. 1998.
- [37] S.Y. Seidel and T.S. Rappaport, "914 MHz path loss prediction models for indoor wireless communications in multifloored buildings," *IEEE Trans. Ant. Prop.*, vol. 40, no. 2, pp. 207-217, Feb. 1992.
- [38] T.K. Blankenship and T.S. Rappaport, "Characteristics of impulsive noise in the 450-MHz band in hospitals and clinics," *IEEE Trans. Ant. Prop.*, vol. 46, no. 2, pp. 194-203, Feb. 1998.
- [39] P. Vlach, B. Segal, J. LeBel, and T. Pavlasek, "Cross-floor signal propagation inside a contemporary ferro-concrete building at 434, 862, and 1705 MHz," *IEEE Trans. Ant. Prop.*, vol. 47, no. 7, pp. 1230-1232, July 1999.
- [40] J. Kivinen, X. Zhao, and P. Vainikainen, "Empirical characterization of wideband indoor radio channel at 5.3 GHz," *IEEE Trans. Ant. Prop.*, vol. 49, no. 8, pp. 1192-1203, Aug. 2001.
- [41] B.P. Donaldson, M. Fattouche, and R.W. Donaldson, "Characterization of in-building UHF wireless radio communication channels using spectral energy measurements," *IEEE Trans. Ant. Prop.*, vol. 44, no. 1, pp. 80-86, Jan. 1996.
- [42] W.J. Vogel and G.W. Torrence, "Propagation measurements for satellite radio reception inside buildings," *IEEE Trans. Ant. Prop.*, vol. 41, no. 7, pp. 954-961, July 1993.
- [43] A. Papoulis, *Probability, Random Variables, and Stochastic Processes*. New York: McGraw-Hill, 1984.

Chapter 4. WPI Indoor Geolocation Systems

“For I am persuaded, that neither death, nor life, nor angels, nor principalities, nor powers, nor things present, nor things to come, Nor height, nor depth, nor any other creature, shall be able to separate us from the love of God, which is in Christ Jesus our Lord.” ^{3/4}Romans 8:38-39

4.0 Introduction

SUPPOSE that we want to build an indoor-to-outdoor geolocation system to localize people or emergency personnel in one or more multistory buildings. The main engineering issue with building such a system is the availability of a suitable infrastructure; thus, a portable ad-hoc network would be desirable. Such a network, would consist of ground-based transmitters (or pseudolites) and portable (or handheld) receivers [1].

Consider a situation in which a building is on fire as depicted in Figure 4.1. For the purposes of our investigation and modeling we can symbolically describe the rescue mission of firefighters either operating in the same floor or operating in different floors as shown in Figure 4.1 [1].

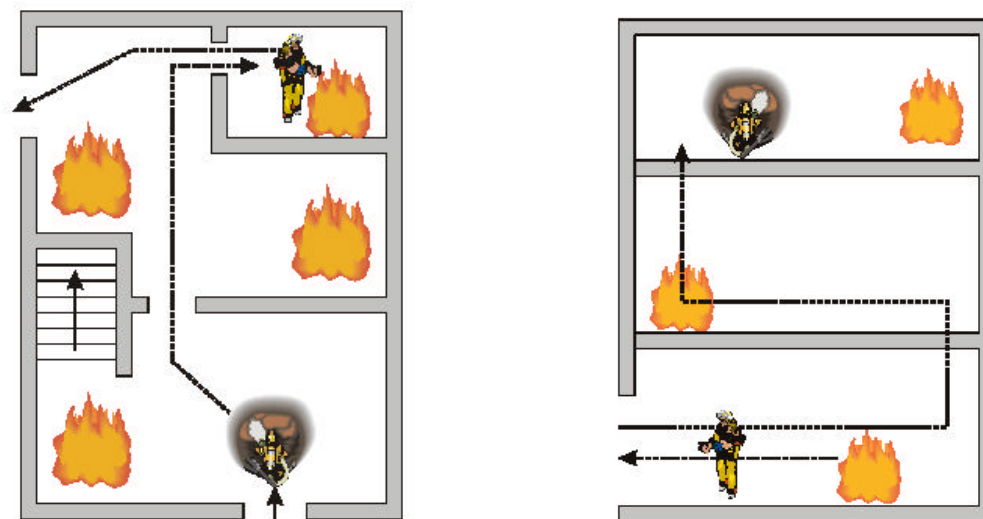


Figure 4.1 Firefighter in rescue mission working in the same floor (left) and at different floors (right)^{3/4} taken from [1].

Each of these firefighters must know the relative position of his peers and be able to communicate with them under severe fire, smoke, and/or interference conditions. In addition, there are people outside the building who conduct and coordinate the mission. Therefore, we recognize three specific situations: (1) outdoor-indoor, (2) the same floor, and (3) in between floors [1].

In order to accomplish these missions we propose the WPI pseudolite based indoor geolocation system which also consists of three segments: the *pseudolite* segment, the *control* segment, and the *user* segment [1]-[12].

The *pseudolite* segment consists of all pseudolites, which are positioned on precise locations on the ground and continuously transmit a spread spectrum signal modulated on a carrier frequency (see Figure 4.2). Suppose that the location of each pseudolite is known but each pseudolite clock bias remains unknown. Therefore, the problem of uploading the pseudolites' clock biases from the *control* segment or from neighboring pseudolite is relatively simple. When the location of the pseudolites is however unknown then an algorithm to determine the location of the pseudolites in place is required before attempting to determine the location of the receiver. The problem of relative synchronization between pseudolites is not addressed here but it is a main problem to these systems and it remains to be solved in the future.

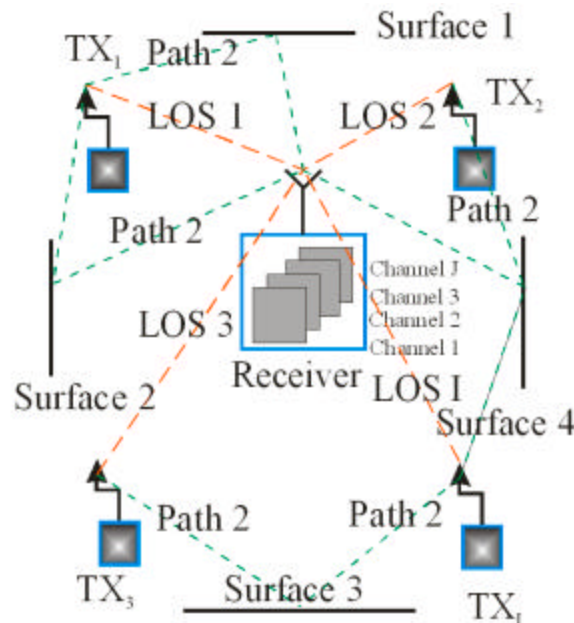


Figure 4.2 The WPI pseudolite indoor geolocation system without the control segment.

The *control* segment consists of one or more monitoring (or base) stations on the ground, which continuously monitor the pseudolite and keep track of the reference time. It is conceivable that the control segment must be synchronized to the GPS time or some other reference time. The study and design of the control segment is not the objective of this work. When the position of each pseudolite is known then the control segment (or base station) needs only to upload the clock corrections to each pseudolite. When the location of each pseudolite is however unknown then base-stations are required to determine the location of each pseudolite first and then upload the pseudolite clock corrections. This again is not the objective of this work.

The *user* segment consists of all the receivers every one of which tracks and computes its 2-D or 3-D position and local time based on the signals coming from at least three or more pseudolites.

The principle of operation of a WPI indoor geolocation system is similar to the principle of operation of GPS or GLONASS in that each system utilizes range information based on the measurement of the time of the arrival between a pseudolite and a receiver. The reader is reminded that GPS employs a CDMA modulation scheme to achieve multiaccess capability and GLONASS employs a FDMA modulation scheme for the same. In Chapters 1 and 2 we discussed most of the limitations of both GPS and GLONASS signal structures for indoor geolocation applications. But GPS and GLONASS provide a wealth of information on system design and implementation. So then the motivation of the WPI indoor geolocation systems is to reuse ideas and concepts from GPS and GLONASS as much as possible to maintain usefulness and enhance the signal structure of GPS and GLONASS to a new signal structure to achieve originality.

There are three WPI indoor geolocation systems that are proposed here and are discussed in Chapters 5 through 7.

A direct sequence spread spectrum (DSSS)/CDMA/FDMA indoor geolocation system (see §4.1) is motivated by GPS and GLONASS signal structure. We have attempted to utilize both code and frequency diversity to achieve better signal separation than the signal separation achieved by GPS and GLONASS individually. In Chapter 5 we analyze the performance objectives of the signal structure of a DSSS/CDMA/FDMA indoor

geolocation system; namely, the bit error probability and the pseudorange and carrier phase error utilizing a low cost and non-optimal receiver signal processing. The main objective behind this signal processing is to show that even under non-optimal receiver signal processing we can achieve a desirable performance of in terms of the bit error probability, pseudorange error and carrier phase error. Section §4.1 and Chapter 5 provide a baseline of a DSSS/CDMA/FDMA indoor geolocation system.

GPS, GLONASS and a DSSS/CDMA/FDMS indoor geolocation system motivate the discussion on a DSSS/OFDM/CDMA/FDMA indoor geolocation system (see §4.2). Here we propose both OFDM and FDMA as frequency diversity and CDMA as code diversity to achieve higher data rate than GPS, GLONASS, or a CDMA/FDMA indoor geolocation system proposed in §4.1. In Chapter 6 we analyze the performance of a DSSS/OFDM/CDMA/FDMA indoor geolocation system utilizing a low cost and non-optimal receiver signal processing. Section §4.2 and Chapter 6 provide a baseline of a DSSS/OFDM/CDMA/FDMA indoor geolocation system.

An OFDM/FDMA indoor geolocation system is the last WPI indoor geolocation system proposed in §4.3 and discussed in Chapters 7. A reduction of system complexity, an improvement of spectrum utilization, and an idea of DSL signal structure are the motivation behind such a system. Section §4.3 and Chapter 7 provide a baseline of an OFDM/FDMA indoor geolocation system.

4.1 A DSSS/CDMA/FDMA Indoor Geolocation System

A DSSS/CDMA/FDMA indoor geolocation system is the first system that we propose, which is intended to overcome the indoor channel impairments by introducing an improved signal structure. This system is motivated by both GPS and GLONASS signal structures and combines these two ideas into one. It is well known (see Chapter 2) that both GPS and GLONASS utilize about 20 MHz of the frequency spectrum in both the L_1 and L_2 frequencies. GPS employs the CDMA modulation scheme as opposed to GLONASS, which utilizes the FDMA modulation scheme. It has been reported in the literature that a combination of these two schemes yields better SNR for the same spectrum allocation (see Appendix B). Nevertheless, modifications on the transmitter and receiver design may be required. These modifications are, however, insignificant

compared to the gain in SNR. The combination of CDMA with FDMA does not change the data rate. Here we discuss the principles of operation (§4.1.1), the transmitter (§4.1.2), and the receiver design (§4.1.3). In Chapter 4 we discuss the system performance evaluation based on the channel model introduced in Chapter 3 and in Chapter 8 we highlight some of the issues of this system.

4.1.1 Principle of Operation of a DSSS/CDMA/FDMA Indoor Geolocation System

The principle of operation of a DSSS/CDMA/FDMA indoor geolocation system is exactly the same as the principle of operation of a GPS/pseudolite indoor geolocation system (see Chapters 1 and 2).

4.1.2 Transmitter

The signal structure of a DSSS/CDMA/FDMA indoor geolocation system is shown in Figure 4.3. The signal structure of each transmitter contains three codes: C code, B code, and P code. The C code is relatively short and it called the synchronization code. As such the C code is unique for every transmitter and we have assumed them to be either Gold or Kasami sequences (see Appendix D). The B code is a much longer code and it is used to protect the signal against interference or jamming. This protection, of course, is to a certain extent. For the reader, who is familiar with the GPS signal structure, the purpose of the C code and B code is almost identical to the purpose of the “C/A” code and “P” code in the GPS signal design. The P code here should not be confused with the “P” code in the GPS signal design. This code has a special purpose in this design. It is used to improve the resolution of the data bit transition. This is the reason why the P code is selected as a maximum length sequence (see Appendix D). The C and P codes are in phase with each other. The B code in 90° offset with either the C or the P code. Assume that the B code requires a bandwidth of W_b . Also assume that the total bandwidth is W . The relation among, W , W_b , f_h , and, f_l , is given by

$$(4.1.1) \quad W = f_h - f_l = W_b + f_l - f_l = W_b + 0.5(I - 1)R_c$$

where f_h is the highest frequency of the allowable spectrum and f_l is the lowest frequency of the allowable spectrum.

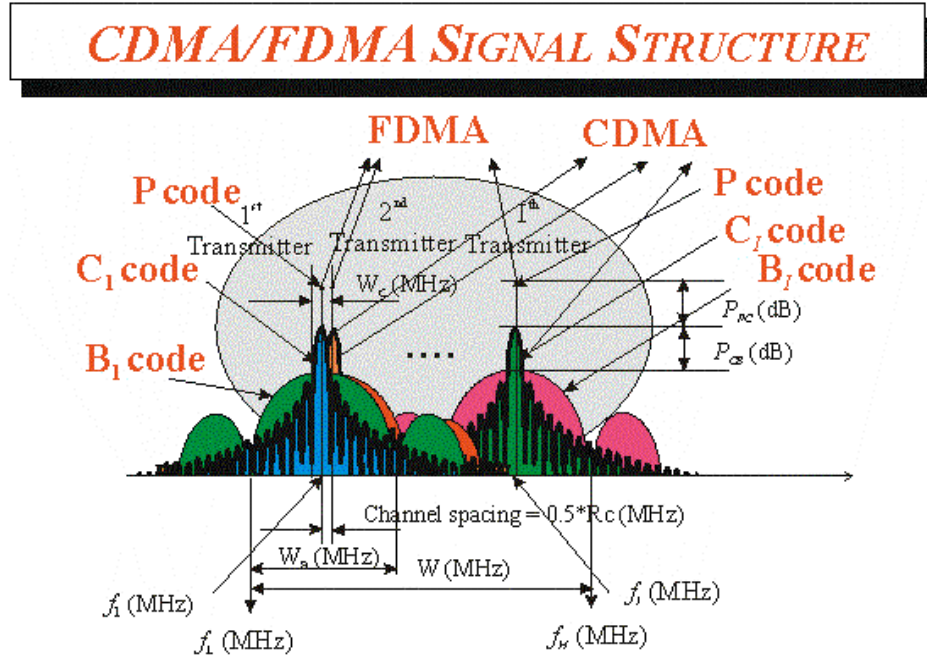


Figure 4.3 The signal structure of a DSSS/CDMA/FDMA indoor geolocation system.

The bandwidth of the C code is W_c , which is close to the chipping rate, R_c . The peak power spectrum gain of the C code is P_{CB} (dB) higher than the peak power spectrum of the B code. And the peak power spectrum gain of the P code is P_{PC} (dB) higher than the peak power spectrum of the C code.

The block diagram of the i th transmitter, $\forall i \in \{1, \dots, I\}$, is shown in Figure 4.4. The transmitted data is generated serially and is encoded with Forward Error Correction (FEC) (see Appendix C). The output of the C and P code generators (see Appendix D) and the output of the FEC enter the left XOR the output of which forms the *quadrature* component of the transmitted signal. The output of the B code generator and the output of the FEC enter the right XOR the output of which forms the *in-phase* component of the transmitted signal. The two XOR outputs and the carrier enter the quadrature phase shift keying (QPSK) modulator the output of which is the composite, transmitted signal. This signal is ready to be amplified and broadcast.

Let the subscript $\lfloor a \rfloor$ depict the greatest integer smaller than or equal to a . Assume that $\mathbf{x} = \{x_{\lfloor m/N_d \rfloor}\}$ denotes the binary sequence representing useful data at a rate of $N_d = R_c/R_d$ chips per data bit, where R_d is the actual data rate. This sequence is encoded with a

half rate convolutional code with generating polynomial matrix \mathbf{G} . Therefore, in view of eq. (B.1.3, Appendix C) the FEC output sequence is given by $\mathbf{y} = \mathbf{x}^t \mathbf{G}$, and can be represented as $\mathbf{y} = \{y_{\lfloor m/2N_d \rfloor}\} = \{y_{\lfloor m/N_s \rfloor}\}$.

Next, let $\mathbf{b} = \{b_m\}$ and $\mathbf{c} = \{c_m\}$ depict either Gold or Kasami periodic pseudorandom spreading sequences of length M_b and M_c respectively, and $\mathbf{p} = \{p_{\lfloor m/N_p \rfloor}\}$ represents an m -sequence of length N and rate R_p chips per P symbol; thus, $N_p = R_c/R_p$. In view of the above assumptions and notation, the output of the first XOR, $\mathbf{z}_1 = \{z_{1m}\}$, can be written as (see Table 4.1 (a))

$$(4.1.2) \quad \mathbf{z}_1 = \mathbf{c} \oplus \mathbf{p} \oplus \mathbf{y} \text{ or } z_{1m} = c_m \oplus p_{\lfloor m/N_p \rfloor} \oplus y_{\lfloor m/N_s \rfloor}.$$

Similarly, the output of the second XOR, $\mathbf{z}_2 = \{z_{2m}\}$, (see Table 4.1 (b)) is given by

$$(4.1.3) \quad \mathbf{z}_2 = \mathbf{b} \oplus \mathbf{y} \text{ or } z_{2m} = b_m \oplus y_{\lfloor m/N_s \rfloor}.$$

Applying the QPSK modulator, shown in Figure 4.5, the signals, $\mathbf{z}_1 = \{z_{1m}\}$ and $\mathbf{z}_2 = \{z_{2m}\}$, are utilized to produce the analog signals, $s_i^c(t)$ and $s_i^s(t)$, as follows

$$(4.1.4) \quad s_i^c(t) \doteq \sum_{m=-\infty}^{\infty} (1 - 2z_{1m}) h(t - mT_c)$$

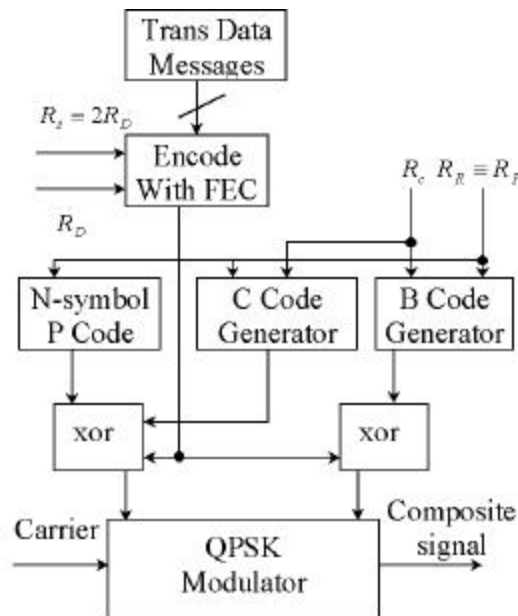


Figure 4.4 A block diagram of a DSSS/CDMA/FDMA transmitter—taken from [12].

$$(4.1.5) \quad s_i^s(t) \triangleq \sum_{m=-\infty}^{\infty} (1 - 2z_{2m})h(t - mT_c).$$

Assuming that the energy per C code chip is E_c and assume that the amplifier gain is $G_a = \sqrt{2E_c}$, which is assumed to be the same for all transmitters, then the i th RF transmitted signal; i.e., the signal broadcast by the i th transmitter, is given by (see [12] and Figure 4.5)

$$(4.1.6) \quad s_i(\mathbf{w}_i, t) = \sqrt{2E_c} [s_i^c(t) \cdot \cos(\mathbf{w}_i t + \mathbf{f}_i) + s_i^s(t) \cdot \sin(\mathbf{w}_i t + \mathbf{f}_i)]$$

Table 4.1 Truth table for the XOR with three inputs and the XOR with two inputs.

P Code (I1)	C Code (I2)	Output FEC (I3)	Output XOR (O1)
0	0	0	0
0	0	1	1
0	1	0	1
0	1	1	0
1	0	0	1
1	0	1	0
1	1	0	0
1	1	1	1

B Code (I1)	Output FEC (I2)	Output XOR (O1)
0	0	0
0	1	1
1	0	1
1	1	0

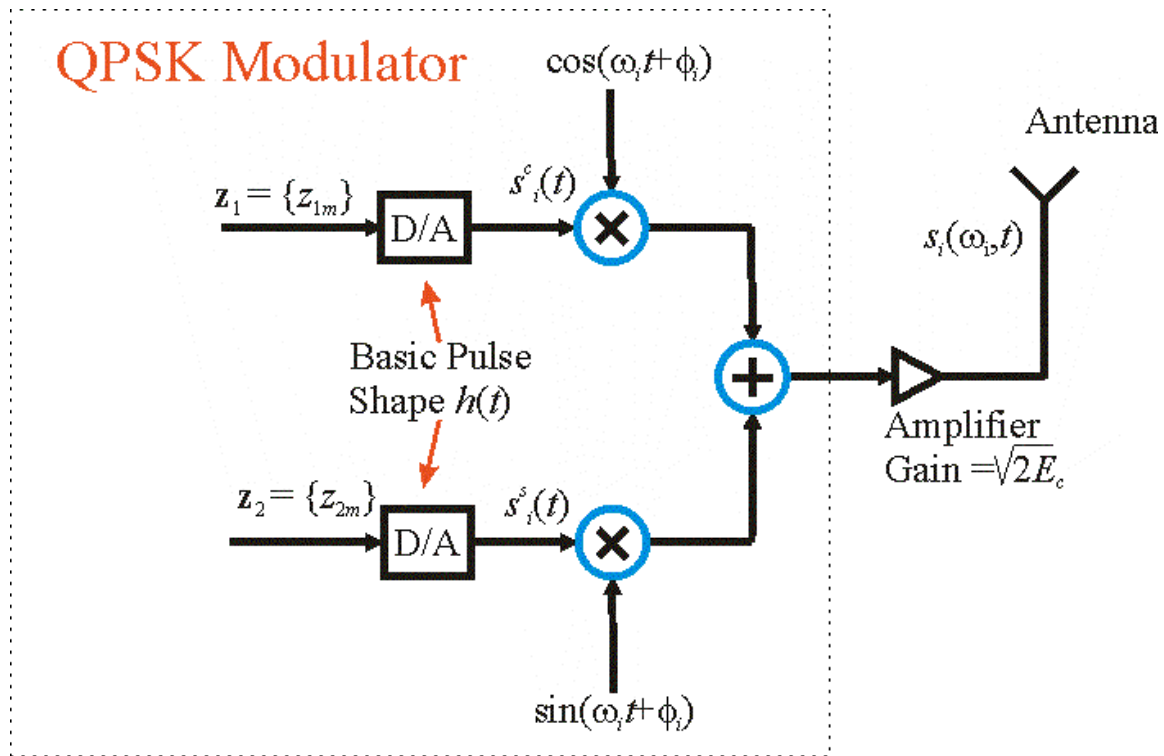


Figure 4.5 A block diagram of a QPSK modulator.

The unknowns in equations (4.1.6), (4.1.4), and (4.1.5) are explained in order: $\mathbf{w}_i = 2\mathbf{p}f_i$, f_i is the carrier frequency of the i th transmitter; t is the time; \mathbf{f}_i is the random phase uniformly distributed over the semi-interval $[0, 2\mathbf{p})$ ($\mathbf{f}_i = \text{un}[0, 2\mathbf{p})$); $h(t)$ is the impulse response of the raised cosine filter, $\int_{-\infty}^{\infty} |h(t)|^2 dt \equiv 1$; and $T_c \equiv 1/R_c$ is the chipping period.

These signals do partially overlap because $f_i = f_1 + 0.5(i-1)R_c$, $\forall i \in \{2, \dots, I\}$, [12]; and thus, the proposed signal structure is designed to overcome this impairment (see Figure 4.3). Employing complex notation the transmitted signal given by equation (4.1.6) can be written as

$$(4.1.7) \quad S_i(\mathbf{w}_i, t) = s_i^c(t) \exp(-j\mathbf{a}_i) + s_i^s(t) \exp\left(j\left[\frac{\mathbf{p}}{2} - \mathbf{a}_i\right]\right) = [s_i^c(t) + js_i^s(t)] \exp(-j\mathbf{a}_i)$$

where $\mathbf{a}_i(t) = \mathbf{w}_i t + \mathbf{f}_i$ is the total phase of the transmitted signal at any given time t and $j = \sqrt{-1}$. We observe that the real part of (4.1.7) is the same as (4.1.6).

A diagram that describes the timing relationship among the B, C, and P codes and the data bit after it is encoded with FEC is shown in Figure 4.6. In this diagram it is assumed that the chipping rate for both the B and the C code is 1.023 MBPS. The C code length is 1023. The length of the B code is not important; however it is much longer than the C code. The P code chipping rate is 1000 BPS; hence the P code chipping period is 1 ms. The P code length is 31. The data rate is 1000/31 BPS and the data bit period is 31 ms [13].

Since the C and the B codes are either Gold or Kasami whose lengths are given by (see Appendix D) [9]-[13]

$$(4.1.8) \quad M_c = 2^{m_c} - 1 \quad \text{and} \quad M_b = 2^{m_b} - 1$$

where m_c is the order of the generating polynomial of the C code and m_b is the order of the generating polynomial of the B code.

Kasami sequences exist only for even m_c or m_b and Gold sequences exist for both even and odd m_c or m_b (see Appendix D).

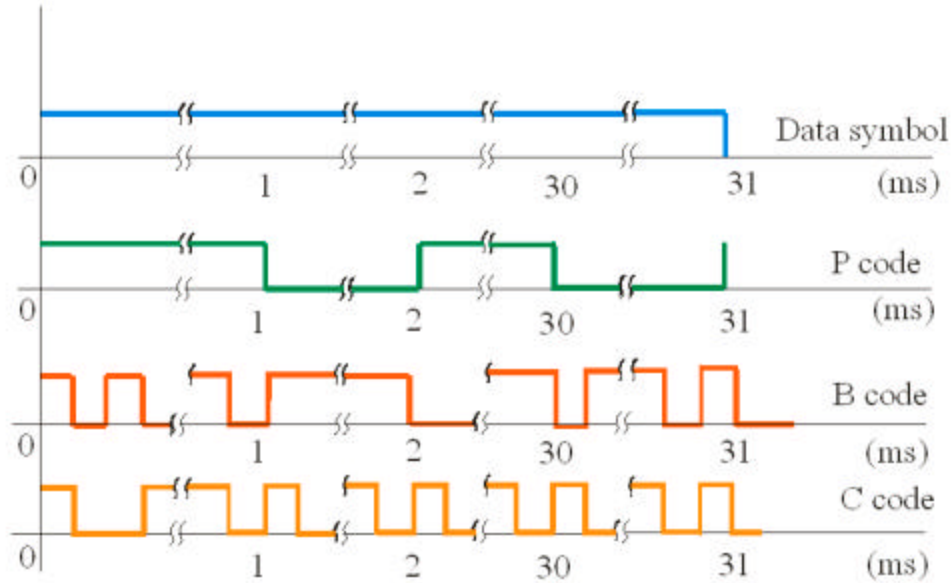


Figure 4.6 The timing diagram of P, C, B, and data symbol - - taken from [13].

Another important aspect in our discussion for this system is that the number of transmitters may impose a restriction to the number of available PRN sequences. The number of PRN sequences, N_c , is equal to

$$(4.1.9) \quad N_c = \begin{cases} M_c + 2, & \text{Gold} \\ \sqrt{M_c + 1}, & \text{Kasami} \end{cases} = \begin{cases} 2^{m_c} + 1, & \text{Gold} \\ 2^{\frac{m_c}{2}}, & \text{Kasami} \end{cases}$$

The modulation scheme of this system is CDMA as long as the number of PRN sequences is greater than or equal to the number of transmitters, i.e.

$$(4.1.10) \quad N_c \geq I.$$

Substituting equation (4.1.9) into (4.1.10) and after some mathematical steps we get

$$(4.1.11) \quad m_c \geq m_{c0} = \begin{cases} \left\lceil \frac{\log I - 1}{\log 2} \right\rceil, & \text{Gold} \\ \left\lceil \frac{2 \log I}{\log 2} \right\rceil, & \text{Kasami} \end{cases}$$

where m_{c0} is the smallest order of the generating polynomial for a given number of transmitters, I , and $\lceil a \rceil$ is the largest number greater than or equal to a .

In Figure 4.7 we plot the smallest number of the generating polynomial, m_{c0} , versus the number of transmitters, I . As we anticipated m_{c0} corresponding to Gold sequences is smaller than m_{c0} corresponding to Kasami sequences. We have arrived at a very important design decision point. The choice that we have to make is simply this: We can either select two different m_{c0} s, one corresponding to the Gold sequences and the other to Kasami sequences, or we can select the same m_{c0} . If we were to make the first decision we would achieve that the smallest number of Gold or Kasami sequences is greater than or equation to I . However, since the code length, the chipping rate, and the data rate are closely linked together then the selection of two different m_{c0} s will ultimately lead to different code lengths, chipping rates, and data rates and hence complicate the assessment process. If we were to select, on the other hand, the same m_{c0} , we will then maintain the same code lengths, chipping rates, and data rates for both systems and thus simplify the assessment process. Therefore, in order to simplify the assessment process we have decided to select the same m_{c0} , corresponding to either Gold or Kasami sequences to keep code lengths, chipping rates, and data rates unchanged.

As indicated in Figure 4.7 for up to 32 transmitters, $m_{c0} = 10$ or $m_c \geq 10$. As we shall see in Chapter 5 this is the number that we have used for the generating polynomial of either Gold or Kasami sequences, $m_c = 10$. The B sequence is a much larger code; therefore, m_b is always greater than m_c . As long as m_b is even and greater than m_c , the number of PRN sequences is always greater than I .

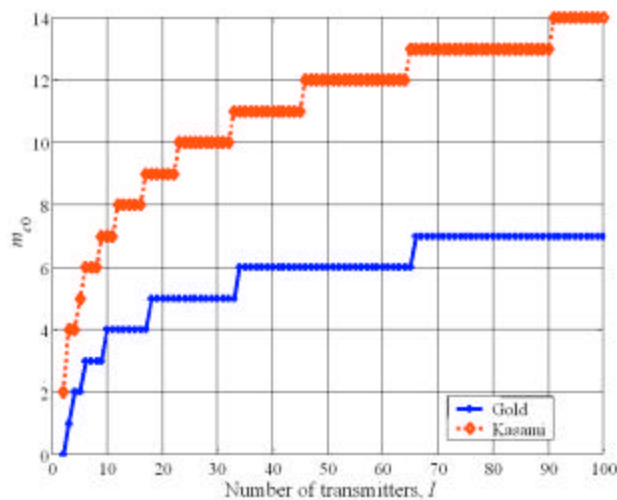


Figure 4.7 The smallest order of generating polynomial, m_{c0} , vs. the number of transmitters, I .

This concludes the discussion on the design of a DSSS/CDMA/FDMA transmitter. Next, we continue our discussion on the design of a DSSS/CDMA/FDMA receiver.

4.1.3 Receiver

The block diagram of a generic DSSS/CDMA/FDMA receiver is shown in Figure 4.8. When designing a receiver, the engineer is going to take into account the principle of operation, the transmitter design, the channel model, and the noise generated from electronics section of the receiver.

Taking into account the principle of operation (see Chapters 1 and 2) a receiver must contain multiple channels to enable simultaneous tracking of multiple transmitters. In this configuration one channel is designated to track the signal coming from a single transmitter. Taking into account the transmitter design a receiver must contain a section that locally replicates the C, P, and B codes and must account for signal structure parameters discussed in the previous section. A receiver design must account for indoor channel models discussed in Chapter 3. The noise generated by the electronics section of the receiver must be accounted in the signal processing. Based on these design constrains (see Appendix F for more details) we propose a DSSS/CDMA/FDMA receiver which contains eight modules as shown in the figure. A C and P code receiver contains these modules: (1) receiver's front end (FE) and baseband sampling (BBS), (2) Doppler removal (DR) and phase rotation (PR), (3) C code I/Q correlators/integrators, (4) P code I/Q correlators/integrators; (5) acquisition and tracking loops, (6) digital oscillator, (7) C code generators, and (8) P code generator.

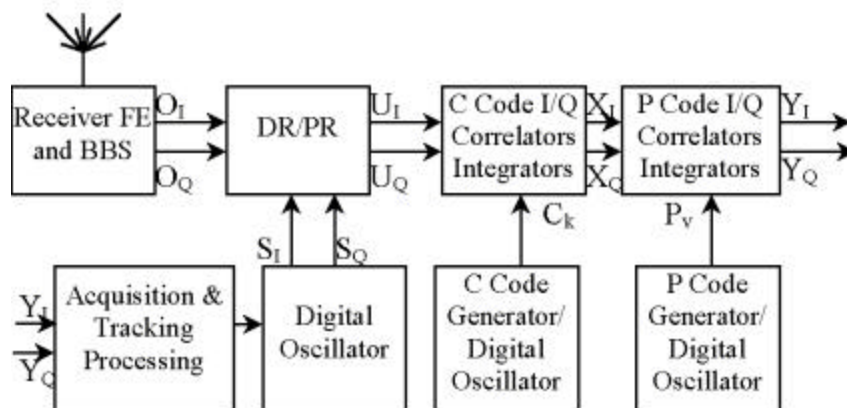


Figure 4.8 A block diagram of a channel of a C and P code receiver.

There may be other modules in the receiver, which are not shown in the figure such as decoding of the communication or navigation messages, synchronization module, navigation solution solver, etc. Therefore, we will only discuss a subset of a receiver design, which enables us to analyze the steps for obtaining an observable and assess the parameters that affect such a process.

In Chapter 3 we have considered the propagation effects that occur as a result of the wave propagation from the transmitting antenna to the receiving antenna. If we assume a transmitting antenna with gain, G_t , and a receiving antenna with gain, G_r , located at a distance, $R_i(t)$, from the transmitting antenna, then the received energy per chip, $E_{ri}(t)$, from the receiving antenna is equal to

$$(4.1.12) \quad E_{ri}(t) = Q(R_i(t), f_i) G_t G_r E_c$$

where $Q(R_i(t), f_i)$ is the propagation power loss factor. For a given frequency, f_i , the propagation power loss factor, $Q(R_i(t), f_i)$, is computed from

$$(4.1.13) \quad Q(R_i(t), f_i)_{dB} = Q(R_0, f_0)_{dB} + 10n \log_{10} \left(\frac{R_0}{R_i(t)} \right) + 10m \log_{10} \left(\frac{f_0}{f_i} \right) + N(0, \sigma)$$

where $R_0 = 1$ m, $f_0 = 1575.42$ MHz, and χ_σ and γ_σ are both zero mean Gaussian random variables. Moreover, the parameter n denotes the slope of the power loss factor, $Q(R_i(t), f_0)_{dB}$, from the distance, $R_i(t)$, and the parameter m denotes the slope of the power loss factor, $Q(R_0, f_i)_{dB}$, from the frequency, f_i . The values of n , m , and $Q(R_0, f_0)_{dB}$ are specified in Chapter 5.

The effects of the total propagation losses, of the transmitting antenna gain, of the receiving antenna gain and of the system geometry are given by equations (4.1.12) and (4.1.13). Taking into account these effects the received noiseless signal, $S_{ri}(\tilde{\omega}_i, t)$, can be written as

$$(4.1.14) \quad S_{ri}(\tilde{\omega}_i, t) = [s_{ri}^c(t) + js_{ri}^s(t)] \cdot \exp(-j\tilde{\alpha}_i)$$

where

$$(4.1.15) \quad s_{ri}^c(t) \triangleq \sqrt{2E_{ri}} \sum_{m=-\infty}^{\infty} d_{[m/N_D]}^{(i)} b_m^{(i)} h(t - mT_c)$$

$$(4.1.16) \quad s_{ri}^s(t) \triangleq \sqrt{2E_{ri}} \sum_{m=-\infty}^{\infty} d_{[m/N_D]}^{(i)} P_{[m/N_P]} c_m^{(i)} h(t - mT_c)$$

$$(4.1.17) \quad \tilde{\mathbf{a}}_i(t) = \tilde{\mathbf{w}}_i t + \mathbf{f}_i$$

$$(4.1.18) \quad \tilde{\mathbf{w}}_i = \mathbf{w}_i (1 \pm \dot{R}_i(t)/c)$$

and $\dot{R}_i(t)$ is the geometric range rate (m/s) between the i th transmitter and the receiver.

If we assume a one-to-one correspondence between channels of the receiver and transmitters; i.e., the channel index is denoted by subscript j , which means that the j th channel is assigned to track the i th transmitted signal.

Considering the propagation effects as the result of the multipath distribution (see Chapter 3) and noise generated by the receiver's front end electronics the received signal, $r_j(t)$, is determined from

$$(4.1.19) \quad r_j(t) = \sum_{i=1}^I \int_{-\infty}^{\infty} C_i(\tau) S_{ri}(\tilde{\omega}_i, t - \tau) d\tau + n(t) \\ = \sum_{i=1}^I \sum_{k=1}^K a_i^k [s_{ri}^c(t - \tau_i^k) + j s_{ri}^s(t - \tau_i^k)] \exp[-j\beta_i^k(t)] + n(t)$$

where

$$(4.1.20) \quad \beta_i^k(t) = \tilde{\omega}_i(t - \tau_i^k) + \phi_i + \theta_i^k.$$

The received signal, given by (4.1.19), goes through several processing stages, which are described in Chapter 5. It is important to emphasize here that the received signal model is independent of the processing performed by the receiver; i.e., the same signal model can potentially lead to a variety of different receivers or receiver designs. In Chapter 5 two different receivers are exploited: one tracking the C code and the other tracking the C and B code. Next, we discuss an improved system, namely a DSSS/OFDM/CDMA/FDMA indoor geolocation system which is motivated by the system we have already introduced.

4.2 A DSSS/OFDM/CDMA/FDMA Indoor Geolocation System

When high data rate is required then a DSSS/OFDM/CDMA/FDMA system can be exploited. The channel spacing can be divided into subchannels, in which the subchannel spacing is equal to the channel spacing divided by number of subchannels. The center frequency of every channel is the transmitter main frequency. In this embodiment the number of subchannels is equal to the number of OFDM frequencies. The number of channels can, however, be different from the number of transmitters. Chapter 6 discusses the analytical development of this system.

Here we discuss the principle of operation (§4.2.1), the transmitter (§4.2.2), and the receiver design (§4.2.3). In Chapter 6 we discuss the system performance evaluation based on the channel model introduced in Chapter 3 and in Chapter 8 we highlight some of the issues of this system.

4.2.1 Principle of Operation

The principle of operation of a DSSS/OFDM/CDMA/FDMA system is the same as the principle of operation of a GPS/pseudolite indoor geolocation system discussed in Chapter 2.

4.2.2 Transmitter

From the communication point of view a DSSS/OFDM/CDMA/FDMA indoor geolocation system must suppress three kinds of interference the Inter Symbol interference (ISI), the Subchannel Access Interference (SAI), and the Mutually Accessed Interference (MAI). The scheme that we propose for this system cancels most of the ISI, SAI, and part of the MAI.

The signal structure of a DSSS/OFDM/CDMA/FDMA indoor geolocation system is depicted in Figure 4.9. The transmitted signal contains only the C code as a spreading code. Assume that the total bandwidth is W . Assume that the C code bandwidth is W_c , which is close to the chipping rate, R_c . Assume that the bandwidth of the i th transmitter signal is W_i and assume that N is the number of OFDM frequencies. The relation among, W , W_i , f_1 , and, f_I , is given by

$$(4.2.1) \quad W = f_h - f_l = W_i + f_l - f_l = W_i + 0.5(I - 1)R_c,$$

where f_h is the highest frequency of the allowable spectrum and f_l is the lowest frequency of the allowable spectrum.

The modulation scheme of this system would be CDMA as long as the number of PRN sequences, N_c , is greater than or equal to the number of transmitters, I , times the number of OFDM frequencies, N , i.e.

$$(4.2.2) \quad N_c \geq N \cdot I.$$

Substituting equation (4.1.9) into (4.2.2) and after some mathematical operation we get

$$(4.2.3) \quad m_c \geq m_{c0} = \begin{cases} \left\lceil \frac{\log(N \cdot I) - 1}{\log 2} \right\rceil, & \text{Gold} \\ \left\lceil \frac{2 \log(N \cdot I)}{\log 2} \right\rceil, & \text{Kasami} \end{cases}$$

where m_{c0} is the smallest order of the generating polynomial for a given number of transmitters, I , and for a given number of OFDM frequencies, N .

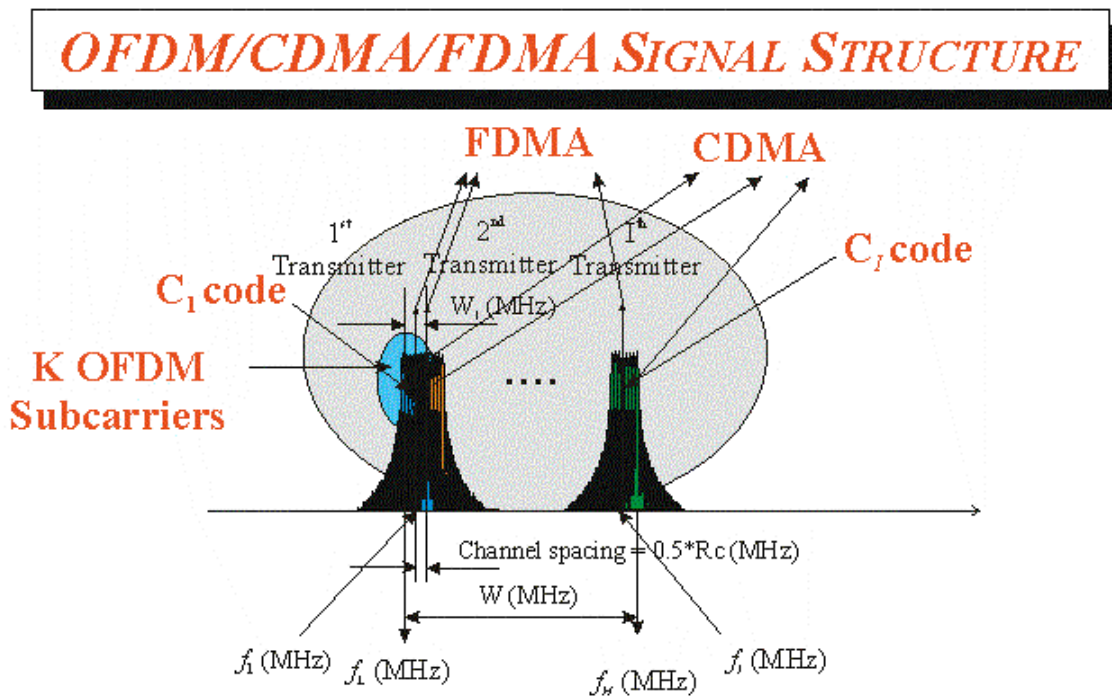


Figure 4.9 The signal structure of a DSSS/OFDM/CDMA/FDMA indoor geolocation system.

Figure 4.10 (a) depicts the smallest order of generating polynomial, m_{c0} , vs. the number of transmitters, I , for $N = 10$. As shown in the figure for up to 32 transmitters $m_{c0} = 17$. Since we have determined that only even m_c are required; therefore, $m_c \geq 18$.

However, if we select $m_c = 18$ then this is going to yield a code length of 262,143 which is going to limit the data rate. To avoid this condition, we change the assumption from every transmitter as a unique set of codes to every transmitter has the same set of codes but there is a unique code corresponding to an OFDM frequency. In this case the order of the generating polynomial is given by

$$(4.2.4) \quad m_c \geq m_{c0} = \begin{cases} \left\lceil \frac{\log N - 1}{\log 2} \right\rceil, & \text{Gold} \\ \left\lceil \frac{2 \log N}{\log 2} \right\rceil, & \text{Kasami} \end{cases}$$

where m_{c0} is the smallest order of the generating polynomial for a given number of OFDM frequencies, N .

Figure 4.10 (b) shows the smallest order of generating polynomial, m_{c0} , vs. the number of OFDM frequencies, N . As shown in the figure for up to 12 OFDM frequencies the smallest, even order of the generating polynomial is $m_{c0} = 8$ or $m_c \geq 8$. In fact, $m_c \geq 8$ is the number that we have selected in our analysis performance parameters in Chapter 6.

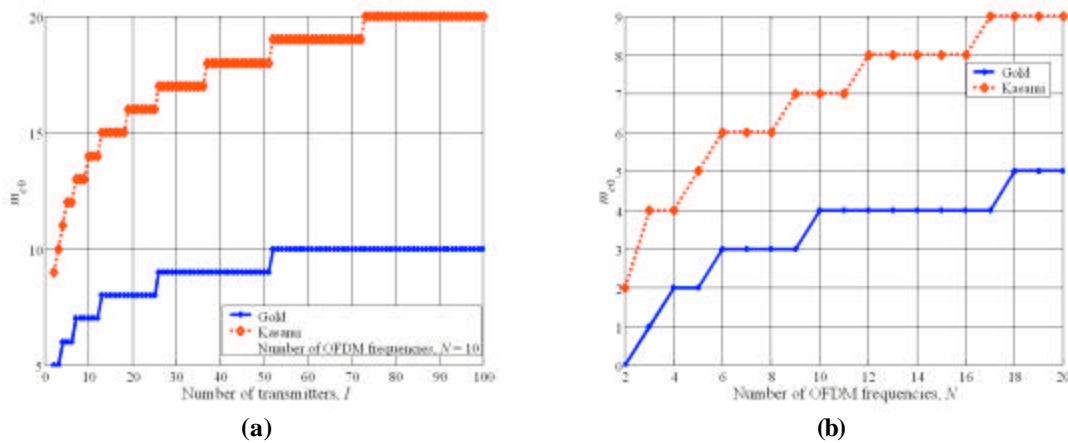


Figure 4.10 The smallest order of generating polynomial, m_{c0} , vs. (a) the number of transmitters, I , (b) the number of OFDM frequencies, N .

Assume that $\mathbf{d}^{i,l} = \{d_{\lfloor m/N_d \rfloor}^{(i,l)}\}$ denotes the binary sequence representing useful data at a rate of N_d chips per symbol where the superscript i depicts the transmitter index, which is also the carrier frequency index because we have assigned one frequency per carrier per transmitter, and l depicts the OFDM frequency index. Let $\mathbf{c}^{i,n} = \{c_m^{(i,n)}\}$ depict periodic pseudorandom spreading sequences of length M_c and n is the index of an OFDM frequency. The sequence $c_m^{(i,n)}$ and $d_{\lfloor m/N_d \rfloor}^{(i,l)} c_m^{(i,n)}$ modulate an impulse train respectively, where the energy per chip is E_c , which is assumed to be the same for all transmitters.

The i th transmitted signal; i.e., the signal broadcast by the i th transmitter, is modeled as (see Figure 4.11)

$$(4.2.5) \quad s_i(\omega_i, t) \hat{=} \sum_{n=1}^N s_{i,n}^c(t) \cos(\omega_n t + \omega_i t + \phi_i) + \sum_{n=1}^N s_{i,n}^s(t) \sin(\omega_n t + \omega_i t + \phi_i)$$

where

$$(4.2.6) \quad s_{i,n}^c(t) \hat{=} \sqrt{2E_c} \sum_{m=-\infty}^{\infty} d_{\lfloor m/N_d \rfloor}^{(i,l)} c_m^{(i,n)} h(t - mT_c)$$

$$(4.2.7) \quad s_{i,n}^s(t) \hat{=} \sqrt{2E_c} \sum_{m=-\infty}^{\infty} c_m^{(i,n)} h(t - mT_c).$$

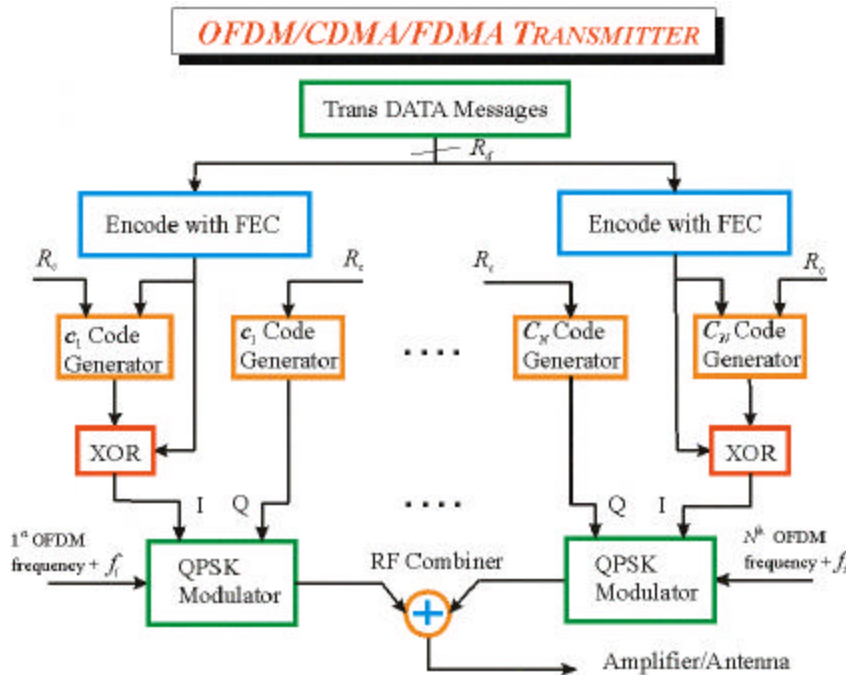


Figure 4.11 A block diagram of a DSSS/OFDM/CDMA/FDMA transmitter.

The unknowns in equations (4.1.6) through (4.2.7) are explained in order: $\omega_n = 2\pi f_n$, f_n is the n th OFDM frequency, t is the time; ϕ_i is the random phase uniformly distributed over the semi-interval $[0, 2\pi)$ ($\phi_i = \text{un}[0, 2\pi)$); $h(t)$ is the impulse response of a raised cosine filter, $\int_{-\infty}^{\infty} |h(t)|^2 dt \equiv 1$; and $T_c \equiv 1/R_c$ is the chip period with R_c being the chipping rate in units of MBPS.

Based on the signal structure discussed in the previous section and employing complex notation we get

$$(4.2.8) \quad S_i(\omega_i, t) = \sum_{n=1}^N [s_{i,n}^c(t) + js_{i,n}^s(t)] \exp[-\alpha_{i,n}(t)]$$

where $\alpha_{i,n}(t) = \omega_i t + \omega_n t + \phi_i$ is the total phase corresponding to the n th OFDM frequency of the i th transmitted signal at any given time t and $j = \sqrt{-1}$, examining that the real part of (4.2.8) is the same as (4.2.5).

4.2.3 Receiver

So far we have discussed the transmitter and the channel model (see Chapter 3). The block diagram of a generic receiver is similar to that of a DSSS/CDMA/FDMA receiver shown in Figure 4.12.

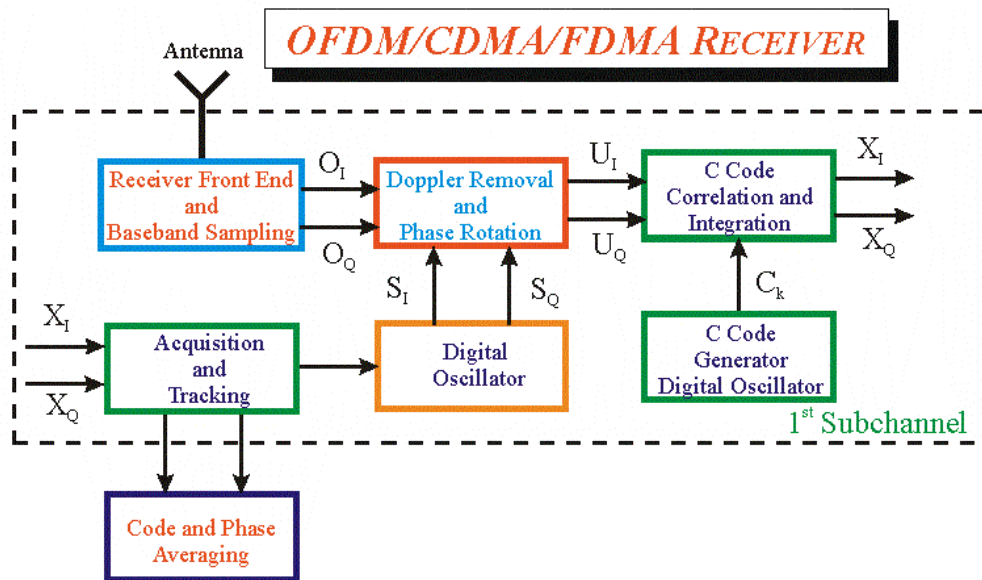


Figure 4.12 A block diagram of a channel a DSSS/OFDM/CDMA/FDMA receiver.

Taking into account the propagation effects, the received noiseless signal, $S_{ri}(\tilde{\omega}_i, t)$, can be written as

$$(4.2.9) \quad S_{ri}(\tilde{\omega}_i, t) = \sum_{n=1}^N [s_{ri,n}^c(t) + js_{ri,n}^s(t)] \exp(-j\tilde{\alpha}_{i,n})$$

or every signal component

$$(4.2.10) \quad S_{ri,n}(\tilde{\omega}_{i,n}, t) = [s_{ri,n}^c(t) + js_{ri,n}^s(t)] \exp(-j\tilde{\alpha}_{i,n})$$

where

$$(4.2.11) \quad s_{ri}^c(t) \triangleq \sqrt{2E_{ri}} \sum_{m=-\infty}^{\infty} d_{[m/N_d]}^{(i),(l)} c_m^{(i),(n)} h(t - mT_c)$$

$$(4.2.12) \quad s_{ri}^s(t) \triangleq \sqrt{2E_{ri}} \sum_{m=-\infty}^{\infty} c_m^{(i),(k)} h(t - mT_c)$$

$$(4.2.13) \quad \tilde{\alpha}_{i,n}(t) = \tilde{\omega}_{i,n} t + \phi_{i,n}$$

$$(4.2.14) \quad \tilde{\omega}_{i,n} = \omega_{i,n} (1 \pm \dot{R}_i(t)/c)$$

and $\dot{R}_i(t)$ is the geometric range rate (m/s) between the i th transmitter and the receiver.

Considering the propagation effects as a result of multipath distribution and the receiver's frontend electronics, the received signal, $r_j(t)$, is given by

$$(4.2.15) \quad r_j(t) = \sum_{i=1}^I \sum_{n=1}^N \int_{-\infty}^{\infty} C_i^n(\tau) S_{ri,n}(\tilde{\omega}_{i,n}, t - \tau) d\tau + n(t) \\ = \sum_{i=1}^I \sum_{n=1}^N \sum_{k=1}^K a_{i,n}^k [s_{ri,n}^c(t - \tau_{i,n}^k) + js_{ri,n}^s(t - \tau_{i,n}^k)] \exp[-j\beta_{i,n}^k(t - \tau_{i,n}^k)] + n(t)$$

where

$$(4.2.16) \quad \beta_{i,n}^k(t - \tau_{i,n}^k) = \tilde{\omega}_{i,n}^k (t - \tau_{i,n}^k) + \phi_{i,n} + \theta_{i,n}^k.$$

The received signal, given by equation (4.2.15), undergoes through several processing stages, which are described in Chapter 6.

It is important to emphasize here that the received signal model is independent of the processing performed by the receiver; i.e., the same signal model can potentially lead to a variety of different receivers or receiver designs.

4.3 An OFDM/FDMA Indoor Geolocation System

Ultra Wide Band (or UWB) systems employ narrow, pulsed signals in the time domain (hence, ultra wideband signals in the frequency domain). The pulse width can be very narrow which eliminates the multi-path effect; thus, making UWB systems attractive in indoor applications. The time of arrival between two consecutive pulses is measured to determine the receiver location. Signal bandwidth is one of the key factors that affects TOA estimation accuracy in multipath propagation environments [16]-[17]. In general, larger bandwidth yields better ranging accuracy. UWB systems, which exploit bandwidths in excess of 1 GHz, have attracted considerable attention as a means of measuring accurate TOA for indoor geolocation applications [18]. The utilization of high frequencies result in high attenuation; therefore, the high and low cutoff frequencies considered for a UWB system are typically focused unlicensed operation in the 2–3 GHz band up to the year 2002 [18]. Results of propagation measurement in a typical modern office building have shown that the UWB signal does not suffer multipath fading [18], which is desirable for accurate TOA estimation in indoor areas.

The actual deployment of UWB systems in the United States is subject to the Federal Communications Commissions (FCC) approval of Feb. 14, 2002 [19]. The main concern of the FCC is the interference between UWB devices, other licensed services and GPS system that operate at {1176.45, 1227.6, 1575.42} MHz frequency bands [20]-[22]. The UWB signal has a low, flat, and noise-like power spectrum similar to a spread spectrum signal [20]-[22]. Therefore, FCC has approved the operation of wall imaging systems below 960 MHz and in the frequency band of 3.1-10.6 GHz (see Figure 4.13) [19].

These systems are designed to detect the location of objects contained within a “wall,” such as concrete structure, the side of a bridge, or the wall of a mine [19]. Nevertheless, operation of these systems is restricted to law enforcement, fire and rescue organizations, scientific research institutions, commercial mining companies and construction companies [19]. However, given the weak GPS satellite signals that must be processed by GPS receivers, the noise-like UWB signal is still considered harmful to GPS systems in close proximity [20]-[22]. For this reason we propose a modified or spectralized UWB

system; namely, an OFDM/FDMA indoor geolocation system, which is presented here and which is discussed in Chapter 7.

4.3.1 Principle of Operation

An OFDM/FDMA (or spectralized UWB) indoor geolocation system utilizes a profile for the configuration of the bandwidth allocation, which determines which portion of the spectrum can be allocated and which cannot be allocated. The following steps describe the basic idea behind the spectralized UWB (or OFDM/FDMA) system (see Figure 4.14). First, we divide the high end UWB spectrum into I blocks of equal bandwidth W . Second, there is a one-to-one mapping between a frequency block and a transmitter; hence, on one hand the modulation scheme of the system is FDMA. On the other hand, each frequency block is composed of tones with consecutive spacing of Δ ; hence, the other aspect of the modulation scheme is OFDM.

There are two reasons why we propose an OFDM/FDMA indoor geolocation system: (1) there is a large, available spectrum equal to 7.5 GHz and (2) the FDMA modulation scheme is well known to achieve the smallest cross-channel interference (ex. GLONASS).

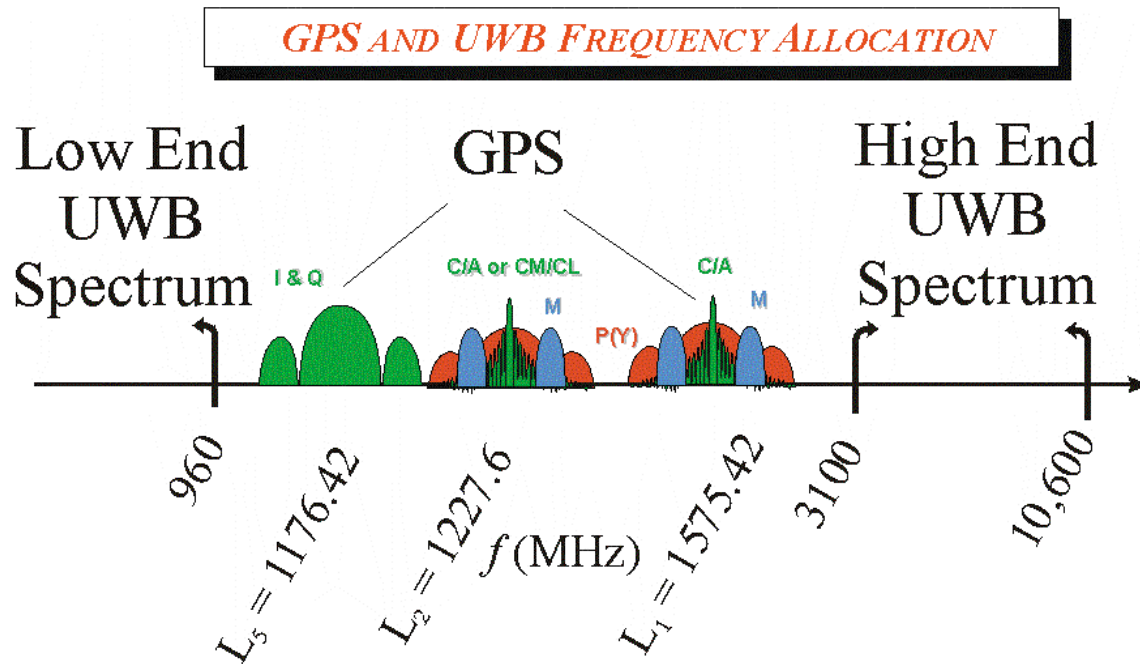


Figure 4.13 GPS and UWB frequency allocation-- taken from [23].

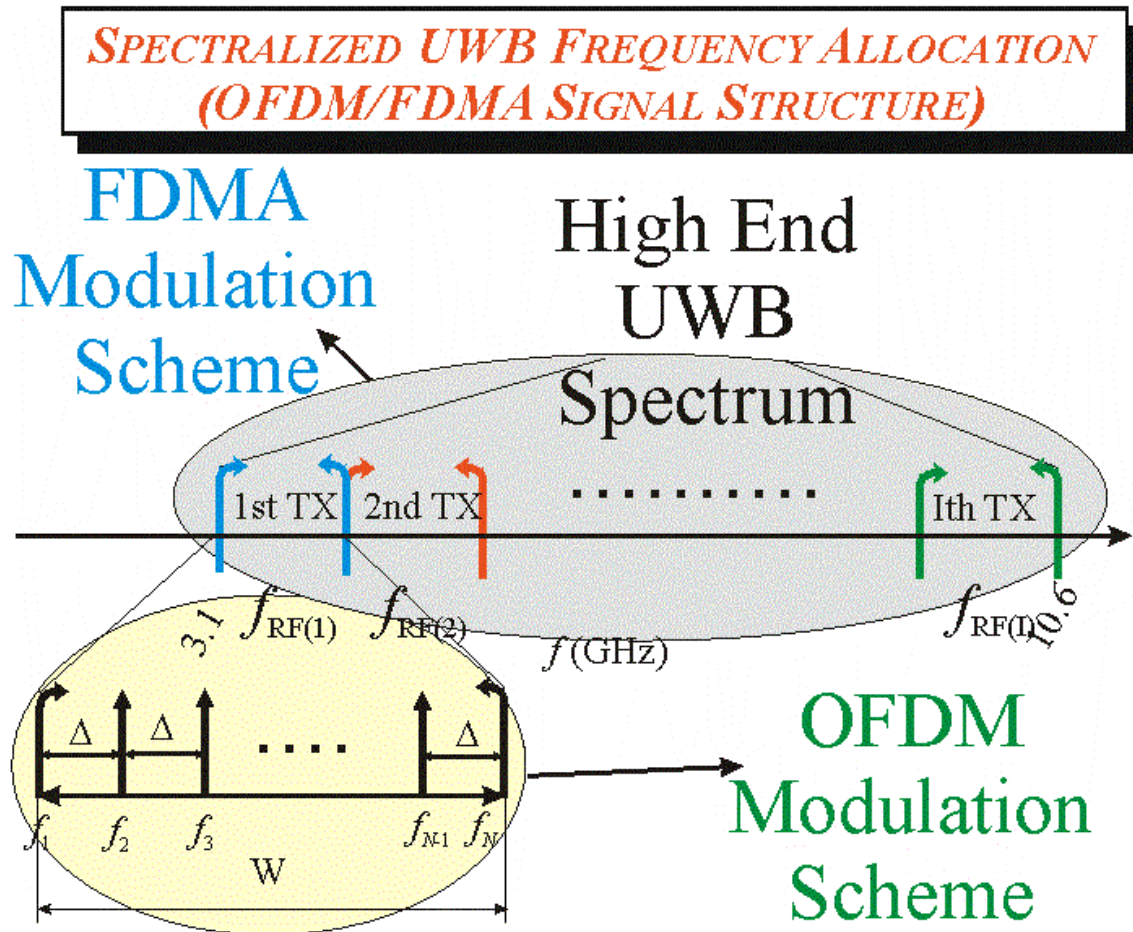


Figure 4.14 GPS and UWB frequency allocation- - taken from [23].

Typically, synchronization is achieved using a pseudorandom sequence, as it is the case with GPS. This is necessary because the phase information from a single sinusoid is lost due to multipath. In the system described below, we employ the characteristics of an OFDM signal to preserve the phase information even in the presence of multipath; thus, eliminating the need of a conventional PRN scheme.

Based on this discussion we propose an OFDM/FDMA indoor geolocation system as illustrated in Figure 4.15. In this figure there are I OFDM/FDMA transmitters and one OFDM/FDMA receiver. The channel (see Chapter 3) enables the signal propagation from a transmitter to the receiver.

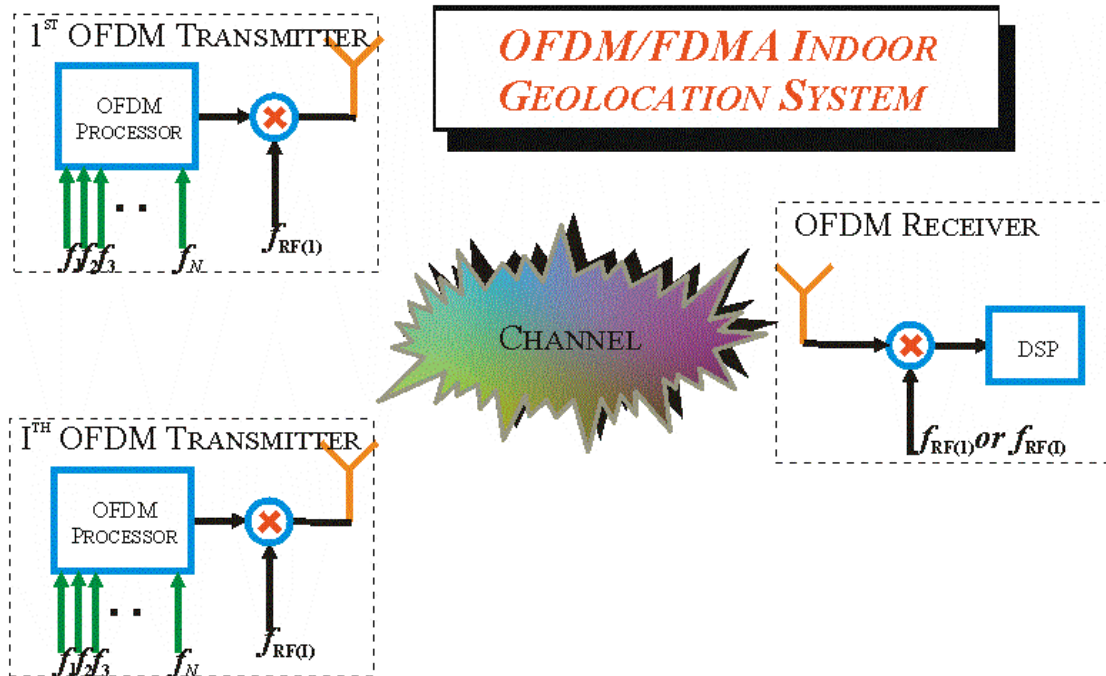


Figure 4.15 A block diagram of an OFDM/FDMA indoor geolocation system.

An OFDM/FDMA receiver contains multiple channels (not to be confused with the propagation medium between the transmitting antenna and receiving antenna). Each channel of the receiver is designated to track a particular OFDM transmitter. Each channel generates an observable based on the OFDM transmitted signal and the locally generated OFDM signal. This observable is in fact a direct measure of the time of arrival between that transmitter and the receiver. From this point on the principle of operation of an OFDM/FDMA indoor geolocation system is the same as the principle of operation of GPS, GLONASS, or WPI indoor geolocation systems that we discussed earlier.

4.3.2 Transmitter

The transmitted signal is a superposition of sinusoids (or tones) equally spaced in the frequency domain. A tone is defined as a narrowband signal whose bandwidth does not exceed 40 kHz. This kind of signal structure is often referred to as OFDM and it is very similar to the Digitally Sampled Line (DSL) waveform. The generation of an OFDM-like signal is depicted in Figure 4.16. There are N OFDM frequencies (or tones) generated by the same clock; therefore all OFDM tones have the same initial phase. These tones are combined with the help of an analog combiner. The combined signal is sampled and digitized employing an analog-to-digital (A/D) converter. At this stage the

signal can go through additional filtering and processing, which is not shown in the figure because it is not relevant to the discussion here. Next, the signal is converted back to the analog domain using a digital-to-analog (D/A) converter and modulated on a RF carrier. The mathematics of the signal structure is discussed next.

Let $S_i(t)$ be the complex OFDM transmitted signal coming from the i th transmitter before up-conversion, which is defined as

$$(4.3.1) \quad S_i(t) = \sum_{n=1}^N \exp(j[\omega_n t + \phi_i])$$

where ω is the radian frequency, ϕ_i is the initial phase, and the subscript n denotes the index of the OFDM frequency (see Figure 4.16).

The transmitted signal (see eq. (4.3.1)) is sampled at the sampling frequency, f_s , producing the discrete-time signal

$$(4.3.2) \quad S_i[m] = \sum_{n=1}^N \exp\left(j\left[\frac{f_n}{f_s} m + \phi_i\right]\right)$$

The crosscorrelation function, $\gamma(k, \tau)$, of the discrete-time signal $S_i[m]$ with a delayed and conjugated version of itself, $S_i[m+k+\tau]$, is defined as

$$(4.3.3) \quad \gamma(k, \tau) = \frac{1}{T} \int_0^{T-\frac{|k|}{N_s}} S_i(t) S_i(t+\tau)^* dt \cong \frac{1}{N_s} \sum_{m=1}^{N_s-|k|} S_i[m] S_i[m+k+\tau]^*$$

where N_s is the number of samples.

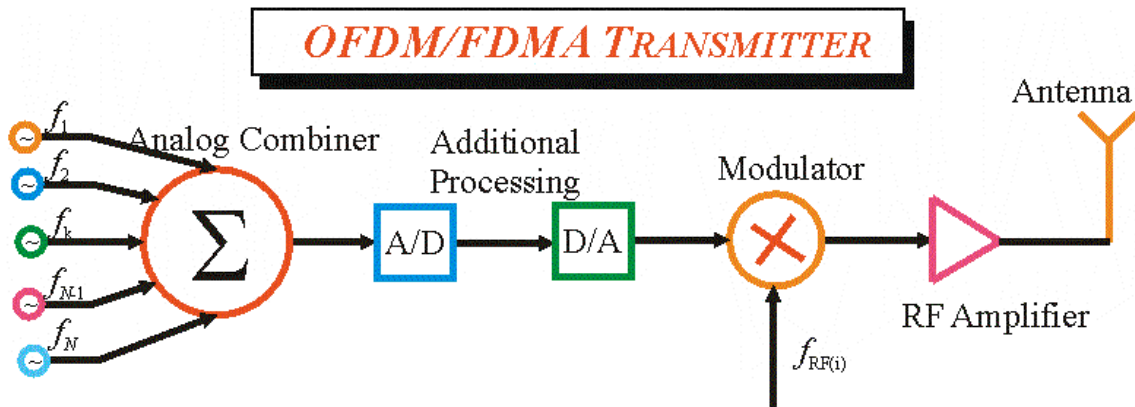


Figure 4.16 A block diagram of an OFDM/FDMA transmitter-- taken from [23].

In order to evaluate equation (4.3.3), we compute the expression inside the sum as follows

$$(4.3.4) \quad S_i[m]S_i[m+k+\tau]^* = \left(j \left[\frac{f_n}{f_s} m + \phi_i \right] \right) \exp \left(j \left[\frac{f_h}{f_s} (m+k+\tau) + \phi_i \right] \right)^* \\ = \sum_{h=1}^N \left[\exp \left(-j \frac{f_h(k+\tau)}{f_s} \right) \sum_{n=1}^N \exp \left(j \frac{(n-h)\Delta}{f_s} m \right) \right]$$

where Δ is the difference between two sinusoids (or tones).

Substituting the results of equation (4.3.4) into equation (4.3.3) yields

$$(4.3.5) \quad \gamma(m, \tau) \gamma(k, \tau) = \sum_{h=1}^N \exp \left(-j \frac{f_h(k+\tau)}{f_s} \right) \sum_{n=1}^N \left[\frac{1}{N_s} \sum_{m=1}^{N_s-|k|} \exp \left(j \frac{(n-h)\Delta}{f_s} m \right) \right].$$

Let β_h denote the sum

$$(4.3.6) \quad \beta_h = \sum_{n=1}^N \left[\frac{1}{N_s} \sum_{m=1}^{N_s-|k|} \exp \left(j \frac{(n-h)\Delta}{f_s} m \right) \right].$$

These coefficients β_h , $\forall h \in \{1, \dots, N\}$, are independent of the delay τ ; therefore, they will be the same for every τ . Hence, equation (4.3.5) can be written as

$$(4.3.7) \quad \gamma(k, \tau) = \sum_{h=1}^N \beta_h \exp \left(-j \frac{f_h(\tau+k)}{f_s} \right).$$

We shall seek a relation between the spacing parameter, Δ , and the sampling frequency, f_s ; such that the coefficient, β_h , has the largest possible value and it is independent of h . If we assume the following

$$(4.3.8) \quad \frac{\Delta}{f_s} \leq \frac{2\pi}{N_s N 10^2}$$

then

$$(4.3.9) \quad \beta_h \cong N \frac{N_s - |k|}{N_s}, \quad \forall h \in \{1, \dots, N\}.$$

The above equality allows writing the crosscorrelation function (4.3.7) as follows

$$(4.3.10) \quad \gamma(k, \tau) \cong N \frac{N_s - |k|}{N_s} \sum_{h=1}^N \exp\left(j \frac{f_h(\tau + k)}{f_s}\right) \text{ for } \frac{\Delta}{f_s} \leq \frac{2\pi}{N_s N 10^2} = \frac{\pi}{50 N_s N}.$$

We shall also seek a relation between the OFDM frequencies, f_h , $\forall h \in \{1, \dots, N\}$, the sampling frequency, f_s ; and the number of samples, N_s . If we assume

$$(4.3.11) \quad \frac{f_h}{f_s} \cong \frac{2\pi}{N_s}$$

then the magnitude of the sum of all the complex exponents in eq. (4.3.10) will have the shape of a sinc function with maximum occurring for $m = -\tau$; thus, the magnitude of this crosscorrelation function serves as a detector statistics.

Now we come back to the discussion of the transmitter design. The signal $S_i[n]$ is passed through a D/A converter, up-converted at the RF frequency, $f_{RF(i)} \equiv f_i$, and amplified with gain $\sqrt{2P_t}$ yielding the RF signal at the transmitter antenna (or at the output of the transmitter)

$$(4.3.12) \quad \tilde{S}_i(t) = \sqrt{2P_t} \sum_{n=1}^N \exp(j[\omega_n t + \omega_{RF(i)} t + \phi_i]),$$

where P_t is the transmitted signal power and $\omega_{RF(i)} = 2\pi f_{RF(i)}$ is the RF radian frequency of the i th transmitter (see Figure 4.16).

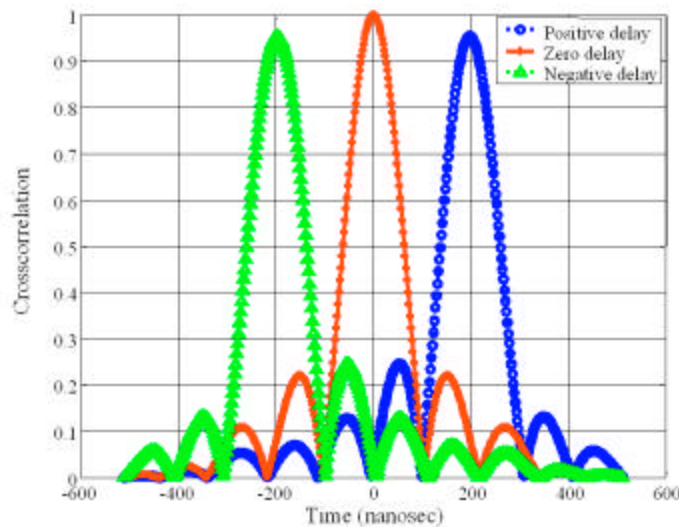


Figure 4.17 Crosscorrelation function g for $t = \{-204.8$ (dash ^), 0 (solid +), 204.8 (dash o) nsec.

Expression (4.3.12) enables us to compute the i th transmitted signal amplitude based only on the transmitter signal structure and design. For example, assume that the transmitter has 10 OFDM frequencies, 1 MHz spaced apart, a 500 MHz sampling frequency and $N_s = 256$ samples. Figure 4.17 illustrates the autocorrelation function γ for delay $\tau = \{-204.8$ (dash ^), 0 (solid +), 204.8 (dash o)} nsec.

The maximum detectable range without ambiguity for this transmitter is

$$(4.3.13) \quad d_{\max} = \frac{(N_s - 1)c}{f_s} = Tc = 153 \text{ m and } T = \frac{(N_s - 1)}{f_s}.$$

As it is shown in Figure 4.17, when the delay between two sequences is zero, then we have the maximum crosscorrelation peak. When $\tau = 0.4T = 204.8$ nsec, the maximum crosscorrelation peak occurs slightly earlier. Also, when $\tau = -0.4T = -204.8$ nsec, the maximum crosscorrelation peak occurs slightly later. However, the closer the maximum crosscorrelation peak is to the center the smaller this time difference becomes.

4.3.3 Receiver

The block diagram of a generic receiver is shown in Figure 4.18. As shown in Figure 4.18, the incoming signal is received through an antenna element, is amplified, filtered, and down-converted to the intermediate frequency. (In actual implementation there may be several down-conversion stages.) A local oscillator drives the locally generated RF reference frequency of every mixer. It is conceivable that this frequency will differ both in absolute value and in rate of change from the actual RF signal frequency; therefore, the frequency of the signal after the down-conversion will exhibit an error with statistics depending on the stability of the local receiver clock and the propagation models. This frequency error is expected to have an impact on the following stages of the receiver. The IF signal is sampled and it is either amplified or attenuated depending on the gain from the automatic gain controller (AGC) (not shown in the figure). Then the signal is ready for digital signal processing in the digital signal processor. The digital signal processor utilizes a locally generated reference OFDM signal (LGS) to produce an estimate of the time delay, pseudorange, Doppler, carrier phase and finally navigation solution. The phase of the LGS is expected to be different from the phase of the OFDM signal from the i th transmitter. Once the time delay is estimated then a coherent phase

lock loop can be used to track the phase of the OFDM signal from the i th transmitter; thus, improving the time delay and navigation solution accuracy.

Taking into account the propagation effects (see equations (4.1.12) and (4.1.13) and Chapter 3) the received noiseless signal reads

$$(4.3.14) \quad \tilde{S}_{ri}(t) = \sqrt{2P_r} \sum_{n=1}^N d_k(t) \exp j(\omega_n t + \tilde{\omega}_i t + \phi_i)$$

$$(4.3.15) \quad P_r = p_i(t)P_t = Q_i(t)G_r G_t P_t$$

$$(4.3.16) \quad \tilde{\omega}_i = \omega_i (1 \pm \dot{R}_i(t)/c).$$

We have assumed a one-to-one correspondence between channels and transmitters; hence, the channel index is denoted by subscript, j , which means that j th receiver channel is assigned to track the i th transmitted signal.

Considering the multipath distribution of the channel and the front end receiver noise, the received signal, $r_j(t)$, is determined from

$$(4.3.17) \quad r_j(t) = \sum_{i=1}^I \int_{-\infty}^{\infty} C_{i,k}(\tau) \tilde{S}_{ri}(t - \tau) d\tau + n(t) = \sqrt{2P_r} \sum_{i=1}^I \sum_{n=1}^N \sum_{k=1}^K a_i^k d_i(t - \tau_i^k) \exp j\beta_i^k(t) + n(t)$$

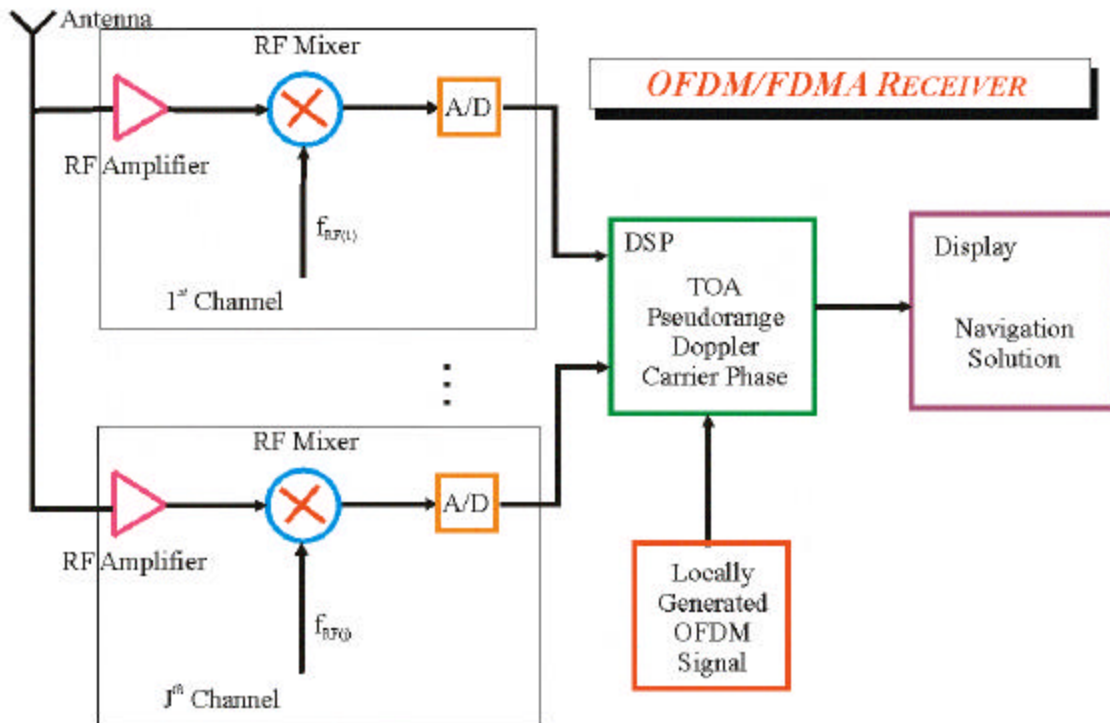


Figure 4.18 A block diagram of an OFDM/FDMA receiver.

where

$$(4.3.18) \beta_i^k(t) = \tilde{\omega}_i(t - \tau_i^k) + \omega_n(t - \tau_i^k) + \phi_i + \theta_i^k.$$

The received signal, given by (4.3.17), undergoes through several processing stages, which are considered separately in Chapter 7. It is important to emphasize here that the received signal model is independent of the processing performed by the receiver; i.e., the same signal model can potentially lead to a variety of different receivers or receiver designs or the model discussed here can be used as a base line for future receiver designs.

CITED REFERENCES AND FURTHER READING:

- [1] I.F. Proгри, W.R. Michalson et al, "A system for tracking and locating emergency personnel inside buildings," in *Proc. ION-GPS*, Salt Lake City, UT, pp. 560-568, Sep. 2000.
- [2] I.F. Proгри and W.R. Michalson, "Performance evaluation of category III precision landing using airport Pseudolites," in *Proc. IEEE PLANS*, San Diego, CA, pp. 262-269, Mar. 2000.
- [3] I.F. Proгри and W.R. Michalson, "A combined GPS satellite/pseudolite system for category III precision landing," in *Proc. IEEE PLANS*, Palm Spring, CA, Apr. 2002.
- [4] W.R. Michalson and I.F. Proгри, "Assessing the accuracy of underground positioning using pseudolites," in *Proc. ION-GPS*, Salt Lake City, UT, pp. 1007-1015, Sep. 2000.
- [5] I.F. Proгри, W.R. Michalson, and J. Hill, "Assessing the accuracy of navigation algorithms using a combined system of GPS satellites and pseudolites," in *Proc. ION-NTM*, Long Beach, CA, pp. 473-481, Jan. 2001.
- [6] I.F. Proгри, J. Hill, and W.R. Michalson, "A Doppler based navigation algorithm," in *Proc. ION-NTM*, Long Beach, CA, pp. 482-490, Jan. 2001.
- [7] I.F. Proгри and W.R. Michalson, "An innovative navigation algorithm using a system of fixed Pseudolites," in *Proc. ION-NTM*, Long Beach, CA, pp. 619-627, Jan. 2001.
- [8] J. Hill, I.F. Proгри, and W.R. Michalson, "Techniques for reducing the near-far problem in indoor geolocation systems," in *Proc. ION-NTM*, Long Beach, CA, pp. 860-865, Jan. 2001.
- [9] I.F. Proгри, J.M. Hill, and W.R. Michalson, "An investigation of the pseudolite's signal structure for indoor applications," in *Proc. ION-AM*, Albuquerque, NM, pp. 453-462, June 2001.
- [10] I.F. Proгри and W.R. Michalson, "The impact of proposed pseudolite's signal structure on the receiver's phase and code error," in *Proc. ION-AM*, Albuquerque, NM, pp. 414-422, June 2001.

- [11] I.F. Progri and W.R. Michalson, "An alternative approach to multipath and near-far problem for indoor geolocation systems," in *Proc. ION-GPS*, Salt Lake City, UT, Sep. 2001.
- [12] I.F. Progri and W. R. Michalson, "Performance evaluation of a DSSS/CDMA/FDMA indoor geolocation system," in review *IEEE Trans. Comm.*, Nov. 2001.
- [13] I.F. Progri, W.R. Michalson, and M.C. Bromberg, "A DSSS/CDMA/FDMA indoor geolocation system," in *Proc. ION-GPS*, Portland, OR, pp. 155-164, Sep. 2002.
- [14] R.A. Valenzuela, "Performance of adaptive equalization for indoor radio communications," *IEEE Trans. Comm.*, vol. 37, no. 3, pp. 291-293, Mar. 1989.
- [15] D.J. Goodman, "Cellular packet communications," *IEEE Trans. Comm.*, vol. 38, no. 8, pp. 1272-1280, Aug. 1990.
- [16] B.W. Parkinson, J.J. Spilker, Jr, et al., *The Global Positioning System-Theory and Applications*, Washington, DC: American Institute of Aeronautics and Astronautics, (vol. 1, chap. 3, "GPS signal structure and theoretical performance") 1996.
- [17] B.W. Parkinson, J.J. Spilker, Jr, et al., *The Global Positioning System-Theory and Applications*, Washington, DC: American Institute of Aeronautics and Astronautics, (vol. 1, chap. 8, "GPS receivers") 1996.
- [18] R. Fontana, "Advances in ultra wideband indoor geolocation systems," *3rd IEEE Wksp. WLAN*, Boston, MA, Sept. 2001.
- [19] Federal Communications Commission, *News*, "New public safety applications and broadband internet access among uses envisioned by FCC authorization of ultra-wideband technology," Washington, DC, Feb. `14, 2002.
- [20] G.R. Opshaug and P. Enge, "GPS and UWB for indoor navigation," in *Proc. ION-GPS*, Salt Lake City, UT, pp. 1427–1433, Sep. 11-14, 2001.
- [21] P. Enge, "A global challenge—protect GNSS noise floor a.k.a. spectrum stewardship," *ION-GPS 2002* (panel presentation), Portland, OR, Sep. 24, 2002.
- [22] K. Pahlavan, X. Li, J.-P. Makela, "Indoor geolocation science and technology," *IEEE Comm. Mag.*, vol. 40, no. 2, pp. 112-118, Feb. 2002.
- [23] I.F. Progri, W.R. Michalson, and D. Cyganski, "An OFDM/FDMA indoor geolocation system," in *Proc. ION-NTM*, Anaheim, CA, Jan. 2003.

Chapter 5. A DSSS/CDMA/FDMA Indoor Geolocation System

“...to pursue mathematical analysis while at the same time turning one’s back on its applications and on intuition is to condemn it to hopeless atrophy.” ^{3/4}R. Courant

5.0 Introduction

THE performance of a DSSS/CDMA/FDMA indoor geolocation system is analyzed in this Chapter. This system contains multiple transmitters and multiple receivers. As we have already discussed in Chapter 4 each transmitted signal contains a single frequency and two unique pseudorandom sequences. Each receiver is capable of simultaneously tracking multiple transmitters. A known pseudorandom sequence of zeros and ones (called *chips*) modulates the transmitted signal phase and it is used to transmit information in form of binary data [1]. The chip modulation is typically accomplished using either the binary phase shift keying (BPSK) or quaternary phase shift keying (QPSK) modulation [1]. Although the QPSK modulation is more complex than the BPSK modulation it is usually employed to prevent signal capture when a strong interferer drives the receiver into saturation [1].

It is well known that a DSSS/CDMA system is susceptible from large mutually accessed interference (MAI). FEC coding (see Appendix C) is utilized in the CDMA systems to enhance the multiple access capability because the processing gain is not affected by the coding rate, thus, performance is improved by coding gain [1]. Nevertheless, a DSSS/CDMA system has good frequency spectrum utilization (large capacity) and good multipath protection because it discriminates the multipath components that are delayed with respect the LOS path by more than one chip duration [1]-[13]. On the other hand, a DSSS/FDMA system has a small MAI in the expense of large spectrum utilization (small capacity) and good multipath protection [1], [5], [14], and [15]. Although a combination of both the CDMA and FDMA can improve the MAI and multipath protection, it still suffers from the bandwidth allocation.

This Chapter is organized as follows. Based on the mathematical model discussed in Chapter 4 we analyze the communication performance based on C code tracking in §5.1. Communication performance includes the bit error probability (BEP) (or bit error rate (BER) as preferred by some). Next, we analyze the communication performance based on tracking both C and B codes §5.2. Next, we analyze the receiver's phase error, receiver's code error, and receiver's frequency error, as part of the navigation performance analyses §5.3. In the context of this investigation the parameters of interests are the ideal signal to noise ratio, synchronization frequency error, synchronization time error, synchronization phase error, number of transmitters, system geometry and system kinematics and dynamics and channel parameters. Quantitative assessment is provided in §5.4. Conclusions and summary is provided in §5.5.

5.1 Communication Performance Analyses (C Code)

The communication performance of the receiver is analyzed relying on the synchronization as a result of tracking of the C code. The C code is relatively short which makes it relatively easy to resolve for its beginning. Having resolved the start of the C code the receiver then attempts to resolve the beginning of the P code. For ease of analyses qualitative computations are performed for an analog receiver assuming that the sampling rate satisfies the Nyquist criterion.

Based on the receiver diagram, shown in Figure 5.1, we can identify 8 (eight) important processing stages, which are analyzed in order. We analyze the receiver's front end and base band sampling is §5.1.1. We discuss the process of Doppler removal and phase rotation in §5.1.2. We analyze the correlation with the locally generated C code in §5.1.3. We discuss the first integration after the correlation with the locally generated C code in §5.1.4. We continue our discussion with the correlation with the locally generated P code in §5.1.5. We analyze the second integration after the correlation with the locally generated P code in §5.1.6. We study the signal plus interference to noise ratio in §5.1.7. And finally, we conclude our analyses with the qualitative of the bit error probability (see §5.1.8).

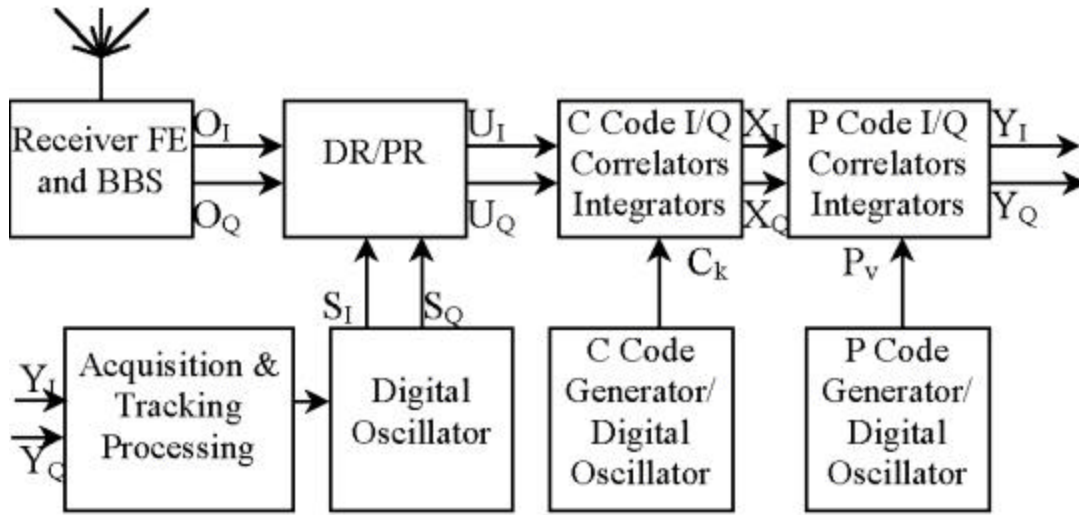


Figure 5.1 Block diagram of the first channel of a DSSS/CDMA/FDMA receiver.

5.1.1 Receiver's Front End and Baseband Sampling

The receiver's front-end section has a two-fold impact on the received signal: a *desired* impact and an *undesired* impact. On one hand, the down-conversion of the received signal to the desired base-band or intermediate frequency (IF) for further signal processing occurs at the receiver's front end and baseband sampling (the *desired* effect). On the other hand, thermal or Johnson noise is introduced in the received signal (*undesired* effect).

We perform the analysis only for the first channel; i.e., we assume that the desired signal ($i=1$) is received at channel ($j=1$), all the remaining adjacent (or interfering) signals $\forall i \in \{2, \dots, I\}$ for that particular channel come from the other transmitters. The analysis is performed for the continuous signal, which should provide the base line for any design method.

The received signal, $r_{j=1}(t) \equiv r(t)$, is down-converted to the base-band frequency and sampled (see Figure 5.2) and the subscript j is no longer used in our analysis. Therefore, the expression for the sampled, received signal at base-band, $o(t)$, can be written as

$$(5.1.1) \quad o(t) = \sum_{i=1}^I \sum_{k=1}^K \sqrt{G_a} a_i^k [s_{ri}^c(t - \tau_i^k) + j s_{ri}^s(t - \tau_i^k)] \exp \left\{ -j [(\tilde{\omega}_i - \hat{\omega}_i)(t - \tau_i^k) + \phi_i + \theta_i^k] \right\} + n_{out}(t)$$

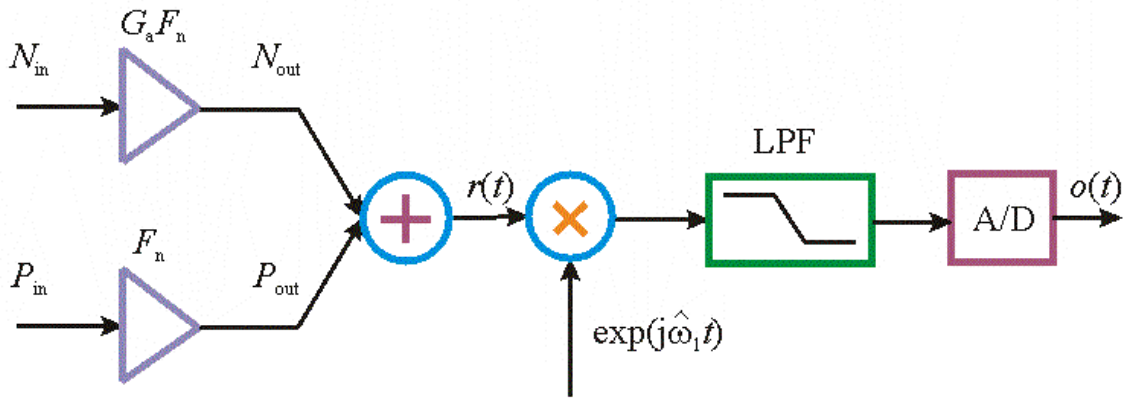


Figure 5.2 Block diagram of the receiver's front end and base band sampling.

where the hat (^) denotes a parameter generated and estimated locally by the receiver and $n_{out}(t)$ is the noise with power spectral density given by (5.1.4) and G_a is the amplifier gain of the electronics section of the receiver, which includes the RF and IF sections.

The *undesired* effect of the receiver's front end is analyzed next. Assume that the available thermal noise power, N_{in} (W), which is proportional to the temperature, T_0 (K), and receiver bandwidth, B_n (Hz), in accordance with [20], is given by

$$(5.1.2) \quad N_{in} = kT_0 B_n$$

where $k = 1.38 \times 10^{-23} \text{ J/K}$, the Boltzmann's constant. The bandwidth of the IF stage is typically considered as the receiver's bandwidth [20]; i.e.

$$(5.1.3) \quad B_n = \frac{\int_{-\infty}^{\infty} |H_{IF}(f)|^2 df}{|H_{IF}(f_c)|^2}$$

where $H_{IF}(f)$ is the frequency response of the IF filter (amplifier) and f_c the maximum response frequency (or the center band frequency).

Normalizing $H_{IF}(f)$ such that $H_{IF}(f_c) = 1$ produces a rectangular filter whose bandwidth is the noise bandwidth, B_n , and a 3-dB separation in hertz on the normalized frequency response, $H_{IF}(f)$, can be exploited to approximate B_n , a practice which is widely used by electronics engineers.

Let F_n denote the noise figure (or the noise factor) by which the actual receiver noise power, N_{out} , is greater than the ideal thermal noise power, N_{in} . These three parameters are the basis of the following closed form expression

$$(5.1.4) \quad N_{out} = G_a F_n N_{in} = G_a F_n k T_o B_n .$$

It is important to emphasize here that the same signal model given by (5.1.1) can be exploited for different signal processing designs (such as coherent, non-coherent, or vector based tracking loops). Next we discuss the removal of Doppler shift from the desired signal and the rotation of the phase of the desired signal.

5.1.2 Doppler Removal and Phase Rotation

Obviously, the signal given by (5.1.1) contains the Doppler shift and its phase is not rotated. Hence, before correlating it with the C code, the Doppler shift must be removed and its phase must be rotated to an acceptable accuracy.

First, during this process the Doppler shift of the desired signal (corresponding to the signal coming out from the first transmitter) is removed and second, the phase of the desired signal is rotated, which yields the signal, $u(t)$, determined from (see Figure 5.3)

$$(5.1.5) \quad u(t) = \sum_{i=1}^I \sum_{k=1}^K \sqrt{G_a} a_i^k [s_{ri}^c(t - \tau_i^k) + j s_{ri}^s(t - \tau_i^k)] \exp(-j\chi_i^k) + n_{out}(t).$$

where

$$(5.1.6) \quad \tilde{\omega}_1 = \hat{\omega}_1 (1 \pm \dot{R}_1(t)/c)$$

$$(5.1.7) \quad \chi_i^k = (\tilde{\omega}_i - \tilde{\omega}_1)(t - \tau_i^k) + \phi_i + \theta_i^k .$$

Let ω_{ei} denote radian error frequency term defined as

$$(5.1.8) \quad \omega_{ei} = \tilde{\omega}_i - \tilde{\omega}_1 = \omega_i (1 \pm \dot{R}_i(t)/c) - \hat{\omega}_1 (1 \pm \dot{R}_1(t)/c)$$

then relation (5.1.7) can be further written as

$$(5.1.9) \quad \chi_i^k = \omega_{ei} (t - \tau_i^k) + \phi_i + \theta_i^k .$$

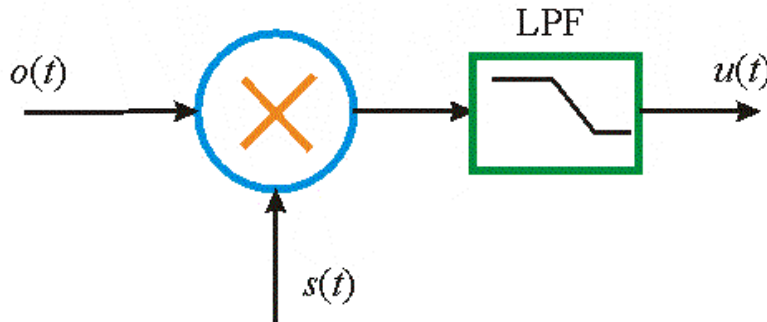


Figure 5.3 Doppler removal and phase rotation block diagram.

The accuracy of removing the Doppler shift and rotating the phase depends upon the radian frequency error, ω_{ei} , and the time delay, τ_i^k . This effect, while unnoticeable at this stage, will become very detrimental during the acquisition and tracking of the C code.

Before acquiring the C code, the receiver performs the correlation with the locally generated C code, which is the topic of the coming subsection.

5.1.3 Correlation with the Locally Generated C Code

The receiver will be able to track the desired code, $c^{(1)}(t)$, from the first channel by exploiting or comparing the received signal with the desired code, $c^{(1)}(t)$. Although, there are several techniques for performing this comparison such as full or partial correlation of the c code, maximum likelihood estimation, or match-filtering etc., we perform our analyses assuming full or complete correlation with the C code due to its simplicity.

Assuming full or complete correlation with the code, $c^{(1)}(t)$ (see Figure 5.4), the signal coming out of this process, $w(t)$, is a superposition of the desired signal component, $w_d(t)$, the Inter Symbol Interference (ISI) term, $w_f(t)$, Mutually Accessed Interference (MAI) component, $w_m(t)$, and the Additive With Gaussian Noise (AWGN) term, $w_n(t)$. The signal, $w(t)$, is analytically expressed as [16]

$$(5.1.10) \quad w(t) = w_d(t) + w_f(t) + w_m(t) + w_n(t)$$

where these individual components are computed from

$$(5.1.11) \quad w_d(t) = \sqrt{G_a} a_1^1 [s_{r1}^c(t - \tau_1^1) + js_{r1}^s(t - \tau_1^1)] \exp(-j\chi_1^1) \cdot c^{(1)}(t)$$

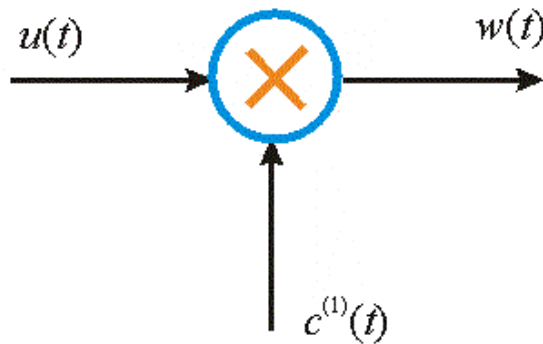


Figure 5.4 Block diagram of the correlation with the locally generated C code.

$$(5.1.12) \quad w_f(t) = \sqrt{G_a} \sum_{k=2}^K a_1^k [s_{r1}^c(t - \tau_1^k) + js_{r1}^s(t - \tau_1^k)] \exp(-j\chi_1^k) \cdot c^{(1)}(t)$$

$$(5.1.13) \quad w_m(t) = \sqrt{G_a} \sum_{i=2}^I \sum_{k=1}^K a_i^k [s_{ri}^c(t - \tau_i^k) + js_{ri}^s(t - \tau_i^k)] \exp(-j\chi_i^k) \cdot c^{(1)}(t)$$

$$(5.1.14) \quad w_n(t) = n_{out}(t) \cdot c^{(1)}(t).$$

When proper alignment is achieved, every component of the desired signal, $w_d(t)$, should yield minimum and constant phase, as opposed to the other component, which should yield random and non-minimum phase. During the integration phase the desired signal component is accumulated and the undesired terms are averaged out as much as possible. The following section provides the necessary mathematical details to support these claims.

5.1.4 (First) Integration after the Correlation with the Locally Generated C Code

Having discussed the correlation with the C code, the receiver performs initially a non-coherent detection; i.e., the first accumulation (integration) is performed, for only one C code repetition period, T_r , until the start of the $c^{(1)}(t)$ sequence is determined (see Figure 5.5). This process is known by the name “acquisition mode.” Then for every block of M_c data the receiver performs the correlation with the $p(t)$ sequence and the second integration until the start of the $p(t)$ sequence is determined. At this point the receiver has entered the “tracking mode.” The outcome of this process determines the data bit transition; hence, it enables the transition from the acquisition to the tracking mode.

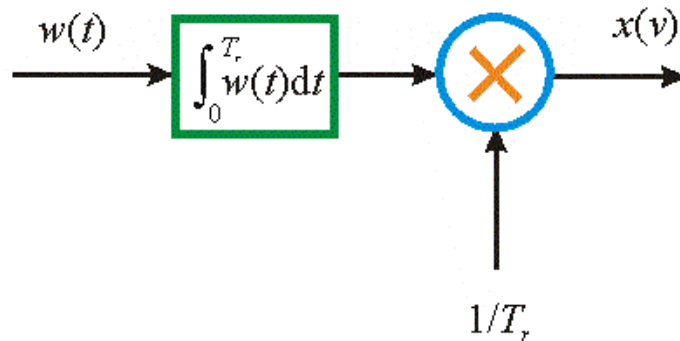


Figure 5.5 Block diagram of the integration after the correlation with the C code.

The signal, $x(v)$, that describes the acquisition mode is given by [16]

$$(5.1.15) \quad x(v) = x_d(v) + x_f(v) + x_m(v) + x_n(v)$$

where each component of $x(v)$, for $j = \{d, f, m, n\}$ and v an integer, is obtained from [16]

$$(5.1.16) \quad x_j(v) = \frac{1}{T_r} \int_0^{T_r} w_j(t) dt.$$

The integration of (5.1.16) requires the computation of the crosscorrelation function, $\phi_m^{(1,i)}(\omega_{ei}, \tau_i^k)$, which is computed by crosscorrelating the sequence $c^{(1)}(t)$ with the function $s_{ri}^s(t - \tau_i^k)$ and the crosscorrelation function, $\gamma_m^{(1,i)}(\omega_{ei}, \tau_i^k)$, which is derived by crosscorrelating the sequence $c^{(1)}(t)$ with the sequence $s_{ri}^c(t - \tau_i^k)$. The crosscorrelation functions, $\phi_m^{(1,i)}(\omega_{ei}, \tau_i^k)$ and $\gamma_m^{(1,i)}(\omega_{ei}, \tau_i^k)$ are defined as [16]

$$(5.1.17) \quad \phi_m^{(1,i)}(\omega_{ei}, \tau_i^k) = \int_0^{T_r} s_{ri}^s(t - \tau_i^k) c^{(1)}(t) \exp(-j\chi_i^k) dt$$

$$(5.1.18) \quad \gamma_m^{(1,i)}(\omega_{ei}, \tau_i^k) = \int_0^{T_r} s_{ri}^c(t - \tau_i^k) c^{(1)}(t) \exp(-j\chi_i^k) dt.$$

These crosscorrelation functions depend on several parameters, such as the time delay, τ_i^k , the frequency error, ω_{ei} , the phase shift, $\phi_i + \theta_i^k$, and code properties, $c_i^{(1)} c_{l-m}^{(i)}$ or $c_i^{(1)} b_{l-m}^{(i)}$. Therefore, a better understanding of these parameters is necessary for a proper calculation of the crosscorrelation functions $\phi_m^{(1,i)}(\omega_{ei}, \tau_i^k)$ and $\gamma_m^{(1,i)}(\omega_{ei}, \tau_i^k)$.

The time delay τ_i^k is a sum of multiple number of chipping periods and a random number between 0 and T_c ; and thus, it can be modeled as

$$(5.1.19) \quad \tau_i^k = mT_c + \delta\tau_i^k, \quad m \in \{0, 1, \dots\} \text{ and } 0 \leq \delta\tau_i^k < T_c.$$

The parameter $\delta\tau$ is called the synchronization parameter and as such it must be taken into account when designing the tracking loops (see Chapter 2). Conceivably, the number m corresponding to the line-of-sight path (or the direct path) is smaller than the number m corresponding to each of the non line-of-sight paths because the line-of-sight path is shorter than each the non line-of-sight paths. Moreover, the number m corresponding to the line-of-sight path is directly linked with the pseudorange measurement accurate to the synchronization parameter, $\delta\tau$.

The frequency error, ω_{ei} , is assumed to be independent of any variable and much smaller than the chipping rate; hence, $f_{ei}/R_c \cong 0$, where $f_{ei} = \omega_{ei}/2\pi$. This is not a bad assumption at this point, knowing that this variable is dependent upon the design of the tracking loops, which is secondary at this stage, because we are trying to provide an analytical performance of the tracking loop(s).

The phase shift, $\phi_i + \theta_i^k$, and code properties, $c_l^{(1)}c_{l-m}^{(i)}$ or $c_l^{(1)}b_{l-m}^{(i)}$ are explored in that after some mathematical steps, the crosscorrelation functions $\varphi_m^{(1,i)}(\omega_{ei}, \tau_i^k)$ and $\gamma_m^{(1,i)}(\omega_{ei}, \tau_i^k)$ can be written as [16]

$$(5.1.20) \quad \begin{aligned} \varphi_m^{(1,i)}(\omega_{ei}, \tau_i^k) &= \frac{\sqrt{2E_{ri}}}{\omega_{ei}} j\kappa_c(\omega_{ei}, \delta\tau_i^k) \exp[-j(\phi_i + \theta_i^k)] \sum_{l=0}^{M_c-1} c_l^{(1)}c_{l-m}^{(i)} \\ &= j|\varphi_m^{(1,i)}(\omega_{ei}, \tau_i^k)| \exp[-j(\phi_i + \theta_i^k)] \end{aligned}$$

$$(5.1.21) \quad \begin{aligned} \gamma_m^{(1,i)}(\omega_{ei}, \tau_i^k) &= \frac{\sqrt{2E_{ri}}}{\omega_{ei}} \kappa_c(\omega_{ei}, \delta\tau_i^k) \exp[-j(\phi_i + \theta_i^k)] \sum_{l=0}^{M_c-1} c_l^{(1)}b_{l-m}^{(i)} \\ &= |\gamma_m^{(1,i)}(\omega_{ei}, \tau_i^k)| \exp[-j(\phi_i + \theta_i^k)] \end{aligned}$$

where

$$(5.1.22) \quad \kappa_c(\omega_{ei}, \delta\tau_i^k) = \int_0^{T_c} \psi_c(t - \delta\tau_i^k) \exp[j\omega_{ei}(t - \delta\tau_i^k)] dt \cong \Psi_c(f_{ei})(1 - R_c \delta\tau_i^k).$$

In light of expressions (5.1.20) and (5.1.21) the desired signal term is given by

$$(5.1.23) \quad x_d(v) = \frac{a_1^1 \sqrt{G_a}}{M_c} \left[|\gamma_m^{(1,1)}(\omega_{e1}, \tau_1^k)| + j|\varphi_m^{(1,1)}(\omega_{e1}, \tau_1^k)| p(v) \right] \exp[-j(\phi_1 + \theta_1^k)].$$

Similarly, the ISI component can be obtained from

$$(5.1.24) \quad x_f(v) = \frac{\sqrt{G_a}}{M_c} \sum_{k=2}^K a_1^k \left[|\gamma_m^{(1,1)}(\omega_{e1}, \tau_1^k)| + j|\varphi_m^{(1,1)}(\omega_{e1}, \tau_1^k)| p(v) \right] \exp[-j(\phi_1 + \theta_1^k)]$$

and the MAI term as follows

$$(5.1.25) \quad x_m(v) = \frac{\sqrt{G_a}}{M_c} \sum_{i=2}^I \sum_{k=1}^K a_i^k \left[|\gamma_m^{(1,i)}(\omega_{ei}, \tau_i^k)| + j|\varphi_m^{(1,i)}(\omega_{ei}, \tau_i^k)| p(v) \right] \exp[-j(\phi_i + \theta_i^k)].$$

Finally, the AWGN term can be written as

$$(5.1.26) \quad x_n(v) = \frac{\sigma_{out} \eta(v)}{\sqrt{M_c}} = \sqrt{\frac{N_{out}}{2M_c}} \eta(v)$$

where \mathbf{h} is WGNs(0,1).

During the acquisition process the receiver can only tell where the start of the C code sequence is. This is going to become clearer in §5.1.7 where we will talk about the signal to interference plus noise ratio as a means of declaring whether the desired signal (i.e., the desired code $c^{(1)}(t)$) is present or absent. On one hand tracking the C code enables the receiver to track the desired signals at the appropriate channels. On the other hand, it enables the receiver to measure the travel time between the receiver and the appropriate transmitter, which is the time difference between the start of the C sequence generated from the transmitter and the start of the C code sequence generated from the receiver. To the extent that acquisition is achieved reliably the receiver can enter the next phase, which is the tracking phase and this is the topic discussed next.

5.1.5 Correlation with the Locally Generated P Code

There are two ways, at least in principle, to determine the data bit transition. The first approach exploits the autocorrelation properties of the N blocks to detect the data bit without utilizing any additional locally generated pseudo random sequence. The second approach improves the autocorrelation property of the N blocks by introducing an additional sequence, $p(t)$ (see Figure 5.6). This and the following section discuss the correlation with the P code and the (second) integration process respectively.

Once the start of the sequence $c^{(1)}(t)$ is determined then we perform the correlation with the $p(t)$ code. The signal, $y(v)$, that describes the correlation with the $p(t)$ code is given by [16]

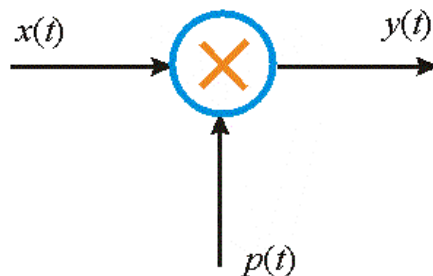


Figure 5.6 Block diagram of the correlation with the locally generated P code.

$$(5.1.27) \quad y(v) = y_d(v) + y_f(v) + y_m(v) + y_n(v)$$

where the desired, ISI, MAI and AGWN components of $y(v)$ are determined from [16]

$$(5.1.28) \quad y_j(v) = x_j(v)p(t), \quad j = \{d, f, m, n\}, \quad v = \{1, \dots, N\}, \quad \text{and } t = oT_p - \mathbf{x}$$

and o is an integer and \mathbf{x} is the unknown P chip delay.

In principle the correlation with the P code is similar to the correlation with the C code other than the differences in codes and their corresponding rates. Therefore, we can conclude here that when proper alignment is achieved then the desired component phase is constant and minimum and the remaining components have non-minimum random phase. When the integration is performed then the desired component is accumulated and the undesired terms are minimized as much as possible. The following section provides the analytical development of this discussion.

5.1.6 (Second) Integration after the P Code Correlation

This is required to determine the data bit transition. The output signal, $z(u)$, during the tracking phase is calculated from (see Figure 5.7) [16]

$$(5.1.29) \quad z(u) = z_d(u) + z_f(u) + z_m(u) + z_n(u)$$

where its components can be written as [16]

$$(5.1.30) \quad z_j(u) = \frac{1}{N} \sum_{v=0}^{N-1} y_j(v), \quad j = \{d, f, m, n\}.$$

We are interested only in the autocorrelation property of the sequence $p(t)$; therefore, it is desired that the sequence $p(t)$ be a maximum length sequence (its autocorrelation peak is $N = 2^n - 1 \ll M_c$, its out-of-phase auto-correlation peak is -1 and its average is 1 [21]).

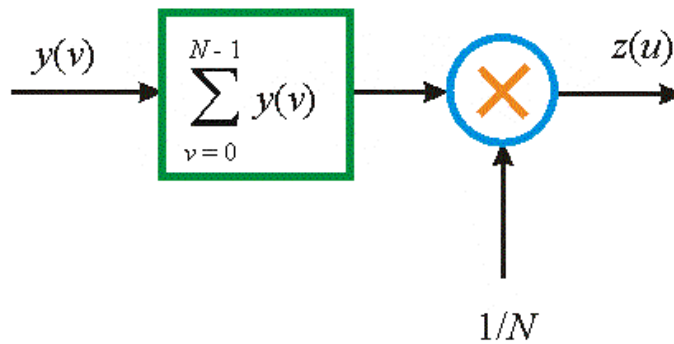


Figure 5.7 Integration with the P code block diagram.

Let $\rho_u(\omega_{e1}, \xi)$ denote the autocorrelation function of $p(t)$ sequence, which includes the effects of synchronization and assuming, that $t = (v + u)T_p - \xi$ then $\rho_u(\omega_{e1}, \xi)$ is given by [16]

$$(5.1.31) \quad \rho_u(\omega_{e1}, \xi) = \kappa_p(\omega_{e1}, \xi) \sum_{v=0}^{N-1} p_v p_{v-u}$$

where $\kappa_p(\omega_{e1}, \xi)$ is the coefficient which accounts for synchronization and is determined from [16]

$$(5.1.32) \quad \kappa_p(\omega_{e1}, \xi) \cong \Psi_P(f_{e1})(1 - R_p \xi).$$

Once the start of the C code is determined than the time can be known to within one-half of a chip. This implies that the unknown P chip delay can be also known to within one-half of a chip of the C code; i.e., $\mathbf{x} \in \text{un}[0, T_c/2]$.

First, utilizing the definition of the autocorrelation function, $\rho(\omega_{e1}, \xi)$, the desired term can be written as [16]

$$(5.1.33) \quad z_d(v) = \frac{a_1^1 \sqrt{G_a}}{M_c N} \left[\sum_{q=0}^{N-1} |\gamma_m^{(1,1)}(\omega_{e1}, \tau_1^1)| p_q + j |\phi_m^{(1,1)}(\omega_{e1}, \tau_1^1)| \rho_u(\omega_{e1}, \xi) \right] \exp[-j(\phi_1 + \theta_1^1)].$$

Utilizing the explanation provided in [16], the desired term can be computed from

$$(5.1.34) \quad z_d(v) = \frac{a_1^1 \sqrt{G_a}}{M_c N} \left[\pm |\gamma_m^{(1,1)}(\omega_{e1}, \tau_1^1)| + j |\phi_m^{(1,1)}(\omega_{e1}, \tau_1^1)| \rho_u(\omega_{e1}, \xi) \right] \exp[-j(\phi_1 + \theta_1^1)].$$

Second, exploiting the definition of the $\rho(\omega_{e1}, \xi)$ into the ISI term produces [16]

$$(5.1.35) \quad z_f(v) = \frac{\sqrt{G_a}}{M_c} \sum_{k=2}^K a_1^k \left[\pm |\gamma_m^{(1,1)}(\omega_{e1}, \tau_1^k)| + j |\phi_m^{(1,1)}(\omega_{e1}, \tau_1^k)| \rho_u(\omega_{e1}, \xi) \right] \exp[-j(\phi_1 + \theta_1^k)].$$

Third, similarly we can compute the MAI component as [16]

$$(5.1.36) \quad z_m(v) = \frac{\sqrt{G_a}}{M_c} \sum_{i=2}^I \sum_{k=1}^K a_i^k \left[\pm |\gamma_m^{(1,i)}(\omega_{ei}, \tau_i^k)| + j |\phi_m^{(1,i)}(\omega_{ei}, \tau_i^k)| \rho_u(\omega_{ei}, \xi) \right] \exp[-j(\phi_i + \theta_i^k)].$$

And finally the noise term is determined from [16]

$$(5.1.37) \quad z_n(u) = \frac{\sigma_{out}}{\sqrt{M_c N}} \mathbf{v}(u)$$

where \mathbf{n} is WGNs(0,1).

Up to now we have been concerned with the analysis of the signal characteristics, which undergoes several processing stages. This is the first important block in the endeavor to evaluate the receiver and the total system performance. The second important block is the useful criterion to assess the system performance; hence, the next two sections (see §5.1.7 and §5.1.8) provide a way of achieving such a goal.

5.1.7 Signal to Interference Plus Noise Ratio

Among several performance criteria, two are the most distinct, suitable, and familiar to spread-spectrum communication engineers: SINR and BEP (while the latter is dependent from SINR). First, SINR demonstrates whether the desired signal can be detected in the presence of noise, MAI, and ISI. Second, depending on the distribution of the interference and noise, BEP provides a measure to the quality of data detection (see §5.1.8), which differentiates one system from another.

The output signal conditional SINR conditioned on $\mathbf{a} \equiv \{a_1^1\} = a$ is defined as the ratio of the desired signal power over the sum of the output ISI, MAI, and AWGN signal power in accordance with the following expression [16]

$$(5.1.38) \quad \text{SINR} = \frac{\text{Desired Power}}{(\text{ISI} + \text{MAI} + \text{AWGN}) \text{ Power}}.$$

To aid our analysis we make for following notation simplifications

$$(5.1.39) \quad \omega_e \equiv \omega_1^e, \quad \tau \equiv \tau_1^1, \quad \text{and} \quad \delta\tau \equiv \delta\tau_1^1.$$

The desired output signal power conditioned on a is determined from:

$$(5.1.40) \quad P_d^z(a, \omega_e, \tau, \xi) = \frac{0.5G_a}{M_c^2 N^2} a^2 \left[\left| \gamma_m^{(1,1)}(\omega_e, \tau) \right|^2 + \left| \phi_m^{(1,1)}(\omega_e, \tau) \right|^2 \rho_u(\omega_e, \xi)^2 \right].$$

Note the explicit dependency of the desired output signal power conditioned on a on the C code unknown time delay τ (because of the misalignment of the code $c^{(1)}(t)$ generated from the receiver and the code $c^{(1)}(t - \tau)$ contained in the received signal), the frequency error, ω_{e1} , and the unknown block time delay, ξ , (because of the misalignment of the $p(t)$ code generated from the receiver with the $p(t - \xi)$ contained in the received blocks).

Note that the proper alignment of the $c^{(1)}(t)$ code is achieved when $m = 0$ and $u = 0$; hence, eq. (5.1.40) can be written as

$$(5.1.41) \quad P_d^z(a, \omega_e, \tau, \xi) = \frac{0.5G_a}{M_c^2 N^2} a^2 \left[\left| \gamma_0^{(1,1)}(\omega_e, \delta\tau) \right|^2 + \left| \phi_0^{(1,1)}(\omega_e, \delta\tau) \right|^2 \rho_0(\omega_e, \xi)^2 \right].$$

The power corresponding to the ISI term is given by

$$(5.1.42) \quad P_f^z(a, \omega_e, \tau, \xi) = 0.5G_a B g \sum_{k=2}^K \left[\left| \gamma_m^{(1,1)}(\omega_e, \tau_1^k) \right|^2 + \left| \phi_m^{(1,1)}(\omega_e, \tau_1^k) \right|^2 \rho_u(\omega_e, \xi)^2 \right]$$

where $g = E \left\{ a_i^{k^2} | \mathbf{a} \right\}$ and $B = 1/M_c^2 N^2$. The argument given for the desired signal term, which shows the dependency of the ISI terms on the C code unknown chip time delay τ_1^k , the frequency error ω_e , and on the block P code unknown chip time delay, ξ , can be applied here as well. Under the assumption that $\tau_1^k > T_c$ then the out-of-phase autocorrelation function, $\phi_m^{(1,1)}(\omega_e, \tau_1^k)$, and the crosscorrelation function, $\gamma_m^{(1,1)}(\omega_e, \tau_1^k)$, satisfy the following inequality [16]

$$(5.1.43) \quad \left| \phi_m^{(1,1)}(\omega_e, \tau_1^k) \right| \leq \phi_a^{(1,1)}(\omega_e, \delta\tau)$$

$$(5.1.44) \quad \left| \gamma_m^{(1,1)}(\omega_e, \tau_1^k) \right| \leq \gamma_c^{(1,1)}(\omega_e, \delta\tau)$$

where $\phi_a^{(1,1)}(\omega_e, \delta\tau)$ is the peak out-of-phase autocorrelation magnitude, $\gamma_c^{(1,1)}(\omega_e, \delta\tau)$ is the peak crosscorrelation magnitude, and $\delta\tau = \text{un}[0, T_c)$. Utilizing the above relationships into (5.1.42) produces

$$(5.1.45) \quad P_f^z(a, \omega_e, \tau, \xi) \leq 0.5G_a B g \tilde{K} \left\{ \left| \gamma_c^{(1,1)}(\omega_e, \delta\tau) \right|^2 + \left| \phi_a^{(1,1)}(\omega_e, \delta\tau) \right|^2 \rho_u(\omega_e, \xi)^2 \right\}$$

where $\tilde{K} = K - 1$.

Similarly, the power corresponding to the MAI term can be written as

$$(5.1.46) \quad P_m^z(a, \Lambda, \xi) = 0.5G_a B g \sum_{i=2}^I \sum_{k=1}^K \left\{ \left| \gamma_m^{(1,i)}(\omega_{ei}, \tau_i^k) \right|^2 + \left| \phi_m^{(1,i)}(\omega_{ei}, \tau_i^k) \right|^2 \rho_u(\omega_{ei}, \xi)^2 \right\}$$

where $\Lambda = \{\tau_2, \dots, \tau_I, \omega_{e1}, \dots, \omega_{eI}\}^{\mathcal{I}}$. Under the assumption that $\tau_i^k > T_c$ then the crosscorrelation function, $\phi_m^{(1,i)}(\omega_{ei}, \tau_i^k)$, and the crosscorrelation function, $\gamma_m^{(1,i)}(\omega_{ei}, \tau_i^k)$, satisfy the following inequality [16]

$$(5.1.47) \quad \left| \phi_m^{(1,i)}(\omega_{ei}, \tau_i^k) \right| \leq \phi_c^{(1,i)}(\omega_{ei}, \delta\tau_i)$$

$$(5.1.48) \quad \left| \gamma_m^{(1,i)}(\omega_{ei}, \tau_i^k) \right| \leq \gamma_c^{(1,i)}(\omega_{ei}, \delta\tau_i)$$

where $\varphi_c^{(1,i)}(\omega_{ei}, \delta\tau_i)$ is the peak crosscorrelation magnitude of $\varphi_m^{(1,i)}(\omega_{ei}, \tau_i^k)$, $\gamma_c^{(1,i)}(\omega_{ei}, \delta\tau_i)$ is the peak crosscorrelation magnitude of $\gamma_m^{(1,i)}(\omega_{ei}, \tau_i^k)$, and $\delta\tau_i = \text{un}[0, T_c)$.

If the misalignments of the code $c^{(1)}(t)$ generated from the receiver and the code $c^{(i)}(t - \tau_i)$ contained in the received signal, for $i = \{2, \dots, I\}$ can be expressed with the help of the vector $\Lambda = \{\tau_2, \dots, \tau_I, \omega_{e1}, \dots, \omega_{eI}\}^T$, then the total receiver power of the MAI terms will show this dependency.

Similarly, after some algebra and under the assumption that $\tau_i^k > T_c$ the power expression of the MAI terms is simplified to

$$(5.1.49) \quad P_m^z(a, \Lambda, \xi) \leq 0.5G_a BgK \sum_{i=2}^I \left[\gamma_c^{(1,i)}(\omega_{ei}, \delta\tau_i)^2 + \varphi_c^{(1,i)}(\omega_{ei}, \delta\tau_i)^2 \rho_0(\omega_{e1}, \xi)^2 \right].$$

The power corresponding to AWGN terms is computed from

$$(5.1.50) \quad P_n^z(a) = \frac{\sigma_{out}^2}{M_c N} = \frac{N_{out}}{2M_c N}.$$

Hence, it follows that the output signal SINR conditioned on a is written, according to [16], as

$$(5.1.51) \quad SINR(a, \tau_1, \Lambda, \xi) = \frac{P_d^z(a, \tau_1, \xi)}{P_f^z(a, \tau_1, \xi) + P_m^z(a, \Lambda, \xi) + P_n^z(a)} = \frac{N_{SINR}}{D_{SINR}}.$$

Substituting (5.1.50), (5.1.49), (5.1.45) and (5.1.41) into (5.1.51) produces

$$(5.1.52) \quad N_{SINR} = 0.5a^2 B E_c^{-1} \left[\gamma_0^{(1,1)}(\omega_e, \delta\tau)^2 + \varphi_0^{(1,1)}(\omega_e, \delta\tau)^2 \rho_0(\omega_{e1}, \xi)^2 \right]$$

$$(5.1.53) \quad D_{SINR} \leq \left\{ 0.5Bg\tilde{K}E_c^{-1} \left[\gamma_c^{(1,1)}(\omega_e, \delta\tau)^2 + \varphi_a^{(1,1)}(\omega_e, \delta\tau)^2 \rho_0(\omega_e, \xi)^2 \right] + 0.5BgKE_c^{-1} \sum_{i=2}^I \left[\gamma_c^{(1,i)}(\omega_{ei}, \tau_i)^2 + \varphi_c^{(1,i)}(\omega_{ei}, \tau_i)^2 \rho_0(\omega_{ei}, \xi)^2 \right] + 0.5F_n (E_b/N_{in})^{-1} \right\}$$

where $E_b = M_c N E_c$ is the total energy per bit. Note the disappearance of the amplifier gain, G_a , from the computation of the SINR.

Assuming that the power loss factor, $Q_i(t)$, is not changing during the data bit transition and that the C code is a Gold sequence [21] then the SINR expression, (5.1.52) and (5.1.53), can be further simplified as

$$(5.1.54) \quad N_{SINR} \geq a^2 \frac{p_1(t) \kappa_c(\omega_e, \delta\tau)^2}{|\omega_e|^2} [B + \kappa_p(\omega_e, \xi)^2]$$

$$(5.1.55) \quad D_{SINR} \leq \frac{4p_1(t)g\tilde{K}\kappa_c(\omega_e, \delta\tau)^2 [\kappa_p(\omega_e, \xi)^2 + N^{-2}]}{M_c |\omega_e|^2} \\ + \frac{4gK [\kappa_p(\omega_e, \xi)^2 + N^{-2}]}{M_c} \sum_{i=2}^I \frac{p_i(t) \kappa_c(\omega_{ei}, \delta\tau_i)^2}{|\omega_{ei}|^2} + \frac{F_n}{2} (E_b/N_{in})^{-1}.$$

Assuming that the C code comes from the small Kasami sequences [21] then we can write the SINR expression, (5.1.52) and (5.1.53), as follows

$$(5.1.56) \quad N_{SINR} \geq \frac{a^2 p_1(t) \kappa_c(\omega_e, \delta\tau)^2}{|\omega_e|^2} [B + \kappa_p(\omega_e, \xi)^2]$$

$$(5.1.57) \quad D_{SINR} \leq \frac{p_1(t)g\tilde{K}\kappa_c(\omega_e, \delta\tau)^2 [\kappa_p(\omega_e, \xi)^2 + N^{-2}]^{-1}}{M_c |\omega_e|^2} \\ + \frac{gK [\kappa_p(\omega_e, \xi)^2 + N^{-2}]}{M_c} \sum_{i=2}^I \frac{p_i(t) \kappa_c(\omega_{ei}, \delta\tau_i)^2}{|\omega_{ei}|^2} + \frac{F_n}{2} (E_b/N_{in})^{-1}.$$

The lower bound expressions on the SINR are particularly useful, because they provide an upper bound expression on BEP (or rate see §5.1.8) and on the receiver's detector degradation ratio, which is the inverse of the SINR and which is, to some extent, a direct measure of the receiver's code and phase error (see §5.3.1 and §5.3.2).

5.1.8 Bit Error Probability

Assuming that the interference is Gaussian distributed we can obtain the expression for BEP conditioned on a and to the extent that this is a good approximation, BEP reads [16]

$$(5.1.58) \quad BEP(a, \tau, \Lambda, \xi) = Q\left(\sqrt{SINR(a, \tau, \Lambda, \xi)}\right)$$

where $Q(x) = (2\pi)^{-1/2} \int_x^\infty e^{-t^2/2} dt$.

The unconditional $BEP(\tau, \Lambda, \xi)$ can be produced by integrating the conditional $BEP(a, \tau, \Lambda, \xi)$ with respect to the density function of a , $p(a) = a \exp(-a^2/2)U(a)$ (see Appendix A of [16]), which reads

$$(5.1.59) \quad BEP(\tau, \Lambda, \xi) \cong 0.5 \left[1 - \left(\frac{\sqrt{\mu}}{\sqrt{\mu} + 1} \right)^{\exp[-\alpha(\sqrt{\mu})]} \right]$$

where $\mu \equiv \frac{1}{2} E\{SINR(a, \tau, \Lambda, \xi)\}$ and the expectation is performed with respect to a .

Knowing that the function BEP given by (5.1.59) is monotonically decreasing with respect to μ then the largest BEP corresponds to the smallest μ ; hence, the upper BEP bound can be obtained from

$$(5.1.60) \quad BEP_{\max}(\tau, \Lambda, \xi) \cong 0.5 \left[1 - \left(\frac{\sqrt{\mu_{\min}}}{\sqrt{\mu_{\min}} + 1} \right)^{\exp[-\alpha(\sqrt{\mu_{\min}})]} \right]$$

where $\mu_{\min} \equiv \frac{1}{2} E\{SINR_{\min}(a, \tau, \Lambda, \xi)\}$ and the expectation is performed with respect to a .

Equation (5.1.60) is particularly useful for hardware implementation because it provides a closed form expression that can be implemented employing any digital signal processor or the state of the art microprocessor design, which utilizes floating-point arithmetic. Nevertheless, for our theoretical performance evaluation we can employ the accurate expression from MATLAB[®].

Thus, we have concluded the analytical evaluation of the receiver performance based only on tracking performance of the C and P code. We have not considered however, the performance based on tracking the frequency and the carrier phase which can be exploited using any of the Delay Lock Loops or Phase Lock Loops, leaving this of part of future studies or publications. We have; nevertheless, considered the performance based on tracking the C and the B code, which is the topic of the following section.

5.2 Communication Performance Analyses (C and B Codes)

So far we have analyzed the communication performance evaluation; i.e., the SINR and BEP based on the tracking performance of the C and P code signal structure and with partial exploitation of the B code signal structure. While, there are several combinations of the C and B code, in this section we explore the impact of the B code signal structure on the communication performance evaluation for a particular combination of the B and

C codes. For this particular combination the B code is assumed to be much longer than the c code. Hence, the B code is very important because it protects the receiver from interference and jamming, although there are limitations to its protection and when we intentionally desire to deny the use of the C code to other users. The B code is a much longer code than the C and P codes are together and this insures a much higher ratio of the autocorrelation peak for the B code over the out of phase autocorrelation and crosscorrelation peak. The correlation with the B code is exploited in §5.2.1. The integration after the B code correlation is presented in §5.2.2. The SINR is analyzed in §5.2.3 and the BEP is exploited in §5.2.4.

5.2.1 Correlation with the Locally Generated B Code

When the correlation with the B code is performed we have resolved not only the start the C code sequence but also the start of the B code sequence to better than a half of the chipping period (or $0.5T_c$). The signal, $a(t)$, that describes the correlation with the $b(t)$ code is given by

$$(5.2.1) \quad a(t) = a_d(t) + a_f(t) + a_m(t) + a_n(t)$$

where the desired, ISI, MAI and AGWN components of $a(t)$ are determined from

$$(5.2.2) \quad a_j(t) = w_j(t)b(t), \quad j = \{d, f, m, n\} \text{ and } v = \{1, \dots, N\}.$$

As mentioned earlier, the correlation with the B code is the first step towards acquiring the B code, which is followed by the integration stage. Due to the perfect synchronization between the C and the B code, the receiver is potentially able to resolve for the start of the B code (see §5.2.2), if the start of the C sequence is known at this time.

5.2.2 (Third) Integration after the Correlation with the Locally Generated B Code

After the correlation with the B sequence is performed, next the receiver's designated channel performs the third integration or the integration after the B code correlation. Nevertheless, before achieving this goal, one important design parameter to be determined is the length of the B code sequence, M_b . Having determined the optimum length of the B code sequence, M_b , the receiver performs the third integration.

The signal, $d(n)$, that describes this mode is given by

$$(5.2.3) \quad d(n) = d_d(n) + d_f(n) + d_m(n) + d_n(n)$$

where every component of $d(n)$, for $j = \{d, f, m, n\}$ and $n = \{1, \dots, M_b\}$, is obtained from

$$(5.2.4) \quad d_j(n) = \frac{1}{T_d} \int_0^{T_d} a_j(t) dt$$

where T_d is the bit transition or the data bit period.

Next, the crosscorrelation function, $\vartheta_m^{(1,i)}(\omega_{ei}, \tau_i^k)$, obtained by crosscorrelating the sequence $b^{(1)}(t)$ with the waveform $s_{ri}^s(t - \tau_i^k)$ and the crosscorrelation function, $\delta_m^{(1,i)}(\omega_{ei}, \tau_i^k)$, derived by crosscorrelating the sequence $b^{(1)}(t)$ with the waveform $s_{ri}^c(t - \tau_i^k)$, are required to compute the components of $d(n)$. The crosscorrelation functions, $\vartheta_m^{(1,i)}(\omega_{ei}, \tau_i^k)$ and $\delta_m^{(1,i)}(\omega_{ei}, \tau_i^k)$, are defined as

$$(5.2.5) \quad \vartheta_m^{(1,i)}(\omega_{ei}, \tau_i^k) = \int_0^{T_d} s_{ri}^s(t - \tau_i^k) b^{(1)}(t) \exp(-j\chi_i^k) dt$$

$$(5.2.6) \quad \delta_m^{(1,i)}(\omega_{ei}, \tau_i^k) = \int_0^{T_d} s_{ri}^c(t - \tau_i^k) b^{(1)}(t) \exp(-j\chi_i^k) dt.$$

After some mathematical steps, assuming that $f_{ei}/R_c \cong 0$ then the crosscorrelation functions $\vartheta_m^{(1,i)}(\omega_{ei}, \tau_i^k)$ and $\delta_m^{(1,i)}(\omega_{ei}, \tau_i^k)$ can be written as

$$(5.2.7) \quad \vartheta_{m,q}^{(1,i)}(\omega_{ei}, \tau_i^k) = \frac{\sqrt{2E_{ri}}}{\omega_{ei}} j\kappa_c(\omega_{ei}, \delta\tau_i^k) \exp[-j(\phi_i + \theta_i^k)] \sum_{l=0}^{M_c-1} b_{l+q}^{(1)} c_{l-m}^{(i)}$$

$$(5.2.8) \quad \delta_m^{(1,i)}(\omega_{ei}, \tau_i^k) = \frac{\sqrt{2E_{ri}}}{\omega_{ei}} \kappa_c(\omega_{ei}, \delta\tau_i^k) \exp[-j(\phi_i + \theta_i^k)] \sum_{l=0}^{NM_c-1} b_l^{(1)} b_{l-m}^{(i)}$$

where $\kappa_c(\omega_{ei}, \delta\tau_i^k)$ is determined from (5.1.22).

In light of equations (5.2.7) and (5.2.8) the desired signal term is computed from

$$(5.2.9) \quad d_d(n) = \frac{a_1^1 \sqrt{G_a}}{NM_c} \left[|\delta_m^{(1,1)}(\omega_{e1}, \tau_1^1)| + j \sum_{q=0}^N |\vartheta_{m,q}^{(1,1)}(\omega_{e1}, \tau_1^1)| p(q) \right] \exp[-j(\phi_1 + \theta_1^1)].$$

After some simplifications the desired signal component can be written as

$$(5.2.10) \quad d_d(n) = \frac{a_1^1 \sqrt{G_a}}{NM_c} \left[|\delta_m^{(1,1)}(\omega_{e1}, \tau_1^1)| \pm j |\vartheta_m^{(1,1)}(\omega_{e1}, \tau_1^1)| \right] \exp[-j(\phi_1 + \theta_1^1)]$$

where $|\vartheta_m^{(1,1)}(\omega_{e1}, \tau_1^1)|$ is the maximum value of $|\vartheta_{m,q}^{(1,1)}(\omega_{e1}, \tau_1^1)|$.

Similarly, the ISI component can be approximated by

$$(5.2.11) \quad d_f(n) = \frac{\sqrt{G_a}}{NM_c} \sum_{k=2}^K a_1^k \left[|\delta_m^{(1,1)}(\omega_{e1}, \tau_1^k)| \pm j |\vartheta_m^{(1,1)}(\omega_{e1}, \tau_1^k)| \right] \exp[-j(\phi_1 + \theta_1^k)]$$

and the MAI term is given by

$$(5.2.12) \quad d_m(n) = \frac{\sqrt{G_a}}{NM_c} \sum_{i=2}^L \sum_{k=1}^K a_i^k \left[|\delta_m^{(1,i)}(\omega_{ei}, \tau_i^k)| \pm j |\vartheta_m^{(1,i)}(\omega_{ei}, \tau_i^k)| \right] \exp[-j(\phi_i + \theta_i^k)].$$

Finally the AWGN term can be written as

$$(5.2.13) \quad d_n(n) = \frac{\sigma_{out} \mathbf{1}(n)}{\sqrt{NM_c}} = \sqrt{\frac{N_{out}}{2NM_c}} \mathbf{1}(n)$$

where $\mathbf{1}$ is WGNs(0,1).

So far the focus of our analysis has been the study of the signal characteristics, which undergoes several processing stages while tracking both the C and the B code. This is the first important step in the endeavor to evaluate the receiver and system performance. The second important step, just like in §5.1.7 and §5.1.8, is the useful criterion to assess the system performance; hence, the next two sections provide the analytical development of the SINR (see §5.2.3) and BEP (see §5.2.4), for the reasons mentioned earlier.

5.2.3 Signal To Interference Plus Noise Ratio

Based on the development of §5.1.7 we determine the SINR for the receiver in accordance to the properties of the B code.

The output signal conditional SINR conditioned on $\mathbf{a} \equiv \{a_i^1\} = a$ is defined similarly as in equation (5.1.38); hence, we can compute the output desired, ISI, MAI, and AWGN signal power. First, the desired output signal power conditioned on a is determined from:

$$(5.2.14) \quad P_d(a, \omega_e, \tau, \xi) = 0.5 G_a B a^2 \left[|\delta_m^{(1,1)}(\omega_e, \tau)|^2 + |\vartheta_m^{(1,1)}(\omega_e, \tau)|^2 \right].$$

Second, the power corresponding to the ISI term is given by

$$(5.2.15) \quad P_f(a, \omega_{e1}, \tau, \xi) = 0.5 G_a B g \sum_{k=2}^K \left[|\delta_m^{(1,1)}(\omega_e, \tau_1^k)|^2 + |\vartheta_m^{(1,1)}(\omega_e, \tau_1^k)|^2 \right]$$

where $g = E\{a_i^{k2} | \mathbf{a}\}$. Under the assumption that $\tau_1^k > T_c$ then the out-of-phase autocorrelation function, $\delta_m^{(1,1)}(\omega_{e1}, \tau_1^k)$, and the crosscorrelation function, $\vartheta_m^{(1,1)}(\omega_{e1}, \tau_1^k)$, satisfy the following inequality

$$(5.2.16) \quad |\delta_m^{(1,1)}(\omega_{e1}, \tau_1^k)| \leq \delta_a^{(1,1)}(\omega_e, \delta\tau)$$

$$(5.2.17) \quad |\vartheta_m^{(1,1)}(\omega_{e1}, \tau_1^k)| \leq \vartheta_c^{(1,1)}(\omega_e, \delta\tau)$$

where $\delta_a^{(1,1)}(\omega_e, \delta\tau)$ is the peak of the out-of-phase autocorrelation magnitude, $\vartheta_c^{(1,1)}(\omega_e, \delta\tau)$ is the peak of the crosscorrelation magnitude, and $\delta\tau = \text{un}[0, T_c)$. Utilizing the above relationships into (5.2.15) produces

$$(5.2.18) \quad P_f(a, \omega_e, \tau, \xi) \leq 0.5G_a g \tilde{K} B \left\{ \delta_a^{(1,1)}(\omega_e, \delta\tau)^2 + \vartheta_c^{(1,1)}(\omega_e, \delta\tau)^2 \right\}$$

where $\tilde{K} = K - 1$.

Similarly, the power corresponding to the MAI term can be written as

$$(5.2.19) \quad P_m(a, \Lambda, \xi) = 0.5G_a g B \sum_{i=2}^I \sum_{k=1}^K \left\{ \delta_m^{(1,i)}(\omega_{ei}, \tau_i^k)^2 + |\vartheta_m^{(1,i)}(\omega_{ei}, \tau_i^k)|^2 \right\}$$

where $\Lambda = \{\tau_2, \dots, \tau_I, \omega_{e1}, \dots, \omega_{eI}\}^T$. Under the assumption that $\tau_i^k > T_c$ then the crosscorrelation function, $\delta_m^{(1,i)}(\omega_{ei}, \tau_i^k)$, and the crosscorrelation function, $\vartheta_m^{(1,i)}(\omega_{ei}, \tau_i^k)$, satisfy the following inequality

$$(5.2.20) \quad |\delta_m^{(1,i)}(\omega_{ei}, \tau_i^k)| \leq \delta_c^{(1,i)}(\omega_{ei}, \delta\tau_i)$$

$$(5.2.21) \quad |\vartheta_m^{(1,i)}(\omega_{ei}, \tau_i^k)| \leq \vartheta_c^{(1,i)}(\omega_{ei}, \delta\tau_i)$$

where $\delta_a^{(1,i)}(\omega_{ei}, \delta\tau_i)$ is the peak of the crosscorrelation magnitude of $\delta_m^{(1,i)}(\omega_{ei}, \tau_i^k)$, $\vartheta_c^{(1,i)}(\omega_{ei}, \delta\tau_i)$ is the peak of the crosscorrelation magnitude of $\vartheta_m^{(1,i)}(\omega_{ei}, \tau_i^k)$, and $\delta\tau_i = \text{un}[0, T_c)$.

If the misalignments of the code $b^{(1)}(k)$ generated from the receiver and the code $b^{(i)}(t - t_i)$ contained in the received signal, for $i = \{2, \dots, I\}$ can be expressed with the help of the vector $\Lambda = \{\tau_2, \dots, \tau_I, \omega_{e1}, \dots, \omega_{eI}\}^T$, then the total receiver power of the MAI term will show this dependency.

Similarly, after some algebra and under the assumption that $\tau_i^k > T_c$ the power expression of the MAI term is simplified to

$$(5.2.22) \quad P_m(a, \Lambda, \xi) \leq 0.5G_a gKB \sum_{i=2}^I \left[\delta_c^{(1,i)}(\omega_{ei}, \delta\tau_i)^2 + \vartheta_c^{(1,i)}(\omega_{ei}, \delta\tau_i)^2 \right].$$

Fourth, the power corresponding to the AWGN term is computed from

$$(5.2.23) \quad P_n(a) = \frac{\sigma_{out}^2}{M_c N} = \frac{N_{out}}{2M_c N}.$$

Hence, it follows that the output signal SINR conditioned on a is determined from

$$(5.2.24) \quad SINR(a, \tau, \Lambda, \xi) = \frac{P_d(a, \tau, \xi)}{P_f(a, \tau, \xi) + P_m(a, \Lambda, \xi) + P_n(a)} = \frac{N_{SINR}}{D_{SINR}}.$$

Substituting (5.2.15), (5.2.18), (5.2.22), and (5.2.23) into (5.2.24) produces

$$(5.2.25) \quad N_{SINR} = 0.5a^2 B E_c^{-1} \left[\delta_0^{(1,1)}(\omega_e, \delta\tau)^2 + \vartheta_c^{(1,1)}(\omega_e, \delta\tau)^2 \right]$$

$$(5.2.26) \quad D_{SINR} \leq \left\{ 0.5g\tilde{K}B E_c^{-1} \left[\delta_c^{(1,1)}(\omega_e, \delta\tau)^2 + \vartheta_c^{(1,1)}(\omega_e, \delta\tau)^2 \right] + 0.5gKB E_c^{-1} \sum_{i=2}^I \left[\delta_c^{(1,i)}(\omega_{ei}, \tau_i)^2 + \vartheta_c^{(1,i)}(\omega_{ei}, \tau_i)^2 \right] + 0.5F_n (E_b/N_{in})^{-1} \right\}$$

where $E_b = M_c N E_c$ is the total bit energy.

Given the power loss factor, $p_i(t)$, and assuming that the B code is a Gold sequence [21] then the SINR equations, (5.2.25) and (5.2.26), can be further simplified as

$$(5.2.27) \quad N_{SINR} \geq a^2 p_1(t) \kappa_c(\omega_e, \delta\tau)^2 |\omega_e|^{-2} [1 + B]$$

$$(5.2.28) \quad D_{SINR} \leq 4p_1(t) g\tilde{K} \kappa_c(\omega_e, \delta\tau)^2 M_c^{-1} |\omega_e|^{-2} [1 + N^{-1}] + 4gKM_c^{-1} [1 + N^{-1}] \sum_{i=2}^I p_i(t) \left[\kappa_c(\omega_{ei}, \delta\tau_i)^2 |\omega_{ei}|^{-2} \right] + 0.5F_n (E_b/N_{in})^{-1}.$$

Assuming that the B code comes from the small set of Kasami sequences [21] then we can write the SINR equations (5.2.25) and (5.2.26), as follows

$$(5.2.29) \quad N_{SINR} \geq a^2 p_1(t) \kappa_c(\omega_e, \tau)^2 |\omega_e|^{-2} [1 + B]$$

$$(5.2.30) \quad D_{SINR} \leq p_1(t) g\tilde{K} \kappa_c(\omega_e, \tau)^2 M_c^{-1} |\omega_e|^{-2} [1 + N^{-1}] + gKM_c^{-1} [1 + N^{-1}] \sum_{i=2}^I p_i(t) \left[\kappa_c(\omega_{ei}, \tau_i)^2 |\omega_{ei}|^{-2} \right] + 0.5F_n (E_b/N_{in})^{-1}.$$

The lower bound expressions on the SINR are particularly useful, because they provide an upper bound expression on the BEP (or BER see §5.2.4) and on the receiver's detector degradation ratio, which is the inverse of the SINR and which is, to some extent, a direct measure of the receiver's code and phase error (see §5.3.1 and §5.3.2).

5.2.4 Bit Error Probability

The development, presented in §5.1.8, can be utilized here as well. Rather than repeat that development here, the reader is referred to that section.

5.3 Navigation Performance Analyses

Thus far we have been concerned with the communication performance analysis, which provides the means of assessing the SINR and BEP. Another important aspect of our analysis is the navigation performance analyses. To evaluate the navigation performance it is necessary to evaluate the receiver's code error (see §5.3.1) and to evaluate the receiver's phase error (see §5.3.2), which directly influences the receiver's position and velocity error.

5.3.1 Receiver's Code Error

An accurate estimate of the receiver's code (or pseudorange) error can only be obtained from analyzing the delay lock loop suitable for the system under investigation. For a discussion on delay locked loops the reader is referred to Chapter 2 (see §2.2.4.2.3), and [22]-[26]. For the purposes of our investigation we only look at a simplified expression of the receiver's code error, which is sufficient to provide a preliminary estimate and thus serve as a baseline for the future design of a delay lock loop.

For a discussion on the delay locked loops and phase lock loops the reader is referred to Chapter 2 (see §2.2.4.2.3), and [22], [25]-[26].

According to Spilker [22], a simplified expression for the receiver's code error can be obtained as follows

$$(5.3.1) \quad \mathbf{s}_c = \frac{cT_c}{\sqrt{SINR}} \text{ (m)}.$$

For analysis purposes we are interested in computing an upper bound expression for the receiver's code error. Since σ_c is a monotonically decreasing with respect to $SINR$

then $SINR_{\min}$ produces $\sigma_{c_{\max}}$; therefore, in our numerical assessment results we compute $\sigma_{c_{\max}}$ instead of σ_c .

5.3.2 Receiver's Phase Error

An accurate estimate of the receiver's phase error can only be obtained from analyzing frequency lock loops and phase lock loops suitable for the system under investigation. For a discussion on frequency lock loops and phase lock loops the reader is referred to Chapter 2 (see §2.2.4.2.4 and §2.2.4.2.5) [22]-[26]. For the purposes of our investigation we only look at a simplified expression on the receiver's phase error, which is sufficient to provide a preliminary estimate and thus serve as a baseline for the future design of frequency lock loops and phase lock loops.

For a discussion on the delay locked loops and phase lock loops the reader is referred to Chapter 2 (see §2.2.4.2.5) [22], [25]-[26].

Similarly, according to Spilker [22], a simplified expression for the receiver's phase error can be obtained as follows

$$(5.3.2) \quad \sigma_{\phi} = \frac{c}{2\pi f_i \sqrt{SINR}} \text{ (m)}.$$

For analysis purposes we are interested in computing an upper bound expression for the receiver's phase error. Since σ_{ϕ} is a monotonically decreasing with respect to $SINR$ then $SINR_{\min}$ produces $\sigma_{\phi_{\max}}$; therefore, in our numerical assessment results we compute $\sigma_{\phi_{\max}}$ instead of σ_{ϕ} .

5.4 Quantitative Assessment

While quantitative assessment is partially discussed in some of our references [16]-[19], we perform here a complete assessment of the impact of the system design parameters; such as the signal to noise ratio, E_b/N_{in} , receiver's noise figure, F_n , number of transmitters, I , number of paths, K , synchronization parameter, $\delta\tau$, and frequency error, f_e , on the upper bound of the BEP and receiver's code and phase error. This section includes the selection of parameters in §5.4.1 and the quantitative requirements on the theoretical performance in §5.4.2.

5.4.1 Selection of Parameters

The system geometry is shown in Figure 5.8. As shown in the figure there are 10 transmitters and one receiver. More discussion about this geometry is provided later in this section.

The selection of the parameters is based on the initial work performed in [16]-[19] and it is applied to every section of the system.

The transmitter parameters are selected from:

- The number of transmitters is $I = 10$.
- The frequency of the desired signal (coming from the 1st transmitter) is 3.069 GHz.
- The chipping rate $R_c = 1.023\text{e}8$ MBPS, the C code repetition rate or the P code chipping rate $R_r \equiv R_p = 1$ MBPS.
- The frequency of the adjacent signal (signal coming from other transmitters) is $f_i = f_1 + 0.5(i-1)R_c$, $\forall i \in \{2, \dots, I\}$, [16]-[19].
- The C code length $M_c = 1023$, the P code length $N = 31$ and the B code length $M_b = 1023 \times 1025$.
- The data rate for this configuration is $R_p = 1/31$ BBPS $\cong 3.2$ KPBS.

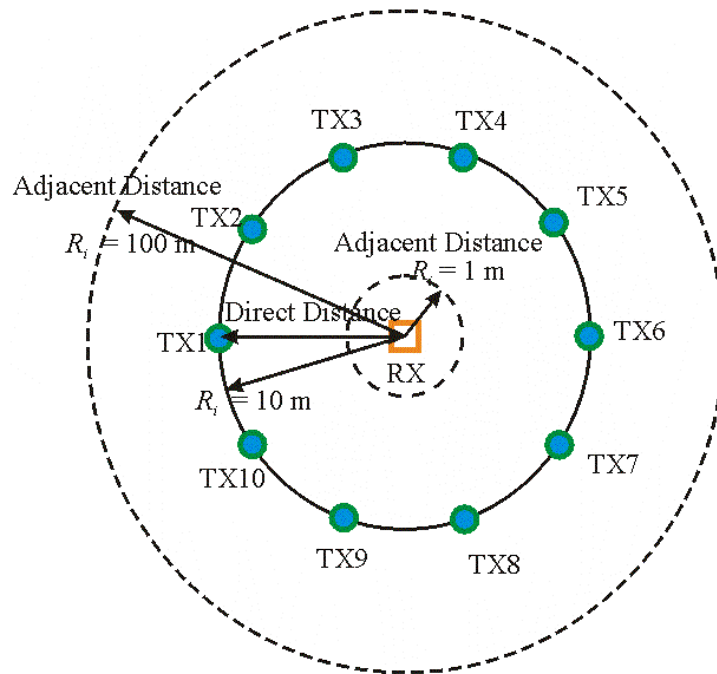


Figure 5.8 Transmitter receiver geometry of both a CDMA and a CDMA/FDMA indoor geolocation systems.

- The transmitting antenna gain is $G_t = 10$ dB.

The channel parameters are selected as follows:

- The reference path loss is $Q_0 = -42.275$ dB. This reference path loss corresponds to $R = 1$ m and $L_1 = 1575.42$ MHz.
- The slope for the path loss function vs. transmitter receiver distance is $n = 3.5$.
- The slope of the path loss function vs. operating frequency is $m = 2.01$.
- The standard deviation of the normal distributed noise, which represents unaccounted factors of the path loss model, is 0.5.
- The number of paths including the line of sight path is 10.
- The average attenuation $a = 0.5$ and $g = 0.25$.
- The roll-off factor for the raised cosine filter is $\delta = 0.5$.

The receiver parameters are selected as follows:

- Doppler shift between the receiver and the i th transmitter is $i \cdot 0.1$ m/s.
- The noise figure, $F_n = 10$, and the calibration temperature is $T_0 = 290$ K.
- The IF filter bandwidth, $B_n = 30$ MHz.
- The synchronization parameter $\delta\tau$ for the C code is $\text{un}[0, T_c)$ nsec. The mean of $\delta\tau$ is given by $\bar{\tau}_c = 0.5T_c$. With the help of $\bar{\tau}_c$ we have selected two distinct values for the synchronization parameter $\delta\tau = \{0, \bar{\tau}_c\}$ which correspond to perfect and average synchronization respectively.
- The synchronization parameter ξ corresponding to the P code misalignment is the same as the synchronization parameter $\delta\tau$, due to the perfect synchronization of the P code with the C code.
- The frequency error is given by $f_e = 0.05$ Hz.
- The receiving antenna gain is $G_r = 10$ dB.

5.4.2 Quantitative Requirements on Theoretical Performance

Quantitative requirements on theoretical performance are given in terms of the quantitative requirements on the communication performance (see §5.4.2.1) and quantitative requirements on navigation performance (see §5.4.2.2).

5.4.2.1 Quantitative Requirements on Communication Performance

The BEP provides the means of assessing the communication performance of a DSSS/CDMA and DSSS/CDMA/FDMA indoor geolocation system. The BEP is given as a function of six important design parameters such as ideal signal to noise ratio, E_b/N_0 (dB), relative adjacent distance, R_i (m), $\forall i \in \{2, \dots, I\}$, number of transmitters, I , number of paths, K , synchronization parameter, $\delta\tau$ (nsec), and frequency error, f_e , (Hz). Figure 5.9 illustrates the synchronization coefficient, κ (see equation (5.1.22)), as a function of the synchronization parameter, $\delta\tau$. As indicated in the figure, perfect synchronization corresponds to $\kappa = 1$ and average synchronization corresponds to $\kappa = 0.5$.

Figure 5.10 depicts the BEP as a function of E_b/N_0 (dB) using (a) Gold and (b) Kasami sequences for a DSSS/CDMA only and DSSS/CDMA/FDMA indoor geolocation system for average and perfect synchronization.

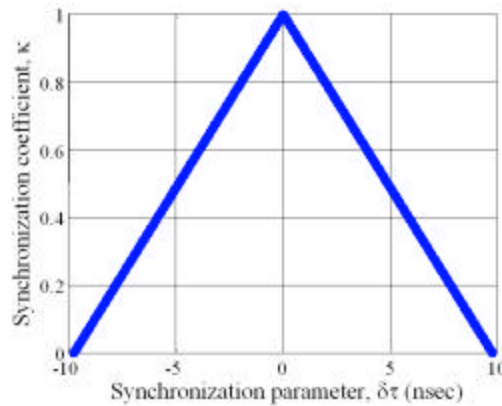


Figure 5.9 The synchronization coefficient vs. synchronization parameter, $\delta\tau$ (nsec).

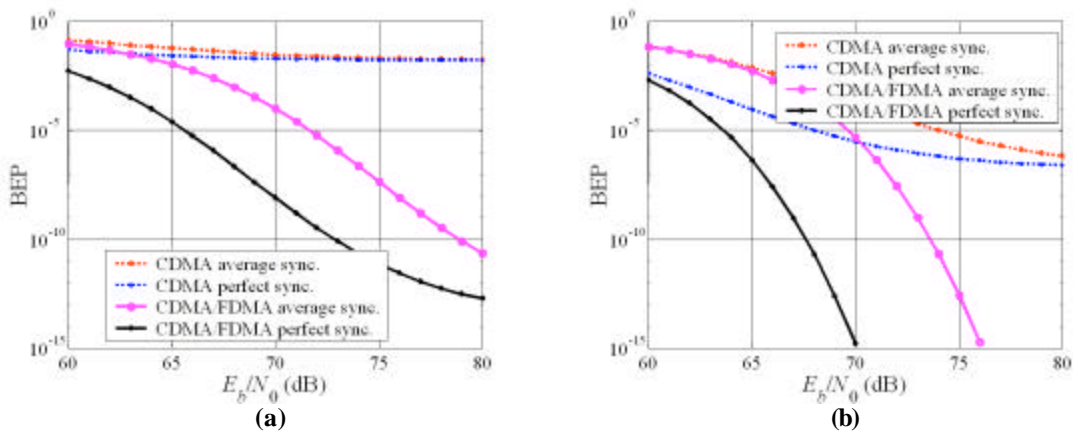


Figure 5.10 BEP vs. ideal SNR, E_b/N_0 (dB), for (a) Gold and (b) Kasami sequences.

We note that for a DSSS/CDMA indoor geolocation system with Gold/Kasami sequences as E_b/N_0 increases from 60 to 80 dB the BEP for average synchronization decreases from 0.1/0.1 to 0.02/1e-6 the BEP for perfect synchronization decreases from 0.09/0.1 to 0.02/3e-7. Clearly, a DSSS/CDMA indoor geolocation with Kasami sequences can achieve a BEP almost 10 times as small as the BEP of the same system with Gold sequences.

For a DSSS/CDMA/FDMA indoor geolocation system with Gold/Kasami sequences as E_b/N_0 increases from 60 to 80 dB the BEP for average synchronization decreases from 0.1/0.1 to 2e-11/0 and the BEP for perfect synchronization decreases from 8e-3/2e-3 to 2e-13/0. At $E_b/N_0 = 70$ dB the DSSS/CDMA/FDMA system with Kasami sequences can achieve an order of magnitude smaller BEP than the same system with Gold sequences.

Figure 5.11 depicts the BEP as a function of relative adjacent distance, R_i (m), $\forall i \in \{2, \dots, I\}$, using (a) Gold and (b) Kasami sequences for a DSSS/CDMA only and DSSS/CDMA/FDMA indoor geolocation system for average and perfect synchronization. For this experiment, in addition to the parameters shown above, E_b/N_0 is equal to 70 (dB).

We note that for a DSSS/CDMA indoor geolocation system with Gold/Kasami sequences as R_i increases from 1 to 100 m the BEP for average synchronization decreases from 0.5/0.5 to 1e-4/1e-5 and the BEP for perfect synchronization decreases from 0.5/0.5 to 1e-8/1e-13. Clearly, a DSSS/CDMA indoor geolocation with Kasami or Gold sequences **cannot** overcome the *near-far* effect.

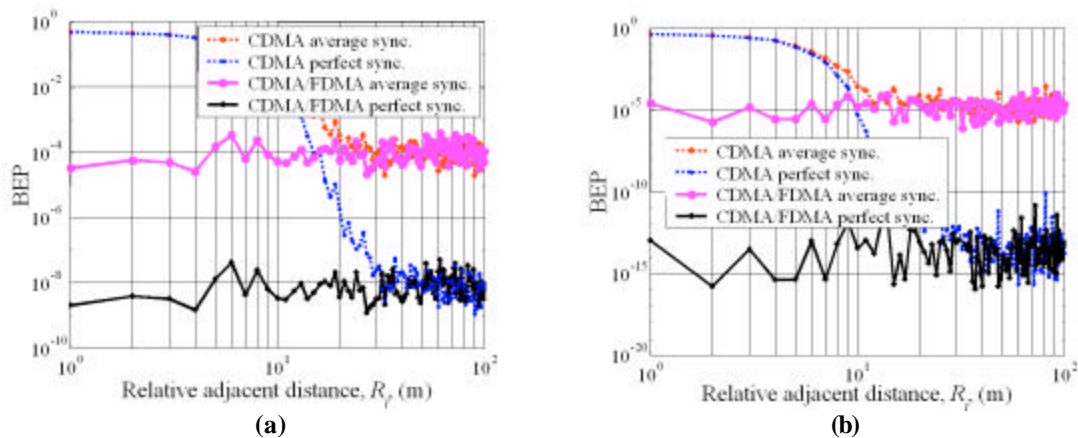


Figure 5.11 BEP vs. relative adjacent distance, R_i (m), for (a) Gold and (b) Kasami sequences.

We note that for a DSSS/CDMA/FDMA indoor geolocation system with Gold/Kasami sequences as R_i increases from 1 to 100 m the BEP for average synchronization remains almost unchanged at $1e-4/1e-5$ and the BEP for perfect synchronization remains almost unchanged $1e-8/1e-13$. Clearly, a DSSS/CDMA/FDMA indoor geolocation with Kasami or Gold sequences **can** overcome the *near-far* effect.

Figure 5.12 depicts the BEP as a function of the number of transmitters, I , using (a) Gold and (b) Kasami sequences for a DSSS/CDMA only and a DSSS/CDMA/FDMA indoor geolocation system for average and perfect synchronization. For this experiment, in addition to the parameters shown above, the E_b/N_0 is equal to 70 (dB). Also the relative distance between the 1st transmitter and receiver is 10 m and the relative distance between each adjacent transmitter and the receiver is 10 m.

We note that for a DSSS/CDMA indoor geolocation system with Gold/Kasami sequences as I increases from 2 to 32 the BEP for average synchronization increases from $9e-9/5e-5$ to $1e-1/1e-2$ and the BEP for perfect synchronization increases from $1e-5/1e-10$ to $1e-1/1e-2$. Clearly, a DSSS/CDMA indoor geolocation with Kasami or Gold sequences **cannot** be used when more than 10 transmitters are required.

We note that for a DSSS/CDMA/FDMA indoor geolocation system with Gold/Kasami sequences as I increases from 2 to 32 the BEP for average synchronization remains almost unchanged at $4e-4/1e-5$ and the BEP for perfect synchronization remains almost unchanged $7e-8/2e-14$. Clearly, a DSSS/CDMA/FDMA indoor geolocation with Kasami or Gold sequences **can** be used when up to 32 transmitters are required.

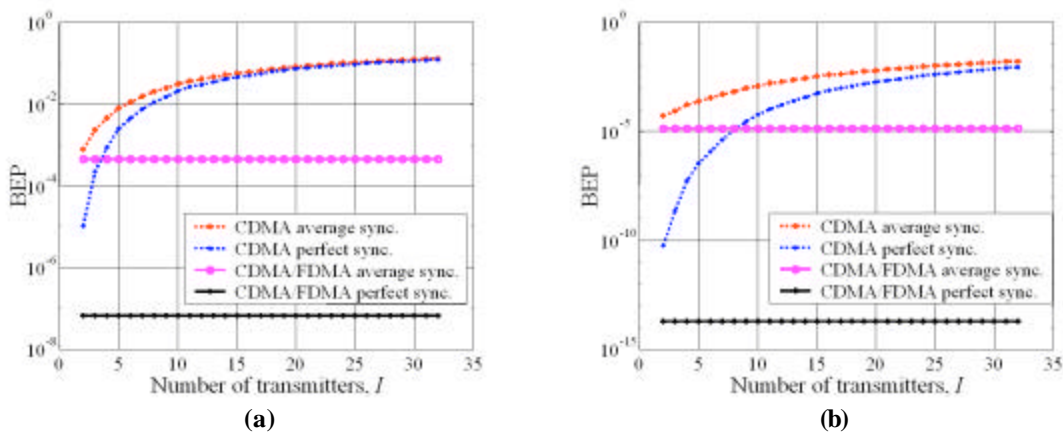


Figure 5.12 BEP vs. number of transmitters, I , for (a) Gold and (b) Kasami sequences.

Figure 5.13 illustrates the BEP as a function of the number of paths, K , using (a) Gold and (b) Kasami sequences for a DSSS/CDMA only and a DSSS/CDMA/FDMA indoor geolocation system for average and perfect synchronization. For this experiment, in addition to the parameters shown above, the E_b/N_0 is equal to 70 (dB). The relative distance between the 1st transmitter and receiver is 10 m and the relative distance between each adjacent transmitter and the receiver is 10 m. The number of transmitters is equal to 10.

We note that for a DSSS/CDMA indoor geolocation system with Gold/Kasami sequences as K increases from 1 to 100 the BEP for average synchronization increases from $2e-4/3e-5$ to $0.5/1e-1$ and the BEP for perfect synchronization increases from $1e-7/1e-13$ to $0.5/1e-1$. Clearly, a DSSS/CDMA indoor geolocation system with Kasami or Gold sequences **cannot** be used when an indoor channel contains more than 10 paths.

We note that for a DSSS/CDMA/FDMA indoor geolocation system with Gold/Kasami sequences as K increases from 1 to 100 the BEP for average synchronization increases from $1e-4/1e-5$ to $1e-2/1e-3$ and the BEP for perfect synchronization increases from $1e-13/0$ to $1e-2/1e-5$. Clearly, a DSSS/CDMA/FDMA indoor geolocation with Kasami or Gold sequences **can** be used when an indoor channel contains up to 30 paths.

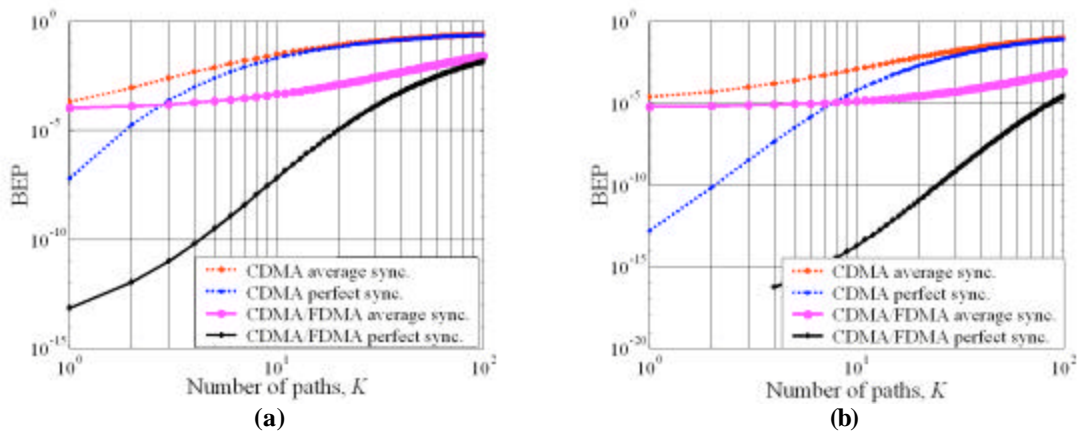


Figure 5.13 BEP vs. number paths, K , for (a) Gold and (b) Kasami sequences.

Figure 5.14 presents the BEP as a function of the synchronization parameter, $\delta\tau$ (nsec), using (a) Gold and (b) Kasami sequences for a DSSS/CDMA only and a DSSS/CDMA/FDMA indoor geolocation system. For this experiment, in addition to the parameters shown above, the E_b/N_0 is equal to 70 (dB). The relative distance between the 1st transmitter and receiver is 10 m and the relative distance between each adjacent transmitter and the receiver is 10 m. The number of transmitters is equal to 10 and the number of paths is equal to 10.

We note that for a DSSS/CDMA indoor geolocation system with Gold/Kasami sequences as τ increases from 0 to 9 nsec the BEP increases from $1e-2/1e-5$ to $0.1/1e-1$. A DSSS/CDMA indoor geolocation system with Kasami or Gold sequences **can** be used when $\delta\tau < 5$ nsec. We note that for a DSSS/CDMA/FDMA indoor geolocation system with Gold/Kasami sequences as $\delta\tau$ increases from 0 to 9 nsec the BEP increases from $5e-8/1e-13$ to $1e-2/1e-3$. A DSSS/CDMA/FDMA indoor geolocation with Kasami or Gold sequences **can** be used when $\delta\tau < 5$ nsec.

Figure 5.15 presents the BEP as a function of the frequency error, f_e (Hz), using (a) Gold and (b) Kasami sequences for a DSSS/CDMA only and a DSSS/CDMA/FDMA indoor geolocation system for average synchronization. For this experiment, in addition to the parameters shown above, the E_b/N_0 is equal to 70 (dB). The relative distance between the 1st transmitter and receiver is 10 m and the relative distance between each adjacent transmitter and the receiver is 10 m. The number of transmitters is equal to 10, the number of paths is equal to 10, and $\delta\tau = 0.5 * T_c = 5$ nsec.

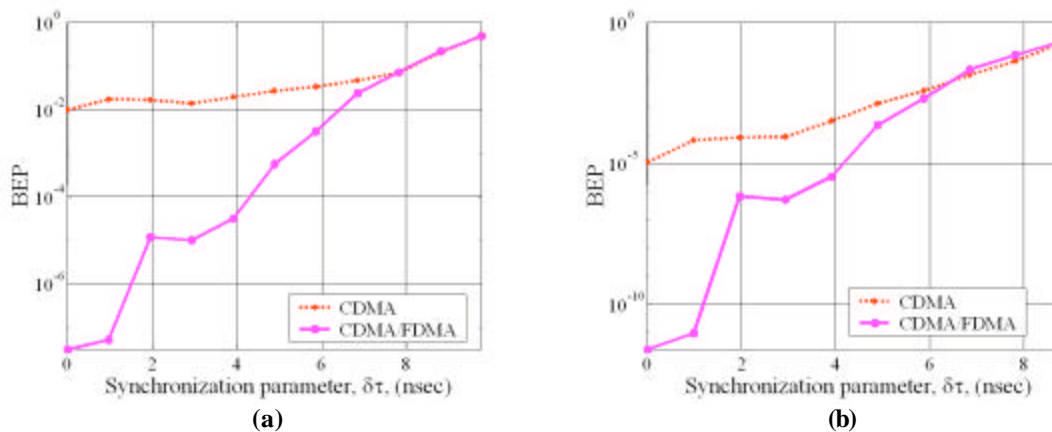


Figure 5.14 BEP vs. synchronization parameter, $\delta\tau$, for (a) Gold and (b) Kasami sequences.

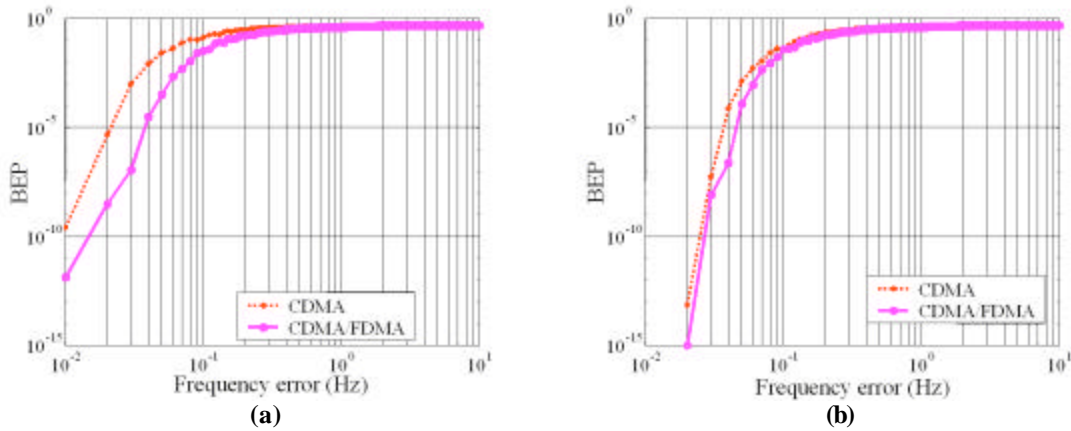


Figure 5.15 BEP vs. frequency error, f_e , (Hz) for (a) Gold and (b) Kasami sequences.

We note that for a DSSS/CDMA indoor geolocation system with Gold/Kasami sequences as f_e increases from 0.01 to 10 Hz the BEP increases from $1e-7/0$ to $0.5/0.5$. A DSSS/CDMA indoor geolocation system with Kasami or Gold sequences **would require** a frequency error smaller than 0.01 Hz.

We note that for a DSSS/CDMA/FDMA indoor geolocation system with Gold/Kasami sequences as f_e increases from 0.01 to 10 Hz the BEP increases from $1e-12/0$ to $0.5/0.5$. A DSSS/CDMA/FDMA indoor geolocation system with Kasami or Gold sequences **would require** a frequency error smaller than 0.1 Hz.

5.4.2.2 Navigation Performance

The pseudorange error and the phase error provide the means of assessing the navigation performance of a DSSS/CDMA and DSSS/CDMA/FDMA indoor geolocation system. The pseudorange error and phase error are given as a function of six important design parameters such as ideal signal to noise ratio, E_b/N_0 (dB), relative adjacent distance, R_i (m), $\forall i \in \{2, \dots, I\}$, number of transmitters, I , number of paths, K , synchronization parameter, $\delta\tau$ (nsec), and frequency error, f_e , (Hz).

Figure 5.16 depicts the pseudorange error as a function of E_b/N_0 (dB) using (a) Gold and (b) Kasami sequences for a DSSS/CDMA only and DSSS/CDMA/FDMA indoor geolocation system for average and perfect synchronization.

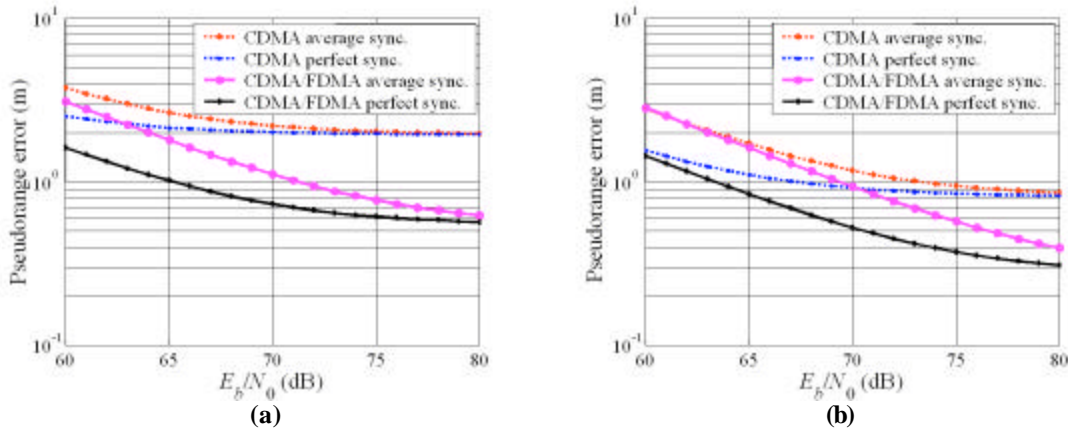


Figure 5.16 Pseudorange error vs. ideal SNR, E_b/N_0 (dB), for (a) Gold and (b) Kasami sequences.

We note that for a DSSS/CDMA system with Gold/Kasami sequences as E_b/N_0 increases from 60 to 80 dB the pseudorange error for average synchronization decreases from 4/2 to 2/0.8 and the pseudorange error for perfect synchronization decreases from 2.5/1.5 to 2/0.8. Clearly, a DSSS/CDMA indoor geolocation with Kasami sequences can achieve a pseudorange error almost 2 times as small as the same system with Gold sequences.

We note that for a DSSS/CDMA/FDMA indoor geolocation system with Gold/Kasami sequences as E_b/N_0 increases from 60 to 80 dB the pseudorange error for average synchronization decreases from 3/2 to 0.6/0.4 the pseudorange error for perfect synchronization decreases from 1.5/1.5 to 0.6/0.3. Clearly, a DSSS/CDMA/FDMA indoor geolocation with Kasami sequences can achieve a pseudorange error almost 2 times as small as the pseudorange error of the same system with Gold sequences.

Figure 5.17 depicts the pseudorange error as a function of relative adjacent distance, R_i (m), using (a) Gold and (b) Kasami sequences for a DSSS/CDMA only and DSSS/CDMA/FDMA indoor geolocation system for average and perfect synchronization. For this experiment E_b/N_0 is equal to 70 (dB).

We note that for a DSSS/CDMA indoor geolocation system with Gold/Kasami sequences as R_i increases from 1 m to 100 m the pseudorange error for average synchronization decreases from 100/50 to 1/1 and the pseudorange error for perfect synchronization decreases from 100/50 to 0.7/0.5. Clearly, a DSSS/CDMA indoor geolocation with Kasami or Gold sequences **cannot** overcome the *near-far* effect.

We note that for a DSSS/CDMA/FDMA indoor geolocation system with Gold/Kasami sequences as R_i increases from 1 to 100 m the pseudorange error for average synchronization remains almost unchanged at 1 m and the pseudorange error for perfect synchronization remains almost unchanged 0.7/0.5 m. Clearly, a DSSS/CDMA/FDMA indoor geolocation with Kasami or Gold sequences **can** overcome the *near-far* effect.

Figure 5.18 depicts the pseudorange error as a function of the number of transmitters, I , using (a) Gold and (b) Kasami sequences for a DSSS/CDMA only and a DSSS/CDMA/FDMA indoor geolocation system for average and perfect synchronization. In addition to the parameters shown above, the E_b/N_0 is equal to 70 (dB). Also the relative distance between the 1st transmitter and receiver is 10 m and the relative distance between each adjacent transmitter and the receiver is 10 m.

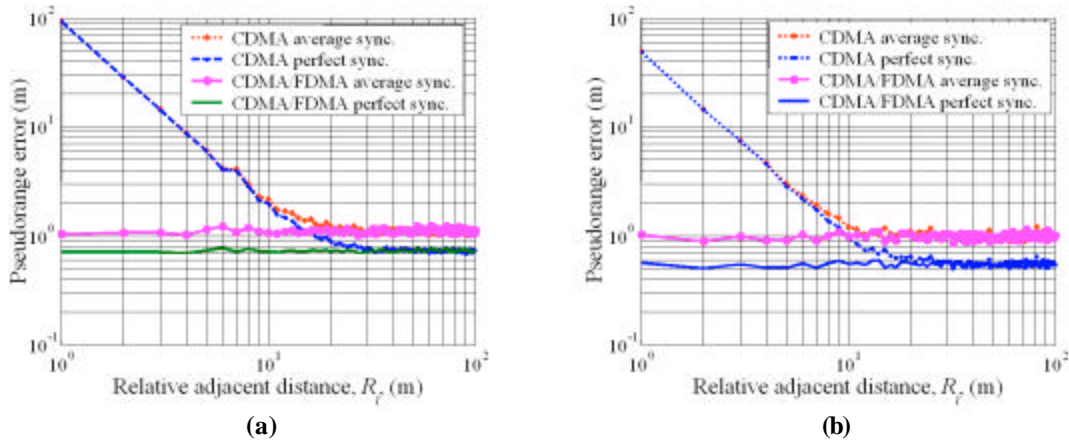


Figure 5.17 Pseudorange error vs. adjacent distance (m) for (a) Gold and (b) Kasami sequences.

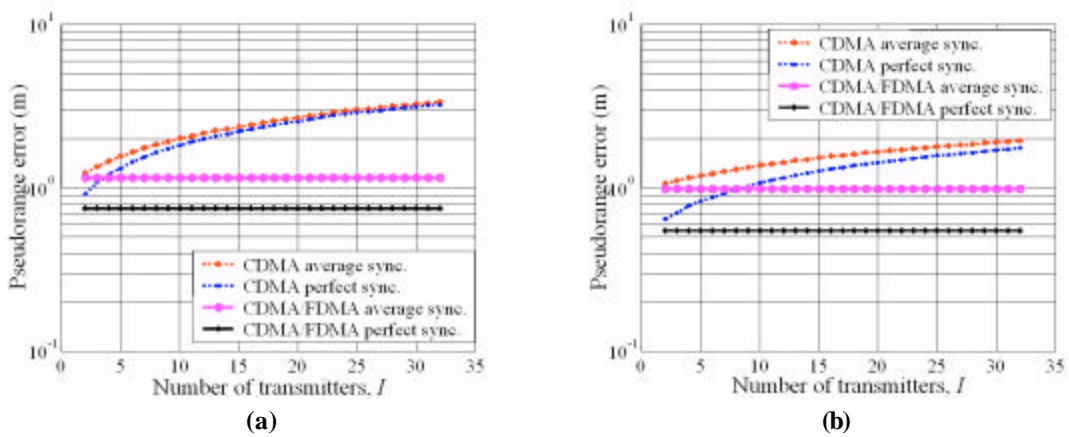


Figure 5.18 Pseudorange error vs. number of transmitters, I , for (a) Gold and (b) Kasami sequences.

We note that for a DSSS/CDMA indoor geolocation system with Gold/Kasami sequences as I increases from 2 to 32 the pseudorange error for average synchronization increases from 1.2/1 to 3.2/2 m and the pseudorange error for perfect synchronization increases from 0.9/0.65 to 3.2/1.8. Clearly, a DSSS/CDMA indoor geolocation with Kasami or Gold sequences **cannot** be used when more than 10 transmitters are required.

We note that for a DSSS/CDMA/FDMA indoor geolocation system with Gold/Kasami sequences as I increases from 2 to 32 the pseudorange error for average synchronization remains almost unchanged at 1.2/1 m and the pseudorange error for perfect synchronization remains almost unchanged 7.5/5.5 m. Clearly, a DSSS/CDMA/FDMA indoor geolocation with Kasami or Gold sequences **can** be used when up to 32 transmitters are required.

Figure 5.19 illustrates the pseudorange error as a function of the number of paths, K , using (a) Gold and (b) Kasami sequences for a DSSS/CDMA only and a DSSS/CDMA/FDMA indoor geolocation system for average and perfect synchronization. For this experiment, in addition to the parameters shown above, the E_b/N_0 is equal to 70 (dB). The relative distance between the 1st transmitter and receiver is 10 m and the relative distance between each adjacent transmitter and the receiver is 10 m. The number of transmitters is equal to 10.

We note that for a DSSS/CDMA indoor geolocation system with Gold/Kasami sequences as K increases from 1 to 100 the pseudorange error for average synchronization increases from 1 m to 6/3 m and the pseudorange error for perfect synchronization increases from 0.7/0.6 m to 6/3 m. Clearly, a DSSS/CDMA indoor geolocation system with Kasami or Gold sequences **cannot** be used when an indoor channel contains more than 10 paths.

We note that for a DSSS/CDMA/FDMA indoor geolocation system with Gold/Kasami sequences as K increases from 1 to 100 the pseudorange error for average synchronization increases from 1/1 m to 2/1.5 m and the pseudorange error for perfect synchronization increases from 0.5/0.45 m to 2/1 m. Clearly, a DSSS/CDMA/FDMA indoor geolocation with Kasami or Gold sequences **can** be used when an indoor channel contains more than 10 paths.

Figure 5.20 presents the pseudorange error as a function of the synchronization parameter, $\delta\tau$ (nsec), using (a) Gold and (b) Kasami sequences for a DSSS/CDMA only and a DSSS/CDMA/FDMA indoor geolocation system. For this experiment, in addition to the parameters shown above, the E_b/N_0 is equal to 70 (dB). The relative distance between the 1st transmitter and receiver is 10 m and the relative distance between each adjacent transmitter and the receiver is 10 m. The number of transmitters is equal to 10 and the number of paths is equal to 10.

We note that for a DSSS/CDMA indoor geolocation system with Gold/Kasami sequences as $\delta\tau$ increases from 0 to 10 nsec the pseudorange error increases from 3/1 m to 6/5 m. A DSSS/CDMA indoor geolocation system with Kasami or Gold sequences **can** be used when $\delta\tau < 5$ nsec.

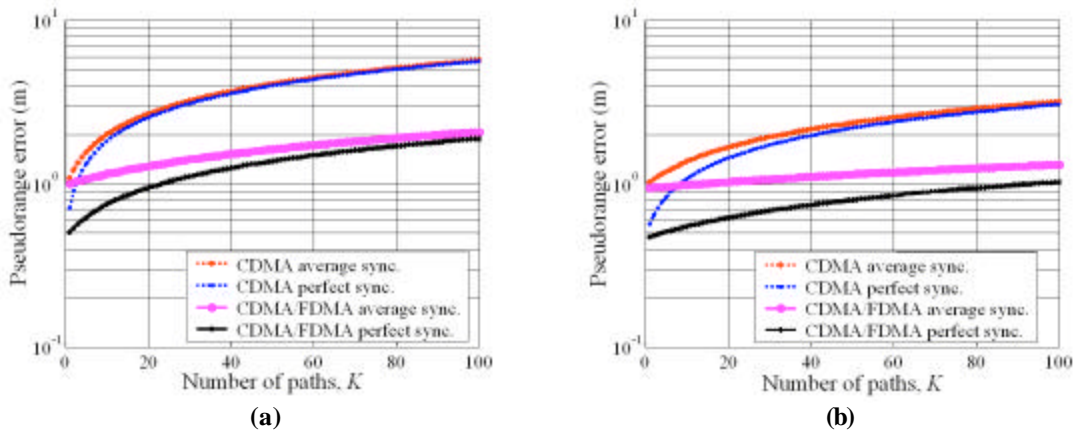


Figure 5.19 Pseudorange error vs. number of paths, K , for (a) Gold and (b) Kasami sequences.

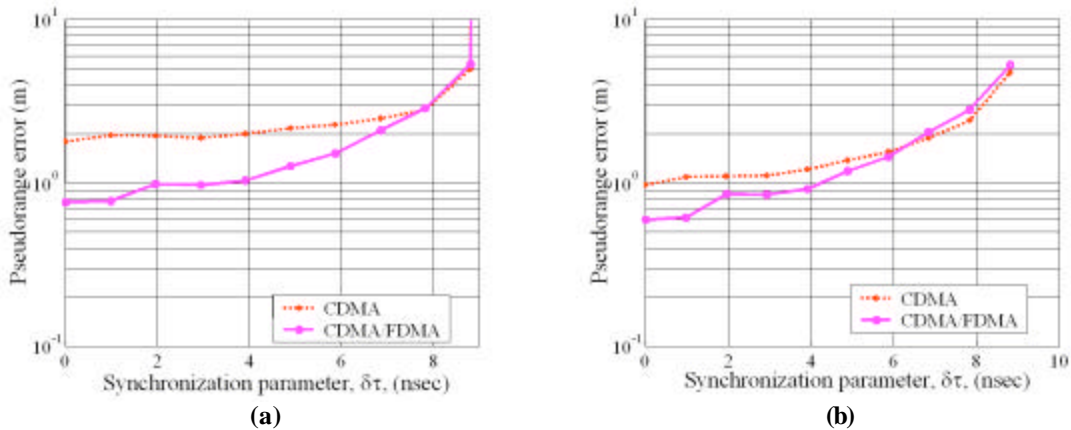


Figure 5.20 Pseudorange error vs. $\delta\tau$ for (a) Gold and (b) Kasami sequences.

We note that for a DSSS/CDMA/FDMA indoor geolocation system with Gold/Kasami sequences as $\delta\tau$ increases from 0 to 9 nsec the pseudorange error increases from 0.7/0.6 to 5/5 m. A DSSS/CDMA/FDMA indoor geolocation with Kasami or Gold sequences **can** be used when $\delta\tau < 5$ nsec.

Figure 5.21 presents the pseudorange error as a function of the frequency error, f_e (Hz), using (a) Gold and (b) Kasami sequences for a DSSS/CDMA only and a DSSS/CDMA/FDMA indoor geolocation system for average synchronization. For this experiment, in addition to the parameters shown above, the E_b/N_0 is equal to 70 (dB). The relative distance between the 1st transmitter and receiver is 10 m and the relative distance between each adjacent transmitter and the receiver is 10 m. The number of transmitters is equal to 10, the number of paths is equal to 10, and $\delta\tau = 0.5 * T_c = 5$ nsec.

We note that for a DSSS/CDMA indoor geolocation system with Gold/Kasami sequences as f_e increases from 0.01 to 10 Hz the pseudorange error increases from 0.7/0.3 to 500/300 m. A DSSS/CDMA indoor geolocation system with Kasami or Gold sequences **would require** a frequency error smaller than 0.01 Hz.

We note that for a DSSS/CDMA/FDMA indoor geolocation system with Gold/Kasami sequences as f_e increases from 0.01 to 10 Hz the pseudorange error increases from 0.6/0.3 m to 200/200 m. A DSSS/CDMA/FDMA indoor geolocation system with Kasami or Gold sequences **would require** a frequency error smaller than 0.1 Hz.

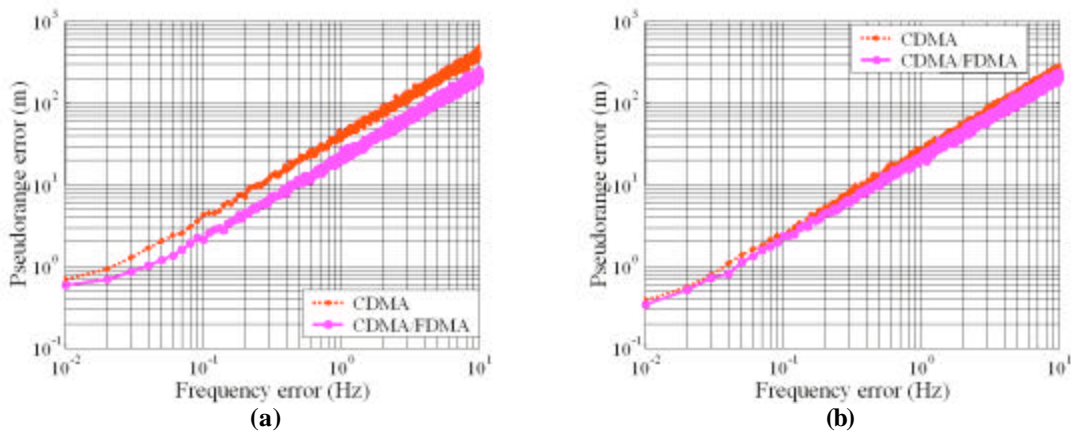


Figure 5.21 Pseudorange error vs. the frequency error (Hz) for (a) Gold and (b) Kasami sequences.

Figure 5.22 depicts the phase error as a function of E_b/N_0 (dB) using (a) Gold and (b) Kasami sequences for a DSSS/CDMA only and DSSS/CDMA/FDMA indoor geolocation system for average and perfect synchronization.

We note that for a DSSS/CDMA system with Gold/Kasami sequences as E_b/N_0 increases from 60 to 80 dB the phase error for average synchronization decreases from 2/1.5 cm to 1.2/0.5 cm and the phase error for perfect synchronization decreases from 1.5/0.8 cm to 1.2/0.4 cm. Clearly, a DSSS/CDMA indoor geolocation with Kasami sequences can achieve a phase error almost 2 times as small as the phase error of the same system with Gold sequences.

We note that for a DSSS/CDMA/FDMA indoor geolocation system with Gold/Kasami sequences as E_b/N_0 increases from 60 to 80 dB the phase error for average synchronization decreases from 1.5/1.5 cm to 3/2 mm the phase error for perfect synchronization decreases from 8/7.5 mm to 3/1.6 mm. Clearly, a DSSS/CDMA/FDMA indoor geolocation with Kasami sequences can achieve a phase error almost 2 times as small as the phase error of the same system with Gold sequences.

Figure 5.23 depicts the phase error as a function of relative adjacent distance, R_i (m), $\forall i \in \{2, \dots, I\}$, using (a) Gold and (b) Kasami sequences for a DSSS/CDMA only and DSSS/CDMA/FDMA indoor geolocation system for average and perfect synchronization. For this experiment, in addition to the parameters shown above, the E_b/N_0 is equal to 70 (dB).

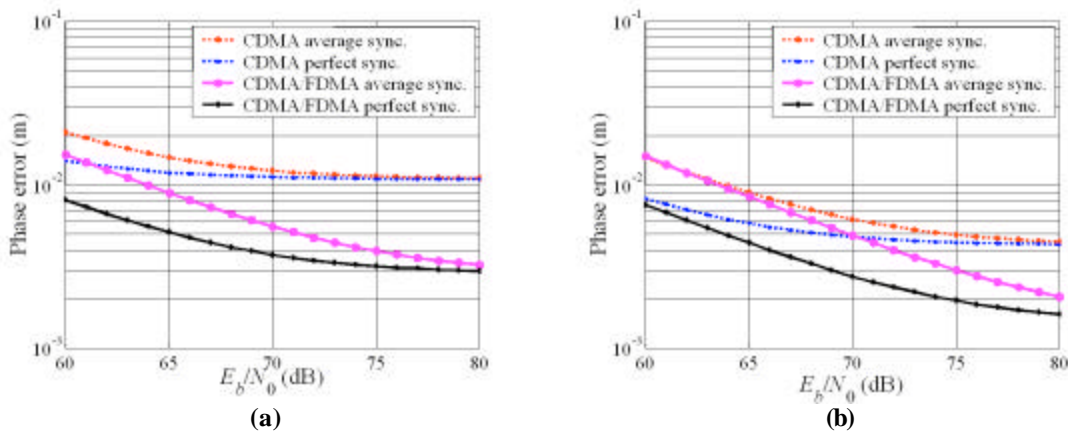


Figure 5.22 Phase error vs. the ideal SNR (dB) for (a) Gold and (b) Kasami sequences.

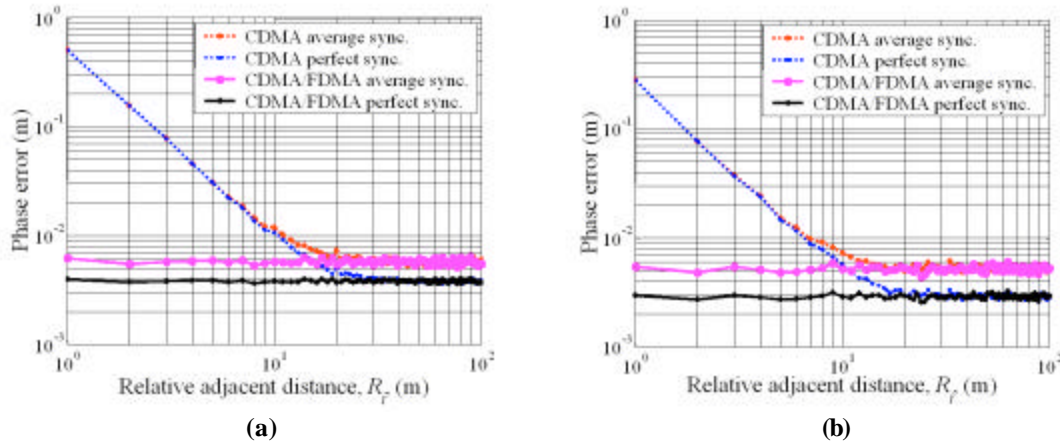


Figure 5.23 Phase error vs. the adjacent distance, R_i , (m) for (a) Gold and (b) Kasami sequences.

We note that for a DSSS/CDMA indoor geolocation system with Gold/Kasami sequences as R_i increases from 1 to 100 m the phase error for average synchronization decreases from 50/30 cm to 5/5 mm and the phase error for perfect synchronization decreases from 50/30 cm to 5/5 mm. Clearly, a DSSS/CDMA indoor geolocation with Kasami or Gold sequences **cannot** overcome the *near-far* effect.

We note that for a DSSS/CDMA/FDMA indoor geolocation system with Gold/Kasami sequences as R_i increases from 1 to 100 m the phase error for average synchronization remains almost unchanged at 5 mm and the phase error for perfect synchronization remains almost unchanged 4/3 mm. Clearly, a DSSS/CDMA/FDMA indoor geolocation with Kasami or Gold sequences **can** overcome the *near-far* effect.

Figure 5.24 depicts the phase error as a function of the number of transmitters, I , using (a) Gold and (b) Kasami sequences for a DSSS/CDMA only and a DSSS/CDMA/FDMA indoor geolocation system for average and perfect synchronization. For this experiment, in addition to the parameters shown above, the E_b/N_0 is equal to 70 (dB). Also the relative distance between the 1st transmitter and receiver is 10 m and the relative distance between each adjacent transmitter and the receiver is 10 m.

We note that for a DSSS/CDMA indoor geolocation system with Gold/Kasami sequences as I increases from 2 to 32 the phase error for average synchronization increases from 6/5 mm to 1.8/1 cm and the phase error for perfect synchronization increases from 5/3 mm to 1.8/1 cm. Clearly, a DSSS/CDMA indoor geolocation with Kasami or Gold sequences **cannot** be used when more than 10 transmitters are required.

We note that for a DSSS/CDMA/FDMA indoor geolocation system with Gold/Kasami sequences as I increases from 2 to 32 the phase error for average synchronization remains almost unchanged at 6/5 mm and the phase error for perfect synchronization remains almost unchanged 4/3 mm. Clearly, a DSSS/CDMA/FDMA indoor geolocation with Kasami or Gold sequences **can** be used when up to 32 transmitters are required.

Figure 5.25 illustrates the phase error as a function of the number of paths, K , using (a) Gold and (b) Kasami sequences for a DSSS/CDMA only and a DSSS/CDMA/FDMA indoor geolocation system for average and perfect synchronization. For this experiment, in addition to the parameters shown above, the E_b/N_0 is equal to 70 (dB). The relative distance between the transmitter and receiver is 10 m and the relative distance between the adjacent transmitters and the receiver is 10 m. The number of transmitters is equal to 10.

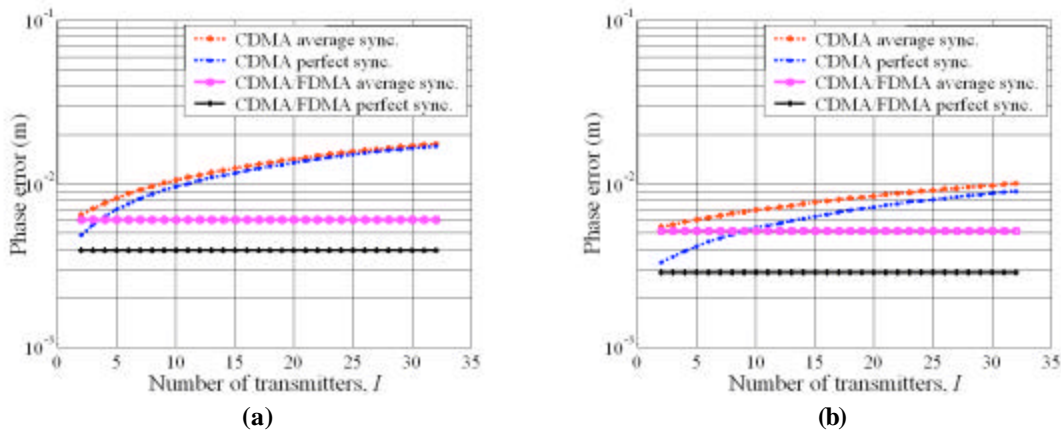


Figure 5.24 Phase error vs. number of transmitters, I , for (a) Gold and (b) Kasami sequences.

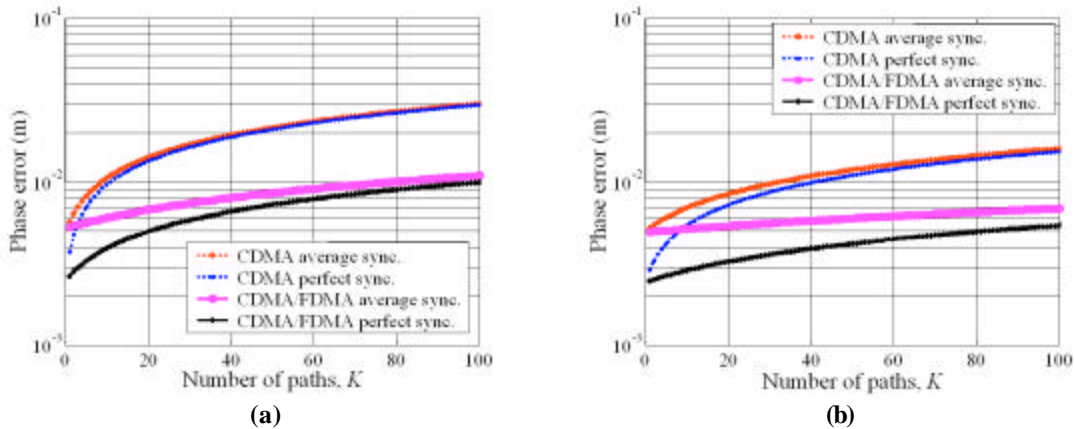


Figure 5.25 Phase error vs. number paths, K , for (a) Gold and (b) Kasami sequences.

We note that for a DSSS/CDMA indoor geolocation system with Gold/Kasami sequences as K increases from 1 to 100 the phase error for average synchronization increases from 5/5 mm to 3/1.6 cm and the phase error for perfect synchronization increases from 4/3 mm to 2/1.6 cm. Clearly, a DSSS/CDMA indoor geolocation system with Kasami or Gold sequences **cannot** be used when an indoor channel contains more than 10 paths.

We note that for a DSSS/CDMA/FDMA indoor geolocation system with Gold/Kasami sequences as K increases from 1 to 100 the phase error for average synchronization increases from 5/5 mm to 1/0.7 cm and the phase error for perfect synchronization increases from 2.5/1.5 mm to 1/0.55 cm. Clearly, a DSSS/CDMA/FDMA indoor geolocation with Kasami or Gold sequences **can** be used when an indoor channel contains more than 10 paths.

Figure 5.26 presents the phase error as a function of the synchronization parameter, $\delta\tau$ (nsec), using (a) Gold and (b) Kasami sequences for a DSSS/CDMA only and a DSSS/CDMA/FDMA indoor geolocation system. For this experiment, in addition to the parameters shown above, the E_b/N_0 is equal to 70 (dB). The relative distance between the 1st transmitter and receiver is 10 m and the relative distance between each adjacent transmitter and the receiver is 10 m. The number of transmitters is equal to 10 and the number of paths is equal to 10.

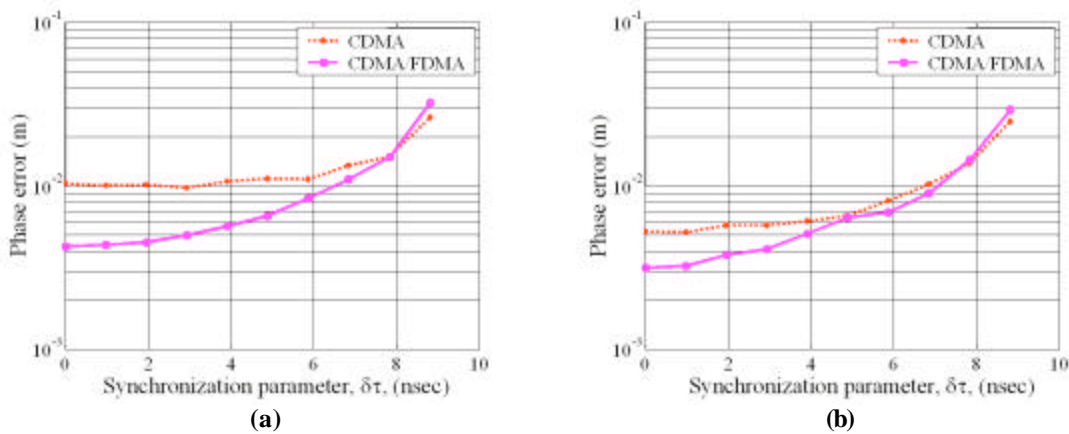


Figure 5.26 Phase error vs. synchronization parameter, $\delta\tau$, for (a) Gold and (b) Kasami sequences.

We note that for a DSSS/CDMA indoor geolocation system with Gold/Kasami sequences as $\delta\tau$ increases from 0 to 9 nsec the phase error increases from 1/0.5 cm to 3/3 cm. A DSSS/CDMA indoor geolocation system with Kasami or Gold sequences **can** be used when $\delta\tau < 5$ nsec. We note that for a DSSS/CDMA/FDMA indoor geolocation system with Gold/Kasami sequences as $\delta\tau$ increases from 0 to 9 nsec the phase error increases from 4/3 mm to 2.8/2.8 cm. A DSSS/CDMA/FDMA indoor geolocation with Kasami or Gold sequences **can** be used when $\delta\tau < 5$ nsec.

Figure 5.21 presents the phase error as a function of the frequency error, f_e (Hz), using (a) Gold and (b) Kasami sequences for a DSSS/CDMA only and a DSSS/CDMA/FDMA indoor geolocation system for average synchronization. For this experiment, in addition to the parameters shown above, the E_b/N_0 is equal to 70 (dB). The relative distance between the transmitter and receiver is 10 m and the relative distance between the adjacent transmitters and the receiver is 10 m. The number of transmitters is equal to 10, the number of paths is equal to 10, and $\delta\tau = 0.5 * T_c = 5$ nsec.

We note that for a DSSS/CDMA indoor geolocation system with Gold/Kasami sequences as f_e increases from 0.01 to 10 Hz the phase error increases from 4/2 mm to 2/1.5 m. We note that for a DSSS/CDMA/FDMA indoor geolocation system with Gold/Kasami sequences as f_e increases from 0.01 to 10 Hz the phase error increases from 3/2 mm to 1/1 m. A normal operation of a DSSS/CDMA indoor geolocation system and a DSSS/CDMA/FDMA indoor geolocation system with Kasami or Gold sequences **would require** a frequency error smaller than 0.01 Hz and 0.1 Hz respectively.

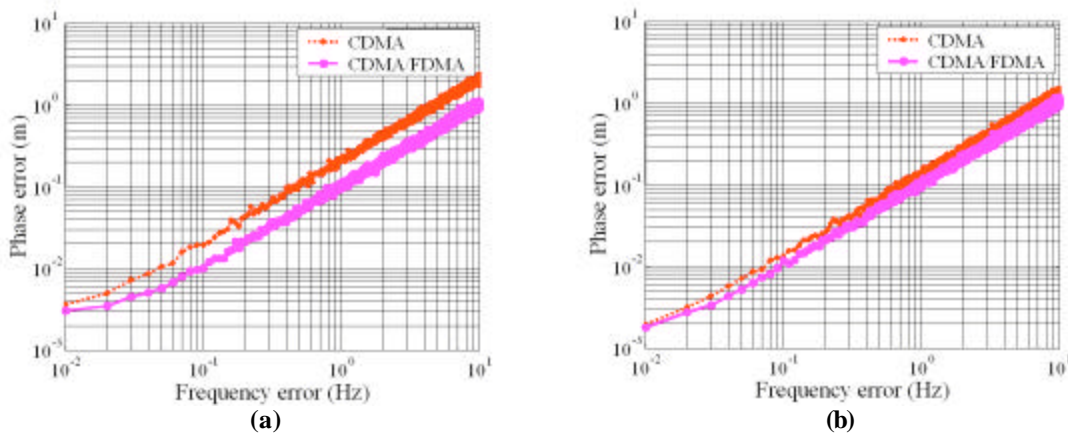


Figure 5.27 Phase error vs. frequency error (Hz) for (a) Gold and (b) Kasami sequences.

5.5 Summary and Conclusions

We have analyzed and discussed the theoretical performance of a DSSS/CDMA only indoor geolocation system and a DSSS/CDMA/FDMA indoor geolocation system. Recall that in Chapter 2 when we discussed a pseudolite indoor geolocation system where we argued that the conventional pseudolite signal structure is inadequate to overcome the *near-far* effect and mitigate the indoor multipath effect. The theoretical performance results indicate that a DSSS/CDMA only system which operates on a frequency different from the L_1 frequency is also inadequate to overcome the *near-far* effect. On the other hand, a DSSS/CDMA/FDMA indoor geolocation system would be successful in eliminating the near-far effect, operating when a large number of transmitters is required, handling severe multipath, and operating under average synchronization requirements.

CITED REFERENCES AND FURTHER READING:

- [1] D.T. Magill, F.D. Natali, and G.P. Edwards, "Spread-spectrum technology for commercial applications," in *Proc. IEEE*, vol. 82, no. 4, pp. 572-584, Apr. 1994.
- [2] A.A.M. Saleh, A.J. Rustako, Jr., L.J. Cimini, Jr., G.J. Owens, and R.S. Roman, "An experimental TDMA indoor radio communications system using slow frequency hopping and coding," *IEEE Trans. Comm.*, vol. 39, no. 1, pp. 152-162, Jan. 1991.
- [3] J. Wang, M. Moeneclaey, and L.B. Milstein, "DS-CDMA with predetection diversity for indoor radio communications," *IEEE Trans. Comm.*, vol. 42, no. 2/3/4, pp. 1929-1938, Feb/Mar/Apr. 1994.
- [4] S. Kandala, E.S. Sousa, and S. Pasupathy, "Multi-user multi-sensor detectors for CDMA networks," *IEEE Trans. Comm.*, vol. 43, no. 2, pp. 946-957, Feb-Apr. 1995.
- [5] G.W. Marsh and J.M. Kahn, "Channel reuse strategies for indoor infrared wireless communications," *IEEE Trans. Comm.*, vol. 45, no. 10, pp. 1280-1290, Oct. 1997.
- [6] Y. Bar-Ness, "Asynchronous multiuser CDMA detector made simpler: novel decorrelator, combiner, canceller, combiner (DC3) structure," *IEEE Trans. Comm.*, vol. 47, no. 1, pp. 115-122, Jan. 1999.
- [7] J. Yang, "Diversity receiver scheme and system performance evaluation for a CDMA system," *IEEE Trans. Comm.*, vol. 47, no. 2, pp. 272-280, Feb. 1999.
- [8] D.I. Kim and J.C. Roh, "Performance of slotted asynchronous CDMA using controlled time of arrival," *IEEE Trans. Comm.*, vol. 47, no. 3, pp. 454-463, Mar. 1999.
- [9] R. Fantacci and A. Galligani, "An efficient RAKE receiver architecture with pilot signal cancellation for downlink communications in DS-CDMA indoor wireless networks," *IEEE Trans. Comm.*, vol. 47, no. 6, pp. 823-827, June 1999.

- [10] K.S. Butterworth, K.W. Sowerby, and A.G. Williamson, "Base station placement for in-building mobile communication systems to yield high capacity and efficiency," *IEEE Trans. Comm.*, vol. 48, no. 4, pp. 658-669, Apr. 2000.
- [11] M.R. Hueda, G. Corral-Briones, and C.E. Rodriguez, "MMSEC-RAKE receivers with resolution reduction of the diversity branches: analysis, simulation, and applications," *IEEE Trans. Comm.*, vol. 49, no. 6, pp. 1073-1081, June 2001.
- [12] F. Adachi, M. Sawahashi, and H. Suda, "Wideband DS-CDMA for next-generation mobile communications systems," *IEEE Comm. Mag.*, vol. 36, no. 9, pp. 56-69, Sep. 1998.
- [13] P. Taaghoul et al., "Satellite UMTS/IMT2000 W-CDMA air interfaces," *IEEE Comm. Mag.*, vol. 37, no. 9, pp. 116-126, Sep. 1999.
- [14] T.-C. Wu, C.-C. Chao, and K.-C. Chen, "Capacity of synchronous coded DS SFH and FFH spread-spectrum multiple-access for wireless local communications," *IEEE Trans. Comm.*, vol. 45, no. 5, pp. 200-212, Feb. 1997.
- [15] D. Dardari and V. Tralli, "High-speed indoor wireless communications at 60 GHz with coded OFDM," *IEEE Trans. Comm.*, vol. 47, no. 11, pp. 1709-1721, Nov. 1999.
- [16] I.F. Progri and W.R. Michalson, "Performance evaluation of a DSSS/CDMA/FDMA indoor geolocation system," in *review IEEE Trans. Comm.*, Nov. 2001.
- [17] I.F. Progri, J.M. Hill, and W.R. Michalson, "An investigation of the pseudolite's signal structure for indoor applications," in *Proc. ION-AM*, June 2001.
- [18] I.F. Progri, and W.R. Michalson, "The impact of proposed pseudolite's signal structure on the receiver's phase and code error," in *Proc. ION-AM*, June 2001.
- [19] I.F. Progri, and W.R. Michalson, "An alternative approach to multipath and near-far problem for indoor geolocation systems," in *Proc. ION-GPS*, Sep. 2001.
- [20] M.L. Skolnik, *Introduction to Radar Systems*, 2nd ed. Boston, MA: McGraw-Hill, 1980.
- [21] D.V. Sarwate and M.B. Pursley, "Crosscorrelation properties of pseudorandom and related sequences," in *Proc. of IEEE*, vol. 68, pp. 593-619, May 1980.
- [22] B.W. Parkinson, J.J. Spilker, Jr, et al., *The Global Positioning System-Theory and Applications*, Washington, DC: American Institute of Aeronautics and Astronautics, (vol. 1, chap. 3, "GPS signal structure and theoretical performance") 1996.
- [23] L.J. Greenstein et al., "Microcells in personal communications systems," *IEEE Comm. Mag.*, vol. 30, no. 12, pp. 76-88, Dec. 1992.
- [24] J.J.G. Fernandes, P.A. Watson, and J.C. Neves, "Wireless LANs: physical properties of infra-red systems vs. mmw systems," *IEEE Comm. Mag.*, vol. 32, no. 8, pp. 68-73, Aug. 1994.
- [25] D.T. Magill, F.D. Natali, and G.P. Edwards, "Spread-spectrum technology for commercial applications," in *Proc. IEEE*, vol. 82, no. 4, pp. 572-584, Apr. 1994.

- [26] J.M. Hill, "Development of an experimental Global Positioning System (GPS) receiver platform for navigation algorithm evaluation," Ph.D. Dissertation, Worcester Polytechnic Institute, Aug. 2001.

Chapter 6. A DSSS/OFDM/CDMA/FDMA Indoor Geolocation System

“They that hate me without a cause are more than the hairs of mine head.” ³/₄Psalm 69:4

6.0 Introduction

ALTHOUGH a DSSS/CDMA/FDMA indoor geolocation system can overcome the *near-far* effect and the multipath propagation effect, it has a low data rate. For such a system, the data rate is to some extent proportional to the chipping rate; i.e., a higher chipping rate increases the data rate and vice versa. This is a major concern for achieving high data rate. So far we have exploited only time diversity. Exploiting other diversities, such as frequency diversity, may provide the infrastructure for achieving higher data rates. In a DSSS/OFDM/CDMA/FDMA indoor geolocation system the data rate increase is achieved at the expense of high system complexity. Moreover, reducing the code length, applied to achieve timing diversity, can also potentially increase the data rate. Shorter codes can potentially deteriorate the time delay estimation by worsening the code autocorrelation and crosscorrelation properties. If we exploit frequency diversity then we may estimate the time of arrival for every OFDM frequency and then average them out to obtain a time of arrival corresponding to the time of flight for a signal coming from a transmitting antenna to the receiving antenna.

There are many similarities between this system and the system analyzed in Chapter 5 that enable us to reuse some parts of Chapter 5 in this Chapter. The discussion of this Chapter starts with the communication performance analyses (see §6.1), continues with navigation performance analyses (see §6.2), goes on with quantitative assessment (see §6.3), and is concluded with a summary and conclusions (see §6.4).

6.1 Communication Performance Analyses

We analyze the communication performance of the receiver relying only on tracking the C code. In contrast to a DSSS/CDMA/FDMA indoor geolocation system (see

Chapter 5) which contained the C, P, and B codes, the system under investigation in this Chapter contains only the C code. The C code is relatively short and thus it is relatively easy to resolve the beginning of the C code, which enables a coarse acquisition between the transmitter and the receiver. Assuming that the sampling rate satisfies the Nyquist criterion, analyses are performed for an equivalent analog receiver to simplify the computations. Based on the diagram, shown in 0, we can identify 6 (six) important processing stages, which are analyzed in order: First, the analysis starts with the receiver's front end and base band sampling (see §6.1.1). Second, the analysis continues with the Doppler removal and phase rotation (see §6.1.2). Third, the discussion includes the correlation with the C code (see §6.1.3). Fourth, the investigation goes on with the integration after the C code correlation (see §6.1.4). Fifth, the discussion continues with the time of arrival estimation (see §6.1.5). Sixth, the analysis goes on with the study of the signal plus interference to noise ratio (see §6.1.6). And seventh, the discussion concludes with the evaluation of the bit error probability (see §6.1.7).

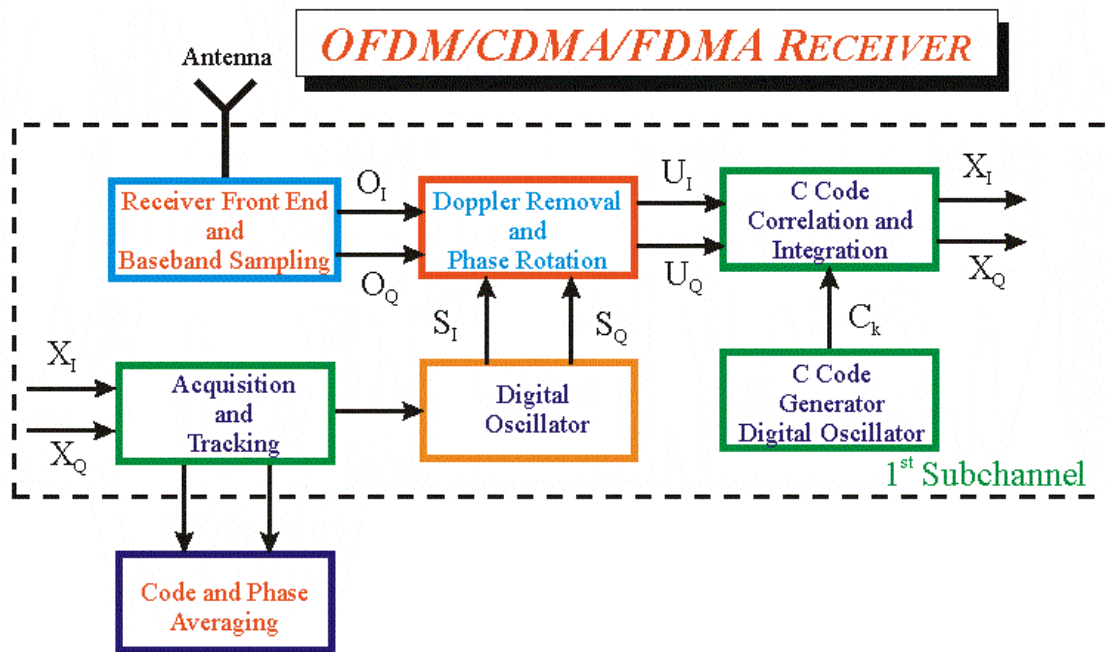


Figure 6.1 A DSSS/OFDM/CDMA/FDMA receiver design.

6.1.1 Receiver's Front End and Baseband Sampling

The receiver's front end section has a two-fold impact on the received signal: a *desired* impact and an *undesired* impact. On one hand, the *desired* impact consists of down-converting the received signal to the desired base-band or intermediate frequency for further signal processing. On the other hand, the *undesired* effect consists of introducing thermal or Johnson noise into the received signal. For a detailed discussion of the undesired impact of the receiver's front end and baseband sampling the reader should refer to §5.2.1.

The received signal, $r_{j=1}(t) \equiv r(t)$, is down-converted to the base-band frequency and sampled (see Figure 6.1 and Figure 6.2) and the subscript j is no longer used in our analysis. Therefore, the expression for the sampled, received signal at base-band frequency, $o(t)$, can be written as

$$(6.1.1) \quad o(t) = \sum_{i=1}^I \sum_{n=1}^N \sum_{k=1}^K \sqrt{G_a} a_{i,n}^k s_{i,n}(t - \tau_{i,n}^k) \exp \left\{ -j \left[(\tilde{\omega}_{i,n} - \hat{\omega}_{1,1}) (t - \tau_{i,n}^k) + \phi_{i,n} + \theta_{i,n}^k \right] \right\} + n_{out}(t)$$

where

$$(6.1.2) \quad s_{i,n}(t) = s_{i,n}^{rc}(t) + j s_{i,n}^{rs}(t)$$

and G_a is the front end amplifier gain. Note that the hat (^) denotes a parameter generated and estimated locally by the receiver and $n_{out}(t)$ is the noise with power spectral density given by equation (5.1.4).

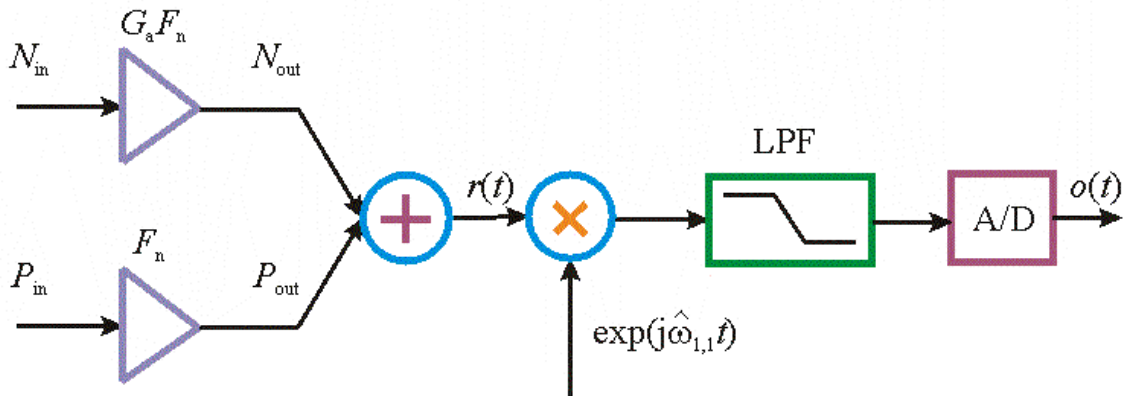


Figure 6.2 Block diagram of the receiver's front end and base band sampling.

6.1.2 Doppler Removal and Phase Rotation

During this process the Doppler shift of the desired signal (corresponding to the signal coming out from the first transmitter) is removed and the phase of the desired signal is rotated, which yields the signal, $u(t)$, determined from (see Figure 6.1 and Figure 6.3),

$$(6.1.3) \quad u(t) = \sum_{i=1}^I \sum_{n=1}^N \sum_{k=1}^K \sqrt{G_a} a_{i,n}^k s_{i,n}(t - \tau_{i,n}^k) \exp(-j\chi_{i,n}^k) + n_{out}(t)$$

where

$$(6.1.4) \quad \tilde{\omega}_{1,1} = \hat{\omega}_{1,1} (1 \pm \dot{R}_1(t)/c)$$

$$(6.1.5) \quad \chi_{i,n}^k = (\tilde{\omega}_{i,n} - \tilde{\omega}_{1,1})(t - \tau_{i,n}^k) + \phi_{i,n} + \theta_{i,n}^k.$$

Let $\omega_{i,n}^e$ denote radian error frequency term defined as

$$(6.1.6) \quad \omega_{i,n}^e = \tilde{\omega}_{i,n} - \tilde{\omega}_{1,1} = \omega_{i,n} (1 \pm \dot{R}_{i,n}(t)/c) - \hat{\omega}_{1,1} (1 \pm \dot{R}_1(t)/c)$$

then equation (6.1.5) can be further written as

$$(6.1.7) \quad \chi_{i,n}^k = \omega_{i,n}^e (t - \tau_{i,n}^k) + \phi_{i,n} + \theta_{i,n}^k.$$

The accuracy of removing the Doppler shift and rotating the phase depends upon the radian error frequency, $\omega_{i,n}^e$, and the time delay, $\tau_{i,n}^k$. This effect, while unnoticeable at this stage, will become very detrimental during the acquisition and tracking of the C code. Before acquiring the C code, the receiver performs the correlation with the C code, which is the topic of the coming subsection.

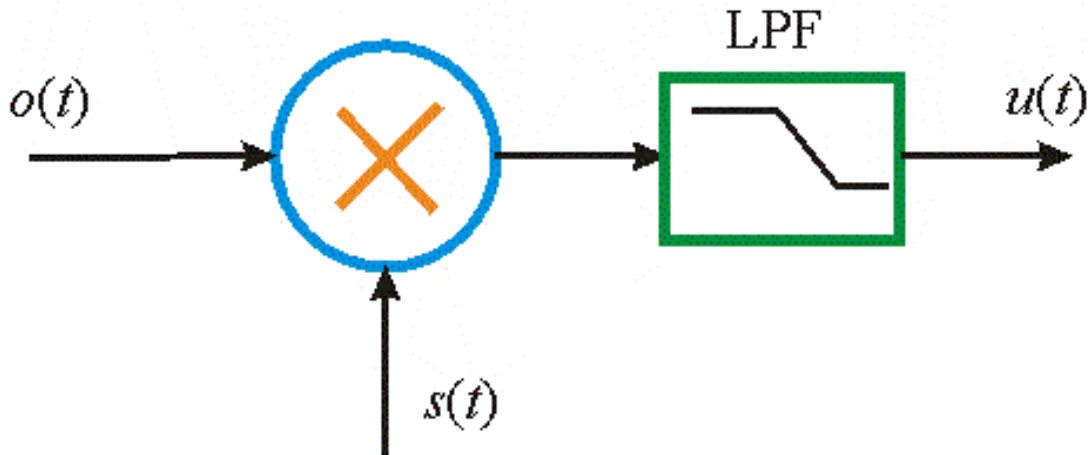


Figure 6.3 Doppler removal and phase rotation block diagram.

6.1.3 Correlation with the Locally Generated C Code

Assuming full or complete correlation with the code, $c^{(1),(1)}(t)$, (see Figure 6.1 and Figure 6.4), the signal coming out of this process, $w(t)$, is the superposition of the desired signal component, $w_d(t)$, the Inter Symbol Interference (ISI) term, $w_f(t)$, the Subchannel Access Interference (SAI), $w_s(t)$, the Mutually Accessed Interference (MAI) component, $w_m(t)$, and the Accumulated White Gaussian Noise (WGN) term, $w_n(t)$, which is analytically expressed as

$$(6.1.8) \quad w(t) = w_d(t) + w_f(t) + w_s(t) + w_m(t) + w_n(t)$$

where these individual components can be separately computed from

$$(6.1.9) \quad w_d(t) = \sqrt{G_a} a_{1,1}^1 s_{1,1}(t - \tau_{1,1}^1) \exp(-j\chi_{1,1}^1) \cdot c^{(1),(1)}(t)$$

$$(6.1.10) \quad w_f(t) = \sqrt{G_a} \sum_{k=2}^K a_{1,1}^k s_{1,1}(t - \tau_{1,1}^k) \exp(-j\chi_{1,1}^k) \cdot c^{(1),(1)}(t)$$

$$(6.1.11) \quad w_s(t) = \sqrt{G_a} \sum_{n=2}^N \sum_{k=1}^K a_{1,n}^k s_{1,n}(t - \tau_{1,n}^k) \exp(-j\chi_{1,n}^k) \cdot c^{(1),(1)}(t)$$

$$(6.1.12) \quad w_m(t) = \sqrt{G_a} \sum_{i=2}^I \sum_{n=2}^N \sum_{k=1}^K a_{i,n}^k s_{i,n}(t - \tau_{i,n}^k) \exp(-j\chi_{i,n}^k) \cdot c^{(1),(1)}(t)$$

$$(6.1.13) \quad w_n(t) = n_{out}(t) \cdot c^{(1),(1)}(t).$$

When proper alignment is achieved, every component of the desired signal, $w_d(t)$, should yield minimum and constant phase, as opposed to the other component, which should yield random and non-minimum phase. This ensures that during the integration phase the undesired terms average out as much as possible. The following section provides the necessary mathematical details to support these claims.

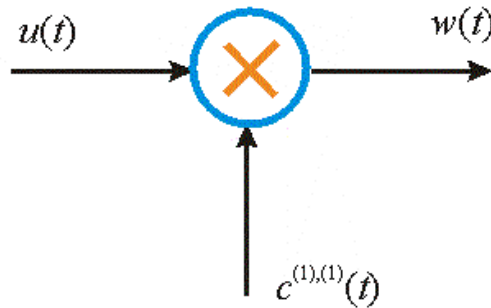


Figure 6.4 Correlation with the C code block diagram.

6.1.4 Integration after the Correlation with the Locally Generated C Code

Having discussed the correlation with the C code, the receiver will initially perform a non-coherent detection by integrating over only one C code repetition period, T_r , until the start of the $c^{(1),(1)}(t)$ sequence is determined. This process is known by the name “*acquisition mode*” (see Figure 6.1 and Figure 6.5).

When all subchannels have acquired the signal then the receiver enters the “*tracking mode*.” The outcome of this procedure determines the data symbol transition; hence, it enables the transition from the acquisition to the tracking mode.

The signal, $x(v)$, that describes the acquisition mode is given by

$$(6.1.14) \quad x(v) = x_d(v) + x_f(v) + x_s(v) + x_m(v) + x_n(v)$$

where every component of $x(v)$, for $j = \{d, f, s, m, n\}$ and v an integer, is obtained from

$$(6.1.15) \quad x_j(v) = \frac{1}{T_r} \int_0^{T_r} w_j(t) dt .$$

The integration of (6.1.15) requires the computation of the crosscorrelation function, $\phi_m^{(1,i),(1,n)}(\omega_{i,n}^e, \tau_{i,n}^k)$, which is computed by crosscorrelating the sequence $c^{(1),(1)}(t)$ with the function $s_{i,n}^{rs}(t - \tau_{i,n}^k)$ and the crosscorrelation function, $\gamma_m^{(1,i),(1,n)}(\omega_{i,n}^e, \tau_{i,n}^k)$, which is derived by crosscorrelating the sequence $c^{(1),(1)}(t)$ with the sequence $s_{i,n}^{rc}(t - \tau_{i,n}^k)$. The crosscorrelation functions, $\phi_m^{(1,i),(1,n)}(\omega_{i,n}^e, \tau_{i,n}^k)$ and $\gamma_m^{(1,i),(1,n)}(\omega_{i,n}^e, \tau_{i,n}^k)$ are defined as

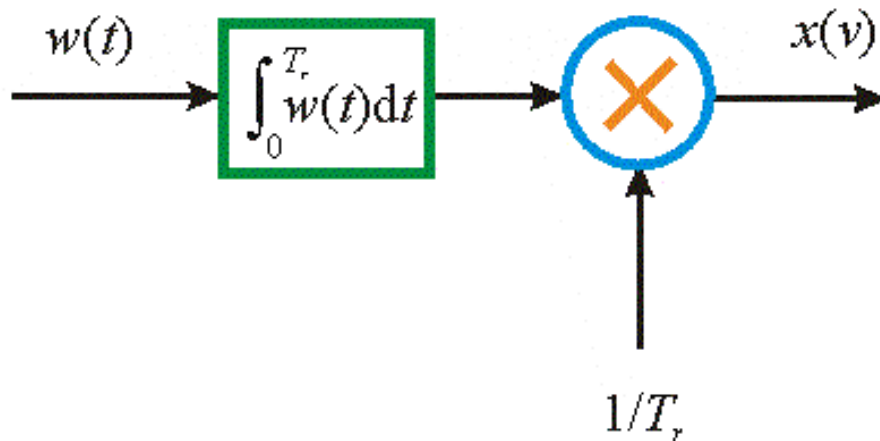


Figure 6.5 Integration of the C code block diagram.

$$(6.1.16) \quad \varphi_m^{(1,i),(1,n)}(\omega_{i,n}^e, \tau_{i,n}^k) = \int_0^{T_r} s_{i,n}^{rs}(t - \tau_{i,n}^k) c^{(1),(1)}(t) \exp(-j\chi_{i,n}^k) dt$$

$$(6.1.17) \quad \gamma_m^{(1,i),(1,n)}(\omega_{i,n}^e, \tau_{i,n}^k) = \int_0^{T_r} s_{i,n}^{rc}(t - \tau_{i,n}^k) c^{(1),(1)}(t) \exp(-j\chi_{i,n}^k) dt.$$

These crosscorrelation functions depend on several parameters, such as the time delay, $\tau_{i,n}^k$, the frequency error, $\omega_{i,n}^e$, the phase shift, $\phi_{i,n} + \theta_{i,n}^k$, and code properties, $c_j^{(1),(1)} c_{j-m}^{(i),(n)}$. Therefore, a better understanding of these parameters is necessary for a proper calculation of the crosscorrelation functions $\varphi_m^{(1,i),(1,n)}(\omega_{i,n}^e, \tau_{i,n}^k)$ and $\gamma_m^{(1,i),(1,n)}(\omega_{i,n}^e, \tau_{i,n}^k)$.

The time delay $\tau_{i,n}^k$ is a sum of multiple number of chipping periods and a random number between 0 and T_c ; and thus, it can be modeled as

$$(6.1.18) \quad \tau_{i,n}^k = mT_c + \delta\tau_{i,n}^k, \quad m \in \{0, 1, \dots\}, \quad \text{and } 0 \leq \delta\tau_{i,n}^k < T_c.$$

The parameter $\delta\tau$ is called the synchronization parameter and as such it must be taken into account when designing the tracking loops (see Chapter 2). Conceivably, the number m corresponding to the line-of-sight path (or the direct path) is smaller than the number m corresponding to each of the non line-of-sight paths because the line-of-sight path is shorter than each the non line-of-sight paths. Moreover, the number m corresponding to the line-of-sight path is directly linked to the pseudorange measurement accurate to the synchronization parameter, $\delta\tau$.

The frequency error, $\omega_{i,n}^e$, is assumed to be independent of any variable and much smaller than the chipping rate; hence, $f_{i,n}^e/R_c \cong 0$, where $f_{i,n}^e = \omega_{i,n}^e/2\pi$. This is not a bad assumption at this point, knowing that this variable depends on the design of tracking loops, which is secondary at this stage, because we are trying to provide an upper bound for the performance of the tracking loop(s).

The phase shift, $\phi_{i,n} + \theta_{i,n}^k$, and code properties, $c_j^{(1),(1)} c_{j-m}^{(i),(n)}$ are explored in that after some mathematical steps, the crosscorrelation functions $\varphi_m^{(1,i),(1,n)}(\omega_{i,n}^e, \tau_{i,n}^k)$ and $\gamma_m^{(1,i),(1,n)}(\omega_{i,n}^e, \tau_{i,n}^k)$ can be written as

$$(6.1.19) \quad \begin{aligned} \varphi_m^{(1,i),(1,n)}(\omega_{i,n}^e, \tau_{i,n}^k) &= \frac{\sqrt{2E_{i,n}^r}}{\omega_{i,n}^e} j\kappa_c(\omega_{i,n}^e, \delta\tau_{i,n}^k) \exp[-j(\phi_{i,n} + \theta_{i,n}^k)] \sum_{j=0}^{M_c-1} c_j^{(1),(1)} c_{j-m}^{(i),(n)} \\ &= j|\varphi_m^{(1,i),(1,n)}(\omega_{i,n}^e, \tau_{i,n}^k)| \exp[-j(\phi_{i,n} + \theta_{i,n}^k)] \end{aligned}$$

$$(6.1.20) \quad \begin{aligned} \gamma_m^{(1,i),(1,k)}(\omega_{i,n}^e, \tau_{i,n}^k) &= \frac{\sqrt{2E_{i,n}^r}}{\omega_{i,n}^e} \kappa_c(\omega_{i,n}^e, \delta\tau_{i,n}^k) \exp[-j(\phi_{i,n} + \theta_{i,n}^k)] \sum_{j=0}^{M_c-1} c_j^{(1),(1)} c_{j-m}^{(i),(n)} \\ &= |\gamma_m^{(1,i),(1,n)}(\omega_{i,n}^e, \tau_{i,n}^k)| \exp[-j(\phi_{i,n} + \theta_{i,n}^k)] = -j\varphi_m^{(1,i),(1,n)}(\omega_{i,n}^e, \tau_{i,n}^k) \end{aligned}$$

where

$$(6.1.21) \quad \kappa_c(\omega_{i,n}^e, \delta\tau_{i,n}^k) = \int_0^T \psi_c(t - \delta\tau_{i,n}^k) \exp[j\omega_{i,n}^e(t - \delta\tau_{i,n}^k)] dt \cong \Psi_c(f_{i,n}^e)(1 - R_c \delta\tau_{i,n}^k).$$

In light of expressions (6.1.19) and (6.1.20) the desired signal term is computed from

$$(6.1.22) \quad x_d(v) = \frac{a_1^1 \sqrt{2G_a}}{M} |\varphi_m^{(1,1),(1,1)}(\omega_{1,1}^e, \tau_{1,1}^k)| \exp[0.25\pi - j(\phi_{1,1} + \theta_{1,1}^k)].$$

The ISI component can be obtained from

$$(6.1.23) \quad x_f(v) = \frac{\sqrt{2G_a}}{M_c} \sum_{k=2}^K a_{1,1}^k |\varphi_m^{(1,1)}(\omega_{1,1}^e, \tau_{1,1}^k)| \exp[0.25\pi - j(\phi_{1,1} + \theta_{1,1}^k)].$$

The SAI component is written as

$$(6.1.24) \quad x_s(v) = \frac{\sqrt{2G_a}}{M} \sum_{n=2}^N \sum_{k=1}^K a_{i,n}^k |\varphi_m^{(1,i),(1,n)}(\omega_{i,n}^e, \tau_{i,n}^k)| \exp[0.25\pi - j(\phi_{i,n} + \theta_{i,n}^k)].$$

The MAI term is given by

$$(6.1.25) \quad x_m(v) = \frac{\sqrt{2G_a}}{M_c} \sum_{i=2}^I \sum_{n=2}^N \sum_{k=1}^K a_{i,n}^k |\varphi_m^{(1,i),(1,n)}(\omega_{i,n}^e, \tau_{i,n}^k)| \exp[0.25\pi - j(\phi_{i,n} + \theta_{i,n}^k)].$$

The AWGN term can be written as

$$(6.1.26) \quad x_n(v) = \frac{\sigma_{out} \eta(v)}{\sqrt{M}} = \sqrt{\frac{N_{out}}{2M}} \eta(v)$$

where \mathbf{h} is WGN(0,1).

During the acquisition process the receiver can only tell where the start of the C code sequence is. This is explained in §2.2.4.1 where we discuss the signal to interference plus noise ratio as a means of declaring whether the desired signal (i.e., the desired code $c^{(1),(1)}(t)$) is present or absent. Tracking the C code enables the receiver to track the

desired signals at the appropriate channels. Tracking the C code also enables the receiver to crudely measure the travel time between the appropriate transmitter and the receiver, which is the time difference between the start of the C sequence generated from the transmitter and the start of the C code sequence generated from the receiver accurate to the standard of the receiver's own clock. To the extent that acquisition is achieved reliably, the receiver enters the "*tracking phase*" which is the next topic of discussion as part of the time of arrival estimation.

6.1.5 Time of Arrival Estimation

After the integration process, every correlator dumps the clock offset from the receiver clock which is a crude estimate of the time of the arrival estimate. The signal coming from each pseudolite (or transmitter) contains N OFDM frequencies; and therefore, the receiver has N correlators per channel to track N PRN codes and determine N time of arrival, $\tau_{n,n}$, $n = \{1, 2, \dots, N\}$, from the i th transmitter to the receiver. A simple averaging can be used at this point to determine the estimate of the time of arrival from the i th transmitter to the receiver

$$(6.1.27) \quad \tau_i = \frac{1}{N} \sum_{n=1}^N \tau_{n,n}.$$

The mean and the variance of τ_i can be determined from [1]

$$(6.1.28) \quad E\{\tau_i\} = \frac{1}{N} \sum_{n=1}^N E\{\tau_{n,n}\}$$

$$(6.1.29) \quad V\{\tau_i\} = \frac{1}{N^2} \sum_{n=1}^N V\{\tau_{n,n}\}.$$

Therefore, a simple averaging can reduce the variance by N . More is said about the time of arrival estimate in §6.2.1.

6.1.6 Signal to Interference Plus Noise Ratio

Among several performance criteria, two are the most distinct, suitable, and familiar to spread-spectrum communication engineers: SINR and BEP (while the latter depends from SINR). First, SINR demonstrates whether the desired signal can be detected in the presence of noise, MAI, SAI, and ISI, treated in this subsection (see Chapter 2, §2.2.4.1). Second, depending on the distribution of the interference and noise, BEP provides a

measure to the quality of data detection (see §6.1.7), which differentiates one communication system from another.

The output signal conditional SINR conditioned on $\mathbf{a} \equiv \{a_{1,1}^1\} = a$ is defined as the ratio of the desired signal power over the sum of the output ISI, SAI, MAI, and AWGN signal power in accordance with the following expression

$$(6.1.30) \quad SINR = \frac{\text{Desired Power}}{(\text{ISI} + \text{SAI} + \text{MAI} + \text{AWGN})\text{Power}}.$$

To aid our analysis we make for following notation simplifications

$$(6.1.31) \quad \omega_e \equiv \omega_{1,1}^e, \quad \tau \equiv \tau_{1,1}^1, \quad \text{and} \quad \delta\tau \equiv \delta\tau_{1,1}^1.$$

Now the desired output signal power conditioned on a is determined from:

$$(6.1.32) \quad P_d^z(a, \omega_e, \tau) = \frac{G_a}{M^2} a \left| \varphi_m^{(1,1),(1,1)}(\omega_e, \tau) \right|^2.$$

Note the explicit dependency of the desired output signal power conditioned on a , on the C code synchronization parameter $\delta\tau$ (because of the misalignment of the code $c^{(1,1)}(t)$ generated from the receiver and the code $c^{(1,1)}(t - \tau)$ contained in the received signal), and on the frequency error, ω_e .

Note also that the proper alignment of the $c^{(1,1)}(t)$ code is achieved when $m = 0$; hence, eq. (6.1.32) can be written as

$$(6.1.33) \quad P_d^z(a, \omega_e, \tau) = \frac{G_a}{M^2} a \left| \varphi_0^{(1,1),(1,1)}(\omega_e, \delta\tau) \right|^2.$$

The power corresponding to the ISI term is given by

$$(6.1.34) \quad P_f^z(a, \omega_e, \tau_{1,1}^2, \dots, \tau_{1,1}^K) = G_a B g \sum_{k=2}^K \left| \varphi_m^{(1,1),(1,1)}(\omega_e, \tau_{1,1}^k) \right|^2$$

where $g = E \left\{ \alpha_{i,n}^k{}^2 | \mathbf{a} \right\}$ and $B = 1/M^2$. The argument given for the desired signal term, which shows the dependency of the ISI terms on the C code delay time, $\tau_{1,1}^k$, the frequency error, ω_e , can be applied here as well. Under the assumption that $\tau_{1,1}^k > T_c$ then the out-of-phase autocorrelation function, $\varphi_m^{(1,1),(1,1)}(\omega_e, \tau_{1,1}^k)$, satisfies the following inequality

$$(6.1.35) \quad \left| \varphi_m^{(1,1),(1,1)}(\omega_e, \tau_{1,1}^k) \right| \leq \varphi_a^{(1,1),(1,1)}(\omega_e, \delta\tau)$$

where $\varphi_a^{(1,1),(1,1)}(\omega_e, \delta\tau)$ is the peak out-of-phase autocorrelation magnitude and $\delta\tau = \text{un}[0, T_c)$. Substituting the above equation into (6.1.34) produces

$$(6.1.36) \quad P_f^z(a, \omega_e, \tau) \leq G_a Bg \tilde{K} \varphi_a^{(1,1),(1,1)}(\omega_e, \delta\tau)^2$$

where $\tilde{K} = K - 1$.

The power corresponding to the SAI term can be written as

$$(6.1.37) \quad P_s^z(a, \Lambda_N) = G_a Bg \sum_{n=2}^N \sum_{k=1}^K \left| \varphi_m^{(1,1),(1,n)}(\omega_{1,n}^e, \tau_{1,n}^k) \right|^2$$

where $\Lambda_N = \{\tau_{1,2}, \dots, \tau_{1,N}, \omega_{1,1}^e, \dots, \omega_{1,N}^e\}^t$. Under the assumption that $\tau_{1,n}^k > T_c$ then the crosscorrelation function, $\varphi_m^{(1,1),(1,n)}(\omega_{1,n}^e, \tau_{1,n}^k)$, satisfies the following inequality

$$(6.1.38) \quad \left| \varphi_m^{(1,1),(1,n)}(\omega_{1,n}^e, \tau_{1,n}^k) \right| \leq \varphi_c^{(1,1),(1,n)}(\omega_{1,n}^e, \delta\tau_{1,n})$$

where $\varphi_c^{(1,1),(1,n)}(\omega_{1,n}^e, \delta\tau_{1,n})$ is the peak crosscorrelation magnitude of $\varphi_m^{(1,1),(1,n)}(\omega_{1,n}^e, \tau_{1,n}^k)$ and $\delta\tau_{1,n} = \text{un}[0, T_c)$.

If the misalignment of the code $c^{(1),(1)}(t)$ generated from the receiver and the code $c^{(1),(n)}(t - \tau_{1,n})$ contained in the received signal, for $n = \{2, \dots, N\}$, can be expressed with the help of the vector, $\Lambda_N = \{\tau_{1,1}, \dots, \tau_{1,N}, \omega_{1,1}^e, \dots, \omega_{1,N}^e\}^t$, then the total receiver power of the SAI terms will show this dependency.

Similarly, after some algebra and under the assumption that $\tau_{1,n}^k > T_c$ the power expression of the SAI terms is simplified to

$$(6.1.39) \quad P_s^z(a, \Lambda_N) \leq G_a Bg K \sum_{n=2}^N \varphi_c^{(1,1),(1,n)}(\omega_{1,n}^e, \delta\tau_{1,n})^2.$$

The power corresponding to the MAI term can be written as

$$(6.1.40) \quad P_m^z(a, \Lambda) = G_a Bg \sum_{i=2}^I \sum_{n=1}^N \sum_{k=1}^K \left| \varphi_m^{(1,i),(1,n)}(\omega_{i,n}^e, \tau_{i,n}^k) \right|^2 \\ = G_a Bg \sum_{i=2}^I \sum_{k=1}^K \left| \varphi_m^{(1,i),(1,1)}(\omega_{i,1}^e, \tau_{i,1}^k) \right|^2 + G_a Bg \sum_{i=2}^I \sum_{n=2}^N \sum_{k=1}^K \left| \varphi_m^{(1,i),(1,n)}(\omega_{i,n}^e, \tau_{i,n}^k) \right|^2$$

where $\Lambda = \{\tau_{i,1}, \dots, \tau_{i,N}, \omega_{i,1}^e, \dots, \omega_{i,N}^e\}^t$. Under the assumption that $\tau_{i,n}^k > T_c$ then the crosscorrelation function, $\varphi_m^{(1,i),(1,n)}(\omega_{i,n}^e, \tau_{i,n}^k)$, satisfies the following inequality

$$(6.1.41) \quad \left| \varphi_m^{(1,i),(1,n)}(\omega_{i,n}^e, \tau_{i,n}^k) \right| \leq \varphi_c^{(1,i),(1,n)}(\omega_{i,n}^e, \delta\tau_{i,n}), \quad n > 1$$

$$(6.1.42) \quad \left| \varphi_m^{(1,i),(1,1)}(\omega_{i,1}^e, \tau_{i,1}^k) \right| \leq \varphi_a^{(1,i),(1,1)}(\omega_{i,1}^e, \delta\tau_{i,1}), \quad n = 1$$

where $\varphi_c^{(1,i),(1,n)}(\omega_{i,n}^e, \delta\tau_{i,n})$ is the peak crosscorrelation magnitude of $\varphi_m^{(1,i),(1,n)}(\omega_{i,n}^e, \tau_{i,n}^k)$, for $\delta\tau_{i,n} = \text{un}[0, T_c)$, and $\varphi_c^{(1,i),(1,1)}(\omega_{i,1}^e, \delta\tau_{i,1})$ is the out-of-phase autocorrelation peak of $\varphi_m^{(1,i),(1,1)}(\omega_{i,1}^e, \tau_{i,1}^k)$.

If the misalignments of the code $c^{(1),(1)}(t)$ generated from the receiver and the code $c^{(i),(n)}(t - \tau_{i,n})$ contained in the received signal, for $i = \{2, \dots, I\}$ and $n = \{2, \dots, N\}$, can be expressed with the help of the vector $\Lambda = \{\tau_{i,2}, \dots, \tau_{i,N}, \omega_{i,1}^e, \dots, \omega_{i,N}^e\}^t$, then the total receiver power of the MAI term will show this dependency.

Similarly, after some algebra and under the assumption that $\tau_{i,n}^k > T_c$ the power expression of the MAI term is simplified to

$$(6.1.43) \quad P_m^z(a, \Lambda) \leq G_a B g K \left(\sum_{i=2}^I \sum_{n=2}^N \varphi_c^{(1,i),(1,n)}(\omega_{i,n}^e, \delta\tau_{i,n})^2 + \sum_{i=2}^I \varphi_a^{(1,i),(1,1)}(\omega_{i,1}^e, \delta\tau_{i,1})^2 \right).$$

The power corresponding to the AWGN terms is computed from

$$(6.1.44) \quad P_n^z(a) = \frac{\sigma_{out}^2}{M} = \frac{N_{out}}{2M}.$$

The output signal SINR conditioned on a is written as

$$(6.1.45) \quad \text{SINR}(a, \tau, \Lambda_N, \Lambda) = \frac{P_d^z(a, \tau)}{P_f^z(a, \tau) + P_s^z(a, \Lambda_N) + P_m^z(a, \Lambda) + P_n^z(a)} = \frac{N_{\text{SINR}}}{D_{\text{SINR}}}.$$

Substituting (6.1.33), (6.1.36), (6.1.39), (6.1.43), and (6.1.44) into (6.1.45) produces

$$(6.1.46) \quad N_{\text{SINR}} = a^2 B E_c^{-1} \varphi_0^{(1,1),(1,1)}(\omega_e, \delta\tau)^2$$

$$(6.1.47) \quad D_{\text{SINR}} \leq \left\{ B g \tilde{K} E_c^{-1} \varphi_a^{(1,1),(1,1)}(\omega_e, \delta\tau)^2 + B g K E_c^{-1} \sum_{n=2}^N \varphi_c^{(1,1),(1,n)}(\omega_{1,n}^e, \delta\tau_{1,n})^2 \right. \\ \left. + B g K E_c^{-1} \left[\sum_{i=2}^I \sum_{n=2}^N \varphi_c^{(1,i),(1,n)}(\omega_{i,n}^e, \delta\tau_{i,n})^2 + \sum_{i=2}^I \varphi_c^{(1,i),(1,1)}(\omega_{i,1}^e, \delta\tau_{i,1})^2 \right] + 0.5 F_n (E_b / N_{in})^{-1} \right\}$$

where $E_b = M E_c$ is the total energy per bit. Note the disappearance of the amplifier gain, G_a , from the computation of the SINR.

Assuming that $p_{i,n}(t) = G_t G_r Q_{i,n}(t)$ is not changing during the data bit transition and that the C code is a Gold sequence [2] then the SINR expression, (6.1.46) and (6.1.47), can be further simplified as

$$(6.1.48) \quad N_{SINR} \geq 2a^2 \frac{p_{1,1}(t) \kappa_c(\omega_e, \delta\tau)^2}{|\omega_e|^2}$$

$$(6.1.49) \quad D_{SINR} \leq \frac{8p_{1,1}(t)g\tilde{K}\kappa_c(\omega_e, \delta\tau)^2}{M_c|\omega_e|^2} + \frac{8gK}{M_c} \sum_{n=2}^N \frac{p_{1,n}(t) \kappa_c(\omega_{1,n}^e, \delta\tau_{1,n})^2}{|\omega_{1,n}^e|^2} \\ + \frac{8gK}{M} \sum_{i=2}^I \sum_{n=1}^N \frac{p_{i,n}(t) \kappa_c(\omega_{i,n}^e, \delta\tau_{i,n})^2}{|\omega_{i,n}^e|^2} + \frac{F_n}{2} (E_b/N_{in})^{-1}.$$

Assuming that the C code is a Kasami sequence [2] then the SINR expression, (6.1.46) and (6.1.47), can be further simplified as

$$(6.1.50) \quad N_{SINR} \geq 2a^2 \frac{p_{1,1}(t) \kappa_c(\omega_e, \delta\tau)^2}{|\omega_e|^2}$$

$$(6.1.51) \quad D_{SINR} \leq \frac{2p_{1,1}(t)g\tilde{K}\kappa_c(\omega_e, \delta\tau)^2}{M_c|\omega_e|^2} + \frac{2gK}{M_c} \sum_{n=2}^N \frac{p_{1,n}(t) \kappa_c(\omega_{1,n}^e, \delta\tau_{1,n})^2}{|\omega_{1,n}^e|^2} \\ + \frac{2gK}{M_c} \sum_{i=2}^I \sum_{n=1}^N \frac{p_{i,n}(t) \kappa_c(\omega_{i,n}^e, \delta\tau_{i,n})^2}{|\omega_{i,n}^e|^2} + \frac{F_n}{2} (E_b/N_{in})^{-1}.$$

The lower bound expressions on the SINR are particularly useful, because they provide an upper bound expression on BEP (or BER see §6.1.7) and on the receiver's detector degradation ratio, which is the inverse of the SINR and which is, to some extent, a direct measure of the receiver's code and phase error (see §6.2.1 and §6.2.2).

6.1.7 Bit Error Probability

Assuming that the interference is Gaussian distributed we can obtain the expression for BEP conditioned on a and to the extent that this is a good approximation, BEP reads

$$(6.1.52) \quad BEP(a, \tau, \Lambda, \xi) = Q\left(\sqrt{SINR(a, \tau, \Lambda, \xi)}\right)$$

where $Q(x) = (2\pi)^{-1/2} \int_x^\infty e^{-t^2/2} dt$.

The unconditional $BEP(\tau, \Lambda, \xi)$ is obtained by integrating the conditional $BEP(a, \tau, \Lambda, \xi)$ with respect to the density function of a , $p(a) = a \exp(-a^2/2)U(a)$ (see Appendix A of [3]), which reads

$$(6.1.53) \quad BEP(\tau, \Lambda, \xi) \cong 0.5 \left[1 - \left(\frac{\sqrt{\mu}}{\sqrt{\mu} + 1} \right)^{\exp[-\alpha(\sqrt{\mu})]} \right]$$

where $\mu \equiv \frac{1}{2} E\{SINR(a, \tau, \Lambda, \xi)\}$ and the expectation is performed with respect to a .

Knowing that the function BEP given by (6.1.53) is monotonically decreasing with respect to μ then the largest BEP corresponds to the smallest μ ; hence, the upper BEP bound can be obtained from

$$(6.1.54) \quad BEP_{\max}(\tau, \Lambda, \xi) \cong 0.5 \left[1 - \left(\frac{\sqrt{\mu_{\min}}}{\sqrt{\mu_{\min}} + 1} \right)^{\exp[-\alpha(\sqrt{\mu_{\min}})]} \right]$$

where $\mu_{\min} \equiv \frac{1}{2} E\{SINR_{\min}(a, \tau, \Lambda, \xi)\}$ and the expectation is performed with respect to a .

Equation (6.1.54) is particularly useful for hardware implementation because it provides a closed form expression that can be implemented employing any digital signal processor or the state of the art microprocessor design, which utilizes either fixed or floating-point arithmetic. Nevertheless, for our theoretical performance evaluation we can employ the accurate expression from MATLAB[®].

Thus, we have concluded the analytical evaluation of the receiver performance based only on tracking performance of the C code. We have not considered however, the performance of the Delay Lock Loops, Frequency Lock Loops, and Phase Lock Loops, but we have provided an upper bound on time, frequency, and phase error and synchronization. The actual design of the Delay Lock Loops, Frequency Lock Loops, and Phase Lock Loops is left for future studies and publications.

6.2 Navigation Performance Analyses

Thus far we have concerned the communication performance analyses as a means of assessing the SINR and BEP. Next, our analyses include the navigation performance;

namely, the receiver's code error (see §6.2.1) and the receiver's phase error (see §6.2.2), which influence directly the receiver's position and velocity error.

6.2.1 Receiver's Code Error

An accurate estimate of the receiver's code (or pseudorange) error can only be obtained from analyzing the delay lock loop suitable for the system under investigation. For a discussion on delay locked loops the reader is referred to Chapter 2 (see §2.2.4.2.3), and [4]-[6]. For the purposes of our investigation we only look at a simplified expression on the receiver's code error, which is sufficient to provide a preliminary estimate and thus serve as a baseline for the future design of a delay lock loop.

According to Spilker [4], a simplified expression for the receiver's code error can be obtained as follows

$$(6.2.1) \quad \mathbf{s}_c = \frac{cT_c}{\sqrt{SINR}} \text{ (m)}.$$

After the simple averaging the variance on receiver's code error is reduced by N (see equation (6.1.29)); thus, we can write

$$(6.2.2) \quad \sigma_c = \frac{cT_c}{\sqrt{N \cdot SINR}} \text{ (m)}.$$

For purposes of our analysis we are interested in computing an upper bound expression for the receiver's code error. Since σ_c is a monotonically decreasing with respect to $SINR$ then $SINR_{\min}$ produces $\sigma_{c\max}$; therefore, in our numerical assessment results we compute $\sigma_{c\max}$ instead of σ_c .

6.2.2 Receiver's Phase Error

An accurate estimate of the receiver's phase error can only be obtained from analyzing frequency lock loops and phase lock loops suitable for our system under investigation. For a discussion on frequency lock loops and phase lock loops the reader is referred to Chapter 2 (see §2.2.4.2.4 and §2.2.4.2.5) [4]-[6]. For the purposes of our investigation we only look at a simplified expression on the receiver's phase error, which is sufficient to provide a preliminary estimate and thus serve as a baseline for the future design of frequency lock loops and phase lock loops.

Similarly, according to Spilker [4], a simplified expression for the receiver's phase error can be obtained as follows

$$(6.2.3) \quad \sigma_{\phi} = \frac{c}{2\pi f_i \sqrt{SINR}} \text{ (m)}.$$

After the simple averaging the variance on receiver's phase error is reduced by N (see equation (6.1.29)); thus, we can write

$$(6.2.4) \quad \sigma_{\phi} = \frac{c}{2\pi f_i \sqrt{N \cdot SINR}} \text{ (m)}.$$

For analysis purposes we are interested in computing an upper bound expression for the receiver's phase error. Since σ_{ϕ} is a monotonically decreasing with respect to $SINR$ then $SINR_{\min}$ produces $\sigma_{\phi_{\max}}$; therefore, in our numerical assessment results we compute $\sigma_{\phi_{\max}}$ instead of σ_{ϕ} .

6.3 Quantitative Assessment

System design parameters; such as the signal to noise ratio, E_b/N_{in} , receiver's noise figure, F_n , number of transmitters, I , number of paths, K , synchronization parameter, $\delta\tau$, and frequency error, f_e , on the upper bound of the BEP and receiver's pseudorange and phase error are exploited in our numerical assessment.

This section includes the selection of parameters in §6.3.1 and the quantitative requirements on the theoretical performance in §6.3.2.

6.3.1 Selection of Parameters

The system geometry is shown in Figure 6.6. As shown in the figure there are 10 transmitters and one receiver. More discussion on the system geometry is provided later in the section.

The selection of these parameters is based on the initial work performed in Chapter 5 and it includes the transmitter parameters, the channel parameters, and the receiver parameters.

The transmitter parameters are selected from:

- The number of transmitters is $I = 10$.
- The number of OFDM frequencies per transmitter is $N = 10$.

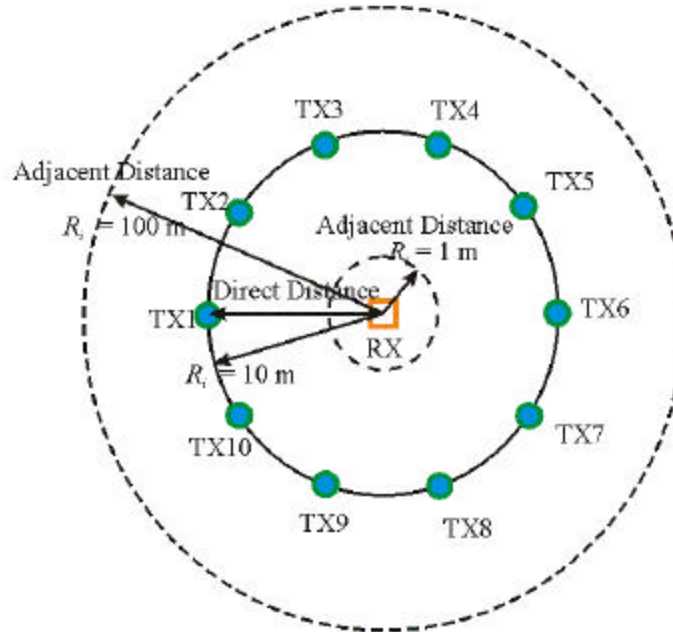


Figure 6.6 Transmitter receiver geometry of an OFDM/CDMA/FDMA indoor geolocation system.

- The difference between the first and the last OFDM frequency is $B = 1$ MHz.
- The 1st OFDM frequency of the desired signal (coming from the 1st transmitter) is 3.1875 GHz.
- The chipping rate $R_c = 127.5$ MBPS and thus the C code repetition rate is $R_r = 0.5$ MBPS.
- The frequency of the adjacent signal (signal coming from other transmitters) is $f_{i,n} = f_1 + 0.5(i-1)R_c + (n-1)B/N$, $\forall n \in \{2, \dots, N\}$, and $\forall i \in \{2, \dots, I\}$.
- The C code length $M_c = 255$ bits.
- The data rate for this system is $N \cdot R_r = 5$ MBPS.
- The transmitting antenna gain is $G_t = 10$ dB.

The channel parameters are selected as follows:

- The reference path loss is $Q_0 = -42.275$ dB. This reference path loss corresponds to $R = 1$ m and $L_1 = 1575.42$ MHz.
- The slope for the path loss function vs. transmitter receiver distance is $n = 3.5$.
- The slope of the path loss function vs. operating frequency is $m = 2.01$.
- The standard deviation of the normal distributed noise, which represents unaccounted factors of the path loss model, is 0.5.

- The number of paths including the line of sight path is 10.
- The average attenuation $a = 0.5$ and $g = 0.25$.
- The roll-off factor for the raised cosine filter is $\delta = 0.5$.

The receiver parameters are selected as follows:

- Doppler shift between the receiver and the i th transmitter is $i*0.1$ m/s.
- The noise figure, $F_n = 10$, and the calibration temperature is $T_0 = 290$ K.
- The IF filter bandwidth, $B_n = 30$ MHz.
- The synchronization parameter $\delta\tau$ for the c code is $\text{un}[0, T_c)$ nsec. The mean of $\delta\tau$ is given by $\bar{t}_c = 0.5T_c$. With the help of \bar{t}_c we have selected two distinct values for the synchronization parameter $\delta\tau = \{0, \bar{t}_c\}$ which correspond to perfect and average synchronization respectively.
- Frequency error is $f_e = 0.05$ Hz.
- The receiving antenna gain is $G_r = 10$ dB.

6.3.2 Quantitative Requirements on Theoretical Performance

Quantitative requirements on theoretical performance are given in terms of the quantitative requirements on the communication performance (see §6.3.2.1) and quantitative requirements on navigation performance (see §6.3.2.2).

6.3.2.1 Quantitative Requirements on Communication Performance

The BEP provides a means of assessing the communication performance of a DSSS/OFDM/CDMA/FDMA indoor geolocation system. The BEP is given as a function of six important design parameters such as ideal signal to noise ratio, E_b/N_0 (dB), relative adjacent distance, R_i (m), number of transmitters, I , number of paths, K , synchronization parameter, $\delta\tau$ (nsec), and frequency error, f_e , (Hz). Figure 6.7 illustrates the synchronization coefficient, κ (see equation (6.1.21)), as a function of the synchronization parameter, $\delta\tau$. As indicated in the figure perfect synchronization corresponds to $\kappa = 1$ and average synchronization corresponds to $\kappa = 0.5$.

Figure 6.8 depicts the BEP as a function of E_b/N_0 (dB) using (a) Gold and (b) Kasami sequences for a DSSS/OFDM/CDMA/FDMA indoor geolocation system for average and perfect synchronization.

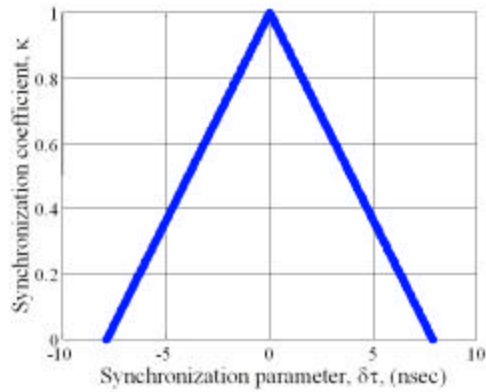


Figure 6.7 The synchronization coefficient vs. synchronization parameter, $\delta\tau$, (nsec).

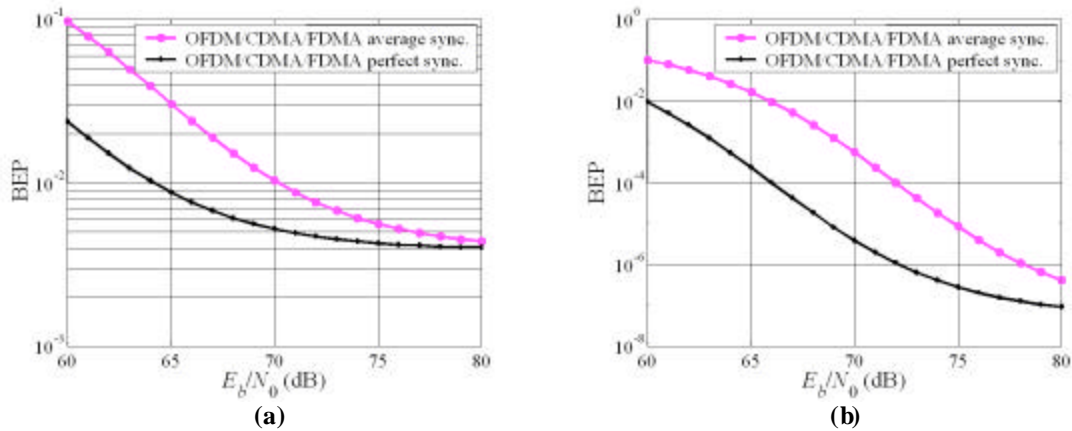


Figure 6.8 BEP vs. ideal SNR, E_b/N_0 (dB), for (a) Gold and (b) Kasami sequences.

We note that for this system with Gold/Kasami sequences as E_b/N_0 increases from 60 to 80 dB the BEP for average synchronization decreases from 0.1/0.1 to $4e-3/4e-6$ and the BEP for perfect synchronization decreases from 0.02/1e-2 to $4e-3/1e-7$. Clearly, a DSSS/CDMA indoor geolocation with Kasami sequences can achieve a BEP almost 10 or more times as small as the BEP of the same system with Gold sequences.

Figure 6.9 depicts the BEP as a function of relative adjacent distance, R_i (m), using (a) Gold and (b) Kasami sequences for a DSSS/OFDM/CDMA/FDMA indoor geolocation system for average and perfect synchronization. For this experiment, in addition to the parameters shown above, E_b/N_0 is equal to 70 (dB). We noted that a DSSS/CDMA indoor geolocation system with Kasami or Gold sequences **could not** overcome the *near-far* effect (see Chapters 2 and 5). We also noted that a DSSS/CDMA/FDMA indoor geolocation with Kasami or Gold sequences **could** overcome the *near-far* effect.

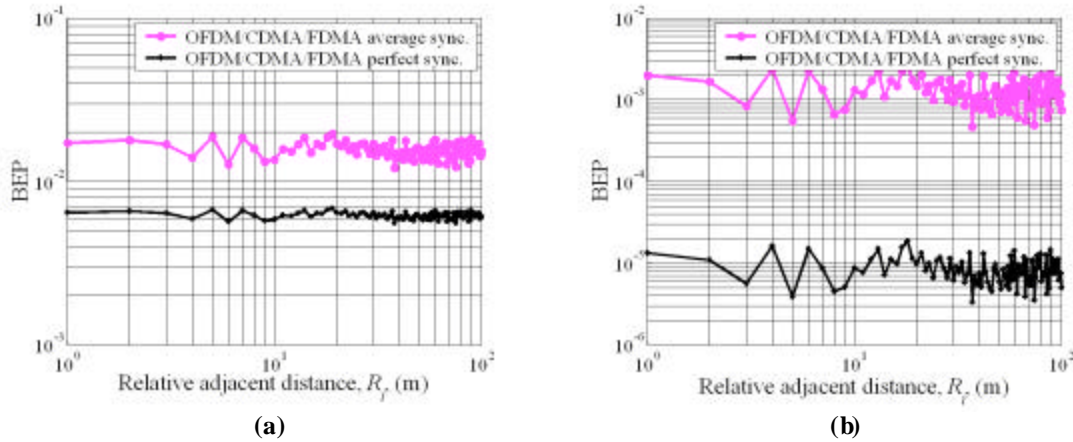


Figure 6.9 BEP vs. relative adjacent distance, R_i (m), for (a) Gold and (b) Kasami sequences.

Now for a DSSS/OFFDM/CDMA/FDMA indoor geolocation system with Gold/Kasami sequences as R_i increases from 1 to 100 m the BEP for average synchronization remains almost unchanged at $1.5e-2/1.4e-3$ (see Figure 6.9) and the BEP for perfect synchronization remains almost unchanged $6e-3/7e-6$. We remind the reader that these results are without the forward error correction encoding which means that once the forward error correction is employed then the BEP is improved by a factor of a thousand to one hundred thousand as indicated in Appendix C.

Nevertheless, the poor communication performance of a DSSS/OFFDM/CDMA/FDMA indoor geolocation system is not due to the *near-far* effect but due to short integration time and short code length. To some extent we have sacrificed communication performance to achieve high data rate. As a conclusion, a DSSS/OFFDM/CDMA/FDMA indoor geolocation system does not suffer from the *near-far* effect. The poor communication performance can be ameliorated by means of a forward error correction encoding.

Figure 6.10 depicts the BEP as a function of the number of transmitters, I , using (a) Gold and (b) Kasami sequences for a DSSS/OFFDM/CDMA/FDMA indoor geolocation system for average and perfect synchronization. For this experiment, in addition to the parameters shown above, the E_b/N_0 is equal to 70 (dB). Also the relative distance between the 1st transmitter and receiver is 10 m and the relative distance between each adjacent transmitter and the receiver is 10 m also. We noted that a DSSS/CDMA indoor

geolocation with Kasami or Gold sequences **could** not be recommended when more than 10 transmitters are required.

We also noted that a DSSS/CDMA/FDMA indoor geolocation with Kasami or Gold sequences **could** be used when more than 32 transmitters are required. Now, for a DSSS/OFFDM/CDMA/FDMA indoor geolocation system with Gold/Kasami sequences as I increases from 2 to 32 the BEP for average synchronization remains almost unchanged at $1.4e-2/1.3e-3$ and the BEP for perfect synchronization remains almost unchanged $6e-3/9e-6$.

The poor performance of this system is not due to the number of transmitters but due to the short integration time and short code length. If forward error correction encoding were utilized then the system communication performance would be improved drastically. Therefore, the number of transmitters does not represent any concern for the communication performance of this system.

Figure 6.11 illustrates the BEP as a function of the number of paths, K , using (a) Gold and (b) Kasami sequences for a DSSS/OFFDM/CDMA/FDMA indoor geolocation system for average and perfect synchronization. For this experiment, in addition to the parameters shown above, the E_b/N_0 is equal to 70 (dB). The relative distance between the 1st transmitter and receiver is 10 m and the relative distance between each adjacent transmitter and the receiver is 10 m also. The number of transmitters is equal to 10. We noted that a DSSS/CDMA indoor geolocation system with Kasami or Gold sequences **could not** be used when an indoor channel contains more than 10 paths.

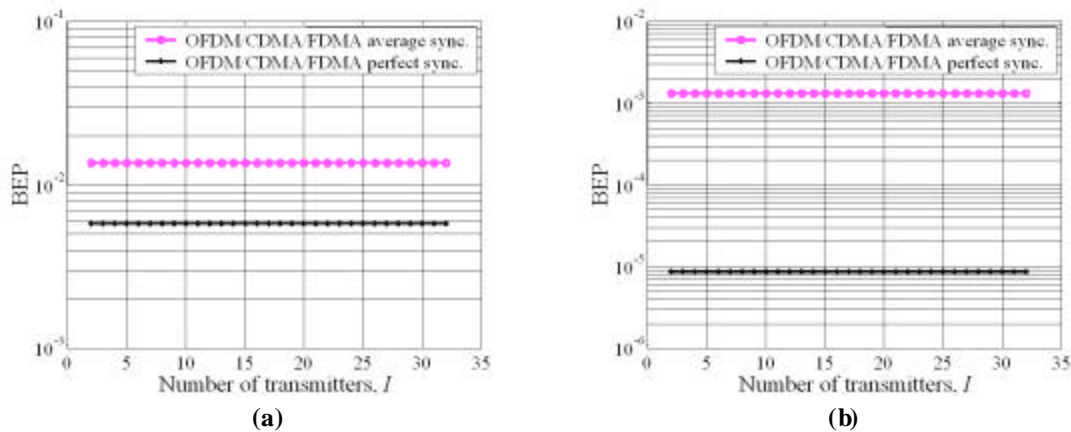


Figure 6.10 BEP vs. number of transmitters, I , for (a) Gold and (b) Kasami sequences.

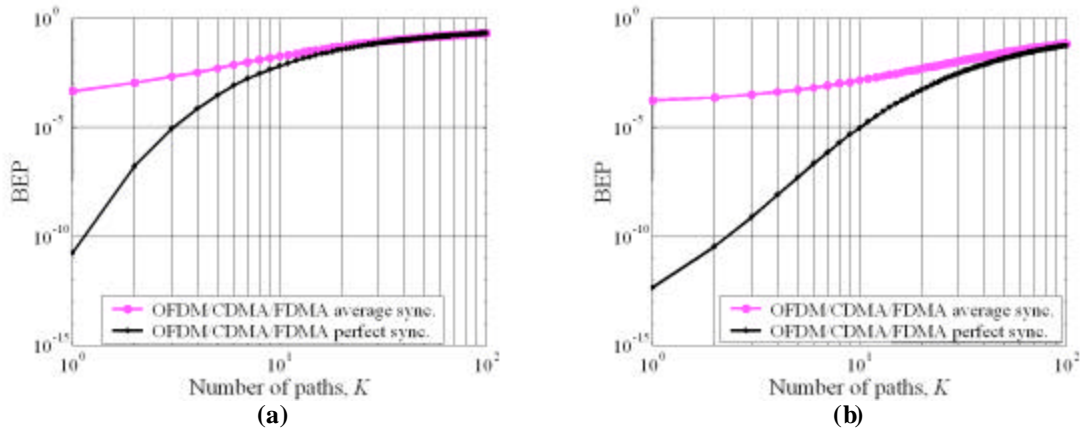


Figure 6.11 BEP vs. number paths, K , for (a) Gold and (b) Kasami sequences.

We also noted that a DSSS/CDMA/FDMA indoor geolocation with Kasami or Gold sequences **could** be used when an indoor channel contains more than 10 paths. Now for an OFDM/CDMA/FDMA indoor geolocation system with Gold/Kasami sequences as K increases from 1 to 100 the BEP for average synchronization increases from $5e-4/2e-4$ to $0.5/0.5$ and the BEP for perfect synchronization increases from $1e-11/5e-13$ to $0.5/0.5$.

Clearly, any system is very susceptible to the number of paths, K . Although the system with Kasami sequences outperforms the system with Gold sequences by a factor of 5 for $K = 10$ both systems require a forward error correction encoding to improve the communication performance. Therefore, a DSSS/OFDM/CDMA/FDMA indoor geolocation system with forward error correction encoding can be employed when the number of resolvable paths is smaller than or equal to 10.

Figure 6.12 presents the BEP as a function of the synchronization parameter, $\delta\tau$ (nsec), using (a) Gold and (b) Kasami sequences for a DSSS/OFDM/CDMA/FDMA indoor geolocation system. For this experiment, in addition to the parameters shown above, the E_b/N_0 is equal to 70 (dB). The relative distance between the 1st transmitter and receiver is 10 m and the relative distance between each adjacent transmitter and the receiver is 10 m also. The number of transmitters is equal to 10 and the number of paths is equal to 10.

We noted that both a DSSS/CDMA and a DSSS/CDMA/FDMA indoor geolocation system with Gold/Kasami sequences **could** be used when $\delta\tau < 5$ nsec. In Figure 6.12 we

note that for a DSSS/OFDM/CDMA/FDMA indoor geolocation system with Gold/Kasami sequences as $\delta\tau$ increases from 0 to 8 nsec the BEP increases from $5e-3/1e-6$ to $5e-1/4e-1$. A normal operation of DSSS/OFDM/CDMA/FDMA indoor geolocation system with forward error correction encoding **would require** $\delta\tau < 4$ nsec.

Figure 6.13 presents the BEP as a function of the frequency error, f_e (Hz), using (a) Gold and (b) Kasami sequences for a DSSS/OFDM/CDMA/FDMA indoor geolocation system for average synchronization. For this experiment, in addition to the parameters shown above, the E_b/N_0 is equal to 70 (dB). The relative distance between the transmitter and receiver is 10 m and the relative distance between the adjacent transmitters and the receiver is 10 m. The number of transmitters is equal to 10, the number of paths is equal to 10, and $\delta\tau = 0.5 * T_c = 4$ nsec.

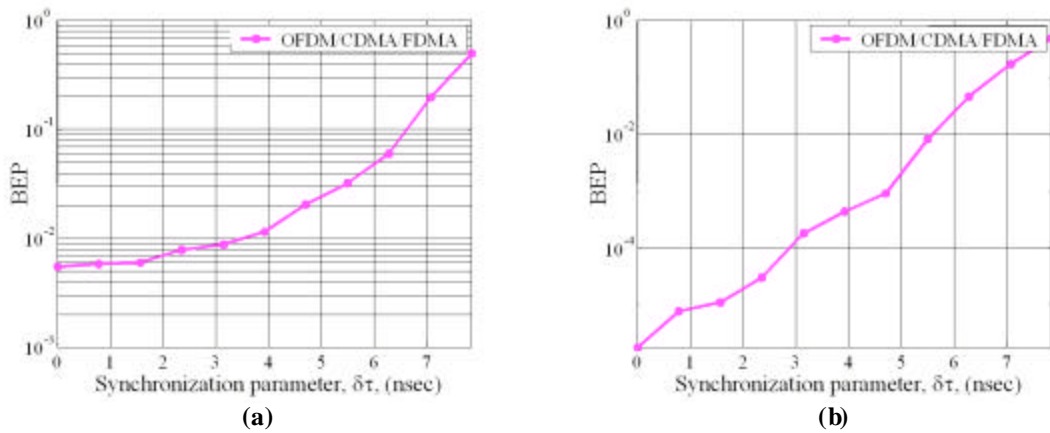


Figure 6.12 BEP vs. synchronization parameter, dt, for (a) Gold and (b) Kasami sequences.

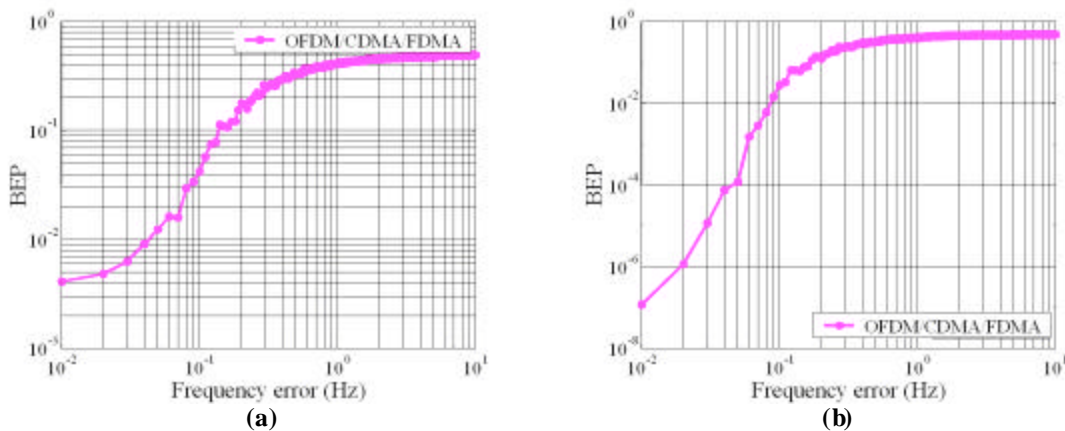


Figure 6.13 BEP vs. frequency error (Hz) for (a) Gold and (b) Kasami sequences.

We noted that a DSSS/CDMA indoor geolocation system with Kasami or Gold sequences **would require** a frequency error smaller than 0.01 Hz. We also noted that a DSSS/CDMA/FDMA indoor geolocation system with Kasami or Gold sequences **would require** a frequency error smaller than 0.1 Hz. Here we note that for a DSSS/OFDM/CDMA/FDMA indoor geolocation system with Gold/Kasami sequences as f_e increases from 0.01 to 10 Hz the BEP increases from $4e-3/1e-7$ to 0.5/0.5.

Again, a DSSS/OFDM/CDMA/FDMA indoor geolocation system is very susceptible to any frequency error changes. If the frequency error is smaller than 0.1 Hz and if forward error correction encoding is utilized then a DSSS/OFDM/CDMA/FDMA indoor geolocation system can be successfully employed to achieve high communication performance.

6.3.2.2 Quantitative Requirements on Navigation Performance

The pseudorange error and the phase error were a means of assessing the navigation performance of a DSSS/CDMA and DSSS/CDMA/FDMA indoor geolocation system as discussed in Chapter 5. The pseudorange error and phase error are given as a function of six important design parameters such as the ideal signal to noise ratio, E_b/N_0 (dB), the relative adjacent distance, R_i (m), number of transmitters, I , number of paths, K , the synchronization parameter, $\delta\tau$ (nsec), and the frequency error, f_e , (Hz).

Figure 6.14 depicts the pseudorange error as a function of E_b/N_0 (dB) using (a) Gold and (b) Kasami sequences for a DSSS/OFDM/CDMA/FDMA indoor geolocation system for average and perfect synchronization.

We note that for this system with Gold/Kasami sequences as E_b/N_0 increases from 60 to 80 dB the pseudorange error for average synchronization decreases from 80/72 cm to 40/22 cm and the pseudorange error for perfect synchronization decreases from 55/40 cm to 40/22 cm.

Clearly, a DSSS/OFDM/CDMA/FDMA indoor geolocation with Kasami sequences can achieve a pseudorange error almost 2 times as small as the same system with Gold sequences. Moreover, the pseudorange error of a DSSS/OFDM/CDMA/FDMA indoor geolocation system is 10 or more times smaller than the pseudorange error of either a DSSS/CDMA or a DSSS/CDMA/FDMA indoor geolocation system. We note that this performance is achieved due to the expense of high system complexity.

Figure 6.15 depicts the pseudorange error as a function of relative adjacent distance, R_i (m), using (a) Gold and (b) Kasami sequences for a DSSS/OFFDM/CDMA/FDMA indoor geolocation system for average and perfect synchronization. For this experiment, in addition to the parameters shown above, E_b/N_0 is equal to 70 (dB).

We noted in Chapter 5 that a DSSS/CDMA indoor geolocation with Kasami or Gold sequences **cannot** overcome the *near-far* effect. We also noted that a DSSS/CDMA/FDMA indoor geolocation with Kasami or Gold sequences **could** overcome the *near-far* effect. We note that for a DSSS/OFFDM/CDMA/FDMA indoor geolocation system with Gold/Kasami sequences as R_i increases from 1 to 100 m the pseudorange error for average synchronization remains almost unchanged at 50/35 cm and the pseudorange error for perfect synchronization remains almost unchanged 42/24 cm.

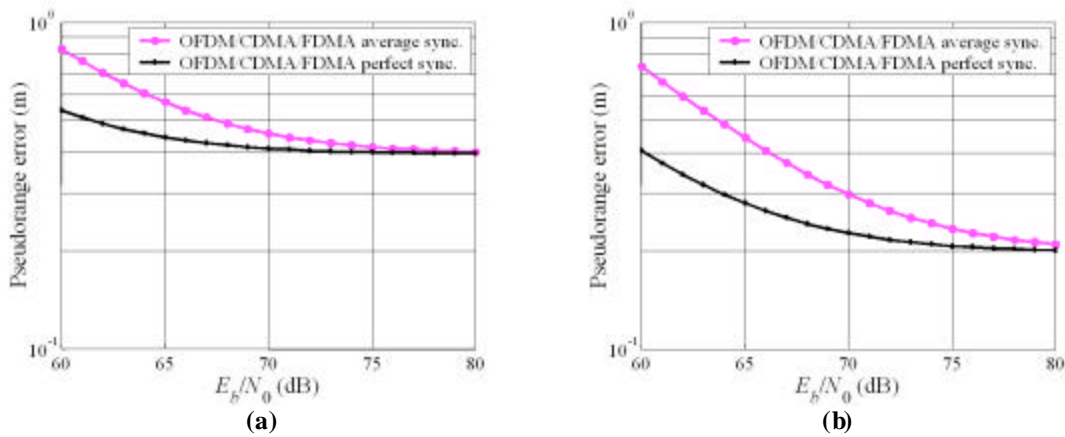


Figure 6.14 Pseudorange error vs. ideal SNR, E_b/N_0 (dB), for (a) Gold and (b) Kasami sequences.

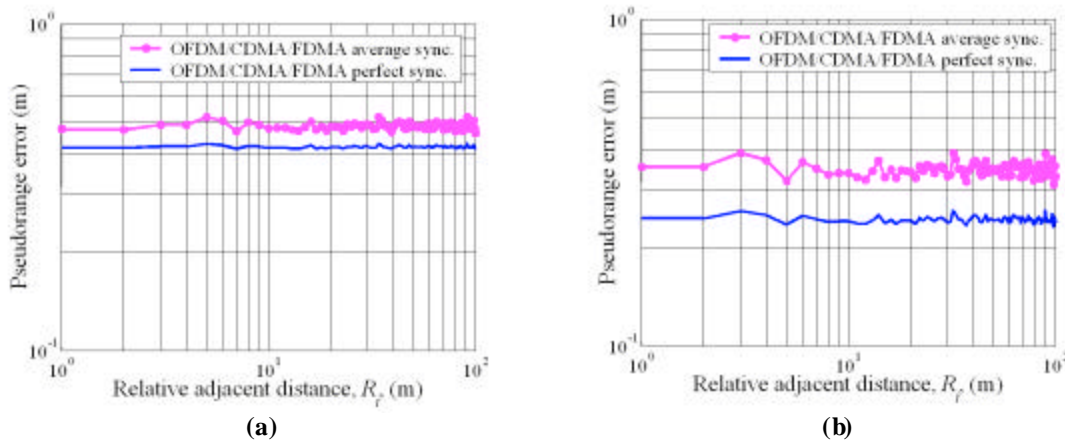


Figure 6.15 Pseudorange error vs. adjacent distance (m) for (a) Gold and (b) Kasami sequences.

Besides the BEP performance, it appears that a DSSS/OFDM/CDMA/FDMA indoor geolocation system can overcome the *near-far* effect and achieve a better navigation performance than a DSSS/CDMA only or a DSSS/CDMA/FDMA indoor geolocation system.

Figure 6.16 depicts the pseudorange error as a function of the number of transmitters, I , using (a) Gold and (b) Kasami sequences for a DSSS/OFDM/CDMA/FDMA indoor geolocation system for average and perfect synchronization. For this experiment, in addition to the parameters shown above, the E_b/N_0 is equal to 70 (dB). Also the relative distance between the 1st transmitter and receiver is 10 m and the relative distance between each adjacent transmitter and the receiver is 10 m.

We noted in Chapter 5 that a DSSS/CDMA indoor geolocation with Kasami or Gold sequences **could not** be used when more than 10 transmitters were required. In Chapter 5 we also noted that a normal operation of DSSS/CDMA/FDMA indoor geolocation with Kasami or Gold sequences **would** require up to 32 transmitters.

We note here that for a DSSS/OFDM/CDMA/FDMA indoor geolocation system with Gold/Kasami sequences as I increases from 2 to 32 the pseudorange error for average synchronization remains almost unchanged at 50/35 cm and the pseudorange error for perfect synchronization remains almost unchanged 42/24 cm.

It appears that a DSSS/OFDM/CDMA/FDMA indoor geolocation system with up to 32 transmitters can achieve better navigation performance than either a DSSS/CDMA or a DSSS/CDMA/FDMA indoor geolocation system.

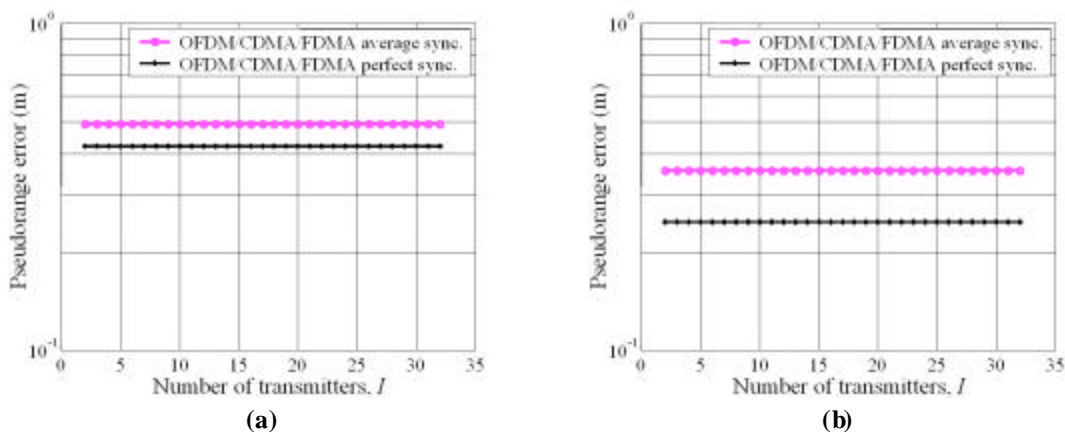


Figure 6.16 Pseudorange error vs. number of transmitters, I , for (a) Gold and (b) Kasami sequences.

Figure 6.17 illustrates the pseudorange error as a function of the number of paths, K , using (a) Gold and (b) Kasami sequences for a DSSS/OFDM/CDMA/FDMA indoor geolocation system for average and perfect synchronization.

For this experiment, in addition to the parameters shown above, the E_b/N_0 is equal to 70 (dB). The relative distance between the 1st transmitter and receiver is 10 m and the relative distance between each adjacent transmitter and the receiver is 10 m. The number of transmitters is equal to 10.

In Chapter 5 we noted that a DSSS/CDMA indoor geolocation system with Gold/Kasami **could not** be used when an indoor channel contains more than 10 paths. However, in Chapter 5 we also noted a normal operation of DSSS/CDMA/FDMA indoor geolocation with Kasami or Gold sequences **would require** an indoor channel with no more than 10 paths.

We note that for a DSSS/OFDM/CDMA/FDMA indoor geolocation system with Gold/Kasami sequences as K increases from 1 to 100 the pseudorange error for average synchronization increases from 30/30 cm to 1.4/0.72 m and the pseudorange error for perfect synchronization increases from 15/15 cm to 1.4/0.7 m.

As indicated by the results in Figure 6.17 a DSSS/OFDM/CDMA/FDMA indoor geolocation system can be successfully employed to achieve a pseudorange error smaller than 2 m when the indoor channel contains up to 10 paths. Moreover, such a system achieves better navigation performance than either a DSSS/CDMA or a DSSS/CDMA/FDMA indoor geolocation system discussed in Chapter 5.

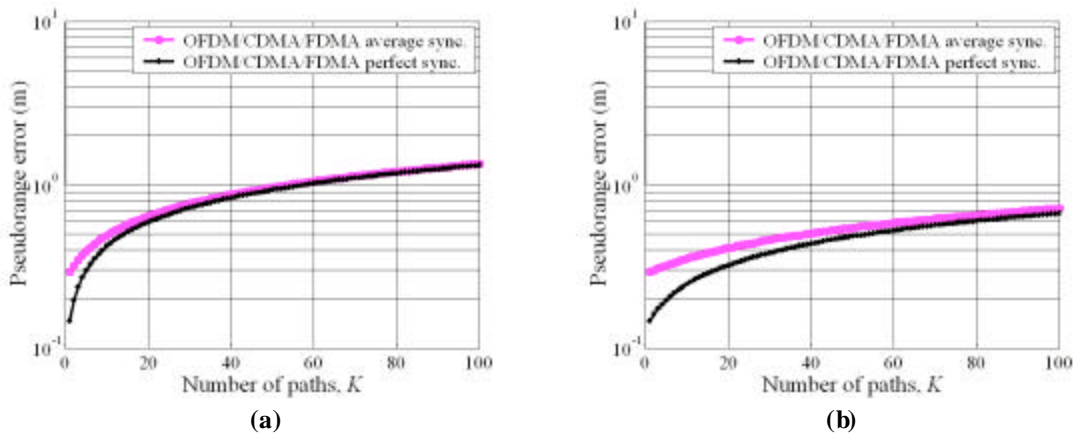


Figure 6.17 Pseudorange error vs. number of paths, K , for (a) Gold and (b) Kasami sequences.

Figure 6.18 presents the pseudorange error versus the synchronization parameter, τ (nsec), using (a) Gold and (b) Kasami sequences for a DSSS/OFDM/CDMA/FDMA indoor geolocation system.

For this experiment, in addition to the parameters shown above, the E_b/N_0 is equal to 70 (dB). The relative distance between the 1st transmitter and receiver is 10 m and the relative distance between each adjacent transmitter and the receiver is 10 m. The number of transmitters is equal to 10 and the number of paths is equal to 10.

In Chapter 5 we noted that a DSSS/CDMA or a DSSS/CDMA/FDMA indoor geolocation system with Gold/Kasami sequences **could** require $\delta\tau < 5$ nsec. For a DSSS/OFDM/CDMA/FDMA indoor geolocation system with Gold/Kasami sequences we note that the pseudorange error increases from 40/22 cm to 1.2/1.1 m as $\delta\tau$ increases from 0 to 8 nsec. A proper operation of a DSSS/OFDM/CDMA/FDMA indoor geolocation with Kasami or Gold sequences **would require** $\delta\tau < 4$ nsec.

Figure 6.19 presents the pseudorange error as a function of the frequency error, f_e (Hz), using (a) Gold and (b) Kasami sequences for a DSSS/OFDM/CDMA/FDMA indoor geolocation system for average synchronization.

For this experiment, in addition to the parameters shown above, the E_b/N_0 is equal to 70 (dB). The relative distance between the transmitter and receiver is 10 m and the relative distance between the adjacent transmitters and the receiver is 10 m. The number of transmitters is equal to 10, the number of paths is equal to 10, and $\delta\tau = 0.5 * T_c = 4$ nsec.

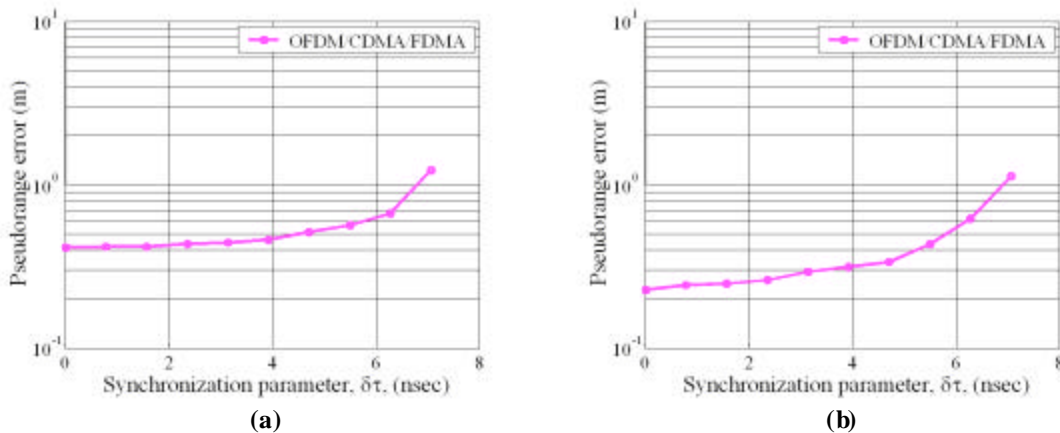


Figure 6.18 Pseudorange error vs. $\delta\tau$ for (a) Gold and (b) Kasami sequences.

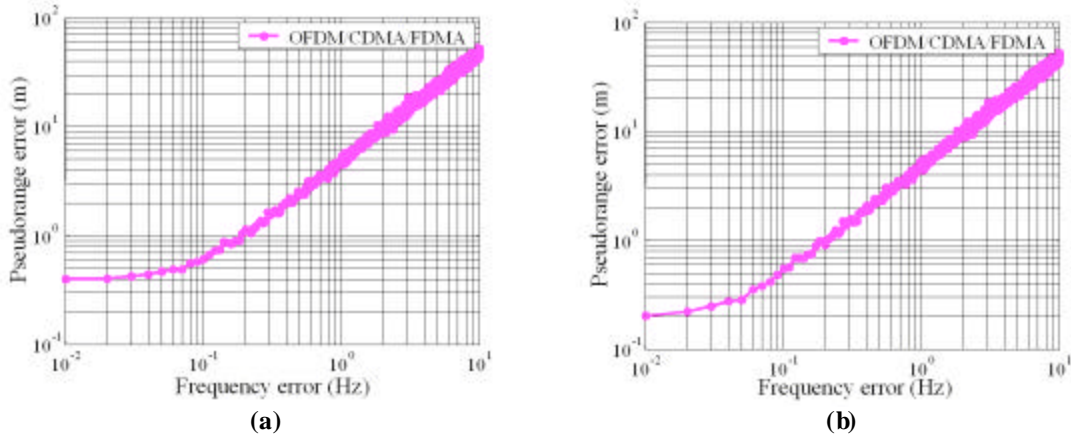


Figure 6.19 Pseudorange error vs. the frequency error (Hz) for (a) Gold and (b) Kasami sequences.

In Chapter 5 we note that a normal operation of a DSSS/CDMA indoor geolocation system with Gold/Kasami sequences **would require** a frequency error smaller than 0.01 Hz. We also noted in Chapter 5 that a normal operation of a DSSS/CDMA/FDMA indoor geolocation system with Kasami or Gold sequences **would require** a frequency error smaller than 0.1 Hz.

We note here that a normal operation of a DSSS/OFDM/CDMA/FDMA indoor geolocation system with Gold/Kasami sequences as f_e increases from 0.01 to 10 Hz the pseudorange error increases from 55/30 cm to 65/55 m. As indicated by the results a normal operation of a DSSS/OFDM/CDMA/FDMA indoor geolocation system would require a frequency error of the order of 0.1 Hz or smaller.

Figure 6.20 depicts the phase error as a function of E_b/N_0 (dB) using (a) Gold and (b) Kasami sequences for a DSSS/OFDM/CDMA/FDMA indoor geolocation system for average and perfect synchronization.

We note that for a DSSS/OFDM/CDMA/FDMA indoor geolocation system with Gold/Kasami sequences as E_b/N_0 increases from 60 to 80 dB the phase error for average synchronization decreases from 5.5/3 mm to 2.5/1.4 mm the phase error for perfect synchronization decreases from 3.5/2.3 mm to 2.5/1.4 mm.

It appears that a DSSS/OFDM/CDMA/FDMA indoor geolocation with Kasami sequences can achieve a phase error almost 2 times as small as the phase error of the same system with Gold sequences. Moreover, such a system achieves a smaller phase error than a DSSS/CDMA or a DSSS/CDMA/FDMA indoor geolocation system.

Figure 6.21 depicts the phase error as a function of relative adjacent distance, R_i (m), using (a) Gold and (b) Kasami sequences for a DSSS/OFDM/CDMA/FDMA indoor geolocation system for average and perfect synchronization. For this experiment, in addition to the parameters shown above, the E_b/N_0 is equal to 70 (dB). In Chapter 5 we noted that a DSSS/CDMA indoor geolocation with Kasami or Gold sequences **could not** overcome the *near-far* effect.

We also noted that a DSSS/CDMA/FDMA indoor geolocation with Kasami or Gold sequences **could** overcome the *near-far* effect. Here we observe that for a DSSS/OFDM/CDMA/FDMA indoor geolocation system with Gold/Kasami sequences as R_i increases from 1 to 100 m the phase error for average synchronization remains almost unchanged at 3/2.1 mm and the phase error for perfect synchronization remains almost unchanged 2.7/1.6 mm.

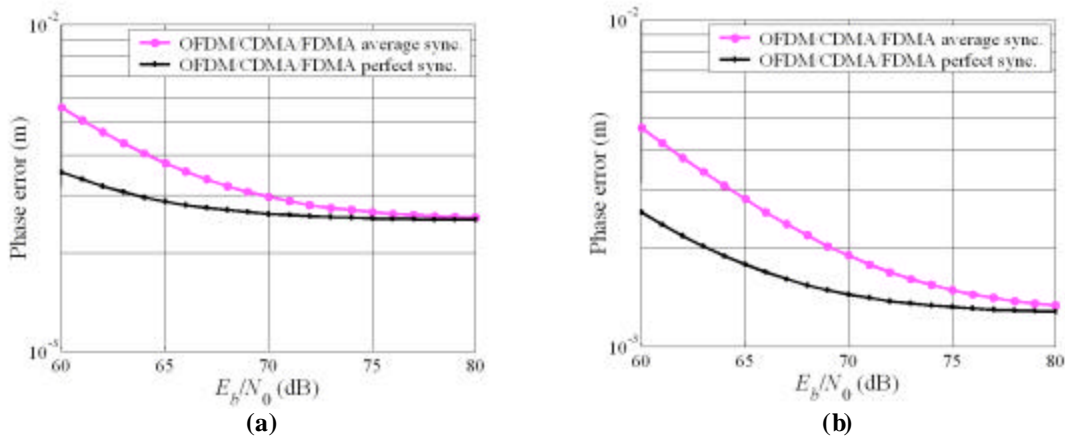


Figure 6.20 Phase error vs. the ideal SNR (dB) for (a) Gold and (b) Kasami sequences.

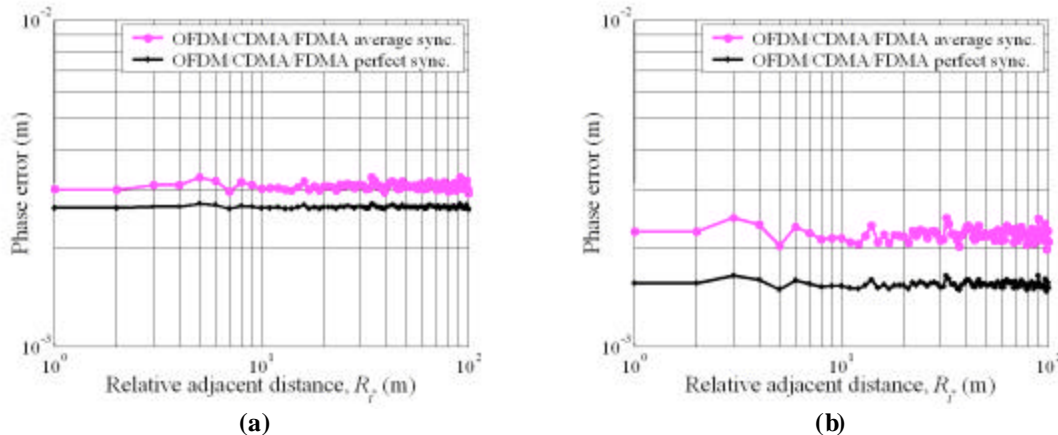


Figure 6.21 Phase error vs. the adjacent distance (m) for (a) Gold and (b) Kasami sequences.

Therefore, a DSSS/OFDM/CDMA/FDMA not only can overcome the *near-far* effect but also at the same time can achieve a smaller phase error than a DSSS/CDMA or a DSSS/CDMA/FDMA indoor geolocation system discussed in Chapter 5.

Figure 6.22 depicts the phase error as a function of the number of transmitters, I , using (a) Gold and (b) Kasami sequences for a DSSS/OFDM/CDMA/FDMA indoor geolocation system for average and perfect synchronization.

For this experiment, in addition to the parameters shown above, the E_b/N_0 is equal to 70 (dB). Also the relative distance between the 1st transmitter and receiver is 10 m and the relative distance between each adjacent transmitter and the receiver is 10 m.

We noted in Chapter 5 that a DSSS/CDMA indoor geolocation with Kasami or Gold sequences **could not** be used when more than 10 transmitters are required. We also noted that a normal operation of a DSSS/CDMA/FDMA indoor geolocation with Kasami or Gold sequences **would require** up to 32 transmitters.

We note here that for a DSSS/OFDM/CDMA/FDMA indoor geolocation system with Gold/Kasami sequences as I increases from 2 to 32 the phase error for average synchronization remains almost unchanged at 3.2/2.1 mm and the phase error for perfect synchronization remains almost unchanged 2.6/1.6 mm.

Thus, for a normal operation of a DSSS/OFDM/CDMA/FDMA indoor geolocation with Kasami or Gold sequences up to 32 transmitters are required and at the same time this system achieves a better navigation performance than either a DSSS/CDMA or a DSSS/CDMA/FDMA indoor geolocation system.

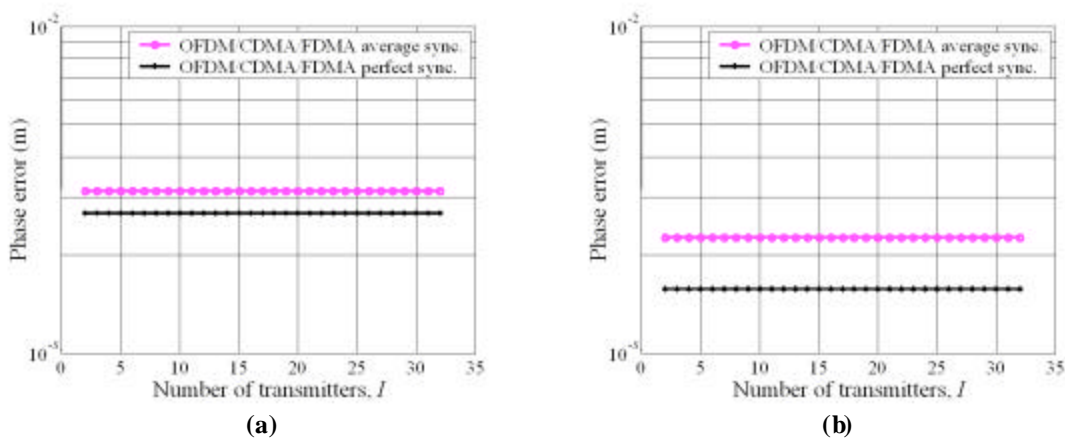


Figure 6.22 Phase error vs. number of transmitters, I , for (a) Gold and (b) Kasami sequences.

Figure 6.23 illustrates the phase error as a function of the number of paths, K , using (a) Gold and (b) Kasami sequences for a DSSS/OFDM/CDMA/FDMA indoor geolocation system for average and perfect synchronization.

For this experiment, in addition to the parameters shown above, the E_b/N_0 is equal to 70 (dB). The relative distance between the 1st transmitter and receiver is 10 m and the relative distance between each adjacent transmitter and the receiver is 10 m. The number of transmitters is equal to 10.

In Chapter 5 we noted that a normal operation of a DSSS/CDMA indoor geolocation system with Kasami or Gold sequences **would require** an indoor channel which contains no more than 10 paths. We also noted that a normal operation of a DSSS/CDMA/FDMA indoor geolocation with Kasami or Gold sequences **would require** an indoor channel, which contains no more than 10 paths.

We note here that for a DSSS/OFDM/CDMA/FDMA indoor geolocation system with Gold/Kasami sequences as K increases from 1 to 100 the phase error for average synchronization increases from 2/1.9 mm to 8/5 mm and the phase error for perfect synchronization increases from 0.9/0.9 mm to 8/4 mm. Therefore, a normal operation of a DSSS/OFDM/CDMA/FDMA indoor geolocation with Kasami or Gold sequences **would require** an indoor channel with no more than 10 paths.

Figure 6.24 presents the phase error as a function of the synchronization parameter, $\delta\tau$ (nsec), using (a) Gold and (b) Kasami sequences for a DSSS/OFDM/CDMA/FDMA indoor geolocation system.

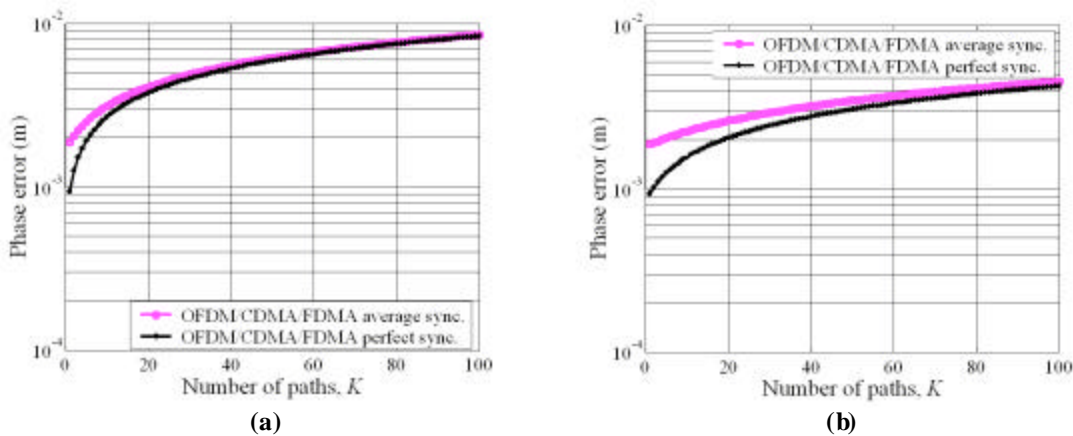


Figure 6.23 Phase error vs. number paths, K , for (a) Gold and (b) Kasami sequences.

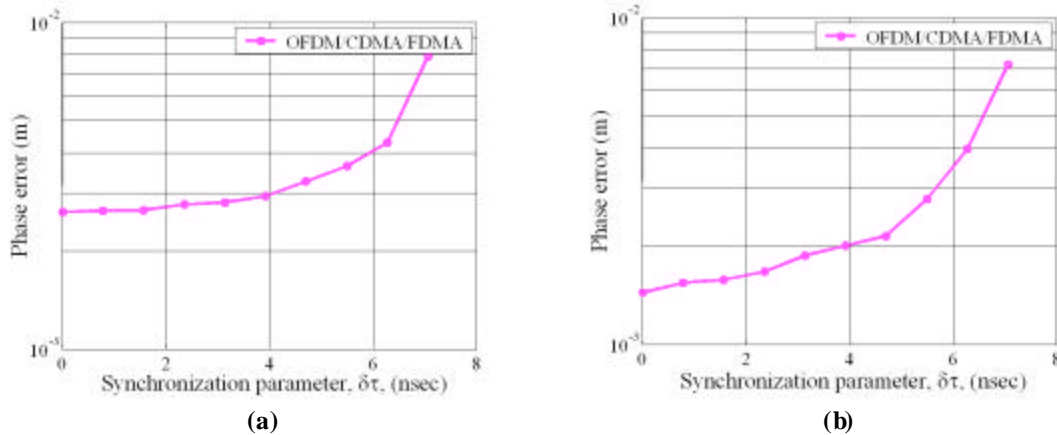


Figure 6.24 Phase error vs. synchronization parameter, $\delta\tau$, for (a) Gold and (b) Kasami sequences.

For this experiment, in addition to the parameters shown above, the E_b/N_0 is equal to 70 (dB). The relative distance between the 1st transmitter and receiver is 10 m and the relative distance between each adjacent transmitter and the receiver is 10 m. The number of transmitters is equal to 10 and the number of paths is equal to 10.

In Chapter 5 we noted that a normal operation of a DSSS/CDMA or a DSSS/CDMA/FDMA indoor geolocation system with Gold/Kasami sequences **would require** $\delta\tau < 5$ nsec. We note that a normal operation of a DSSS/OFDM/CDMA/FDMA indoor geolocation system with Gold/Kasami sequences as $\delta\tau$ increases from 0 to 9 nsec the phase error increases from 2.6/1.5 mm to 8/7 mm. As indicated earlier a normal operation of a DSSS/OFDM/CDMA/FDMA indoor geolocation with Kasami or Gold sequences **would require** $\delta\tau < 4$ nsec.

Figure 6.19 presents the phase error as a function of the frequency error, f_e (Hz), using (a) Gold and (b) Kasami sequences for a DSSS/OFDM/CDMA/FDMA indoor geolocation system for average synchronization.

For this experiment, in addition to the parameters shown above, the E_b/N_0 is equal to 70 (dB). The relative distance between the 1st transmitter and receiver is 10 m and the relative distance between each adjacent transmitter and the receiver is 10 m. The number of transmitters is equal to 10, the number of paths is equal to 10, and $\delta\tau = 0.5 * T_c = 4$ nsec.

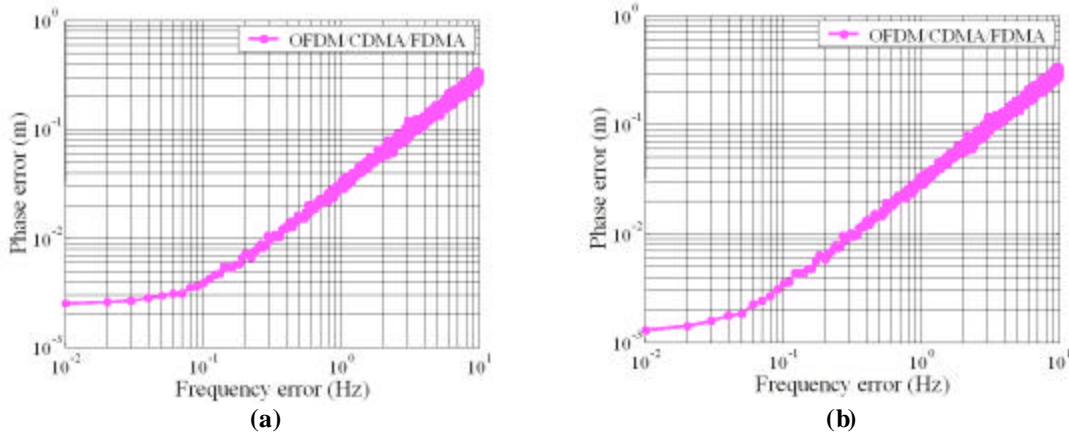


Figure 6.25 Phase error vs. frequency error (Hz) for (a) Gold and (b) Kasami sequences.

In Chapter 5 we noted that a normal operation of a DSSS/CDMA indoor geolocation system with Kasami or Gold sequences **would require** a frequency error smaller than 0.01 Hz. We also noted that a normal operation of a DSSS/CDMA/FDMA indoor geolocation system with Kasami or Gold sequences **would require** a frequency error smaller than 0.1 Hz.

We note that for an OFDM/CDMA/FDMA indoor geolocation system with Gold/Kasami sequences as f_e increases from 0.01 to 10 Hz the phase error increases from 2.5/1.5 mm to 30/25 cm. Therefore, a normal operation of a DSSS/CDMA/FDMA indoor geolocation system with Kasami or Gold sequences **would require** a frequency error smaller than 0.1 Hz.

6.4 Summary and Conclusions

We have analyzed and discussed the quantitative requirements on the theoretical performance of an OFDM/CDMA/FDMA indoor geolocation system. Recall that in Chapter 5 when we discussed the theoretical performance results indicate that a DSSS/CDMA only system which operates on a frequency different from the L_1 frequency and we have concluded that this system is inadequate to overcome the *near-far* effect. In Chapter 5 we also have discussed that a DSSS/CDMA/FDMA indoor geolocation system would be successful in eliminating the *near-far* effect, operating when a large number of transmitters is required, handling severe multipath, and operating under average synchronization requirements. As we have mentioned earlier a

DSSS/CDMA/FDMA indoor geolocation system has several restrictions such as low data rate (~3.2 KBPS) and high signal bandwidth. A DSSS/OFDM/CDMA/FDMA indoor geolocation system can operate with a data rate up to 5 MBPS which makes this system very attractive to achieve both communication and navigation applications. The communication performance evaluation of such a system is not very good if no forward error correction encoding is employed. The main concern of such a system is its complexity in comparison to a DSSS/CDMA or DSSS/CDMA/FDMA indoor geolocation system.

CITED REFERENCES AND FURTHER READING:

- [1] A. Papoulis, *Probability, Random Variables, and Stochastic Processes*. New York: McGraw-Hill, 1984.
- [2] D.V. Sarwate and M.B. Pursley, "Crosscorrelation properties of pseudorandom and related sequences," in *Proc. of IEEE*, vol. 68, pp. 593-619, May 1980.
- [3] I.F. Progri and W.R. Michalson, "Performance evaluation of a DSSS/CDMA/FDMA indoor geolocation system," in review *IEEE Trans. Comm.*, Nov. 2001.
- [4] B.W. Parkinson, J.J. Spilker, Jr, et al., *The Global Positioning System-Theory and Applications*, Washington, DC: American Institute of Aeronautics and Astronautics, (vol. 1, chap. 3, "GPS signal structure and theoretical performance") 1996.
- [5] D.T. Magill, F.D. Natali, and G.P. Edwards, "Spread-spectrum technology for commercial applications," in *Proc. IEEE*, vol. 82, no. 4, pp. 572-584, Apr. 1994.
- [6] J.M. Hill, "Development of an experimental Global Positioning System (GPS) receiver platform for navigation algorithm evaluation," Ph.D. Dissertation, Worcester Polytechnic Institute, Aug. 2001.

Chapter 7. An OFDM/FDMA Indoor Geolocation System

“Study to show thyself approved unto God, a workman that needeth not to be ashamed, rightly dividing the word of truth.” ⁴² Timothy 2:15

7.0 Introduction

ALTHOUGH a DSSS/OFDM/CDMA/FDMA indoor geolocation system that we discussed in Chapter 6 was an evolution of a DSSS/CDMA/FDMA indoor geolocation system discussed in Chapter 5, in terms of higher data rates it introduces much more complexity and it requires much more computation power. The system under discussion here is intended to achieve similar performance with much less complexity. This system is called an OFDM/FDMA system because it employs the OFDM modulation scheme for a single transmitter and the FDMA modulation scheme for multiple transmitters.

Recently broadband wireless access (BWA) solutions are proposed based on the OFDM access in IEEE 802.16 [1]. These BWA solutions will compete with the traditional cable modem and Digital Subscriber Line (DSL) technologies, which are strongly entrenched in the “last mile” access environment [1]. About 28 million homes and businesses are forecasted to deploy fixed wireless access [1]. While the majority of these deployments will be for communication purposes (such as video, voice, and data) a good percentage will be equipped with some sort of localization technology. Some suggest that the two-way multi-channel and multi-service distribution system (MMDS), which operates in the bands of 150 MHz to 2.5 GHz or 12 MHz to 2.1 GHz, is viewed as the most appropriate for BWA solutions in the United States [1]. A group of US companies formed the Broadband Wireless Internet Forum (BWIF) as a program of the IEEE Industry Standard and Technology organization to address the shortcomings of MMDS (although the program proceedings are proprietary information [1]). In order to

efficiently mitigate the effect of fading and multipath the operation in 2-11 GHz bands is supported under the project IEEE 802.16a [1].

The actual deployment of UWB systems in the United States is subject to the Federal Communications Commissions (FCC) approval of Feb. 14, 2002 [2]. The main concern of the FCC is the interference between UWB devices, other licensed services and GPS system that operate at {1176.45, 1227.6, 1575.42} MHz frequency bands [3]-[5]. The UWB signal has a low, flat, and noise-like power spectrum similar to a spread spectrum signal [3]-[5]. Therefore, FCC has approved the operation of wall imaging systems below 960 MHz and in the frequency band of 3.1-10.6 GHz [2].

In Chapter 4 we presented the mathematical model of an OFDM/FDMA indoor geolocation system. The communication performance analyses are given in §7.1, where we discuss the receiver's front end and intermediate frequency sampling and the digital signal processing. Next we continue our discussion with the navigation performance analyses (see §7.2), where are particularly interested in the time delay estimation, pseudorange and phase error estimation. This chapter is concluded with a summary and conclusion section (see §7.3). In addition we provide a list of useful references.

7.1 Communication Performance Analyses

A block diagram of an OFDM/FDMA receiver for the OFDM transmitter shown in Figure 4.16 is shown in Figure 7.1. Based on the discussion presented in Chapter 4 and Figure 7.1 the communication performance analyses include the receiver's front end and intermediate frequency sampling (see §7.1.1) and the digital signal processing (see §7.1.2). The receiver's front end and intermediate frequency sampling consists of down-converting the radio frequency signal into the intermediate frequency and then sampling. The digital signal processing consists of the crosscorrelation estimation in the digital signal processor, which leads to the time delay estimation (see §7.2.1) and pseudorange estimation (see §7.2.2).

7.1.1 Receiver's Frond End and Intermediate Frequency Sampling

The receiver's front-end section has a two-fold impact on the received signal: a *desired* impact and an *undesired* impact. On one hand, the *desired* impact consists of

down-converting the received signal to the desired intermediate frequency for further signal processing. On the other hand, the *undesired* effect consists of introducing thermal or Johnson noise into the received signal. For a detailed discussion of the undesired impact of the receiver's front end and baseband (here intermediate frequency) sampling the reader should refer to §5.2.1.

The received signal, $r_{j=1}(t) \equiv r(t)$, is down-converted to the intermediate frequency and sampled and then digitized (see Figure 7.2) and the subscript j is no longer used in our analysis. Therefore, the expression for the received signal at the intermediate frequency, $o(t)$, can be written as

$$(7.1.1) \quad o(t) = \sqrt{2G_a} \sum_{i=1}^I \sqrt{P_{ri}} \sum_{n=1}^N \sum_{k=1}^K a_i^k d_i(t - \tau_i^k) \exp j[(\tilde{\omega}_i - \hat{\omega}_i)(t - \tau_i^k) + \omega_n(t - \tau_i^k) + \phi_i + \theta_i^k] + n_{out}(t)$$

and G_a is the front end amplifier gain. Note that the caret (^) symbol denotes a parameter generated or estimated locally by the receiver and $n_{out}(t)$ is the noise with power spectral density given by (5.2.3), which includes the impact of the noise figure (see §5.2.1).

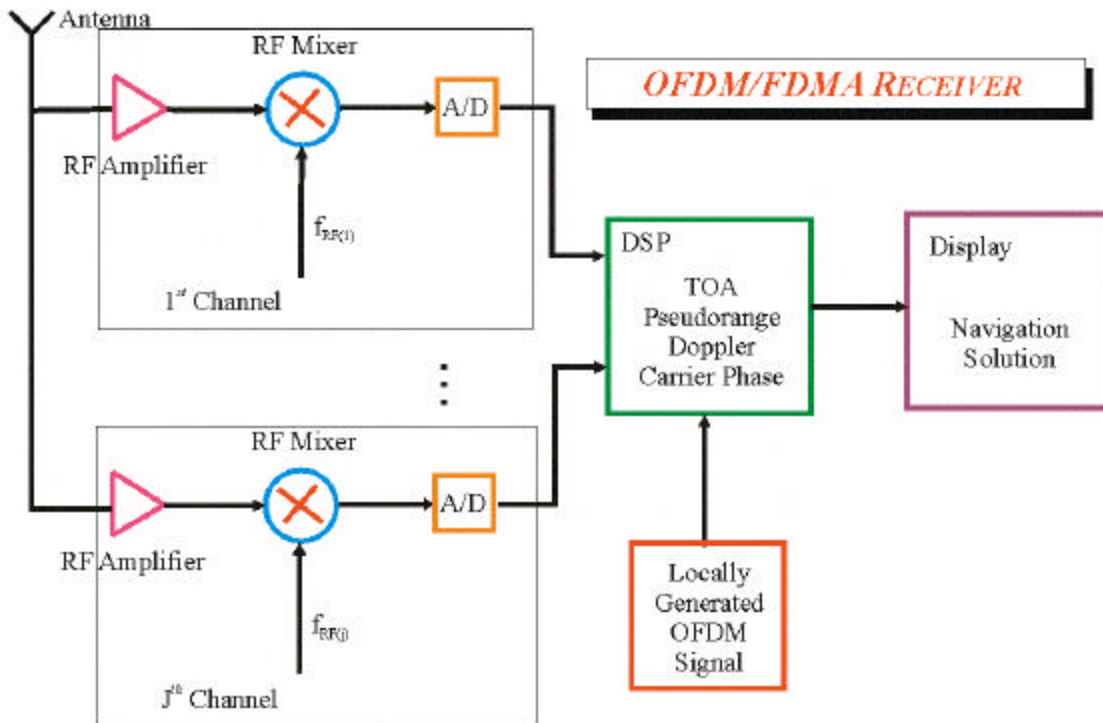


Figure 7.1 The block diagram of an OFDM/FDMA receiver.

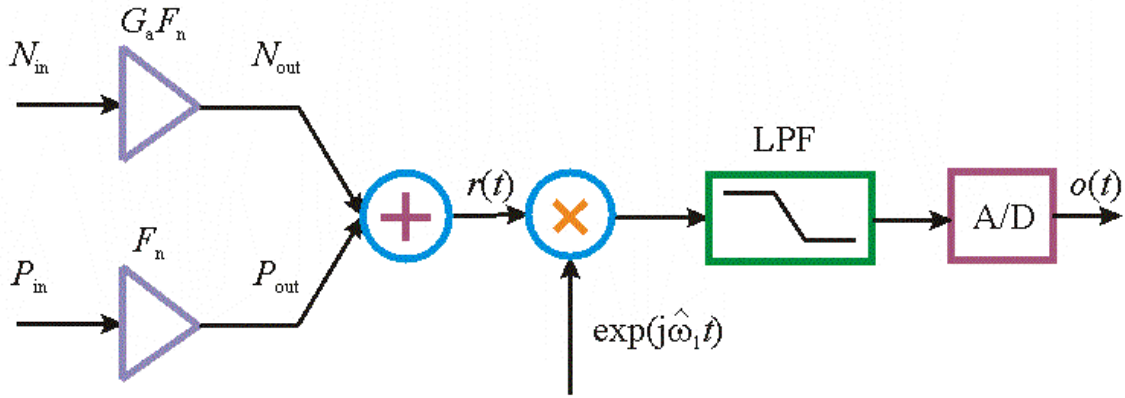


Figure 7.2 The block diagram of the receiver's front end and intermediate frequency sampling.

In order to perform some analysis we have to simplify our notation for the received signal given by eq. (7.1.1). Therefore, we rewrite equation (7.1.1) as follows:

$$\begin{aligned}
 (7.1.2) \quad o(t) = & \sqrt{2P_i G_a} \sqrt{p_1(t)} \sum_{n=1}^N a_1^1 d_1(t - \tau_1^1) \exp j[\omega_1^e(t - \tau_1^1) + \omega_n(t - \tau_1^1) + \phi_1 + \theta_1^1] \\
 & + \sqrt{2P_i G_a} \sqrt{p_1(t)} \sum_{n=1}^N \sum_{k=2}^K a_1^k d_1(t - \tau_1^k) \exp j[\omega_1^e(t - \tau_1^k) + \omega_n(t - \tau_1^k) + \phi_1 + \theta_1^k] \\
 & + \sqrt{2P_i G_a} \sum_{i=2}^I \sqrt{p_i(t)} \sum_{n=1}^N \sum_{k=1}^K a_i^k d_i(t - \tau_i^k) \exp j[\omega_i^e(t - \tau_i^k) + \omega_n(t - \tau_i^k) + \phi_i + \theta_i^k] + n_{out}(t)
 \end{aligned}$$

where, ω_i^e , is the radian frequency error defined as

$$(7.1.3) \quad \omega_i^e = \tilde{\omega}_i - \hat{\omega}_1.$$

Based on equation (7.1.2) we recognize four components (or terms) of the received signal $o(t)$: the *desired* component, the inter symbol interference term, the mutually accessed interference term, and the noise component. For notation simplicity, the above expression can be written as

$$(7.1.4) \quad o(t) = A \exp j[\omega^e(t - \tau) + \phi + \theta] \sum_{n=1}^N \exp j[\omega_n(t - \tau)] + i(t)$$

where

$$(7.1.5) \quad \mathbf{f} \equiv \mathbf{f}_1, \mathbf{q} \equiv \mathbf{q}_1^1, \mathbf{t} \equiv \mathbf{t}_1, \omega^e \equiv \omega_1^e \text{ and } A \equiv \sqrt{2P_i G_a} \sqrt{p_1(t)} a_1^1 d_1(t - \tau)$$

and $i(t)$ is the interference signal which is assumed to be normally (or Gaussian) distributed keeping in mind the central limit theorem and the filtering that occurs after the mixer (or down-conversion).

The signal $o(t)$ is sampled at the rate (or sampling frequency) f_s ; thus, producing a discrete-time signal

$$(7.1.6) \quad o[m] = A \exp j \left[\frac{f^e}{f_s} (m - \tau) + \phi + \theta \right] \sum_{n=1}^N \exp j \left[\frac{f_k}{f_s} (m - \tau) \right] + i[m].$$

The signal $o[m]$ can be written in a more simplified expression as

$$(7.1.7) \quad o[m] = A \exp j \left[\frac{f^e}{f_s} (m - \tau) + \theta \right] S[m - \tau] + i[m] = \hat{S}[m - \tau] + i[m].$$

The signal given by (7.1.6) is the first input into the digital signal processor and the locally generated OFDM signal the second input. These two inputs are processed to form the desired signal detection function as shown in Figure 7.1 the output of which is the time delay estimation.

7.1.2 Digital Signal Processing

The principle (or the idea) behind the processing that occurs in the digital signal processor is similar to the concept that is treated in the transmitter section (see §4.3.2). The detection statistics on the receiver is based on the crosscorrelation function, $\gamma(k, \tau)$, between the received signal $o[m]$ and the locally generated OFDM signal $S[m + k]$

$$(7.1.8) \quad \begin{aligned} \gamma(k, \tau) &\equiv \frac{1}{N_s} \sum_{m=1}^{N_s - |k|} o[m] S[m + k]^* \\ &= \frac{1}{N_s} \sum_{m=1}^{N_s - |k|} \hat{S}[m - \tau] S[m + k]^* + \frac{1}{N_s} \sum_{m=1}^{N_s - |k|} i[m] S[m + k]^*. \end{aligned}$$

The crosscorrelation function at the receiver contains two components: a *desired* component and an *undesired* (or *unwanted*) component. The desired component results from considering the multiplication

$$(7.1.9) \quad \begin{aligned} \hat{S}_i[m - \tau] S_i[m + k]^* &= A \exp j \theta \exp j \left[\frac{f^e}{f_s} \tau \right] \exp j \left[\frac{f^e}{f_s} m \right] \\ &\quad \sum_{l=1}^K \left[\exp \left(-j \frac{f_l(k + \tau)}{f_s} \right) \sum_{n=1}^N \exp \left(j \frac{(n - l) \Delta}{f_s} m \right) \right]. \end{aligned}$$

The undesired component is obtained from the multiplication between $i[m]$ and $S[m + k]$ as

$$(7.1.10) \quad v[k] = \frac{1}{N_s} \sum_{m=1}^{N_s-|k|} i[m]S[m+k]^* .$$

Substituting the results of equations (7.1.9) and (7.1.10) into equation (7.1.8) yields

$$(7.1.11) \quad \gamma(k, \tau) = A \exp j\theta \exp j \left[\frac{f^e}{f_s} \tau \right] \sum_{l=1}^N \exp \left(-j \frac{f_l(m+\tau)}{f_s} \right) \\ \sum_{n=1}^N \left[\frac{1}{N_s} \sum_{m=1}^{N_s-|k|} \exp \left(j \frac{(n-l)\Delta + f^e}{f_s} m \right) \right] + v[k].$$

We observe three major impairments in the crosscorrelation function, $\gamma(k, \tau)$: (1) multipath, (2) frequency error, and (3) receiver noise and interference. Under assumptions similar to those applied in the transmitter design, the receiver detection function $\gamma(k, \tau)$ can be approximated as

$$(7.1.12) \quad \gamma(k, \tau) \cong N \frac{N_s - |k|}{N_s} A \exp j\theta \exp j \left[\frac{f^e}{f_s} \tau \right] \sum_{n=1}^N \exp \left(j \frac{f_n(\tau+k)}{f_s} \right) + v[k] \text{ for} \\ \frac{\Delta + f^e}{f_s} \leq \frac{2\pi}{NK10^2} .$$

Here we conclude our discussion of the communication performance and discuss a quantitative assessment next.

7.1.3 Quantitative Assessment

As an example we consider an OFDM/FDMA indoor geolocation system depicted in Figure 7.3. This system consists of three transmitters and one receiver, which are all positioned in the same line. The receiver location is defined as the origin of the system. The coordinates of the 1st, 2nd, and 3rd transmitters are -130.47 m, 0 m, and 130.467 m respectively. The receiver is however located at 0 m.

We have assumed that the transmitted signal power is at 0 dB. The IF signal coming from the 1st, 2nd, and 3rd transmitters are illustrated in Figure 7.4, Figure 7.5, and Figure 7.6 respectively. Each signal contains 10 sinusoids with 1 MHz spacing between two consecutive sinusoids. Therefore, the bandwidth of each IF OFDM signal is 10 MHz wide. The first signal is delayed in time by 435.2 nsec that corresponds to a distance of -130.47 m. The second signal is generated in true time that corresponds to a distance of

0 m. The third signal is advanced by 435.2 nsec that corresponds to a distance of 130.47 m. In reality there is neither a negative distance nor a negative time. However, to distinguish between the first and the second transmitter we have made such assumptions. For the true principle of operation of such a system the reader should refer to §1.2, §2.2.1, and §2.5.1. The purpose of this quantitative assessment is only to show how an observable can be obtained and what would be the accuracy on that observable.

OFDM/FDMA INDOOR GEOLOCATION SYSTEM

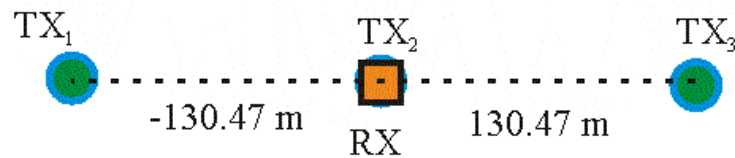


Figure 7.3 An example of an OFDM/FDMA indoor geolocation system- - modified from [6].

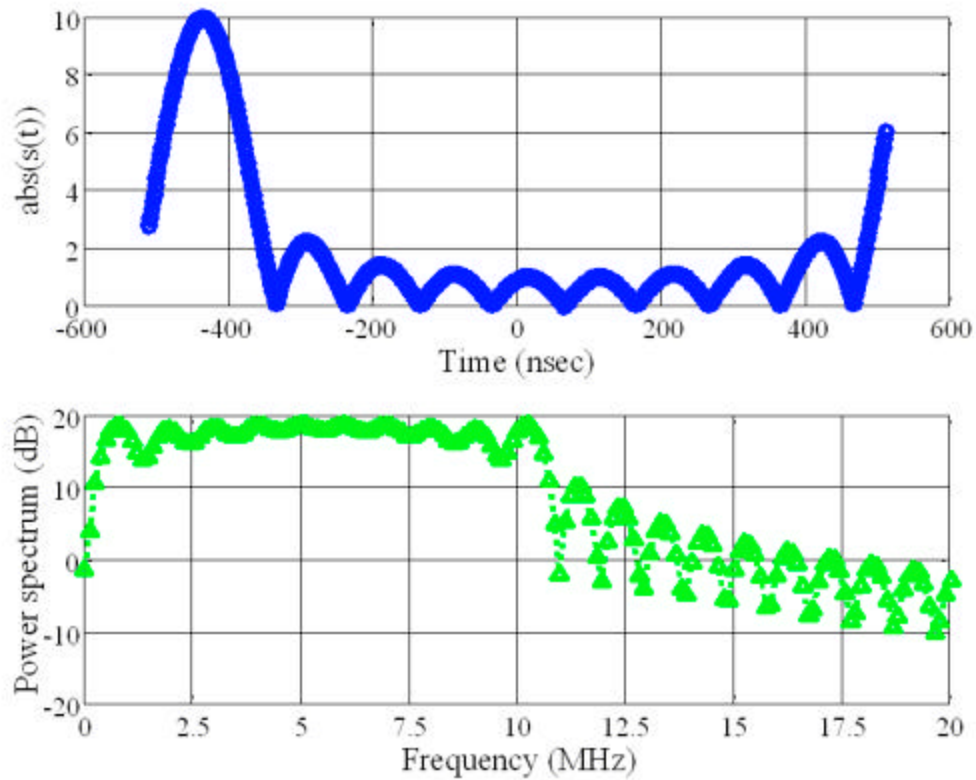


Figure 7.4 The IF signal from the 1st transmitter in the time and frequency domain.

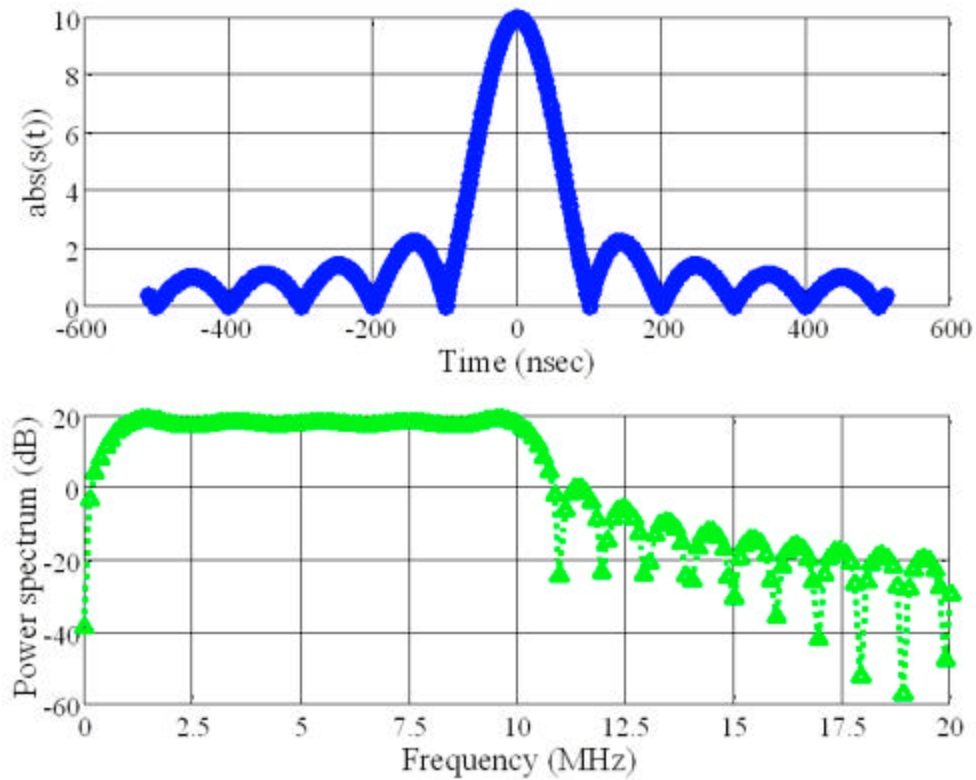


Figure 7.5 The IF signal from the 2nd transmitter in the time and frequency domain.

If we were to crosscorrelate the three IF signals with an OFDM signal, normalize the crosscorrelation function, and plot the crosscorrelation function versus time, we would obtain the result shown in Figure 7.7. As shown in the figure each crosscorrelation function peaks at $\tau = \{-435.2$ (blue o), 0 (red +), 435.2 (green ^)}. Therefore, the crosscorrelation peak would indicate the “distance” between each transmitter and the receiver.

Figure 7.8 illustrates the total RF signal in the time and frequency domain. Each IF OFDM signal is unconverted at 3.105 GHz, 3.125 GHz, and 3.145 GHz respectively. As shown in Figure 7.8, two consecutive RF frequencies are 20 MHz apart; hence, there is little overlap between the waveforms of two separate transmitters. As we have indicated in Chapter 4 this is known as the OFDM/FDMA modulation scheme and this waveform is crucial for achieving channelization between a transmitter and a channel of the receiver. Next, we consider the result of channel losses to this transmitted signal.

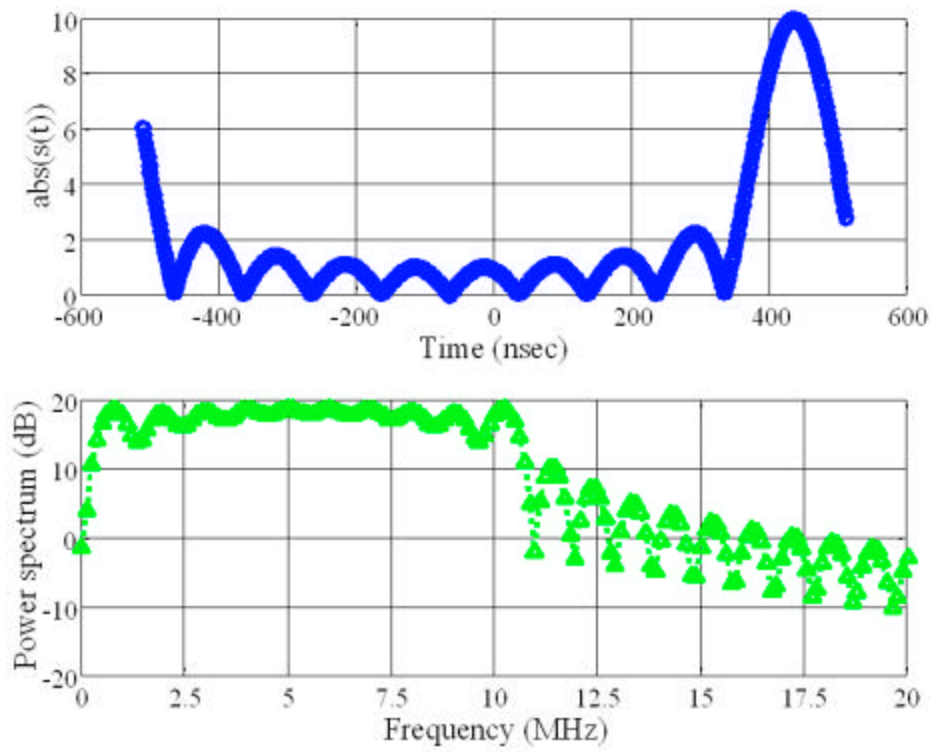


Figure 7.6 The IF signal from the 3rd transmitter in the time and frequency domain.

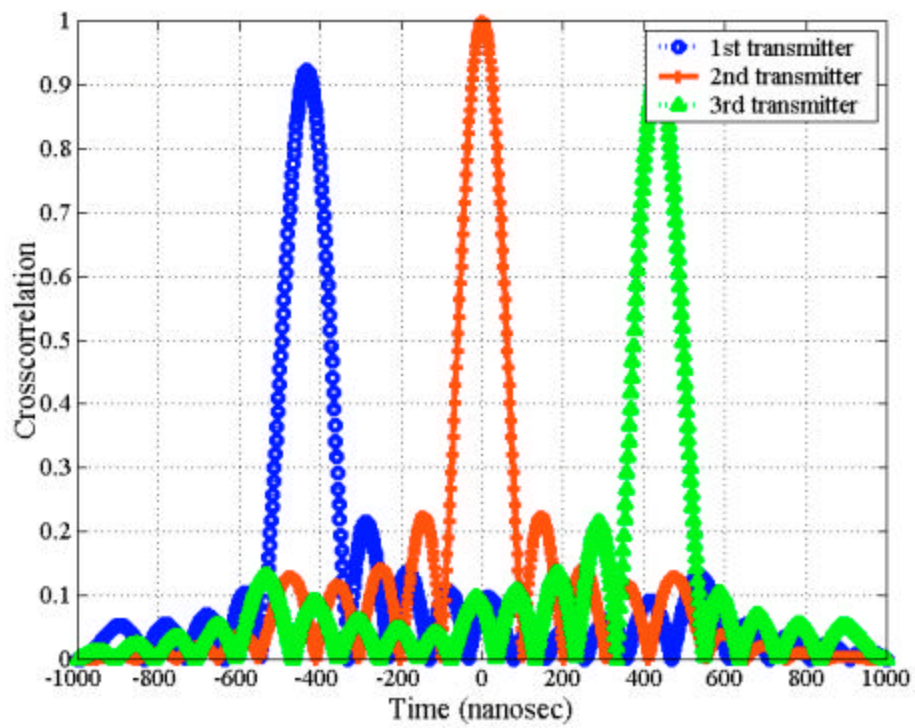


Figure 7.7 The crosscorrelation function g for $t = \{-435.2$ (blue o), 0 (red +), 435.2 (green ^)} nsec.

We assume that the power spectrum density of the normally distributed interference is 10 dB above the signal power, which is at 0 dB. Hence, the received signal at the receiver's antenna port looks like the waveform shown in Figure 7.9. Figure 7.10, Figure 7.11, and Figure 7.12 depict the received signal after down-conversion in the 1st, 2nd, and 3rd channel at the receiver respectively. We have indicated in these figures that the bandwidth between 0-15 MHz of the spectrum of the waveform of 1st, 2nd, and 3rd channel would correspond to the 1st, 2nd, and 3rd transmitter respectively. We have also indicated that further signal processing would be required to filter out or window out unwanted signals. As we have mentioned earlier in an OFDM/FDMA receiver (see Figure 7.1), this receiver generates a replica of an ideal IF OFDM signal which is used to estimate the time of arrival between each transmitter and the receiver. This is the processing that occurs next.

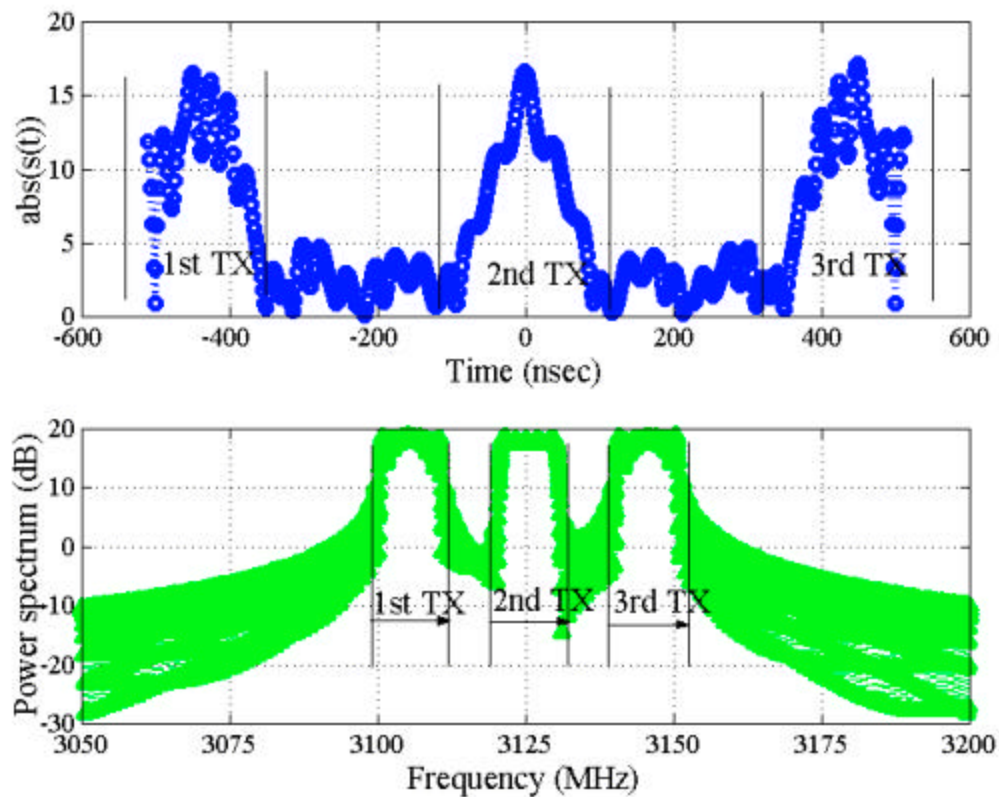


Figure 7.8 The total noiseless RF signal in the time and frequency domain.

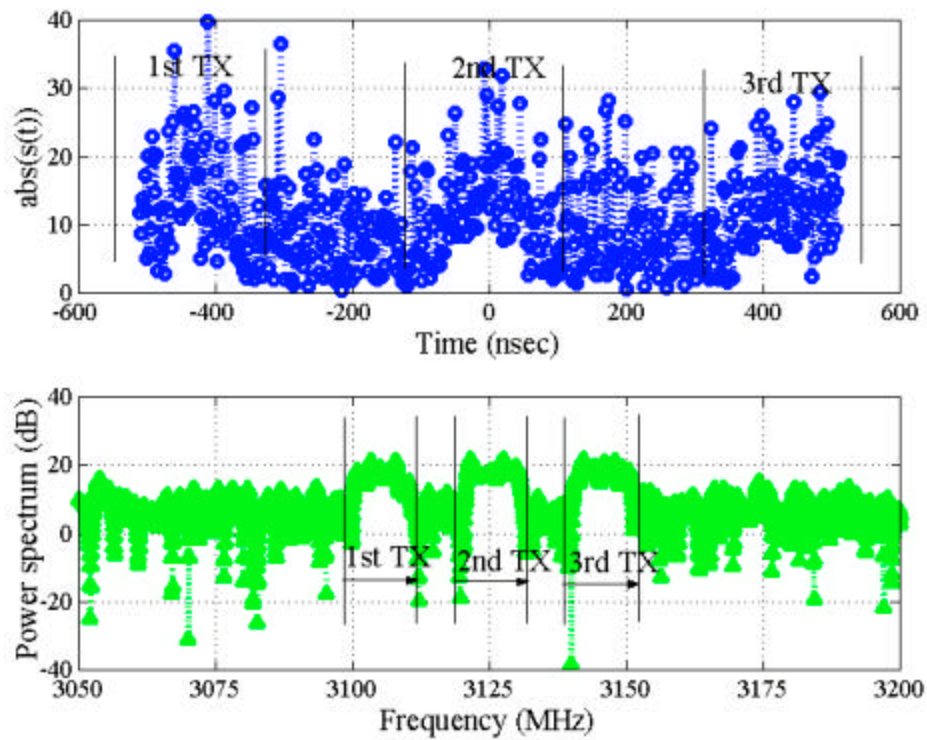


Figure 7.9 The total noisy RF signal in the time and frequency domain.

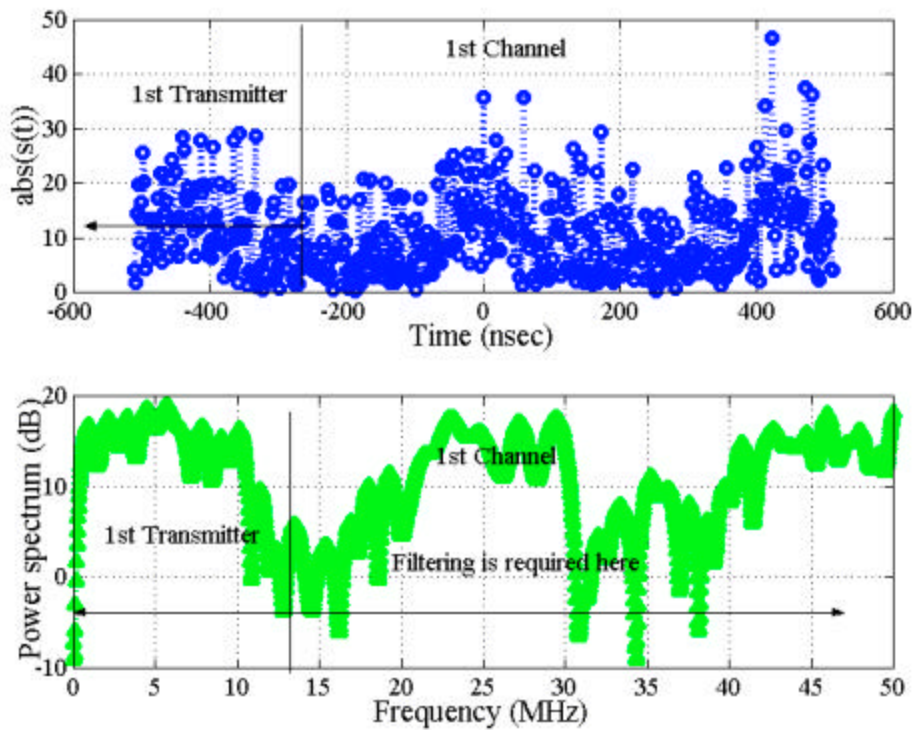


Figure 7.10 The received noisy IF signal of the 1st channel in the time and frequency domain.

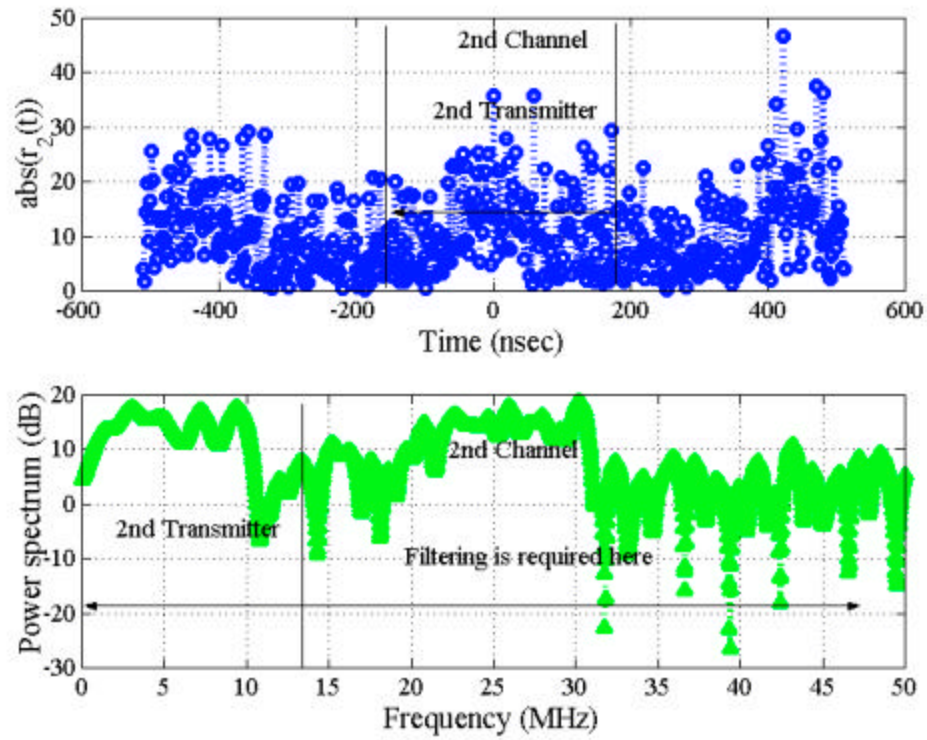


Figure 7.11 The received noisy IF signal of the 2nd channel in the time and frequency domain.

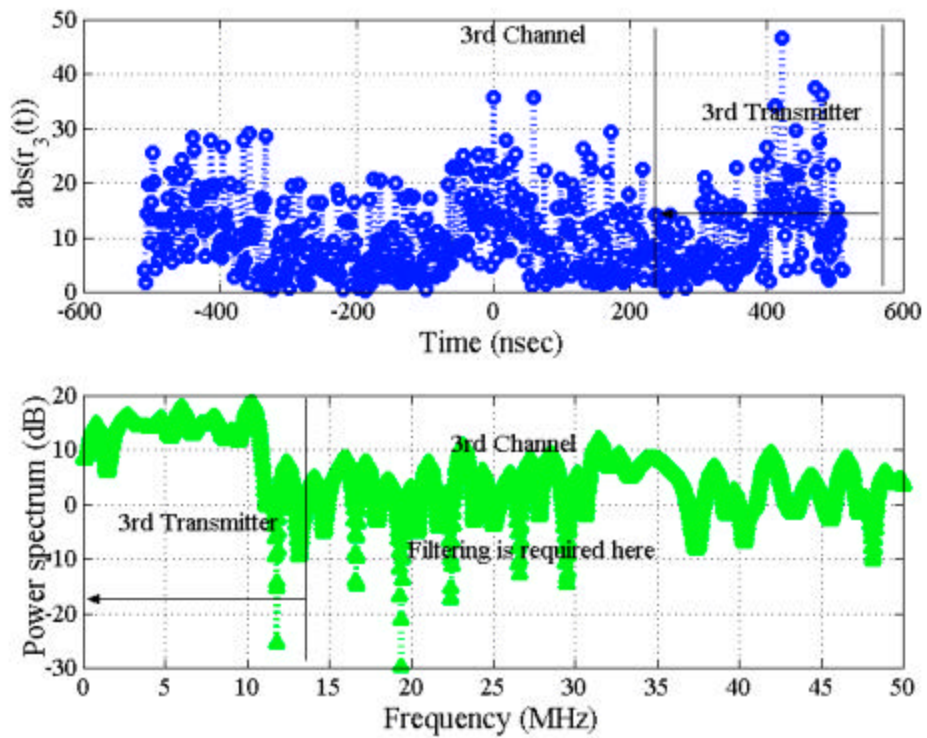


Figure 7.12 The received noisy IF signal of the 3rd channel in the time and frequency domain.

A snapshot of the crosscorrelation $g(m, t)$ at the receiver side is shown in Figure 7.13. As a result of the multipath error, the frequency error, and the receiver noise the crosscorrelation function at the receiver is distorted (see Figure 7.13) compared to the ideal crosscorrelation function at the transmitter (see Figure 7.7).

How accurately we will estimate the crosscorrelation peak from the center is the subject of the upcoming section.

7.2 Navigation Performance Analyses

An OFDM/FDMA indoor geolocation system is very different from any conventional GPS like systems that we have discussed in the previous two chapters because it does not use any pseudorandom related sequences; therefore, its signal is not a spread spectrum signal. Therefore, we should look more carefully into the concept of measurement generation and navigation solution using an OFDM/FDMA signal structure. There are two topics that we discuss here include (1) a quantitative approach for time delay estimation (see §7.2.1) and (2) a quantitative approach for pseudorange error (see §7.2.2).

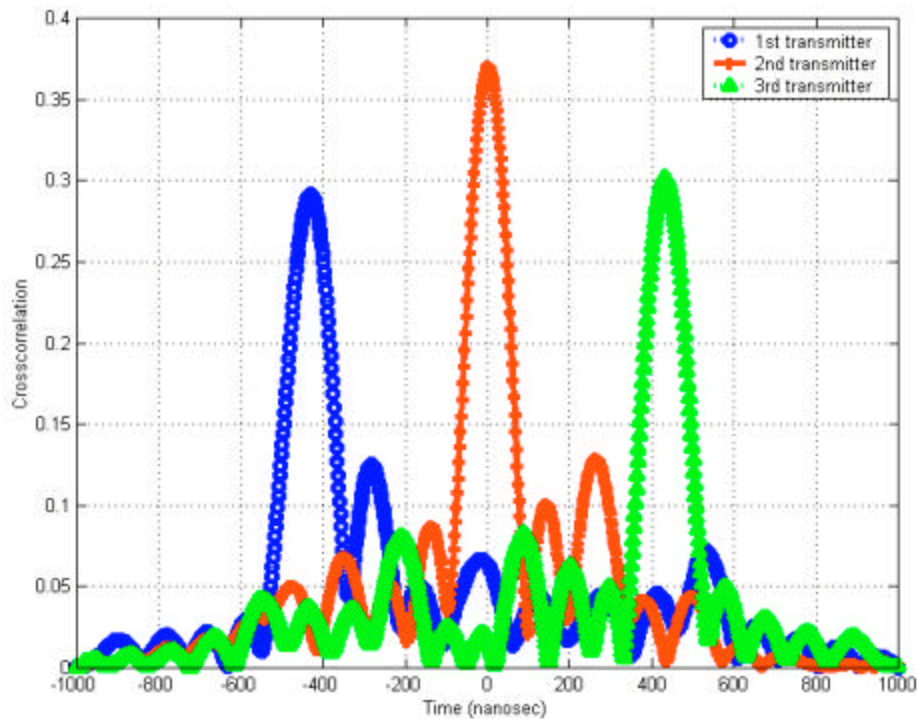


Figure 7.13 The crosscorrelation function g for $t = \{-435.2$ (blue o), 0 (red +), 435.2 (green ^)} nsec.

7.2.1 A Quantitative Approach for Time Delay Estimation

The time delay, τ , is defined as the sum of the signal time of travel (or arrival), τ_o , with the transmitter clock bias, τ_t , (or offset from the reference time) and with the receiver clock bias, τ_r , (or offset from the reference time), which analytically reads

$$(7.2.1) \quad \tau = \tau_t + \tau_o + \tau_r.$$

If we assume that we can achieve some means of synchronization between transmitters (either using a master GPS receiver, local area network (LANs), or some other means) then the transmitter clock bias, τ_t , is estimated separately to enable the computation of the navigation solution.

Consider the numerical example presented in both transmitter and communication sections (see §4.3.2 and §7.1.2). The time delay can be measured without ambiguity if the maximum distance between the transmitter and receiver is less than 153.6 m (see equation 4.3.13). Comparing the results of Figure 7.13 with the results of Figure 7.7 we conclude that the location of the crosscorrelation peaks is preserved to a large extent. We also observe that the actual distance of the crosscorrelation peak from the center does not reflect the true time delay due to the nonlinear nature of the crosscorrelation function.

The algorithm for computing the time delay is provided in the following steps:

1. Initialize the transmitter and channel models
2. Compute the IF locally generated OFDM signal at its own local time t
3. Set $m = 0$ and $\tau = 0$
4. Set (step index) index = 0
5. While ($|m - M - 1| > 1$ or index < 3) do
 6. Compute the crosscorrelation function $\mathbf{g}(m, t)$ given by equation (7.1.12).
 7. Find the maximum value, \mathbf{g}_{\max} , and its corresponding index, m
 8. Compute the intermediate time delay, $dum = (m - M - 1)/f_s$
 9. Compute the actual time delay, $\tau = \tau + dum$
 10. Update the local time, $t = t + dum$
 11. Compute the IF locally generated signal using the new time t
 12. Increment the step index, index = index + 1
13. End

14. Output the time delay

This algorithm is supposed to converge in no more than two or three steps. If it does not converge than at the third step the computational loop of the algorithm is supposed to be interrupted.

Figure 7.14 illustrates the crosscorrelation function, g , after the algorithm has converged and the time delay from each transmitter is given by $\tau = \{-434$ (blue o), -2 (red +), 436 (green ^)} nsec.

Since the time delay estimates are statistical parameters we conducted the experiment 1000 times and plotted the cumulative distribution functions in Figure 7.15. We also computed the sample mean

$$(7.2.2) \quad \mu_{\tau} = \{-435.53, 0.4, 435.03\} \text{ nsec,}$$

and standard deviation

$$(7.2.3) \quad \sigma_{\tau} = \{8.4, 0.8, 0.3\} \text{ nsec.}$$

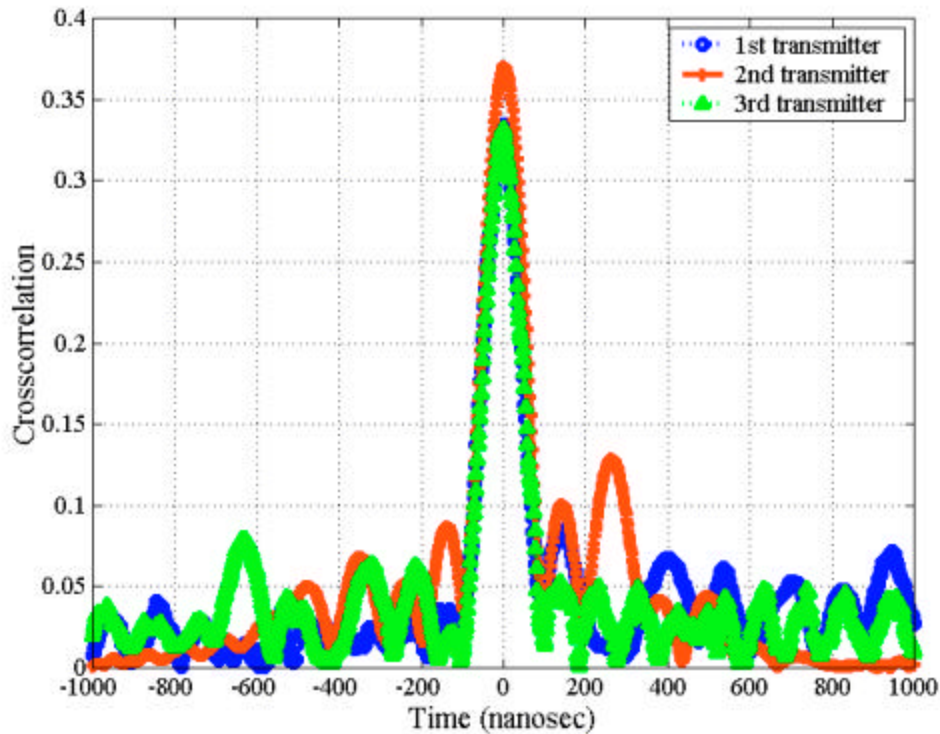


Figure 7.14 A snap shot of the crosscorrelation function g for $t = \{-434$ (blue o), -2 (red +), 436 (green ^)} nsec after the algorithm as converged.

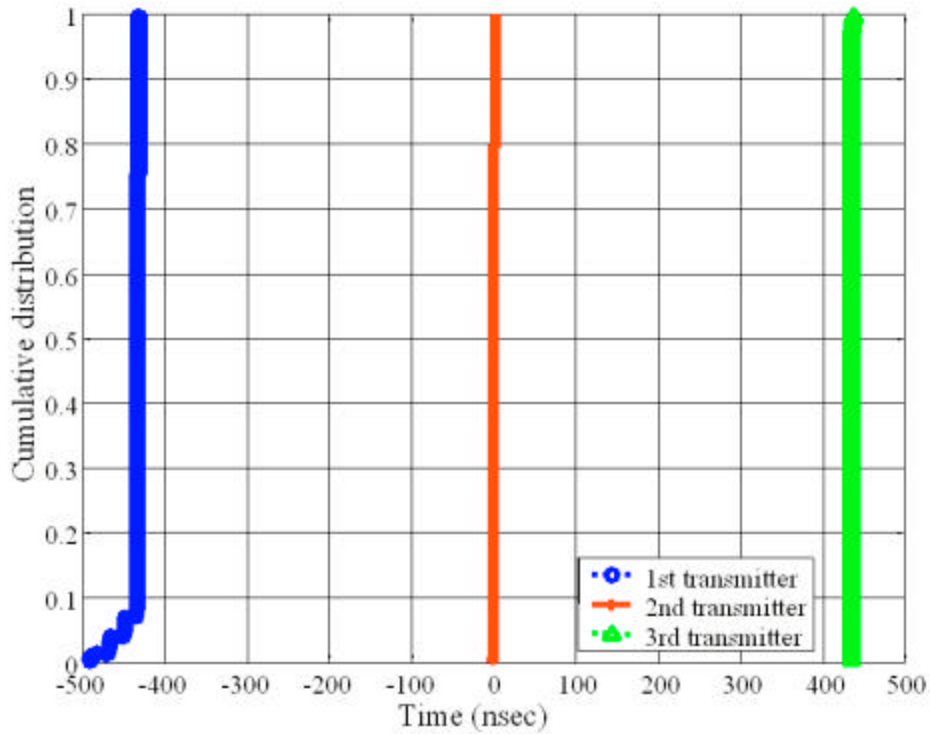


Figure 7.15 The cumulative distribution function corresponding to the three scenarios for 1000 runs.

These results appear to be consistent with the previous publications that the rms delay spread for indoor wireless systems is in the range of tens of nanoseconds [7]–[10].

The time delay estimation is the first important measurement for producing the navigation solution. As we shall see in the following section this measurement can be interpreted as a pseudorange measurement.

7.2.2 Pseudorange Estimation and Pseudorange Error

By definition the pseudorange measurement, ρ , is a quantity which results from the multiplication of the time delay estimation (see equation (7.2.1)) with the speed of light, c ; i.e.

$$(7.2.4) \quad \rho = c \cdot \tau = c \cdot \tau_i + c \cdot \tau_o + c \cdot \tau_r.$$

On the other hand, if we write the time delay, τ , as

$$(7.2.5) \quad \tau = \mu_\tau \pm \sigma_\tau$$

then the pseudorange error based on eq. (7.2.4) reads

$$(7.2.6) \quad \rho = c \cdot \tau = c \cdot \mu_{\tau} \pm c \cdot \sigma_{\tau} = \mu_{\rho} \pm \sigma_{\rho}.$$

Therefore, the pseudorange sample mean, μ_{ρ} , and standard deviation, σ_{ρ} , for the experiment under investigation are:

$$(7.2.7) \quad \mu_{\rho} = \{-130.6, 0.12, 130.91\} \text{ m}$$

$$(7.2.8) \quad \sigma_{\rho} = \{2.5, 0.24, 0.08\} \text{ m}.$$

We note that the pseudorange error is independent of the time delay estimation; i.e., whether the time delay estimation is positive, zero, or negative the pseudorange error is almost 2 – 3 m. Nevertheless, the pseudorange error is very large. Therefore, we should seek alternate measurements to insure precise indoor geolocation. And one such measurement results from estimating the phase of the carrier, which would be the subject of future work.

The cumulative distribution function of the pseudorange error is plotted in Figure 7.16. We observe more error associated with the first observable than with the second and third.

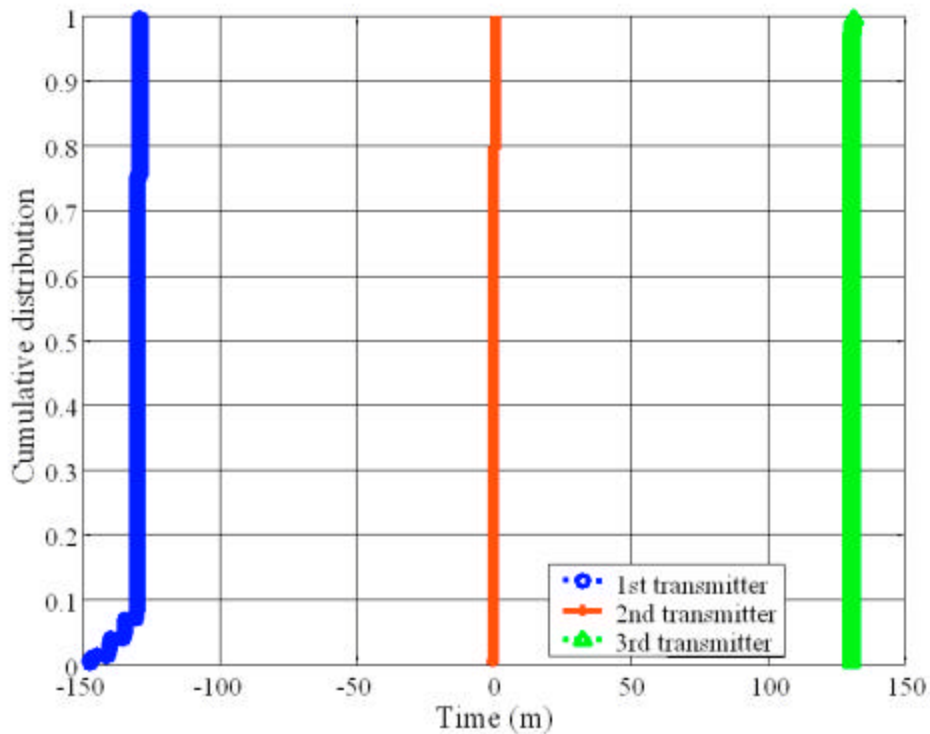


Figure 7.16 The cumulative distribution function corresponding to the three scenarios for 1000 runs.

7.3 Summary and Conclusions

There are several lessons learned from this investigation. We have shown that it is possible to design an OFDM/FDMA indoor geolocation system. There are several advantages for developing such a system:

- There is a 7.5 GHz bandwidth available for such systems.
- The design of an OFDM/FDMA indoor geolocation system appears to be conceptually simpler than the design of a GPS like indoor geolocation system.
- The pseudorange error of an OFDM/FDMA indoor geolocation system is about 2.3 m (1 sigma) which is much better than the accuracy of a GPS like indoor geolocation system.

Nevertheless, there are also some disadvantages to an OFDM/FDMA indoor geolocation system.

- The theoretical maximum detectable range depends on the number of OFDM tones and on the sampling frequency (see equation 4.3.13).

Further developments and implementations of this system will be presented in future publications.

CITED REFERENCES AND FURTHER READING:

- [1] I. Koffman and V. Roman, "Broadband wireless access solutions based on OFDM access in IEEE 802.16," *IEEE Comm. Mag.*, vol. 40, no. 4, pp. 96-103, Apr. 2002.
- [2] Federal Communications Commission, *News*, "New public safety applications and broadband internet access among uses envisioned by FCC authorization of ultra-wideband technology," Washington, DC, Feb. 14, 2002.
- [3] G.R. Opshaug and P. Enge, "GPS and UWB for indoor navigation," in *Proc. ION-GPS*, Salt Lake City, UT, pp. 1427-1433, Sep. 11-14, 2001.
- [4] P. Enge, "A global challenge—protect GNSS noise floor a.k.a. spectrum stewardship," *ION-GPS 2002* (panel presentation), Portland, OR, Sep. 24, 2002.
- [5] K. Pahlavan, X. Li, J.-P. Makela, "Indoor geolocation science and technology," *IEEE Comm. Mag.*, vol. 40, no. 2, pp. 112-118, Feb. 2002.
- [6] I.F. Progri, W.R. Michalson, and D. Cyganski, "An OFDM/FDMA indoor geolocation system," in *Proc. ION-NTM*, Anaheim, CA, Jan. 2003.
- [7] R. Prasad, H.S. Misser, and A. Kegel, "Performance evaluation of direct-sequence spread spectrum multiple-access for indoor wireless communication in a Rician fading channel," *IEEE Trans. Comm.*, vol. 43, no. 2, pp. 581-592, Feb-Apr. 1995.

- [8] G.J.M. Janssen, P.A. Stigter, and R. Prasad, "Wideband indoor channel measurements and BER analysis of frequency selective multipath channels at 2.4, 4.75, and 11.5 GHz," *IEEE Trans. Comm.*, vol. 44, no. 10, pp. 1272-1288, Oct. 1996.
- [9] J.G. Durgin, T.S. Rappaport, and H. Xu, "Measurements and models for radio path loss and penetration loss in and around homes and trees at 5.85 GHz," *IEEE Trans. Comm.*, vol. 46, no. 11, pp. 1484-1496, Nov. 1998.
- [10] M. Kavehrad and P.J. McLane, "Spread spectrum for indoor digital radio," *IEEE Comm. Mag.*, vol. 25, no. 6, pp. 32-40, June 1987.

Chapter 8. Conclusions and Future Work

“But the wisdom that is from above is first pure, then peaceable, gentle, and easy to be entreated, full of mercy and good fruits, without partiality, and without hypocrisy.

And the fruit of righteousness is sown in peace of them that make peace.”³⁴James 3:17-18

8.0 Introduction

BY now the reader is introduced to the concept of an indoor geolocation system; namely, its principle of operation, transmitter, channel, and receiver design and the issues associated with obtaining an observable to achieve indoor navigation. As we already know from Chapter 2 and 3, the main issues of designing a radio based indoor geolocation system are directly linked with the signal waveforms and parameters under the term of signal structure. Motivated by the success of GPS, GLONASS, and GPS-like pseudolite systems we have addressed many of the limitations associated with GPS, GLONASS, and GPS-like pseudolite signal structures for indoor positioning. In the context of providing something novel and useful we have proposed three indoor geolocation systems two of which are motivated by GPS and GLONASS signal structure and principle of operation and one of them is motivated by the DSL and GLONASS signal structure and GPS or GLONASS principle of operation. We made this main assumption because: (1) GPS, GLONASS and other systems are the state of the art technology and have proven to be successful and reliable outdoors (2) modifications of the GPS and GLONASS signal structure to the extent that the principle of operation is kept the same as GPS and GLONASS would hopefully result in a reasonable complexity of a receiver design.

This Chapter is organized as follows. First, we discuss the benefits a CDMA/FDMA indoor geolocation system and contrast the signal structure of this system with the GPS and GPS like signal structure (see §8.1). Second, we discuss the benefits an OFDM/CDMA/FDMA indoor geolocation system and contrast the signal structure of this system with the GPS and GPS like signal structure (see §8.2). Third, we discuss the

benefits an OFDM/FDMA indoor geolocation system and contrast the signal structure of this system with the GPS and GPS like signal structure (see §8.2). Fourth, we discuss a number of avenues that this work will eventually lead in the near future.

8.1 A DSSS/CDMA/FDMA Indoor Geolocation System

Motivated by GPS and GLONASS limitations indoor and the need of indoor positioning system, the study of the signal structure of a CDMA/FDMA indoor geolocation system and its performance has been our goal for quite some time [1]–[13]. In essence we believe that a CDMA/FDMA indoor geolocation system as discussed in Chapters 4 and 5 is a solution to the *near-far* effect and multipath effects because it utilizes both frequency and code diversity to achieve multiaccess capability in contrast the GPS which employs only the code diversity and GLONASS only the frequency diversity. In the case of GPS the signal waveforms fully overlap and therefore the multiaccess is achieved only through code properties. In the case of GLONASS the signal waveforms partially overlap and the GLONASS signal structure is a better solution than the GPS signal structure. Nevertheless, as it is currently designed the overlap between the GLONASS signals is a problem for indoor positioning. As we have discussed in Chapters 4 and 5 the overlap between the signals of a CDMA/FDMA system is small enough that an observable can be obtained under an indoor Rayleigh fading channel. The *near-far* effect is eliminated as a result of the frequency and code diversity. The *multipath* effect is eliminated as a result of frequency, code diversity, and high chipping rate. For a CDMA/FDMA indoor geolocation system to accommodate up to 32 pseudolites (or transmitters) within circle of a 100-m radius, 10 multipath components, 1-m adjacent transmitter receiver distance in indoor Rayleigh fading channel the ideal signal to noise ration should be 70 dB, chipping rate of 102.3 MBPS, timing synchronization of 5 nsec, and frequency synchronization of 0.1 Hz. In addition the spacing between the carrier frequency of one transmitter with the carrier frequency of another transmitter should be a multiple of one-half of the chipping rate. In addition the spreading codes should be selected as follows: the C code should be selected from the small set of Kasami sequences with a length of 1023 chips. The P code should be a maximum length sequence of length 31. The B code should be a sequence of length

1023×1025 chips. The data rate of this system is approximately 3.2 KPBS and roughly 200-MHz bandwidth for the C code. Therefore, a DSSS/CDMA/FDMA indoor geolocation system is a solution to indoor navigation and communication but not necessarily the optimal one. An alternative solution to both indoor navigation and communication is a DSSS/CDMA/FDMA indoor geolocation system, which we have discussed in Chapters 4 and 6.

8.2 A DSSS/OFDM/CDMA/FDMA Indoor Geolocation System

A DSSS/OFDM/CDMA/FDMA indoor geolocation system is motivated by its predecessor a DSSS/CDMA/FDMA indoor geolocation system. The goal of this system is to increase the data rate. In order to achieve this requirements we proposed in Chapter 4 and 6 a DSSS/OFDM/CDMA/FDMA indoor geolocation system that can achieve up to 10 MBPS date rate while maintaining the signal characteristics mitigate both indoor multipath Rayleigh fading and *near-far* effect. Again we have very high requirements on channel bandwidth of the order of 254 MHz. Since, there is about 7.5 GHz spectrum allocated by the FCC for indoor positioning devices then a total number of transmitters that can operate simultaneously would be approximately 27. Nevertheless, this number is close to our requirements of 32 transmitters within a circle of 100-m radius. At the same time the system complexity is increased. We believe that a DSSS/OFDM/CDMA/FDMA indoor geolocation system is a better solution to both indoor navigation and communications but with higher risks for implementation than a DSSS/CDMA/FDMA indoor geolocation system.

8.3 An OFDM/FDMA Indoor Geolocation System

An OFDM/FDMA indoor geolocation system is a system that we have recently started to investigate [14]. The system that we propose in Chapters 4 and 7 is purely a navigation system. It requires only 10 MHz bandwidth per transmitter. Since, there are about 7.5 GHz unused bandwidth in the bands of 3.1 – 10.6 GHz we can obtain up to 600 transmitters. It still remains to investigate the communications aspects of such a system, which should not be a problem given that this structure is successfully used in a DSL line.

8.4 Assessment of All WPI Indoor Geolocation Systems

The assessment of the three WPI indoor geolocation systems is given in terms of the data rate capability and pseudorange and phase error performance. Figure 8.1 illustrates the data rate, R_d , versus the order of the generating polynomial for both a DSSS/CDMA/FDMA indoor geolocation system and a DSSS/OFDM/CDMA/FDMA indoor geolocation system. As indicated by the figure, a DSSS/OFDM/CDMA/FDMA indoor geolocation system has a data rate that is about 2.5 orders of magnitude higher than the data rate of a DSSS/CDMA/FDMA indoor geolocation system for the same order of the generating polynomial, m .

Table 8.1 depicts the quantitative requirements of the pseudorange error for a DSSS/CDMA indoor geolocation system, a DSSS/CDMA/FDMA indoor geolocation system, a DSSS/OFDM/CDMA/FDMA indoor geolocation system, and an OFDM/FDMA indoor geolocation system. Based on the pseudorange error performance, as indicated Table 8.1, a DSSS/OFDM/CDMA/FDMA indoor geolocation system with Kasami sequences is superior to all the remaining indoor geolocation systems.

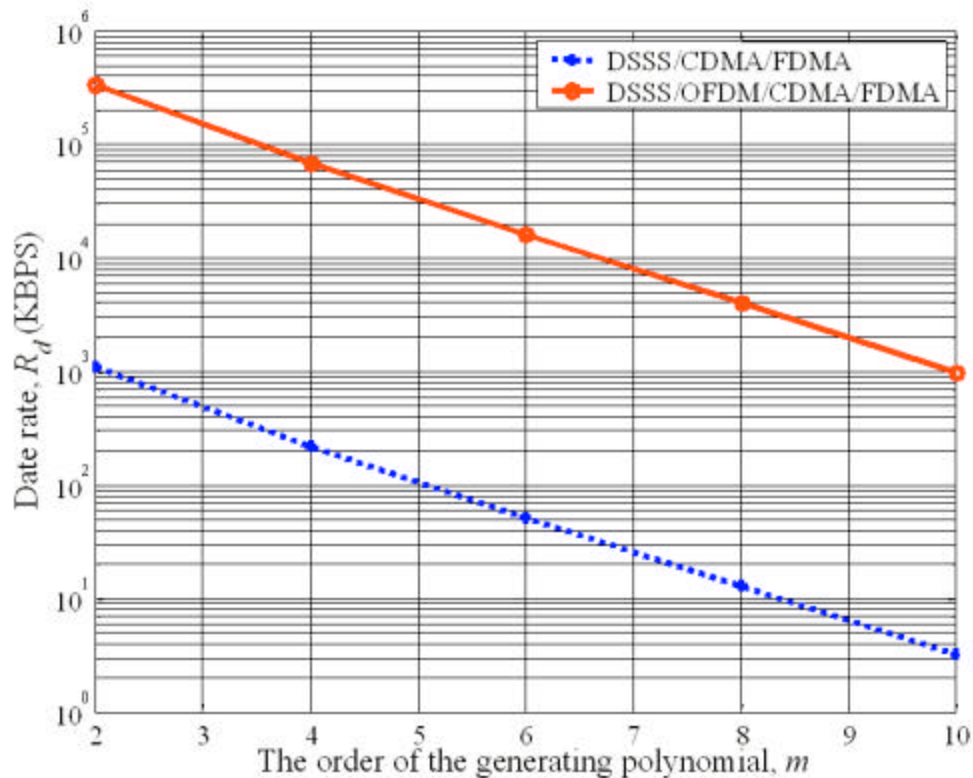


Figure 8.1 Data rate, R_d , vs. the order of the generating polynomial, m .

Table 8.2 depicts the quantitative requirements of the phase error for a DSSS/CDMA indoor geolocation system, a DSSS/CDMA/FDMA indoor geolocation system, a DSSS/OFDM/CDMA/FDMA indoor geolocation system, and an OFDM/FDMA indoor geolocation system. Based on the phase error performance, as indicated Table 8.2, a DSSS/OFDM/CDMA/FDMA indoor geolocation system with Kasami sequences is superior to all the remaining indoor geolocation systems.

To achieve high data rate, as indicated in Figure 8.1, the signal structure of a DSSS/OFDM/CDMA/FDMA indoor geolocation system is superior to the signal structure of a DSSS/CDMA indoor geolocation system or a DSSS/CDMA/FDMA indoor geolocation system.

To achieve small pseudorange error, as indicated in Table 8.1, the signal structure of a DSSS/OFDM/CDMA/FDMA indoor geolocation system with Kasami sequences is superior to the signal structure of all other indoor geolocation systems.

To achieve small phase error, as indicated in Table 8.2, the signal structure of a DSSS/OFDM/CDMA/FDMA indoor geolocation system with Kasami sequences is superior to the signal structure of all other indoor geolocation systems. Therefore, the signal structure of a DSSS/OFDM/CDMA/FDMA indoor geolocation system with Kasami sequences is the best system in terms of both communication performance and navigation performance.

In terms of bandwidth requirements, an OFDM/FDMA indoor geolocation system requires almost an order of magnitude smaller signal bandwidth than either a DSSS/CDMA/FDMA or a DSSS/OFDM/CDMA/FDMA indoor geolocation system.

Table 8.1 Quantitative results for the pseudorange error performance.

CDMA		CDMA/FDMA		OFDM/CDMA/FDMA		OFDM/FDMA
Gold	Kasami	Gold	Kasami	Gold	Kasami	
2 m	1.5 m	1 m	0.8 m	0.5 m	0.3 m	2 m

Table 8.2 Quantitative results for the phase error performance.

CDMA		CDMA/FDMA		OFDM/CDMA/FDMA		OFDM/FDMA
Gold	Kasami	Gold	Kasami	Gold	Kasami	
1 cm	6 mm	7 mm	<6 mm	3 mm	<2 mm	N/A

8.5 Future Work

There are a lot of avenues to be followed based on the research presented here. The most obvious is to build the three systems that we have proposed in Chapters 4 through 7 and verify the validity of our assumptions. These systems can be either built separately or jointly. Within each system we suspect that the transmitter and the receiver would be a project in itself. Moreover, synchronization is another issue, which must be addressed. In the mean time, the communication or networking protocol needs to be defined for every system. Another important contribution in the future would be to repeat this work for closed indoor environments.

CITED REFERENCES AND FURTHER READING:

- [1] I.F. Progri, W.R. Michalson et al, "A system for tracking and locating emergency personnel inside buildings," in *Proc. ION-GPS*, Salt Lake City, UT, pp. 560-568, Sep. 2000.
- [2] I.F. Progri and W.R. Michalson, "Performance evaluation of category III precision landing using airport Pseudolites," in *Proc. IEEE PLANS*, San Diego, CA, pp. 262-269, Mar. 2000.
- [3] I.F. Progri and W.R. Michalson, "A combined GPS satellite/pseudolite system for category III precision landing," in *Proc. IEEE PLANS*, Palm Spring, CA, Apr. 2002.
- [4] W.R. Michalson and I.F. Progri, "Assessing the accuracy of underground positioning using pseudolites," in *Proc. ION-GPS*, Salt Lake City, UT, pp. 1007-1015, Sep. 2000.
- [5] I.F. Progri, W.R. Michalson, and J. Hill, "Assessing the accuracy of navigation algorithms using a combined system of GPS satellites and pseudolites," in *Proc. ION-NTM*, Long Beach, CA, pp. 473-481, Jan. 2001.
- [6] I.F. Progri, J. Hill, and W.R. Michalson, "A Doppler based navigation algorithm," in *Proc. ION-NTM*, Long Beach, CA, pp. 482-490, Jan. 2001.
- [7] I.F. Progri and W.R. Michalson, "An innovative navigation algorithm using a system of fixed Pseudolites," in *Proc. ION-NTM*, Long Beach, CA, pp. 619-627, Jan. 2001.
- [8] J. Hill, I.F. Progri, and W.R. Michalson, "Techniques for reducing the near-far problem in indoor geolocation systems," in *Proc. ION-NTM*, Long Beach, CA, pp. 860-865, Jan. 2001.
- [9] I.F. Progri, J.M. Hill, and W.R. Michalson, "An investigation of the pseudolite's signal structure for indoor applications," in *Proc. ION-AM*, Albuquerque, NM, pp. 453-462, June 2001.
- [10] I.F. Progri and W.R. Michalson, "The impact of proposed pseudolite's signal structure on the receiver's phase and code error," in *Proc. ION-AM*, Albuquerque, NM, pp. 414-422, June 2001.

- [11] I.F. Proгри and W.R. Michalson, "An alternative approach to multipath and near-far problem for indoor geolocation systems," in *Proc. ION-GPS*, Salt Lake City, UT, Sep. 2001.
- [12] I.F. Proгри and W. R. Michalson, "Performance evaluation of a DSSS/CDMA/FDMA indoor geolocation system," in review *IEEE Trans. Comm.*, Nov. 2001.
- [13] I.F. Proгри, W.R. Michalson, and M.C. Bromberg, "A DSSS/CDMA/FDMA indoor geolocation system," in *Proc. ION-GPS*, Portland, OR, pp. 155-164, Sep. 2002.
- [14] I.F. Proгри, W.R. Michalson, and D. Cyganski, "An OFDM/FDMA indoor geolocation system," in *Proc. ION-NTM*, Anaheim, CA, Jan. 2003.

Appendix A. History and Background

“*The glory of young men is their strength: and the beauty of old men is the grey head.*”—Prov. 20:29

A.0 Introduction

THE material presented here is neither original nor unheard of. Because most of it can be found in most books of history and science; therefore, we do not deserve any credit for presenting it here. In the context of a geolocation system, nevertheless, it might be attractive to the reader to see how the ancient idea of measuring distance has evolved to the modern idea of measuring time and then translating this to distance measurements.

A.1 History and Background

A.1.1 *Ancient Era*

In ancient Greece science was simply a branch of general philosophy; therefore, most of philosophers were concerned with both the physical and the abstract sciences. Thales of Miletus (635-546 BC), for example, who believed that water is the source of everything, died fittingly by falling down a well. He, among other thing, measured the distances between ships and the height of mountains, and he was also credited with predicting solar eclipses [1]. It is believed that Greek mathematics developed under the influence both of speculative thought and religious mysticism. Supposedly, Thales had learned the rudiments of arithmetic and geometry in Egypt [1]. But, it was Pythagoras, who having made a number of original advances, launched the *Theory of Numbers*, formulated the theorem about the square of the hypotenuse of the right-angle triangle, which are the bases of the Euclidian Geometry that emerged later [1]. Aristotle contributed systematic works in both physics and biology. Eudoxus, discovered the Theory of Proportions and the method of exhaustion for measuring the curvilinear surfaces. With Euclides of Alexandria whose *Elements* is said ‘to have reigned longer than any other book save the Bible began the new era of systematized geometry’.

Moreover, he was noted as the great mathematical systematizer and he was noted to have provided lasting proofs for all existing knowledge [1]. Later, Archimedes and Eratosthenes of Cyrene (276-196 BC), who in calculating the earth's diameter at 252,000 stades or 7,850 miles, erred (or was mistaken) by less than 1 per cent [1]. (*Note here that distance measurement will become the centerpiece of modern localization.*)

A.1.2 Medieval Era

In medieval times the science was inextricably mixed in with theology. The awareness of time and space then was radically different from our own [1]. It is believed that time was measured by the irregular motions of day and night, of the seasons, of sowing and reaping; i.e., primitively, by mere observation of the eye without relying on any scientific evidence or methodology. Only the Church (not to be confused with the word Church used in the New Testament) had sacredly the privilege to measure the time based on fixed hours and calendars. There were no means of testing conventional geographical wisdom of men because they traveled so slowly and so seldom. The main idea of the world was simply this: Jerusalem lay at the center of the three continents—Asia, Africa, and Europe, which were attributed to the sons of Noah: Shem, Ham, and Japheth respectively. And beyond the continents lay the encompassing ocean, and beyond the ocean the line were heaven and earth merged imperceptibly into one. Such was the wisdom and horizon of medieval men. Nevertheless, even in this dark period of human history, there were great inventions such as the *clock*. Giovanni da Dondi (1318-89), Professor of Astronomy at Padua, was indisputably the first *clock* maker. Although, clock is mentioned as early as Dante in his *Paradiso*, and other records of *clock* are found in London's St Paul's in 1286 and in Milan in 1308, Dondi's treatise provides the earliest detailed description of clockwork [1]. This description presented a seven-dialed astronomical clock, regulated by an escapement of the crown-wheel-and-verge type [1]. (The reader is reminded that the accurate measure of *time* is translated into accurate measure of *distance* in modern localization.)

On the other fields of science, most of the landmark achievements came from the work of scattered individuals. The experiments of Roger Bacon in optics and machines formed part of his general attack on corruption and superstition. Pierre de Maricourt (Peter the

Stranger), Bacon's master, produced a fundamental treatise on magnetism during the Angevin siege of *Lucera di Calabria* (Lucera of Calabria) in 1269. Witello, or Vitello (1230-80), a Silesian, wrote a fundamental treatise on optics, *il Perspectiva* (the Perspective). By dividing the mechanical operations of the eye from the coordinating function of the mind he opened the way of modern psychology [1]. (Certainly with *optics* starts the observation of propagation effects such as *reflection*, *refraction*, and *diffraction*.)

A.1.3 Scientific Revolution

Between the mid-sixteenth and mid-seventeenth centuries, the scientific revolution is generally held to have taken place and it has been called 'the most important event in European History since the rise of Christianity' [2]. Science with its forte in astronomy, and in those sciences such as mathematics, optics, and physics, followed a natural progression from Renaissance humanism and was assisted to some extent by Protestant attitudes [1]. The scientific revolution changed the mankind's view both of human nature and the human predicament starting with the observations made on the tower of the capitular church of Frombork (Frauenburg) in Polish Prussia in the second decade of the sixteenth century; and culminating at a meeting of the Royal Society at Gresham College in London on 28 April 1686 [1].

Although Copernicus, Bacon, and Galileo were undoubtedly the highest achievers of human thought, it would be a misnomer, to call this period the so-called 'age of Copernicus, Bacon, and Galileo' because in most respect that was still the age of the alchemists, the astrologers, and the magicians. Davies on one hand claims that 'the alchemists misunderstood the nature of matter', and on the other hand he disclaims that 'researchers who have being the constructive aspect of alchemy are tainted by the lunacy which they try to describe' [1]-[2]. Nevertheless, the discoveries of Copernicus, Bacon, and Galileo were a breakthrough never seen before in human history.

Nikolaj Kopernik (Copernicus, 1473-1543) proved that the Sun, not the Earth, lay at the center of the solar system by detailed experiments and measurements. Johann Kepler (1571-1630) established the elliptical shape of planetary orbits and enunciated the laws of motion underlying Copernicus. But Galileo Galilei really brought Copernicus to the

wider public because he was among the first to avail himself of the newly invented telescope. Moreover, Galilei also contributed the kinematic principle, which in common engineering terms is known as the relation between the position and the velocity of a moving, physical body. This principle will become the backbone of Isaac Newton theory enunciating the laws of physics and including second order derivatives for the motion of physical bodies. (Without the knowledge produced from the works of Kopernik, Kepler, Galilei and Newton it would be impossible to even conceptually build the simplest Satellite Navigation System or a Geolocation System for that matter).

Practical science, to our disadvantage, remained in its infancy during the era when the Copernican theory was in dispute. Frances Bacon, the father of scientific method, made some important assertions in his *Advancement of Learning* (1605), the *Nuvum Organum* (1620), and the *New Atlantis* (1627), that knowledge should proceed by orderly and systematic experimentation and by inductions based on experimental data, which is a common practice in scientific methodology even today.

Two dazzling Frenchmen, René Descartes (1596-1650) and Blaise Pascal (1623-62), and their successor, Benedictus Spinoza (1632-77), a.k.a. as ‘philosophers with a mathematical bent’, made other important advances and contributions [1]. Descartes is most associated with his contribution to the analytical geometry (Amsterdam, 1644), and whose Cartesian system was named after him and so popular today. Pascal is also known for his contribution in physics and Spinoza in philosophy. (Analytical geometry lay at its center in all the study of mechanics and provides the framework for most coordinate systems.)

The scientific revolution opened the door to a new era, the *Enlightenment*, which enabled the scientific knowledge to make great strides. Undisputedly, the central giant of the period was Sir Isaac Newton (1642-1727), President of the [British] Royal Society. In his *Principia* in 1687, his description about the laws of Motion and Gravity provided the basis of physics and the working of the universe for over 200 years [1]. To him is attributed the invention of differential calculus, which he called ‘fluxions’, and he also conducted the first experiments in 1666 into the nature of Light, placing a glass of prism behind a hole in the blind of his window in Trinity College, Cambridge. In mathematics

the Leipziger Gottfried Leibniz (1646-1716) may well have discovered calculus independently before Newton did, and rightfully giving him the honor by calling the Newton-Leibniz calculus. Another giant in mathematics, Leonhard Euler (1707-83), who is said that 'Euler calculated as other men breathed, or eagles soar', discovered any number of theorems, invented the calculation of sines, completed the search for the numerical evaluation of the pi, and posited the existence of transcendental numbers [1]. Davies mentioned that Euler wrote 886 scientific works and 4,000 letters, at an average rate of two printed pages per day over five decades. Not surprisingly, the Russian journal *Commentarii Academiae Scientiarum Imperialis Petropolitanae* was still publishing the backlog of his articles forty-five years after his death. 'Euler's Theorem', which we take so much for granted in our complex algebra calculations, demonstrated the connection between the exponential and trigonometric functions: $\exp(ix) = \cos x + i \sin x$ [1]. The only peer in the history of mathematics, who could measure up to Euler, was C. F. Gauss (1777-1855), who was born in Brunswick ten years latter after Euler left Berlin.

A.1.4 *Dynamo*

Nineteenth century is fittingly called the '*dynamo* or the *powerhouse of the world*' because its dynamism far exceeded anything that was previously known in the world. In the same period, science and technology marched ahead as never seen before. Although the discoveries made were not as fundamental as those of Copernicus's, Newton's, or Einstein's were, the amount of knowledge gained was equal to map out whole new continents [1]. With the exception of one or two American of genius, it was entirely dominated by Europeans, and the most distinguished names belong to the fields of physics, chemistry, medicine, and biology [1].

During the same period communication systems improved as well. For the first time, the creation of a unified postal services made correspondence available to all. Postal stamps appeared with Great Britain's 'Penny Black' on 1 May 1840, later introduced in Zurich and Geneva (1843), in France and Bavaria (1849), in Prussia, Austria, and Spain (1850), in Sweden (1855), in Russia and Romania (1858), in Poland (1860), and in Island (1873) [1]. The invention of electric telegraph (1835), of the telephone (1877), and of radio (1890) rendered long-distance communications instantaneously and safely [1]. (For

the first time radio based systems rendered safe long-distance communications under severe weather or terrain conditions.)

A.1.5 *Greatest Scientific Discoveries between 1800- 1951*

Some of the scientific discoveries between 1800–1951 are: (1) E. L. Malus, polarization of light, Strasburg, 1808; (2) A. J. Fresnell, frequency of light, France, 1815; (3) H. C. Oested, electromagnetism, Copenhagen, 1819; (4) G. Ohm, electrical resistance, Cologne, 1827; (5) M. Faraday, electrical induction, London, 1831; (6) C. J. Doppler, acoustics, Prague, 1842; (7) G. R. Kirchhoff, spectral analysis, Heidenberg, 1859; (8) H. Hertz, electromagnetic waves, Karlsruhe, 1888; (9) H. Lorentz, electron theory, Leiden, 1895; (10) W. Röntgen, X-rays, Wuzburg, 1895; (11) J. J. Thompson, electron, Cambridge, 1897; (12) P. and M. Curie, radioactivity, Paris, 1898; (13) M. Plank, quantum theory, Berlin, 1900; (14) A. Einstein, theory of relativity, Zurich, 1905; (15) H. K. Onnes, superconductivity, Leiden, 1911; (16) E. Rutherford, atomic structure, Manchester, 1911; (17) W. Heisenberg, quantum mechanics, Copenhagen, 1925; and (18) O. Hahn, nuclear fission, Berlin, 1938 [1].

A.1.6 *Greatest Technological Inventions Between 1800- 1951*

Some of the technological inventions between 1800–1951 are: (1) A. Volta, electric battery, Bologna, 1800; (2) C. Babbage, mechanical calculator, Cambridge, 1834; (3) L. Foucault, gyroscope, Paris, 1852; (4) J. Reis, telephone, Friedrichsdorf, 1861; (5) W. von Siemens, dynamo, Berlin, 1867; (6) E. Berliner, microphone, Germany, 1877; (6) C. von Linde, refrigerator, Munich, 1877; (7) W. von Siemens, electric locomotive, Berlin, 1879; (8) H. S. Maxim, machine-gun, London, 1883; (9) G. Daimler, petrol engine, Connstatt, 1884; (10) Daimler and Benz, motor car, Mannheim, 1885; (11) C. Ader, aeroplane, France, 1890; (12) G. Marconi, radio transmitter, London, 1901; (13) K. E. Tsiolkovsky, rocketry, Moskcov, 1903; (14) Breguet-Richet, helicopter, France 1907; (14) British Army, military tank, Cambrai, 1915; (15) J. Logie Baird, television, London, 1924; (16) F. Whittle, jet engine, Cranwell, 1930; (17) Air Ministry, radar, Dover, 1940; (18) Wilkes and Renwick, EDSAC, computer, Manchester, 1946; (19) Power Ministry, nuclear power station, Calder Hall, 1956 [1].

A.1.7 Modern Localization Idea

Such discoveries and inventions provided the basis, the means of the technology and the understanding of geolocation systems we discuss in this work.

Thus, we have arrived in the present era and demand for geolocation systems. In the context of this chapter, the word ‘present’ is referred to a time period from as early as 1900 up to the current time of the publication of this work.

We briefly mentioned that modern localization idea is based upon *the precise measurement of time rather than distance*. Although in Newton physics time and distance are intrinsically related with the help of another component, which is called velocity, the latter must account for the system in which the observation is performed. It was Einstein who with his principle of special relativity enunciated the greatest achievement in modern physics. He postulated that the speed of light is constant despite the condition of the observer. On one hand, indisputably the electromagnetic wave was the best candidate for distance measurement because it propagates in almost any media as long as it had the proper frequency with a velocity equal to 299,792,458 m/sec in free space. On the other hand, a precise measure of time resulted from the atomic reaction of some materials such as rubidium/cesium/etc. At least from the theoretical perspective, it was possible to precisely measure both time and distance in free space. What was required next was the embodiment of these principles into physical devices and the greatest of them all is called *radio*.

On 28 September 1901, Reginald Fessenden applied for a patent on a means of reception of wireless signals by beats, for which he coined the term ‘*heterodyne*’. He was granted the U.S. Patent No. 706,740 on 12 August 1902 [3]. Fessenden proposed in sending Morse signals simultaneously on two carriers differing in frequency by a small amount. Not long after this, about 1907, it was soon realized that one of the signals could be replaced by a *locally generated oscillation*. The heterodyne principle has since rendered many amazing applications in wireless communications, notably the *superheterodyne* circuit, the standard circuit in radio receivers [3].

The twentieth century is known to all as the century of science, engineering, as the century of great dreams and worst nightmares. Today the knowledge in both science and

engineering is tremendous and the rate that this knowledge is increasing is overwhelming too. Nevertheless, in Chapter 1 we discuss some of the state of the art geolocation systems in great detail.

CITED REFERENCES AND FURTHER READING:

- [1] N. Davies, *Europe a History*, New York, NY: Oxford University Press, 1996.
- [2] H. Butterfield, *The Origins of Modern Science, 1300-1800*, London, 1947.
- [3] F. Nebeker, "September and October in EE history," *IEEE The Institute*, vol. 25, pp. 9, Oct. 2001.

Appendix B. Transmitter Design Considerations

“He that hath knowledge spareth his words: and a man of understanding is of an excellent spirit.”—Prov. 17:27

B.0 Introduction

As we have mentioned in Chapter 1 a transmitter is an apparatus that broadcasts one or more ranging signals. For personal communication systems a transmitter broadcasts a communication (voice, data, and video) signal. For geolocation systems a transmitter can either be a moving object such as a satellite or a fixed object in the ground such as a pseudolite. In the effort to combine both personnel communication systems and geolocation systems together we shall treat a transmitter as a pseudolite and vice versa. From the communication and signal structure point of view we exploit transmitters based in its signal structure presented in Figure B.1. As shown in Figure B.1 transmitters can be designed exploiting either one or a combination of *code*, *frequency*, *time* (delay), *amplitude*, *phase*, *pulse*, *encoding*, *antenna*, and *polarization* diversities. The advantages and disadvantages of each modulation technique in connection with indoor geolocation and communication are discussed in order.

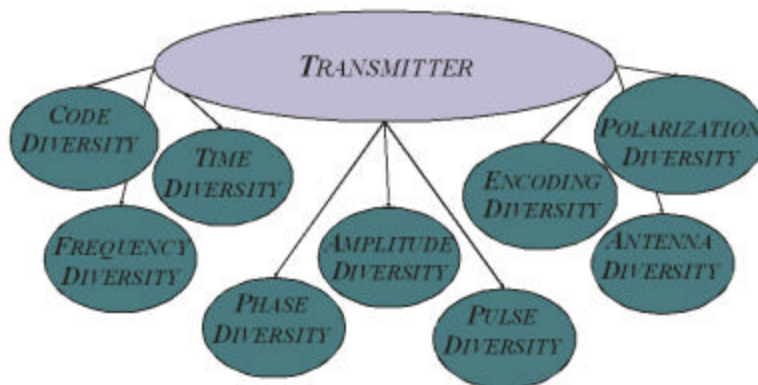


Figure B.1 An overview of transmitter modulation techniques.

B.1 Code Diversity

Code diversity is the modulation scheme, which exploits the code properties such as code autocorrelation and crosscorrelation. Code diversity can be further classified into *binary* (meaning two voltage levels) or *M-ary* (more than two voltage levels).

Two of the classical references in the study of binary code properties are the works by Sarwate and Pursley [1] and Enge and Sarwate [2]. There are several properties of the code autocorrelation and crosscorrelation discussed by Sarwate and Pursley [1]; nevertheless, they all depend to some extent on the *code family* (or type) and *code length*. Moreover, binary codes can be further classified into *periodic* and *aperiodic*. On one hand, code autocorrelation has two performance measures: *autocorrelation peak* and *out-of-phase autocorrelation peak* [1]. On the other hand, code crosscorrelation has one performance measure *crosscorrelation peak* [1]. In general, the code autocorrelation peak improves faster with the increase of the code length than the out-of-phase and crosscorrelation peaks do. Some code families have better ratio of the autocorrelation over either the out-of-phase autocorrelation peak or the crosscorrelation peak [1]; however, some families with poorer code properties provide a larger number of codes than some other families with better code properties. All these should be taken into consideration for designing a particular transmitter (pseudolite). The communication and geolocation systems that exploit code diversity are known as CDMA. Although with this modulation scheme we can achieve large system capacity due to a large number of transmitters, this is achieved in expense of large channel bandwidth due to long code length. Therefore, due to multiaccess interference an important problem occurs which is known as the *near-far effect*. Hence, we have arrived to a very important conclusion that the *near-far effect* is primarily dependent on the *code family and length*. Alone, this technique has limitations in eliminating the *near-far effect*.

The next technique is known as the M-ary. Although this technique is known to improve the bandwidth efficiency; nevertheless, it still retains the *near-far effect* problems of the binary sequences. For example, Pahlavan discusses a direct sequence spread spectrum system (DSSS) which provides resistance to multipath and utilizes

coding and diversity combining to improve bandwidth efficiency [3]. He also employs an M-ary signaling to further improve the bandwidth efficiency [3].

Magill, Natali, and Edwards provide an excellent review on the spread spectrum (SS) signaling [4]. While these techniques were widely used by the military, due to the advancement of the digital signal processing they are proliferating more and more in the commercial markets. Some of the properties of SS signaling properties that make it attractive for commercial applications are: (1) signal hiding and non-interference with conventional systems; (2) anti-jam and interference resistance; (3) privacy; (4) accurate ranging (self synchronization); (5) multi access; and (6) multipath mitigation [4]. There are two SS techniques that are carefully treated: direct sequence (DS) SS and frequency hopping (FH) SS (see the discussion in the following section) [4].

In conclusion code diversity can provide larger capacity and bandwidth efficiency with limited *near-far* capability.

B.2 Frequency Diversity

Frequency diversity is the modulation scheme based on the signal frequency operation. Unlike code diversity, *frequency diversity* has a major restriction—it is regulated the Federal Communication Commission (FCC). In the context of indoor geolocation systems three are of the most important modulation schemes that exploit *frequency diversity*: FDMA, *orthogonal frequency division modulation* (OFDM) [5], and *frequency hopping* (FH).

For example, Proгри and Michalson exploit a hybrid FDMA/CDMA scheme to overcome the *near-far* and the multipath effect [6]-[9]; hence, FDMA provides robustness against frequency selective multipath fading and to some extent narrow band interference [6]-[9].

Dardari and Tralli discusses high-speed indoor wireless communications at 60 GHz with coded OFDM by taking into account the propagation conditions in an actual environment [10]. Local performance and coverage figures have been suitably defined and the effects of code choice, frequency diversity, system clustering, and antenna sectorization have been studied and new algorithms to evaluate coding performance have

been introduced [10]. It has been shown that a system using 32 subcarriers, code-rate 0.5, sectored antennas, and 10 dBm of transmitted power in linear conditions can support packet transmission up to 155 MBPS with coverage of 84% [10].

Saleh summarizes the theoretical and experimental results on an experimental indoor radio communications system based on slow frequency hopping and coding to overcome the frequency selective multipath and narrowband interference [11]. Wang and Moeneclaey propose a hybrid direct sequence, slow frequency hopped, spread spectrum multiple access (DS/SFH-SSMA) operating over a Rician-fading channel which is less vulnerable to multi-access interference power than DS; and thus, more suitable to overcome the *near-far* problem [12]. Wang and Moeneclaey conclude that for both coherent and non-coherent receivers, frequency diversity and coding should be exploiting to achieve a satisfactory BER performance [12].

In conclusion, *frequency diversity* can be exploited to overcome frequency selective multipath fading, narrowband interference, overcome near-far effect, and increase the data rate. The only drawback is the lack of unallocated frequency spectrum.

B.3 Time Diversity

Time diversity is the modulation scheme, which utilizes a fraction of time to communicate between a designated transmitter and a designated receiver. *TDMA* and *signal pulsing* are two well know time diversity modulation schemes.

For example, Saleh appears to favor the TDMA technique due to its service flexibility stand point as opposed to the FDMA and spread spectrum CDMA which employ a fixed bit rate format [11].

Stanford and Ohio universities have employed signal pulsing to overcome the near-far effect [13].

Therefore, in summary time diversity can provide service flexibility; i.e., variable bit rate and overcome the near-far effect.

B.4 Phase Diversity

Phase diversity is the modulation scheme, which exploits the phase information. Phase information is achieved when there is a coherent reception; therefore, phase modulation should only be considered in the context of coherent reception.

For example, the work by Driessen and Greenstein [14] is a classical treatise of modulation techniques for high-speed wireless indoor systems using narrowbeam antennas. Due to the ubiquitous multipath encountered in indoor environment high data rates cannot be achieved easily [14]; hence, the aim of Driessen and Greenstein research is to break the multipath barrier "... to devise techniques whereby other factors (power, cost, etc) alter the limiting attainable bit-rates [14]." Based on the analysis considered here 2 level PSK schemes (coherent with pilot tones or differential) is favored among the other modulation schemes for narrow beam transmission indoors [14].

In conclusion, phase diversity can be exploited if very high data rate is required when it is possible to establish coherent reception.

B.5 Amplitude Diversity

Amplitude diversity is the modulation scheme, which exploits amplitude information. This modulation scheme suffers from the Inter Symbol Interference (ISI) and alone it is the least attractive. The most popular amplitude diversity is the quadrature amplitude modulation (QAM) which has better performance than the amplitude modulation (AM).

B.6 Pulse Diversity

Pulse diversity is the modulation technique, which exploits the pulse shape information. The most popular is the *pulse position modulation* (PPM) or its derivatives utilized in infrared communication [15]-[23].

For example, in order to overcome the bandwidth requirements of the PPM Shiu and Kahn [23] propose differential pulse-position modulation (DPPM) for power-efficient optical communication. The authors also discuss the chip-rate and multichip-rate to combat ISI. DPPM always achieves higher power efficiency and lower hardware

complexity than PPM does [23]. These make DPPM a favorable candidate to replace PPM in many applications [23].

In conclusion pulse diversity should be exploited for infrared or laser (optical) communication.

B.7 Encoding Diversity

Encoding diversity is the scheme, which improves the data robustness in fading and noisy channels. There are several encoding techniques that should be exploit; however, this is secondary and it is not going to be the focus of this work. For example, forward error correction (FEC) should be exploited to preserve the data information in multipath fading channels (see Appendix C).

B.8 Antenna Diversity

Antenna diversity is based on the space information achieved from the different location of the antenna elements. Antenna diversity is becoming more and more popular due to a number of improvements that it offers such as capacity increase, bandwidth efficiency, power decrease, and superior performance against narrowband interference and frequency selective and flat fading multipath.

For example, an indoor communication system proposed by Saleh appears also to employ antenna diversity to gain immunity against very-slow-time varying and frequency selective multipath fading and to some extent to narrow band interference [11]. He is also asserting that signaling rate can almost be doubled through the use of antenna diversity [11].

B.9 Polarization Diversity

Polarization diversity is the modulation scheme, which exploits the polarization diversity to yield better multipath interference mitigation. Nevertheless, this kind of modulation is not going to be exploited here anyway.

CITED REFERENCES AND FURTHER READING:

- [1] D.V. Sarwate and M.B. Pursley, "Crosscorrelation properties of pseudorandom and related sequences," in *Proc. of IEEE*, vol. 68, pp. 593-619, May 1980.
- [2] P.K. Enge and D.V. Sarwate, "Spread-spectrum multi-access performance of orthogonal codes: linear receivers," *IEEE Trans. Comm.*, vol. COM-35, 1309-1399, Dec. 1987.
- [3] K. Pahlavan and M. Chase, "Spread-spectrum multiple-access performance of orthogonal codes for indoor radio communications," *IEEE Trans. Comm.*, vol. 38, no. 5, pp. 574-577, May 1990.
- [4] D.T. Magill, F.D. Natali, and G.P. Edwards, "Spread-spectrum technology for commercial applications," in *Proc. IEEE*, vol. 82, no. 4, pp. 572-584, Apr. 1994.
- [5] I. Koffman and V. Roman, "Broadband wireless access solutions based on OFDM access in IEEE 802.16," *IEEE Comm. Mag.*, vol. 40, no. 4, pp. 96-103, Apr. 2002.
- [6] I.F. Proгри, J.M. Hill, and W.R. Michalson, "An investigation of the pseudolite's signal structure for indoor applications," in *Proc. ION-AM*, Albuquerque, NM, pp. 453-462, June 2001.
- [7] I.F. Proгри and W.R. Michalson, "The impact of proposed pseudolite's signal structure on the receiver's phase and code error," in *Proc. ION-AM*, Albuquerque, NM, pp. 414-422, June 2001.
- [8] I.F. Proгри and W.R. Michalson, "An alternative approach to multipath and near-far problem for indoor geolocation systems," in *Proc. ION-GPS*, Salt Lake City, UT, Sep. 2001.
- [9] I.F. Proгри and W. R. Michalson, "Performance evaluation of a DSSS/CDMA/FDMA indoor geolocation system," in review *IEEE Trans. Comm.*, Nov. 2001.
- [10] D. Dardari and V. Tralli, "High-speed indoor wireless communications at 60 GHz with coded OFDM," *IEEE Trans. Comm.*, vol. 47, no. 11, pp. 1709-1721, Nov. 1999.
- [11] A.A.M. Saleh, A.J. Rustako, Jr., L.J. Cimini, Jr., G.J. Owens, and R.S. Roman, "An experimental TDMA indoor radio communications system using slow frequency hopping and coding," *IEEE Trans. Comm.*, vol. 39, no. 1, pp. 152-162, Jan. 1991.
- [12] J. Wang and M. Moeneclaey, "Hybrid DS/SFH-SSMA with predetection diversity and coding over indoor radio multipath Rician-fading channels," *IEEE Trans. Comm.*, vol. 40, no. 10, pp. 1654-1662, Oct. 1992.
- [13] B.W. Parkinson, J.J. Spilker, Jr, et al., *The Global Positioning System-Theory and Applications*, Washington, DC: American Institute of Aeronautics and Astronautics, (vol. 1, chap. 2, "Overview of GPS operation and design") 1996.

- [14] P.F. Driessen and L.J. Greenstein, "Modulation techniques for high-speed wireless indoor systems using narrowbeam antennas," *IEEE Trans. Comm.*, vol. 43, no. 10, pp. 2605-2612, Oct. 1995.
- [15] M.D. Audeh and J.M. Kahn, "Performance evaluation of baseband OOK for wireless indoor infrared LAN's operating at 100 Mb/s," *IEEE Trans. Comm.*, vol. 43, no. 6, pp. 2085-2094, June 1995.
- [16] M.D. Audeh, J.M. Kahn, and J.R. Barry, "Performance of pulse-position modulation on measured non-directed indoor infrared channels," *IEEE Trans. Comm.*, vol. 44, no. 6, pp. 654-659, June 1996.
- [17] G.W. Marsh and J.M. Kahn, "Performance evaluation of experimental 50-Mb/s diffuse infrared wireless link using on-off keying with decision-feedback equalization," *IEEE Trans. Comm.*, vol. 44, no. 11, pp. 1496-1504, Nov. 1996.
- [18] D.C.M. Lee, J.M. Kahn, and M.D. Audeh, "Trellis-coded pulse-position modulation for indoor wireless infrared communications," *IEEE Trans. Comm.*, vol. 45, no. 9, pp. 1080-1087, Sep. 1997.
- [19] J.B. Carruthers and J.M. Kahn, "Modeling of nondirected wireless infrared channels," *IEEE Trans. Comm.*, vol. 45, no. 10, pp. 1260-1268, Oct. 1997.
- [20] G.W. Marsh and J.M. Kahn, "Channel reuse strategies for indoor infrared wireless communications," *IEEE Trans. Comm.*, vol. 45, no. 10, pp. 1280-1290, Oct. 1997.
- [21] D.C.M. Lee and J.M. Kahn, "Coding and equalization for PPM on wireless infrared channels," *IEEE Trans. Comm.*, vol. 47, no. 2, pp. 255-260, Feb. 1999.
- [22] M.D. Audeh, J.M. Kahn, and J.R. Barry, "Decision-feedback equalization of pulse-position modulation on measured nondirected indoor infrared channels," *IEEE Trans. Comm.*, vol. 47, no. 4, pp. 500-503, Apr. 1999.
- [23] D. Shiu and J.M. Kahn, "Differential pulse-position modulation for power-efficient optical communication," *IEEE Trans. Comm.*, vol. 47, no. 8, pp. 1201-1210, Aug. 1999.

Appendix C. Forward Error Correction (FEC)

“Now the just shall live by faith.”—Heb 10:38

C.0 Forward Error Correction

FIRST, it is possible to encode I binary source digits into u binary code words by mapping $u = 2^l$ orthogonal signals to reduce the probability of bit error. However, this encoding increases the bandwidth proportionally with u , which introduces more noise into the system, ultimately resulting in an inefficient improvement in the probability of bit error. FEC encoding provides an optimum solution to this problem by minimizing the probability of bit error at the smallest possible bandwidth increase. It is well known that the number of errors that can be detected is equal to the Hamming distance, d_H , which is the minimum number of bit positions by which code words of a particular code are different. However, the maximum number of errors that can be corrected is equal to $(d_H - 1)/2$ [1]. Next, we discuss some categories of FECs and the process for encoding and decoding of a specific category of FEC.

The FEC main categories are block coding, cyclic codes (Read Solomon codes), and convolutional codes [1]-[4]. For example, for Wide Area Augmentation System (WAAS) applications, the WAAS signal is encoded with FEC (convolutional code) with rate, $R = 0.5$, and a constraint length, $N = 7$, and 3-bit soft decision [2]. For the purposes of this investigation we cover only *convolutional codes* because first, both block coding and cyclic codes are *primarily non-binary* codes and second the convolutional codes are *primarily binary* codes and have been previously utilized in geolocation applications [2].

Let I denote the source digits before entering the FEC encoder and u the digits of the sequence coming out of the FEC encoder. The code R rate of the output of a convolutional encoder is defined as [1]

$$(C.1.1) \quad R = \frac{I}{u}$$

The constraint length, N , of a convolutional code is defined as [1]

$$(C.1.2) \quad N \equiv L_s$$

where L_s is the length of the shift registers (see Figure C.1).

A generator polynomial matrix \mathbf{G} describes the connections between modulo-2 adders and shift registers. Let \mathbf{X} be the code word corresponding to the input sequence entering the convolutional encoder. Then the code word corresponding to the output sequence, \mathbf{Y} , exiting the convolutional encoder is defined as [1]

$$(C.1.3) \quad \mathbf{Y} = \mathbf{X}^T \mathbf{G} .$$

As shown in Figure C.1 there are two generator polynomials that form the generator polynomial matrix \mathbf{G} : one that represents the upper connections from the shift register and the other the lower connections from the shift register. The best $R = 0.5$ convolutional codes can be generated using the data from Table C.1 for convolutional codes with rates other than $R = 0.5$ the reader may refer to Appendix B of [1].

The left column of Table C.1 is the constraint length N . The second column of Table C.1 represents the two generator polynomials in octal representation. The third left column represents the corresponding generator polynomials in binary representation. Whenever there is a '1' in the generating polynomial (third column of Table C.1) then there is a physical connection at the corresponding location of the shift register and the modulo two adder and whenever there is a '0' in the generating polynomial there is no physical connection at the location of the shift register and the modulo two adder. For example, for $N = 3$ the best convolutional code is created using $g_1 = [1 \ 1 \ 1]$ and $g_2 = [1 \ 0 \ 1]$; i.e., there are *three* connections connecting each location of the shift register to the upper modulo two adder and there are only *two* connections connecting only the first and the last locations of the shift register to the modulo two adder. The fourth column of Table C.1 represents the free distance, d , (not to be confused with the Hamming distance, d_H) and the fifth through the ninth columns represent the total information weight of all paths with weight d through $d + 4$. More is said about these columns later.

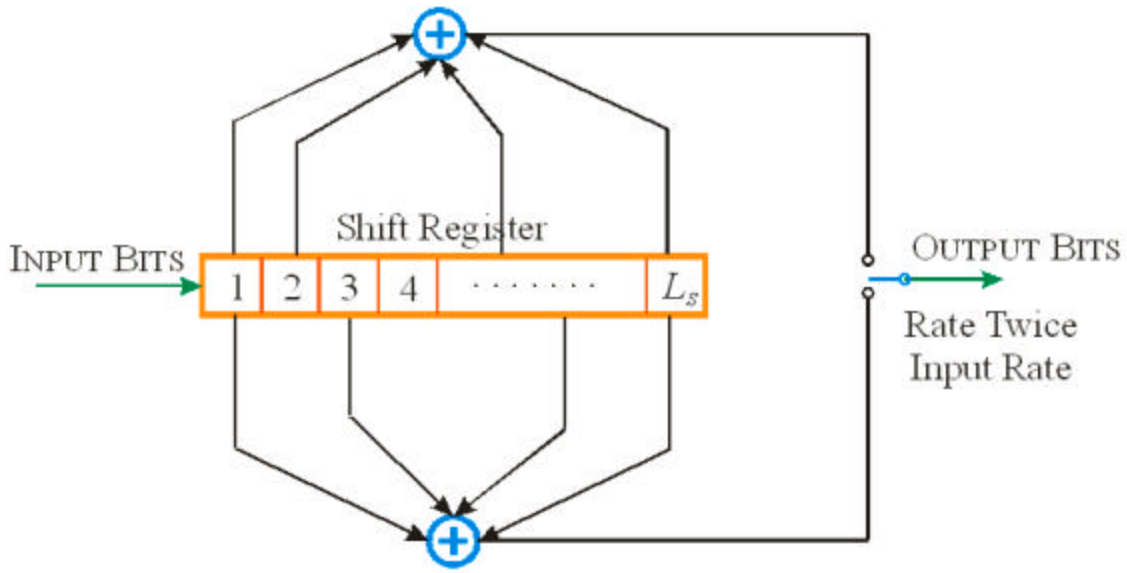


Figure C.1 A $R=0.5$, convolutional code with constrain length of L_s .

A convolutional encoder is in fact a finite state machine and the state is determined by the most recent $v = N-1$ symbols shifted into the encoder shift register and therefore it is a number from 0 to 2^v-1 [1]. The state diagram of a convolutional code with $R = 1/2$ and constraint length of $N = 4$ is shown in Figure C.2.¹

Table C.1 Generators (in Octal) and weight structure of an $R = 0.5$ convolutional code—taken and modified from [1].

N	Generators (octal)	Generators (binary)	d	w_d	w_{d+1}	w_{d+2}	w_{d+3}	w_{d+4}
3	7, 5	111, 101	5	1	4	12	32	80
4	17, 15	1111, 1101	6	2	7	18	49	130
5	35, 23	11101, 10011	7	4	12	20	72	225
6	75, 53	111101, 101011	8	2	36	32	62	332
7	171, 133	1111001, 1011011	10	36	0	211	0	1404
8	371, 247	11111001, 10100111	10	2	22	60	148	340
9	753, 561	111101011, 101110001	12	33	0	281	0	2179

¹ Because the $R = 0.5$ and $N = 3$ convolutional code is discussed extensively in [1] we have decided to discuss here the $R = 0.5$ and $N = 4$ convolutional code structure and properties.

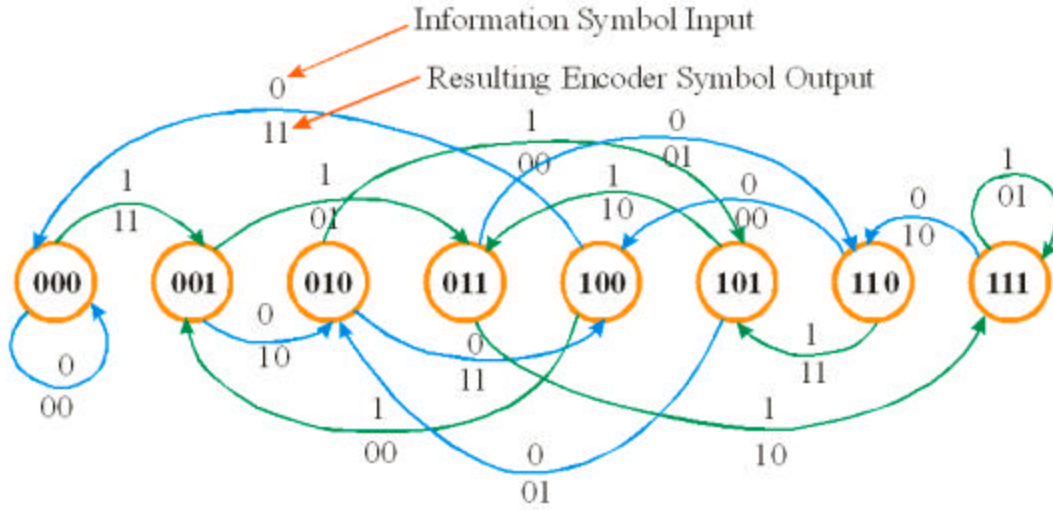


Figure C.2 State diagram for an $R = 1/2, N = 4$, convolutional code.

The state diagram of Figure C.2 can be exploited to produce a signal flow graph as shown in Figure C.3 because the theory of signal flow graphs have been applied to the study of convolutional structure and performance [1]. Assuming the all-zero transmitted sequence, the paths of interest are those which start and end in the zero state and do not return to the zero state anywhere in between [1]. The length of the input sequence, the weight of the input sequence, and the weight of the output sequence are often determined from each one of these paths [1]. For example, consider the signal flow graph that results from the state diagram of Figure C.2 as shown in Figure C.3. Let L denote the length of the input sequence, W denote the weight of the input sequence, and O denote the weight of the output sequence. Each branch in the flow graph in Figure C.3 has a gain, g , given by $LW^{w_i}O^{w_o}$, where w_i is the input weight required to drive the encoder between two nodes connected by the branch and w_o is the output weight associated with the branch. Since the paths that start and end in state zero and do not go through zero in between are the paths of interest then the self loop on zero state is removed and the state is split into an input and an output [1]. The gain of this graph is computed using the standard methods, which results in the following generating function

$$(C.1.4) \quad T(L,W,O) = \frac{L^4WO^6(LW - O - LWO^2)}{1 - LWO(L+1) + L^3W^2O^2 - L^4W^2O^2 - L^3WO^3 - L^3W^2O^4 + L^4W^2O^4}$$

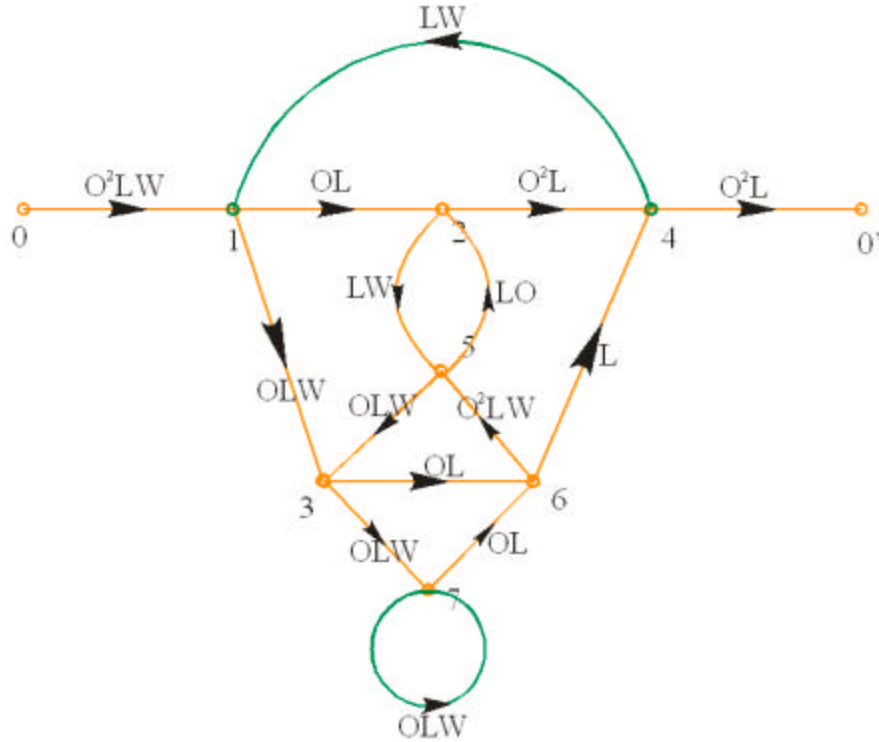


Figure C.3 Signal flow graph for an $R = 1/2, N = 4$, convolutional code.

Let $L = 1$ we get

$$(C.1.5) \quad T(W, O) = \frac{WO^6(W + O - WO^2)}{1 - 2WO - WO^3}$$

Expanding by long division the above equation can be written as

$$(C.1.6) \quad T(W, O) = (W^2O^6 + WO^7 - W^2O^8)(1 + WO[2 + O^2] + W^2O^2[2 + O^2]^2 + \dots) \\ = W^2O^6 + WO^7 - W^2O^8 + (W^3O^7 + W^2O^8 - W^3O^9)(2 + O^2) \\ + (W^4O^8 + W^3O^9 - W^4O^{10})(2 + O^2)^2.$$

Hence, there is one path of input weight 2 and output weight 6. There are three paths two of input weight 3 and one of input weight 1 and all of output weight 7. Now we define the *free-distance*, d , of the code as the weight of the *minimum [output] weight* path which begins and ends in state zero [1]. There are three paths that start in state zero and end in state zero: 0-1-4-0', 0-1-3-6-4-0', and 0-1-3-7-6-4-0'. The first path has an output weight of 7, the second of 6, and the third of 7. Hence, the free-distance for this $R = 1/2, N = 4$ convolutional code is 6 just like shown in Table C.1 fourth column.

Another useful method for obtaining the transfer (or generating) function, given by eq. (C.1.4), would be through the use of state equations

$$(C.1.7) \quad \mathbf{x} = \mathbf{Ax} + \mathbf{b}u$$

$$(C.1.8) \quad y = \mathbf{cx} + du$$

where

$$(C.1.9) \quad \mathbf{A} = \begin{bmatrix} 0 & 0 & 0 & LW & 0 & 0 & 0 \\ LO & 0 & 0 & 0 & LO & 0 & 0 \\ LWO & 0 & 0 & 0 & LWO & 0 & 0 \\ 0 & LO^2 & 0 & 0 & 0 & L & 0 \\ 0 & LW & 0 & 0 & 0 & LWO^2 & 0 \\ 0 & 0 & LO & 0 & 0 & 0 & LO \\ 0 & 0 & LWO & 0 & 0 & 0 & LWO \end{bmatrix}, \quad \mathbf{b} = \begin{bmatrix} LWO^2 \\ 0 \\ 0 \\ 0 \\ 0 \\ 0 \\ 0 \end{bmatrix},$$

$$(C.1.10) \quad \mathbf{c} = [0 \ 0 \ 0 \ LO^2 \ 0 \ 0 \ 0], \text{ and } d = 0.$$

The transfer function can be obtained as

$$(C.1.11) \quad T(L, W, O) = \mathbf{c}(\mathbf{I} - \mathbf{A})^{-1}\mathbf{b}.$$

A simple illustration in MATLAB for computing the transfer function given by eq. (C.1.11) is shown in Figure C.4.

According to eq. (C.1.6) there is one path of weight 6, three of weight 7, etc [1]. This information is used later to determine the probability of event error. Now, we define the total information weight, w_j , of all paths of weight j as the coefficient of O^j and is determined from:

$$(C.1.12) \quad \left. \frac{\partial T(W, O)}{\partial W} \right|_{W=1} = \sum_{j=0}^{\infty} w_j O^j$$

After some calculus manipulations the above equation is given by

$$(C.1.13) \quad \left. \frac{\partial T(W, O)}{\partial W} \right|_{W=1} = 2O^6 + 7O^7 + 18O^8 + \dots$$

The weight coefficients obtained in eq. (C.1.13) are in agreement with those provided in the 2nd row and in the 5th through 7th column of Table C.1.

```

MATLAB Editor/Debugger - [Appendix-C.m - C:\Documents...
File Edit View Debug Tools Window Help
Stack:
% Ph.D. Dissertation Appendix C
% Copyright (c) 2002, 2003 by Ilir F. Progri

clear all;
close all;
format compact;

L = sym('L');
W = sym('W');
O = sym('O');

% Enter the matrix A
A = [ 0 0 0 0 L*W 0 0 0;
      L*O 0 0 0 0 L*O 0 0;
      L*W*O 0 0 0 0 L*W*O 0 0;
      0 L*O^2 0 0 0 0 0 L;
      0 L*W 0 0 0 0 L*W*O^2 0;
      0 0 L*O 0 0 0 0 L*O;
      0 0 L*W*O 0 0 0 0 L*W*O];

N = length(A);

% Form the matrix I - A
B = eye(N,N) - A;

% Form the vector c
c = [ 0 0 0 L*O^2 0 0 0];

% Form the vector b
b = [L*W*O^2; 0; 0; 0; 0; 0; 0];

% Compute the transfer function
T = c*inv(B)*b

```

Figure C.4 An illustration in MATLAB for computing the transfer function $T(L,W,O)$.

Thus far we have explained in great detail the meaning of all the columns of Table C.1. It remains to discuss the probability of event error and the convolutional code performance. The performance of the convolutional code is estimated in terms of union bounds and computer simulations [1]. Union bounds is the performance measure that relates the bit error probability (BEP) (more commonly used as bit error rate (BER)) without encoding to the BER with encoding as shown in Figure C.5. Assuming a binary symmetric channel (BSC) with a channel symbol error rate BER_{NCC} (i.e., the BER without any encoding), the BER_{WCC} (i.e., the BER with convolutional encoding) of a $R=0.5$ convolutional code is given by [1],

$$(C.1.14) \quad BER_{WCC} < \sum_{j=d}^{\infty} w_j D^j \Big|_{D=2\sqrt{BER_{NCC}(1-BER_{NCC})}} \approx \sum_{j=d}^{d+4} w_j D^j \Big|_{D=2\sqrt{BER_{NCC}(1-BER_{NCC})}} .$$

Utilizing the data from Table C.1 and the expression (C.1.14) we estimated the performance of an $R = 0.5$ convolutional code; i.e., the BER_{WCC} vs. the BER_{NCC} for a convolutional code with constraint length $N = \{3, 5, \dots, 9\}$ and the result of this work is plotted in Figure C.5.

As shown in Figure C.5 the convolutional code improves tremendously the BER. For example, for a typical channel if the BER rate without convolutional code is $1e-5$ the convolutional code of $N = \{3, 4, \dots, 9\}$ would improve the BER = $\{2.5e-14, 1e-14, 2.8e-18, 3.5e-19, 2.22e-22, 1.26e-23, 7.63e-27\}$. Obviously, if the channel is erroneous or for $BER_{NCC} > 0.1$ then the $BER_{WCC} > 0.1$ (not shown in Figure C.5 but implied and computed), which indicates that convolutional encoding is helpful for channels with $BER_{NCC} \leq 0.2$ and it is very helpful for channels with $BER_{NCC} \leq 0.3$. Here we conclude our discussion on FEC and $R = 0.5$ convolutional codes.

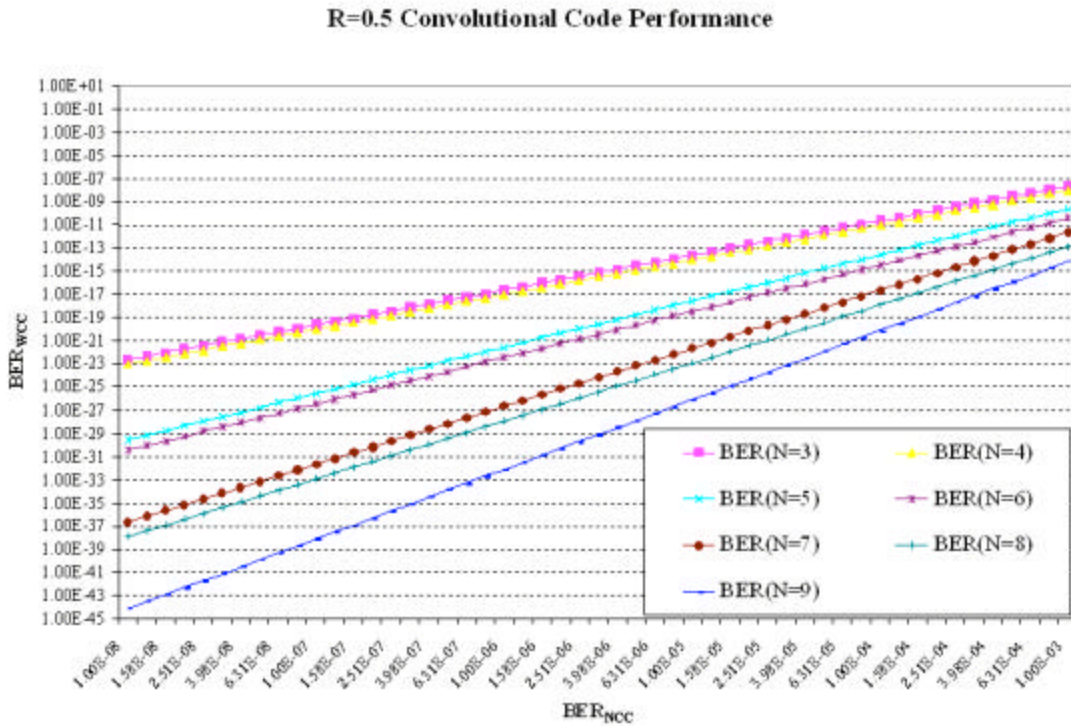


Figure C.5 The BER_{WCC} vs. BER_{NCC} for a 0.5 rate convolutional code with $N = \{3, 5, \dots, 9\}$.

CITED REFERENCES AND FURTHER READING:

- [1] G.C. Clack, Jr. and J. Bibb Cain, *Error Correcting Coding for Digital Communications*. New York, NY: Plenum Press, 1981.
- [2] P.K. Enge and A.J. Van Dierendonck, "Wide area augmentation system," in *Global Positioning System: Theory and Applications*, vol. 164, Washington, DC: AIAA, 1996.
- [3] R.G. Gallager, *Information Theory and Reliable Communications*. New York: Wiley, 1968.
- [4] W.W. Peterson and E.J. Weldon, *Error Correcting Codes*. Cambridge, MA: MIT Press, 1972.

Appendix D. Spreading Codes

“The fear of the LORD is the instruction of wisdom; and before honour is humility.”—Prov. 15:33

D.0 Spreading Codes

THE generation of the spreading C, P, and B, codes (see Chapter 4) is performed using shift registers with linear feedback [1]. The spreading sequences that we are interested in are Gold and Kasami sequences [1]-[6], which are derived from a very important class of pseudorandom (PN) sequences called maximum length shift register sequences (or m -sequences). A general m -stage shift register with linear feedback is used for generating m -sequences as shown in Figure D.1. The m -sequence code generator contains one m -stage shift register and one modulo 2 adder. Stages connected for generating the m -sequence for $m = \{2,3,\dots,34\}$ are tabulated in Table D.1. From Table D.1 it is interesting to observe that the number of stages connected to modulo 2 adder can be either 2 or 4 with position 1 being always connected.

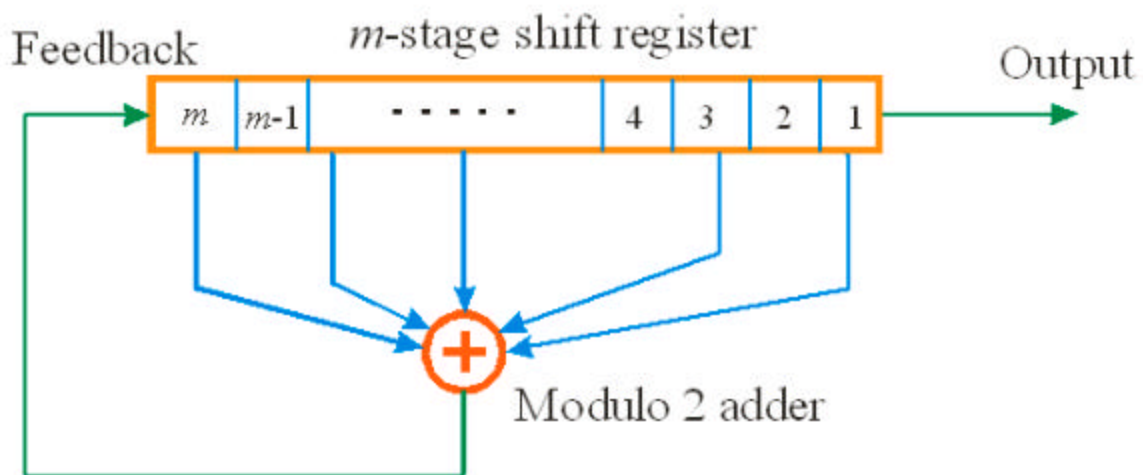


Figure D.1 An m -stage shift register with linear feedback—taken from [1].

Table D.1 Shift register connections for generating m -sequences—taken from [1]

m	Stages connected to modulo-2 adder	m	Stages connected to modulo-2 adder	m	Stages connected to modulo-2 adder
2	1, 2	13	1, 10, 11, 13	24	1, 18, 23, 24
3	1, 3	14	1, 5, 9, 14	25	1, 23
4	1, 4	15	1, 15	26	1, 21, 25, 26
5	1, 4	16	1, 5, 14, 16	27	1, 23, 26, 27
6	1, 6	17	1, 15	28	1, 26
7	1, 7	18	1, 12	29	1, 28
8	1, 5, 6, 7	19	1, 15, 18, 19	30	1, 8, 29, 30
9	1, 6	20	1, 18	31	1, 29
10	1, 8	21	1, 20	32	1, 11, 31, 32
11	1, 10	22	1, 22	33	1, 21
12	1, 7, 9, 12	23	1, 19	34	1, 8, 33, 34

In geolocation and DSSS applications the binary sequence $\{c'_m\} = \{0,1\}$ is mapped into a corresponding binary sequence with elements $\{c_m\} = \{\pm 1\}$, which is called a *bipolar sequence*, to avoid multiplications with zero simply by $c_m = 1 - 2c'_m$. Let us discuss eight important properties of m -sequences.

1. The m -sequence length (in bits) is equal to $M = 2^m - 1$ bits [1].
2. There are exactly M nonzero sequences generated by $f(x)$ and they are just the M different phases of c ; i.e., $c, Tc, T^2c, T^3c, \dots, T^{M-1}c$, where T^m is a left cyclic shift operator or $(T^k c)_m = c_{m+k}$ [1].
3. Given distinct integers m and n , $0 \leq m, n < M$, there exists a unique k , such that $0 < k < N \cap k \neq i, j$ and [1]

$$T^m c \oplus T^n c = T^k c.$$

This property is known as the *shift-and-add* property and it is the necessary and sufficient condition for a sequence of period M to be an m -sequence.

4. The number of ones in c is called the Hamming weight of c and it is equal to $\mathbf{h}_c = 2^{m-1} = (M + 1)/2$ [1].
5. The autocorrelation function, \mathbf{j}_c , of the bipolar sequence is defined as [1]-[4]

$$(D.1.2) \quad \varphi_c(m) = \sum_{n=0}^{M-1} c_n c_{n+m} = \varphi_c(m+M), \quad \forall m \in \{0, \dots, M-1\}$$

where M is the period of the sequence and the autocorrelation function $\varphi_c(m)$, which satisfies

$$(D.1.3) \quad \mathbf{j}_c(m) = \begin{cases} M, & m = 0 \bmod M \\ -1, & m \neq 0 \bmod M \end{cases}.$$

The $\mathbf{j}_c(0)$ is called the *autocorrelation peak* and $\mathbf{j}_c(m)$, $1 \leq m \leq M-1$, is called the *out of phase autocorrelation peak* (or the *off-peak*). The peak ratio $\mathbf{j}_c(m)/\mathbf{j}_c(0) = -1/M$ decreases proportionally with M ; hence, the m -sequence is the closest to the ideal pseudorandom sequence with autocorrelation properties similar to white noise.

6. Among M sequences generated by $p(x)$ there is only one sequence, \tilde{c}_m , which satisfies the property $\tilde{c}_m = \tilde{c}_{2m}, \forall m \in \mathbf{Z}$ [1]. This unique sequence, \tilde{c}_m , is called a *characteristic m -sequence*, or the *characteristic phase* of the m -sequence c .
7. Consider the sequence, b , formed by taking every q^{th} bit of c (i.e., $b_m = c_{qm}, \forall m \in \mathbf{Z} \cap q \in \mathbf{Z}^+$); the sequence b is said to be a decimation by q of c is denoted by $c[q]$ [1]. Also, denote the *greatest common divisor* of the integers m and n by $\mathbf{r}(m, n)$. If $c[q]$ is not identically zero (i.e., $c[q] \neq 0$) then its period is equal to $M/\mathbf{r}(m, n)$ and $c[q]$ is generated by the polynomial $\hat{p}(x)$ whose roots are the q^{th} powers of the roots of $p(x)$ [1].
8. Assume that $\mathbf{r}(M, q) = 1$. If $b = c[q]$ then for all $n \geq 0$,

$$(D.1.4) \quad \tilde{c}[2^n q] = \tilde{c}[2^n q \bmod M] = \tilde{b}$$

and

$$(D.1.5) \quad c[2^n q] = u[2^n q \bmod M] = T^m b$$

for some m that depends on n [1].

Although some of these properties may not seem obvious they are carefully discussed in [1] and applied in [1]-[4]. Nevertheless, all m -sequences have two major drawbacks: (1) they are vulnerable to enemy interception and (2) they are impractical for CDMA and geolocation applications. On one hand, m -sequences are vulnerable to enemy interception because the enemy can determine the linear feedback by observing the $2m$ chips from the m -sequences and thus can decode the data. This vulnerability of the m -

sequence can be solved the encryption or scrambling. And on the receiver, the decryption and de-scrambling is applied. On the other hand, for CDMA and geolocation applications the crosscorrelation of the PN sequences are as important and the autocorrelation properties which is discussed next.

Suppose that b and c are two m -sequences of period $M = 2^m - 1$ and $b = c[q]$. The crosscorrelation function between b and c is defined as [1]

$$(D.1.6) \quad \mathbf{j}_{b,c}(m) = \sum_{n=0}^{M-1} b_n c_{n+m} = \mathbf{j}_{b,c}(m+M), \quad \forall m \in \{0, \dots, M-1\}.$$

It is relatively easy to see that $\mathbf{j}_{b,c}(m)$ is an odd integer and that $|\mathbf{j}_{b,c}(m)| \leq M$ [1]. Moreover, if b and c are generated by reciprocal polynomials then $\mathbf{j}_{b,c}(m) = -1 \pmod{4}$; otherwise, $\mathbf{j}_{b,c}(m) = -1 \pmod{8}$ [1]. The average of the crosscorrelation function $\mathbf{j}_{b,c}(m)$ is always +1 or

$$(D.1.7) \quad \sum_{m=0}^{M-1} \mathbf{j}_{b,c}(m) = +1.$$

A very important identity of the crosscorrelation function is given below and the proof can be found in [1]

$$(D.1.8) \quad \sum_{m=0}^{M-1} \mathbf{j}_{b,c}(m) [\mathbf{j}_{b,c}(m+n)]^* = \sum_{m=0}^{M-1} \mathbf{j}_b(m) [\mathbf{j}_c(m+n)]^*$$

and setting $n = 0$ gives,

$$(D.1.9) \quad \sum_{m=0}^{M-1} |\mathbf{j}_{b,c}(m)|^2 = \sum_{m=0}^{M-1} \mathbf{j}_b(m) [\mathbf{j}_c(m)]^*.$$

Utilizing the above identity and property 5 of the autocorrelation function produces [1]

$$(D.1.10) \quad \sum_{m=0}^{M-1} |\mathbf{j}_{b,c}(m)|^2 = M^2 + M - 1 = 2^{2m} - 2^m - 1.$$

There exists one integer l for which,

$$(D.1.11) \quad |\mathbf{j}_{b,c}(l)| > 2^{(m+1)/2} - 1 = \sqrt{2} 2^{m/2} - 1 > 2^{m/2} - 1.$$

A very important property of the crosscorrelation function is given by [1]

$$(D.1.12) \quad \mathbf{j}_{\tilde{b},\tilde{c}}(m) = \mathbf{j}_{\tilde{b},\tilde{c}}(2^n m) = \mathbf{j}_{\tilde{b},\tilde{c}}(2^n m \pmod{M}), \quad \forall n \geq 0.$$

Therefore, it is sufficient to know the values of the crosscorrelation function for only a few selected values because the remaining values can be determined based on the above

property and the following technique. First, find the decimation of \tilde{b} that produces \tilde{x} and the decimation of \tilde{x} that produces \tilde{y} ; then, if $\tilde{x} = \tilde{b}[r]$, $\tilde{y} = \tilde{x}[q]$, and $\tilde{c} = \tilde{b}[q]$, the following is obtained [1]

$$(D.1.13) \quad \mathbf{j}_{\tilde{x},\tilde{y}}(rm) = \mathbf{j}_{\tilde{b},\tilde{c}}(m) \quad \text{and} \quad \mathbf{j}_{\tilde{x},\tilde{y}}(m) = \mathbf{j}_{\tilde{b},\tilde{c}}(r'm)$$

where $rr' = 1 \pmod{M}$.

For geolocation application it is not necessary to know all the values of the crosscorrelation function, $\mathbf{j}_{b,c}(m)$, for each m ; nevertheless, it may be sufficient to know the set of values taken on by $\mathbf{j}_{b,c}(m) = u$ for each u in this set. This is referred to as the *crosscorrelation spectrum* or just *spectrum*. For example, the *autocorrelation spectrum* is *two valued* [1]

$$\begin{aligned} M &\text{ occurs } 1 \text{ time} \\ -1 &\text{ occurs } M-1 \text{ times.} \end{aligned}$$

The crosscorrelation spectra for the pair (b,c) is the same as for the pair $(T^i b, T^i c)$ and in particular for the pair (\tilde{b}, \tilde{c}) [1]. From eq. (D.1.13) the crosscorrelation spectra depends only on the decimation q and not upon the individual m -sequences [1]. Also, if $qq' = 1 \pmod{M}$ then both decimations q and q' give rise to the same crosscorrelation spectra [1].

Theorem 1: Let b and c denote m -sequences of period $M = 2^m - 1$. If $c = b[q]$ or $b = c[q]$, where either $q = 2^k + 1$ or $q = 2^{2k} - 2^k + 1$, and if $e = \mathbf{r}(m,k)$ is such that if m/e is *odd*, then the *spectrum* of $\mathbf{j}_{b,c}(m)$ is three valued and is given by [1]

$$\begin{aligned} -1 + 2^{(m+e)/2} &\text{ occurs } 2^{m-e-1} + 2^{(m-e-2)/2} \text{ times,} \\ -1 &\text{ occurs } 2^m - 2^{m-e} - 1 \text{ times,} \\ -1 - 2^{(m+e)/2} &\text{ occurs } 2^{m-e-1} - 2^{(m-e-2)/2} \text{ times.} \end{aligned}$$

The reader is reminded that if e is large, $\mathbf{j}_{b,c}(m)$ takes on large values but only a few times and if e is small then $\mathbf{j}_{b,c}(m)$ takes on smaller values but more frequently [1].

Theorem 2: Let b and c denote m -sequences of period $M = 2^m - 1$, where m is a multiple of 4. If $c = b[q]$, where either $q = -1 + 2^{(m+2)/2} = t(m) - 2$, then the *spectrum* of $\mathbf{j}_{b,c}(m)$ is four valued and [1]

$$\begin{aligned} -1 + 2^{(m+2)/2} & \text{ occurs } (2^{m-1} - 2^{(m-2)/2})/3 & \text{ times,} \\ -1 + 2^{m/2} & \text{ occurs } 2^{m/2} & \text{ times,} \\ -1 & \text{ occurs } 2^{m-1} - 2^{(m-2)/2} - 1 & \text{ times,} \\ -1 - 2^{m/2} & \text{ occurs } (2^m - 2^{m/2})/3 & \text{ times.} \end{aligned}$$

The reader is reminded that since $m \equiv 0 \pmod{4}$, the best three-valued crosscorrelation spectrum provided by Theorem 1 has crosscorrelation magnitudes as large as $1 + 2^{(m+e)/2}$ where $e \geq 4$. However, the crosscorrelation magnitudes in Theorem 2 are bounded by $-1 + 2^{(m+2)/2} = t(m) - 2$ [1].

Suppose that b and c are reciprocal pairs of m -sequences (i.e., generated by reciprocal polynomials) then [1]

$$(D.1.14) \quad |\mathbf{j}_{b,c}(m)| \leq 2^{(m+2)/2} - 1.$$

When m is even inequality (D.1.14) can be written as

$$(D.1.15) \quad -t(m) + 2 \leq \mathbf{j}_{b,c}(m) \leq t(m) - 2.$$

When m odd (i.e., $m = 2k + 1$) then

$$(D.1.16) \quad -\sqrt{2}2^{k+1} = -\sqrt{2}[t(2k) - 2] \leq \mathbf{j}_{b,c}(m) \leq \sqrt{2}2^{k+1} = \sqrt{2}[t(2k) - 2]$$

which means that the bound is larger by $\sqrt{2}$.

Let \mathbf{j}_c denote the maximum crosscorrelation magnitude for a given pair of m -sequences b and c of period $M = 2^m - 1$, $m \geq 3$. The most important results concerning \mathbf{j}_c , can be summarized as follows [1]:

- When m is odd, or when $m \equiv 2 \pmod{4}$, $\mathbf{j}_c = t(m)$ for preferred pairs of m -sequences.

- When m is even and $m \not\equiv 0 \pmod{4}$, $\mathbf{j}_c = t(m) - 2$ for reciprocal pairs of m -sequences.
- When $m \equiv 0 \pmod{4}$, $\mathbf{j}_c = t(m) - 2$ for pairs of m -sequences specified in Theorem 2.

It is interesting to note that when m is odd, $\mathbf{j}_c \geq t(m)$ for *any* pair of m -sequences; hence, the preferred pair achieve the minimum possible value of \mathbf{j}_c odd m .

Now that we have discussed the crosscorrelation spectra it remains to find the sets of binary sequences with small crosscorrelation values because for most of the geolocation applications more than two pairs of m -sequences are required.

A *maximal connected set*, M_m , of m -sequences is called a *largest* collection of m -sequences that has the property that every pair is a preferred pair [1]. In Table D.2 we list the information on all m -sequences and maximal connected set of sequences for $m = \{3,4,\dots,16\}$. Table D.2 contains six columns, which are explained in order. The first column contains the size of the generating polynomial or the *primitive*. The second column contains the period of m -sequence, $M = 2^m - 1$, which is an odd number. The third column contains the number of all possible m -sequences that have a period M . The fourth column contains the crosscorrelation magnitude for the set of all m -sequences. The fifth column contains the maximal connected set of m -sequences. And the sixth column contains approximately the crosscorrelation magnitude for the maximal connected set. Note that for all $m = 4k$ the maximal connected set contain zero sequences, as opposed to when m is a prime number then the maximal connected set contains the highest possible number. Anyway, even for m prime number, the maximal connected set is still a very small number (six for $m = 7$) and not useful for geolocation applications. Therefore, larger sets that contain non-maximal-length sequences as well as maximal-length sequences must be obtained, which would sacrifice the out-of-phase autocorrelation peak to yield small crosscorrelation peak. This is where Gold, Kasami, and other sequences come to play a very important role.

Table D.2 *M*-sequences and maximal connected set for $m = \{3,4,\dots,16\}$ - taken from [1].

m	$M = 2^m - 1$	Number of m -sequences	φ_c for set of all m -sequences	M_m	$t(m) = 1+2^{\lfloor (m+2)/2 \rfloor}$
3	7	2	5	2	5
4	15	2	9	0	9
5	31	6	11	3	9
6	63	6	23	2	17
7	127	18	41	6	17
8	255	16	95	0	33
9	511	48	113	2	33
10	1023	60	383	3	65
11	2047	176	287	4	65
12	4095	144	1407	0	129
13	8191	630	≥ 703	4	129
14	16383	756	≥ 5631	3	257
15	32767	1800	≥ 2047	2	257
16	65535	2048	≥ 4095	0	513

A set of Gold sequences of period, $M = 2^m - 1$, consists of $M + 2$ sequences for which $\mathbf{j}_c = \mathbf{j}_a = t(m)$ [1]. Let us see how a Gold sequence can be constructed.

Suppose that the generating polynomial $f(x)$ factors into $h(x)h(x)$, where $h(x)$ and $h(x)$ have no factors in common. Then the set of all sequences generated by $f(x)$ is the set of all sequences of the form $g = b \oplus c$ where b is some sequence generated by $h(x)$ and c is some sequence generated by $h(x)$ and b and/or c may be zero sequence(s) [1]. Based on the property 2 of m -sequences we get that either

$$(D.1.17) \quad g = T^i b, \text{ or } g = T^j c, \text{ or } g = T^i b \oplus T^j c$$

where $0 \leq i, j \leq M - 1$ and where $T^i b \oplus T^j c$ denotes the sequence whose k th element is $b_{k+i} \oplus c_{k+j}$; therefore, the sequence g is some phase of some sequence in the set $G(b,c)$ defined by [1]

$$(D.1.18) \quad G(b,c) \triangleq \{b, c, b \oplus c, b \oplus Tc, b \oplus T^2c, \dots, b \oplus T^{M-1}c\}.$$

It is easier to see that $G(b,c)$ contains $M + 2$ sequences of period M .

Theorem 3: Let $\{b,c\}$ denote a preferred pair of m -sequences of period $M = 2^m - 1$. Generated by the primitive binary polynomial $h(x)$ and $h(x)$ respectively. The set defined in (D.1.18) is called a set of Gold sequences. For every pair of sequences $y, z \in G(b,c)$, the three-valued *crosscorrelation spectrum* is $\varphi_{y,z}(l) \in \{-1, -t(m), t(m) - 2\}$, $\forall l \in \mathbf{Z}$ and the three-valued *autocorrelation spectrum* is $\varphi_y(l) \in \{-1, -t(m), t(m) - 2\}$, $\forall l \neq 0 \pmod M$. The polynomial $f(x) = h(x)h(x)$ generates every sequence of $G(b,c)$, which is simply a

modulo 2 adding (term by term modulo 2) of the output sequence generated by $h(x)$ with the one generated by $\hat{h}(x)$ (see Figure D.2).

Let $\mathbf{j}_{\max} = \max\{\mathbf{j}_a, \mathbf{j}_c\}$ for a set of Gold sequences defined by Theorem 3 and eq. (D.1.18). A bound on \mathbf{j}_{\max} due to Sidelnikov states that for any set of M or more binary sequences of period M [1]

$$(D.1.19) \quad \phi_{\max} > \sqrt{2M - 2}.$$

For $M = 2^m - 1$ then the bound is given by [1]

$$(D.1.20) \quad \phi_{\max} > \sqrt{2^{m+1} - 4} \geq 2^{(m+1)/2} - 2 \text{ or } \phi_{\max} > 2^{(m+1)/2} - 1.$$

When m is odd then the right hand side of (D.1.20) is equal to $t(m) - 2$. Since, \mathbf{j}_{\max} is an odd integer then for any set of M or more binary sequences of period $M = 2^m - 1$ and m odd, [1]

$$(D.1.21) \quad \phi_{\max} \geq t(m).$$

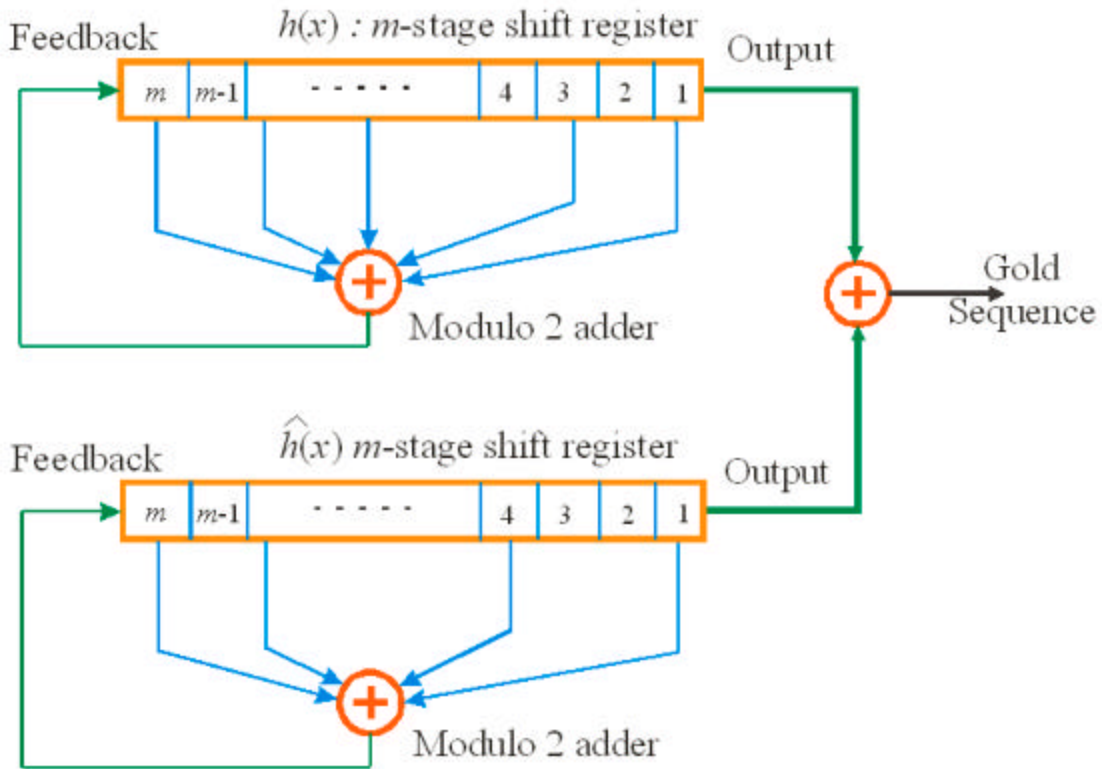


Figure D.2 Generation of a Gold sequence as depicted in Theorem 3.

On the other hand, for Gold sequences $j_{\max} = t(m)$; thus, Gold sequences form an *optimal* set with respect to the bounds (D.1.19) through (D.1.21) when m is odd. Table D.3 lists primitive polynomials $h(x)$ and $h(x)$ in octal representation for generating a Gold sequence when the degree of the polynomial $m = \{5,6,\dots,34\}$. For example, for $m = 5$ $h(x) = 45$ (octal) and $h(x) = 75$ (octal). For m even the right hand side of (D.1.20) is smaller than $t(m)$ by approximately $\sqrt{2}$; hence, Gold sequences are not the optimal set for m even. The small set of Kasami sequences that are discussed next are, on the other hand, the optimal set for m even.

Another important class of sequences, which has properties similar to Gold sequences, is discussed now.

Theorem 4: Let m be even and let q be an integer such that $r(q,M) = 3$. Let c denote an m -sequence of period $M = 2^m - 1$ generated by $h(x)$, and let $b^{(k)}$, $k = \{0,1,2\}$, denote the result of decimation $T^k c$ by q . Property 7 of m -sequences implies that the $b^{(k)}$ sequences have period $M' = M/3$ and are generated by the polynomial $h(x)$ whose roots are q th powers of the roots of $h(x)$. Suppose that y denote a nonzero sequence generated by $f(x) = h(x)h(x)$, then $y = T^i c$ or $y = T^j b^{(k)}$ or $y = T^i c \oplus T^j b^{(k)}$ where $0 \leq i < M$, $0 \leq j < M'-1$, and $0 \leq k \leq 2$. Any sequence of period M generated by the polynomial $f(x)$ is some phase of some sequence in the set $H_q(c)$ defined by [1]

$$(D.1.22) \quad H_q(c) = \{c, c \oplus b^{(0)}, \dots, c \oplus T^{M'-1} b^{(0)}, c \oplus b^{(1)}, \dots, c \oplus T^{M'-1} b^{(1)}, \\ c \oplus b^{(2)}, \dots, c \oplus T^{M'-1} b^{(2)}\}$$

Table D.3 The primitive polynomials (octal) for generating Gold sequences.

m	Generating polynomials (octal)	m	Generating polynomials (octal)	m	Generating polynomials (octal)
5	45, 75	13	100003, 102043	23	200000011, 200000017
6	103, 155	16	210013, 234313	26	400000107, 430216473
7	211, 217	17	400011, 400017	27	1000000047, 1001007071
8	435, 551	18	1000201, 1002241	28	2000000011, 2104210431
9	1021, 1131	19	2000047, 2020471	29	4000000005, 4004004005
10	2011, 2415	20	4000011, 4001051	30	10040000007, 10115131333
11	4005, 4445	21	10000005, 10040205	31	20000000011, 20000000017
12	10123, 15647	22	20000003, 20001043	32	40020000007, 40460216667
13	20033, 23261	23	40000041, 40404041	33	10000020001, 100020024001
14	42103, 43333	24	100000207, 125245661	34	20100000007, 201472024107

Note that $H_q(c)$ contains $M + 1 = 2^m$ sequences of period M . Suppose that c is generated by $h(x)$ and $b = c[t(m)]$ is generated by $h(x)$, where the roots of $h(x)$ are the $t(m)$ th power of the roots of $h(x)$. According to Gold, for any sequence y generated by $f(x) = h(x)h(x)$ [1]

$$(D.1.23) \quad 2^{m-1} - 2^{\lfloor m/2 \rfloor} \leq \mathbf{h}_y \leq 2^{m-1} + 2^{\lfloor m/2 \rfloor} \text{ or } |\mathbf{h}_y - 2^{m-1}| \leq 2^{\lfloor m/2 \rfloor}.$$

Two cases can be discussed here. If $m \neq 0 \pmod{4}$, $h(x)$ is a primitive polynomial and $G(b,c)$ constructed has $\mathbf{j}_{\max} = t(m)$. However, if $m = 0 \pmod{4}$, $r(t(m),M) = 3$ is thus Theorem 4 must be applied and the set obtained is called Gold-like and is denoted by $H_{t(m)}(c)$. The crosscorrelation spectrum for the sequence $H_{t(m)}(c)$ is given by $\{-1, -t(m), t(m) - 2, -s(m), s(m) - 2\}$, where $s(m)$ is defined for even m only and is given by

$$(D.1.24) \quad s(m) = 1 + 2^{m/2} = 0.5[t(m) + 1].$$

Theorem 5: Let m be even and let c denote an m -sequence of period $M = 2^m - 1$ generated by $h(x)$. Consider the sequence $b = c[s(m)] = c[2^{m/2} + 1]$, which based on property 7 has period $2^{m/2} - 1$. The b sequence is generated by $h'(x)$ whose roots are the $s(m)$ th powers of the roots of $h(x)$. Furthermore, since $h'(x)$ is a polynomial of degree $m/2$; hence, b is an m -sequence of period $M' = 2^{m/2} - 1$. Now consider the sequence, y , generated by the polynomial $h(x)h'(x)$ of period M and degree $m + m/2 = 3m/2$. Any such sequence, y , (see Figure D.3) must be one of the forms $\{T^i c, T^j b, T^i c \oplus T^j b\}$, $0 \leq i < M$, $0 \leq j < M$, which is some phase of some sequence in the *small set of Kasami sequences*, $K_S(c)$, defined by [1]

$$(D.1.25) \quad K_S(c) \triangleq \{c, c \oplus b, c \oplus Tb, \dots, c \oplus T^{M'-1}b\}.$$

Table D.4 lists primitive polynomials $h(x)$ and $h'(x)$ in octal representation for generating a Gold sequence when the degree of the polynomial $m = \{6, 8, \dots, 30\}$. For example, for $m = 6$ $h(x) = 103$ (octal) and $h'(x) = 15$ (octal).

The crosscorrelation spectrum of $K_S(c)$ taken on three values in the set $\{-1, -s(m), s(m) - 2\}$; thus, the crosscorrelation magnitude satisfies [1],

$$(D.1.26) \quad \phi_{\max} = s(m) = 2^{m/2} + 1 = 0.5(t(m) + 1).$$

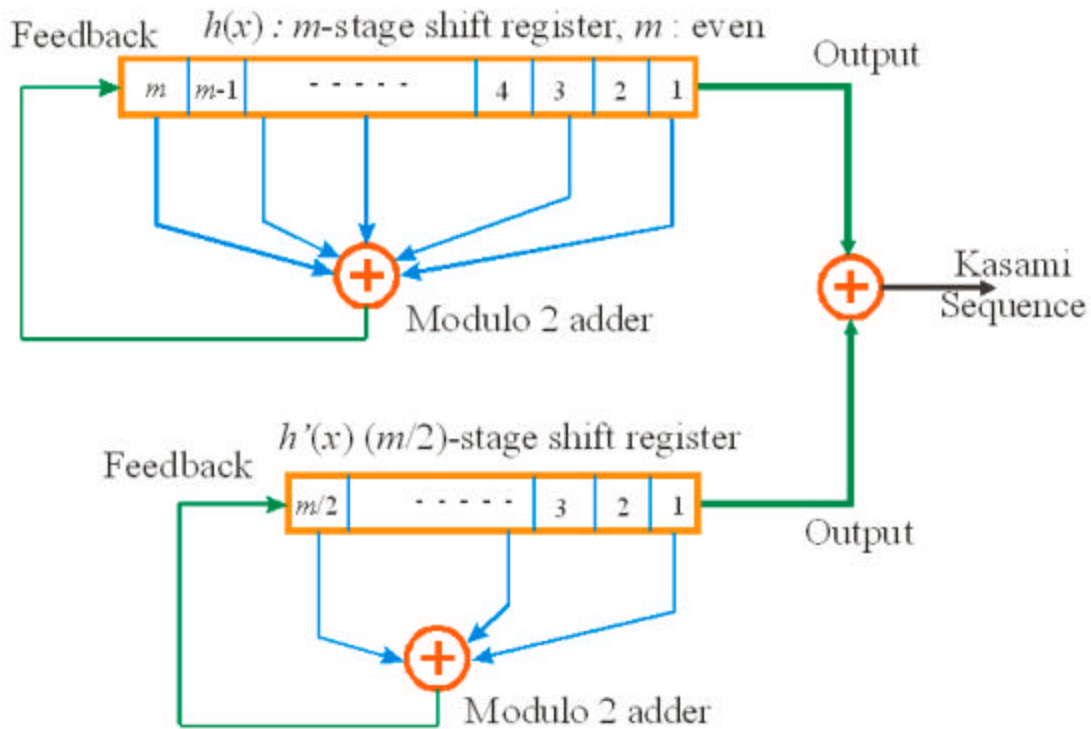


Figure D.3 Generation of a small set Kasami sequence as depicted in Theorem 4.

Table D.4 The primitive polynomials (octal) for generating Kasami sequences.

m	Generating polynomials (octal)	m	Generating polynomials (octal)	m	Generating polynomials (octal)
6	103, 15	16	210013, 717	26	400000107, 37743
8	435, 23	18	1000201, 1207	28	2000000011, 67737
10	2011, 75	20	4000011, 2605	30	10040000007, 175241
12	10123, 141	22	20000003, 4707		
14	42103, 203	24	100000207, 12727		

We notice two important consequences of the small set of Kasami sequences: (1) the number of sequences in the set is $2^{m/2} = \sqrt{M+1}$ sequences, while the set discussed previously contain $M+2$ sequences and (2) the crosscorrelation magnitude is approximately smaller by half than the crosscorrelation magnitude discussed previously. If a set contains K binary sequences of period M then Sidelnikov and Welch provided a formula for lower bound on the crosscorrelation magnitude, j_c , and out-of-phase autocorrelation magnitude, j_a , [1]

$$(D.1.27) \quad \phi_{\max} \hat{=} \max \{ \phi_a, \phi_c \} \geq M \sqrt{\frac{K-1}{MK-1}}.$$

Applying the above result to the set of $2^{m/2}$ sequences of period $2^m - 1$ implies that [1]

$$\begin{aligned}
(D.1.28) \quad \phi_{\max} &\geq (2^m - 1) \sqrt{\frac{2^{m/2} - 1}{(2^m - 1)2^{m/2} - 1}} = (2^{m/2} - 1) \sqrt{\frac{(2^{m/2} + 1)^2 (2^{m/2} - 1)}{(2^m - 1)2^{m/2} - 1}} \\
&= (2^{m/2} - 1) \sqrt{\frac{2^{3m/2} + 2^m - 2^{m/2} - 1}{2^{3m/2} - 2^{m/2} - 1}} > 2^{m/2} - 1.
\end{aligned}$$

Also, since \mathbf{j}_{\max} is an odd integer then the above bound can be improved to [1]

$$(D.1.29) \quad \phi_{\max} \geq 2^{m/2} + 1 = s(m).$$

Therefore, for m even, the small set of Kasami sequences, $K_S(c)$, achieves the smallest possible \mathbf{j}_{\max} ; hence, $K_S(c)$ is an optimal collection of binary sequences with respect to the bound (D.1.29).

Theorem 6: Let m be even and let $h(x)$ denote a primitive binary polynomial of degree m that generates the m -sequences, b , of period $M = 2^m - 1$. Let $y = b[s(m)]$ denote the m -sequence of period $M' = 2^{m/2} - 1$ generated by the primitive polynomial $h'(x)$ of degree $m/2$ and let $h(x)$ denote the polynomial of degree m that generates $b[t(m)]$. Then the set of sequences of period M generated by the $h(x)h(x)h'(x)$, called *the large set of Kasami sequences*, $K_L(b)$, is as follows [1]:

(a) if $m \equiv 2 \pmod{4}$, then

$$(D.1.30) \quad K_L(b) = G(b, c) \cup \left[\bigcup_{i=0}^{M'-1} \{T^i y \oplus G(b, c)\} \right]$$

where $c = b[t(m)]$ and $G(b, c)$ is defined in (D.1.18).

(b) if $m \equiv 0 \pmod{4}$, then

$$(D.1.31) \quad K_L(b) = H_{t(m)}(b) \cup \left[\bigcup_{i=0}^{M'-1} \{T^i y \oplus H_{t(m)}(b)\} \right] \cup \{c^{(j)} \oplus T^j y : 0 \leq j \leq 2, 0 \leq k < M'/3\}$$

where $c^{(j)}$ is the result of decimating $T^j y$ by $t(m)$ and $H_{t(m)}(b)$ is defined in (D.1.22).

Two important remarks of *the large set of Kasami sequences* are underlined in order. First, the crosscorrelation spectrum of the $K_L(b)$ is on either case the set $\{-1, -t(m), t(m)-2, -s(m), s(m)-2\}$; and thus, $\mathbf{j}_{\max} = t(m)$. Second, the when $m \equiv 2 \pmod{4}/0 \pmod{4}$, $K_L(b)$ contains $(M'+1)(M+2)/(M'+1)(M+1)+M'$ sequences respectively. Therefore, for the same crosscorrelation bound, $\mathbf{j}_{\max} = t(m)$, the large set of Kasami sequences can achieve

a much larger set than the set of Gold sequences because the latter one is included in the former one.

Applying the Sidelnikov and Welch lower bound formula for the large set of Kasami sequences we get

$$(D.1.32) \quad \phi_{\max} \geq 2^{m/2} + 1 = s(m).$$

Therefore, the large set of Kasami sequences is sub-optimal with respect to the bound (D.1.32) because $t(m) > s(m)$ for m even.

CITED REFERENCES AND FURTHER READING:

- [1] J.G. Proakis and M. Salehi, *Communication Systems Engineering*, Upper Saddle River, New Jersey: Prentice Hall, 1994.
- [2] D.V. Sarwate and M.B. Pursley, "Crosscorrelation properties of pseudorandom and related sequences," in *Proc. of IEEE*, vol. 68, pp. 593-619, May 1980.
- [3] P.K. Enge and D.V. Sarwate, "Spread-spectrum multi-access performance of orthogonal codes: linear receivers," *IEEE Trans. Commun.*, vol. COM-35, 1309-1399, Dec. 1987.
- [4] I.F. Proгри, J.M. Hill, and W.R. Michalson, "An investigation of the pseudolite's signal structure for indoor applications," in *Proc. ION-AM*, June 2001.
- [5] I.F. Proгри, and W.R. Michalson, "The impact of proposed pseudolite's signal structure on the receiver's phase and code error," in *Proc. ION-AM*, June 2001.
- [6] I.F. Proгри, and W.R. Michalson, "An alternative approach to multipath and near-far problem for indoor geolocation systems," in *Proc. ION-GPS*, Sep. 2001.

Appendix E. Channel Considerations

“Whoso findeth a wife findeth a good thing, and obtaineth favour of the LORD.”—Prov. 17:22

E.0 Introduction

MORE or less there are two approaches for modeling the Wireless Communication Channel (WCC): (1) ray-tracing approach (or model) and (2) statistical approach. First, the ray-trace approach is based on the analytical description of a certain polarized electromagnetic wave propagating in a layered, lossy media characterized by reflection, refraction, and diffraction (or scattering). Second, the statistical approach is based on the analytical and stochastic description of the WCC impulse response. While the first approach is particularly useful in understanding the path losses, the second one is useful in understanding the nature of the multipath effect. There are efforts made to come up with a unified WCC ray-trace model as well as efforts made to come up with a unified WCC statistical model. There are also some efforts made to reconcile both models into one. When necessary we will mention either one of these efforts; nevertheless, that this is currently an open issue in the wireless community to be solved in the future.

An overview of the indoor WCC is shown in Figure E.1. The signal (i.e., the electromagnetic wave) travelling through an indoor communication channel is diffracted (or scattered), reflected, and refracted. Also the signal energy (or power) is reduced (or “absorbed”). Different media absorb different amount of the signal energy and this phenomenon results in different power loss factor. The two most accepted indoor communication channel models are the *ray-tracing* model and the *statistical* model. The *ray tracing* model is the most accurate yet the most computationally intensive because it models the propagation effects of every path which includes the effects we have just mentioned. The *statistical* model, however, is less accurate yet less computationally intensive. For fast and easy calculations the statistical model can be employed as opposed for more accurate computations the ray-trace model can be employed.

Nevertheless, both models have two things in common: the *path loss* and the *multipath effect*. There is another less known channel model—*auto regressive (AR)*—which stands in between ray tracing model and statistical model. While both the ray-tracing model and the statistical model processing the data in the time domain, the AR does it in the frequency domain. In our discussion we have included also the *interference* effect. The indoor communication channel model is yet to be complete and universally accepted for two reasons: (1) lack of measurements and (2) lack of accurate simulation models fully compliant with the existing measurements. In the following chapter we attempt to provide a broader picture on these issues.

E.1 Path Loss

Below we give two definitions of the path loss: (1) used for radio frequencies and (2) used for optical frequencies. The path loss is defined as the ratio of the average transmitted power to the average received power, provided that the transmitting antenna used in the field is comparable to the type used to arrive at the path loss model. Second, the path loss is defined as the ratio of the transmitted average optical power to the average optical power received by a 1-cm² having an acceptance half-angle of 70° [1].

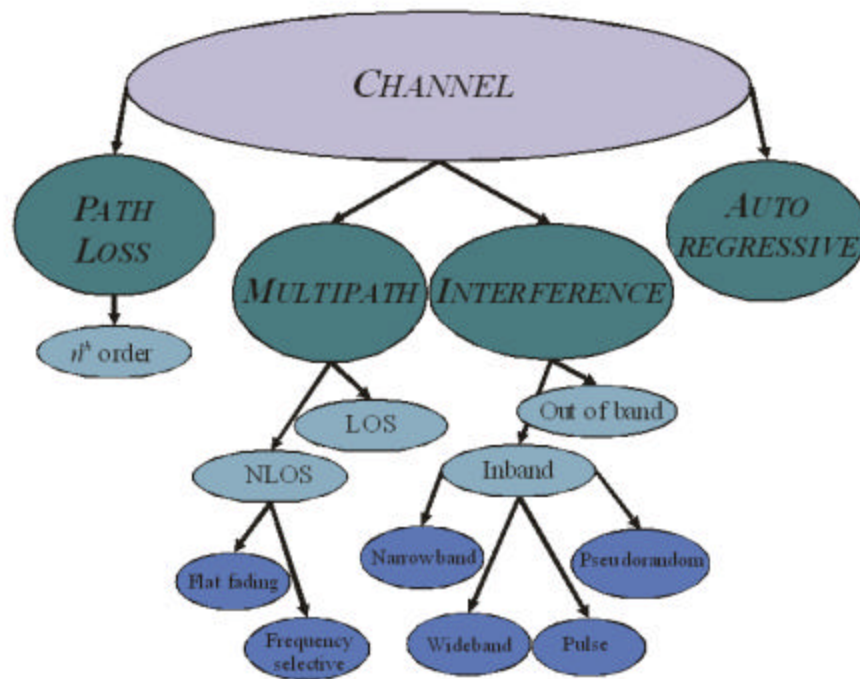


Figure E.1 An overview of the indoor communication channel.

We discuss here as part of the system introduction only the contributors in modeling the path loss and leaving the mathematics that underline the path loss model(s) to be discussed in Chapter 3. The indoor environment is a layered media and as a result it can exhibit a higher power loss factor than the outdoor environment. While the power loss factor, outdoors, is computed and measured to be between 2 – 3; the power loss factor, indoors, is between 1 (LOS) – 6.5 (NLOS). Similarly, the degree of scattering, reflection, and refraction is expected and is measured to be higher indoors than outdoors.

Rappaport defines the power loss as the relative power attenuation (dB) seen by a receiver with respect to a convenient (close) reference distance between the transmitter and receiver (usually 1 km for HF frequencies, or 1 m for wideband propagation measurements inside office buildings) [2]. Along the lines of the statistical channel models, Rappaport et al. assert that there are two compelling reasons why the indoor channel should be modeled as a statistical channel as opposed to a deterministic channel: (1) the number of potential reflectors and (2) the location of each potential scatterer [2]-[3]. He then presents an approach for modeling indoor channels based on the first and second-order statistics both the LOS and OBS channels [2]-[3]. These statistics are the mean excess delay and the rms delay spread [2]-[3]. The mean excess delay is simply the first moment of the power delay profile and the rms delay spread is the square root of the second moment of the power delay profile [2]-[3]. For some particular scenarios the statistical channel model appear to provide a very good agreement with the experimental results from propagation measurements from five factory buildings [2]-[3]. Another important result from the safety standpoint is that manmade noise is not a problem for indoor radio factory systems operating at frequencies higher than 1 GHz and that fading characteristics are highly correlated with the local topography in the workplace [2]-[3].

The work by Rappaport et al. [4] indicates that the directional circularly polarized (CP) antennae always reduce the rms delay spread when compared to omni-directional and directional linearly polarized (LP) antennae in LOS [4]. Therefore, CP may be an effective technique for minimizing the small-scale variation of the multipath delay spread [4], [5].

In a work by Kahn, Krause, and Carruthers [1] an infrared indoor system is discussed. The focus of this work consists primarily in the study and measurement of the channel response for the line of sight and diffuse link configurations and then the computation of the channel impulse response, path losses, and rms delay spreads amounting to approximately 100 different channels from 5 different rooms and for frequency ranging from 2 to 300 MHz [1]. It is shown a strong penalty between the rms delay spread and the multipath power penalty [1]. Moreover, it is shown that non-directed infrared channels employing intensity modulation do not exhibit multipath fading; hence, whose representation can be justified as linear time invariant [1].

A work by Carruthers and Kahn considers modeling of non-directed wireless infrared channels by characterizing only two important parameters: (1) optical path loss and (2) rms delay spread [6]. The authors propose and analyze several functional indoor infrared channel models for the impulse response [6]. Moreover, by employing ceiling-bounce functional model, Carruthers and Kahn have developed a computationally efficient way of predicting the path loss and multipath power of diffuse links based on the location of the transmitter and receiver within a room [6].

Hashemi has conducted a remarkable survey on the indoor radio propagation channel [7]. He discussed that the path losses are reported in the literature modeled in at least four different ways that are analyzed in Chapter 3 in great detail. Moreover, all of them taken together provide inconclusive remarks, which suggests that the modeling of indoor channel path loss is currently an open issue.

Babich and Lombardi have statistically analyzed and characterized the indoor propagation channel by measuring narrow-band path loss at the digital enhanced cordless telecommunications (DECT) frequency (1.89 GHz) [8]. They have applied goodness-of-fit to the measured data and have found out that either the Weibull or Nakagami distribution can better approximate the local path loss distribution in most environments [8]. Nevertheless, they have made a good effort to show that when the signals and interferers are coherent/noncoherent and Rician then a general, simple, approximate expression for the cumulative distribution function of the signal-to-interference ratio can

be obtained, which is known as noncoherent and coherent Prasad approximations [8]-[33].

Durgin, Rappaport, and Xu have conducted measurements and have developed models based on these measurements for radio outdoor path loss, tree loss, and indoor penetration loss at 5.85 GHz; namely, the US National Information Infrastructure (NII) band [34]. Detailed measurements (270 local area path loss measurements and over 270,000 instantaneous power measurements) were performed in the 5.85 GHz NII band for three typical middle- to upper-middleclass houses and for deciduous and coniferous stands of trees [34]. Specific effects of foliage, house shadowing, transmitter receiver separation, and receiver height were quantified for outdoor path loss in residential areas [34]. This work also determined how exterior shadowing, house construction, and floor plan influence the penetration of radio waves into homes [34]. Results show that, at 5.85 GHz, home penetration attenuates signals at an average of 14 dB, tree shadowing attenuates signals between 11 and 16 dB, and close-in house shadowing attenuates signals between 15 and 21 dB, depending on the height of the receive antenna [34]. These measurements and models may aid the development of future outdoor-to-indoor communication systems, which operate at NII band [34].

E.2 Multipath

Multipath is encountered when signal propagates from a transmitter to a receiver through more than one path. The direct line of sight path (DLOS) is usually the strongest path and the other paths are called the obstructed paths (OP) or simply multipath (MP). One way of classifying the multipath impact for indoor geolocation would be according to Pahlavan et al [31]. To relate the performance of traditional GPS receivers into more complex RAKE-type receivers he classifies the frequency fading multipath profiles in three categories: (1) the DLOS path is the direct dominant path (DDP); (2) the DLOS path is not the direct dominant path (NDDP); (3) undetectable direct paths (UDP) [31]. Moreover, for the first category (DDP) both the GPS and RAKE-type receivers work properly [31]. For the second category (NDDP) only the RAKE-type receivers work properly [31]. And for the third category (UDP) neither receiver works properly [31].

Tannous investigates the nature of multipath indoors and according to his research the estimation of the correlation dimension of multipath propagation signals may indicate the presence of strange attractors [35]. Although the model that he proposes for the indoor channel is very complicated because it can be described by a set of at most 5 nonlinear differential equations, it reveals an important aspect of the true nature of multipath in indoor environments [35].

The endeavor to model the radio channel based on experimental data is continued by Yegani and McGillem, who in [36] present an excellent approach for modeling the factory radio channel as a statistical, discrete channel. The channel properties can be fully characterized exploiting three important parameters: the path gain coefficient, the path interarrival times, and the path number. First, the path gain coefficients can be model using any of the Reyleigh, Rician, or lognormal distributions [36]. The Reyleigh distribution provides a good fit for scenarios with *heavy* clutter as opposed to the Rician distribution, which models the path gain coefficients for scenarios with *light* clutter [36]. Nevertheless, for data with no threshold at the receiver, the lognormal model appears to provide a better fit than either the Reyleigh or the Rician distribution [36]. Second, the interarrival times can be model using the Weibull distribution [36]. And third, it was determined empirically that the number of paths (or signals) distribution fits the Beta distribution [36].

Bargallo and Roberts [37] claim that semi-analytic results obtained using exponential multipath profile for spread-spectrum indoor radio channels are closer to the simulation results based on actual measurements for indoor radio channels than those obtained assuming constant profile multipath.

E.3 Auto-Regressive

Howard and Pahlavan propose an auto-regressive (AR) modeling for indoor radio propagation [38]. They demonstrate both analytically and experimentally that a second order process is sufficient to represent the important statistical characteristics of the channel both in the time and the frequency domain [38]. They argue that the second-order AR based indoor channel modeling requires fewer parameters than the time domain modeling [39]-[49], [4]; therefore, once the AR gains and phases are determined then it

would be considerably easier to simulate the channel model in the computer [38]. According to Howard and Pahlavan the location of the poles represent the arrival of a cluster of paths, and the angle of the pole represent the arrival time, and the closeness to the unit circle indicates the relative strength of the cluster [38]. Therefore, a two-pole AR process is identified with two clusters and it is shown in [38] that this model is sufficient to model indoor radio propagation channels based on over 800 global, local, and mixed measurements.

Hassan-Ali and Pahlavan propose a new statistical model for site-specific indoor radio propagation prediction based on geometric optics and geometric probability [50]. This model is supposed to perform worse than the ray-tracing model and better than the statistical models [50].

E.4 Interference

Vogel, Hao, and Torrence bring an interesting fact on the fluorescent light interaction with personal communication signals [51]. According to Vogel, Hao, and Torrence the fluorescent light absorb and reflect radio waves in the band of 1 ~ 2 GHz [51]. A variation of 3dB/2dB on the peak-to-peak amplitude and 10°/20° phase for the in-line/orthogonal path was encountered [51].

Butterworth, Sowerby, and Williamson have studied the base station placement for in-building mobile DS-CDMA communication systems to yield high capacity and efficiency [52]. Correlated shadowing is identified as being a ‘key’ in-building propagation characteristic that has the potential to strongly influence system performance [52]. Propagation models that included correlated shadowing are shown to produce the most accurate estimates of outage probability when there are a number of interferers facing a user [52]. Base station deployment is shown to be a dominant factor influencing the levels of correlated shadowing, and consequently, base station deployment is shown to have major implications on system performance [52].

CITED REFERENCES AND FURTHER READING:

- [1] J.M. Kahn, W.J. Krause, and J.B. Carruthers, "Experimental characterization of non-directed indoor infrared channel," *IEEE Trans. Comm.*, vol. 42, no. 2, pp. 1929-1938, Feb-Apr. 1995.
- [2] T.S. Rappaport, "Indoor radio communications for factories of the future," *IEEE Comm. Mag.*, vol. 27, no. 2, pp. 15-24, May 1989.
- [3] T.S. Rappaport, S.Y. Seidel, and K. Takamizawa, "Statistical channel impulse response models for factory and open plan building radio communicate system design," *IEEE Trans. Comm.*, vol. 39, no. 5, pp. 794-807, May. 1991.
- [4] T.S. Rappaport and D.A. Hawbaker, "Wide-band microwave propagation parameters using circular and linear polarized antennas for indoor wireless channels," *IEEE Trans. Comm.*, vol. 40, no. 2, pp. 240-245, Feb. 1992.
- [5] J.B. Andersen, T.S. Rappaport, and S. Yoshida, "Propagation measurements and models for wireless communications channels," *IEEE Comm. Mag.*, vol. 33, no. 1, pp. 42-49, Jan. 1995.
- [6] J.B. Carruthers and J.M. Kahn, "Modeling of nondirected wireless infrared channels," *IEEE Trans. Comm.*, vol. 45, no. 10, pp. 1260-1268, Oct. 1997.
- [7] H. Hashemi, "The indoor radio propagation channel," in *Proc. IEEE*, vol. 81, no. 7, pp. 943-968, July 1993.
- [8] F. Babich and G. Lombardi, "Statistical analysis and characterization of the indoor propagation channel," *IEEE Trans. Comm.*, vol. 48, no. 3, pp. 455-464, Mar. 2000.
- [9] M. Kavehrad and P.J. McLane, "Spread spectrum for indoor digital radio," *IEEE Commun. Mag.*, vol. 25, no. 6, pp. 32-40, June 1987.
- [10] S.Y. Seidel and T.S. Rappaport, "914 MHz path loss prediction models for indoor wireless communications in multifloored buildings," *IEEE Trans. Ant. Prop.*, vol. 40, no. 2, pp. 207-217, Feb. 1992.
- [11] D. Tholl, M. Fattouche, R.J.C. Builtitude, P. Melancon, and H. Zaghloul, "A comparison of two radio propagation channel impulse response determination techniques," *IEEE Trans. Ant. Prop.*, vol. 41, no. 4, pp. 515-517, April 1993.
- [12] Y. Wang, S. Safavi-Naeini, S.K. Chaudhuri, "A hybrid technique based on combining ray tracing and FDTD methods for site-specific modeling of indoor radio wave propagation," *IEEE Trans. Ant. Prop.*, vol. 48, no. 5, pp. 743-754, May 2000.

- [13] T. Lo, J. Litva, and H. Leung, "A new approach for estimating indoor radio propagation characteristics," *IEEE Trans. Ant. Prop.*, vol. 42, no. 10, pp. 1369-1376, Oct. 1994.
- [14] Y. Chang-Fa, W. Boau-Cheng, and K. Chuen-Jyi, "A ray-tracing method for modeling indoor wave propagation and penetration," *IEEE Trans. Ant. Prop.*, vol. 46, no. 6, pp. 907-919, June 1998.
- [15] W. Honcharenko, H.L. Bertoni, and J.L. Dailing, "Bilateral averaging over receiving and transmitting areas for accurate measurements of sector average signal strength inside buildings," *IEEE Trans. Ant. Prop.*, vol. 43, no. 5, pp. 508-512, May 1995.
- [16] T.K. Blankenship and T.S. Rappaport, "Characteristics of impulsive noise in the 450-MHz band in hospitals and clinics," *IEEE Trans. Ant. Prop.*, vol. 46, no. 2, pp. 194-203, Feb. 1998.
- [17] B.P. Donaldson, M. Fattouche, and R.W. Donaldson, "Characterization of in-building UHF wireless radio communication channels using spectral energy measurements," *IEEE Trans. Ant. Prop.*, vol. 44, no. 1, pp. 80-86, Jan. 1996.
- [18] T.S. Rappaport, "Characterization of UHF multipath radio channels in factory buildings," *IEEE Trans. Ant. Prop.*, vol. 37, no. 8, pp. 1058-1069, Aug. 1989.
- [19] P. Vlach, B. Segal, J. LeBel, and T. Pavlasek, "Cross-floor signal propagation inside a contemporary ferro-concrete building at 434, 862, and 1705 MHz," *IEEE Trans. Ant. Prop.*, vol. 47, no. 7, pp. 1230-1232, July 1999.
- [20] B.M. Green and M.A. Jensen, "Empirical characterization of wideband indoor radio channel at 5.3 GHz," *IEEE Trans. Ant. Prop.*, vol. 48, no. 7, pp. 1017-1024, July 2000.
- [21] J. Kivinen, Zhao Xiongwen, and P. Vainikainen, "Empirical characterization of wideband indoor radio channel at 5.3 GHz," *IEEE Trans. Ant. Prop.*, vol. 49, no. 8, pp. 1192-1203, Aug. 2001.
- [22] Y. Karasawa and H. Iwai, "Formulation of spatial correlation statistics in Nakagami-Rice fading environments," *IEEE Trans. Ant. Prop.*, vol. 48, no. 1, pp. 12-18, Jan. 2000.
- [23] O. Norklit, P.D. Teal, and R.G. Vaughan, "Measurement and evaluation of multi-antenna handsets in indoor mobile communication," *IEEE Trans. Ant. Prop.*, vol. 49, no. 3, pp. 429-437, Mar. 2001.
- [24] U. Dersch, J. Troger, and E. Zollinger, "Multiple reflections of radio waves in a corridor," *IEEE Trans. Ant. Prop.*, vol. 42, no. 11, pp. 1571-1574, Nov. 1994.
- [25] W.J. Vogel and G.W. Torrence, "Propagation measurements for satellite radio reception inside buildings," *IEEE Trans. Ant. Prop.*, vol. 41, no. 7, pp. 954-961, July 1993.

- [26] V. Degli-Eposti, G. Lombardi, C. Passerini, and G. Riva, "Wide-band measurement and ray-tracing simulation of the 1900-MHz indoor propagation channel: comparison criteria and results," *IEEE Trans. Ant. Prop.*, vol. 49, no. 7, pp. 1101-1110, July 2001.
- [27] M.S. Varela and M.G. Sanchez, "Study of a frequency diversity system for indoor digital TV," *IEEE Trans. Broad.*, vol. 46, no. 2, pp. 165-170, June 2000.
- [28] L.J. Greenstein et al., "Microcells in personal communications systems," *IEEE Comm. Mag.*, vol. 30, no. 12, pp. 76-88, Dec. 1992.
- [29] J.J.G. Fernandes, P.A. Watson, and J.C. Neves, "Wireless LANs: physical properties of infra-red systems vs. mmw systems," *IEEE Comm. Mag.*, vol. 32, no. 8, pp. 68-73, Aug. 1994.
- [30] S. Dehghan and R. Steele, "Small cell city," *IEEE Comm. Mag.*, vol. 35, no. 8, pp. 52-59, Aug. 1997.
- [31] K. Pahlavan, P. Krishnamurthy, and A. Beneat, "Wideband radio propagation modeling for indoor geolocation applications," *IEEE Comm. Mag.*, vol. 36, no. 4, pp. 60-65, Apr. 1998.
- [32] W. Webb, "Broadband fixed wireless access as a key component of the future integrated communications environment," *IEEE Comm. Mag.*, vol. 39, no. 9, pp. 115-121, Sep. 2001.
- [33] R. Prasad, A. Kegal, and C. Rönne, "Performance analysis of a sectorized mobile microcellular radio system with diversity and forward error correction coding," in *Proc. IEEE VTC '94*, 1994.
- [34] J.G. Durgin, T.S. Rappaport, and H. Xu, "Measurements and models for radio path loss and penetration loss in and around homes and trees at 5.85 GHz," *IEEE Trans. Comm.*, vol. 46, no. 11, pp. 1484-1496, Nov. 1998.
- [35] C. Tannous, R. Davies, and A. Angus, "Strange attractors in multipath propagation," *IEEE Trans. Comm.*, vol. 39, no. 5, pp. 629-631, May. 1991.
- [36] P. Yegani and C.D. McGillem, "A statistical model for the factory radio channel," *IEEE Trans. Comm.*, vol. 39, no. 10, pp. 1445-1454, Oct. 1991.
- [37] J.M. Bargallo and J.A. Roberts, "Performance of BPSK and TCM using the exponential multipath profile model for spread-spectrum indoor radio channels," *IEEE Trans. Comm.*, vol. 43, no. 2, pp. 615-623, Feb-Apr. 1995.
- [38] S.J. Howard and K. Pahlavan, "Autoregressive modeling of wide-band indoor radio propagation," *IEEE Trans. Comm.*, vol. 40, no. 9, pp. 1540-1552, Sep. 1992.
- [39] D. Dardari and V. Tralli, "High-speed indoor wireless communications at 60 GHz with coded OFDM," *IEEE Trans. Comm.*, vol. 47, no. 11, pp. 1709-1721, Nov. 1999.

- [40] G.J.M. Janssen, P.A. Stigter, and R. Prasad, "Wideband indoor channel measurements and BER analysis of frequency selective multipath channels at 2.4, 4.75, and 11.5 GHz," *IEEE Trans. Comm.*, vol. 44, no. 10, pp. 1272-1288, Oct. 1996.
- [41] H.L. Bertoni, W. Honcharenko, L.R. Macel, and H.H. Xia, "UHF propagation prediction for wireless personal communications," in *Proc. IEEE*, vol. 82, no. 9, pp. 1333-1359, Sep. 1994.
- [42] G.L. Turin, "Communication through noisy, random multipath varying channels," in *1956 IRE Convention Record*, part 4, pp. 154-166.
- [43] G.L. Turin, *et al.* "A statistical model of urban multipath propagation," *IEEE Trans. Veh. Technol.*, vol. VT-21, pp. 1-9, Feb. 1972.
- [44] H. Suzuki, "A statistical model for urban radio propagation," *IEEE Trans. Commun.*, vol. COMM-25, pp. 673-685, July 1977.
- [45] H. Hashemi, "Simulation of the urban radio propagation channel," *IEEE Trans. Veh. Technol.*, vol. VT-28, pp. 213-224, Aug. 1979.
- [46] L.R. Macel, H.L. Bertoni, and H.H. Xia, "Unified approach to prediction of propagation over building of all ranges of base station antenna height," *IEEE Trans. Veh. Technol.*, vol. 42, pp. 41-45, Feb. 1993.
- [47] G.D. Ott and A. Plitkins, "Urban path-loss characteristics at 820 MHz," *IEEE Trans. Veh. Technol.*, vol. VT-27, pp. 189-197, 1978.
- [48] T. Iwama *et al.*, "Investigation of propagation characteristics above 1 GHz for microcell land mobile radio," in *Proc. IEEE Veh. Technol. Conf.*, pp. 396-400, 1990.
- [49] H.H. Xia and H.L. Bertoni, "Diffraction of cylindrical and plane waves by an array of absorbing half screens," *IEEE Trans. Ant. Prop.*, vol. 40, pp. 170-177, Feb, 1992.
- [50] M. Hassan-Ali and K. Pahlavan, "A new statistical model for site-specific indoor radio propagation prediction based on geometric optics and geometric probability," *IEEE Trans. W. Comm.*, vol. 1, no. 1, pp. 112-124, Jan. 2002.
- [51] W.J. Vogel, L. Hao, and G.W. Torrence, "Fluorescent light interaction with personal communication signals," *IEEE Trans. Comm.*, vol. 43, no. 2, pp. 194-197, Feb-Apr. 1995.
- [52] K.S. Butterworth, K.W. Sowerby, and A.G. Williamson, "Base station placement for in-building mobile communication systems to yield high capacity and efficiency," *IEEE Trans. Comm.*, vol. 48, no. 4, pp. 658-669, Apr. 2000.

Appendix F. Receiver Design Considerations

“He that getteth wisdom loveth his own soul: he that keepeth understanding shall find good.”—Prov. 18:8

F.0 Introduction

DIFFERENT receiver designs are shown in Figure F.1. As presented in Figure F.1 receivers can be build exploiting any of the combinations of *equalization, code, frequency, time, amplitude, phase, antenna, blind, and other* diversities. The advantages and disadvantages of each receiver technique in connection with indoor geolocation and communication are discussed in order.

F.1 Equalization

Saleh asserts that signaling rate can almost be even quadrupled through the use of adaptive equalization [1].

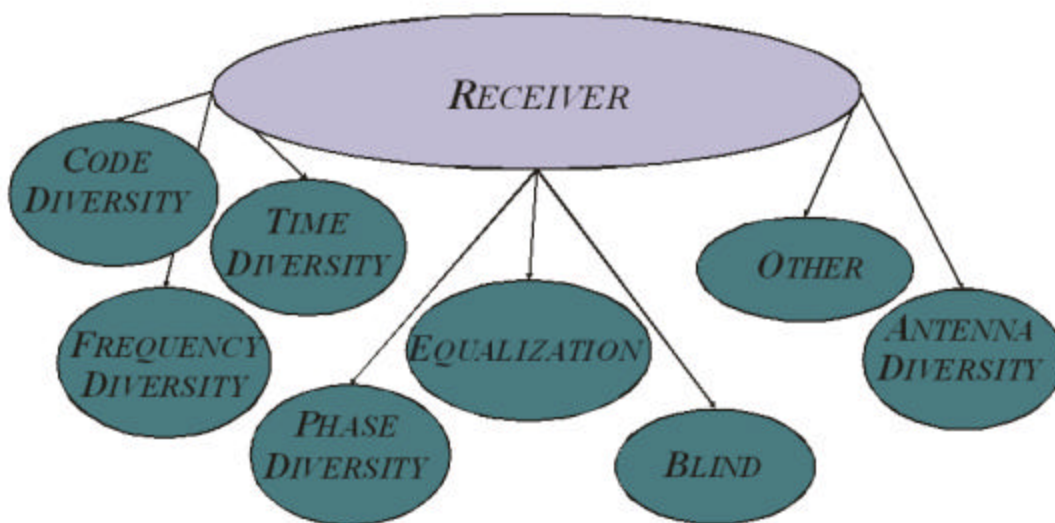


Figure F.1 An overview of indoor communication and localization receiver designs.

Pahlavan, Howard, and Sexton analyze the performance of the binary phase shift key (BPSK) and BPSK with decision feedback equalization (DFE) modems operating in five different indoor industry and business areas [2]. It was observed that for all five areas data rate in the order on 10 MBPS are obtainable with a DFE having three feedback and three forward taps as opposed 1 MBPS without any equalization [2]. This is another example that stresses the importance of equalization on the receiver side.

Lo, Falconer, and Sheikh are concerned with co-channel interference (CCI) in multipath fading environment and propose the direct recursive least squares (RLS) decision feedback equalizer to militate the CCI in the presence of multipath [3].

Audeh and Kahn [4] investigate a wireless indoor infrared LAN operating at 100 MBPS using baseband nonreturn-to-zero (NRZ) and on-off-keying (OOK) modulation. They also employ an adaptive decision feedback equalizer based on least mean squares algorithm to recover most of the performance degradation caused by multipath [4]. They also evaluate the timing recovery of the phase lock loop, which operates independent of the adaptive equalizer and quickly and accurately recovers the sampling phase with minor performance degradation [4]. The authors also present an approach for mitigating the low-frequency noise impact induced by the fluorescent light [4]. Overall results support the feasibility of the infrared indoor communication for data rates of the order of 100 MBPS [4].

Audeh, Kahn, and Barry [5] examine the performance of pulse-position modulation (PPM) on measured non-direct indoor infrared channels with inter symbol interference (ISI). They also examine bit rates of 10 MBPS to 30 MBPS and employ the maximum likelihood sequence detection (MLSD), which yields that 16-PPM provides superior performance than 2, 4, or 8 PPM and OOK modulation scheme [5].

Marsh and Kahn present in [6] the performance evaluation of experimental 50-MBPS diffuse infrared wireless link using on-off keying with decision-feedback equalization. They favor the OOK for achieving low BERs in the presence of background noise, ISI, and shadowing [6]. The decision feedback equalizer yields a reduction of the multipath effects, conclusion, which is supported both from the theory and experimental result [6].

Lee, Kahn, and Audeh discuss the Trellis-coded pulse-position modulation (PPM) for indoor wireless infrared communications [7]. They claim that the maximum likelihood sequence detection (MLSD) of trellis-coded PPM is a very effective in eliminating the multipath effect for indoor infrared channels [7].

The work by Lee and Kahn is a treatise on coding and equalization for PPM on wireless infrared channels [8]. The authors have analyzed the performance of trellis-coded pulse position modulation with block decision-feedback equalization (BDFE) and parallel decision-feedback decoding (PDFD) on indoor, wireless infrared channels [8]. They showed that the reduced complexities of BDFE and PDFD as compared to maximum-likelihood sequence detection allow for better codes whose increased coding gain more than compensates for the penalty due to suboptimal detection [8]. These net gains were quantified in performance over a range of dispersive channels, indicating where BDFE and PDFD provide the best performance [8].

Audeh, Kahn, and Barry reconsider the decision-feedback equalization of pulse-position modulation on measured nondirected indoor infrared channels [9]. Earlier work [5] has shown that the maximum likelihood sequence detector (MLSD) yields significant performance for IR indoor wireless communication system; nevertheless, this is achieved in expense to higher system complexity. Here the authors reconsider the same system by employing a sub-optimal, reduced complexity optimization techniques and they provide performance analysis for zero-forcing (ZF) chip-rate and symbol-rate DFE's [9]. Based on their investigation, the performance of a symbol-rate ZF-DFE closely approaches that of the MLSD [9].

A novel, asynchronous multiuser CDMA detector which includes a novel decorrelator, combiner, canceller, combiner (DC^3) structure is discussed by Bar-Ness [10]. The new detector uses a one-shot decorrelator followed by a maximum SNR data combiner of other user (current and previous) bits, an adaptive canceller, and an output data bit combiner [10]. The one-shot code may use a particular code to be inserted at the input of the receiver and, hence, simplifies bit synchronization [10]. The detector's output performance is almost the same as that of the synchronous user detector, and, thus, there

is no need to repeat the one-shot matched filter for each user separately [10]. This fact results in a simple structure with tremendous hardware savings [10].

The measurements performed by Frigon and Daneshrad support the idea of DFE and antenna array for indoor radio design [11].

F.2 Frequency Diversity

Wang and Moeneclaey explore a multiple hops fast frequency hopped spread spectrum multiple access (FFH-SSMA) system for indoor radio communication [12]. The system proposed by Wang and Moeneclaey consists of three units: transmitter, channel, and receiver [12]. The transmitter encodes the data via a Reed-Solomon scheme, and modulates employing an M-ary frequency-shift-keying (MFSK) [12]. The channel is represented as either Rayleigh or Rician slowly fading [12]. And the receiver employs diversity by linearly combining the squared envelopes of the different frequency hops of the same MFSK symbol [12]. It is concluded that for signal to noise ratio much greater than 0 dB; i.e., in order to overcome the *near-far* problem, the receiver performs equally well operating in either Rayleigh or Rician fading channel and under this conditions the multipath Rayleigh fading is equivalent to multipath Rician fading [12]. On the other hand, when the multiaccess interference is small the bit error rate (BER) performance is better under Rician fading channel than under Rayleigh fading channel due to the presence of specular components [12]. Moreover, the multiple hops per symbol system is not sensitive to the number of path which is in contrast with the conventional DS systems whose performance degrades with the increase of the number of paths [12]. In addition the RS coding appears to improve the BER performance with number of M-ary [12].

Alles and Pasupathy explore an indoor wireless communication system operating in 20-60 GHz band which are biased toward the power efficiency than bandwidth efficiency [13]. The authors consider a two-wave Rayleigh fading channel to derive the optimum detector structure and develop a simple suboptimum detector [13]. Moreover, the suboptimum detector is optimum when the delay of the second wave is known and whenever the equally energy signals have a normalized complex autocorrelation of either zero or unity at that delay [13]. The results presented here appear to indicate that the

frequency diversity provides robustness for the signal with multipath fading [13]. The method presented here can be extended for M-ary signals [13].

A work by Wu, Chao, and Chen considers the capacity of synchronous coded DS slow frequency-hopped (SFH) and fast frequency-hopped (FFH) spread-spectrum multiple-access (SSMA) for wireless local communications for high and low data rates [14]. For high data rate communications, wide band DS-SSMA systems appear to outperform in capacity the hybrid frequency division multiple access (FDMA)/SSMA systems [14]. For low data rate communications the fading statistics determines which system has larger capacity [14]. On the other hand, hybrid FDMA/SFH SSMA systems have larger capacity than wide band DS-SSMA; nevertheless, FFH SSMA systems could not provide satisfactory performance due to correlation among hopping bands [14].

Dardari and Tralli discusses high-speed indoor wireless communications at 60 GHz with coded OFDM by taking into account the propagation conditions in an actual environment [15]. Local performance and coverage figures have been suitably defined and the effects of code choice, frequency diversity, system clustering, and antenna sectorization have been studied and new algorithms to evaluate coding performance have been introduced [15]. It has been verified that in the NLOS points, a suitable coding can considerably reduce fading effects, but large propagation losses have a negative impact on link budget when a sufficient antenna gain is not introduced [15]. The use of sectorization has been found to be a flexible solution, which increases the received signal strength without a significant reduction of the available frequency diversity [15]. It has been shown that a system using 32 subcarriers, code-rate 0.5, sectored antennas, and 10 dBm of transmitted power in linear conditions can support packet transmission up to 155 MBPS with a coverage of 84% [15].

F.3 Code Diversity

Wang, Moeneclaey, and Milstein propose a direct sequence code division multiple access (DS-CDMA) system operating under a Rician fading channel, which is more common in factories in contrast to a Rayleigh fading channel which is more suitable for the interoffice radio channels [16]. In this work both the coherent and non-coherent phase shift keying modulation schemes are considered as well as predetection multipath

diversity to improve the BER [16]. The base station is assumed to control the average transmission power, within its particular cell, to overcome the *near-far* problem [16]. An important parameter for the Rician fading channel is the ratio (H) of the specular component power to the Rayleigh fading power. For typical factory environments the value of H changes from 2–7 dB. It appears that tremendous improvement can be obtained utilizing predetection multipath diversity for both the coherent and non-coherent receivers [16]. For small/large values of H the coherent receiver underperforms/outperforms the noncoherent receiver and for some intermediate values of H both receivers achieve similar BER performance. Nevertheless, the coherent receiver is very sensitive to the variations of H and is more complicated than the non-coherent receiver; thus, making the non-coherent scheme the preferred design for the receiver [16].

A classical work by Prasad, Misser, and Kegel [17] considers the diversity, coding, and spreading as ways of improving the performance of direct-sequence spread spectrum multiple-access for indoor wireless communication system in a Rician fading channel. The authors note that maximum ratio combining yields superior performance as compared to selection diversity [17]. In general, an increase of the rms delay spread increases the number of resolvable paths; hence, a decrease of the system performance [17]. If the number of resolvable paths is required to be smaller than the order of diversity than additional antennae are required as well, which constitutes a drawback of the diversity scheme [17]. On the other hand, forward error correction (FEC) codes and spread spectrum codes require considerable amount of channel bandwidth [17]. Therefore, improvements in diversity, coding, and spreading sequences require additional hardware and logic, which results in higher system cost [17].

Fantacci and Galligani discuss in [18] an efficient RAKE receiver architecture with pilot signal cancellation for downlink communications in DS-CDMA indoor wireless networks. This is among the first papers on the IEEE Transactions on Communications that discusses the DS-CDMA for indoor wireless communications. While this scheme is researched and implemented for outdoor applications and systems such as the GPS, cellular and mobile, it was considered less popular due to its large system Mutually Accessed Interference (MAI) [18]. One approach of canceling the MAI is provided in

the paper by Fantacci and Galligani [18], which considers a pilot signal cancellation for downlink communications.

Yang has evaluated the performance of a CDMA system with a diversity receiver scheme [19]. She uses the frame error rate (FER) instead of the BER as a performance measure because when more users are present, the FER is more sensitive to channel characteristics than BER is [19]. Based on her simulation results, when the multipath delay spread is less than the chip interval the antenna diversity is essential for improving the system performance [19].

Kim and Roh discuss the performance of slotted asynchronous CDMA using controlled time of arrival, which is similar to a wireless indoor system [20].

Hueda, Corral-Briones, and Rodriguez have shown that significant extra diversity gain can be achieved when a RAKE receiver (RR) with reduction of the interval between diversity branches is used in combination with an MMSEC [21]. This technique is attractive when the bandwidth of the spread-spectrum signal is not sufficiently large to give rise to path diversity (e.g., IS-95 in indoor radio channels) [21]. By means of theoretical analysis and computer simulations, they have shown that an important performance improvement can be achieved in a typical indoor office environment [21]. They also showed that a RR to one quarter of the chip interval for the IS-95 parameters is enough to provide almost all of the achievable improvement [21]. In practice, a RR to less than one quarter of the chip interval is not useful as a result of uncorrelated noise components such as quantization noise from A/D converters [21]. To allow a simple practical implementation, a suboptimal structure of the MMSEC was also proposed. Simulations of this receiver scheme in the forward link of the digital cellular standard IS-95, demonstrated that a gain of 4.9 dB over a classical MRC-RAKE receiver at an FER of 0.01 can be obtained. It is important to realize that this gain is achieved without the need of multiple antennae [21]. Furthermore, the additional processing required by the RR technique takes place at the output of the RAKE at a low sampling rate (for example, 19.2 kHz for an IS-95 receiver) [21]. Finally, they have found that if the proposed receiver is used in combination with a distributed antenna system, a significant increase of the capacity of DS-CDMA systems can be obtained [21].

F.4 Antenna Diversity

The utilization of antenna arrays for mobile and indoor users is well known [22]-[26]. An antenna array increases the number of degrees of freedom in the system, which results in better multipath and interference mitigation in expense of an increased size, cost, and system complexity.

Fernandes, Watson, and Neves discussed the wireless LANs: physical properties of infra-red (IR) systems vs. millimeter wave (mmw) systems [22]. Their contribution is very pertinent in the context of the assessment of indoor communication systems [22]. First, on one hand the use of transceiver antenna diversity can improve multipath mitigation for the mmw systems but not for the IR systems. On the other hand, the use of the transceiver antenna diversity can improve shadowing and blocking for both systems [22]. Second, frequency diversity can provide significant improvement for the mmw system but almost no improvement at all for the IR systems [22]. Third, channel equalization can yield significant improvement for the mmw systems and is impractical for the IR systems [22]. Fourth, the cost for building a mmw system would be smaller than the cost for building an IR system for achieving the same bit rate (less than 10 MBPS) [22].

Kandala, Sousa, and Pasupathy [24] propose a multi-user multi-sensor detectors for CDMA networks emphasizing the diversity to improve the performance of both cellular networks and personal communications systems. They have developed sub-optimal receivers based on both the multi-user detection and diversity concepts to mitigate the *near-far* effect and increase the network capacity [24].

An interesting work by Driessen [25], gigabit/s indoor wireless systems with directional antennas is explored. The author investigates the multipath effect on the size of the beam-width for a given maximum data rate [25]. According to Driessen simple FSK and PSK modems can be used instead of more costly and complex “anti-multipath” modems to achieve data rates above 1 GBPS [25].

Li, Ingram, and Rausch [26] have considered the relative performance of a number of different BS beamformer/DFE configurations for 100-MBPS QPSK using a clustered statistical indoor propagation model. They have observed a significant SNR

improvement for the beam-former case relative to the single omni-directional antenna case when enough DFE FF taps are provided to fully exploit the in-band diversity in all cases [26]. They have determined that tapering was not beneficial in this TDMA interference-free environment [26]. While performance improves as the total number of beams increases, beyond 56 beams, the improvements are small; therefore, cost is likely to heavily influence the choice of the total number of beams [26].

F.5 Phase Diversity

Roberts and Bargallo discuss the performance of a Differential Phase Shift Keying (DPSK) indoor wireless system operating in Rician fading channel [27]. Besides the typical BER performance, the loss and the packet error probability are also shown, which are of interest in packet communication [27]. The loss is the amount of additional signal power in Rician fading channel compared to the Additive White Gaussian Noise (AWGN) channel [27]. When the loss is large then additional mitigation techniques should follow [27].

Janssen, Stigter, and Prasad [28] have conducted measurements for wideband indoor channels and analyzed the BER performance for frequency selective multipath channels at 2.4, 4.75, and 11.5 GHz for data rates up to 50 MBPS. They have also developed an analytical model for an indoor coherent binary phase shift keying (BPSK) receiver [28].

A work by Benvenuto and Salloum [29] evaluates the Multitrellis Viterbi algorithm (MVA) for indoor systems using narrowbeam antennas and two modulation schemes 2-PSK and 4-PSK. This algorithm is compared against a slicer detector threshold (DT) considering two carrier recovery methods: (1) data directed (DD), which sets the phase of the recovered carrier to zero and (2) pilot toning (PT), which sets the phase of the recovered signal equal to the original signal [29]. It is observed that the 4-PSK VMA system is more robust than the 2-PSK system [29].

Jonqyin and Reed have conducted a nice survey on the performance of multiple differential phase-shift keying (MDPSK), multiple phase shift keying (MPSK), and noncoherent multiple frequency shift-keying (MFSK) in wireless Rician fading channels [30]. The analysis performance results consider the symbol error probability for a given

Rayleigh, Rician parameter K between 6-12 dB, AWGN, the multiple coding order or index $M = \{2,4,8,16\}$, and different modulation schemes [30].

F.6 Time Diversity

Marsh and Kahn [31] discuss channel reuse for base station strategies for indoor infrared wireless communications based on the following techniques: (1) Time division multiple access (TDMA) using on-off keying (OOK) or PPM; (2) FDMA using BPSK or QPSK; and (3) CDMA using OOK with direct sequence spreading by m-sequences or optical orthogonal codes (OOC) [31].

They define a parameter γ , which equals the signal-to-noise ratio (SNR) for unit optical path gain and is proportional to the square of the transmitted average optical power [31]. Employing measured path loss data TDMA with OOK or 2-PPM, and CDMA using OOC's all require approximately the same γ to achieve a worst-case bit-error rate (BER) of 10^{-9} within a cell in a system using hexagonal cells and a reuse factor of three, for cell radii above 3 m [31]. Using TDMA with 4-PPM results in a 6-dB decrease in the required value of γ [31]: CDMA using m-sequences requires an increase in γ of 5 dB over TDMA using OOK, and FDMA with BPSK requires an increase of 12 dB [31]. For a given reuse factor N in the noise-limited regime, the required value of γ decreases in inverse proportion to N^2 for TDMA schemes and inversely with N for FDMA and CDMA schemes [31]. For cell radii below 3 m, cochannel interference dominates the systems using TDMA, FDMA, and CDMA with an OOC, resulting in an irreducible BER above 10^{-9} at cell radii below 1.5 m [31]. Only CDMA with m-sequences does not develop an irreducible BER, making it the only choice for cell radii below 1.5 m [31].

F.7 Blind

Cui, Falconer, and Sheikh [32] have investigated the blind adaptation of antenna arrays using a simple algorithm based on small frequency offsets based on the idea by Agee [33]. A novel and simple algorithm is proposed for blind adaptive extraction of a binary phase-shift keying (BPSK) signal in the presence of interference by

cyclostationary signal processing using an antenna array [32]. The algorithm operates in an interference limited system in which the desired and interfering signals have identical symbol rates, but are modulated on slightly different carrier frequencies [32],[34]. Compared to existing blind algorithms, which also exploit the cyclostationarity of the received signal, the new algorithm provides a simpler and faster converging means to estimate the channel phase for diversity combining [32]-[34]. The proposed algorithm is relatively simple and very promising in applications to indoor wireless communication where interference rejection and increased spectrum efficiency are the objectives. Analysis and simulation results are presented to confirm interference rejection capabilities [32]-[34].

F.8 Other

Jang, Vojcic, and Pickholtz [35] propose a joint transmitter-receiver optimization in synchronous multiuser communications over multipath channels. They claim that transmitter optimization in addition to receiver optimization contributes significantly in improving the system performance and in multipath mitigation [35]. Joint optimization is defined as a linear transformation of the transmitted signal at the transmitter and as a linear transformation of the received signal at the receiver subject to minimizing the multiaccess and multipath interference [35]. They have shown that the joint transmitter-receiver optimization outperforms significantly either one of the single transmitter and receiver separately [35].

Tellambura, Johnson, Guo, and Barton while studying the frequency-offset estimation for HIPERLAN came across to something very peculiar: the estimator is shown to approach the Cramer–Rao bound for frequency-offset estimation over a multipath channel and the performance for a HIPERLAN system simulation example with an offset of 150 kHz is within 0.5 dB of that of a system with zero frequency offset [36].

Just when I thought that my knowledge in the Quantum Theory was lost, Fleury, presents a wonderful treatise on an uncertainty relation for WSS processes and its application to WSSUS systems [37]. This principle (similar to the one established by Heisenberg) states basically that there exists an uncertainty relation between the

coherence interval and the spectral spread of zero-mean WSS processes whose spectrum has a finite, second moment [37].

CITED REFERENCES AND FURTHER READING:

- [1] A.A.M. Saleh, A.J. Rustako, Jr., L.J. Cimini, Jr., G.J. Owens, and R.S. Roman, "An experimental TDMA indoor radio communications system using slow frequency hopping and coding," *IEEE Trans. Comm.*, vol. 39, no. 1, pp. 152-162, Jan. 1991.
- [2] K. Pahlavan, S.J. Howard, and T.A. Sexton, "Decision feedback equalization of the indoor radio channel," *IEEE Trans. Comm.*, vol. 41, no. 1, pp. 164-170, Jan. 1993.
- [3] N.W.K. Lo, D.D. Falconer, and A.U.H. Sheikh, "Adaptive equalization for co-channel interference in a multipath fading environment," *IEEE Trans. Comm.*, vol. 43, no. 2, pp. 1441-1453, Feb, Mar, and Apr. 1995.
- [4] M.D. Audeh and J.M. Kahn, "Performance evaluation of baseband OOK for wireless indoor infrared LAN's operating at 100 Mb/s," *IEEE Trans. Comm.*, vol. 43, no. 6, pp. 2085-2094, June 1995.
- [5] M.D. Audeh, J.M. Kahn, and J.R. Barry, "Performance of pulse-position modulation on measured non-directed indoor infrared channels," *IEEE Trans. Comm.*, vol. 44, no. 6, pp. 654-659, June 1996.
- [6] G.W. Marsh and J.M. Kahn, "Performance evaluation of experimental 50-Mb/s diffuse infrared wireless link using on-off keying with decision-feedback equalization," *IEEE Trans. Comm.*, vol. 44, no. 11, pp. 1496-1504, Nov. 1996.
- [7] D.C.M. Lee, J.M. Kahn, and M.D. Audeh, "Trellis-coded pulse-position modulation for indoor wireless infrared communications," *IEEE Trans. Comm.*, vol. 45, no. 9, pp. 1080-1087, Sep. 1997.
- [8] D.C.M. Lee and J.M. Kahn, "Coding and equalization for PPM on wireless infrared channels," *IEEE Trans. Comm.*, vol. 47, no. 2, pp. 255-260, Feb. 1999.
- [9] M.D. Audeh, J.M. Kahn, and J.R. Barry, "Decision-feedback equalization of pulse-position modulation on measured nondirected indoor infrared channels," *IEEE Trans. Comm.*, vol. 47, no. 4, pp. 500-503, Apr. 1999.
- [10] Y. Bar-Ness, "Asynchronous multiuser CDMA detector made simpler: novel decorrelator, combiner, canceller, combiner (DC³) structure," *IEEE Trans. Comm.*, vol. 47, no. 1, pp. 115-122, Jan. 1999.

- [11] J.-F. Frigon, and B. Daneshrad, "Field measurements of an indoor high-speed QAM wireless system using decision feedback equalization and smart antenna array," *IEEE Trans. W. Comm.*, vol. 1, no. 1, pp. 134-144, Jan. 2002.
- [12] J. Wang and M. Moeneclaey, "Multiple hops/symbol FFH-SSMA with MFSK modulation and Reed-Solomon coding for indoor radio," *IEEE Trans. Comm.*, vol. 41, no. 5, pp. 793-801, May. 1993.
- [13] M. Alles and S. Pasupathy, "Suboptimum detection for the two-wave Rayleigh-fading channel," *IEEE Trans. Comm.*, vol. 42, no. 11, pp. 2947-2958, Nov. 1994.
- [14] T.-C. Wu, C.-C. Chao, and K.-C. Chen, "Capacity of synchronous coded DS SFH and FFH spread-spectrum multiple-access for wireless local communications," *IEEE Trans. Comm.*, vol. 45, no. 5, pp. 200-212, Feb. 1997.
- [15] D. Dardari and V. Tralli, "High-speed indoor wireless communications at 60 GHz with coded OFDM," *IEEE Trans. Comm.*, vol. 47, no. 11, pp. 1709-1721, Nov. 1999.
- [16] J. Wang, M. Moeneclaey, and L.B. Milstein, "DS-CDMA with predetection diversity for indoor radio communications," *IEEE Trans. Comm.*, vol. 42, no. 2/3/4, pp. 1929-1938, Feb/Mar/Apr. 1994.
- [17] R. Prasad, H.S. Misser, and A. Kegel, "Performance evaluation of direct-sequence spread spectrum multiple-access for indoor wireless communication in a Rician fading channel," *IEEE Trans. Comm.*, vol. 43, no. 2, pp. 581-592, Feb-Apr. 1995.
- [18] R. Fantacci and A. Galligani, "An efficient RAKE receiver architecture with pilot signal cancellation for downlink communications in DS-CDMA indoor wireless networks," *IEEE Trans. Comm.*, vol. 47, no. 6, pp. 823-827, June 1999.
- [19] J. Yang, "Diversity receiver scheme and system performance evaluation for a CDMA system," *IEEE Trans. Comm.*, vol. 47, no. 2, pp. 272-280, Feb. 1999.
- [20] D.I. Kim and J.C. Roh, "Performance of slotted asynchronous CDMA using controlled time of arrival," *IEEE Trans. Comm.*, vol. 47, no. 3, pp. 454-463, Mar. 1999.
- [21] M.R. Hueda, G. Corral-Briones, and C.E. Rodriguez, "MMSEC-RAKE receivers with resolution reduction of the diversity branches: analysis, simulation, and applications," *IEEE Trans. Comm.*, vol. 49, no. 6, pp. 1073-1081, June 2001.
- [22] J.J.G. Fernandes, P.A. Watson, and J.C. Neves, "Wireless LANs: physical properties of infra-red systems vs. mmw systems," *IEEE Comm. Mag.*, vol. 32, no. 8, pp. 68-73, Aug. 1994.

- [23] L.C. Godara, "Applications of antenna arrays to mobile communications. I. Performance improvement, feasibility, and system considerations," in *Proc. IEEE*, vol. 85, no. 7, pp. 1031-1060, July 1997.
- [24] S. Kandala, E.S. Sousa, and S. Pasupathy, "Multi-user multi-sensor detectors for CDMA networks," *IEEE Trans. Comm.*, vol. 43, no. 2, pp. 946-957, Feb-Apr. 1995.
- [25] P.F. Driessen, "Gigabit/s indoor wireless systems with directional antennas," *IEEE Trans. Comm.*, vol. 44, no. 8, pp. 1034-1043, Aug. 1996.
- [26] K.-H. Li, M.A. Ingram, and E.O. Rausch, "Multibeam antennas for indoor wireless communications," *IEEE Trans. Comm.*, vol. 50, no. 2, pp. 192-194, Feb. 2002.
- [27] J.A. Roberts and J.M. Bargallo, "DPSK performance for indoor wireless Rician fading channels," *IEEE Trans. Comm.*, vol. 42, no. 2/3/4, pp. 592-596, Feb/Mar/Apr. 1994.
- [28] G.J.M. Janssen, P.A. Stigter, and R. Prasad, "Wideband indoor channel measurements and BER analysis of frequency selective multipath channels at 2.4, 4.75, and 11.5 GHz," *IEEE Trans. Comm.*, vol. 44, no. 10, pp. 1272-1288, Oct. 1996.
- [29] N. Benvenuto and A. Salloum, "Multitrellis Viterbi algorithm for indoor systems using narrowbeam antennas," *IEEE Trans. Comm.*, vol. 45, no. 8, pp. 900-902, Aug. 1997.
- [30] S. Jongyin and I.S. Reed, "Performance of MDPSK, MPSK, and noncoherent MFSK in wireless Rician fading channels," *IEEE Trans. Comm.*, vol. 47, no. 6, pp. 813-816, June 1999.
- [31] G.W. Marsh and J.M. Kahn, "Channel reuse strategies for indoor infrared wireless communications," *IEEE Trans. Comm.*, vol. 45, no. 10, pp. 1280-1290, Oct. 1997.
- [32] J. Cui, D.D. Falconer, and A.U.H. Sheikh, "Blind adaptation of antenna arrays using a simple algorithm based on small frequency offsets," *IEEE Trans. Comm.*, vol. 46, no. 1, pp. 61-70, Jan. 1998.
- [33] B.G. Agee, "The property-restoral approach to blind adaptive signal extraction," Ph.D. dissertation, University of California, Davis, 1989.
- [34] N.W.K. Lo, "Adaptive Equalization for a Multipath Fading Channel in the Presence of Interference," Ph.D. dissertation, Dept. of Systems and Computer Eng., Carleton University, May 1994.
- [35] W.M. Jang, B.R. Vojcic, and R.L. Pickholtz, "Joint transmitter-receiver optimization in synchronous multiuser communications over multipath channels," *IEEE Trans. Comm.*, vol. 46, no. 2, pp. 269-278, Feb. 1998.

- [36] C. Tellambura, I.R. Johnson, Y.J. Guo, and S.K. Barton, "Frequency-offset estimation for HIPERLAN," *IEEE Trans. Comm.*, vol. 47, no. 8, pp. 1137-1139, Aug. 1999.
- [37] B.H. Fleury, "An uncertainty relation for WSS processes and its application to WSSUS systems," *IEEE Trans. Comm.*, vol. 44, no. 12, pp. 1632-1634, Dec. 1996.

References

*“For thus saith the high and lofty One that inhabiteth eternity, whose name is Holy; I dwell in the high and holy place, with him also that is of a contrite and humble spirit, to revive the spirit of the humble, and to revive the heart of the contrite ones.”*³⁴Isaiah 57:15

A

- F. Adachi, M. Sawahashi, and H. Suda, “Wideband DS-SS-SS for next-generation mobile communications systems,” *IEEE Comm. Mag.*, vol. 36, no. 9, pp. 56-69, Sep. 1998.
- B.G. Agee, “The property-restoral approach to blind adaptive signal extraction,” Ph.D. dissertation, University of California, Davis, 1989.
- D. Akos, “A software radio approach to Global Navigation Satellite System receiver design,” Ph.D. dissertation, Ohio University, August 1997.
- R.J. Alexander, “Navigation requirements for oceanography,” *J. Inst. Nav.*, vol. 10, no. 2, pp. 161-166, summer 1963.
- M. Alles and S. Pasupathy, “Suboptimum detection for the two-wave Rayleigh-fading channel,” *IEEE Trans. Comm.*, vol. 42, no. 11, pp. 2947-2958, Nov. 1994.
- J.B. Andersen, T.S. Rappaport, and S. Yoshida, “Propagation measurements and models for wireless communications channels,” *IEEE Comm. Mag.*, vol. 33, no. 1, pp. 42-49, Jan. 1995.
- Anon., Department of Defense, *Global Positioning System (GPS) Standard Positioning Service (SPS)*, Signal Specification, Dec. 8, 1993.
- Anon., “Minimum aviation system performance standards—DGNS instrument approach system: special category I (SCAT-I),” RTCA/DO-217, RTCA, Inc., Washington, DC, Aug. 27, 1993.
- Anon, “JCAB MTSAT functions and current status,” the 4th meeting of the allpirc advisory Y group, Montreal, 6 - 8 February 2001.
- Anon., “Location technologies for GSM, GPRS, and WCDMA networks,” SnapTrack™ a QUALCOM company, white paper.
- Anon. “UWB threatens from the sideline,” ION-GPS 2002, Show Daily, p. 2, Wed., Sep. 25, 2002.
- Antenna Engineering Handbook*, H. Jasik, Ed., MacGraw-Hill, New York, 1961.
- M.D. Audeh and J.M. Kahn, “Performance evaluation of baseband OOK for wireless indoor infrared LAN's operating at 100 Mb/s,” *IEEE Trans. Comm.*, vol. 43, no. 6, pp. 2085-2094, June 1995.

- M.D. Audeh, J.M. Kahn, and J.R. Barry, "Performance of pulse-position modulation on measured non-directed indoor infrared channels," *IEEE Trans. Comm.*, vol. 44, no. 6, pp. 654-659, June 1996.
- M.D. Audeh, J.M. Kahn, and J.R. Barry, "Decision-feedback equalization of pulse-position modulation on measured nondirected indoor infrared channels," *IEEE Trans. Comm.*, vol. 47, no. 4, pp. 500-503, Apr. 1999.

B

- F. Babich and G. Lombardi, "Statistical analysis and characterization of the indoor propagation channel," *IEEE Trans. Comm.*, vol. 48, no. 3, pp. 455-464, Mar. 2000.
- J. Bahl and P. Bhartia, *Microstrip Antennas*. Norwood, MA: Artech House, 1980
- P. Bahl and V. Padmanabhan, "RADAR: an in-building RF-based user location and tracking system," *IEEE INFOCOM*, Israel, Mar. 2000.
- C.A. Balanis, *Advanced Engineering Electromagnetics*. New York: Wiley, 1989.
- J. Bao-Yen Tsui, *Fundamentals of Global Positioning Systems Receivers, A Software Approach*. New York, NY: Wiley Inter-Science, May 2000.
- J.M. Bargallo and J.A. Roberts, "Performance of BPSK and TCM using the exponential multipath profile model for spread-spectrum indoor radio channels," *IEEE Trans. Comm.*, vol. 43, no. 2, pp. 615-623, Feb-Apr. 1995.
- Y. Bar-Ness, "Asynchronous multiuser CDMA detector made simpler: novel decorrelator, combiner, canceller, combiner (DC3) structure," *IEEE Trans. Comm.*, vol. 47, no. 1, pp. 115-122, Jan. 1999.
- J.R. Barry, *Wireless Infrared Communications*, Boston: Kluwer Academic Publishers, 1994.
- C. Bartone and F., Van Graas, "Ranging airport pseudolite for local area augmentation," *IEEE Trans. Aer. Elect. Sys.*, vol. 36, pp. 278 -286, Jan. 2000.
- C.G. Bartone and S. Kiran, "Flight test results of an integrated wideband airport pseudolite for the local area augmentation system," *J. Inst. Nav.*, vol. 48, no. 1, pp. 35-48, Spring 2001.
- S. Benedetto, E. Biglieri, and V. Castellani, *Digital Transmission Theory*. Englewood Cliffs, NJ: Prentice-Hall, 1987.
- N. Benvenuto and A. Salloum, "Multitrellis Viterbi algorithm for indoor systems using narrowbeam antennas," *IEEE Trans. Comm.*, vol. 45, no. 8, pp. 900-902, Aug. 1997.
- H.L. Bertoni, W. Honcharenko, L.R. Macel, and H.H. Xia, "UHF propagation prediction for wireless personal communications," in *Proc. IEEE*, vol. 82, no. 9, pp. 1333-1359, Sep. 1994.
- R.E. Best, *Phase-Locket Loops*. New York: McGraw-Hill, 1984.
- R.E. Best, *Phase Locked Loops: Design, Simulations, and Applications*. 4th Ed. Mc-Graw Hill, Jun. 1999.

- V.K. Bhargava, D. Hancoun, R. Matyas, and P.P. Nuspl, *Digital Communications by Satellite*. New York, NY: John Wiley & Sons, 1981.
- T.K. Blankenship and T.S. Rappaport, "Characteristics of impulsive noise in the 450-MHz band in hospitals and clinics," *IEEE Trans. Ant. Prop.*, vol. 46, no. 2, pp. 194-203, Feb. 1998.
- J. Blau, "Wi-Fi hotspot networks sprout like mushrooms," *IEEE Spectrum Mag.*, pp18-20, Sep. 2002.
- D.E. Boegeman, "The offset method of sonar ranging," *J. Inst. Nav.*, vol. 17, no. 1, pp. 47-51, spring 1970.
- J. Boersma, "On certain multiple integrals occurring in wave-guide scattering problem," *SIAM J. Math. Anal.*, vol. 9, no. 2, pp. 377-393, 1978.
- P. Boisvert, "The ambient electromagnetic environment in metropolitan hospitals," MS thesis, Dept. Elect. Eng., McGill Univ., Montreal, Canada, 1991.
- M.S. Braach, "On the characterization of multipath error in satellite-based precision approach and landing systems," Ph.D. dissertation, Ohio University, Athens, OH, June 1992.
- K. Brayer, Ed., *Data Communications via Fading Channels*. New York: IEEE Press, 1975.
- A. Brown, F. Van Diggelen, and C. LaBerge, "Test results of a GPS/pseudolite precision approach and landing system," in *Proc. ION-GPS*, pp. 157-853, 1993.
- R.C. Brown and P.Y.C. Hwang, *Introduction to Random Signals and Applied Kalman Filtering*. 3rd ed., New York: John Wiley & Sons, 1981.
- H. Butterfield, *The Origins of Modern Science, 1300-1800*, London, 1947.
- K.S. Butterworth, K.W. Sowerby, and A.G. Williamson, "Base station placement for in-building mobile communication systems to yield high capacity and efficiency," *IEEE Trans. Comm.*, vol. 48, no. 4, pp. 658-669, Apr. 2000.

C

- D.E. Campbell, "Precise acoustic navigation and position keeping," *J. Inst. Nav.*, vol. 17, no. 2, pp. 124-135, summer 1970.
- W. Carrara, R. Goodman, and R. Majewski, *Spotlight Synthetic Aperture Radar*. Boston, MA: Artech House, 1995.
- J.B. Carruthers and J.M. Kahn, "Modeling of nondirected wireless infrared channels," *IEEE Trans. Comm.*, vol. 45, no. 10, pp. 1260-1268, Oct. 1997.
- K.W. Cattermole, *Principles of Pulse Code Modulation*, London: Illife Books, 1969.
- J.A. Cestone, "Deep submergence navigation," *J. Inst. Nav.*, vol. 15, no. 1, pp. 3-15, spring 1968.
- J.A. Cestone and E.st. George, jr., "Hydrospheric navigation," *J. Inst. Nav.*, vol. 19, no. 3, pp. 199-208, fall 1972.
- J.A. Cestone, R.J. Cyr, G. Roesler, and E.st. George, jr., "Latest highlights in acoustic underwater navigation," *J. Inst. Nav.*, vol. 24, no. 1, pp. 7-39, spring 1977.

- Y. Chang-Fa, W. Boau-Cheng, and K. Chuen-Jyi, "A ray-tracing method for modeling indoor wave propagation and penetration," *IEEE Trans. Ant. Prop.*, vol. 46, no. 6, pp. 907-919, June 1998.
- G.C. Clack, Jr. and J. Bibb Cain, *Error Correcting Coding for Digital Communications*. New York, NY: Plenum Press, 1981.
- C.A. Cohen et al., "Real-time cycle ambiguity resolution using a pseudolite for precision landing of aircraft using GPS," in Proc. DSNS, Amsterdam, The Netherlands, Mar.-Apr. 1993.
- R.E. Collin, *Field Theory of Guided Waves*. New York: McGraw-Hill, 1960.
- R.E. Collin, *Antennas and Radiowave Propagation* New York: McGraw-Hill, 1985.
- C.E. Cook, *Radar Signals: An Introduction to Theory and Application*. New York: Academic Press, 1967.
- G.R. Cooper and C.D. McGillem, *Modern Communications and Spread Spectrum*. New York: McGraw-Hill, 1986.
- J. Cui, D.D. Falconer, and A.U.H. Sheikh, "Blind adaptation of antenna arrays using a simple algorithm based on small frequency offsets," *IEEE Trans. Comm.*, vol. 46, no. 1, pp. 61-70, Jan. 1998.
- J. Curlander and R. McDonough, *Synthetic Aperture Radar*. New York: Wiley, 1991.
- N.C. Currie, R.D. Hayes, and R.N. Trebits, *Millimeter-Wave Radar Clutter*. Boston, MA: Artech House, 1992.

D

- A.S. Dale, P. Daly, and I.D. Kitching, "Understanding signals from GLONASS satellites," *Inter. J. of Sat. Comm.*, vol. 7, no. 1, pp. 11-22, 1989.
- P. Daly, I.D. Kitching, D. Allan, and T. Pepler, "Frequency and time stability of GPS and GLONASS clocks," *Inter. J. of Sat. Comm.*, vol. 9, no. 1, pp. 11-22, 1991.
- M.H. Damon, "SANS, ships acoustic navigation system," *J. Inst. Nav.*, vol. 19, no. 1, pp. 11-18, spring 1972.
- D. Dardari and V. Tralli, "High-speed indoor wireless communications at 60 GHz with coded OFDM," *IEEE Trans. Comm.*, vol. 47, no. 11, pp. 1709-1721, Nov. 1999.
- N. Davies, *Europe a History*, New York, NY: Oxford University Press, 1996.
- N. Davies, K. Cheverst, K. Mitchell, and A. Efrat, "Using and determining location in a context-sensitive tour guide," *Comp.*, vol. 34, pp 35-41, Aug. 2001.
- R.J. Davies, "In-building UHF propagation studies," M.Sc. thesis, Univ. Calgary, 1989, unpublished.
- P.T. Davis and C.R. McGuffin, *Wireless Local Area Networks: Technology, Issues, and Strategies*. New York: McGraw-Hill, 1995.

- V. Degli-Eposti, G. Lombardi, C. Passerini, and G. Riva, "Wide-band measurement and ray-tracing simulation of the 1900-MHz indoor propagation channel: comparison criteria and results," *IEEE Trans. Ant. Prop.*, vol. 49, no. 7, pp. 1101-1110, July 2001.
- S. Dehghan and R. Steele, "Small cell city," *IEEE Comm. Mag.*, vol. 35, no. 8, pp. 52-59, Aug. 1997.
- D.M.J. Devasirvatham, C. Banerjee, R.R. Murray, and D.A. Rappaport, "Two frequency radio-wave propagation measurements in Brooklyn," in *Proc. IEEE Int. Conf. on Universal Personal Commun.*, pp. 23-27, Dallas, TX, 1992.
- U. Dersch, J. Troger, and E. Zollinger, "Multiple reflections of radio waves in a corridor," *IEEE Trans. Ant. Prop.*, vol. 42, no. 11, pp. 1571-1574, Nov. 1994.
- B.P. Donaldson, M. Fattouche, and R.W. Donaldson, "Characterization of in-building UHF wireless radio communication channels using spectral energy measurements," *IEEE Trans. Ant. Prop.*, vol. 44, no. 1, pp. 80-86, Jan. 1996.
- P.F. Driessen and L.J. Greenstein, "Modulation techniques for high-speed wireless indoor systems using narrowbeam antennas," *IEEE Trans. Comm.*, vol. 43, no. 10, pp. 2605-2612, Oct. 1995.
- G.D. Dunlap, "Major developments in marine navigation during the last 25 years," *J. Inst. Nav.*, vol. 18, no. 1, pp. 63-76, spring 1971.
- E. Durbin, "Current development in the Loran C system," *J. Inst. Nav.*, vol. 9, no. 2, pp. 138-150, summer 1962.
- J.G. Durgin, T.S. Rappaport, and H. Xu, "Measurements and models for radio path loss and penetration loss in and around homes and trees at 5.85 GHz," *IEEE Trans. Comm.*, vol. 46, no. 11, pp. 1484-1496, Nov. 1998.

E

- W. Elenbass, *Fluorescent Lamps*. London: Macmillan, 2nd ed., 1971.
- P. Enge, "A global challenge—Protect GNSS noise floor a.k.a. spectrum stewardship," *ION-GPS 2002* (panel presentation), Portland, OR, Sep. 24, 2002.
- P.K. Enge and D.V. Sarwate, "Spread-spectrum multi-access performance of orthogonal codes: linear receivers," *IEEE Trans. Comm.*, vol. COM-35, 1309-1399, Dec. 1987.

F

- R. Fantacci and A. Galligani, "An efficient RAKE receiver architecture with pilot signal cancellation for downlink communications in DS-CDMA indoor wireless networks," *IEEE Trans. Comm.*, vol. 47, no. 6, pp. 823-827, June 1999.

- Federal Communications Commission, Memorandum Opinion and Order FCC 97-402, Revision of the Commission's Rules To Ensure Compatibility with Enhanced 911 Emergency Calling Systems, Washington, DC, adopted December 1, 1997, revised Sep. 1999.
- Federal Communications Commission, *News*, "New public safety applications and broadband internet access among uses envisioned by FCC authorization of ultra-wideband technology," Washington, DC, Feb. 14, 2002.
- L.B. Felsen and N. Marcuvitz, *Radiation and Scattering of Waves*. Englewood Cliffs, NJ: Prentice-Hall, 1973.
- J. Fen, "A precise RF positioning system," *Pres. at ION-NES*, Jan. 17, 2001.
- J. Fen, "Security system," *United States Patent*, no. 5,374,936, Dec. 20, 1994.
- J.J.G. Fernandes, P.A. Watson, and J.C. Neves, "Wireless LANs: physical properties of infra-red systems vs. mmw systems," *IEEE Comm. Mag.*, vol. 32, no. 8, pp. 68-73, Aug. 1994.
- B.H. Fleury, "An uncertainty relation for WSS processes and its application to WSSUS systems," *IEEE Trans. Comm.*, vol. 44, no. 12, pp. 1632-1634, Dec. 1996.
- J.P. Fitch, *Synthetic Aperture Radar*. New York: Springer-Verlag, 1988.
- R. Fontana, "Advances in ultra wideband indoor geolocation systems," *3rd IEEE Wksp. WLAN*, Boston, MA, Sept. 2001.
- J.-F. Frigon, and B. Daneshrad, "Field measurements of an indoor high-speed QAM wireless system using decision feedback equalization and smart antenna array," *IEEE Trans. W. Comm.*, vol. 1, no. 1, pp. 134-144, Jan. 2002.

G

- R. Gagliardi, *Introduction to Communication Engineering*. New York: Wiley, 1978.
- R.C. Galijan and G.V. Lucha, "A suggested approach for augmenting GNSS category III approaches and landings: the GPS/GLONASS and GLONASS pseudolite system," in *Proc. ION-GPS*, pp. 157-853, 1993.
- R.G. Gallager, *Information Theory and Reliable Communications*, New York: Wiley, 1968.
- F.M. Gardner, *Phaselock Techniques*. New York: John Wiley, 1979.
- R.D. Gitlin, J.F. Hayes, and S.B. Weinstein, *Data Communications Principles*. New York: Plenum, 1992.
- L.C. Godara, "Applications of antenna arrays to mobile communications. I. Performance improvement, feasibility, and system considerations," in *Proc. IEEE*, vol. 85, no. 7, pp. 1031-1060, July 1997.
- W. Goj, *Synthetic Aperture Radar and Electronic Warfare*. Dedham, MA: Artech House, 1989.
- D.J. Goodman, "Cellular packet communications," *IEEE Trans. Comm.*, vol. 38, no. 8, pp. 1272-1280, Aug. 1990.

- T.A. Goulet, "The use of pulsed Doppler sonar for navigation of manned deep submergence vehicles," *J. Inst. Nav.*, vol. 17, no. 2, pp. 136-141, summer 1970.
- B.M. Green and M.A. Jensen, "Empirical characterization of wideband indoor radio channel at 5.3 GHz," *IEEE Trans. Ant. Prop.*, vol. 48, no. 7, pp. 1017-1024, July 2000.
- L.J. Greenstein et al., "Microcells in personal communications systems," *IEEE Comm. Mag.*, vol. 30, no. 12, pp. 76-88, Dec. 1992.
- L.W. Griswold, "Underwater logs," *J. Inst. Nav.*, vol. 15, no. 2, pp. 127-135, summer 1968.

H

- H. Hashemi, "Simulation of the urban radio propagation channel," *IEEE Trans. Veh. Technol.*, vol. VT-28, pp. 213-224, Aug. 1979.
- H. Hashemi, "The indoor radio propagation channel," in *Proc. IEEE*, vol. 81, no. 7, pp. 943-968, July 1993.
- M. Hassan-Ali and K. Pahlavan, "A new statistical model for site-specific indoor radio propagation prediction based on geometric optics and geometric probability," *IEEE Trans. W. Comm.*, vol. 1, no. 1, pp. 112-124, Jan. 2002.
- S.S. Haykin, *Adaptive Filter Theory*. Englewood Cliffs, NJ: Prentice-Hall, 1987.
- S. Haykin, *An Introduction to Analog and Digital Communications*. New York: Wiley, 1989.
- C. Hegarty, "GPS-Galileo signal compatibility," *ION-GPS 2002* (panel presentation), Portland, OR, Sep. 24, 2002.
- C.W. Helstrom, *Elements of Signal Detection and Estimation*. Englewood Cliffs, NJ: Prentice-Hall, 1995.
- M. Higgins and D.M. Harrell, "Integrated navigation for deep ocean positioning," *J. Inst. Nav.*, vol. 35, no. 1, pp. 1-13, spring 1988.
- J. Hill, I.F. Progni, and W.R. Michalson, "Techniques for reducing the near-far problem in indoor geolocation systems," in *Proc. ION-NTM*, Long Beach, CA, pp. 860-865, Jan. 2001.
- J.M. Hill, "Development of an experimental Global Positioning System (GPS) receiver platform for navigation algorithm evaluation," Ph.D. Dissertation, Worcester Polytechnic Institute, Aug. 2001.
- D.M. Holmes, "Surface controlled-deep ocean navigation techniques for precise bottom site determination and relocation," *J. Inst. Nav.*, vol. 12, no. 4, pp. 287-298, winter 1965-66.
- W. Honcharenko, H.L. Bertoni, and J.L. Dailing, "Bilateral averaging over receiving and transmitting areas for accurate measurements of sector average signal strength inside buildings," *IEEE Trans. Ant. Prop.*, vol. 43, no. 5, pp. 508-512, May 1995.
- S.J. Howard, "Frequency domain characteristics and autoregressive modeling of the indoor radio channel," Ph.D. dissertation, Worcester Polytech. Inst., 1991.

S.J. Howard and K. Pahlavan, "Autoregressive modeling of wide-band indoor radio propagation," *IEEE Trans. Comm.*, vol. 40, no. 9, pp. 1540-1552, Sep. 1992.

M.R. Hueda, G. Corral-Briones, and C.E. Rodriguez, "MMSEC-RAKE receivers with resolution reduction of the diversity branches: analysis, simulation, and applications," *IEEE Trans. Comm.*, vol. 49, no. 6, pp. 1073-1081, June 2001.

I

IRN-200C-001, ICD-GPS-200C, 13 Oct 1995.

T. Iwama *et al.*, "Investigation of propagation characteristics above 1 GHz for microcell land mobile radio," in *Proc. IEEE Veh. Technol. Conf.*, pp. 396-400, 1990.

J

R. Jain, *The Art of Computer Systems Performance Analysis (Techniques for Experimentation Design, Measurements, Simulation, and Modeling)*. New York, NY: John Wiley & Sons, 1991 ("Chap. 29, Commonly Used Distributions").

W. Jakes, Jr., *Microwave Mobile Communications*. New York: Wiley-Interscience, 1974.

W.M. Jang, B.R. Vojcic, and R.L. Pickholtz, "Joint transmitter-receiver optimization in synchronous multiuser communications over multipath channels," *IEEE Trans. Comm.*, vol. 46, no. 2, pp. 269-278, Feb. 1998.

G.J.M. Janssen, P.A. Stigter, and R. Prasad, "Wideband indoor channel measurements and BER analysis of frequency selective multipath channels at 2.4, 4.75, and 11.5 GHz," *IEEE Trans. Comm.*, vol. 44, no. 10, pp. 1272-1288, Oct. 1996.

S. Jongyjin and I.S. Reed, "Performance of MDPSK, MPSK, and noncoherent MFSK in wireless Rician fading channels," *IEEE Trans. Comm.*, vol. 47, no. 6, pp. 813-816, June 1999.

K

J.M. Kahn, W.J. Krause, and J.B. Carruthers, "Experimental characterization of non-directed indoor infrared channel," *IEEE Trans. Comm.*, vol. 42, no. 2, pp. 1929-1938, Feb-Apr. 1995.

S. Kandala, E.S. Sousa, and S. Pasupathy, "Multi-user multi-sensor detectors for CDMA networks," *IEEE Trans. Comm.*, vol. 43, no. 2, pp. 946-957, Feb-Apr. 1995.

E.D. Kaplan, *Understanding GPS: Principles and Applications*. Boston, MA: Artech House, 1996.

Y. Karasawa and H. Iwai, "Formulation of spatial correlation statistics in Nakagami-Rice fading environments," *IEEE Trans. Ant. Prop.*, vol. 48, no. 1, pp. 12-18, Jan. 2000.

M. Kavehrad and P.J. McLane, "Spread spectrum for indoor digital radio," *IEEE Commun. Mag.*, vol. 25, no. 6, pp. 32-40, June 1987.

J.B. Keller, "Geometrical theory of diffraction," *J. Opt. Soc. Amer.*, vol. 52, pp. 116-131, 1962.

- R.S. Kennedy, *Fading Dispersive Communication Channel*. New York: Wiley-Interscience, 1969.
- G.E. Keiser, *Local Area Networks*. New York: McGraw-Hill, 1989.
- D.E. Kerr, Ed., *Propagation of Short Radio Waves*. New York: McGraw-Hill, vol. 13, 1951 (Radiation Lab. Series).
- D.I. Kim, "On the performance of common spreading code CDMA packet radio systems with multiple capture capability," Ph.D. dissertation, Dept. Elect. Eng., Univ. Southern California, Los Angeles, CA, 1990.
- D.I. Kim and J.C. Roh, "Performance of slotted asynchronous CDMA using controlled time of arrival," *IEEE Trans. Comm.*, vol. 47, no. 3, pp. 454-463, Mar. 1999.
- J. Kivinen, X. Zhao, and P. Vainikainen, "Empirical characterization of wideband indoor radio channel at 5.3 GHz," *IEEE Trans. Ant. Prop.*, vol. 49, no. 8, pp. 1192-1203, Aug. 2001.
- D. Klein and B.W. Parkinson, "The use of pseudo-satellites for improving GPS performance," in *Global Positioning System*, vol. II., pp. 135-146, Silver Spring, MD: Institute of Navigation, 1986.
- R. Klukas, G. Lachapelle, and M. Fattouche, "Estimation noise of a cellular telephone positioning system," *J. Inst. Nav.*, vol. 47, no. 3, pp. 167-174, fall 2000.
- R. Klukas, "Cellular telephone positioning using GPS time synchronization," in *Proc. ION-GPS*, Kansas City, MO, pp. 1405-1414, Sep. 1997.
- I. Koffman and V. Roman, "Broadband wireless access solutions based on OFDM access in IEEE 802.16," *IEEE Comm. Mag.*, vol. 40, no. 4, pp. 96-103, Apr. 2002.
- J.A. Kong, *Electromagnetic Waves Theory*. New York: Wiley, 1986.
- M.D. Kotzin, "Short-range communications using diffusely scattered infrared radiation," Ph.D. dissertation, Northwestern Univ., June 1981.
- K. Kovac, "GNSS signal compatibility and interoperability: GPS person's view," *ION-GPS 2002* (panel presentation), Portland, OR, Sep. 24, 2002.
- J.D. Kraus, *Antennas*, 1st ed. New York: McGraw-Hill, 1950, 2nd ed., 1988.
- K. Kurmiveda et al., "A complete IF software GPS receiver," in *Proc. ION-GPS*, Salt Lake City, UT, pp. 789-829, Sep. 2001.

L

- D.C.M. Lee, J.M. Kahn, and M.D. Audeh, "Trellis-coded pulse-position modulation for indoor wireless infrared communications," *IEEE Trans. Comm.*, vol. 45, no. 9, pp. 1080-1087, Sep. 1997.
- D.C. Lee, "Power-efficient coded modulation for wireless infrared communication," Ph.D. Dissertation, Univ. California, Berkeley, 1998.
- D.C.M. Lee and J.M. Kahn, "Coding and equalization for PPM on wireless infrared channels," *IEEE Trans. Comm.*, vol. 47, no. 2, pp. 255-260, Feb. 1999.

- E.A. Lee and D.G. Messerschmitt, *Digital Communications*, Second Edition, Boston: Kluwer Academic Publishers, 1994.
- H.E. Lee, "Application of optimal estimation techniques to acoustic transponder navigation systems," *J. Inst. Nav.*, vol. 22, no. 3, pp. 201-207, fall 1975.
- W.C.Y. Lee, *Mobile Communications Design Fundamentals*. New York: Howard W. Sams, 1986.
- W.C.Y. Lee, *Mobile Cellular Telecommunications Systems*. New York: McGraw-Hill, 1989.
- C.-S. Li, "Emerging pervasive technologies for e-commerce," in *Proc. IEEE ISCAS*, pp. 7.3.1-7.3.14, 2001.
- K.-H. Li, M.A. Ingram, and E.O. Rausch, "Multibeam antennas for indoor wireless communications," *IEEE Trans. Comm.*, vol. 50, no. 2, pp. 192-194, Feb. 2002.
- W.C. Lindsey and M.K. Simon, *Telecommunication Systems Engineering*. Englewood Cliffs, NJ: Prentice-Hall, 1973.
- J.-P. Linnartz, *Narrowband Land-Mobile Radio Networks*. Boston, MA: Artech House, 1993.
- N.W.K. Lo, "Adaptive Equalization for a Multipath Fading Channel in the Presence of Interference," Ph.D. dissertation, Dept. of Systems and Computer Eng., Carleton University, May 1994.
- N.W.K. Lo, D.D. Falconer, and A.U.H. Sheikh, "Adaptive equalization for co-channel interference in a multipath fading environment," *IEEE Trans. Comm.*, vol. 43, no. 2, pp. 1441-1453, Feb, Mar, and Apr. 1995.
- T. Lo, J. Litva, and H. Leung, "A new approach for estimating indoor radio propagation characteristics," *IEEE Trans. Ant. Prop.*, vol. 42, no. 10, pp. 1369-1376, Oct. 1994.
- Y.T. Lo and S.W. Lee Ed., *Antenna Handbook*. New York: Van-Nostrand Reinhold, 1988.
- R.M. Lollock, "Global Positioning System (GPS) Modernization," civil GPS service interface committee, Washington, DC, 27-29 Mar. 2001. (unclassified presentation)
- C. Lopez-Bravo and M.-D. Cano, "Galileo: The European satellite radio navigation system," *Global Comm. News.*, vol. 40, no. 7, pp. 2-4, Jul. 2002.
- R.W. Lucky, J. Salz, and E.J. Weldon, Jr., *Principles of Data Communication*. New York: McGraw Hill, 1968.

M

- L.R. Macel, H.L. Bertoni, and H.H. Xia, "Unified approach to prediction of propagation over building of all ranges of base station antenna height," *IEEE Trans. Veh. Technol.*, vol. 42, pp. 41-45, Feb. 1993.
- L.R. Macel and H.L. Bertoni, "Cell shape for microcellular systems in residential and commercial environments," in *IEEE Conf. on Universal Personal Communications*, pp. 723-727, Ottawa, Ont., Canada, 1993.

- L.R. Macel and H.L. Bertoni, "Cell shape for microcellular systems in residential and commercial environments," *IEEE Trans. Veh. Technol.*, vol. 43, no. 2, pp. 270-278, 1994.
- K.V. Mackenzie, "Early history of deep submergence navigation a board Trieste," *J. Inst. Nav.*, vol. 17, no. 2, pp. 3-12, spring 1970.
- T.S.M. Maclean and Z. Wu, *Radiowave Propagation over Ground*. London, U.K.: Chapman Hall, 1993.
- D.T. Magill, F.D. Natali, and G.P. Edwards, "Spread-spectrum technology for commercial applications," in *Proc. IEEE*, vol. 82, no. 4, pp. 572-584, Apr. 1994.
- R.J. Mailloux, *Phased Array Antenna Handbook*. Boston: Artech House, 1994.
- G.W. Marsh, "High-speed wireless infrared communication links," Ph.D. dissertation, Univ. California, Berkeley, Dec. 1995.
- G.W. Marsh and J.M. Kahn, "Performance evaluation of experimental 50-Mb/s diffuse infrared wireless link using on-off keying with decision-feedback equalization," *IEEE Trans. Comm.*, vol. 44, no. 11, pp. 1496-1504, Nov. 1996.
- G.W. Marsh and J.M. Kahn, "Channel reuse strategies for indoor infrared wireless communications," *IEEE Trans. Comm.*, vol. 45, no. 10, pp. 1280-1290, Oct. 1997.
- C. Matchumoto, "PinPoint debuts local positioning system," *EE Times*, Sept. 14, 1998.
- G.A. McGraw, "Analysis of pseudolite code interference effects for aircraft precision approaches," in *Proc. ION AM*, Colorado Springs, CO, June 1994.
- D.L. Mckeown, "Survey techniques for acoustic positioning arrays," *J. Inst. Nav.*, vol. 22, no. 1, pp. 59-67, spring 1975.
- W.R. Michalson and I.F. Progri, "Assessing the accuracy of underground positioning using pseudolites," in *Proc. ION-GPS*, Salt Lake City, UT, pp. 1007-1015, Sep. 2000.
- T. Miller, "Radio frequency interference suppression for foliage penetration radar imaging," MS thesis, Ohio State University, Columbus, OH, Dec. 1994.
- P. Misra and P. Enge, *Global Positioning System-Signals Measurements and Performance*, Lincoln, MA: Ganga-Jamuna Press, 2001.
- M. Moeglein and N. Krasner, "An introduction to SnapTrack™ server-aided GPS technology," in *Proc. ION-GPS*, pp. 333-342, Sep. 1998.
- A.G. Mourad and N.A. Frazier, "Improving navigational systems through establishment of a marine geodetic range," *J. Inst. Nav.*, vol. 14, no. 2, pp. 187-194, summer 1967.
- J.B. Murdoch, *Illumination Engineering*, New York: Macmillan, 1985.

N

- F. Nebeker, "September and October in EE history," *IEEE The Institute*, vol. 25, pp. 9, Oct. 2001.

- O. Norklit, P.D. Teal, and R.G. Vaughan, "Measurement and evaluation of multi-antenna handsets in indoor mobile communication," *IEEE Trans. Ant. Prop.*, vol. 49, no. 3, pp. 429-437, Mar. 2001.

O

- A.V. Oppenheim and R.W. Schaffer, *Discrete-Time Signal Processing*. Englewood Cliffs, NJ: Prentice-Hall, 1989.
- G.R. Opshaug and P. Enge, "GPS and UWB for indoor navigation," in *Proc. ION-GPS*, Salt Lake City, UT, pp. 1427-1433, Sep. 11-14, 2001.
- G.D. Ott and A. Plitkins, "Urban path-loss characteristics at 820 MHz," *IEEE Trans. Veh. Technol.*, vol. VT-27, pp. 189-197, 1978.

P

- K. Pahlavan and M. Chase, "Spread-spectrum multiple-access performance of orthogonal codes for indoor radio communications," *IEEE Trans. Comm.*, vol. 38, no. 5, pp. 574-577, May 1990.
- K. Pahlavan, S.J. Howard, and T.A. Sexton, "Decision feedback equalization of the indoor radio channel," *IEEE Trans. Comm.*, vol. 41, no. 1, pp. 164-170, Jan. 1993.
- K. Pahlavan and A.H. Levesque, *Wireless Information Networks*. New York: Wiley, 1995.
- K. Pahlavan, P. Krishnamurthy, and A. Beneat, "Wideband radio propagation modeling for indoor geolocation applications," *IEEE Comm. Mag.*, vol. 36, no. 4, pp. 60-65, Apr. 1998.
- K. Pahlavan, X. Li, J-P. Makela, "Indoor geolocation science and technology," *IEEE Comm. Mag.*, vol. 40, no. 2, pp. 112-118, Feb. 2002.
- A. Papoulis, *Probability, Random Variables, and Stochastic Processes*. New York: McGraw-Hill, 1984.
- H. Park, "Coded modulation and equalization for wireless infrared communications," Ph.D. dissertation, Georgia Inst. Technol., 1997.
- B. Parkinson and S.W. Gilbert, "NAVSTAR: Global Positioning System—ten years later," in *IEEE*, vol. 71, pp. 1177-1186, Oct. 1983.
- B.W. Parkinson and K.T. Fitzgibbon, "Optimal locations of pseudolites for differential GPS," *J. Inst. Nav.*, vol. 33, no. 4, pp. 259-283, winter 1986-87.
- B. Parkinson, K. Gromov, T. Stansell, and R. Beard, "A history of satellite navigation," in *Proc. ION-AM*, pp. 17-65, Colorado Springs, Co, June 1995.
- B.W. Parkinson, J.J. Spilker, P. Axelrad, and P. Enge, *Global Positioning System: Theory and Applications*, vol. 1 and 2, Washington, DC: AIAA, 1996.
- J.D. Parson, *The Mobile Radio Propagation Channel*, New York: Halsted Press, 1992.

- B.B. Peterson, C.G. Kmieciak, H. Nguyen, and B. Kaspar, "Indoor geolocation system operational test results," *J. Inst. Nav.*, vol. 47, no. 3, pp. 157-166, Fall 2000.
- W.W. Peterson and E.J. Weldon, *Error Correcting Codes*. Cambridge, MA: MIT Press, 1972.
- H.V. Poor, *An Introduction to Signal Detection and Estimation*. 2nd ed., New York: Dowden & Culver, 1994.
- R. Prasad, A. Kegal, and C. Rönne, "Performance analysis of a sectorized mobile microcellular radio system with diversity and forward error correction coding," in *Proc. IEEE VTC '94*, 1994.
- R. Prasad, H.S. Misser, and A. Kegal, "Performance evaluation of direct-sequence spread spectrum multiple-access for indoor wireless communication in a Rician fading channel," *IEEE Trans. Comm.*, vol. 43, no. 2, pp. 581-592, Feb-Apr. 1995.
- J.G. Proakis, *Digital Communications*. 1st, 2nd, and 3rd, ed., New York: McGraw-Hill, 1983, 1989, and 1995.
- J.G. Proakis and D.G. Manolakis, *Digital Signal Processing: Principles, Algorithms and Applications*, 2nd ed. New York: Macmillan, 1992.
- J.G. Proakis and M. Salehi, *Communication Systems Engineering*, Upper Saddle River, New Jersey: Prentice Hall, 1994.
- I.F. Proгри, W.R. Michalson et al, "A system for tracking and locating emergency personnel inside buildings," in *Proc. ION-GPS*, Salt Lake City, UT, pp. 560-568, Sep. 2000.
- I.F. Proгри and W.R. Michalson, "Performance evaluation of category III precision landing using airport Pseudolites," in *Proc. IEEE PLANS*, San Diego, CA, pp. 262-269, Mar. 2000.
- I.F. Proгри and W.R. Michalson, "A combined GPS satellite/pseudolite system for category III precision landing," in *Proc. IEEE PLANS*, Palm Spring, CA, Apr. 2002.
- I.F. Proгри, W.R. Michalson, and J. Hill, "Assessing the accuracy of navigation algorithms using a combined system of GPS satellites and pseudolites," in *Proc. ION-NTM*, Long Beach, CA, pp. 473-481, Jan. 2001.
- I.F. Proгри, J. Hill, and W.R. Michalson, "A Doppler based navigation algorithm," in *Proc. ION-NTM*, Long Beach, CA, pp. 482-490, Jan. 2001.
- I.F. Proгри and W.R. Michalson, "An innovative navigation algorithm using a system of fixed Pseudolites," in *Proc. ION-NTM*, Long Beach, CA, pp. 619-627, Jan. 2001.
- I.F. Proгри, J.M. Hill, and W.R. Michalson, "An investigation of the pseudolite's signal structure for indoor applications," in *Proc. ION-AM*, Albuquerque, NM, pp. 453-462, June 2001.
- I.F. Proгри and W.R. Michalson, "The impact of proposed pseudolite's signal structure on the receiver's phase and code error," in *Proc. ION-AM*, Albuquerque, NM, pp. 414-422, June 2001.
- I.F. Proгри and W.R. Michalson, "An alternative approach to multipath and near-far problem for indoor geolocation systems," in *Proc. ION-GPS*, Salt Lake City, UT, Sep. 2001.

- I.F. Proгри and W. R. Michalson, "Performance evaluation of a DSSS/CDMA/FDMA indoor geolocation system," in review *IEEE Trans. Comm.*, Nov. 2001.
- I.F. Proгри, W.R. Michalson, and M.C. Bromberg, "A DSSS/CDMA/FDMA indoor geolocation system," in *Proc. ION-GPS*, Portland, OR, pp. 155-164, Sep. 2002.
- I.F. Proгри, "Special report: magnitude and phase relationship," EE2311, WPI, Nov. 25, 2002.
- I.F. Proгри, W.R. Michalson, and D. Cyganski, "An OFDM/FDMA indoor geolocation system," in *Proc. ION-NTM*, Anaheim, CA, Jan. 2003.
- M.B. Pursley, "Spread spectrum multiple access communications," in *Multi-User Communications*, G. Longo, Ed. Vienna and New York: Springer-Verlag, 1981.

Q

- S.U.H. Qureshi, "Adaptive equalization," Ch. 12 of *Advanced Digital Communications* by K. Feher, Englewood Cliffs, NJ: Prentice-Hall, 1987.

R

- G. Rand, "Sonar and the fourth dimension," *J. Inst. Nav.*, vol. 6, no. 4, pp. 203-216, spring 1959.
- T.S. Rappaport, "Characterization the UHF factory multipath channels," Ph.D. dissertation, School of Elec. Eng., Purdue Univ., West Lafayette, IN, Dec. 1987.
- T.S. Rappaport, "Indoor radio communications for factories of the future," *IEEE Comm. Mag.*, vol. 27, no. 2, pp. 15-24, May 1989.
- T.S. Rappaport, "Characterization of UHF multipath radio channels in factory buildings," *IEEE Trans. Ant. Prop.*, vol. 37, no. 8, pp. 1058-1069, Aug. 1989.
- T.S. Rappaport, S.Y. Seidel, and K. Takamizawa, "Statistical channel impulse response models for factory and open plan building radio communicate system design," *IEEE Trans. Comm.*, vol. 39, no. 5, pp. 794-807, May. 1991.
- T.S. Rappaport and D.A. Hawbaker, "Wide-band microwave propagation parameters using circular and linear polarized antennas for indoor wireless channels," *IEEE Trans. Comm.*, vol. 40, no. 2, pp. 240-245, Feb. 1992.
- T.S. Rappaport, *Wireless Communications: Principles and Practice*. NJ: Prentice-Hall, 1996.
- R. Rau, "Postprocessing tools for ultra-wideband SAR images," Ph.D. dissertation, Georgia Inst. Tech., Atlanta, 1998.
- M.S. Reynolds, "A phase measurement radio positioning system for indoor use," MS Thesis, Dep. Elec. and Comput. Eng., MIT, Cambridge, MA, Feb. 1999.
- S.O. Rice, "Mathematical analysis of random noise," *Bell. Sys. Tech. J.*, vol. 23, pp. 282-332, 1944 and pp. 46-156, 1954.
- M.J. Riezenman, "The ABCs of the IEEE 802.11," *IEEE Spectrum Mag.*, p. 20, Sep. 2002.

- J.A. Roberts, "Packet Radio Performance over Fading Channels," Ph.D. dissertation, Dep. Elec. Eng. Comput. Sci., Santa Carla Univ., Santa Carla, CA, May 1979.
- J.A. Roberts and J.M. Bargallo, "DPSK performance for indoor wireless Rician fading channels," *IEEE Trans. Comm.*, vol. 42, no. 2/3/4, pp. 592-596, Feb/Mar/Apr. 1994.
- A.J. Rustako, Jr., N. Amitay, G.J. Owens, and R.S. Roman, "Radio propagation at microwave frequencies for line-of-sight microcellular mobile and personal communications," *IEEE Trans. Veh. Technol.*, vol. 40, pp. 203-210, 1991.

S

- A.A.M. Saleh and R.A. Valenzuela, "A statistical model for indoor multipath propagation," *IEEE J. Select. Areas Comm.*, vol. SAC-5, pp. 128-137, Feb. 1987.
- A.A.M. Saleh, A.J. Rustako, Jr., L.J. Cimini, Jr., G.J. Owens, and R.S. Roman, "An experimental TDMA indoor radio communications system using slow frequency hopping and coding," *IEEE Trans. Comm.*, vol. 39, no. 1, pp. 152-162, Jan. 1991.
- B. Saltzer, "A deep submergence divers' navigation system," *J. Inst. Nav.*, vol. 17, no. 1, pp. 76-82, spring 1970.
- D.V. Sarwate and M.B. Pursley, "Crosscorrelation properties of pseudorandom and related sequences," in *Proc. of IEEE*, vol. 68, pp. 593-619, May 1980.
- L. Schuchman, B.D. Elrod, and A.J. Van Dierendonck, "Applicability of an augmented GPS for navigation in the national airspace system," in *Proc. IEEE*, vol. 77, pp. 1709-1727, Nov, 1989.
- M. Schwartz, W.R. Bennet, and S. Stein, *Communication Systems and Techniques*. New York: McGraw-Hill, 1966.
- S.Y. Seidel, "UHF indoor radio channel models for manufacturing environments," Master thesis in Elec. Eng., Virginia Polytech. Inst. State Univ., Blacksburg, VA, Aug. 1989.
- S.Y. Seidel and T.S. Rappaport, "914 MHz path loss prediction models for indoor wireless communications in multifloored buildings," *IEEE Trans. Ant. Prop.*, vol. 40, no. 2, pp. 207-217, Feb. 1992.
- T.A. Sexton and K. Pahlavan, "Channel modeling and adaptive equalization of indoor radio channels," *IEEE J. Select. Areas Comm.*, vol. SAC-5, pp. 128-137, Feb. 1987.
- T.A. Sexton, "Channel modeling and high speed data transmission performance for indoor radio channel," Ph.D. dissertation, Worcester Polytechnic Institute, Aug. 1989.
- P.A. Sharples, "The modeling of terrain diffraction phenomena at microwave frequencies," Ph.D. dissertation, Univ. Birmingham, Birmingham, U.K., 1989.
- L. Shaynblat and N. Krasner, "Description of a wireless integrated SmartServer™/client system architecture," in *Proc. ION-AM*, pp. 667-675, Cambridge, MA, June 1999.

- D. Shiu and J.M. Kahn, "Differential pulse-position modulation for power-efficient optical communication," *IEEE Trans. Comm.*, vol. 47, no. 8, pp. 1201-1210, Aug. 1999.
- M.K. Simon, J.K. Omura, R.A. Scholtz, and B.K. Levitt, *Spread Spectrum Communications*, vol. 3. Rockville, MD: Comput. Sci., 1984 and 1994.
- K. Siwiak, *Radio Wave Propagation and Antennas for Personal Communications*. New York: Artech House, 1995.
- M.L. Skolnik, *Introduction to Radar Systems*, 2nd ed. Boston, MA: McGraw-Hill, 1980.
- E.N. Skomal, *Man-Made Radio Noise*. New York: Van Nostrand Reinhold, 1978.
- E.N. Skomal and A.A. Smith, *Measuring the Radio Frequency Environment*. New York: Van Nostrand Reinhold, 1985.
- M. Soumekh, *Synthetic Aperture Radar Signal Processing with MATLAB Algorithms*. New York: Wiley, 1999.
- J.J. Spilker, *Digital Communications by Satellite*. Englewood Cliffs, NJ: Prentice-Hall, 1977.
- B.A. Stain and W.L. Tsang, "Pseudolite-aided GPS: a comparison," in *Proc. IEEE PLANS*, pp. 329-333, 1988.
- B.A. Stain and W.L. Tsang, "COTS GPS C/A-code receivers with pseudolites for range PSL applications," in *Proc. IEEE PLANS*, pp. 101-107, 1990.
- J.S. Stambaugh and R.B. Thibault, "Navigation requirements for autonomous underwater vehicles," *J. Inst. Nav.*, vol. 39, no. 1, pp. 79-92, spring 1992.
- T. Stansell, Jr., "RTCM SC-104 recommended pseudolite signal specification," in *Global Positioning System*, vol. III. Silver Spring, MD: Institute of Navigation, 1986.
- R. Steele, *Mobile Radio Communications*. London, U.K.: Pentech Press, 1992.
- F.G. Stremler, *Introduction to Communication Systems*. Reading, MA: Addison-Wesley, 1982.
- W.L. Stutzman and G.A. Thiele, *Antenna Theory and Design*. New York: Wiley, 1981.
- G.L. Stüber, *Principles of Mobile Communication*. Dordrecht, NL: Kluwer Academic, 1996.
- J. Sun, "Analyses of digital transmissions over wireless fading channels," Ph.D. dissertation, Commun. Sci. Inst., Univ. Southern California, Feb. 1996.
- H. Suzuki, "A statistical model for urban radio propagation," *IEEE Trans. Comm.*, vol. COMM-25, pp. 673-685, July 1977.

T

- P. Taaghoul et al., "Satellite UMTS/IMT2000 W-CDMA air interfaces," *IEEE Comm. Mag.*, vol. 37, no. 9, pp. 116-126, Sep. 1999.
- C. Tannous, R. Davies, and A. Angus, "Strange attractors in multipath propagation," *IEEE Trans. Comm.*, vol. 39, no. 5, pp. 629-631, May. 1991.
- J.D. Taylor, *Introduction to Ultrawide-Band (UWB) Radar Systems*. Boca Raton, FL: CRC Press, 1995.

- C. Tellambura, I.R. Johnson, Y.J. Guo, and S.K. Barton, "Frequency-offset estimation for HIPERLAN," *IEEE Trans. Comm.*, vol. 47, no. 8, pp. 1137-1139, Aug. 1999.
- D. Tholl, M. Fattouche, R.J.C. Builtitude, P. Melancon, and H. Zaghloul, "A comparison of two radio propagation channel impulse response determination techniques," *IEEE Trans. Ant. Prop.*, vol. 41, no. 4, pp. 515-517, April 1993.
- M.J. Tonkel, "Navigation in ocean surveys," *J. Inst. Nav.*, vol. 14, no. 4, pp. 368-375, winter 1967-68.
- G.L. Turin, "Communication through noisy, random multipath varying channels," in *1956 IRE Convention Record*, part 4, pp. 154-166.
- G.L. Turin, *et al.* "A statistical model of urban multipath propagation," *IEEE Trans. Veh. Technol.*, vol. VT-21, pp. 1-9, Feb. 1972.
- E.E. Turner, B.J. Thompson, and O.H. Jackson, "The Raytheon acoustic Doppler navigator," *J. Inst. Nav.*, vol. 13, no. 3, pp. 210-221, autumn 1966.
- W.H.W. Tuttlebee, Ed., *Cordless Telecommunications Worldwide*. New York: Springer-Verlag, 1997.

U

V

- R.A. Valenzuela, "Performance of adaptive equalization for indoor radio communications," *IEEE Trans. Comm.*, vol. 37, no. 3, pp. 291-293, Mar. 1989.
- A.J. Van Dierendonck, B.D. Elrod, and W.C. Melton, "Improving the integrity, availability and accuracy of GPS using pseudolites," in *Proc. NAV*, Royal Institute of Navigation, London, UK, Oct. 1989.
- A.J. Van Dierendonck, "The role of pseudolites in the implementation of differential GPS," in *Proc. IEEE PLANS*, pp. 370-377, 1990.
- R. Van Nee, "Multipath and multi-transmitter interference in spread-spectrum communication and navigation systems," Ph.D. dissertation, Delft University of Technology, Delft, The Netherlands, 1995.
- M.S. Varela and M.G. Sanchez, "Study of a frequency diversity system for indoor digital TV," *IEEE Trans. Broad.*, vol. 46, no. 2, pp. 165-170, June 2000.
- S. Verdú, "Recent progress in multiuser detection," in *Advances in Communication and Signal Processing*. New York: Springer-Verlag, 1989.
- A.J. Viterbi, *CDMA, Principles of Spread Spectrum Communication*. Reading, MA: Addison Wesley, 1995.

- P. Vlach, "Measurement, prediction, and analysis of the radio frequency electromagnetic environment outside and inside hospitals," Master's thesis, Dept. Elect. Eng., McGill Univ., Montreal, Canada, 1994.
- P. Vlach, B. Segal, J. LeBel, and T. Pavlasek, "Cross-floor signal propagation inside a contemporary ferro-concrete building at 434, 862, and 1705 MHz," *IEEE Trans. Ant. Prop.*, vol. 47, no. 7, pp. 1230-1232, July 1999.
- W.J. Vogel and G.W. Torrence, "Propagation measurements for satellite radio reception inside buildings," *IEEE Trans. Ant. Prop.*, vol. 41, no. 7, pp. 954-961, July 1993.

W

- J. Wang and M. Moeneclaey, "Hybrid DS/SFH-SSMA with predetection diversity and coding over indoor radio multipath Rician-fading channels," *IEEE Trans. Comm.*, vol. 40, no. 10, pp. 1654-1662, Oct. 1992.
- J. Wang and M. Moeneclaey, "Multiple hops/symbol FFH-SSMA with MFSK modulation and Reed-Solomon coding for indoor radio," *IEEE Trans. Comm.*, vol. 41, no. 5, pp. 793-801, May. 1993.
- J. Wang, M. Moeneclaey, and L.B. Milstein, "DS-CDMA with predetection diversity for indoor radio communications," *IEEE Trans. Comm.*, vol. 42, no. 2/3/4, pp. 1929-1938, Feb/Mar/Apr. 1994.
- Y. Wang, S. Safavi-Naeini, S.K. Chaudhuri, "A hybrid technique based on combining ray tracing and FDTD methods for site-specific modeling of indoor radio wave propagation," *IEEE Trans. Ant. Prop.*, vol. 48, no. 5, pp. 743-754, May 2000.
- Webster's New World Dictionary of the American Language*. College Edition, Cleveland, OH: World Publishing Co., 1957.
- W. Webb, "Broadband fixed wireless access as a key component of the future integrated communications environment," *IEEE Comm. Mag.*, vol. 39, no. 9, pp. 115-121, Sep. 2001.
- D.R. Wehner, *High Resolution Radar*. Norwood, MA: Artech House, Inc, 1987.
- M.J. Wenninger, *Spherical Models*. New York: Cambridge Univ. Press, 1979.
- M. Win and R. Scholtz, "On the performance of ultra-wide bandwidth signals in dense multipath environment," *IEEE Comm. Letters*, vol. 2, no. 2, Feb. 1998, pp. 51-53.
- S. Wisotsky AND J.A. Dolan, "Subloran-a sonic underwater long range aid to navigation employing cross-correlation of FM-CW signals," *J. Inst. Nav.*, vol. 13, no. 2, pp. 148-153, Summer 1966.
- T.-C. Wu, C.-C. Chao, and K.-C. Chen, "Capacity of synchronous coded DS SFH and FFH spread-spectrum multiple-access for wireless local communications," *IEEE Trans. Comm.*, vol. 45, no. 5, pp. 200-212, Feb. 1997.

X

H.H. Xia and H.L. Bertoni, "Diffraction of cylindrical and plane waves by an array of absorbing half screens," *IEEE Trans. Ant. Prop.*, vol. 40, pp. 170-177, Feb, 1992.

Y

J. Yang, "Diversity receiver scheme and system performance evaluation for a CDMA system," *IEEE Trans. Comm.*, vol. 47, no. 2, pp. 272-280, Feb. 1999.

P. Yegani and C.D. McGillem, "A statistical model for line-of-sight (LOS) factory radio channels," in *Proc. Vehicular Techn. Conf. VTC'89*, pp. 496-503, San Francisco, May 1989.

P. Yegani and C.D. McGillem, "A statistical model for the factory radio channel," *IEEE Trans. Comm.*, vol. 39, no. 10, pp. 1445-1454, Oct. 1991.

J.W. Youngberg, "A novel method for extending GPS to underwater applications," *J. Inst. Nav.*, vol. 38, no. 3, pp. 263-271, fall 1991.

Z

C.A. Zelle, "Radiowave propagation over irregular terrain using the parabolic equation method," Ph.D. dissertation, Univ. Birmingham, Birmingham, U.K., 1996.

Y. Zhao, "Standardization of mobile phone positioning for 3G systems," *IEEE Comm. Mag.*, vol. 40, no. 7, pp. 108-116, Jul. 2002.